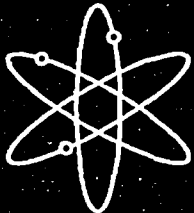




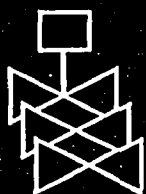
Proceedings of the 2003 Nuclear Safety Research Conference



Held at
Marriott Hotel at Metro Center
Washington, DC
October 20-22, 2003



U.S. Nuclear Regulatory Commission
Office of Nuclear Regulatory Research



Proceedings prepared by
Brookhaven National Laboratory



AVAILABILITY OF REFERENCE MATERIALS IN NRC PUBLICATIONS

NRC Reference Material

As of November 1999, you may electronically access NUREG-series publications and other NRC records at NRC's Public Electronic Reading Room at <http://www.nrc.gov/reading-rm.html>. Publicly released records include, to name a few, NUREG-series publications; *Federal Register* notices; applicant, licensee, and vendor documents and correspondence; NRC correspondence and internal memoranda; bulletins and information notices; inspection and investigative reports; licensee event reports; and Commission papers and their attachments.

NRC publications in the NUREG series, NRC regulations, and *Title 10, Energy*, in the Code of *Federal Regulations* may also be purchased from one of these two sources.

1. The Superintendent of Documents
U.S. Government Printing Office
Mail Stop SSOP
Washington, DC 20402-0001
Internet: bookstore.gpo.gov
Telephone: 202-512-1800
Fax: 202-512-2250
2. The National Technical Information Service
Springfield, VA 22161-0002
www.ntis.gov
1-800-553-6847 or, locally, 703-605-6000

A single copy of each NRC draft report for comment is available free, to the extent of supply, upon written request as follows:

Address: Office of the Chief Information Officer,
Reproduction and Distribution
Services Section
U.S. Nuclear Regulatory Commission
Washington, DC 20555-0001
E-mail: DISTRIBUTION@nrc.gov
Facsimile: 301-415-2289

Some publications in the NUREG series that are posted at NRC's Web site address <http://www.nrc.gov/reading-rm/doc-collections/nuregs> are updated periodically and may differ from the last printed version. Although references to material found on a Web site bear the date the material was accessed, the material available on the date cited may subsequently be removed from the site.

Non-NRC Reference Material

Documents available from public and special technical libraries include all open literature items, such as books, journal articles, and transactions, *Federal Register* notices, Federal and State legislation, and congressional reports. Such documents as theses, dissertations, foreign reports and translations, and non-NRC conference proceedings may be purchased from their sponsoring organization.

Copies of industry codes and standards used in a substantive manner in the NRC regulatory process are maintained at—

The NRC Technical Library
Two White Flint North
11545 Rockville Pike
Rockville, MD 20852-2738

These standards are available in the library for reference use by the public. Codes and standards are usually copyrighted and may be purchased from the originating organization or, if they are American National Standards, from—

American National Standards Institute
11 West 42nd Street
New York, NY 10036-8002
www.ansi.org
212-642-4900

Legally binding regulatory requirements are stated only in laws; NRC regulations; licenses, including technical specifications; or orders, not in NUREG-series publications. The views expressed in contractor-prepared publications in this series are not necessarily those of the NRC.

The NUREG series comprises (1) technical and administrative reports and books prepared by the staff (NUREG-XXXX) or agency contractors (NUREG/CR-XXXX), (2) proceedings of conferences (NUREG/CP-XXXX), (3) reports resulting from international agreements (NUREG/IA-XXXX), (4) brochures (NUREG/BR-XXXX), and (5) compilations of legal decisions and orders of the Commission and Atomic and Safety Licensing Boards and of Directors' decisions under Section 2.206 of NRC's regulations (NUREG-0750).

DISCLAIMER: Where the papers in these proceedings have been authored by contractors of the U. S. Government, neither the U.S. Government nor any agency thereof, nor any U.S. employee makes any warranty, expressed or implied, or assumes any legal liability or responsibility for any third party's use or the results of such use, of any information, apparatus, product, or process disclosed in these proceedings, or represents that its use by such third party would not infringe privately owned rights. The views expressed in these proceedings are not necessarily those of the U. S. Regulatory Commission.

Proceedings of the 2003 Nuclear Safety Research Conference

Held at
Marriott Hotel at Metro Center
Washington, DC
October 20-22, 2003

Manuscript Completed: May 2004
Date Published: June 2004

Compiled by: S. Monteleone, Meeting Coordinator

S. Nesmith, NRC Project Manager

Office of Nuclear Regulatory Research
U.S. Nuclear Regulatory Commission
Washington, DC 20555-0001

Proceedings prepared by
Brookhaven National Laboratory



**NUREG/CP-0185, has been reproduced
from the best available copy.**

ABSTRACT

This report contains papers presented at the 2003 Nuclear Safety Research Conference at the Marriott Hotel at Metro Center in Washington, DC, October 20-22, 2003. The papers were presented in each of the conference's technical sessions and at poster sessions over the course of the three days. They describe progress and results of programs in nuclear safety research conducted in this country and abroad. International participation in the meeting included papers presented by researchers from France, Germany, Japan, Norway, Russia and Spain.

The titles of the papers and the names of the authors have been updated and may differ from those that appeared in the final program of the meeting.

**PROCEEDINGS OF THE
2003 NUCLEAR SAFETY RESEARCH CONFERENCE
OCTOBER 20-22, 2003**

Contents

	<u>Page</u>
Abstract	iii
Registered Attendees	ix

MONDAY, OCTOBER 20, 2003

**RISK-INFORMED REGULATION /REALISTIC CONSERVATISM SESSION
H. Hamzehee, M. Reinhart (NRC), Co-Chairs**

Experience with PRA in the Generic Issues Program	1
H. Vandermolen (NRC)	
A Pilot Application of a Risk-Informed Approach for Certification of Dry Cask Storage of Spent Fuel	11
K. Gruss, M. Waters, C. Lui (NRC)	
Option 3: Risk-Informed Alternative to 10CFR50.46 and GDC 35	23
E. McKenna, J. Lane (NRC)	
Fire Risk Research Program: Advances Supporting Risk-Informed Regulation	29
J. Hyslop (NRC)	

TUESDAY, OCTOBER 21, 2003

**ADVANCED REACTORS SESSION
S. Rubin, J. Lyons (NRC), Co-Chairs**

NRC's Advanced Reactor Research Program	37
J. Flack (NRC)	
DOE Advanced Nuclear Reactor Research: A Summary	43
J. Lake, R. Schultz (INEEL)	
Status of Thermal-Hydraulic Research Activities Related to Advanced Reactors	65
S. Bajorek (NRC)	

BEHAVIOR OF SPENT FUEL IN DRY CASKS SESSION

R. Meyer, C. Interrante (NRC), Co-Chairs

Cladding Behavior during Dry Cask Handling and Storage 71
H. Tsai and M. Billone (ANL)

Mechanical Properties of Irradiated Zircaloy-4 for Dry Cask Storage
Conditions and Accidents 85
R. Daum, S. Majumdar, M. Billone (ANL)

HIGH BURNUP FUEL BEHAVIOR DURING REACTOR ACCIDENTS SESSION

R. Meyer (NRC), R. Yang (EPRI), Co-Chairs

LOCA Results for Advanced-Alloy and High-Burnup Zircaloy Cladding 97
Y. Yan, T. Burtseva, M. Billone (ANL)

LOCA Behavior of E110 Alloy 123
L. Yegorova, K. Lioutov (Kurchatov Institute),
V. Smirnov, A. Goryachev, V. Chesanov (RIA)

Recent Data on M5™ Alloy Under Loca Conditions 141
J. Mardon (Framatome), N. Waeckel (EDF-Septen)

Effects of Pellet Expansion and Cladding Hydrides on
PCMI Failure of High Burnup LWR Fuel during Reactivity Transients 161
T. Fuketa, et al. (JAERI)

CABRI CIPO-1 Preliminary Test Results 173
J. Melis, et al. (IRSN)

OPERATING EXPERIENCE EVALUATION SESSION

J. Ibarra (NRC), Chair

Overview of Research Findings on the Mitigating Systems Performance Index (MSPI) 177
D. Dube (NRC)

Boron Dilution Tests / PKL 185
K. Umminger, B. Brand (Framatome ANP)

WEDNESDAY, OCTOBER 22, 2003

**MATERIALS DEGRADATION - PRESENT STATUS AND FUTURE DIRECTIONS SESSION
W. Cullen (NRC), Chair**

NDE for Reactor Pressure Vessel Head Replacements	207
S. Doctor, G. Schuster (PNNL)	
Predicting the Occurrence of Corrosion Failures in Nuclear Power Components with Emphasis on Applications of Alloy 690	221
R. Staehle (U. Minnesota), J. Gorman (Dominion Engineering)	
Anticipating Materials Problems; Field Experience and Laboratory Studies	233
W. Shack, O. Chopra, H. Chung (ANL)	
Strategic Planning for RPV Head Nozzle PWSCC	251
G. White, S. Hunt (Dominion Engineering)	

POSTER SESSIONS - MONDAY, TUESDAY, WEDNESDAY

Latest Results of the US Nuclear Regulatory Commission Pressurized Thermal Shock Rule Re-evaluation Project	273
T. Dickson (ORNL), M. Kirk, C. Santos (NRC)	
The Effects of Aliovalent Elements on Nodular Oxidation of Zr-Base Alloys	283
H. Chung (ANL)	
LOCA Testing at Halden, Trial Runs in IFA-650	299
V. Lestinen, E. Kolstad, W. Wiesenack (OECD Halden Reactor Project)	
A Scaling Method for RIA Data	311
R. Meyer (NRC)	
Recent Results from LOCA Study at JAERI	321
F. Nagase, T. Fuketa (JAERI)	
Key Input Variables for RIA Simulations: A Study Based on FRAPCON and SCANAIR Codes	333
F. Barrio, L. Herranz (CIEMAT)	

Nuclear Safety Research Conference

October 20-22, 2003 - Washington, DC USA

Organized by the U.S. Nuclear Regulatory Commission

Office of Nuclear Regulatory Research

Registered Attendees

Parvalz Akhtar
Canadian Nuc. Safety Comm.
PO Box 1046, Station B
Ottawa, Ontario K1P 5S9 Canada
Phone: 613 995 3093
Fax:
E-mail: akhtarp@cnsccsn.gc.ca

Mark Allen
Sandia National Lab
PO Box 5800, MS 0748
Albuquerque, NM 87185 USA
Phone: 505 844 7197
Fax: 505 844 2829
E-mail: msallen@sandia.gov

Jan Almberger
Vattenfall Fuel

Stockholm, SE16287 Sweden
Phone: 46 8 739 5444
Fax: 46 8 178640
E-mail: jan.almberger@vattenfall.co

John Alvia
Anatech Corp.
5435 Oberlin Drive
San Diego, CA 92121 USA
Phone: (858) 455-6350
Fax:
E-mail: john@anatech.com

Samim Anghale
University of Florida
202 NSC
Gainesville, FL 32611 USA
Phone: 352 392 8653
Fax: 352 392 8656
E-mail: anghale@ufl.edu

Alvin Ankrum
Pacific Northwest National Lab
PO Box 999
Richland, WA 99352 USA
Phone: 509 372 4095
Fax:
E-mail: alvin.ankrum@pnl.gov

Alex Avvakumov
NSI-RRC Kurchatov Institute
123182 Kurchatov Square 1
Moscow, Russian Federation
Phone: 7 095 196 7466
Fax: 7 095 196 1702
E-mail: avvakumov@nsi.kiae.ru

Markus Baier
Technical University Munich
Walther-Meissner Str. 2
Garching, 85748 Germany
Phone: 49 89 13903
Fax: 49 89 13900
E-mail: baier@isar.tuom.de

Julio Barcelo
CSN
Justo Dorado 11
Madrid, 28040 Spain
Phone: 34 91 346 03 35
Fax: 34 91 346 03 78
E-mail: jbvnet@csn.es

Registered Attendees

Joel Bardelay
IRSN
BP 17
Fontenay aux Roses, Cedex 92262
France
Phone: 33 1 5835 7568
Fax: 33 1 5835 7971
E-mail: joel.bardelay@irsn.fr

Al Barone
Parallax
10200 Century Blvd.
Gemantown, MD USA
Phone: 301 428-1493
Fax: 301 428-1498
E-mail: abarone@parallaxnet.com

Felix Barrio
CIEMAT
Avda. Complutense 22
Madrid, 28040 Spain
Phone: 34 91 346 6000
Fax: 34 91 346 6233
E-mail: felix.barrio@ciemat.es

Robert Beall
Constellation Energy Group
1650 Calvert Cliffs Pkwy
Lusby, MD 20657 USA
Phone: 410 495 4018
Fax: 410 495 4498
E-mail: robert.h.beall@constellation.

Ralph Best
JAI Corp.
2750 Prosperity Avenue
Fairfax, VA 22031 USA
Phone: (703) 645-0445
Fax:
E-mail: rbest@jaicorp.com

Carl Beyer
Pacific Northwest National Lab
PO Box 999
Richland, WA 99352 USA
Phone: 509 372 4605
Fax: 509 372 6485
E-mail: carl.beyer@pnl.gov

Linda Billings
SETI Inst. / NASA HQ
3654 Vacation La
Arlington, VA 22207 USA
Phone: 202 479 4311
Fax: 202 484 8251
E-mail: lbillings@seti.org

Michael Billone
Argonne National Lab
9700 S. Cass Ave.
Argonne, IL 60439 USA
Phone: 630 252 7146
Fax: 630 252 9232
E-mail: billone@anl.gov

Jeffrey Binder
Oak Ridge National Lab

Oak Ridge, TN USA
Phone: 865 576 3879
Fax:
E-mail: binderjl@ornl.gov

Thomas Blejwas
Sandia National Lab
PO Box 5800, MS0736
Albuquerque, NM 87185-0736 USA
Phone: 505 844 0577
Fax: 505 844 0955
E-mail: teblejw@sandia.gov

Bernhard Brand
Framatome ANP GmbH
Freyeslebenstr 1
Erlangen, 91058 Germany
Phone: 49 9131 1892593
Fax: 49 9131 1892851
E-mail: bernhard.brand@framatome-

Charles Brinkman
Westinghouse
12300 Twinbrook Pkwy, Ste 330
Rockville, MD 20852 USA
Phone: 301 881 7040
Fax: 301 881 7043
E-mail: brinkmcb@westinghouse.co

Registered Attendees

Dr. Brinkmann
Framatome ANP GmbH
Freyesle Str. 1
Erlangen, 91050 Germany
Phone: 49 9131 6630
Fax: 49 9131 6685
E-mail: gerd.brinkmann@framatome-

Geoff Brown
Serco Assurance
Thomson House, Risley, Warrington
Cheshire, WA3 6AT United Kingdom
Phone: 44 1925 254473
Fax: 44 1925 254536
E-mail: geoff.brown@sercoassuranc

Edward Burns

5627 Beacon St
Pittsburgh, PA 15217-2011 USA
Phone: 703 236 2752
Fax: 703 236 1930
E-mail: emburns@earthlink.net

John Butler
Nuclear Energy Institute
1776 I St, NW
Washington, DC 20006 USA
Phone: 202 739 8108
Fax:
E-mail: jcb@nei.org

Jose Butragueno
CSN
Justo Dorado, 11
Madrid, 28040 Spain
Phone: 34 1 91 3460 407
Fax: 34 1 91 3460 588
E-mail: jlbcc@csn.es

Patricia Campbell
Winston & Strawn
1400 L St., NW
Washington, DC 20005 USA
Phone: 202 371 5828
Fax: 202 371 5950
E-mail: pcambell@winston.com

Bernard Carlucc
Framatome-ANP
10 rue Juliette Recamier
Lyon, 69456 France
Phone: 33 4 7274 7066
Fax: 33 4 7274 7330
E-mail: bernard.carlucc@framatome-

Earl Carnes
US Department of Energy
1000 Independence Ave
Washington, DC 20585-0270 USA
Phone: 301 903 5255
Fax:
E-mail: earl.carnes@hq.doe.gov

S.Y. Chen
Argonne National Lab
9700 So Cass Ave
Argonne, IL 60439 USA
Phone: 630 252 7695
Fax: 630 252 4611
E-mail: sychen@anl.gov

Shih-Kuel Chen
TECRO/Science Division
4201 Wisconsin Ave., NW
Washington, DC 20016 USA
Phone: 202 895 1932
Fax: 202 895 1939
E-mail: skchen@tecrosd.org

Kuang-Tsan Chiang
Southwest Research Institute
6220 Culebra Road
San Antonio, Texas USA
Phone: 210 522-2309
Fax: 210 522-5184
E-mail: kchiang@swri.org

T.Y. Chu
US Department of Energy
1000 Independence Ave
Washington, DC 20585 USA
Phone: 202 586 5883
Fax:
E-mail: t.y.chu@nnsa.doe.gov

Registered Attendees

Bub-Dong Chung
KAERI
Dukjin 150, Yusong-Gu
Daejon, Korea
Phone: 82 42 868 0223
Fax: 82 42 861 2535
E-mail: bdchung@kaeri.re.kr

Hae-Dong Chung
Korea Institute of Nuclear Safety
19 Kugsungdong Yusungku
Daejon, Korea
Phone:
Fax: 82 42 861 2535
E-mail: k047chd@kins.re.kr

Hee Chung
Argonne National Lab
9700 So Cass Ave.
Argonne, IL 60439 USA
Phone:
Fax:
E-mail:

Sun-Kyo Chung
KEPCO Nuclear Fuel Co.
493 Dukjin-dong, Yuseong-ku
Taejeon, 305-353 Korea
Phone: 81 42 868 1830
Fax: 81 42 863 4430
E-mail: skchung@knfc.co.kr

Gerard Cognet
CEA Saclay
CEA/DEN/DSNI Batiment 121
Gif sur Yvette, 91191 France
Phone: 33 1 6908 5712
Fax: 33 1 6908 5870
E-mail: gerard.cognet@cea.fr

Rodney Cook
New Tenn. Energy Svcs.
6178 Chase Rd
Millington, TN 38053 USA
Phone: 901 353 1860
Fax:
E-mail: rodmcook@msn.com

John Cunningham
MPR Associates, Inc.
320 King Street
Alexandria, VA 223143230 USA
Phone: (703) 519-0200
Fax: 703 519-0224
E-mail: jcunningham@mpr.com

Diane D'Arrigo
NIRS
1424 16th St NW, Ste 404
Washington, DC 20036 USA
Phone: 202 328 0002
Fax:
E-mail: dianed@nirs.org

Robert Daum
Argonne National Lab
9700 So Cass Ave., Bldg. 212
Argonne, IL 60439 USA
Phone: 630 252 9188
Fax: 630 252 9232
E-mail: rdaum@anl.gov

Benoit DeBoeck
AVN
Rue Walcourt 148
Brussels, B1070 Belgium
Phone: 32(2)5280121
Fax: 32(2)5280101
E-mail: bdb@avn.be

Joseph DeBor
Aeroflex Corp.
3630 N. 21st Ave
Arlington, VA 22207 USA
Phone: 703 524 3222
Fax:
E-mail: josephdebor@mindspring.co

David Diamond
Brookhaven National Lab
Bldg. 130, 32 Lewis Rd.
Upton, NY 11973-5000 USA
Phone: 631 344 2604
Fax: 631 344 3957
E-mail: ddiamond@bal.gov

Registered Attendees

Steven Doctor
Pacific Northwest National Lab
PO Box 999, MSIN K5-26
Richland, WA 99352 USA
Phone: 509 375 2495
Fax: 509 375 6437
E-mail: steven.doctor@pnl.gov

Stephen Domotor
US Department of Energy
1000 Independence Ave, SW
Washington, DC 20585 USA
Phone: 202 586 0871
Fax: 202 586 3915
E-mail: stephen.domotor@eh.doe.gov

Bert Dunn
Framatome ANP
PO Box 10935
Lynchburg, VA 24506-0935 USA
Phone: 434 832 2427
Fax: 434 832 2531
E-mail: bert.dunn@framatome-anp.c

Kurt Edsinger
EPRI
3412 Hillview Ave.
Palo Alto, CA USA
Phone: 650 855 1026
Fax:
E-mail: kedsinge@epri.com

Sophie Ehster
Framatome-ANP
10 rue Juliette Recamier
Lyon, 69456 France
Phone:
Fax:
E-mail: sophie.ehster@framatome-a

Robert Einziger
Argonne National Lab
434 Saratoga Dr
Aurora, IL 60504 USA
Phone: 630 236 9824
Fax:
E-mail: re_einziger@hotmail.com

Fred Emerson
Nuclear Energy Institute
1776 I St, NW
Washington, DC USA
Phone: 202 739 8086
Fax:
E-mail: fae@nel.org

Tony Eng
US Department of Energy
19901 Germantown Rd
Germantown, MD 20874 USA
Phone: 301 903 4210
Fax: 301 903 4594
E-mail: tony.eng@eh.doe.gov

Thecla Fabian
Nuclear Waste News
8737 Colesville Rd., Ste 1100
Silver Spring, MD 20910 USA
Phone: 301 587 6300
Fax: 301 587 1081
E-mail: tfabian@bpinews.com

Herbert Feinroth
Gamma Engineering Corp.
15815 Crabbs Branch Way
Rockville, MD 20855 USA
Phone: 301 840 8415
Fax: 301 840 1479
E-mail: hfeinroth@gamma-eng.com

Madeline Feltus
US Department of Energy
19901 Germantown Rd
Germantown, MD 20874 USA
Phone: 301 903 2308
Fax: 301 903 5057
E-mail: madeline.feltus@hq.doe.gov

Karl Fleming
Consultant
616 Sereno View Rd
Encinitas, CA 92024 USA
Phone: 858 455 9500
Fax: 858 452 7831
E-mail: fleming@ti-sd.com

Registered Attendees

Robert Fontaine
KAPL, Inc.

USA
Phone: 518 295 4592
Fax:
E-mail: bobfont@nycap.rr.com

Kazuo Fujiki
JAERI
1825 K St, NW, Ste 508
Washington, DC 20006 USA
Phone: 202 293 4551
Fax: 202 293 4553
E-mail: fujiki@hems.jaeri.go.jp

Yoshitaka Fujisawa
Chubu Electric Power
900 17th St, NW
Washington, DC 20852 USA
Phone: 202 775 1960
Fax: 202 331 9256
E-mail: fujisawa.yoshitaka@chuden.c

Toyoshi Fuketa
JAERI
2-4 Shirakjata-Shirane
Tokai-mura, Ibaraki-ken 319-1195
Japan
Phone: 81 29 2825277
Fax: 81 29 2825429
E-mail: fuketa@hems.jaeri.go.jp

John Galembush
Westinghouse Electric
4350 Northern Pike
Monroeville, PA 15146 USA
Phone: 412 374 5036
Fax: 412 374 4011
E-mail: galemjls@westinghouse.com

F. Gantenbein
IRSN
BP 17
Fontenay-aux-Roses Cedex, 92262
France
Phone: 33158 357816
Fax: 33158 355971
E-mail: francoise.gantenbein@irsn.fr

Pablo Garcia Sedano
Iberinco
Avenida de Burgos 8-B
Madrid, 28036 Spain
Phone: 34 91 767 5201
Fax: 34 91 767 5080
E-mail: pgs@iberinco.com

Andrew Glendening
Penn State Univ.
120 Steidle Bldg
University Park, PA 16802 USA
Phone: 814 574 1592
Fax:
E-mail: alg216@psu.edu

Carl Gogolak
USDHS/EML
201 Varick St., 5th Fl
New York, NY 10014 USA
Phone: 212 620 3635
Fax: 212 620 3600
E-mail: cvg@eml.doe.gov

D.A. Griffiths
Serco Assurance
Thomson House, Risley, Warrington
Cheshire, WA3 6AT England
Phone: 01925 2564263
Fax: 01925 254536
E-mail: david.griffiths@sercoassuran

Gregory Gromov
SSTC
35-37 Radgospna Street
Kiev, Ukraine
Phone: 380 44 4524435
Fax: 380 44 452 4925
E-mail: gromov@l.kiev.ua

Rodney Grow
Utility Resource Assocs
1901 Research Blvd., Ste 405
Rockville, MD 20850 USA
Phone: 301 294 0866
Fax: 301 294 7879
E-mail: rlgrow@urac.com

Registered Attendees

Yue Guan
ASTM, Inc.
2136 Gallows Road
Dunn Loring, VA 22027 USA
Phone: (703) 744-1070
Fax: 703 206-0092
E-mail: guan@astm-inc.com

Paul Gunter
Nuclear Information & Resource Svc
1424 16th St NW, #404
Washington, DC 20036 USA
Phone: 202 328 0002
Fax: 202 462 2183
E-mail: pgunter@nirs.org

Jaejoo Ha
KAERI
Dukjin 150
Daejeon, Korea
Phone: 82 42 868 2755
Fax: 82 42 868 8256
E-mail: jjha@kaeri.re.kr

Brian Haagensen
PSHA, Inc.
27 Charter Oak Dr
East Lyme, CT 06333 USA
Phone: 860 739 0333
Fax: 860 739 9346
E-mail: bhaagensen@psa-inc.com

Lothar Hahn
GRS
Schwertnergasse 1
Koln, 50667 Germany
Phone: 49 221 206 8705
Fax: 49 221 206 8704
E-mail: hah@grs.de

Tadayuki Hakata
Nuclear Safety Commission
3-1-1 Kasumigaseki Chiyoda-Itu
Tokyo, 100-8970 Japan
Phone: 81 3 3581 9841
Fax: 81 3 3581 9836
E-mail: thakata@op.cao.go.jp

Anthony Hamins
NIST
100 Bureau Dr., Stop 8663
Gaithersburg, MD 20899-8663 USA
Phone: 301 975 6598
Fax: 301 975 4052
E-mail: anthony.hamins@nist.gov

Tom Harrison
McGraw-Hill
1200 G Street NW
Washington, DC 200053802 USA
Phone: (202) 383-2165
Fax: (202) 383-2125
E-mail: tharr@mh.com

Jack Haugh
EPRI
3412 Hillview Avenue
Palo Alto, CA 94303 USA
Phone:
Fax:
E-mail:

Yuichi Hayashi
Kansai Electric
3200 Daniel Lane, Apt 302
Monroeville, PA 15146 USA
Phone: 412 374 4931
Fax: 412 374 5456
E-mail: yhayashi@adelphia.net

Brady Haynes
US Department of Energy
10831 Amherst Ave Unit B
Silver Spring, MD 20902 USA
Phone: 202 781 6299
Fax:
E-mail: haynesca_99@yahoo.com

James Higgins
Brookhaven National Lab
Bldg. 130, PO Box 5000
Upton, NY 11973 USA
Phone: 631 344 2432
Fax: 631 344 4900
E-mail: higgins@bnl.gov

Registered Attendees

Paul Highberger
JAI Corp.
2750 Prosperity Ave., Ste 220-B
Fairfax, VA 22031 USA
Phone: 202 488 2307
Fax: 202 488 6721
E-mail: paul.highberger@rw.doe.gov

Masashi Hirano
JAERI
2-4 Shirakata Shirane
Tokai-mura, Naka-gun 319-1106
Japan
Phone: 81 29 282 5146
Fax: 81 29 282 5408
E-mail: hirano@popsvr.tokai.jaeri.go.

Brendan Hoffman
Public Citizen's CME Program

Washington, DC USA
Phone: 202 454 5130
Fax:
E-mail: bhoffman@citizen.org

Jeanne Holm
Jet Propulsion Lab
4800 Oak Grove Dr., MS 202-204
Pasadena, CA 91109 USA
Phone: 818 354 8282
Fax: 818 394 4510
E-mail: jeanne.m.holm@jpl.nasa.gov

Jerald Holm
Framatome ANP

, USA
Phone: 509 375 8142
Fax:
E-mail: jerald.holm@framatome-anp.

Heikki Holmstrom
VTT Processes
Tekniikantie 4 C
Espoo, 02150 Finland
Phone: 358 9 4565050
Fax: 358 9 4565000
E-mail: heikki.holmstrom@vtt.fi

William Horak
Brookhaven National Lab
Bldg. 475B
Upton, NY 11973-5000 USA
Phone: 631 344 2627
Fax: 631 344 7650
E-mail: horak@bnl.gov

Daniel Horner
McGraw-Hill
1200 G St., NW, Ste 1000
Washington, DC 20005 USA
Phone: 202 383 2164
Fax: 202 383 2187
E-mail: daniel_horner@platts.com

Yoji Hosokawa
IAEA
PO Box 100, Wagramerstrasse 5
Vienna, A1400 Austria
Phone: 431 2600 22762
Fax: 431 26007 22762
E-mail: y.hosokawa@iaea.org

Alejandro Huerta
CNSNS
Dr. Barragan 779
Mexico City, 03020 Mexico
Phone: 52 55 5095 3245
Fax: 52 55 5095 3295
E-mail: ahuertab@cnsns.gob.mx

Edwin Hunt
Dominion Engineering, Inc.
11730 Plaza America Drive
Reston, VA 20190 USA
Phone: (703) 437-1155
Fax:
E-mail: shunt@domeng.com

Hamilton Hunter
Oak Ridge National Lab
1 Bethel Valley Rd
Oak Ridge, TN 37831-6171 USA
Phone: 865 574 6297
Fax: 865 241 0607
E-mail: hunterht@ornl.gov

Registered Attendees

Jose Izquierdo
CSN
C/ Justo Dorado 11
Madrid, 28040 Spain
Phone: 34 91 346 0237
Fax: 34 91 346 0596
E-mail: jmir@csn.es

Rich Janati
PA Bur. of Radiation Prot.
PO Box 8469
Harrisburg, PA 17105-8469 USA
Phone: 717 787 2163
Fax: 717 783 8965
E-mail: rjanati@state.pa.us

Josef Jansky
BTB - Jansky GmbH
Gerlinger Str. 151
Leonberg, 71229 Germany
Phone: 49 7152 41058
Fax: 49 7152 3087 22
E-mail: btb@btbjansky.com

Miroslava Jansky
BTB - Jansky GmbH

Phone:
Fax:
E-mail:

Jae-Hoon Jeong
KEPCO Nuclear Fuel Co.
493 Dukjin-dong, Yuseong-ku
Taejon, 305-353 Korea
Phone: 81 42 868 1832
Fax: 81 42 863 4430
E-mail: jhjeong@knfc.co.kr

Tae Eun Jin
Korea Power Eng'g Co.
360-9 Mabuk-ri Kusong-myon
Yongin, Kyunggi-do 449-713 Korea
Phone: 82 31 289 4282
Fax: 82 31 289 3189
E-mail: jinte@ns.kopec.co.kr

Jon Johnson
Nuclear Safety & Eng'g

USA
Phone: 301 330 9280
Fax:
E-mail: johnsonjonr@aol.com

Judith Johnsrud
Sierra Club
433 Orlando Avenue
State College, PA 16803 USA
Phone: (814) 237-3900
Fax:
E-mail: johnsrud@uplink.net

Storm Kauffman
Naval Reactors
1240 Isaac Hull Avenue
Washington, DC 203768041 USA
Phone: (202) 781-6225
Fax: (202) 781-6430
E-mail: kauffmanst@navsea.navy.mil

John Kelly
Sandia National Lab
PO Box 5800, MS-0734
Albuquerque, NM 87185-0734 USA
Phone: 505 844 8993
Fax: 505 844 1480
E-mail: jekelly@sandia.gov

M. Khatib-Rahbar
Energy Research, Inc.
P.O. Box 2034
Rockville, MD 20874 USA
Phone: (301) 881-0866
Fax: 301 881-0867
E-mail: mkr@eri-world.com

Hee-Dong Kim
KAERI
150 Duckjindong Yusong
Daejeon, Korea
Phone: 82 42 868 2664
Fax: 82 42 868 8256
E-mail: hdkin@kaeri.re.kr

Registered Attendees

Hho Kim
Korea Institute of Nuclear Safety
19 Kusong-Dong
Taejon, Korea
Phone: 82 42 868 0230
Fax: 82 42 861 9945
E-mail: kimjh@kins.re.kr

In-Goo Kim
Korea Institute of Nuclear Safety
PO Box 114, Yusong
Daejon, Korea
Phone: 82 42 868 0151
Fax:
E-mail: igkim@kins.re.kr

Woong Sik Kim
Korea Institute of Nuclear Safety
PO Box 114, Yusong
Daejon, Korea
Phone: 82 42 868 0327
Fax: 82 42 861 9945
E-mail: wskim@kins.re.kr

Ronald King
Argonne National Lab
PO Box 2528
Idaho Falls, ID 83403-2528 USA
Phone: 208 533 7541
Fax: 208 533 7996
E-mail: ronald.king@anl.gov

Bernadette Kirk
Oak Ridge National Lab
PO Box 2008
Oak Ridge, TN 37831-6171 USA
Phone: 865 574 6176
Fax: 865 241 4046
E-mail: kirkbl@ornl.gov

Erik Kolstad
OECD Halden Reactor Project
PO Box 173
Halden, N-1751 Norway
Phone: 47 69 212335
Fax: 47 69 212201
E-mail: erik.kolstad@hrp.no

Don Koss
Penn State Univ.
202 B Steidle Bldg
University Park, PA USA
Phone: 814 865 5447
Fax:
E-mail: koss@ems.psu.edu

Zdenek Kriz
Nuclear Research Institute
Rez, 250 68 Czech Republic
Phone: 420 26617 3428
Fax: 420 26617 3464
E-mail: krz@ujv.cz

Junichi Kurakami
Japan Nuclear Cycle Dev. Inst.
1825 K St., NW, Ste 508
Washington, DC 20006 USA
Phone: 202 338 3770
Fax: 202 338 3771
E-mail: kurakami@jnc-dc.org

Karl Kussmaul
MPA Univ. of Stuttgart
32 Pfaffenwaldring
Stuttgart, D70569 Germany
Phone: 49 711 685 7075
Fax: 49 711 685 3053
E-mail: kussmaul@mpa.uni-stuttgart.

James Lake
INEEL
PO Box 1625, MS 3860
Idaho Falls, ID 83415-3860 USA
Phone: 208 526 7670
Fax: 208 526 2930
E-mail: lakeja@inel.gov

Vince Langman
AECL
2251 Speakman Dr.
Mississauga, Ontario L5K 1B2 Canada
Phone: 905 823 9060
Fax: 905 403 7337
E-mail: langmanv@aecl.ca

Registered Attendees

William Lanouette
US GAO
441 G St., NW (2T23)
Washington, DC 20548 USA
Phone: 202 512 6882
Fax: 202 512 6880
E-mail: lanouettew@gao.gov

Nanci Laroche
Canadian Nuc. Safety Comm.
280 Slater St.
Ottawa, Ontario K4K1H5 Canada
Phone: 613 995 2609
Fax: 613 995 5086
E-mail: larochen@cnsccsn.gc.ca

Donald Lawson
Bechtel Bettis, Inc.
PO Box 79
West Mifflin, PA 15122 USA
Phone: 412 476 5644
Fax: 412 476 6843
E-mail: lawsondl@bettis.gov

Timothy Leahy
INEEL
PO Box 1625
Idaho Falls, ID 83415-3850 USA
Phone: 208 526 4944
Fax: 208 526 2930
E-mail: tjl2@inel.gov

Stanley Levinson
Framatome ANP
3315 Old Forest Rd
Lynchburg, VA 24501 USA
Phone: 434 832 2768
Fax: 434 832 2683
E-mail: stanley.levinson@framatome

Kirill Lioutov
NSI-RRC Kurchatov Institute
123182 Kurchatov Square 1
Moscow, Russian Federation
Phone: 7 095 196 9635
Fax: 7 095 196 1702
E-mail: kirill@nsi.kiae.ru

Yung Liu
Argonne National Lab
9700 S. Cass Ave.
Argonne, IL 60439 USA
Phone: 630 252 5127
Fax: 630 252 3250
E-mail: yyliu@anl.gov

Robert Lojk
Canadian Nuc. Safety Comm.
P.O. Box 1046
Ottawa, Ontario K1P 5S9 Canada
Phone: (613) 995-7253
Fax: 613 995-5086
E-mail: lojkr@cnsccsn.gc.ca

Gustaf Lowenhielm
Swedish Nuc. Pow. Inspectorate

Stockholm, SE-10658 Sweden
Phone: 46 8 698 8496
Fax: 46 8 661 9086
E-mail: gustaf.lowenhielm@ski.se

Albert Machiels
EPRI
3412 Hillview Avenue
Palo Alto, CA 94304-1395 USA
Phone: 650 855-2054
Fax: 650 855-2002
E-mail: amachiel@epri.com

Daniel Magallon
CEA
CEA-Cadarache, BP 1, Bat 708
Saint Paul lez Durance, 13108 France
Phone: 33 4 4225 4920
Fax:
E-mail: daniel.magallon@cea.fr

Bernie Maguire
VPA Corp.
1721 Raleigh Hill Rd
Vienna, VA 22182 USA
Phone: 703 620 2111
Fax: 703 620 9072
E-mail: bermaguire@aol.com

Registered Attendees

Robert Maiers
PA Bur. of Radiation Prot.

, USA
Phone: 717 786 8979
Fax:
E-mail: rmaiers@state.pa.us

Alain Maillat
IRSN
BP1
Saint Paul Lez Durance, 13108
CEDEX France
Phone: 33 44 2253637
Fax: 33 44 2252971
E-mail: alain.maillat@irsn.fr

Valery Malofeev
NSI-RRC Kurchatov Institute
123182 Kurchatov Square 1
Moscow, Russian Federation
Phone: 7 095 196 7466
Fax: 7 095 196 1702
E-mail: malofeev@nsi.kiae.ru

Jean-Paul Mardon
Framatome ANP France
10, Rue Juliette Recamier
Lyon, Cedex 06 69456 France
Phone: 33 4 7274 8150
Fax: 33 4 7274 8145
E-mail: jeanpaul.mardon@framatom

Alexander Marion
Nuclear Energy Institute
1776 I Street, NW
Washington, DC 200063708 USA
Phone: (202) 739-8080
Fax: 202 533-0164
E-mail: am@nel.org

Mahmoud Massoud
Calvert Cliffs NPP
1650 Calvert Cliffs Pkwy.
Lusby, MD 20716 USA
Phone: 410 495 6522
Fax: 410 495 4498
E-mail: mahmoud.massoud@constel

Borut Mavko
J. Stefan Institute
Jamova 30
Ljubljana, 1000 Slovenia
Phone: 386 1 5885 330
Fax:
E-mail: borut.mavko@ijs.si

Kathryn McCarthy
INEEL
PO Box 1625
Idaho Falls, ID 83415 USA
Phone: 208 526 9392
Fax: 208 526 2930
E-mail: km3@inel.gov

Robin McCollum
Bechtel Bettis, Inc.
PO Box 79
West Mifflin, PA 15122 USA
Phone: 412 476 6356
Fax: 412 476 6364
E-mail: mccollum@bettis.gov

Colin McCormick
Rep. Ed Markey (MA-7th)
2108 Rayburn House Office Bldg
Washington, DC 20515 USA
Phone: 202 225 2836
Fax:
E-mail: colin.mccormick@mail.house

Jean-Claude Melis
IRSN
Bldg 250 - BP 3
Saint Paul Lez Durance, 13115
France
Phone: 33 4 4225 3722
Fax: 33 4 4225 2971
E-mail: jean-claude.melis@irsn.fr

Jeff Meredith
Exchange Monitor
1725 K St., NW
Washington, DC 20006 USA
Phone: (202) 296-2814
Fax: 202 296-2805
E-mail: meredith@exchangemonitor.

Registered Attendees

James Meyer
Information Systems Labs
11140 Rockville Pike, Ste 500
Rockville, MD 20852 USA
Phone: (301) 255-2269
Fax: 301 468-0883
E-mail: jmeyer@islinc.com

Lauren Miura
E&E Publishing, LLC
122 C st. NW
Washington, DC 20001 USA
Phone: (202) 737-4340
Fax: 202 737-5299
E-mail: lmiura@eenews.net

Robert Montgomery
Anatech Corp.
5435 Oberlin Drive
San Diego, CA 92121 USA
Phone: (858) 455-6350
Fax: 858 455-1094
E-mail: rob@anatech.com

Glenn Morris
US Department of Energy
NE-30 Germantown Building
Washington, DC 205851290 USA
Phone: (301) 903-9527
Fax: 301 903-5057
E-mail: glenn.morris@hq.doe.gov

Bruce Mrowca
Information Systems Labs
11140 Rockville Pike
Rockville, MD 20852 USA
Phone: (301) 255-2268
Fax: 301 468-0883
E-mail: bmrowca@islinc.com

Vinod Mubayi
Brookhaven National Lab
PO Box 5000, Bldg. 475C
Upton, NY 119735000 USA
Phone: (631) 344-2056
Fax: (631) 344-5730
E-mail: mubayi@bnl.gov

Joseph Murphy
Consultant
10 First Ct.
Rockville, MD 20850 USA
Phone: 301 762 2418
Fax:
E-mail: josamurphy@msn.com

Randy Nanstad
Oak Ridge National Lab
P.O. Box 2008
Oak Ridge, TN 37831 USA
Phone: (865) 574-4471
Fax:
E-mail: nanstadrk@ornl.gov

Tomaz Nemeč
Slovenian Nuclear Safety Admin.
Zelezna cesta 16, PO Box 5759
Ljubljana, SI 1001 Slovenia
Phone: 386 1 472 1145
Fax:
E-mail: tomaz.nemec@gov.si

Jean-Christophe Niel
IRSN
BP 17
Fontenay aux Roses, 92269 France
Phone: 33 1 5835 8664
Fax: 33 1 4253 9126
E-mail: jean-chrostophe.niel@irsn.fr

Mamoro Nishiyama
JEPIC
1120 Connecticut Ave, NW, Ste 1070
Washington, DC 20036 USA
Phone: 202 955 5610
Fax: 202 955 5612
E-mail: kyuden@jepic.com

Mitchell Nissley
Westinghouse Electric Co.
PO Box 355
Pittsburgh, PA 15230 USA
Phone: 412 374 4303
Fax: 412 374 4011
E-mail: nissleme@westinghouse.co

Registered Attendees

Friday Ogunluya
University of Lagos
21 Obalende Rd SW Ikoyi
Lagos, 23401 Nigeria
Phone: 234 1 2673586
Fax: 234 1 2674642
E-mail: mikkyfara@yahoo.com

Yukimitsu Okano
Inst. of Nuclear Safety Systems
64 Sata, Mihama-cho
Mikata-gun, Fukui 919-1205 Japan
Phone: 81 770 37 9100
Fax: 81 770 37 2008
E-mail: okano@inss.co.jp

Nino Oliva
CANDU Owners Group, Inc.
480 University Ave, Ste 200
Toronto, Ontario L3T 5E8 Canada
Phone: 416 595 1888
Fax: 416 595 1022
E-mail: nino.oliva@candu.org

Larry Ott
Oak Ridge National Lab
1 Bethel Valley Rd, Bld 5700
Oak Ridge, TN 37831-6167 USA
Phone: 865 574 0324
Fax: 865 574 2032
E-mail: ottlj@ornl.gov

Odelli Ozer
EPRI
PO Box 10412
Palo Alto, CA 94303 USA
Phone: 650 855 2089
Fax: 650 855 1026
E-mail: oozer@epri.com

Cecil Parks
Oak Ridge National Lab
Bethel Valley Rd
Oak Ridge, TN 37831 USA
Phone: 865 574 5280
Fax: 865 574 3527
E-mail: parkscv@ornl.gov

Charles Patterson
Global Nuclear Fuel
3901 Castle Hayne Rd
Wilmington, NC 28402 USA
Phone: 910 675 6065
Fax: 910 362 6065
E-mail: chuck.patterson@gnf.com

Manfred Petroll
PR Square
5108 Cherokee Avenue
Alexandria, VA 223122001 USA
Phone: (703) 354-5127
Fax: (703) 354-5127
E-mail: mpetrollryan@telocity.com

Jean-Louis Pettitclerc
IRSN
BP 17
Fontenay-aux-roses, 92262 France
Phone: 33 1 5835 8177
Fax:
E-mail: jean-louis.pettitclerc@irsn.fr

Carolyn Phillips
Naval Reactors
Isaac Hall Avenue WNY
Washington, DC USA
Phone: (202) 781-6309
Fax:
E-mail:

Larry Phillips
Consultant
118 Monroe St
Rockville, MD 20850 USA
Phone: 301 294 3069
Fax:
E-mail: larryephillips55@cs.com

Tony Pietrangelo
Nuclear Energy Institute
1776 I St, NW
Washington, DC USA
Phone: 202 739 8081
Fax:
E-mail: arp@nel.org

Registered Attendees

Li-Chi Po
Micro-Simulation Technology
10 Navajo Ct
Montville, NJ, 07045 USA
Phone: 973 263 7327
Fax: 973 402 9456
E-mail: Info@microsimtech.com

Gerald Potts
Global Nuclear Fuel
102 Trombay Dr
Wilmington, NC 28412 USA
Phone: 910 675 5708
Fax: 910 675 6966
E-mail: gerald.potts@gnf.com

Dan Prelewicz
Information Systems Labs
11140 Rockville Pike
Rockville, MD 20852 USA
Phone: (301) 468-6425
Fax:
E-mail: danp@islinc.com

Manuel Quecedo
ENUSA
Santiago Rusinol 12
Madrid, 28003 Spain
Phone: 34 9 1347 4264
Fax: 34 9 1347 4215
E-mail: mqq@enusa.es

Anita Ragan
Tokyo Electric Power Co.
1901 L St NW, Ste 720
Washington, DC 20036 USA
Phone: 202 457 0790
Fax: 202 457 0810
E-mail: anita@wash.tepco.com

Charles Ramsey
US Department of Energy
12004 Amber Ridge Cir. # 304
Germantown, MD 20876 USA
Phone: 301 903 5999
Fax: 301 903 2596
E-mail: chuck.ramsey@hq.doe.gov

Nancy Ranek
Argonne National Lab
955 L'Enfant Plaza North, SW
Washington, DC 20024 USA
Phone: 202 488 2417
Fax: 202 488 2413
E-mail: ranekn@anl.gov

Joe Rashid
ANATECH
5435 Oberlin Dr
San Diego, CA 92121 USA
Phone: 858 455 6350
Fax: 858 455 1094
E-mail: joe@anatech.com

Patrick Raynaud
Penn State Univ.
320 E. Beaver Avenue
State College, PA 16801 USA
Phone: (814) 883-5236
Fax:
E-mail: par182@psu.edu

Cal Reid
Bechtel Power

Frederick, MD USA
Phone: (301) 228-6533
Fax:
E-mail: creid@bechtel.com

Jason Remer
US Department of Energy

USA
Phone: (301) 903-4416
Fax:
E-mail: jason.remer@hq.doe.gov

Michel Reocreux
IRSN
IRSN/DRS/DIR, BP3
St Paul Lez Durance, 13115 France
Phone: 33 4 4225 3148
Fax: 33 4 4225 6346
E-mail: michel.reocreux@irsn.fr

Registered Attendees

Jacques Repussard
IRSN
BP 17
Fontenay aux Roses, Cedex 92262
France
Phone: 01 58 358489
Fax: 01 58 357152
E-mail: jackques.repussard@irsn.fr

Jose Rey
CSN
c/ Justo Dorado, 11
Madrid, 28013 Spain
Phone: 34 91 3460215
Fax:
E-mail: jmrj@csn.es

James Riccio
Greenpeace
702 H St NW, Ste 300
Washington, DC 20001 USA
Phone: 202 319 2487
Fax: 202 462 4507
E-mail: jim.riccio@wdc.greenpeace.o

Ian Rickard
Westinghouse Electric Co.
2000 Day Hill Rd.
Windsor, CT 06095 USA
Phone: 860 731 6289
Fax:
E-mail: ian.c.rickard@us.westinghou

Thomas Riekert
TUV Nord
Grobe Bahnstr 31
Hamburg, 22525 Germany
Phone: 49 40 8557 2610
Fax: 49 40 8557 2429
E-mail: triekert@tuev-nord.de

David Ritter
Public Citizen
215 Pennsylvania Avenue, SE
Washington, DC 20003 USA
Phone: (202) 454-5176
Fax: 202 547-7392
E-mail: dritter@citizen.org

Kenneth Rogers
KCR
6202 Perthshire Ct
Bethesda, MD 20817 USA
Phone: 301 530 4489
Fax: 301 530 4033
E-mail: kcrogers@aol.com

Tom Rosseel
Oak Ridge National Lab
PO Box 2008
Oak Ridge, TN 37831 USA
Phone: 865 574 5380
Fax: 865 574 6095
E-mail: rosseeltm@ornl.gov

Jacques Royen
OECD NEA
LeSeine - Saint Germain 12 Blvd des
Issy-les-Moulineaux, F92130 France
Phone: 33 1 4524 1052
Fax: 33 1 4524 1129
E-mail: jacques.royen@oecd.org

George Rudy
Integrated Systems Technology
11 W Crum Rd
Walkersville, MD 21793 USA
Phone: 301 845 8874
Fax: 301 845 8874
E-mail: gcrudy@earthlink.net

John Russell
CNWRA
12300 Twinbrook Pkwy, Ste 210
Rockville, MD 208521606 USA
Phone: (301) 881-0289
Fax: 301 881 0294
E-mail: jlrussell@cnwra.swri.edu

Farideh Saba
Information Systems Labs
11140 Rockville Pike
Rockville, MD 20852 USA
Phone: (301) 255-2262
Fax: (301) 468-0883
E-mail: fsaba@islinc.com

Registered Attendees

Julio Salgado
Mexican Nuc. Reg. Body
La Viga 1898 B-004
Mexico City, 09810 Mexico
Phone: 5255 5095 3235
Fax: 5255 5095 3293
E-mail: jrsgalado@cnsns.gob.mx

Paloma Sarria
Numark Associates, Inc.
1220 19th Street, NW
Washington, DC 200362405 USA
Phone: (202) 466-2700
Fax: 202 466-3669
E-mail: psarria@numarkassoc.com

Pierre Saverot
JAI Corp.
2750 Prosperity Ave, Ste 220B
Fairfax, VA 22031 USA
Phone: 703 645 0440
Fax: 703 645 0445
E-mail: psaverot@jaicorp.com

Anselm Schaefer
ISAR Institute, Tu Munchen
Walther-Meissner Str. 2
Garching, 85748 Germany
Phone: 49 89 2891 3939
Fax: 49 89 2891 3949
E-mail: schaefer@iisar.de

Paul Scheinert
Bechtel Bettis, Inc.
PO Box 79
West Mifflin, PA 15122 USA
Phone: 412 476 5974
Fax: 412 476 6843
E-mail: pascheinert@aol.com

E. Scott deMartinville
IRSN
PO 6 Fontenay-aux-Roses
Fontenay, 92268 France
Phone: 00 33 1 5835 8202
Fax:
E-mail: scott-de-martinville@irsn.fr

John-Tae Seo
Korea Power Eng'g Co.
150 Deokjin-Dong, Yuseong-Gu
Daejeon, 305-353 Korea
Phone: 82 42 868 4006
Fax: 82 42 861 1485
E-mail: jtseo@kopec.co.kr

Charles Serpan
NRC Retired
5510 Bradley Blvd
Bethesda, MD 20814 USA
Phone: 301 656 2268
Fax:
E-mail: pcserpan@olg.com

William Shack
Argonne National Lab
9700 South Cass Avenue
Argonne, IL 604394838 USA
Phone: (630) 252-5137
Fax: 630 252-4798
E-mail: wjshack@anl.gov

Farshid Shahrokhi
Framatome ANP
3315 Old Forest Rd. POB 10935
Lynchburg, VA 24506 USA
Phone: 434 832 2923
Fax: 434 832 2683
E-mail: f.shahrokhi@framatome-anp.

An-Dong Shin
Korea Institute of Nuclear Safety
, USA
Phone: 301 570 5201
Fax:
E-mail: k354sad@hotmail.com

Fred Silady
Technology Insights
6540 Lusk Blvd., Ste C-102
San Diego, CA 92121 USA
Phone: 858 455 9500
Fax: 858 452 7831
E-mail: silady@ti-sd.com

Registered Attendees

Julie Simpson
Oak Ridge National Lab
PO Box 2008
Oak Ridge, TNL 37831-6162 USA
Phone: 865 574 0422
Fax: 865 241 4069
E-mail: simpsonjj@ornl.gov

Robert Sisk
Westinghouse/Nuclear Fuels
PO Box 355
Pittsburgh, PA 15230-0355 USA
Phone: 412 374 6206
Fax: 412 374 2045
E-mail: sisklr@westinghouse.com

William Slagle
Westinghouse Electric
4350 Northern Pike, MS ECED 4-24
Monroeville, PA 15146-2886 USA
Phone: 412 374 2088
Fax: 412 374 2045
E-mail: slaglewh@westinghouse.com

Roger Staehle
Staehle Consulting
22 Red Fox Rd
North Oaks, MN 55127 USA
Phone: 651 482 9493
Fax: 651 484 5735
E-mail: rwstaehle@rwstaehle.com

David Steininger
EPRI
PO Box 10412, 3412 Hillview Ave
Palo Alto, CA 95054 USA
Phone: 650 855 2019
Fax:
E-mail: dsteinin@epri.com

Marek Stepniewski
Vattenfall Fuel AB
Jamtlandsgatan 99
Stockholm, 162-87 Sweden
Phone: 46 8 739 5489
Fax: 46 8 877879
E-mail: marek.stepniewski@vattenfal

Peter Storey
Health & Safety - NII
Room 313, St Peter's House
Merseyside, L203LZ United Kingdom
Phone: 44 0151 951 4172
Fax: 44 0151 951 4100
E-mail: peter.storey@hse.gsi.gov.uk

Roger Stoudt
Framatome-ANP
3315 Old Forest Rd
Lynchburg, VA 24501 USA
Phone: 434 832 2644
Fax:
E-mail: roger.stoudt@framatome-anp

Al Strasser
Aquarius Services Corp.
17 Pokahoe Dr.
Sleepy Hollow, NY 10591 USA
Phone: 914 366 8875
Fax: 914 366 8876
E-mail: stras69@att.net

Gordon Szeto
Naval Reactors

, USA
Phone: 202 781 5834
Fax:
E-mail: szetogn@navsea.navy.mil

Vinh Tang
CNSC
PO Box 1046, Station B
Ottawa, Ontario Canada
Phone: 613 995 3946
Fax: 613 943 1292
E-mail: tangv@cnscccsn.gc.ca

Amy Taylor
US Department of Energy
19901 Germantown Road
Germantown, MD 20874 USA
Phone: (301) 903-7722
Fax:
E-mail: amy.taylor@hq.doe.gov

Registered Attendees

Victor Teschendorff
GRS
Forschungsinstitute
Garching, 85748 Germany
Phone: 49 89 32004 406
Fax: 49 89 32004 599
E-mail: tes@grs.de

Hugh Thompson, Jr.
Talisman International LLC
1000 Potomac St NW, Ste 300
Washington, DC 20007 USA
Phone: 202 471 4244
Fax: 202 471 4360
E-mail: hthompson@talisman-intl.co

Petteri Tiippana
STUK, Rad. & Nuc. Safety
PO Box 17
Helsinki, 00881 Finland
Phone: 358 9 759 88654
Fax: 358 9 759 88382
E-mail: petteri.tiippana@stuk.fi

Erik Titland
Consultant
512 Idlewild Rd
Bel Air, MD 21014 USA
Phone: 410 879 0718
Fax: 410 838 8970
E-mail:

Nicolas Tricot
IRSN
BP 17
Fontenay aux Roses, Cedex 92262
France
Phone: 33 1 5835 9034
Fax: 33 1 5835 9599
E-mail: nicolas.tricot@irsn.fr

Sheldon Trubatch
Attorney
4222 River Rd NW #1
Washington, DC 20016 USA
Phone: 202 363 3924
Fax: 202 363 3924
E-mail: lawofficesofsheldontrubatch

Hanchung Tsai
Argonne National Lab
9700 S. Cass Ave
Argonne, IL 60439 USA
Phone: 630 252 5176
Fax: 630 252 9232
E-mail: htsai@anl.gov

Robert Tsai
Exelon Generation Co.
4300 Winfield Rd.
Warrenville, IL 60555 USA
Phone: 630 657 2162
Fax: 630 657 4331
E-mail: robert.tsai@exeloncorp.com

James Tulenko
University of Florida
202 Nuclear Science Center
Gainesville, FL 32611 USA
Phone: 352 392 1401
Fax: 352 392 3380
E-mail: jimtulenko@mail.com

Gregory Twachtman
McGraw-Hill
1200 G St., NW
Washington, DC 20005 USA
Phone: (202) 382-2166
Fax: 202 383-2187
E-mail: gregory_twachtman@platts.c

Bob Twilley
Framatome ANP
3315 Old Forest Rd
Lynchburg, VA 24501 USA
Phone: 434 832 4019
Fax:
E-mail: bob.twilley@framatome-anp.

Klaus Umminger
Framatome ANP GmbH
Freyeslebenstr 1
Erlangen, 91058 Germany
Phone: 49 9131 189 5539
Fax: 49 9131 189 2851
E-mail: klaus.umminger@framatome

Registered Attendees

Keijo Valtonen
STUK, Reactor & System Eng'g.
PO Box 14
Helsinki, 00881 Finland
Phone: 358 9 759 88331
Fax: 358 9 759 88382
E-mail: keijo.valtonen@stuk.fi

Willem van Doesburg
HSK Swiss NSI
PO Box 5232
Villigen HSK, 5232 Switzerland
Phone: 41 56 3103862
Fax: 41 56 3104979
E-mail: willem.vandoesburg@hsk.psi

Teresa Vazquez
CSN
C/ Justo Dorado 11
Madrid, 28040 Spain
Phone: 34 91 346 0260
Fax: 34 91 346 0496
E-mail: tvm@csn.es

Michel Vidard
EDF Septen
12-14 Ave Dutrievoz
Lyon, Rhone Alpes 69628 France
Phone: 33 4 7282 7565
Fax: 33 4 7282 7701
E-mail: michel.vidard@edf.fr

Christer Viktorsson
Swedish Nuc. Pow. Inspectorate

Stockholm, SE-106 58 Sweden
Phone: 46 8 698 8421
Fax: 46 8 661 9086
E-mail: christer.viktorsson@ski.se

Gary Vine
EPRI
2000 L St NW, Ste 805
Washington, DC 20036 USA
Phone: 202 293 6347
Fax: 202 293 2697
E-mail: gvine@epri.com

Nicolas Waeckel
EDF
12-14 Avenue Dutrievoz
Villeurbanne, 69628 France
Phone: 33 4 7282 7244
Fax: 33 4 7282 7711
E-mail: nicolas.waeckel@edf.fr

Sergio Waller
CNSNS
Dr. Barragan 779
Mexico City, 03020 Mexico
Phone: 52 55 5095 3240
Fax: 52 55 5095 3295
E-mail: swaller@cnsns.gob.mx

Dean Wang
Information Systems Labs
11140 Rockville Pike
Rockville, MD 20852 USA
Phone: (301) 255-2279
Fax:
E-mail: dwang@isilinc.com

Jenny Weil
McGraw-Hill
1200 G St NW, Ste 1000
Washington, DC 20005 USA
Phone: 202 383 2161
Fax: 202 383 2187
E-mail: jenny_weil@platts.com

Robert Weiner
KW Consulting, Inc.
PO Box 101567
Pittsburgh, PA 15237 USA
Phone: 412 422 7732
Fax: 412 422 8471
E-mail: bob@kwconsulting.com

Andrew White
AECL
Chalk River Labs
Chalk River, Ontario K0J 1J0 Canada
Phone: 613 584 8811
Fax: 613 584 8220
E-mail: whitea@aecl.ca

Registered Attendees

Glenn White
Dominion Engineering, Inc.
11730 Plaza America Drive
Reston, VA 20190 USA
Phone: (703) 437-1155
Fax:
E-mail: gwhite@domeng.com

Tomoho Yamada
Institute of Applied Energy
1120 Connecticut Ave NW
Washington, DC 20036 USA
Phone: 202 955 6058
Fax: 202 955 5612
E-mail: yamada@iae.or.jp

Yong Yan
Argonne National Lab
9700 S Cass Ave.
Argonne, IL 60439 USA
Phone: 630 252 9560
Fax: 630 252 9232
E-mail: yan@anl.gov

Rosa Yang
EPRI
3412 Hillview Ave
Palo Alto, CA 94304 USA
Phone: 650 855 2481
Fax: 650 855 1026
E-mail: ryang@epri.com

Larissa Yegorova
NSI-RRC Kurchatov Institute
123182 Kurchatov Square 1
Moscow, Russian Federation
Phone: 7 095 196 7283
Fax: 7 095 196 1702
E-mail: yegorova@nsi.kiae.ru

Jim York
Bechtel SAIC Company, LLC
995 North L'Enfant Plaza, SW
Washington, DC 20024 USA
Phone: (202) 488-2303
Fax: 202 488-2323
E-mail: Jim.york@rw.doe.gov

Kenneth Young
LLNL
7000 East Ave
Livermore, CA 94550 USA
Phone: 925 422 4499
Fax: 925 423 8413
E-mail: kcyoung@llnl.gov

Robert Youngblood
Information Systems Labs
11140 Rockville Pike, Ste 500
Rockville, MD 20852 USA
Phone: 301 255 2270
Fax: 301 468 0883
E-mail: ryoungblood@islinc.com

Dino Zanobetti
University of Bologna

, Italy
Phone: 39 051 2093479
Fax:
E-mail: dino.zanobetti@mail.ing.unib

Jinzhao Zhang
Tractebel
Avenue Ariane 7
Brussels, 1200 Belgium
Phone: 32 2 773 9843
Fax: 32 2 773 8900
E-mail: jinzhao.zhang@tractebel.com

Kazys Zilys
VATESI

Sermuksniu 3, Vilnius 2600 Lithuania
Phone: 3705 266 1621
Fax: 3705 261 4487
E-mail: zilys@vatesi.lt

Martin Zimmerman
Paul Scherrer Institut

Villigen, CH 5232 Switzerland
Phone: 41 56 310 2733
Fax: 41 56 310 2327
E-mail: martin.zimmermann@psi.ch

Registered Attendees

Paul Zmola
C&P Engineering
4620 N. Park Ave, Ste 1605E
Chevy Chase, MD 20815 USA
Phone: 301 656 5756
Fax: 301 656 5756
E-mail:

"Experience with PRA in the Generic Issues Program"

Harold J. Vandermolen
Regulatory Effectiveness Assessment and Human Factors Branch
Division of Systems Analysis and Regulatory Effectiveness
Office of Nuclear Regulatory Research
U.S. Nuclear Regulatory Commission

Abstract

The Generic Issues Program first began formally in response to a Commission directive in October of 1976. In 1983, it became one of the first programs to make successful use of probabilistic risk information to aid in agency decision making. In the 20 years since the program became quantitative, approximately 840 issues have been processed.

Although there is far less reactor licensing activity than in the 1970s, new issues continue to be identified from research programs and operational experience, and the generic issue program remains very active. Moreover, probabilistic techniques have advanced considerably since the program began.

Generic issues tend to involve rather vexing questions of safety and regulation, and an efficient and effective means of addressing these issues is very important if regulatory effectiveness is to be achieved. If an issue proves to pose a genuine, significant safety question, then swift, effective, enforceable, and cost-effective action needs to be taken to eliminate an accident before it happens. Conversely, if an issue is of little safety significance, the issue should be dismissed in an expeditious manner, avoiding unnecessary expenditure of resources and regulatory uncertainty.

The generic issues program's administrative procedures were revised and codified in an NRC management directive in December of 2001, in an attempt to streamline the process. Simultaneously, attempts were made to make use of more modern PRA techniques. In the two years since the process was revised, a number of new generic issues have been processed through the system. The experience gained, both with the new procedures and with the use of more modern PRA techniques, will be discussed.

Definition of a Generic Issue. A generic issue is formally defined¹ as "a regulatory matter involving the design, construction, operation, or decommissioning of several, or a class of, NRC licensees or certificate holders that is not sufficiently addressed by existing rules, guidance, or programs." This rather legalistic definition has several practical corollaries:

First, a generic issue must involve safety or burden reduction. Questions regarding licensing procedures or administrative matters may be valid concerns, but are not addressed in this program. Most issues are explicitly oriented toward safety.

Second, the issue must involve at least two docket, or it will be plant-specific rather than generic. Plant-specific issues are addressed within the context of a specific docket.

Third, the potential safety (or burden-reduction) question must not be covered by existing regulations and guidance. If the issue is covered by existing regulations and/or guidance, it is considered a compliance issue and is addressed by the appropriate program office.

Thus, the effect of a generic issue is to change the body of regulations and associated guidance (e.g., regulatory guides). The intent of the generic issues program is to address weaknesses and improvements in this body of regulatory documentation.

History of the Generic Issue Program. The Generic Issues program was first started in response to a Commission directive of October 8, 1976,² which directed the staff to develop "a program plan for resolution of generic issues and completion of technical projects." This is not a new program; it has been in progress for about 27 years.

The program was further formalized by Section 210 of the Energy Reorganization Act of December 12, 1977, which stated, "The Commission shall develop a plan providing for specification and analysis of unresolved safety issues relating to nuclear reactors and shall take such action as may be necessary to implement corrective measures with respect to such issues." Not every generic issue is considered an "unresolved safety issue," but nevertheless, the existence of the generic issues program keeps the agency in compliance with this requirement.

The program was set out more formally with the publication of the entire set of generic issues and their priorities in NUREG-0933³. The program was affirmed by the Commission in 1983⁴ and again in 1993⁵. More importantly, even after 27 years, new generic issues continue to be proposed.

Origins of Generic Issues. Historically, generic issues have been proposed from several distinct sources, as shown in Table 1.

Table 1. Origins of Generic issues

- | | |
|-----------------------------------|---------------------------|
| ● CP/OL reviews | ● Nuclear Power Industry |
| ● ACRS concerns | ● Public |
| ● TMI-2 accident | ● Part 21 notification |
| ● Operating experience | ● Accident Investigations |
| ● Differing Professional Opinions | ● Event Investigations |
| ● Staff concerns | |

In recent times, most new generic issues have originated from event investigations, staff concerns, and programs which monitor operating experience.

It is not difficult to propose a generic issue. However, the generic issue program is not intended for immediate or emergency action. Such concerns are better addressed by other programs; generic issues tend to be long-term projects that may require extended analysis or

experimental work. It should be noted that the target end dates of individual generic issues are reported to the Congress, and the agency has committed itself to address these issues on schedule.

Process. The generic issue process is governed by Management Directive 6.4¹. The various stages are shown graphically in Figure 1.

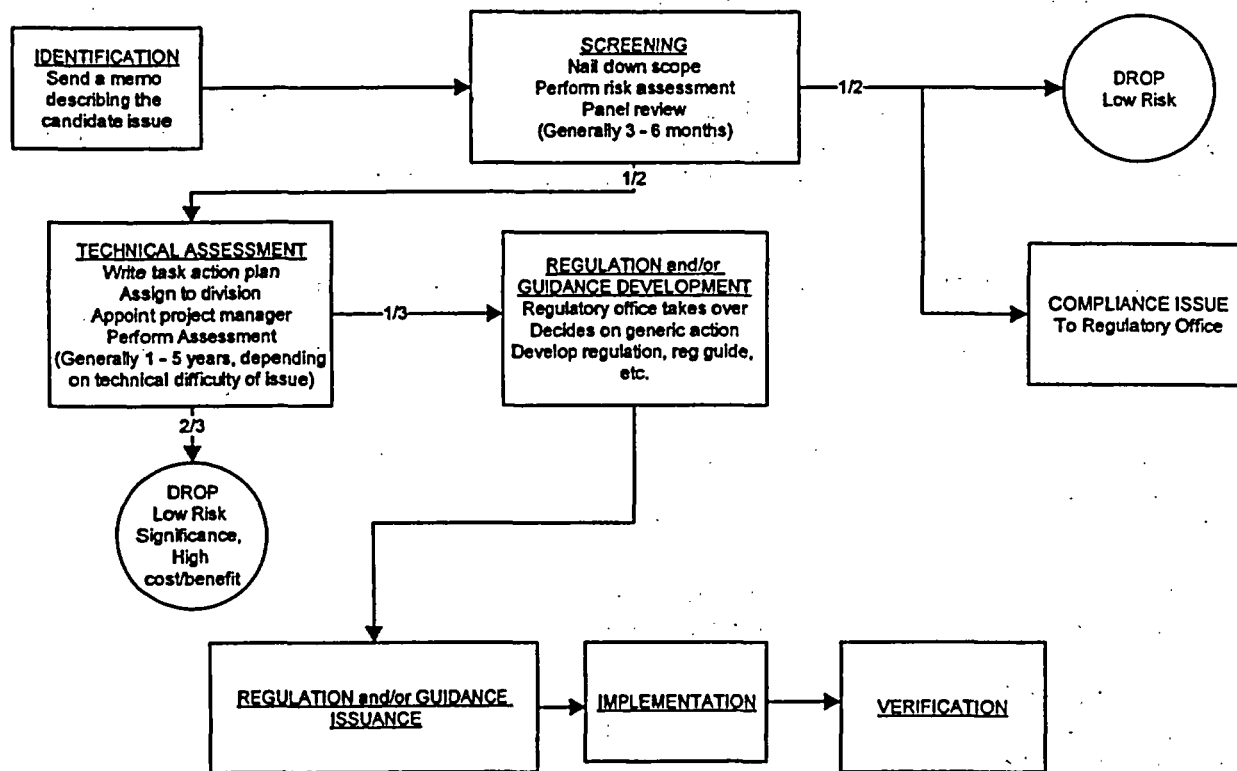


Figure 1
Generic Issue Stages

After a candidate generic issue is identified, a screening analysis is performed. This is an abbreviated analysis, done in-house, using probabilistic techniques if it is practical to do so, and may incorporate some conservatism. If the analysis indicates that the safety significance of the issue exceeds certain thresholds, the issue goes on to a technical assessment stage. It is at this stage where a task action plan for the issue will be generated, and the new generic issue becomes a new research project with its own project manager, budget, milestones, etc.

The technical assessment stage may just involve modeling or simulation calculations, or it may include data searches, investigations, or even experimental work, depending on the technical nature of the issue. Thus, the technical assessment stage may span several years and consume significant staff and financial resources. Moreover, the estimates of safety significance will be as realistic as is practical. It is not at all unusual for an issue to be dropped on low safety significance based on this technical assessment, even though the screening calculations (which are allowed to contain some conservatism) indicated that the issue had the potential for substantial safety significance.

If the technical assessment does indicate that the generic issue has significant safety significance, and that some regulatory action is justified, the issue is turned over to the appropriate program office (usually the Office of Nuclear Reactor Regulation) for appropriate action. The status of the issue will still be tracked in the generic issues tracking system maintained by the Office of Nuclear Regulatory Research, but the lead responsibility is taken over by the program office, which will choose and issue the appropriate regulatory vehicle (e.g., information notice, generic letter, or even rulemaking). The issue is not formally closed out until the regulatory action is issued and, if applicable, implemented at the various sites and verified.

Generic Issue Screening Analysis. It is the screening analysis which makes some unique uses of probabilistic risk analysis. Probabilistic techniques are also used in the technical assessment, to support a regulatory analysis and/or cost/benefit study, but these analyses are governed by NUREG/BR-0184, *Regulatory Analysis Technical Evaluation Handbook*.⁶

The generic issues program was one of the first at the agency to make use of probabilistic techniques. Originally, the purpose was to put the then-large number of unresolved issues into a priority order. Currently, the number of incoming issues is much more manageable, but experience has shown that a probabilistic analysis has several significant advantages.

First, there is no substitute for a mathematical analysis such as this to enforce rationality in investigation and management. When first proposed, candidate generic issues are often unfocused and vague, and the probabilistic screening process eliminates the confusion.

Second, the process provides a documented, risk-informed basis for the decision. This is particularly important for issues which are dropped from further consideration.

Third, experience has shown that any disputes on the decision tend to rapidly focus on the treatment of a specific parameter or sequence. This generally leads to a reasonably rapid resolution, based on specific technical considerations.

The ability to perform probabilistic screening analyses has greatly improved over the last several years. The availability of PRA codes (such as the Sapphire code⁷) which run on a personal computer permits calculations complete with error analyses, calculations which would have necessitated mainframe runs several years ago. The Generic Issues Program usually uses the Sapphire code, developed by the Idaho National Engineering and Environmental Laboratory. The Sapphire code is capable of analyzing linked fault trees and event trees, and can perform a complete error analysis.

Most generic issue screening calculations are performed by making modifications to an existing "base" PRA, to observe the change in core damage frequency, etc. For calculations such as this, the five probabilistic risk analyses in NUREG-1150⁸ have been loaded into the Sapphire code. For almost all screening analyses, these five PRA models are sufficient as a "base" calculation.

In cases where the five NUREG-1150 PRAs do not model the systems of interest, the Standard Plant Analysis Risk (SPAR) models are also available⁹. The SPAR models are a large set of PRA models which were originally developed for accident precursor analysis purposes. The set of SPAR models covers almost all domestic operating reactors. Although

these models are usually used with the GEM code for precursor analysis, the GEM code is in reality the Sapphire code running in a special mode. Thus, the SPAR models can be readily "brought up" in the Sapphire code for use as base PRAs.

Nature of the Analysis. A probabilistic risk analysis generally calculates the total core damage frequency (or other risk parameters) associated with the operation of the plant. For generic issue screening purposes, the parameter of interest is not just the total core damage frequency, but instead is the change in core damage frequency associated with the generic issue. In addition to the effect on core damage frequency, estimates of the change in large early release frequency (LERF) and/or public risk (in terms of total whole-body person-rem per reactor-year) may be made, depending on the technical nature of the issue, and on which parameter is limiting. The management directive for generic issues contains threshold criteria for all three¹. When possible, an error analysis is also performed on these parameters. Specific guidance for such calculations are provided in NUREG-1489¹⁰. Experience with these calculations over the years has shown that most generic issue analyses fall into five broad areas:

Change in initiator frequency. Probably the most common type of analysis involves a change in the frequency of an initiating event. Such calculations are relatively straightforward in theory. The analyst would simply change the initiating event frequencies of the affected event trees and observe the change in the frequencies of the end states. Since the change in each end state is directly proportional to the change in the initiating event frequency, it is often possible to calculate the change in end state frequency by hand.

However, if an error analysis is desired, simply subtracting the original end state frequency from the modified end state frequency will not provide an error distribution for the difference. The usual practice is to re-calculate the end state frequencies with the initiating event frequency set to the change in initiator frequencies (and all other, unaffected event trees excluded). Because of the proportionality of the effect on end state frequencies, the calculated results from such an event tree are in turn a direct calculation of the change in end state frequencies. Once such an event tree is set up, the Monte Carlo error analysis capabilities of the Sapphire code can be used to calculate the error distributions of the gathered end states, which is what is desired.

Change in system reliability. A generic issue which affects the reliability of a particular plant system can be analyzed in a similar manner, by using a split fraction for the unavailability of this system equal to the change in reliability. This type of calculation can be much more elaborate than a simple change in initiator frequency because typically this system unavailability will be present in more than one event tree. All of the event trees will have to be re-calculated, and the end state frequencies summed.

Change in component reliability. A generic issue which involves a change in the reliability of a specific class of components (e.g., all motor-operated valves of a certain type) can be perhaps the most far-reaching in the sense that a particular component type might be used in many different systems in the plant. In such a case, the change in unavailability will affect many fault trees, which will in turn affect many event trees.

Such an analysis would in most cases not be practical without the use of a computer model. To perform such an analysis, the basic events of interest must be changed in the model's data

library. Then, the fault and event trees must be re-solved (to make sure that the truncation cutoffs are appropriate) and re-quantified.

The error analysis is more difficult for this type of analysis. It is necessary to accumulate sample runs both with and without the change in component reliability, using exactly the same seed for the random number generators. Fortunately, the Sapphire code has the capability to output such intermediate results. Once these files are generated, the analyst must form a distribution of differences.

In practice, this type of analysis has become rare. This is primarily due to the advent of the maintenance rule. Because of this rule, such issues are now usually classified as compliance issues, and are not handled by the generic issues program.

Discovery of a new phenomenon or accident sequence. To analyze this type of issue, the analyst will usually generate a new event tree. This can be a rather involved process, but the availability of the existing fault trees for the various systems is a great help.

The error analysis is straightforward in the sense that the whole event tree is "new;" there is no subtraction to be performed. The error analysis capabilities of the Sapphire code can be used directly.

New system interaction. In principle, this type of generic issue can be analyzed by appropriately modifying the existing base PRA model, by linking event trees or using the rules editor in the Sapphire code. No such issue has presented itself in recent years, and thus there is no experience to report, which is unfortunate from the viewpoint of the PRA analyst, but fortunate from the viewpoint of the overall safety program.

Common Problems. Experience has shown that there are a number of difficulties that the analyst may encounter. The first is that the Sapphire code itself, although widely used, may sometimes "crash" or "freeze" when used in these rather novel ways. This is sometimes an annoyance, but has not proven to be a significant problem, to the credit of the writers of the code itself.

It is also not unusual to discover problems or even mistakes in the base PRA model. Such problems are almost invariably discovered in accident sequences that would normally be well below the truncation level used in the PRA. Thus, the discovery of such a "glitch" would not invalidate any conclusion made on the basis of the PRA itself. However, because generic issue analyses often promote these dropped sequences to a point where they are no longer truncated out, some rather minor problems may present some inconvenience.

In a similar vein, it should be noted that approximations which are perfectly appropriate for the purposes of the base PRA, which is generally to calculate the risk associated with the existence and operation of the plant, may not be appropriate for the purpose of generic issue analysis. The most common problem is the truncation level. For example, most plant PRAs calculate total core damage frequencies somewhere between 10^{-5} to 10^{-3} events per reactor-year. For generic issues, in most cases the core damage frequency screening threshold is 10^{-5} per reactor-year, and roughly half of the incoming candidate issues will be less than this threshold. Clearly, a generic issue screening analysis will need a truncation level well below that needed by a standard plant PRA.

Sparseness of information is a common problem. Candidate generic issues are usually not well documented with data when first identified, and there may be large uncertainties in some of the parameters. Yet, the purpose of a screening analysis is not to perform the best, most accurate analysis possible, but instead to explore the potential significance and feasibility of the issue. The usual rule of thumb used within the staff is to make maximum use of all readily-available information, which in practice means information (drawings, dimensions, failure data) which is available within the agency. Site visits, surveys, etc. are usually not considered appropriate for a screening analysis. This leads to a certain tension between the quality of the analysis vs. the approximations necessary because of the limited available information. In practice, it is often necessary to use conservative assumptions, in accordance with the recommended practices of NUREG-1489¹⁰. This situation is most common when analyzing a new phenomenon or accident sequence, as described above. It is often necessary to assume that the phenomenon does indeed occur, even if the existing evidence is not completely convincing, which transforms the probabilistic calculation into an importance measure for the phenomenon, rather than a completely realistic analysis of the new phenomenon. Because of this, it is not uncommon for a screening analysis to conclude that a new generic issue should be pursued further, but for the ensuing technical analysis, which will have more resources available, to subsequently conclude that the issue should be dropped from further consideration.

Finally, some difficulties can arise because a new event tree written to describe a new generic issue can be quite complex. Experience has shown that it is unwise to rush such analyses, and that an independent review is a well-justified precaution.

Recommendations. Not surprisingly, it is recommended that sound PRA practices be followed, particularly as documented in NUREG-1489¹⁰. As always, probabilistic models should not be used as a "black box," but instead the wise analyst will try to maintain some engineering insight. Within the generic issues program, common practice is to print out and review the top few sequences, and to calculate by hand a point estimate for at least one sequence. In this way, the analyst can have some assurance that he or she really understands what is going on.

Recent Generic Issues. Some recent examples include the following:

GI-185, Control of Reactivity Following Small-Break LOCAs in PWRs. GI-185 has to do with a small-break LOCA in a PWR. It is possible in some circumstances to get into a reflux boiling mode, where the core is covered, but the primary system water level is low. The coolant boils in the core, and condenses in the steam generators. There is no immediate threat, but after approximately half an hour, it is possible to have a situation where there is concentrated boric acid in the core, and deborated water in the steam generator. Now, if the system is refilled or if a reactor coolant pump is re-started, a slug of relatively cool, deborated water will be transported into the core. If this happens near the beginning of the fuel cycle, the control rods might not have enough worth to keep the core subcritical, and a reactivity transient is possible. Screening of this issue involved a completely new event tree. Currently, the issue is in the technical assessment stage.

GI-193, BWR ECCS Suction Concerns. GI-195 has to do with a large break LOCA in a BWR. It is well known that the resulting blowdown into the suppression pool in the torus is a very violent event, and there has been considerable effort in the past to make sure that the various

structures can survive it. However, an alert staffer pointed out that, in some plants, the ECCS pumps that take suction from the pool will be starting up just about the time that the pool water is at the point of maximum swell from the drywell atmosphere, and there may be a problem with air entrainment. This issue has just completed the screening process. The analysis was performed by modifying the existing large break LOCA event tree.

GI-195, Hydrogen Combustion in Foreign BWR Piping. GI-195 has to do with some problems with hydrogen. In a BWR, there will be some elemental hydrogen and oxygen from radiolysis mixed in with the steam. If there is a length of pipe connected to the steam space that points upward and is a bit cooler, and has no flow in it, it is possible for an explosive mixture to accumulate. At 1000 psi and 500 degrees F, it does not take much energy for ignition. There have been some events in foreign BWRs where such detonations have caused pipes to rupture, fortunately on the other side of check valves. This issue is currently in the screening process. The analysis is being done by modifying the initiating event frequencies for the event trees for the intermediate break LOCA and the safety/relief blowdown transient.

The screening analyses for all three of these generic issues are being published in NUREG-0933³, which is available on the NRC web site.

Conclusion. The generic issues program is still very active, and likely to remain so in the future. The program is one of the first to make use of probabilistic analysis techniques, and the availability of this technology is one of the primary reasons for the success of the program. Conversely, the generic issues program continues to identify new challenges in the use of these techniques, and unique approaches to these analyses are often required.

References.

1. Management Directive 6.4, *Generic Issues Program*, US Nuclear Regulatory Commission, December 2001.
2. NUREG-0410, *NRC Program for the Resolution of Generic Issues Related to Nuclear Power Plants*, January 1978.
3. NUREG-0933, *A Prioritization of Generic Safety Issues*, December 1983, and Supplements 1 to 27.
4. Memorandum for W. J. Dircks, Executive Director for Operations, from S. J. Chilk, Secretary, United States Nuclear Regulatory Commission, *SECY-83-221 - Prioritization of Generic Safety Issues*, December 9, 1983.
5. SECY-93-108, *Revised Guidelines for Prioritization of Generic Safety Issues*, April 28, 1993.
6. NUREG/BR-0184, *Regulatory Analysis Technical Evaluation Handbook*, January 1997.
7. NUREG/CR-6116, *Systems Analysis Programs for Hands-on Integrated Reliability Evaluations (SAPHIRE)*, July 1994.

8. NUREG-1150, *Severe Accident Risks: An Assessment for Five U. S. Nuclear Power Plants*, December 1990.
9. S. M. Long, P. D. O'Reilly, E. G. Rodrick, and M. B. Sattison, *Current Status of the SAPHIRE Models for ASP Evaluations*, presented at the Probabilistic Safety Assessment & Management (PSAM IV) conference, New York, 1998.
10. NUREG-1489, *A Review of NRC Staff Uses of Probabilistic Risk Assessment*, March 1994.

[This page left intentionally blank]

A PILOT APPLICATION OF A RISK-INFORMED APPROACH FOR CERTIFICATION OF DRY CASK STORAGE OF SPENT FUEL

K.A. Gruss, M. Waters, C. Lui
U.S. Nuclear Regulatory Commission, Washington, DC, 20852, USA

ABSTRACT

The Nuclear Regulatory Commission's (NRC's) Office of Nuclear Material Safety and Safeguards (NMSS) initiated a pilot study to (1) test the effectiveness of a proposed risk-informed decision-making (RIDM) process and the associated draft guidance documents, and (2) identify insights for risk informing staff guidance for conducting licensing reviews for spent fuel storage. The proposed RIDM process is a systematic and transparent process that utilizes risk insights (e.g., total individual accident risks, quantitative health guidelines) along with other information (e.g., defense-in-depth, safety margins, cost-benefit information, competing risks, ALARA, etc.) to make risk-informed decisions. This paper presents the results of a pilot study that utilized the proposed RIDM process and recently issued standard review plan guidance related to conducting confinement reviews for the certification of spent fuel storage casks at independent spent fuel storage installations (ISFSIs).

INTRODUCTION

The NRC staff, guided by the Commission, has long recognized the need to develop a framework for risk-informing its regulatory activities. The 1995 Policy Statement on the use of Probabilistic Risk Assessment¹ (PRA) called for an increase in the use of PRA technology in all regulatory matters, consistent with the state-of-the-art PRA methods and data, in a manner that complements NRC's deterministic approach and supports NRC's traditional defense-in-depth philosophy. The policy statement also recognized that a single approach for incorporating risk analysis into the regulatory process would not be appropriate, given the nature and consequences of the use of nuclear materials in NMSS.

The staff developed and proposed an approach to risk-inform NMSS regulatory activities in SECY-99-100, "Framework for Risk-Informed Regulation in the Office of Nuclear Material Safety and Safeguards²." This approach was designed to: (1) focus NRC and licensee resources on areas commensurate with their importance to safety; (2) provide a framework for using risk information; and, (3) use risk information, when amenable, to provide flexibility for making decisions and managing the work load in NMSS more effectively. The framework defined the potential areas where risk-informing can play a role in the regulation of NMSS activities and, as part of its implementation, the staff proposed to develop risk metrics and goals to help guide the risk-informed activities. In a Staff Requirements Memorandum dated June 28, 1999³, the Commission approved the staff's proposal in SECY-99-100 to develop risk metrics and goals and address risk management consistent with other Agency policies.

As NMSS moved forward in its risk-informing activities, the staff recognized that the ways in which risk information could be used would vary across its diverse programs, and that it would not, in general, be necessary nor cost-effective to either have the NRC staff, or require licensees, to perform risk assessments. In light of this, NMSS developed a screening process,

which uses a set of screening considerations, to help decide whether a risk-informed approach would be feasible and beneficial. The effectiveness of the screening considerations was evaluated through a series of case studies^{4,5}. Insights gained from those case studies and other information led to the development of the proposed RIDM process which is described in more detail below.

In collaboration with the NRC's Office of Nuclear Regulatory Research (RES) and the Brookhaven National Laboratory (BNL), NMSS has completed three draft guidance documents that support the use of the proposed RIDM process. One of the documents (referred to as Screening Consideration Guidance) discusses the use of a set of screening considerations that can be used by the staff to determine whether a regulatory application, activity or process should be risk-informed. The screening considerations can help the staff to evaluate both the benefits and feasibility of implementing a risk-informed approach. Another guidance document provides an overview of the techniques for performing risk assessments for activities in the materials and waste arenas. A third document (referred to as Decision-Making Guidance) describes the process and decision-making algorithms to guide the staff to decide whether to implement a proposed regulatory action or issue using a risk-informed approach. Two NMSS pilot studies have been completed to test these three draft guidance documents, one on risk-informing a piece of dry cask storage standard review plan guidance (the subject of the pilot study reported in the paper) and the other on regulation of chemical agent detectors and monitors.

APPROACH

The proposed RIDM process was applied retrospectively to NMSS licensing confinement review guidance for dry cask storage, which is contained in Interim Staff Guidance No. 18 (ISG-18), "The Design/Qualification of Final Closure Welds on Austenitic Stainless Steel Canisters as Confinement Boundary for Spent Fuel Storage and Containment Boundary for Spent Fuel Transportation⁶." The issuance of ISG-18 allowed the storage cask designers to seek relief from conducting off-site dose calculations related to hypothetical releases from all-welded stainless steel storage canisters. It also allowed licensees to seek relief from having to conduct certain helium leakage tests on double confinement closure lid welds for selected storage canisters. By focusing on this recent staff action and by exercising the proposed RIDM process and draft guidance documents, the staff thought it might be possible to enhance the draft RIDM guidance and illuminate risk insights that could be used to further risk-inform the confinement review or the dry cask storage standard review guidance. It should be noted that the purpose for pilot study was not to re-open regulatory decisions pertaining to ISG-18. Rather, as stated above, the objective was to test the proposed RIDM process and draft guidance against actual NMSS decisions.

The proposed RIDM process is a systematic and transparent process that utilizes risk insights (e.g., total individual accident risks, quantitative health guidelines) along with other information (e.g., defense-in-depth, safety margins, cost-benefit information, competing risks, ALARA, etc.) to make risk-informed decisions. The principles from Regulatory Guide 1.174, "An Approach for Using Probabilistic Risk Assessments in Risk-Informing Decisions on Plant-Specific Changes to the Licensing Basis⁷" and NUREG-BR-0058, "Regulatory Analysis Guidelines of the USNRC⁸," are embodied in the proposed RIDM process but have been adapted, as appropriate, to fit NMSS decision-making needs.

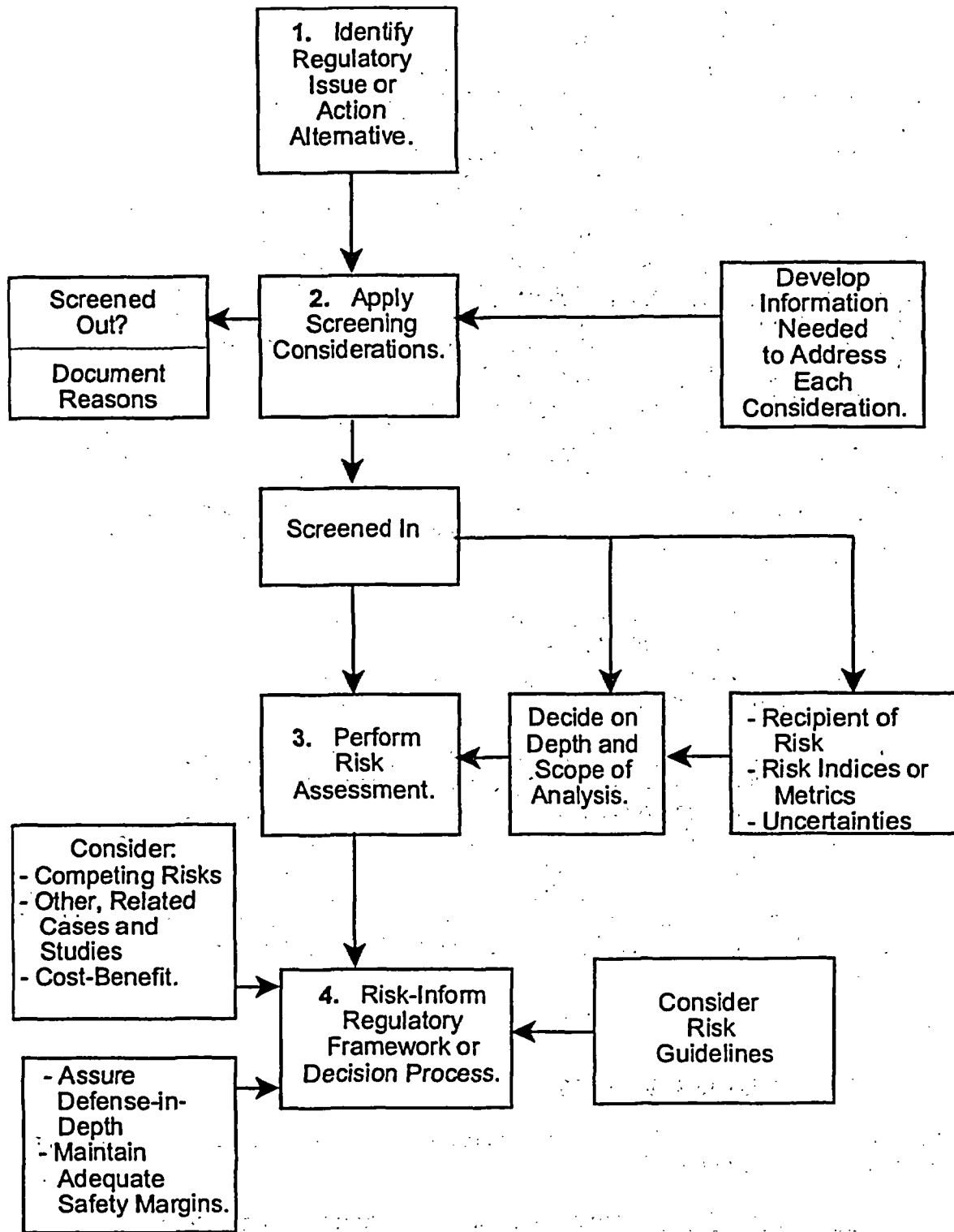


Figure 1. Proposed Risk-Informed Decision-Making Process

The proposed RIDM approach consists of four major steps as shown in Figure 1. Briefly described, the process begins with the identification of a proposed regulatory action or issue (Step 1) to which the screening considerations are applied (Step 2). The screening considerations address both the benefit and feasibility of risk-informing an activity. To assess the benefit of a risk-informed approach, the screening considerations test whether the use of risk information would enhance safety, improve effectiveness and efficiency, reduce unnecessary regulatory burden, or help to communicate a regulatory decision. To assess the feasibility aspects, the screening considerations test whether risk-informing could be accomplished in a cost-beneficial way and examine whether there are other factors, such as legislative or jurisdictional issues, that would preclude or limit the effective use of a risk-informed approach. The outcome of the screening considerations is a determination of whether the activity is amenable to being risk-informed. If a proposed regulatory action is screened-out through the screening consideration process, the reasons for screening it out should be documented. However, if a proposed regulatory action is screened-in, existing risk information is evaluated along with a consideration of the uncertainties (Step 3). If necessary, additional risk information may need to be developed. The risk information along with other information that include the following are factored into the overall decision (Step 4): costs and benefits information related to implementation of the proposed regulatory action, considerations of maintaining adequate defense-in-depth and safety margins as well as other competing risks. Background information that led to the development of the proposed RIDM process can be found in Reference 4, 5 and 9.

Although the 4 steps are listed in a serial fashion, in practice, it is generally carried out in an iterative way. For example, the candidate alternatives may be identified as a process moves forward. In that case, some of the work from the previous steps would need to be revised to ensure that the decision maker has all the necessary risk information at the end of the process.

Accordingly, the pilot study was organized into four major steps: (1) definition of the proposed regulatory action, (2) application of the screening considerations, (3) evaluation of risk information to assess the changes in risks associated with the proposed regulatory action, and (4) an evaluation of the factors that support making a decision including risk and other information. At various steps in the process, the staff expressed uncertainty about the conclusiveness of some of the outcomes of those steps. However, it decided to proceed with the risk-informed process so that it could test the effectiveness of the complete proposed RIDM process and draft RIDM guidance documents. The results obtained during each step are discussed below.

RESULTS

Definition of the Proposed Regulatory Action

The staff developed the following statement of the proposed regulatory action and the basis for considering a risk-informed approach.

Proposed Regulatory Action: Remove the need for leakage testing of certain double confinement closure lid welds of, and calculation of off-site doses due to hypothetical releases from, all-welded austenitic stainless steel canisters and

modify existing staff guidance for conducting confinement reviews of those canisters.[‡]

Basis: Based on the acceptance criteria relating to weld design and specification contained in Interim Staff Guidance No. 15 (ISG-15), "Materials Review,"¹⁰ the staff believes that there is reasonable assurance that no credible leakage would occur from the final closure welds of austenitic stainless steel spent fuel storage canisters when following the ASME code requirements. Therefore, the staff believes the review guidance can be modified to eliminate the need for certain leakage tests on double confinement closure lid welds for selected storage canisters and performing dose analyses related to releases from all-welded canisters as long as the welding criteria in ISG-15 are met. The objectives for implementing this action include: (1) Increase efficiency and effectiveness by reducing unnecessary (or low risk-significant) staff review and inspection of confinement calculations and leak testing requirements; (2) Reduce the burden on cask users by eliminating unnecessary (or low risk-significant) leak tests via reducing doses to workers; Reduce the burden to storage cask designers by eliminating unnecessary confinement analyses; and (3) Maintain public confidence in NRC's regulatory role by improving our rationale for confinement safety with a more consistent technical basis.

The staff also identified several alternatives to the proposed regulatory action that involved various combinations of activities (i.e., analyses, licensing review, leakage testing, inspection) by the NMSS staff, the storage cask designers, and personnel who perform the leakage tests. The proposed regulatory action represents an option where none of the activities are required. At the other end of the spectrum is the no-action alternative which includes all of the following: storage cask designers to conduct confinement calculations for welded casks, NMSS staff to review confinement calculation associated with releases, licensees to conduct leakage tests on welded casks, and NRC inspectors to conduct inspections on the procedures and related aspects of leak testing the canister final closure weld. This latter alternative was the approach taken by the staff before ISG-18 was implemented.

Application of the Screening Considerations

The screening considerations are listed in Table 1 and their application is described in more detail in the draft Screening Consideration Guidance. These considerations were used to assess the benefits and feasibility of using a risk-informed approach to address the proposed regulatory action that was identified in Step 1.

In response to screening considerations 1-4, the staff identified several benefits and determined that the primary benefits of implementing the proposed regulatory action were associated with improving efficiency and effectiveness and reducing unnecessary regulatory burden. Reduced regulatory burden would be achieved because the storage cask designers would not need to

[‡] As noted in the preceding section, the pilot study was initiated after ISG-18 was implemented. Therefore, NMSS staff has already adopted the approach contained in the proposed regulatory action statement.

Table 1. Screening Considerations

BENEFITS OF A RISK-INFORMED REGULATORY APPROACH

- (1) Could a risk-informed regulatory approach help to resolve a question with respect to maintaining or improving the activity's safety?
- (2) Could a risk-informed regulatory approach improve the efficiency or the effectiveness of the NRC regulatory process?
- (3) Could a risk-informed regulatory approach reduce unnecessary regulatory burden for the applicant or licensee?
- (4) Would a risk-informed approach help to effectively communicate a regulatory decision?

If the answer to any of the above is yes, proceed to additional considerations; if not, the activity is considered to be screened out.

FEASIBILITY OF IMPLEMENTING A RISK-INFORMED APPROACH

- (5) Do information (data) and/or analytical models exist that are of sufficient quality or could they be reasonably developed to support risk-informing a regulatory activity?

If the answer to criterion 5 is yes, proceed to additional considerations; if not, the activity is considered to be screened out.

- (6) Can startup and implementation of a risk-informed approach be realized at a reasonable cost to the NRC, applicant or licensee, and/or the public, and provide a net benefit?

If the answer to criterion 6 is yes, proceed to additional consideration; if not, the activity is considered to be screened out.

- (7) Do other factors exist which would limit the utility of implementing a risk-informed approach?

If the answer to criterion 7 is no, a risk-informed approach may be implemented; if the answer is yes, the activity may be given additional consideration or be screened out.

perform the off-site dose calculations and the storage cask licensees would not be required to conduct certain leakage tests on double confinement closure lid welds for selected all-welded canisters. The NRC would gain efficiency and effectiveness because the staff would not have to review storage cask designer confinement calculation associated with the off-site dose consequences from hypothetical releases from the cask. NRC inspectors would also not be required to review the off-site dose calculation or conduct inspections on the procedures and related aspects of leak testing the canister final closure weld.

Relative to screening consideration 5, the staff identified many sources of information that exist to support risk-informing the proposed. Available risk information included a draft storage pilot PRA, a report that evaluated the mechanisms for early disposal cask failures¹¹ and another report that assessed the failure probability of welded closure lids for one type of storage cask. The draft storage pilot PRA that was used in this pilot study to estimate the health risks and conduct cost-benefit analyses was developed specifically to establish a methodology for calculating the risks to the public from a single cask involved in various accidents. Limited in scope, it contains a calculation of the individual accident risks to members of the public associated with accidents relative to a single site and one cask design. It does not address the variability in risks associated with different all-welded storage canister designs or other sites. It also does not contain estimates of the uncertainties in the risks or the uncertainty bands for various parameters used to calculate the risks. Other sources of information identified by the staff include: material properties for stainless steel canisters and welded joints; data on strength of welded joints; calculation methods for assessing off-site dose consequences; information on the costs associated with NRC staff performing confinement reviews and inspections, vendors to perform confinement calculations, and licensees conducting leakage tests; general dry cask storage cask performance information; and, information on doses to workers who perform leakage tests. The staff proceeded to screening consideration 6 since there appeared to be sources of relevant information.

The staff conducted a quantitative cost-benefit analysis to respond to screening consideration 6. A fairly detailed quantitative cost-benefit analysis was performed to identify who received the health risks and the costs (expended and saved) and whether a net (positive) benefit could be realized if the proposed regulatory action was implemented. Following the NRC's value impact approach, which is contained in References 8 and 12, the staff estimated the net costs/savings associated with the proposed regulatory action. The health impacts to the public and worker (e.g., routine and accident risks which were converted to costs) and the costs (either expended or saved) to the NRC, industry and public were calculated using the best available information. The calculations were performed using realistic estimates with the perspective of evaluating the costs and benefits relative to all potentially affected the members of society (e.g., NRC, industry, public) and the environment. The staff used a factor of \$2,000/person-rem to convert estimated doses to an equivalent cost associated with the doses. The health risks and costs were estimated for the entire (realistically estimated) life cycle.

The results of the cost-benefit analysis showed that:

- there was a very small monetary expense associated with the risk of exposure due to leakage from a storage canister (primarily due to the low leakage probability and low consequence assumed);

- the largest impact was associated with the costs to NRC to actually implement the proposed Regulatory Action;
- the largest benefit was associated with the industry not having to conduct leakage tests on the spent fuel storage casks; and
- there was a net positive (monetary) benefit to be gained by society if the proposed Regulatory Action was implemented.

With respect to screening consideration 7, the staff could not identify any particular "Other Factor" that would prevent the proposed regulatory action from being risk-informed.

Favorable responses were obtained for all of the screening considerations so the proposed regulatory action was "screened-in," meaning that a determination that a risk-informed approach would be beneficial and feasible with respect to resolving the regulatory issue identified in Step 1.

Total Individual Accident Risks to the Public and Workers

The staff calculated the total individual accident risks (expressed as the probabilities of acute fatalities, latent cancer fatalities, and severe injury) to the public and workers associated with the implementation of the proposed regulatory action. The total individual accident risk, $R_{total}^{accident}$, is comprised of two components, namely, the baseline risk of dry cask storage before implementing the proposed regulatory action ($R_{baseline}$) and the changes in risks associated with implementing the proposed regulatory action (ΔR_{ISG-18}) which are added together, i.e.,

$$R_{total}^{accident} = R_{baseline} + \Delta R_{ISG-18}$$

Using information contained in the draft storage pilot PRA, the total individual accident risks were evaluated for three populations most at risk: members of the public located at 100 meters (denoted as "public"), workers located at the site of the cask that is involved in an accident (denoted as "Worker1") and workers co-located at the ISFSI site in an administrative building 100 meters from the cask (denoted as "Worker2"). Although it is unlikely that members of the public would be located 100 meters from an ISFSI, the staff made this assumption to maintain consistency with the available dose calculations contained in Reference 13, which were estimated for individuals located at 100 meters from a hypothetical ISFSI. The doses to the Worker2 population were also estimated at 100 meters to maintain consistency with available dose calculations.

For the calculations of the total individual accident risks, the staff made the following assumptions. The staff assumed that the scenarios and initiating event frequencies were applicable to all ISFSIs even though the scenarios and event frequencies used in the draft storage pilot PRA were estimated for a single site and may not apply generically to other ISFSI sites. The staff used a log-log relationship to extrapolate the inhalation doses as a function of distance (i.e., a one order of magnitude closer release would lead to a one order of magnitude increase in dose). The staff did not include the contribution from direct radiation doses emanating from the storage casks to the workers. Additionally, an estimate of the baseline leakage probability on a per cask basis was taken from a report that assessed the failure probability of welded closure lids for one type of storage cask. The staff also made best

estimate assumptions for the amount of time that the populations most at risk were potentially exposed to the risk and the number of casks that would be placed into service at all of the ISFSIs over the lifetime of the industry, since no existing information to support these numbers was available.

The uncertainties associated with the calculation of the total individual accident risks to the public and workers were not explicitly quantified. The uncertainties were evaluated using the following qualitative approach. For accident risks associated with dry cask storage, the staff group identified the following factors that could lead to orders of magnitude differences in the uncertainty: conservative estimates used for the source term in the absence of realistic data, and factors presumed to be applicable to all ISFSI sites (e.g., weather variability, weather variability, evacuation and emergency responses) that did not account for site variability. To fulfill the objective of testing all of the steps of the proposed RIDM process, the staff made the assumption that the uncertainty was represented by two-orders of magnitude in the risk estimates (i.e., the total uncertainty was expressed as the point estimate of the risk plus or minus two orders of magnitude). Thus, the staff intended that this uncertainty account for the aforementioned sources of uncertainty.

Overall, the proposed regulatory action results in a very small increase (i.e., a fraction of an order of magnitude change) in the risks to the public and workers (i.e., probabilities of acute and latent cancer fatalities and severe injuries as expressed as the total individual accident risks).

It should be noted that the information used to calculate the risks (e.g., a report that assessed the failure probability of welded closure lids for one type of storage cask, the draft storage pilot PRA, Reference 13) was not specifically developed for the purposes of conducting the pilot study. Since the main objective of the pilot study was to use existing information to test the effectiveness and concepts of the draft RIDM guidance documents, it was outside the scope of the pilot study to develop a new risk assessment and quantify the uncertainties. Therefore, the staff used the best available risk information to extrapolate and estimate values of parameters used in the risk calculations to test the effectiveness of the whole RIDM process. For example, the draft storage pilot PRA was developed specifically to establish a methodology for calculating the risks to the public from a single cask involved in various accidents. Limited in scope, it contains a calculation of the individual accident risks to members of the public associated with accidents relative to a single site and one cask design and does not address the variability in risks associated with different all-welded storage canister designs or other sites or estimate the uncertainties in the risks. Overall, the staff used somewhat conservative, but reasonable, estimates when there was no available, directly applicable information.

Evaluation of Factors Support a Risk-Informed Decision

The following four pieces of information were used to decide whether the proposed regulatory action should be implemented:

1. Risk information (including the total individual accident risks calculated in Step 3),
2. Public and worker doses,
3. Philosophies of defense-in-depth and safety margins, and
4. Other factors (including competing risks, cost-benefit analysis and related information).

Risk-Information - In accordance with the draft RIDM guidance, the total individual accident risks calculated in Step 3 were compared to NMSS' draft risk guidelines (i.e., quantitative health guidelines (QHG)) using the decision-making algorithms in the draft Decision-Making Guidance. The underlying principle of the draft risk guidelines is the notion that nuclear facilities and activities and associated regulatory changes should not pose a significant additional risk to members of the public and workers. The draft risk guidelines, which have been developed only for accidents, establish a reference level for determining when a decision results in an insignificant or tolerable level of risk. In principle, for any proposed regulatory action that is evaluated using the proposed RIDM process, the risks associated with that action are calculated and compared to the draft risk guidelines using the decision-making algorithms described in Section 2.1 of the draft Decision-Making Guidance. That decision-making algorithm essentially provides method for comparing the calculated total individual accident risks to the QHGs. If the calculated total individual accident risks are less than the risk guideline, the proposed regulatory action could be implemented from a risk perspective because it imposes an insignificant risk. There are other cases where the calculated risks are greater than the proposed QHGs. In some of those cases, it may not be beneficial or feasible (e.g., from a cost-beneficial perspective) to implement the proposed regulatory actions.

For the pilot study, the staff determined that the total individual accident risks were less than the values of the QHGs. This comparison guided the staff to conclude that the risk information (i.e., total individual accident risks and proposed QHGs) supports implementation of the proposed regulatory action.

Public and Worker Doses - The staff assessed whether the proposed regulatory action resulted in unacceptably high doses to the public and the workers relative to the regulations contained in 10 CFR Part 72. If the proposed regulatory action resulted in an increase in the dose to the public or workers that exceed any of the regulatory limits, then the proposed regulatory action should not be implemented.

Regarding an assessment of the impacts of the proposed change on annual routine doses, the staff first referred to the dose and hypothetical release calculations contained in the Holtec HI-STORM Final Safety Analysis Report (FSAR)¹⁴ to establish the baseline doses. For normal storage operations, the baseline routine dose (20.5 mrem) plus the change in routine dose associated with the proposed regulatory action (0.4 mrem, using the upper bound) produces a total routine dose to members of the public that is less than the 10 CFR Part 72 regulatory limit (25 mrem). The information contained in the FSAR also assures that the worker routine doses will be maintained as low as reasonably achievable and less than the regulatory limits. It should be noted that leakage from any cask is not considered to be a routine condition. Rather, leakage from a cask constitutes a condition that is more typical of an accident condition. Therefore, the staff included the risks associated with having a leaking cask on an ISFSI pad in the calculations of the total individual accident risk.

Defense-In-Depth and Safety Margins - The estimates of the total individual accident risks to the public and workers were, in some cases, orders of magnitude lower than the proposed QHG values. From that information alone, it might be concluded that removal of one layer of assurance (i.e., the requirements for conducting certain leakage tests and performing hypothetical off-site dose calculations) does not significantly compromise the defense-in-depth approach for all-welded stainless steel casks. If the proposed regulatory action is implemented,

adequate defense-in-depth is maintained because there is reasonable assurance that the following physical barriers and administrative controls are not affected by the proposed regulatory action. The spent fuel cladding will remain intact and serve as an additional barrier under normal and off-normal conditions. The cask confinement boundary is comprised of two independent seal welds designed in accordance with ASME Boiler and Pressure Vessel Code, which utilizes design stress limits that assure adequate safety margins, a quality assurance program and nondestructively examinations to assure adequate cask construction. The radiological environmental monitoring equipment at the site is maintained and alarms when appropriate. The licensee meets the other non-leak testing technical specifications and maintains the ISFSI at all times in accordance with the Certificate of Compliance. The licensees will operate by following their emergency response program when appropriate. Finally, the NRC conducts periodic inspections to assure the licensees are in compliance with the 10 CFR Part 72 regulations.

None of these elements of defense-in-depth are affected by the implementation of the proposed regulatory action. Therefore, eliminating the requirements for conducting certain leakage tests for the final closure welds and performing hypothetical off-site dose calculations will not adversely compromise the defense-in-depth controls listed above for dry cask storage.

Other Factors - The primary sources of risk are related to potential releases from leaking casks which were factored into the total individual accident risk. The staff did not identify any competing risks that would prevent implementation of the proposed regulatory action.

The cost-benefit analysis was refined using more accurate information. A net positive (monetary) benefit was calculated, representing an overall cost savings that would be realized if the proposed regulatory action was implemented. That is, the net benefit represents the cost savings associated with implementing the proposed regulatory action relative to maintaining the status quo approach of requiring certain leakage test and off-site dose calculations.

CONCLUSIONS

The objective of this pilot study was to identify potential modifications to the draft RIDM guidance documents to support future uses of the RIDM process. The staff tested the effectiveness of the proposed RIDM process and the supporting draft guidance, the logic of the proposed RIDM decision-making algorithms, and the draft NMSS risk guidelines. The staff recommended numerous changes to enhance the draft RIDM guidance documents. Based on the successful test of the proposed RIDM process, NMSS will modify the draft guidance documents to reflect the experience and the comments documented in this report, and NMSS could use the insights gained to guide RES in modifying the draft storage pilot PRA.

The proposed RIDM process led the staff to conclude that the proposed regulatory action (i.e., providing relief to licensees from having to conduct leakage tests and to storage cask designers from having to perform off-site dose calculations associated with hypothetical releases from certain canisters) should be implemented. This conclusion is consistent with the staff's earlier decision to implement ISG-18. NMSS issued ISG-18 primarily based on the consideration that adequate safety would be maintained even though the requirements for the leakage test and off-site dose calculations were lifted. The application of the proposed RIDM process helped to illuminate other benefits associated with implementing ISG-18, namely, a reduction in

unnecessary regulatory burden to the industry and enhanced NRC and industry efficiency and effectiveness.

REFERENCES

1. U.S. Nuclear Regulatory Commission. "Use of Probabilistic Risk Assessment in Nuclear Regulatory Activities: Final Policy Statement," Federal Register, Vol. 60, No.158, August 16, 1995, Washington, D.C.
2. U.S. Nuclear Regulatory Commission. "Framework for Risk-Informed Regulation in the Office of Nuclear Material Safety and Safeguards," SECY-99-100. March 31, 1999.
3. U.S. Nuclear Regulatory Commission. Memorandum from A. Vietti-Cook to W.T. Travers, U.S. Nuclear Regulatory Commission, "Staff Requirements – SECY-99-100 – Framework for Risk-Informed Regulation in the Office of Nuclear Material Safety and Safeguards," June 28, 1999.
4. L. E. Kokajko and R. M. Shane, "The Case Study Approach to Risk-Informing Regulation of Nuclear Materials and Waste," presented at the Probabilistic Safety Assessment and Management 6, San Juan, Puerto Rico, June 23-28, 2002, Elsevier Science Ltd., 2002.
5. C. H. Lui, A. Wong and L. E. Kokajko, "Risk Informing Nuclear Waste: A Case Study on the Regulation of Spent Fuel Interim Storage," presented at the Probabilistic Safety Assessment and Management 6, San Juan, Puerto Rico, June 23-28, 2002, Elsevier Science Ltd., 2002.
6. U.S. Nuclear Regulatory Commission. Interim Staff Guidance - 18, Revision 0, "The Design/Qualification of Final Closure Welds on Austenitic Stainless Steel Canisters as Confinement Boundary for Spent Fuel Storage and Containment Boundary for Spent Fuel Transportation," April 2003.
7. U.S. Nuclear Regulatory Commission. Regulatory Guide 1.174, "An Approach for Using Probabilistic Risk Assessment in Risk-Informed Decisions on Plant-Specific Changes to the Licensing Basis," November 2002, Rev 1.
8. U.S. Nuclear Regulatory Commission. "Regulatory Analysis Guidelines of the U.S. Nuclear Regulatory Commission, NUREG/BR-0058, July 2002."
9. C. Lui, M.V. Federline, "Overview of U.S. Nuclear Regulatory Commission Program on Risk-Informing Materials and Waste Arenas," presented at the Probabilistic Safety Assessment and Management 6, San Juan, Puerto Rico, June 23-28, 2002, Elsevier Science Ltd., 2002.
10. U.S. Nuclear Regulatory Commission. Interim Staff Guidance - 15, "Materials Evaluation," January 2002.
11. Center for Nuclear Waste Regulatory Analysis. "Assessment of Mechanisms for Early Waste Package Failures," CNWRA 2003-05, March 2003.
12. U.S. Nuclear Regulatory Commission. "Regulatory Analysis Technical Evaluation Handbook, Final Report," NUREG/BR-0184, January 1997.
13. U.S. Nuclear Regulatory Commission. "Best-Estimate Offsite Dose from Dry Storage Cask Leakage," SMSAB-00-03, June 2000.
14. Holtec International, Inc., "HI-STAR Final Safety Analysis Report," Revision 1, December 23, 2002.

**Option 3:
Risk-Informed Alternative to 10CFR50.46 and GDC 35**

Eileen McKenna, NRR/NRC
John C. Lane, RES/NRC

Issue Background and History

NRC staff deliberations regarding the possibility of rulemaking changes to 10 CFR 50.46 date from approximately 1997. The following list provides the principal staff communications, known as SECY papers:

1. SECY-98-300, "Options for Risk-Informed Revisions to 10 CFR Part 50 - "Domestic Licensing of Production and Utilization Facilities," December 1998. This is the first SECY paper which described three "high level" options for risk-informing 10 CFR Part 50. Option 1 simply consisted of leaving Part 50 as is. Option 2 involved making changes in the scope of structures, systems and components related to special treatment rules (the current rulemaking activity for 10 CFR 50.69). Option 3, described herein, involved making changes to specific regulatory requirements, such as 10 CFR 50.44 and 50.46.
2. SECY-99-264, "Proposed Staff Plan for Risk-Informing Technical Requirements in 10 CFR Part 50," November 1999, described the overall staff plan for Option 3.
3. SECY-00-0198, "Status Report on Study of Risk-Informed Changes to the Technical Requirements of 10 CFR Part 50 (Option 3) and Recommendations on Risk-Informed Changes to 10 CFR 50.44 (Combustible Gas Control)," provided a description of proposed changes to 50.44 and a proposed framework for considering other changes to Part 50.
4. SECY-01-0133, "Status Report on the Study of Risk-Informed Changes to the Technical Requirements of 10 CFR Part 50 (Option 3) and Recommendations on Risk-Informed Changes to 10 CFR 50.46 (ECCS Acceptance Criteria)," provided preliminary feasibility studies recommending risk-informed changes to Part 50.46.
5. SECY-02-0057, "Update to SECY-01-0133, "Fourth Status Report on Study of Risk-Informed Changes to the Technical Requirements of 10 CFR Part 50 (Option 3) and Recommendations on Risk-Informed Changes to 10 CFR 50.46 (ECCS Acceptance Criteria)," provided specific recommendations for changes to 50.46 in the areas of ECCS break size definition, ECCS acceptance criteria, ECCS reliability and ECCS evaluation model. On March 31, 2003, the Commission provided the latest staff requirements memorandum (SRM) providing their guidance to the staff.

Stakeholder Input

A number of public meetings have been held to provide a forum for discussing staff perspectives and to obtain feedback from industry and the public. Meetings were held in 2003 on June 9 and July 24 to discuss the staff's and industry's interpretation of the SRM issued in March 2003. Industry noted key areas with which they expressed concern, such as, the scope of allowed changes, PRA scope and quality and the appropriate use of best estimate models. On September 5, 2003, the Nuclear Energy Institute (NEI) issued a draft "white paper" which proposed, for staff consideration, an approach for risk-informing Part 46 by applying results from the on-going staff effort to redefine the large break LOCA. The industry paper also referred to the February 6, 2002 industry petition for rulemaking (PRM) which recommended language allowing for revision to the large break LOCA design basis up to and including "an alternate maximum break size defined by an approved risk-informed process."

Overview of 50.46 (Including Appendix K and GDC 35) Issues

An understanding of the implications of a major revision to 10 CFR 50.46 begins with an understanding of existing requirements. The regulations stipulate that every light water reactor licensed by NRC must possess an emergency core cooling system (ECCS). ECCS functional parameters may be divided into four topics: ECCS LOCA break size definition, ECCS reliability, ECCS acceptance criteria and ECCS evaluation model.

Current statutes pertaining to *ECCS LOCA Break Size Definition* require that ECCS response be determined for a variety of LOCA sizes and locations characterized by accidents resulting in a loss of reactor coolant at a rate in excess of the capability of the reactor coolant makeup system. The accidents must include pipe breaks in the reactor coolant system (RCS) pressure boundary up to and including a break equivalent in size to a double-ended rupture of the largest pipe in the RCS. The Commission directed the staff to perform a comprehensive LOCA failure analysis and frequency estimation and to propose revised break sizes as a function of frequency of occurrence. As a result of these revisions, the staff is to provide a proposed rule allowing for a risk-informed alternative to the present maximum LOCA break size.

Additional guidance was provided by the Commission to help establish guidelines for developing new requirements. One important consideration is the need to preserve defense-in-depth. Section 2.2.1 of Regulatory Guide (RG) 1.174 contains a discussion of the concept of defense in depth along with suggestions as to how it can be assured. Defense-in-depth may be assured if the following provisions are satisfied:

- A reasonable balance is preserved between prevention of core damage, prevention of containment failure, and consequence mitigation.
- Over-reliance on programmatic activities to compensate for weaknesses in plant design is avoided.
- System redundancy, independence, and diversity are preserved commensurate with the expected frequency, consequences of challenges to the system, and uncertainties (e.g., no risk outliers).

- Defenses against potential common cause failures are preserved, and the potential for the introduction of new common cause failure mechanisms is assessed.
- Independence of barriers is not degraded.
- Defenses against human errors are preserved.
- The intent of the General Design Criteria in Appendix A to 10 CFR Part 50 is maintained.

The staff is also encouraged to consider the RG 1.174 acceptance guidelines for core damage frequency (CDF) and large early release frequency (LERF) in evaluating appropriate levels of plant risk increments resulting from plant changes as a part of a redefinition rule.

ECCS Reliability assures system safety function can be accomplished over a wide range of accident conditions including conservatisms afforded by inclusion of the availability and unavailability of offsite and onsite power; and including a single active failure of a component. The Commission directed the staff to consider replacing current LOCA/LOOP requirements, which require design capability for concurrent LOCA and LOOP, with a functional ECCS requirement commensurate with the actual LOCA frequencies.

ECCS Acceptance Criteria establishes the standards for ECCS cooling performance following a postulated LOCA. It includes codified requirements including a peak reactor fuel temperature limit of 2200°F, maximum cladding oxidation limit of 17% times the original cladding thickness, maximum hydrogen generation equivalent to 1% of all zirconium metal contained in the core. In addition, the core must maintain a coolable geometry for the long-term. The Commission directed the staff to provide a performance-based acceptance criteria for fuel rod integrity, commensurate with existing provisions requiring a long-term coolable geometry.

The requirements pertaining to the *ECCS Evaluation Model* stipulate that the model upon which the ECCS is designed must contain the characteristics described in 10 CFR 50 Appendix K, must be realistic and must include an uncertainty evaluation. The Commission emphasized that any plant changes based upon changes in the design basis LOCA break sizes should include a requirement for the use of best-estimate analysis methods.

Staff Activities

In support of the March 2003 SRM, the staff is completing a comprehensive LOCA failure analysis and frequency re-estimation which will be use as input to a risk-informed proposed rule. The SRM provides the staff with the following "ground rules" to be included in rulemaking activities:

1. The proposed rule should provide a voluntary risk-informed alternative to the present 10 CFR 50.46 by establishing a risk cutoff for break sizes to be removed from the design basis.
2. As mentioned previously, any proposed functional changes should be risk-informed and consistent with the principles of RG 1.174.

3. ECCS functional reliability should be commensurate with the frequency of accident in which ECCS success would prevent core damage or a large early release.
4. No changes to functional requirements should be made unless fully risk informed. Specifically, no changes should be made to ECCS coolant flow rates or containment capabilities to mitigate accidents.
5. Only non-significant contributors to risk should be handled through severe accident management initiatives.
6. The staff should strive to employ realistically conservative estimates, with appropriate margins for uncertainty.
7. The underlying PRA should be full scope and high quality. It should include Level 2 results, external events, all modes of operation and be subjected to a peer review and ultimately, NRC endorsement.
8. Beyond the initial redefinition of LOCA frequencies, the staff should periodically (every 10 years) re-estimate LOCA frequencies and failure types (every 5 years).
9. Approved operational changes resulting from the flexibility granted via the new rule should be reversible if a future re-estimation of risk shows unacceptable frequency increases.

ECCS LOCA Break Size—The staff is working to define the metric to be used in determining the new design basis maximum break size. One possibility under consideration is the use of LOCA frequency as the basis. In other words, breaks with a frequency of occurrence below a certain threshold might be excluded from the design basis. The staff must also determine the appropriate acceptance criteria for allowing plant changes resulting from the new flexibility gained as a result of the smaller design basis break size. The staff will consider existing criteria, such as those provided in RG 1.174, in arriving at a recommendation.

As with any plant change, the staff must determine the appropriate level of information required of licensees to enable a regulatory decision. This is especially challenging here because the changes may be far reaching and may impact plant response in areas beyond those associated with large break LOCA response. The Commission also requires that plant changes made as part of the 50.46 rulemaking be reversible. Reversibility has typically not been a consideration in the staff review of plant changes.

Other important issues requiring resolution include the extent to which best-estimate models and computer analysis codes should be used in re-examining the plant performance following the redefinition of the large break. The staff needs to consider whether all analyses should now use best-estimate codes or whether “traditional” Appendix K model assumptions may be used for break sizes smaller than the new maximum break size. Also, the staff will need to determine whether other sections of 10 CFR Part 50 should also be revised for conformity with new risk-informed Part 50.46.

It appears that there is consensus agreement that at least some mitigation capability should be provided for pipe breaks that are now part of the design basis but would be removed under the new rule. No definitive proposal has been established as to what this mitigative capability should be but it is clear that it should be enough to provide adequate assurance to the public that plant safety is maintained at a high level despite the plant changes resulting from the rule change. An example of a mitigative criteria would be one which would prevent vessel failure as determined by a realistic thermal hydraulic analysis. Another possible criteria would be one which would prevent fuel rod failure from leading to a loss of a coolable reactor geometry. An issue with the development of these criteria, however, is that the state-of-art computer methods necessary to analyze a plant's ability to satisfy them may not yet be available. It is important to also note that it is the new plant configuration, including the changes allowed by the new rule, which should be subjected to any such mitigation criteria, but at this time, a comprehensive list of proposed plant changes is not known.

ECCS Acceptance Criteria—In the area of fuel performance vis-a-vis ECCS performance, the staff is proceeding with the development of an optional performance based approach to meeting the ECCS acceptance criteria. The new approach might be designed to demonstrate that adequate post-quench cladding ductility is maintained. It will also allow the use of cladding materials other than Zircaloy or ZIRLO without the need for licensees to submit an exemption request. Licensees would still be expected to provide a satisfactory basis to allow the staff to conclude that the new performance based criteria are met.

ECCS Evaluation Model—The Commission, in its March 2003 SRM, disapproved the staff's proposal to provide a voluntary alternative to Appendix K, ECCS Evaluation Models, which specifies the features necessary for the staff to approve ECCS models. The change would have replaced the 1971 ANS decay curve with the 1994 standard. This change would essentially have replaced a multiplier from the older standard with a new requirement for an uncertainty analysis. Regulatory Guide 1.157 discusses the use of uncertainty analysis for realistic ECCS models. The Commission did, however, encourage licensees to use best estimate evaluation models when evaluating the adequacy of changes made to their plants to ensure conformance with acceptance criteria.

ECCS Reliability—The Commission approved the staff's recommendation proposing rulemaking for a new, voluntary provision to risk inform GDC 35, Emergency Core Cooling, related to coincident loss-of-offsite-power (LOSP) along with large break LOCA. The dependence, which appears to be somewhat plant specific, between LOCA and coincident LOOP, is being evaluated along with reliability and uncertainty issues. One problem encountered is the relative paucity of data regarding LOCA-LOOP. Both grid related and plant-centered factors are being considered in assessing the probability of LOOP given LOCA. Acceptable methods and assumptions must be developed in order to accurately estimate the plant-specific probability of LOOP. The staff also intends to examine delayed LOOP, a situation in which the LOOP does not occur at the same moment the LOOP does, but occurs a finite time later, will also be investigated.

The staff is also studying a broader change to the single failure criterion. GDC 35 requires the ECCS safety function to be accomplished assuming a single active failure. The staff is evaluating the basis for revising or replacing the single failure criterion in the alternate rule, but only as it affects ECCS performance. The single failure criterion also impacts plant systems beyond ECCS. For example, GDCs 17, 34, 38, 41 and 44 also contain requirements related to

the single failure criterion. Regulatory Guide 1.53, "Application of Single-Failure Criterion to Safety Systems," discusses the issue in relation to electrical systems.

Conclusion

The staff plans to provide the Commission with their response to the SRM, which will, among other things, discuss the important issues relevant to the rulemaking. Key issues are: PRA scope, reversibility, defense-in-depth, applicability to future plants, plant monitoring and the extent of actual plant changes. Additional public meetings will be held to obtain stakeholder input.

FIRE RISK RESEARCH PROGRAM: ADVANCES SUPPORTING RISK-INFORMED REGULATION

J.S. Hyslop, Senior Risk and Reliability Analyst
Probabilistic Risk Analysis Branch
Office of Nuclear Regulatory Research

The fire risk research program is continuing to provide critical support to risk-informed, fire protection regulatory activities at the U.S. Nuclear Regulatory Commission (NRC) for nuclear power plants. These activities are related to inspection, the Reactor Oversight Process (ROP), and fire protection rulemaking. The relevant technical issues range from associated circuits to broad applications of fire risk analysis (FRA) methods, tools, data, and fire models. A discussion of the technical advances supporting these activities, as well as the anticipatory research programs driving these advances, follow in this paper.

I. Introduction

The fire risk research program is supporting many risk-informed, fire protection regulatory activities that are underway for nuclear power plants. These supported activities span inspection, oversight, and rulemaking. In particular, the resumption of inspection of associated circuits is being focused by risk considerations. An associated circuit is a circuit corresponding to a component directly outside of the 10 CFR Part 50, Appendix R, protected safe shutdown path. Associated circuits remain an inspection issue since their failure can fail the protected train. An example of the impact of a failed associated circuit on the protected train is a flow diversion failing the protected train.

The second activity supported by the fire risk research program is the ROP [1]. The ROP is a risk-informed process for determining the agency response to an inspection finding or performance indicator. No performance indicators have been developed for the ROP with respect to fire protection. The ROP only incorporates a tool for assessing the significance of fire protection inspection findings. This tool, the fire protection significance determination process (SDP), is being revised.

The third supported activity is the technical implementation of the risk-informed, performance-based fire protection rulemaking[2] endorsing National Fire Protection Association (NFPA) Standard 805. This rulemaking provides a voluntary alternative to those regulations in Appendix R, allowing a risk-informed, performance based approach for the entire plant fire protection program.

II. Associated Circuits

Several types of associated circuit issues exist. The type considered in this paper is that which produces a spurious operation of equipment, such as a repositioning of a motor-operated valve. These spurious operations occur as a result of a fire-induced hot short, i.e. particular conductors shorting electrically due to the breakdown of insulation. Hot shorts may occur between those conductors within a single cable (intra-cable), or between conductors from different cables (inter-cable). Prior to the U.S. Nuclear Regulatory Commission (NRC) temporarily suspending inspection of associated circuits[3,4], all

associated circuits leading to spurious operation were candidates for inspection. No distinction was made due to the likelihood of spurious operation due to related cable or circuit features.

The scope of cable and circuit features have been narrowed for resumption of inspection by probability considerations. The Office of Nuclear Regulatory Research (RES) has participated in a public meeting[5] with the Office of Nuclear Reactor Regulation (NRR), industry, and the Electric Power Research Institute (EPRI) to identify those cable and circuit features leading to high probability of spurious actuations. The conclusion of this meeting was that the highest probability cable/circuit features leading to spurious actuation were intra-cable hot shorts (regardless of cable insulation).

Much of the basis of these conclusions was based upon industry tests[6], supplemented by RES testing apparatus[7], to evaluate the likelihood of spurious actuations and those relevant cable/circuit features[8]. Also RES has conducted a multi-year research effort [9] to understand the technical issue of circuit analysis and review the relevant data, including the more recent industry tests.

Many cable and circuit analysis features were identified besides those of highest probability in the public meeting in which NRC and industry participated. In particular, a set of features was identified as having low risk and another set was determined as being of indeterminate risk, i.e. low risk significance or needing further research to determine the risk significance. For example, inter-cable hot shorts between thermoset cables were determined as being of indeterminate risk, and inter-cable shorts between armored cable was determined to have low risk. Hot shorts between cables having thermoplastic insulation is of particular interest with respect to resumption of inspections. Thermoplastic insulation is particularly susceptible to spurious actuation since it deforms under high temperature conditions produced by fire. Based upon available data, RES will be reviewing those categories of low and indeterminate risk to determine if any circuit features should be added to inspections once they resume. RES is participating in ongoing international activities in COOPRA, the Cooperative PRA group, a potential candidate for conducting additional circuit analysis tests.

The number of spurious actuations to consider simultaneously for inspection was determined by expert judgment within the public meeting described above. The presence of multiple spurious actuations was supported by the above mentioned industry tests. Although a determination of the number of spurious actuations has been made for inspection, the technical basis for determining the number to consider for an FRA remains a challenge. In particular, the number of spurious actuations to be considered is plant specific, and depends upon the particular application in question. Work is ongoing to address this issue for FRA.

III. Fire Protection SDP Revision

The fire protection SDP is a tool for evaluating the risk significance of fire protection inspection findings[10]. The revision will improve the technical basis and enhance reproducibility of analytical results. The revision benefits from a time-based framework where fire growth, fire suppression, and degradations in fire protection defense-in-depth due to inspection findings are viewed in the time domain. The time based framework relies heavily upon estimates of time to damage from fires due to various configurations and ignition sources.

Technical advances in many areas supported by RES have occurred in the fire protection SDP revision. The definition of fire frequency has been improved by identifying those fires which have the potential to challenge safety. Traditionally, challenging fires were determined by modifying a component fire frequency representative of all fires with a generic industry-wide severity factor. Fire frequency is now defined with more refined criteria applied in the initial evaluation of fire events. For example, potentially challenging fires consist of those fires which did not challenge safety in one plant configuration, but could have in another. Also, fires requiring multiple fire extinguishers to extinguish a fire constitute challenging fires. This treatment of fire frequency avoids the concern of double counting since suppression is not credited in the both the quantification of fire frequency and suppression.

The categorization of plant components according to fire scenario bins has also been refined. Ignition sources have been grouped according to the potential to damage equipment, resulting in distinctions between wet and dry transformers and between low and high voltage cabinets. To further support the development of fire scenarios, expert judgement based upon available data has been used to determine low probability, high confidence fires. After all, those low probability, high consequence fires may drive risk under certain plant configurations.

The analysis of detection and suppression in the fire SDP considers use of historical evidence regarding fire durations. Fire duration curves are developed based upon bins of components which are expected to produce similar fire scenarios or upon locations such as the main control room. The result of such corresponding analyses are probabilities of manual suppression for particular fire sources. Many prior analyses have only considered fire brigade response times, excluding the effectiveness of the fire brigade or delay in extinguishing the fire. The historical evidence approach explicitly treats the likelihood of long duration fires based upon past experience.

IV. Fire Protection Rulemaking (NFPA 805)

RES will be developing guidance for evaluations of fire models and FRA methods, tools, and data to support reviews of changes to the plant fire protection program. Fire models are comprised of two components: the models themselves and inputs to the models. Verification and validation (V&V) of the fire models will be performed via ASTM E 1355-97, "Standard Guide for Evaluating the Predictive Capability of Deterministic Fire Models." This standard clearly indicates that V&V is performed on a fire scenario basis. In that light, RES and NRR are discussing the types of scenarios to be considered.

The fire models range from relatively simple models based primarily upon empirical equations to more sophisticated, computational fluid dynamics (CFD) approaches relying extensively upon solving fire dynamics conservation equations. The simple models produce homogeneous determinations of fire effects; the complex models produce local effects. The simple models based upon empirical correlations are the EPRI FIVE Revision 1[11] and NRR Fire Dynamics Tools[12]. A more complex fire model which divides the region into several zones is the National Institutes of Standard (NIST) CFAST code[13]. Finally, the more rigorous, CFD code which is undergoing V&V is the NIST Fire Dynamics Simulator[14].

The second component of models is the input. Inputs such as room dimensions, ventilation, and heat release rate (HRR) of the fire source are provided during the initial phase of fire growth. Inputs are also provided after the initial phase of fire growth for phenomenon which cannot be modeled acceptably by the fire model. An example of an input which occurs after the initial phase of fire growth for some models is

the characterization of HRR for secondary fires. The modeling of fires which have propagated to secondary fire combustibles is particularly challenging.

Guidance for review of FRA methods, tools, and data will also be provided. Those issues covered are fire-induced initiators, fire frequency/severity, detection/suppression, circuit analysis, human reliability analysis, and the choice of plant model. Issues associated with frequency, detection/suppression, and circuit analysis have been partially discussed in this paper under the fire protection SDP revision. Human reliability analysis covers not only those issues related to internal events models, but also the impact of smoke, high temperature, and toxic gas, including the use of a self-contained breathing apparatus. The choice of plant model is important since fire procedures, as opposed to emergency operating procedures (EOPs), may direct the operators to remove from service plant equipment to avoid the impact of fire induced spurious operations. Eventually, analyses to support changes in the plant fire protection program will be based upon the American Nuclear Society (ANS) full power fire risk standard[15] under development, which RES is supporting.

V. Anticipatory Research

RES has significant research programs to develop guidance and insights into fire modeling, and FRA methods, tools, and data. These research programs form the foundation for advances discussed previously for risk-informed regulation. First of all, RES is participating in fire modeling benchmark and validation exercises. The program, the International Collaborative Project to Evaluate Fire Models for Nuclear Power Plant Applications [16], consists of multi-national blind benchmark exercises and has been performed for two types of fire scenarios. In addition to the models noted above that are undergoing V&V, FLAMME_S, MAGIC, COCOSYS, CFX, JASMINE, COPBR-3D were also used for these benchmark exercises. The first exercise, related to cable tray fires[17], consists of two phases. The first phase is characterized by moving a fire source within a room to determine the minimum horizontal distance which produces cable damage within a set of cable trays. Cable damage is determined by exceeding the cable temperature threshold for damage. The second phase consists of assuming ignition of those cable trays, with a representative HRR, and evaluating the hot gas layer and radiative fire effects at the redundant set of cable trays across the room. The outcome of the blind benchmark exercise is that the predictions of hot gas layer and plume temperatures were generally similar for the models used. The second exercise is based upon large, oil pool fires which occur in turbine halls[18]. Unlike the cable tray scenario, the predictive capability of the fire models was challenged by the gratings and hatches found in large turbine halls.

RES has also conducted fire tests at NIST which evaluated fire effects in a single compartment based upon heptane and toluene fires. Vertical and horizontal cable trays and a junction box were included in the compartment as targets. Over 350 channels of data for model validation were acquired during the test series. Data is currently being analyzed and compared to blind predictions from the cable tray exercise. Additional fire testing is being planned with the Institute for Protection and Nuclear Safety at the large scale DIVA facility in Cadarache, France. These tests are being conducted to gather data which will enable analysts to validate codes evaluating fire propagation and effects between different compartments.

Another major activity providing the basis for technical advances in risk-informed regulation is the joint NRC/EPRI fire risk requantification study [19, 20]. This program is developing state-of-art guidance for conduct of FRA. This study broadly addresses technical issues for full power operations, including large early release frequency. This program is being conducted with two licensees' FRAs which enable NRC

and EPRI to test the guidance for viability and effectiveness. Fire-induced initiators, fire frequency/severity (including challenging fires), fire scenario development (including initial fire characteristics such as HRR), fixed fire protection suppression systems, fire brigade, spurious operations, and human reliability are addressed in this study. A possible extension of this effort to cover low power and shutdown operational modes is currently being considered by EPRI and NRC. Furthermore, RES has addressed circuit analysis issues in another extensive, research program [9,21].

VI. Conclusion

The fire risk research program provides critical support to regulatory activities in fire protection for nuclear power plants. The activities identified in this paper and supported by RES are identification of associated circuit features for resumption of inspections, evaluations of fire protection inspection findings for the Reactor Oversight Process, and the technical implementation of the risk-informed, performance-based fire protection rulemaking endorsing NFPA 805.

Anticipatory research provides the foundation for the advances for these regulatory activities. Research is ongoing in the areas of fire modeling, and FRA methods, tools, and data. In the area of fire modeling, a range of fire models of varying complexity are being verified and validated under ASTM E 1355-97, "Standard Guide for Evaluating the Predictive Capability of Deterministic Fire Models. The joint NRC/EPRI fire risk requantification study is producing state-of-art guidance for the conduct of FRA. The fire protection SDP revision has already benefitted from this joint NRC/EPRI program. The technical implementation of the fire protection rulemaking is strongly dependent on both activities for its success.

Risk considerations lead to more realistic safety decisions. Inspection of associated circuits will be focused on those features enhancing the likelihood of spurious actuations. The fire protection SDP will be improved through better methods of analysis. Implementation of the NFPA 805 fire protection rulemaking, which provides for an integrated safety analysis of changes to the plant fire protection program, will be refined through effective guidance for regulatory reviews.

VII. Acknowledgment

The author acknowledges review and comments provided by Dr. Monideep Dey of the Office of Nuclear Regulatory Research, NRC. Dr. Dey is responsible for fire modeling under the fire risk research program.

VIII. References

1. U.S. Nuclear Regulatory Commission, "Recommendations for Reactor Oversight Improvements," Commission papers SECY-99-007, January 8, 1999 and SECY-99-07A, March 22, 1999.
2. U.S. Nuclear Regulatory Commission, "Proposed Rule: Revision of 10CFR 50.48 to Permit Light-Water Reactor to Voluntarily Adopt National Fire Protection Association (NFPA) Standard 805, "Performance-Based Standard for Fire Protection for Light-Water Reactor Electric Generating Plants, 2001 Edition" (NFPA 805) as an Alternative Set of Risk-Informed, Performance-Based Fire Protection Requirements (WITS 199900032)," SECY-02-0132, July 15, 2002.
3. U.S. Nuclear Regulatory Commission, Enforcement Manual, Section 8.1.7.1.

4. Memorandum to Gary M. Holahan, Director, Division of Systems Safety and Analysis, Office of Nuclear Reactor Regulation from John N. Hannon, Plant Systems Branch, Division of Systems Safety and Analysis, Office of Nuclear Reactor Regulation, "Rationale for Temporarily Halting Certain Associated Circuits Inspection Lines of Inquiry during Fire Protection Baseline Triennial Inspections," dated November 29, 2000 (ADAMS ML003773142).
5. Memorandum to Cynthia A. Carpenter, Chief, Inspection Program Branch, Division of Inspection Program Management, Office of Nuclear Reactor Regulation from John N. Hannon, Plant Systems Branch, Division of Systems Safety and Analysis, Office of Nuclear Reactor Regulation, "Proposed Risk-Informed Inspector Guidance for Post-Fire Safe-Shutdown Associated Circuit Inspections," dated March 19, 2003 (ADAMS ML030780326).
6. Electric Power Research Institute, Characterization of Fire-Induced Circuit Faults - Results of Cable Fire Testing, EPRI TR 1003326, December 2002.
7. U.S. Nuclear Regulatory Commission, Cable Insulation Resistance Measurements Made During Cable Fire Tests, NUREG/CR-6776, SAND2002-0447P, June 2002.
8. Electric Power Research Institute, Spurious Actuation of Electrical Circuits Due to Cable Fires - Results of an Expert Elicitation, EPRI TR 1006961, 2002.
9. U.S. Nuclear Regulatory Commission, Circuit Analysis - Failure Mode and Likelihood Analysis, NUREG/CR-6834, SAND2002-1942P, September 2003.
10. U.S. Nuclear Regulatory Commission, Inspection Manual Chapter 0609, Appendix F.
11. Electric Power Research Institute, "Fire Modeling Guide for Nuclear Power Plant Applications," Technical Report 1002981, August 2002.
12. U.S. Nuclear Regulatory Commission, Fire Dynamics Tools (FDT^s) Quantitative Fire Hazard Analysis Methods for the U.S. Nuclear Regulatory Commission Fire Protection Inspection Program, Draft Report for Comment, NUREG-1805, Vols. 1 and 2, June 2003.
13. R.D. Peacock et. al., "Consolidated Model of Fire Growth and Smoke Transport," NIST Technical Note 1299, National Institute of Standards and Technology, Gaithersburg, Maryland, February 1993.
14. K.B. McGratton, H.R. Baum, R.G. Rehm, Fire Dynamics Simulator - Technical Reference Guide, NISTIR 6467, January 2000.
15. American Nuclear Society, "Fire PRA Methodology Standard," BSR/ANS 58.21, La Grange Park, Illinois.
16. Dey, M.K., "International Collaborative Project to Evaluate Fire Models for Nuclear Power Plant Applications: Summary of Planning Meeting," NUREG/CP-0170.

17. U.S. Nuclear Regulatory Commission, Evaluation of Fire Models for Nuclear Power Plant Applications: Cable Tray Fires, NUREG-1758, June 2002.
18. NUREG report (under development).
19. Nowlen, S.P., Najafi, B., "Methods Advances in the EPRI/USNRC Fire Risk Requantification Study," Conference Proceedings, SmiRT 17, Post Conference Seminar #21, Fire Safety in Nuclear Power Plants and Installations, Piestany, Slovakia, August 25-28, 2003.
20. Addendum to NRC/EPRI Memorandum of Understanding on Cooperative Nuclear Safety Research, Fire Risk (Rev. 1), May 18, 2001.
21. J.S. Hyslop, "Fire Risk Research Program: Addressing Key Uncertainties," NUREG/CP-0180, Proceedings of the 2002 Nuclear Safety Research Conference, Washington, D.C. 28-30 October 2002.

NRC's ADVANCED REACTOR RESEARCH PROGRAM

**John H. Flack, Chief
Regulatory Effectiveness Assessment and Human Factors Branch
Division of Systems Analysis and Regulatory Effectiveness
Office of Nuclear Regulatory Research
U.S. Nuclear Regulatory Commission**

Abstract

NRC's Office of Nuclear Regulatory Research (RES) performed an infrastructure assessment on which to base an advanced reactor research plan. The infrastructure assessment specifically focused on gaps or shortcomings in regulatory methods, analytical tools, data, and expertise as they relate to advanced reactor technology. The assessment centered around NRC's implementation of the four cornerstones of reactor safety: accident prevention, accident mitigation, barrier protection, and offsite protection. Key research areas were linked to the cornerstones and assessed in the context of six advanced reactor designs and the technical and safety challenges they presented. This paper summarizes the approach used to identify the research areas, and identifies key challenges that need to be addressed by the research program.

In response to Commission concerns about the Agency's preparedness for licensing advanced reactor designs, the staff issued SECY-01-0188 "Future Licensing and Inspection Readiness Assessment [FLIRA]. The FLIRA report committed the staff to the development of a research plan, and ultimately an advanced reactor research infrastructure to support the regulation of new reactor designs. To identify infrastructure needs, an assessment was performed to help identify technology gaps and means to fill the gaps in the form of methods, tools, data, and expertise. The assessment originated from a generic perspective, but the scope specifically included six advanced designs that are either under NRC review or being planned for pre-application or design certification. These designs included the Pebble Bed Modular Reactor (PBMR), General Atomics' Gas Turbine-Modular Helium Reactor (GT-MHR), the Westinghouse International Reactor Innovative and Secure (IRIS), the Westinghouse AP-1000, General Electric's ESBWR, and the Atomic Energy of Canada Limited Advanced CANDU Reactor 700 (ACR-700). Framatome's SWR-1000 design is expected to be added in the near future. Generation IV (Gen IV) designs which are currently being considered for research and development by the Department of Energy (DOE), were not explicitly included because of their early stage of development. Nevertheless, a nexus does exist in many technical areas between Gen IV and advanced reactor designs currently under review.

To various degrees, advanced designs involve new and innovative features. Some of the designs are not based on light-water reactor (LWR) technology where NRC has a considerable experience base. These new non-LWR designs are expected to respond passively to transients and accidents, require fewer operator actions, involve new materials and fuels, and a number of independent reactor cores or modules. As summarized below but contained in detail in SECY-03-0059, [NRC's Advanced Reactor Research Program], new regulatory tools, methods, and facilities will be needed to address the technology that forms the basis of these advanced designs. Nevertheless, a large fraction of the infrastructure that has already been developed and is in place for LWRs, also provides a solid foundation from which to build an

infrastructure for advanced designs. It should be noted, however, that not all research needs to be done by the NRC. Applicants and cooperative agreements with other organizations, both domestic and international, play a key role in preparing the NRC for advanced plants.

The infrastructure assessment performed by the NRC in preparation for advanced reactor designs involved a thorough review of NRC's regulatory research capabilities. Within this context, it is recognized that even a well-funded and appropriately focused research program cannot transform the regulatory process for advanced nuclear power plants into a process where decisions flow exclusively from scientific and technical knowledge. Consideration of defense-in-depth and safety margins will always remain an important part of regulatory decisions to offset limitations in state-of-the-art knowledge and understanding. Advanced reactor licensing will continue to involve a complex blend of applying technical knowledge within the context of Commission policy and prudent regulatory decisions. Therefore, priorities set within the program did take into consideration the relative importance of the activity and its relationship to understanding safety issues, the risk significance of the issues, and cost-benefit. This will be especially important as new technologies are introduced or new safety issues are identified.

High-temperature Gas Cooled Technology

NRC's research infrastructure today primarily supports the licensing and regulation of LWRs. Although several areas were identified where the current infrastructure would need to be improved to address advanced light-water reactor (ALWR) technical and safety issues, most of the infrastructure gaps relate to high temperature gas-cooled reactors (HTGRs). Although HTGR infrastructure development has been largely scaled back as a result of the withdrawal of the PBMR from pre-application review, nevertheless, many of our HTGR infrastructure needs will require a long-term commitment to be ready for licensing applications. Development of codes and standards, evaluation of high temperature materials in their operating environment, radiation testing of reactor fuel, and thermal hydraulic code development, for example, involve activities that extend over many years. It is therefore essential that a long-term perspective in these areas be maintained. In the near-term, this involves awareness of international activities, and application of Phenomena Identification and Ranking Tables (PIRTs) to help identify and prioritize research needs. PIRTs help to focus resources on those tests and analysis that would contribute significantly to NRC's knowledge and understanding the relative safety significance, and the importance of the research to the development of policy recommendations.

Advanced Light Water Technology

During the Advanced Pressurized Water Reactor 600 (AP-600) review, and to a limited extent the Simplified Boiling-Water Reactor (SBWR) review, the staff gained valuable experience and insights regarding the performance of passive reactor components through an extensive program in the USA and overseas. Over the past several years the NRC consolidated and improved its thermal-hydraulic and severe accident codes, and these are ready to support the review of ALWRs. Notwithstanding, additional models and assessment will be needed for advanced designs, particularly the IRIS and ACR-700 designs. Somewhat less are the needs for ESBWR. It is envisioned that NRC's research infrastructure will continue to change to accommodate new design features and associated issues. The need to address technical and safety issues, and the tools, methods, data, and expertise that will be required to identify resolution pathways continue to be an important part of the planning process.

Planning Activities

To effectively identify key technical areas and safety issues, and the infrastructure needed to address these technical and safety issues, the staff used a top down approach, separating the work into strategic arenas: Nuclear Reactor Safety, Nuclear Materials Safety, Nuclear Waste Safety and Safeguards. Figure 1 depicts the top down process starting with the top goal of establishing an effective and efficient regulatory process to protect public health and safety, and ending at the lowest level being the identification of research items and activities. As shown, most of the research infrastructure is associated with the Reactor Safety arena, although work is evolving in support of other initiatives outside the Office of Nuclear Regulatory Research. A brief summary of research supporting the strategic arenas is provided below.

Nuclear Reactor Safety

Using our current framework to define research activities and products, technical disciplines and areas were linked to four components of safety: accident prevention, accident mitigation, barrier protection, and offsite protection. Using this approach, six key technical areas were identified under nuclear reactor safety and used to explore research infrastructure needs:

1. **Accident Analysis** – includes identification of accident scenarios and associated mitigation systems, structures, components, and human actions. The three technical disciplines that support this area include Probabilistic Risk Assessment (PRA), human factors, and advanced instrumentation and control (I&C). PRA models and techniques are used for both identifying significant accident scenarios and focusing the reactor systems analysis on areas that are risk important. Challenging research areas included addressing limitations in data and operating experience required for risk quantification of advanced designs. The impact of human performance and role of I&C within the context of accident analysis is also challenging as industry plans to capitalize on advancements in computer technology to reduce the need for operator involvement in plant operation and accident response.
2. **Reactor Systems Analysis** – Understanding plant performance over a wide variety of transient and accident conditions requires the reliance on validated analytic tools. The level of effort required to upgrade NRC analysis tools varies from a modest level of effort for some ALWRs, to a significant level of effort for HTGRs. Activities include thermal-fluid dynamics modeling, nuclear analysis, and severe accident and source term analysis. Challenging technical areas specific to HTGRs include analysis of helium-cooled, graphite-moderated reactors with multi-phase (helium with air and water ingress) fluid flow under convection, conduction, and radiative heat transfer conditions for irregular and complex geometries. Additionally, for both HTGRs and ALWRs, our knowledge and understanding of passive system performance over a wide spectrum of accident conditions will need to be confirmed using existing experimental facilities. Activities have been planned that expand our current infrastructure to address accident phenomena associated with advanced passive designs.

Advanced Reactor Research Infrastructure Key Research Areas and Areas for Examination

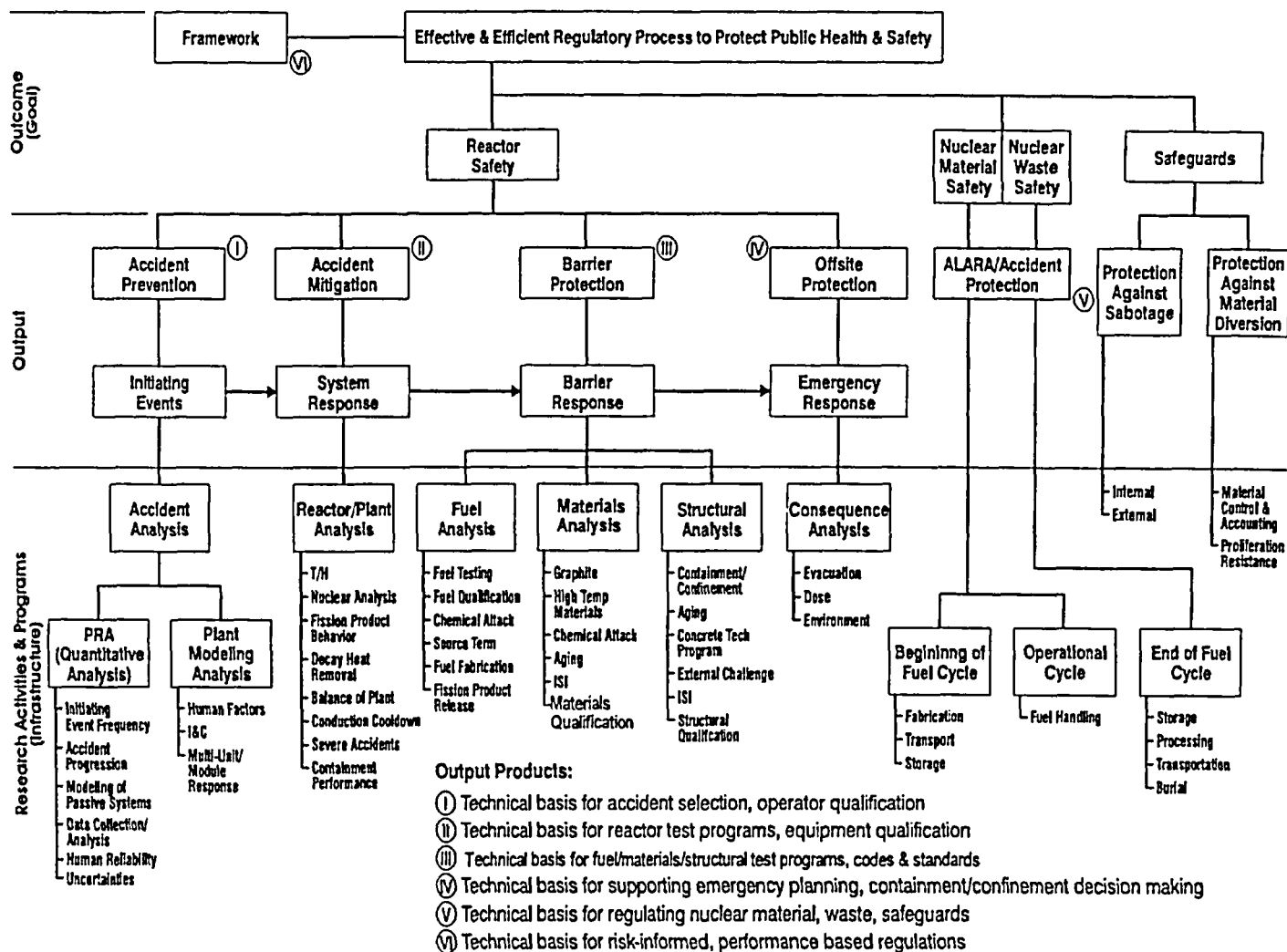


Figure 1 Key Research Areas for Examination

3. **Fuels Analysis** – Critical to the safety of HTGRs is the coated fuel particles which provide the principal safety barrier and primary containment function against fission product release. Due to the high cost of fuel testing within the U.S., NRC is seeking to enter into cooperative agreements with international organizations. Additionally, plans are being developed to implement cooperative agreements on development and validation of analytical tools for assessing fuel particle behavior and fission product release. These tools will aid NRC in understanding margins to failure and source terms. For ALWRs, extension of code capability to higher burnups (up to and beyond 75 gigawatt days per ton (Gwd/t)), and research into new cladding properties are both being planned.

4. **Materials Analysis – Understanding material integrity over a wide variety of environmental conditions requires reliable data and tools. Materials integrity of the pressure boundary and structural components will dictate the useful life expectancy of a plant. Research activities in this area primarily focus on metallic and graphite components under high temperature operating and accident conditions. Data will be generated or captured through cooperative agreements to address issues involving high temperature fatigue, creep, and creep-fatigue in HTGR coolant environments; thermal aging; sensitization of austenitic alloys; degradation by carburization, decarburization, and oxidation of metals. The information would be used to support inservice inspections, to calculate component probability of failure for PRAs, and address issues related to the performance and degradation of graphite under high irradiation levels. Work has begun on development of a consensus specification standard for nuclear grade graphite and for evaluating the engineering bases of the current engineering design codes for high temperature components. A high priority is being placed on national codes and standards for the design and fabrication of metallic and graphite components for service in high temperature and coolant impurity environments.**
5. **Structural Analysis – Historically, the NRC has been committed to the use of U.S. industry consensus standards for the structural analysis, design, construction, and licensing of commercial nuclear power facilities. For advanced designs, this knowledge base will be expanded to address new issues involving aging, degradation, and impact of external events on advanced designs. Areas of interest include seismic hazard assessment and the impact of seismic events on the reactor vessel and core support structures, and seismic soil-structure interaction analysis of deeply embedded structures. The staff is also seeking to understand the effects of high temperature on the properties of concrete and implication of modular construction on safety performance. Cooperative research efforts are being pursued that will capitalize on international experience.**
6. **Consequence Analysis – Understanding the risk to public health and safety requires the performance of off-site consequence analysis. The mix of radionuclides and the chemical forms of the releases from severe accidents occurring in advanced reactors will likely be different than releases from LWRs. The NRC MELCOR and MELCOR Accident Consequence Code System codes are considered suitable to assess the offsite consequences of a severe accident in LWRs. For HTGRs, additional data will be needed to assess these codes. Activities have been planned that would expand the use of these tools to address differences in advanced designs and their chemical forms.**

Many of the activities and associated infrastructure needs described above relate to non-LWR designs. Application of NRC's current infrastructure which is primarily based on LWR technology has generated a number of policy issues for non-LWRs. SECY-03-0047 [Policy Issues Related to Licensing Non-Light Water Reactor Designs] provided to the Commission on March 28, 2003 identified seven policy issues with options and recommended positions for resolution. On-going research to develop a technology-neutral framework for advanced designs will play a key role in resolution of many of these policy issues.

Nuclear Materials Safety

In the nuclear materials safety arena, the staff focused on differences between advanced reactors and current operating reactors. Areas where differences could play an important role include criticality safety, radionuclide inventories, decay heat, radiation sources, shielding, and detection. Most infrastructure needs center on improving nuclear data libraries, validating and modeling criticality conditions, crediting burnup, and predicting decay heat and radiation sources in spent fuel. A number of international cooperative opportunities are being pursued in this area.

Nuclear Waste Safety

Differences between advanced reactors and current generation plants in the nuclear waste arena primarily result from differences in long-lived radionuclide inventories and associated source term releases, waste forms (ceramic), higher fuel burnup and enrichment parameters, increased storage volumes of spent fuel and materials (e.g., graphite), and transportation of an increased amount of advanced reactor spent fuel. Most of the information generated in these areas will be used to support the development of regulatory criteria (e.g., regulations, regulatory guides, policy guidance, and standard review plan sections).

Summary

The nuclear industry has been exploring new and revolutionary reactor design concepts to simultaneously attain safety performance and economic improvement. Many of these designs involve innovative features that are not based on current light-water reactor (LWR) technology. To be prepared for design reviews, the staff performed an infrastructure assessment to identify gaps in expertise, analytic tools, methods, and facilities. On April 18, 2003, the assessment and associated research plans were transmitted to the Commission in SECY-03-0059, titled "NRC's Advanced Reactor Research Program." Cooperative agreements with other organizations play a key role in meeting the infrastructure needs. Research that supports design certification review schedules and the technical bases for regulatory decisions were given the highest priority. Activities that increase NRC's understanding of new phenomena and their impact on safety margins were also given a high priority.

Additionally, on March 28, 2003, the staff transmitted to the Commission SECY-03-0047, titled "Policy Issues Related to Licensing Non-Light-Water Reactor Designs." This paper contained recommendations on seven technical policy issues that resulted from pre-application reviews of non-LWRs. These seven issues relate to the need for an enhanced licensing approach to address key aspects of advanced reactor design and operation that differ substantially from the currently operating reactors. These recommendations are the first step in setting Commission direction and provide a basis for further work. Research activities that focus on improving NRC's advanced reactor infrastructure (described in SECY-03-0059) will play a key role in addressing the challenges that result from the seven policy issues.

DOE Advanced Nuclear Reactor Research: A Summary

James A. Lake, PhD & Richard R. Schultz, PE
Idaho National Engineering & Environmental Laboratory
Idaho Falls, ID 83415

ABSTRACT

The relationship between the Generation IV Program and the Advanced Fuel Cycle Initiative (AFCI) is described and the links between the Generation IV Program and the Nuclear Hydrogen Initiative are outlined. The Generation IV Program, and its high-level research and development (R&D) needs, are summarized and examples of DOE advanced reactor research are given in the areas of: analysis tools, modeling TRISO fuel irradiation performance, and obtaining more accurate cross-section data. Each of the six Generation IV systems has a unique set of technical challenges that stem from fuels, materials, power conversion, and system design & evaluation considerations. The AFCI and Generation IV programs are beginning to confront the interesting and challenging demands that must be overcome to meet the future energy needs of the United States.

INTRODUCTION

As reflected in the *National Energy Policy*, nuclear energy has a strong role in the future of the nation's energy security needs. Nuclear power presently produces approximately one-fifth of all U.S. electric power and is the only available technology that can economically produce large quantities of energy without emitting harmful pollutants, including those associated with global climate change. These desirable attributes give nuclear energy a cornerstone position, not only in the U.S. energy portfolio, but also in the world's energy portfolio. Consequently, on September 20, 2002 U.S. Energy Secretary Spencer Abraham announced that: "The United States and nine other countries have agreed to develop six Generation IV nuclear energy concepts.¹" The Department of Energy also noted: "...the systems are expected to 'represent significant advances in economics, safety, reliability, proliferation-resistance, and waste minimization.'"

Thus, the Generation IV systems² were specified to deliver outstanding: sustainability, economic competitiveness, safety & reliability, and proliferation resistance & physical protection (PRPP). These four attributes are fundamental to the overarching goals of the Generation IV Program and its necessary, ongoing, long-term R&D. Summary descriptions of these four attributes are:

- **Sustainability:** the requirement that resources must be conserved, the environment must be protected, the ability of future generations to meet their needs must not be impaired, and no unjustified burdens must be placed on them.
- **Economic competitiveness:** the ability to economically compete in an unregulated energy market.

¹ *Nuclear News*, November, 2002, pp. 20 to 26

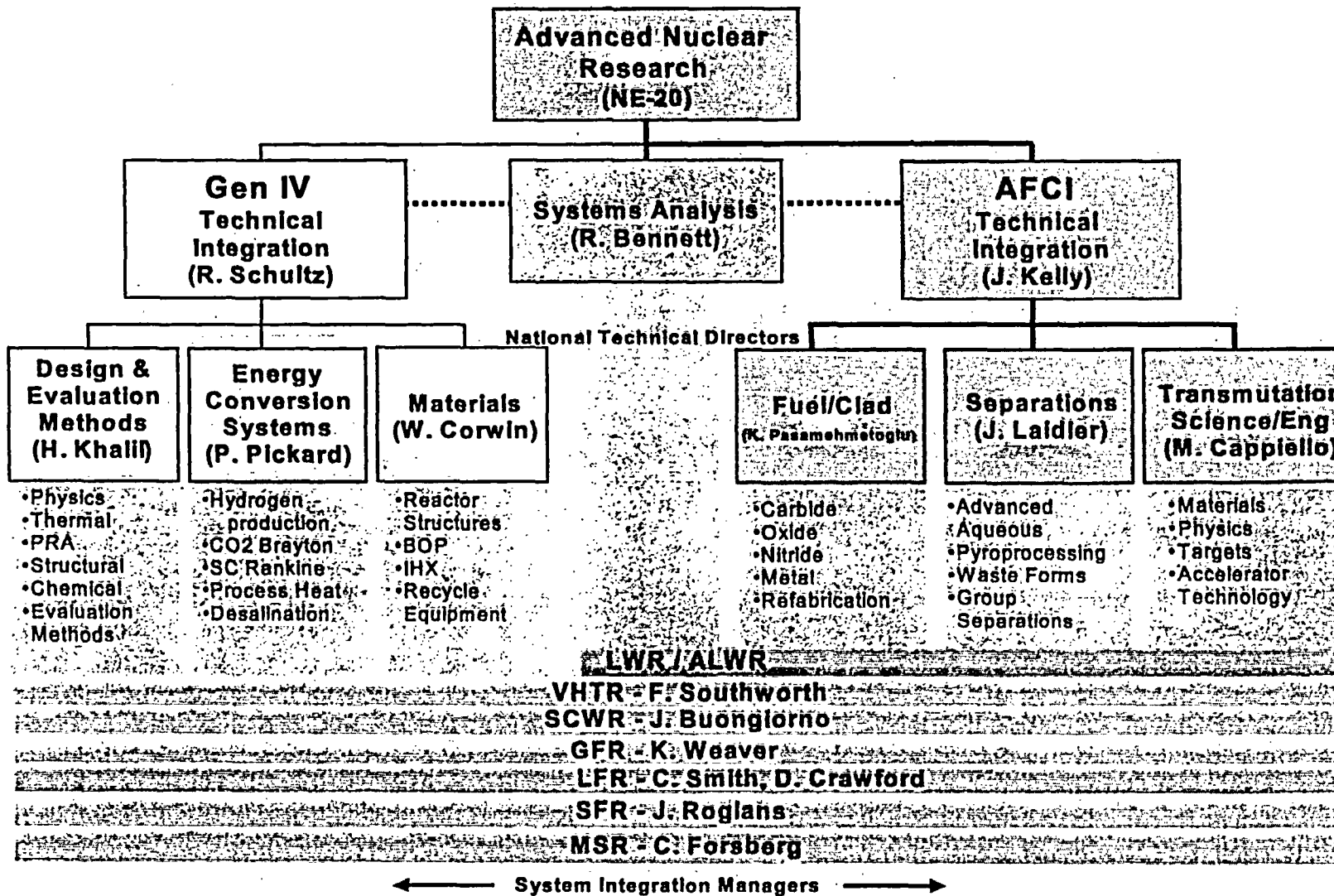
² Very high temperature reactor (VHTR—also called the Next Generation Nuclear Plant: NGNP); supercritical water reactor (SCWR); gas-cooled fast reactor (GFR); lead-cooled fast reactor (LFR); sodium-cooled fast reactor (SFR), and molten salt reactor (MSR).

- **Safety & reliability:** the requirement that safety margins are adequate at all times, accidents are prevented, and off-normal conditions do not deteriorate into severe accidents. Hence, the Generation IV systems will rely chiefly on passive safety systems—which are driven by natural forces.
- **Proliferation resistance & physical protection:** design specifications that meet the requirements of the Nuclear Nonproliferation Treaty from the time the raw material is mined to when it is fabricated, used in the advanced system, and finally recycled and sent for disposal. Although this standard is true for on-line systems, the Generation IV systems will impose this requirement by making the fuel configuration/process more difficult to harvest for non-peaceful use, e.g., by using more proliferation-resistant fuel materials.

Because fundamental ingredients in the successful implementation of the Generation IV Nuclear Energy Systems Program stem from a complementary advanced, full-featured nuclear fuel-cycle, the Advanced Fuel Cycle Initiative (AFCI) includes the wherewithal to (a) reduce the spent fuel volume, (b) separate long-lived, highly toxic elements, i.e., actinides such as plutonium and americium, from the remainder of the spent fuel residual, and (c) reclaim the spent fuel's valuable energy. The AFCI and the Generation IV Nuclear Energy Systems Program are sister efforts (see Figure 1 for organizational structure) that form the backbone of the U.S. national nuclear energy policy implementation. The complementary nature of the two efforts is illustrated in Table 1 with respect to the four key attributes of the advanced nuclear systems. The Generation IV effort makes use of abundant fuels (sustainability) and relies on innovative engineering designs to meet the goals in the other three areas. The AFCI supports the Generation IV effort by providing the means to recover additional energy from spent fuel and by focusing on the means to reduce both the cost and the need for additional waste repositories (sustainability).

Table 1. Complementary Nature of AFCI & Generation IV Goals

Focus Areas	Generation IV	AFCI
Sustainability	Ensure adequate fuel resources and reserves are available for many years.	Recover energy value from commercial spent nuclear fuel; hence this effort translates to converting spent nuclear fuel to a fuel reserve for operational Generation IV systems.
PRPP	Ensure fuels are exceptionally proliferation resistant.	<ol style="list-style-type: none"> 1. Reduce the inventories of civilian plutonium in the U.S.—thus reducing quantity of material available for destructive purposes. 2. Reduces the toxicity of high-level nuclear waste bound for geologic disposal—thus reducing usefulness of waste for harmful purposes.
Economic Competitiveness	Make systems economically competitive with all energy alternatives.	<ol style="list-style-type: none"> 1. Reduces the cost of geologic disposal of commercial spent nuclear fuel. 2. Enables more effective use of the currently proposed geologic repository so that it will serve the needs of the U.S. for the next century.
Safety & reliability	Rely on passive safety systems and generally simpler, more reliable technology than Generation III plants.	Reduces the toxicity and lifetime of high-level nuclear waste bound for geologic disposal—thus reducing the probability of public exposure under accident conditions.



US Universities and Industry

Generation IV International Forum

Figure 1. Organizational Chart: Generation IV Program and Advanced Fuel Cycle Initiative (AFCI)

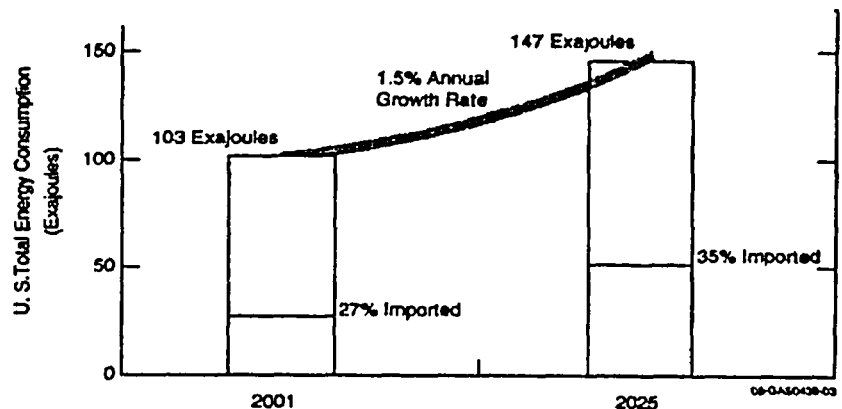
Implementation of the Generation IV Nuclear Energy Systems Program and the AFCI is underway. The programs are based on (1) the long-term outlook for nuclear energy in the United States, (2) the advice of the Nuclear Energy Research Advisory Committee during the two-year development of the Generation IV Technology Roadmap, and (3) the need for the Generation IV Program to be integrated with other nuclear energy programs of the Department. The organizations of both the AFCI and the Generation IV Program are shown in Figure 1. Both programs are governed by the U.S. Department of Energy and include a cooperative effort between six national laboratories: Argonne National Laboratory (ANL), Idaho National Engineering & Environmental Laboratory (INEEL), Lawrence Livermore National Laboratory (LLNL), Los Alamos National Laboratory (LANL), Oak Ridge National Laboratory (ORNL), and the Sandia National Laboratory (SNL).

HISTORICAL CONTEXT

From the early beginnings of nuclear energy in the 1940s to the present, the United States has led the development of three generations of nuclear energy. The first three generations of nuclear energy have been successful in the following ways: (a) Nuclear energy supplies a significant share of electricity for today's needs—over 20% of U.S. and 16% of world demand. (b) Nuclear energy plays a large role in the U.S. economy. In 2002, the 103 operating U.S. nuclear power plants generated 790 billion kilowatt-hours of electricity, valued at \$50 billion. (c) Through the use of nuclear energy, the United States has avoided over three billion tons of air emissions since 1970. (d) U.S. nuclear plants are highly reliable and in 2001 produced electricity for 1.68 cents per kilowatt-hour on average. This low cost is second only to hydroelectric power among baseload generation options. (e) In return for access to peaceful nuclear technology, over 180 countries have signed the Non-Proliferation Treaty to help ensure that peaceful nuclear activities will not be diverted to making nuclear weapons.

Although nearly all U.S. light water reactors are expected to file for 20-year license extensions it is clear that additional nuclear energy systems are needed—based on the U.S. 1.5% annual growth rate (see Figure 2). In order to meet 21st century energy needs, advanced nuclear systems must meet the Generation IV safety, economics, waste, and proliferation resistance goals via a robust research, development, and demonstration program. Advances in all of these areas can contribute to increasing the long-term sustainability of nuclear energy.

The outlook for energy demand in the United States underscores the need to increase the share of nuclear energy production. The *2003 Annual Energy Outlook* projects an annual growth rate of 1.5% in total energy consumption to the year 2025 (see Figure 2). At the same time, domestic energy production will grow only 0.9% per year, creating a widening gap to be filled by energy imports. Further, most of the projected domestic energy



Source: 2003 Annual Energy Outlook

Figure 2. Growing U.S. Energy Demand & Imports

production increase is assumed to be provided by coal and natural gas. Thus, the outlook implies an increasing burden from carbon emissions with the potential for long-term consequences from global climate change, as well as an increasing dependence on foreign energy sources. There is therefore a strong energy security as well as environmental quality motivation for seeking to increase the share of nuclear-generated electricity above its current 20% level.

The outlook for energy demand within the transportation sector of energy use also provides an opportunity for nuclear energy in hydrogen production. *Energy Outlook* projects an annual growth of 2.0% per year for the transportation sector (see Figure 3), while the electricity and heating sectors will grow at 1.4% and 1.2%, respectively.

Transportation is almost exclusively dependent on petroleum. Fluctuations in fuel prices of 30% has caused several 'energy shocks' since the 1970s. This volatility creates a significant need for diversifying the transportation energy sector with new fuels, such as hydrogen for use in emissions-free fuel cells that power electric vehicles. In early 2003 President Bush announced initiatives to develop hydrogen-powered cars and clean fuel sources. Large-scale production of hydrogen by nuclear energy would be free of greenhouse gas emissions. To achieve these benefits, new nuclear energy systems that are capable of hydrogen production at competitive prices need to be developed.

Thus, two long-term technology development objectives for nuclear energy in the U.S. are derived from the needs identified above: (1) Develop advanced nuclear energy systems that can address the barriers to growth and significantly increase the share of nuclear electric generation while increasing their sustainability in the long term, and (2) Develop systems for nuclear-assisted hydrogen production that can diversify the energy supply for the transportation sector and reduce the dependence on petroleum.

Beginning in January 2000, ten countries joined together to form the Generation IV International Forum (GIF³) to develop future-generation nuclear energy systems that can be licensed, constructed, and operated to provide competitively priced and reliable energy products while satisfactorily addressing nuclear safety, waste, proliferation, and public perception concerns. The overarching objective for these new nuclear energy systems—known as Generation IV—is to have them available for international deployment between 2015 and 2030.

THE ROADMAP

From its beginning, the GIF discussed the R&D necessary to support next-generation nuclear energy systems. From those discussions a technology roadmap to guide the Generation IV effort

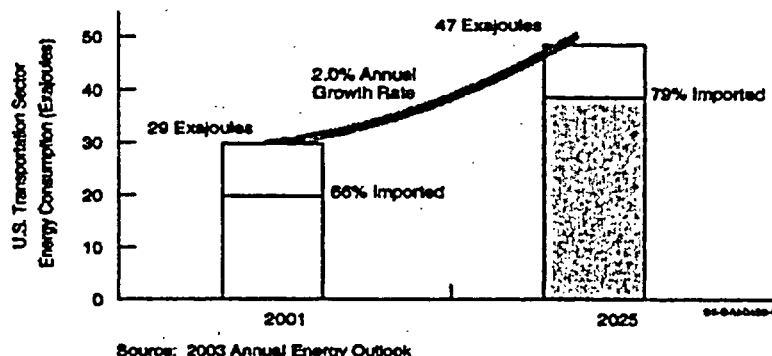


Figure 3. Growing U.S. Transportation Sector Energy Demand & Imports

³ Argentina, Brazil, Canada, Euratom, France, Japan, the Republic of Korea, the Republic of South Africa, Switzerland, the United Kingdom, and the United States currently constitute the GIF. New members can be added by a process outlined in the GIF charter.

began and was completed in two years with the participation of over 100 experts from the GIF countries. The effort ended in December 2002 with issue of the final Generation IV Technology Roadmap.⁴

The roadmap evaluated over 100 future systems proposed by researchers around the world. The scope of the R&D described in the roadmap covers the six most promising Generation IV systems. It is important to note that each GIF country will focus on those systems and the subset of R&D activities that are of greatest interest to them. Thus, the roadmap provides a foundation for formulating national and international program plans on which the GIF countries will collaborate to advance Generation IV systems.

The roadmap identified six most promising systems. Two employ a thermal neutron spectrum with coolants and temperatures that enable electricity production with high efficiency (the Supercritical Water Reactor—SCWR and the Very High Temperature Reactor—VHTR⁵). Three employ a fast neutron spectrum to enable more effective management of nuclear materials through recycling of most components in the discharged fuel (the Gas-cooled Fast Reactor—GFR, the Lead-cooled Fast Reactor—LFR, and the Sodium-cooled Fast Reactor—SFR). The Molten Salt Reactor (MSR) employs a circulating liquid fuel mixture that offers considerable flexibility for recycling nuclear materials.

PRIORITIES FOR THE GENERATION IV PROGRAM

For each of the six systems above, the roadmap develops the R&D needs in considerable detail and highlights the major R&D issues, benefits, and risks. The specific R&D issues and risks, identified in the roadmap and also identified by the NERAC Subcommittee on Generation IV Technology R&D Planning, had a strong bearing on the prioritization of the systems versus the U.S. needs and technology objectives discussed above. From these studies and interactions, the following two U.S. principal priorities emerged (as identified in the Implementation Plan⁶):

Priority 1: *Develop a Next Generation Nuclear Plant (NGNP) to achieve economically competitive energy products, including electricity and hydrogen production in the mid-term.*

The NGNP is presently based on the Generation IV Very High Temperature Reactor (VHTR) design, i.e., a prismatic- or pebble-bed, high-temperature gas-cooled reactor that is able to economically produce hydrogen and electricity. The high priority on developing a capability for nuclear-assisted hydrogen production with the NGNP reflects the excellent potential for this system to provide a major competitive advance toward the long-standing need to diversify the energy supply of the U.S. transportation sector, and to do this in a manner that is essentially emissions-free. Successful development and demonstration of an economically competitive, emissions-free nuclear-assisted hydrogen supply will be the focus of a government-laboratory-industry-international collaboration to design, develop, construct and operate a NGNP by 2016

⁴ "A Technology Roadmap for Generation IV Nuclear Energy Systems," Generation IV International Forum, GIF-002-00, December 2002, available at <http://www.inel.gov/initiatives/generation.shtml>, accessed February 2003.

⁵ The VHTR concept, when used to power a hydrogen production plant, is presently being promoted as the Next Generation Nuclear Plant (NGNP).

⁶ "The U.S. Generation IV Implementation Strategy," *U.S. Department of Energy*, September, 2003, available at <http://nuclear.gov/geniv/gen-ivstrategy.html>, accessed January 2004.

that is dedicated to hydrogen and high efficiency electricity production research and demonstration.

The NGNP program is projected to complete its key R&D by about 2012. This is partially enabled by many prior developments in high-temperature gas-cooled reactors internationally. As a result, completion and startup of a demonstration NGNP is targeted for 2016. The startup test program will include an extensive integral system safety test and demonstration phase that will form part of the safety basis for future U. S. Nuclear Regulatory Commission commercial licensing. The development of a NGNP would have a number of associated benefits including the establishment of a technical basis for development of a fast-spectrum gas reactor as discussed in the next section.

Priority 2: Develop a fast reactor to achieve significant advances in sustainability for the long term.

The priority on fast reactors reflects their excellent potential to make significant gains in reducing the volume and radiotoxicity, and increasing the manageability of spent nuclear fuel. With a successful fast reactor program, the U.S. may be able to avoid the need for a second domestic geological repository for many decades. Fast reactors also hold the potential for extending the useful energy yield of the world's finite uranium supply many-fold, if needed in the very long term.

The chief issues in the development of a next-generation fast-spectrum reactor for use in the United States are its economic competitiveness and management of the overall risks to workers and the public from the deployment of a closed fuel cycle. The most promising fast-spectrum Generation IV systems are the Gas Fast Reactor (GFR), the Lead Fast Reactor (LFR), and the Sodium Fast Reactor (SFR). Among these, the initial priority is that the LFR and GFR will be given the most emphasis in order to resolve technical issues and uncertainties, since these reactors offer strong potential benefits that have not been fully demonstrated. The SFR is already at a fairly advanced state of development, with many of its technologies having been demonstrated internationally. All of these systems should be brought to a state where a down selection can be undertaken based on demonstrated performance of their economics, safety and reliability, sustainability, and proliferation resistance and physical protection. The Generation IV Program gives major emphasis to advancing the LFR and GFR, as well as efforts to monitor the progress of the SFR internationally.

Advancing All of the Generation IV Systems: The priorities identified in the Implementation Plan specify the direction of the major thrusts in the Generation IV program. However, the program also addresses those systems not in the forefront of U.S. development, but which have significant international interest in their potential. The roadmap identified six most promising systems, four of which are mentioned above. The additional two are the Supercritical-Water-Cooled Reactor⁷ (SCWR) and the Molten Salt Reactor (MSR). The SCWR employs water above the critical temperature and pressure that affords a considerable increase in thermal efficiency as well as major simplifications and savings in the balance of plant. The MSR employs a circulating liquid fuel mixture that offers considerable flexibility for recycling actinides, and may provide a favorable alternative to accelerator-driven systems. The Generation IV Program includes significant international collaborative efforts on the SCWR, and exploratory collaborations on the MSR.

⁷ The high thermal efficiency of the SCWR makes it a candidate to generate economically-competitive electricity—a U.S. priority 1 objective.

TIMEFRAMES FOR THE GENERATION IV SYSTEMS

Proposed timelines for the two priorities are shown in Figure 4. For the development of a NGNP in Priority 1, a 15-year timeline is to be implemented. This balances the benefit of demonstrating a large-scale economically competitive nuclear hydrogen system with the technical issues and risks establishing an aggressive schedule for its development. Key R&D will require about 5 years, followed by a 10-year demonstration phase. For the development of a fast-spectrum reactor in Priority 2, a 20–25-year timeline is to be implemented. This fits with the expected future need for radiotoxicity reduction and closure of the U.S. nuclear fuel cycle, and allows the progression of several most promising candidates to a downselection in about a decade, followed by a demonstration of all elements of a closed fuel cycle within about a decade thereafter.

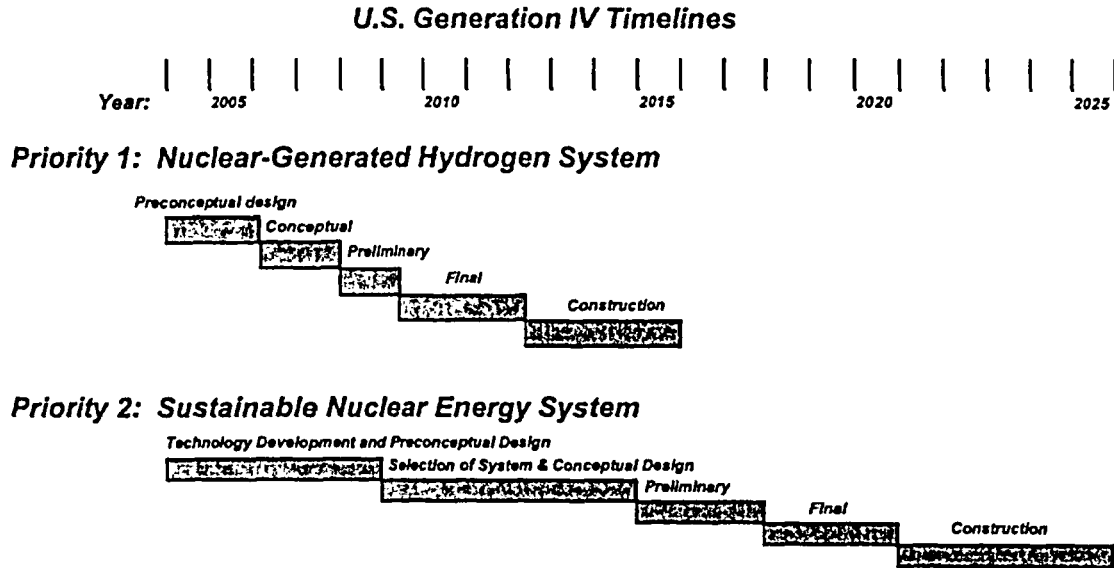


Figure 4. Timelines for U.S. Priority 1 & 2 Systems

A key benefit of the GIF is the members' desire to collaborate on R&D, greatly reducing the resources needed by any individual country. While the GIF is now working to develop the project teams and implementing arrangements that will undertake and govern the R&D collaborations, the details of their expected resource needs are not well developed.

During the roadmap process, the working groups prepared draft conceptual estimates of total R&D resources. These were based on expert judgment, and not detailed cost analysis. Assumptions were made about the systems having relatively successful advances without contingency for setbacks or changes in approach. The research programs were estimated to require 15–20-year timelines that included both viability and performance phase R&D. Following these two phases, given the successful resolution of all issues, a system could enter a demonstration phase. This was estimated to generally require six or more years with funding for licensing, construction, and startup of the demonstration system. Commercialization would follow the successful demonstration.

RESEARCH & DEVELOPMENT: ADVANCED REACTOR SYSTEMS

The R&D requirements, to enable DOE's advanced nuclear energy programs to achieve their objectives, are summarized in Table 2⁸ as a function of the systems aimed at achieving priorities 1 and 2 and major R&D requirement areas. Thus the NGNP and the SCWR have been grouped together as the candidate systems aimed at satisfying priority 1 and the GFR and LFR have been grouped together as the candidate systems aimed at achieving the priority 2 goals. The SFR has been left off the chart since its R&D needs are better understood as a result of U.S. and international experience.

NGNP & SCWR: Fuels for the SCWR do not require extensive R&D. Hence the focus, for thermal reactor fuels, is on the NGNP where it has been shown that NGNP fuels, fabricated in the United States, have been inferior in quality and presently are not commercial-grade. Further discussion of this point is given in the examples discussed in more detail below. Since the U.S. has not fabricated a TRISO fuel with adequate quality for the NGNP, one of the first priorities is to demonstrate a quality fuel fabrication process and quality-assurance approach for manufacturing the NGNP fuel. In addition, because the TRISO fuel will be irradiated over its lifetime, it is important to both demonstrate the fuel's ability to perform in such an environment and also to develop the capability to confidently model the effect of irradiation on the fuel for all conditions. Finally, the waste repository needs must be determined. Materials research will focus on performing confirmatory demonstrations⁹ showing the vessel, vessel internals, insulation, and all reactor components are capable of withstanding the high-temperature operational conditions. An intermediate heat exchanger (IHX) capable of operation at 1000 °C must be developed and demonstrated as capable of long-term, reliable operation for hydrogen production.

The capability to efficiently utilize the energy in the NGNP high temperature exhaust stream to produce hydrogen must be demonstrated. A major part of this research area (energy conversion) also includes the demonstration of a thermally-efficient heat exchanger design—since the heat exchanger will be used to transfer the energy necessary to the hydrogen production plant from the gas-cooled reactor system.

Finally, the analytical tools required to show the NGNP and the SCWR are capable of efficient and safe operation under all conditions must be validated, developed further if necessary, and approved for performing licensing calculations. The process for validating and gaining approval for the analytical tools may require the design and conduct of a number of experiments to provide data at conditions representative of the NGNP and SCWR. This area of research, termed "system design & evaluation," will also require the rigorous definition of correlations for gas flow in the transition region and for supercritical water at various heat transfer conditions—both operational and off-normal. Once a preliminary validation of the analytical tools has been accomplished, the tools can be used to select the reference design, i.e., nominally either a prismatic or pebble-bed gas-cooled design. Following selection of the reference design, both design and licensing calculations can be performed for the most likely reactor design configuration once the final validation is completed successfully and the passive safety system performance can be both demonstrated and studied. In addition to developing plant behavior modeling capability, it is also essential to develop an economics-modeling capability to enable reliable cost projections to be made.

⁸ Examples of ongoing research are given for the topics in red font.

⁹ NGNP only for vessel, control rods, and intermediate heat exchanger.

Table 2. Correlation between Crosscut R&D & Systems Needs

	Fuels	Materials	Energy Conversion	System Design & Evaluation
NGNP & SCWR	<ul style="list-style-type: none"> • Demonstrate fuel fabrication processes & QA approach • Demonstrate & model fuel irradiation performance • Identify waste repository needs 	<ul style="list-style-type: none"> • Confirm materials adequate for high temps in vessel, internals, insulation, control rods, etc. • Develop & demonstrate high temperature heat exchanger materials 	<ul style="list-style-type: none"> • Identify & demonstrate most efficient means to produce H₂ • Demonstrate thermally-efficient intermediate heat exchanger (IHX) 	<ul style="list-style-type: none"> • Develop & verify analysis methods, data, & codes • Perform analysis & trade studies to select reference design (prismatic or pebble-bed) • Demonstrate passive safety performance operability • Confirm economic viability
GFR & LFR	<ul style="list-style-type: none"> • Confirm fuel fabrication techniques • Demonstrate fuel irradiation performance • Develop capability to fabricate carbide & nitride fuels • Demonstrate fuel & matrix material recyclability 	<ul style="list-style-type: none"> • Demonstrate materials compatible with operational conditions • Demonstrate materials operational in corrosive environment 	<ul style="list-style-type: none"> • Investigate H₂ production cycles • Perform confirmatory demonstration of Brayton cycle • Develop IHX technology • Develop and demonstrate balance-of-plant 	<ul style="list-style-type: none"> • Develop & verify analysis capability • Optimize safety systems & confirm reactivity control and transient behavior • Develop correlations and properties for working fluid • Demonstrate passive safety performance capability • Reduce uncertainty of heat transfer & fluid flow regimes • Define deployment strategy & economic models

* NGNP specific ** GFR specific *** LFR specific

GFR & LFR: In general terms, the R&D requirements for the GFR and LFR are similar to the NGNP and SCWR. For example, although the fuel configuration will be different for these systems, all of the systems must have demonstrated capability for producing the necessary fuels that are peculiar to the advanced system under consideration. Consequently, only special requirements specific to the GFR and LFR will be mentioned in these paragraphs with respect to fuel, materials, energy conversion, and system design & evaluation.

The GFR designs will require development of the capability to fabricate both carbide and nitride fuels. In addition, the recyclability potential for both the fuel and the matrix material must be demonstrated.

Materials compatible with corrosive working fluids such as supercritical CO₂ (an alternate coolant under consideration for the GFR) and lead-based working fluids (for the LFR) must be identified and demonstrated.

Energy conversion for the GFR and LFR will likely be accomplished using the Brayton cycle. Consequently it is important to demonstrate the use of Brayton cycle components with both fast-reactor designs. Development and demonstration of the balance-of-plant components for both systems are also required. Finally, the feasibility of producing hydrogen using the LFR will be investigated.

Systems design & evaluation needs for the GFR and LFR are similar to the NGNP and SCWR. However, with respect to the LFR, since it will likely be a small modular design, intended in part for deployment in remote regions, a deployment strategy must be developed.

To illustrate some of the unique R&D requirements for the advanced reactor systems, several examples are given in the subsequent paragraphs.

ONGOING RESEARCH & DEVELOPMENT

A summary of R&D aimed at:

1. Developing the calculational capability to select the proper reference designs, characterize the design performance, and ultimately license the selected designs,
2. Modeling TRISO fuel irradiation performance, and
3. Obtaining improved and/or missing cross-section data for minor actinides that may be present in large quantities in reactor cores

is given in the following three examples.

Analytical Tool Development and Validation: One of the characteristics of the NGNP, GFR, and LFR advanced reactor systems is the working fluid remains single-phase for the great majority of the transients and also at steady-state conditions. Hence computation fluid dynamics (CFD) codes will be used extensively to analyze these systems. Even the SCWR, which will revert to two-phase conditions when accident transients are underway has many opportunities to use CFD codes to analyze transients of interest.

Typical phenomena and regions that will require analysis in an advanced VHTR are shown in Figure 5 for one possible variant of the NGNP. Figure 6 shows an illustration that indicates a

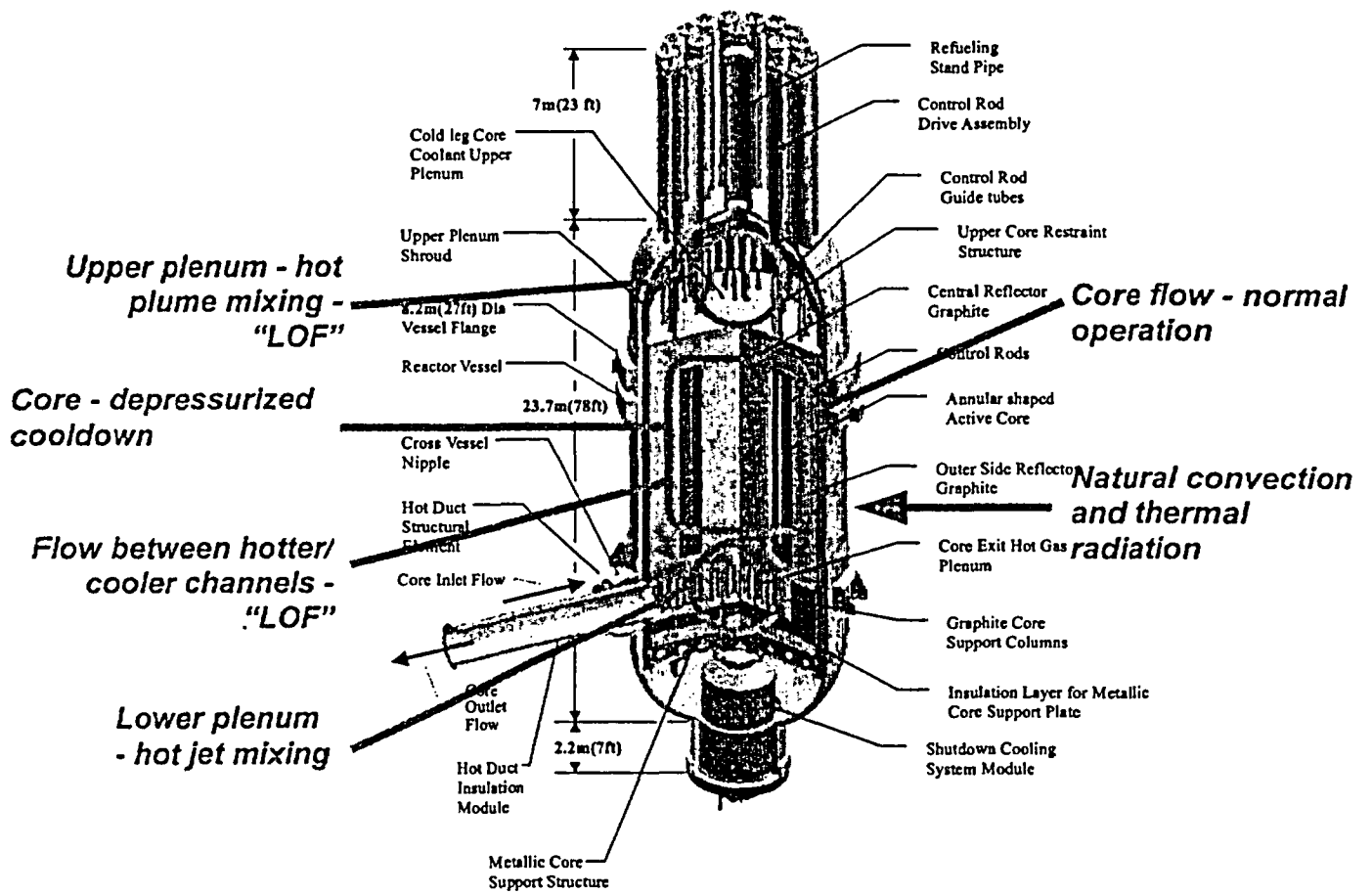


Figure 5. Typical regions that will require analysis in advanced VHTR

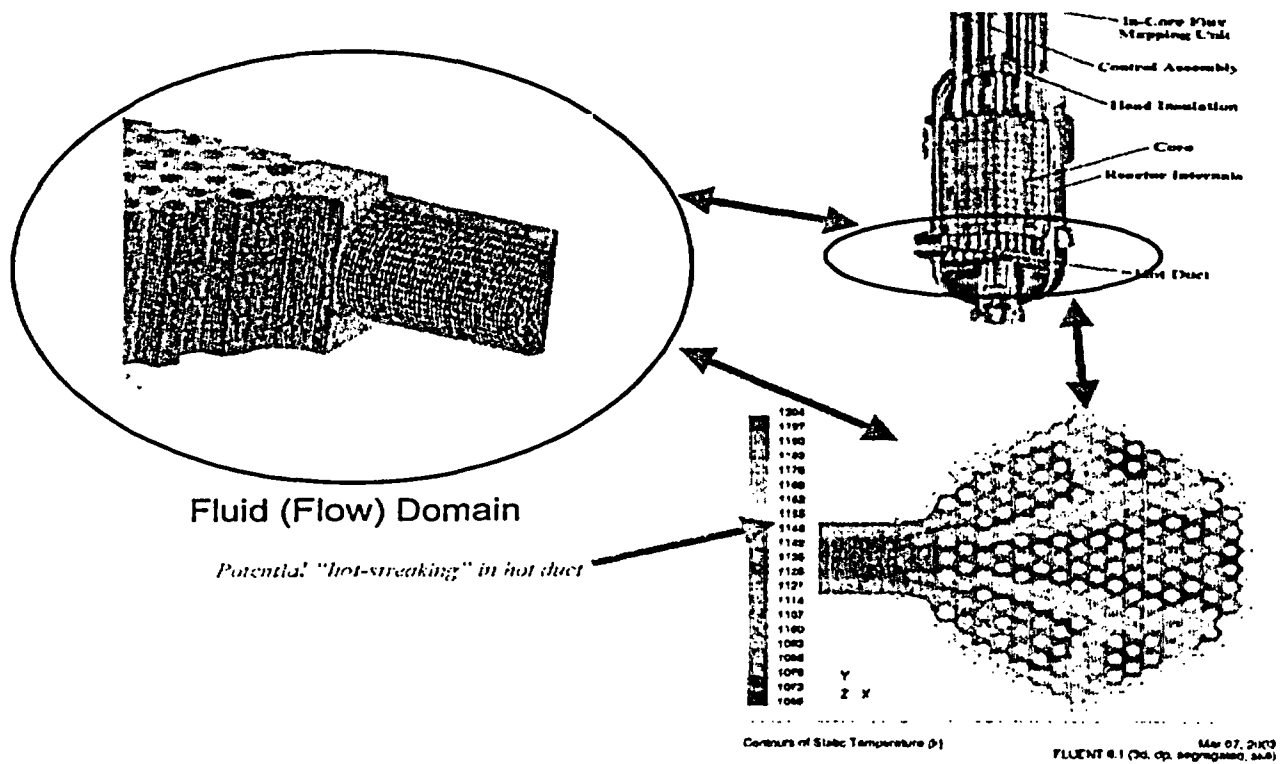


Figure 6. Advanced high temperature gas reactor analysis (preliminary) of lower plenum temperature distribution—to study “hot-streaking”

way in which CFD codes will be used to analyze the advanced reactors. The preliminary analysis, produced in a collaborative effort between the Fluent Corporation, General Atomics Corporation, and INEEL shows the hot gas temperature profile in a horizontal plane in the lower plenum of the GT-MHR. The calculation was performed for two reasons: (i) to examine the temperature variation to obtain a preliminary look at the peak temperatures that might pass through the reactor hot duct and thus impinge on the turbine blades in the GT-MHR power conversion unit and (ii) to perform a benchmark study to validate a new analysis tool which is under development for the advanced reactor system design studies. The new tool, shown in Figure 7, enables a one-dimensional model of the balance-of-plant to be coupled to a three-dimensional model of a component using the Fluent CFD code (Schultz & Weaver 2003).

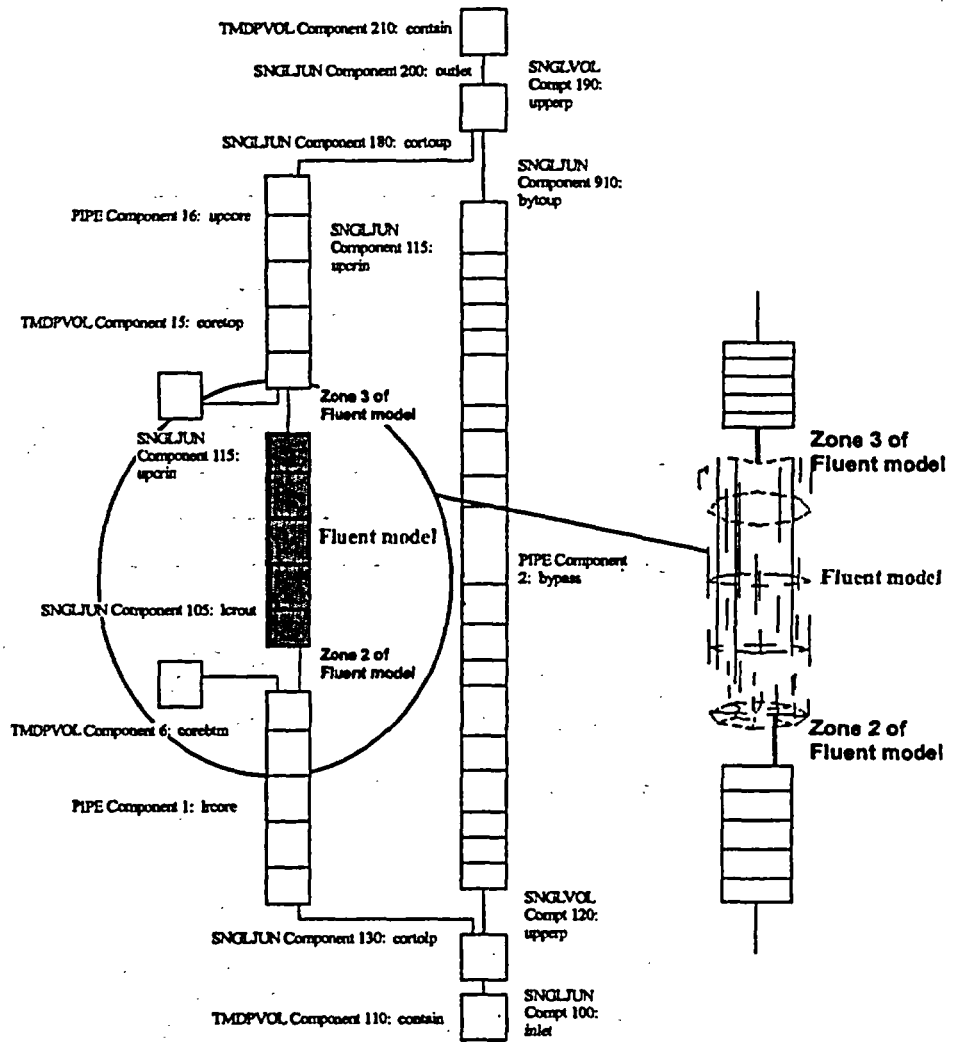


Figure 7. Coupled systems analysis and computational fluid dynamics (CFD) software—to enable analysis of complete advanced systems

Modeling TRISO fuel irradiation performance: An effort is underway to develop a mechanistic state-of-the-art fuel performance model that will enable researchers to model relevant failure mechanisms observed in coated particle fuel, to explain past poor performance of U.S. coated particle fuel, and to provide a better linkage between fuel performance and fuel product and process specifications used to manufacture the fuel. This effort stems from the historically, poor performance of TRISO fuel produced in the U.S. versus that produced in Germany. The contrast between the two is shown in Figure 8 where the release/born ratio of Kr-85m at fuel end-of-life (EOL) for the German fuel is over two orders of magnitude lower than the U.S. fuels. This parameter, indicative of the degree of fuel failures, is a primary indicator that not only must U.S. fuel fabrication techniques be improved, but also that U.S. fuel modeling capabilities must be improved to enable us to accurately calculate the fuel quality levels and lifetime behavioral characteristics.

The TRISO fuel configuration, shown in Figure 9, accumulates fission products within the coated-kernel volume. If the outer wall remains intact then the fissions products are isolated from the environment and thus are not of concern for potential release to the environment during normal operations or accident conditions. Failure of the outer pyro-carbon layer appears to be related to the coating rates used to fabricate the U.S. and the German fuels. The German fuels,

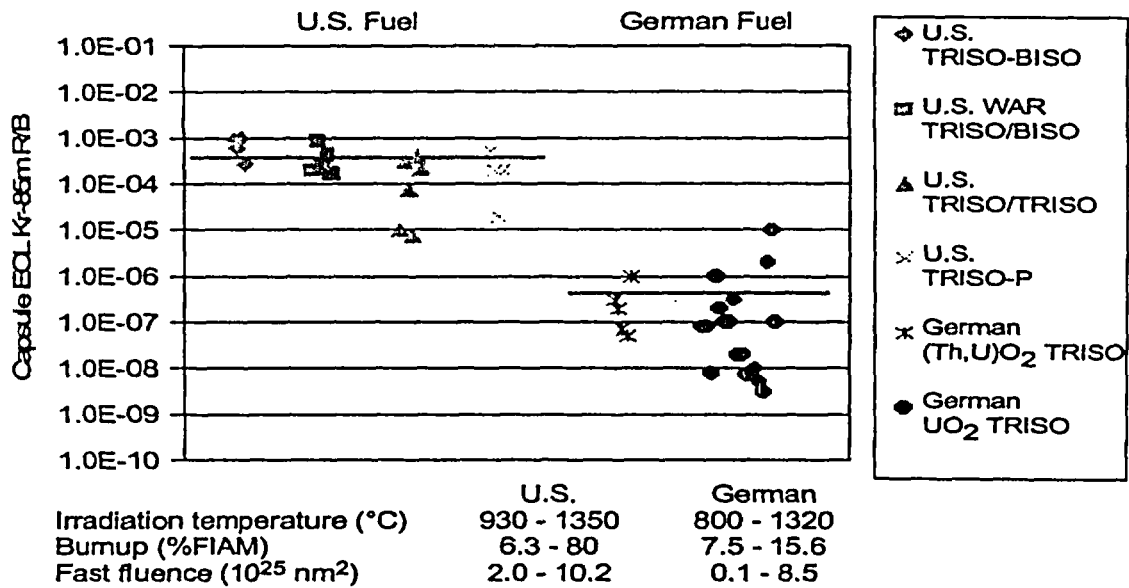


Figure 8. Comparison of German and U.S. end-of-life gas release measurements for numerous irradiation capsules: why additional fuel work is required

made using rapid coating rates (see Figure 10) have low anisotropy while the U.S. fuels were made using low coating rate and have high anisotropy and thus are more susceptible to cracking. These findings, documented in Petti, et al 2003, require further study, research, and especially demonstration. Successful completion of a detailed computational model will enable researchers to couple the TRISO fuel fabrication parameters to fuel irradiation and accident performance for the NGNP.

Confirmation of successful design and fabrication procedures will be achieved by conducting irradiation experiments in the Advanced Test Reactor (see Figure 11).

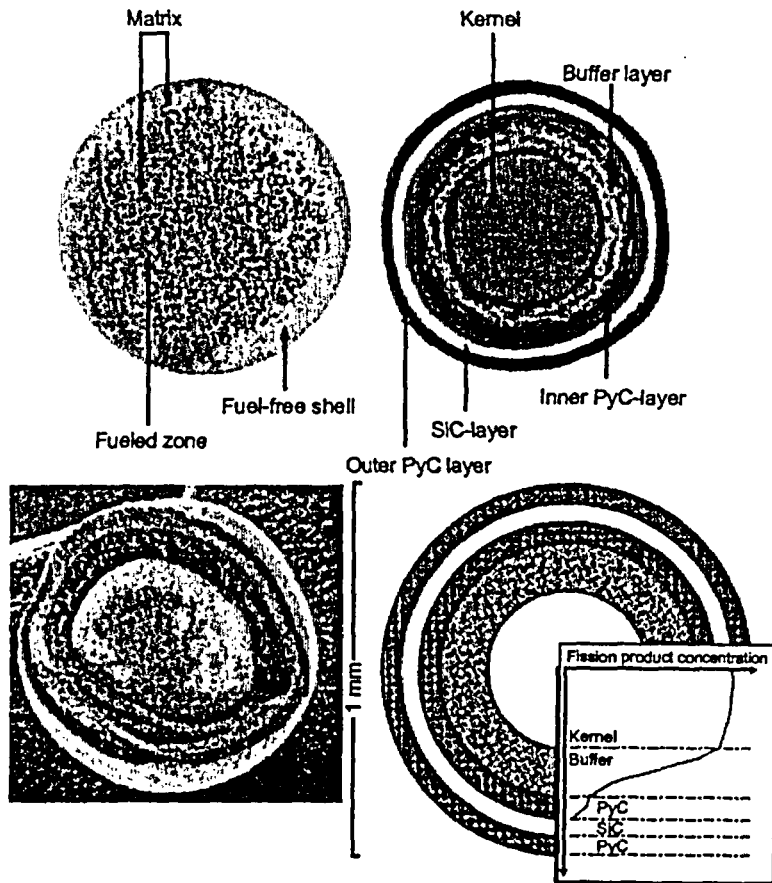


Figure 9. TRISO fuel geometry and typical fission product concentration

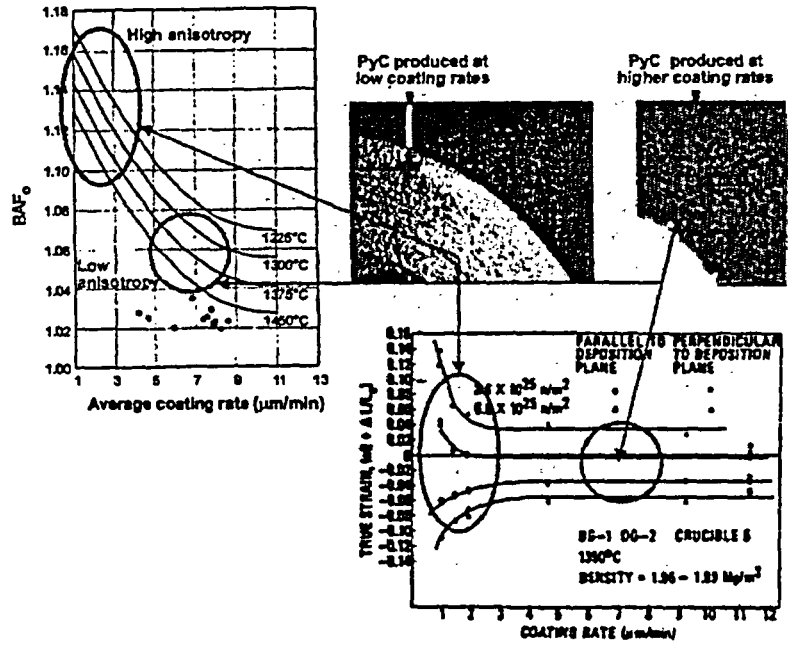


Figure 10. Impact of fabrication differences on irradiation performance

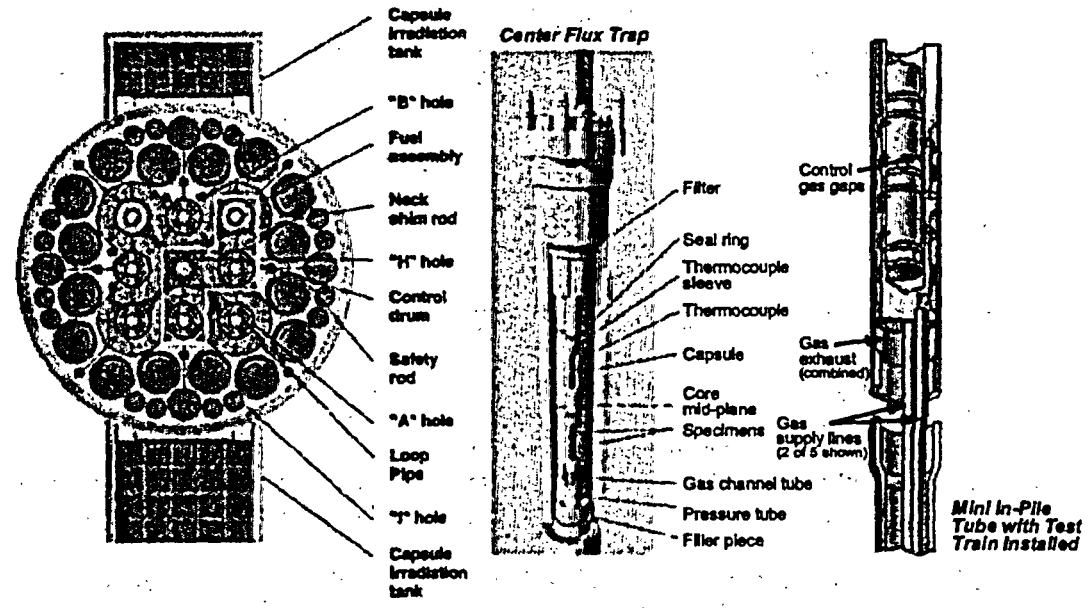


Figure 11. Advanced Test Reactor material irradiation configuration

Expansion & Validation of Nuclear Cross-section Data for Actinides: Nuclear data measurements are needed for high-burnup cores and advanced nuclear systems with recycled fuels when minor actinides become major constituents. Cross-section uncertainties and gaps in the measured data (see Figure 12—from Brown, et al, 1970; Hoffmann, et al, 1976; and Plattard, et al, 1975—note large variation in measured data at ~100 eV energy levels in the cross-section data and the lack of data at energy levels less than 25 eV for ^{237}Np) are presently too large for many of the minor actinides. These data uncertainties result in large uncertainties in calculated core physics performance (e.g., criticality, burn-up reactivity...) and safety parameters (reactivity feedback coefficients, control system worth...). Hence major improvements in the nuclides beyond ^{235}U , ^{238}U , and ^{239}Pu are essential to the design and safety of Generation IV systems. The example given in Figure 12, for ^{237}Np , shows the measured data are not always consistent and large uncertainties exist even for the critical mass (e.g., for ^{237}Np the critical mass is: 60 ± 20 kg, that is, 1000 times the uncertainty of ^{235}U -fueled systems).

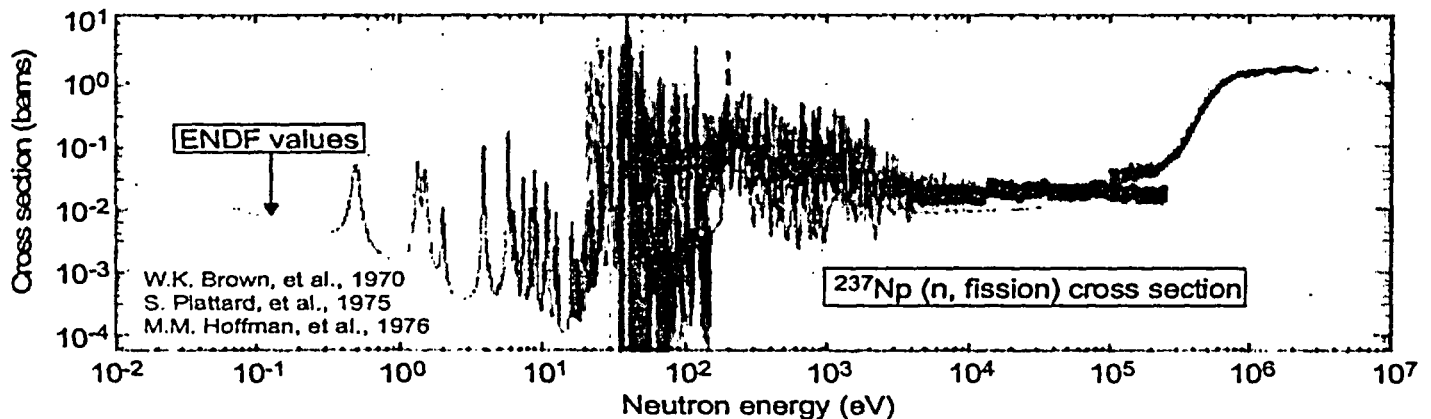


Figure 12. Cross-section data for Neptunium 237

RESEARCH & DEVELOPMENT: HYDROGEN PRODUCTION

In November, 2002, DOE issued the National Hydrogen Roadmap and identified the activities required to use hydrogen to its full potential to meet the U.S. needs for energy security, diversity, and environmental quality. As noted in the hydrogen roadmap: "...realization of a hydrogen economy faces multiple challenges. Unlike gasoline and natural gas, hydrogen has no existing large-scale supporting infrastructure—and building one will require major investment."

The DOE Hydrogen Program is contained within the Offices of Nuclear Energy, Science, and Technology (NE), Science (SC), Fossil Energy (FE), and Energy Efficiency and Renewable Energy (EE), which has the lead organizational role for the DOE as shown in Figure 13. These offices are now working together to accomplish the overall program goals—and the intersection of their nuclear-related efforts resides in the Nuclear Hydrogen Initiative (NHI).

The immediate focus of the DOE hydrogen program is on distributed production to meet short-term needs most cost effectively. To meet longer term needs, there is significant effort to provide competitive renewable feedstocks and energy sources, to develop centralized production from coal with sequestration, and to develop high-temperature processes using advanced nuclear reactors.

- Nuclear hydrogen systems interface R&D will address the essential high-temperature thermal transport, heat exchanger, and materials issues to couple the high-temperature reactor to the process plant.

Since all nuclear hydrogen production approaches being considered in the NHI (high-temperature electrolysis and thermochemical) avoid the production of greenhouse gases and can be based on domestic resources, the primary issue for nuclear hydrogen is the development of cost-effective systems that produce hydrogen at a cost that is competitive with gasoline.

High Temperature Electrolysis (HTE): HTE technology is presently being developed by DOE's Office of Energy Efficiency & Renewable Energy (EE) and Office of Nuclear Energy, Science, and Technology (NE). Electrolysis is the most straightforward approach currently available to produce hydrogen directly from water. Conventional electrolyzers are available today with electrical to hydrogen conversion efficiencies of 70% at a cost of about \$400/kWe installed. When coupled with conventional electricity production with an efficiency of 30% to 35%, the net hydrogen production efficiency is of the order of 20% to 25%. HTE, or steam electrolysis, has the potential for much higher efficiency. Thermal energy is used to produce high-temperature steam, which results in a reduction of the electrical energy required for electrolysis and, therefore, a reduction in the total energy required for hydrogen generation with the potential for net hydrogen production efficiencies exceeding 50%. Electrolysis requires low-cost, efficient electricity. Additionally, HTE requires an energy source that provides the highest possible temperatures, consistent with materials capabilities. The temperature range currently being considered is nominally 750 °C to 950 °C. HTE can be accomplished using similar materials and technology to those used in solid-oxide fuel cells (SOFC). Large-scale applications would be composed of many small electrolyzer modules. The cost effectiveness of scaling the modular electrolysis process is the major technical challenge for HTE.

Thermochemical Cycle Technology: Thermochemical cycle technology is relatively immature and only a few cycles have been demonstrated at the laboratory-scale. Although there is greater uncertainty in the outcome of R&D, there is also potential for significant process improvement based on advances in materials and chemical technology over the past two decades. Based on the information that is available, promising cycles have been identified for further investigation based on performance potential and demonstrated technical viability. Two "families" of thermochemical cycles emerged as the most promising thermochemical options and have been classified as baseline methods: the first priority is the sulfur-based family and the second priority is the calcium-bromide family. These processes have potential for high efficiencies (greater than 50%), have process steps that have been demonstrated to show feasibility, and can be developed by 2016.

The first priority baseline process is the sulfur-based family. Sulfur-Iodine, Hybrid-Sulfur, and Sulfur-Bromine Hybrid cycles are sulfur-based variations that have demonstrated high performance and are the focus of ongoing research in the United States, Japan and France. The sulfur-based cycles are the first priority, because they are projected to have high efficiencies at NGNP temperatures, are the most highly developed and supported, and much of the R&D is potentially applicable to multiple cycle variations, thus reducing overall risk.

The process-specific R&D areas for sulfur-iodine and hybrid sulfur are summarized as follows (see Figure 14—courtesy of Dr. Charles Forsberg of ORNL):

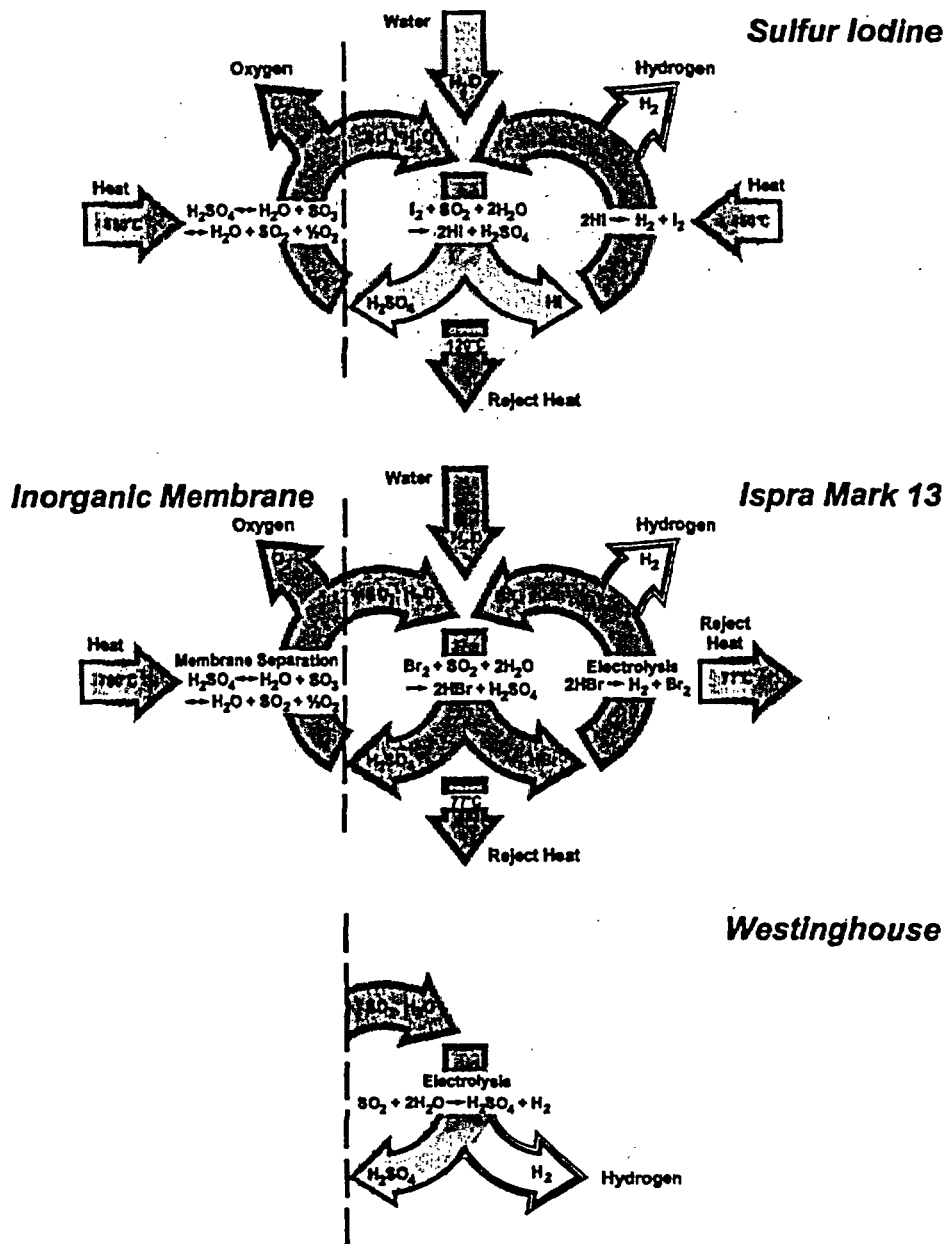


Figure 14. Sulfur Family of Thermochemical Cycles for Hydrogen Production

- *Sulfur Iodine Cycle* – This all-liquids-and-gases cycle involves three primary thermochemical steps. Unique technical issues associated with this specific cycle include efficient separation of hydrogen iodide, minimizing the recycle rates of chemicals within the process per unit of hydrogen produced, and reducing the inventories of iodine within the process; which, although not consumed, is expensive and toxic. Multiple alternative technical solutions (primarily using membranes) have been proposed to address these challenges. The distillation of HI from solution is the most difficult process issue for this cycle. The NHI work will examine both reactive and extractive (H_3PO_4) distillation and investigate recent Japanese proposals for the use of electrolysis as an alternative technology.
- *Sulfur-Bromine Hybrid* -- The sulfur-bromide hybrid process is the sulfur family contingency option. This all-liquids-and-gases cycle involves two thermochemical steps and one electrolysis step. It was demonstrated in a laboratory-scale experiment operated in ISPRA for 1.5 years producing 100 l/h. However, the projected efficiencies are slightly lower than the hybrid sulfur cycle. The hybrid sulfur cycle is chosen relative to this cycle because the process is more efficient, primarily because the electrolytic cell power consumption is less (0.6V vs. 0.8V), and it is a simpler process. Reduction of energy requirements for the electrolytic step is the most important R&D area. Initial work on sulfur-bromine will focus on updated flowsheet analyses.

The second thermochemical baseline process is the calcium-bromine thermochemical cycles. The calcium-bromine family (UT-3, Japan, Star, U.S.) involves lower peak temperatures and solid-gas reactions, and all process steps have been demonstrated. This family is identified as third priority (after the sulfur family thermochemical processes and HTE) because it is not projected to have as high an overall efficiency as the sulfur cycles.

The nuclear generated hydrogen-specific R&D is aimed at focusing resources on processes that have the highest probability of producing hydrogen at costs that are competitive with gasoline. Both thermochemical and high-temperature electrolysis processes have been identified with the

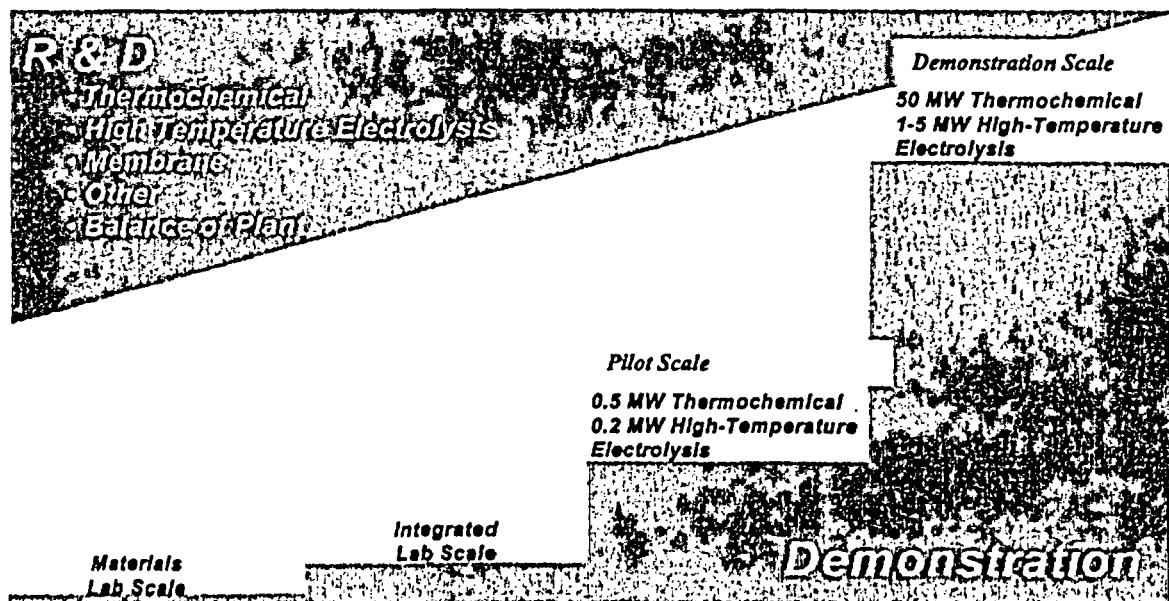


Figure 15. Nuclear hydrogen production scale-up requirements

potential to achieve this objective and both may be powered by nuclear power.

Initially, a broad research effort is required. The planned R&D effort will include laboratory-scale demonstrations, where it is justified by the available information, in addition to analytical evaluations of those processes with promise. This approach will provide a more consistent and complete assessment to base future R&D funding and scaling decisions. NHI research will follow a systematic approach to develop the required information for the sequence of scaling decisions. Confirmation of performance potential based on consistent thermodynamic analyses of candidate cycles will be confirmed in laboratory-scale tests to support pilot plant scaling decisions (see Figure 15). Pilot plant demonstrations for the selected processes will confirm engineering viability and establish a basis for process cost estimates. Pilot plant performance and cost information will provide a basis for selection of the NGNP nuclear-heated engineering demonstration. The plant, presently thought to be a 50 MW thermochemical and/or 1 MW to 5 MW HTE demonstration, would be located outside of the Emergency Planning Zone for the nuclear plant driver although possible interactions between the hydrogen and nuclear plants will be methodically analyzed.

SUMMARY

The Advanced Fuel Cycle Initiative and the Generation IV Nuclear Energy System R&D Programs are underway. The two efforts are complementary and involve contributors at the national laboratories, universities, industry, and international partners. Each Generation IV system has a unique set of technical challenges that stem from fuels, materials, power conversion, and system design & evaluation considerations. The AFCI and Generation IV programs are confronting the interesting and challenging demands that must be overcome to meet the future energy needs of the United States. All indicators are that a substantial fraction of the energy needs for the U.S. in the 21st century can be met using advanced nuclear systems that are economically competitive and that have a more than sufficient fuel supply for both this generation of Americans and future generations—while using proliferation resistant fuel forms and while operating more safely and reliably than ever before. The future for nuclear power in the U.S. and the world is indeed bright.

REFERENCES

- Brown, W. K., D.R. Dixon, D.M. Drake, "Fission Cross Section of Np237 From Pommard," *Nucl. Phys.* A156, 609 (1970).
- Hoffman, M. M., W.M. Sanders, M.D. Semon, "Fission, Scattering and Capture Cross Sections For 237-Neptunium," *Bull. Amer. Phys. Soc.* 21, 655 (JE3) (1976).
- Petti, D.A., et al, "Key Differences in the Fabrication, Irradiation, and High Temperature Accident Testing of US and German TRISO-Coated Particle Fuel, and Their Implications on Fuel Performance," *Nuclear Engineering and Design*, (232), 281-297 (2003).
- Plattard, S., Y. Pranal, J. Blons, X. Mazur, "Np-237 Fission Cross-Section Measurement Between 100 keV and 2 MeV," *All Union Conf. On Neutron Physics*, Kiev (1975).
- Schultz, R. R. and W. L. Weaver, "Using the RELAP5-3D^o Systems Analysis Code with Commercial and Advanced CFD Software," *Proceedings of the 11th International Conference on Nuclear Engineering*, Tokyo, Japan, (2003).
- U.S. Department of Energy, *The U.S. Generation IV Implementation Strategy*, (2003)
- U.S. Department of Energy, *Report to Congress—The Advanced Fuel Cycle Initiative, The Future Path for Spent Fuel Treatment and Transmutation Research*, (2003).
- U.S. Department of Energy, *A Technology Roadmap for Generation IV Nuclear Energy Systems*, (2003).

[This page left intentionally blank]

Status of Thermal-Hydraulic Research Activities Related to Advanced Reactors

Stephen M. Bajorek

Senior Technical Advisor

Division of Systems Analysis and Regulatory Effectiveness

Office of Nuclear Regulatory Research

Ph.: (301) 415-7574 / FAX: (301) 415-5160 / smb4@nrc.gov

Abstract

The Office of Research (RES) is anticipating or is actively participating in the review of several advanced reactor designs. Efforts have been more significant for the AP1000 and ESBWR designs, with the AP1000 under review for Design Certification, and the ESBWR nearing the end of the pre-Design Certification phase of its review. Other designs, including the ACR-700, IRIS, SWR-1000, GT-MHR and PBMR, are also under consideration especially for those design features and thermal-hydraulic processes that may require development of the research infrastructure. Each of these designs appear to offer significant improvements in safety by taking advantage of the prior testing, analysis, and operational experience gained from existing plants. Most of these advanced reactor designs rely on natural processes to insure that the core remains adequately cooled and containment integrity is maintained in the event of an accident. This reliance on natural processes and on unique and novel design features often requires new experimental testing, model development, and enhancement of thermal-hydraulic code capabilities.

This paper discusses each of these advanced reactor designs, and summarizes the thermal-hydraulic processes of particular interest and indicates where additional research may be necessary. Work performed in the Office of Research over the last year with relevance to advanced reactors, and plans for continuing research are outlined.

Introduction

Over the past several years, there has been a re-emergence in design and licensing activity for advanced reactors. Currently, the staff is anticipating or is actively reviewing several new designs; AP1000, ESBWR, SWR-1000, ACR-700, IRIS, GT-MHR, and PBMR. Table 1 summarizes the general design of each. These designs offer significant improvements in safety by taking advantage of prior testing, analysis, and operational experience gained from existing plants. Advanced reactor designs generally rely on natural processes to insure that the core remains adequately cooled and containment integrity is maintained in the event of an accident. In some of these designs, the large break loss of coolant accident (LOCA) is eliminated and the limiting accident scenario becomes a small LOCA or transient.

Each of these new designs promise significant safety benefits, however, their unique features create new challenges to thermal-hydraulic analysis. Physical processes such as natural circulation with low driving heads, condensation in the presence of a non-condensable gas, and entrainment and de-entrainment play an important role in several advanced plant accident scenarios. The following sections discuss the thermal hydraulic issues that are important to advanced light water reactors and are being addressed as part of the staff's code development and review effort.

Table 1: Advanced Reactors for Design Certification Consideration

Design	Applicant	Type
AP1000	Westinghouse	Advanced Passive PWR
ESBWR	General Electric	Advanced Passive BWR
SWR-1000	Framatome-ANP	Advanced Passive BWR
ACR-700	AECL	Light-Water Cooled, Heavy-Water Moderated PWR
IRIS	Westinghouse	Advanced Passive PWR
PBMR	Eskom	Advanced Gas Reactor
GT-MHR	General Atomics	Advanced Gas Reactor

First, it is informative to consider the question, "Why are there thermal-hydraulic issues?" The nuclear industry has invested considerable resources in experimental test programs and in the development of advanced computational methods. One's initial expectation is that previous work should be sufficient to resolve any thermal-hydraulic problem. With advanced reactors, however, there are several reasons why new research may be necessary:

- (1) Most of these advanced reactors utilize novel design features. While engineering judgement leads to the conclusion that these new features are beneficial, they must be considered over a broad range of conditions. Because of a lack of operational experience, it is not always clearly evident that the performance of new devices and passive safety systems will be as intended.
- (2) Some accident scenarios are eliminated by design. In some cases for example, the traditional large break LOCA is not a possibility. As a result, the focus of attention shifts to a new critical accident scenario. For designs in which the large break LOCA analysis previously limited the core power, some other accident scenario must be identified and evaluated in detail. The most critical accident scenario and limiting failure is not always readily identifiable.
- (3) Passive safety features generally result in a dependence on natural circulation and small driving heads. While this is a major objective of these new safety systems, thermal-hydraulic codes generally have difficulty in simulating transients that progress slowly and without large driving potentials. Small uncertainties in thermal-hydraulic models when propagated over long periods of

time can result in large differences in predicted system performance. Thus, thermal-hydraulic code assessment needs may change for these new plant designs.

(4) The state of the art in boiling, condensation and two-phase flow remains weak for some important physical processes. In spite of extensive research and development, it is difficult to assess with certainty processes such as subcooled nucleate boiling, flow pattern transition in rod bundles, condensation in the presence of a non-condensable gas, and two-phase separation. Many correlations developed for boiling and two-phase flow are known to be geometry dependent and as the geometry and surface conditions change, existing models and correlations may become very inaccurate.

Status of RES Thermal-Hydraulic Activities

Of the designs under consideration, the AP1000, ESBWR, and ACR-700 have received the most attention and have been the subject of the most development work. The AP1000 is in the Design Certification stage of its review, and the ESBWR is well into its pre-Design Certification stage. The ACR-700 is also in the pre-Design Certification stage. The AP1000 has been under review for some time and the staff expects to complete its Final Safety Evaluation Report in 2004. The remaining designs (SWR-1000, IRIS, GT-MHR, and PBMR) have received relatively little in the way of a formal review, but significant planning is underway in order to improve the research infrastructure in anticipation of their submittal to the staff.

The following sections provide a brief description of the main thermal-hydraulic issues related to each design, and a summary of research efforts directed at their resolution over the past year.

AP1000: The AP1000 is an advanced pressurized water reactor (PWR) that relies on passive systems for emergency core cooling. Much of the basis for AP1000 performance was established in the review of the previously certified AP600 design. Most of the test and analysis programs that supported AP600 also apply to the AP1000, which incorporates several design modifications to accommodate the 75% increase in core power. One of the key features of the AP1000 design is the Automatic Depressurization System (ADS), which rapidly reduces primary pressure so that water from the In-containment Refueling Water Storage Tank (IRWST) can flow to the vessel in case of a loss of coolant accident (LOCA). Thermal-hydraulic processes that affect performance of the ADS, and are of significant research interest include the hot leg flow patterns, entrainment from horizontal-stratified flows to the ADS, and entrainment and de-entrainment of water in the upper plenum. Each of these phenomena affect the two-phase pressure drop through the ADS and the net rate of mass loss from the primary system.

To investigate these processes, work has been conducted using the ATLATS facility at Oregon State University to investigate phase separation and two-phase flow patterns for conditions similar to those expected in the hot leg of the AP1000. The ATLATS data provided information to develop a new correlation for phase separation at an upward facing off-take, and showed that the flow patterns were influenced by the steam generator inlet plenum and could not be characterized by conventional flow pattern maps.

The APEX facility, also at Oregon State University, was also used to investigate performance of the AP1000 and to provide data on entrainment to the ADS-4 system. This facility was upgraded as part of a U. S. Department of Energy (DOE) grant to approximate the AP1000's higher power and design modifications. NRC sponsored tests included several transients involving breaks of the direct vessel injection (DVI) line with multiple failures in the passive safety systems. These beyond design basis tests helped to identify safety margin limits and provided unique entrainment data. Additional tests were conducted, sponsored by the DOE, to provide information on AP1000 performance under design basis accident conditions.

ESBWR: The ESBWR is an advanced boiling water reactor (BWR) that also relies on passive systems to maintain adequate core cooling. The design is similar to the SBWR design that received considerable attention from the staff in the early 1990's. While that review was not completed, it serves an important role in defining the major thermal-hydraulic phenomena for an advanced BWR. Thermal-hydraulic research issues include performance of the Passive Containment Cooling (PCC) heat exchangers, which must condense steam in the presence of non-condensable gas. Long term containment pressure is also affected by the distribution of non-condensables and phenomena that affect the wetwell vapor pressure.

In order to provide an independent audit capability, and to improve the ability to model the close relationship between vessel and containment thermal-hydraulics, the TRACE (TRAC/RELAP Advanced Computational Engine) and CONTAIN codes were coupled. As part of the SBWR review, the CONTAIN code had been improved in order to provide a more accurate representation of advanced BWR containment processes and thus coupling the two codes took advantage of prior development efforts.

The PUMA facility at Purdue University is being used to provide new data for code validation. Several modifications have been made to the facility to better represent the ESBWR configuration. A series of integral tests are being conducted to provide independent information on ESBWR performance.

SWR-1000: The SWR-1000 is also an advanced, passive BWR. It has numerous similarities with the ESBWR, and as such, thermal-hydraulic phenomena with large uncertainties in ESBWR have high importance in the SWR-1000. Thus, condensation in the presence of a non-condensable gas and its impact on passive containment cooling is a candidate for additional research in SWR-1000. Also important in the SWR-1000 are the performance of several novel design features such as the Passive Pressure Pulse Transmitter, which is a novel device for actuation of various safety signals.

Because of the similarities between ESBWR and SWR-1000, the code development and validation being performed for ESBWR applies to SWR-1000. Coupling of TRACE and CONTAIN is considered necessary for independent audit calculations of the SWR-1000 as well as for ESBWR. Additional work will be undertaken to address SWR-1000 specific issues once the design is submitted for pre-Design Certification review.

ACR-700: The ACR-700 is an advanced CANDU reactor, with the important distinction that the fuel is light water cooled. Moderation is performed by heavy water in the calandria, the volume of

which is significantly reduced compared to previous CANDU reactors. The ACR-700 has a negative void coefficient, and a negative power coefficient over its operating range. Of particular challenge to the staff in evaluating the ACR-700 thermal-hydraulics are post-critical heat flux and quench in horizontal fuel channels, and modeling the two-phase distribution in the inlet and outlet headers that supply water to the fuel channels. Each of these may require testing and model development. Because both light water and heavy water are used in the same system, there may be unique challenges in modeling kinetic and thermal-hydraulic feedback.

Review of the ACR-700 presents a significant challenge to the NRC research infrastructure and its development. Thermal-hydraulic codes such as TRACE and its predecessors, TRAC and RELAP, were developed for light water reactors with vertically oriented rod bundles. Constituent models and correlations, such as flow pattern maps, were specifically developed for this orientation. Because of this and other fundamental differences between the ACR-700 and other light water reactors, a Phenomena Identification and Ranking Table (PIRT) is being developed for critical accident scenarios. This will provide the basis for model development and experimental testing in the support of ACR-700 review.

IRIS: The International Reactor Innovative and Secure (IRIS) is an advanced pressurized water reactor. Unlike other PWRs however, the reactor coolant pumps, the pressurizer, and steam generators are internal to the reactor vessel. As a result, typical Class IV accidents are either eliminated or reduced in consequence. Several thermal-hydraulic issues may merit new research, including two-phase performance of the integral helical coil steam generators and interaction between the primary and a containment that is designed to withstand relatively high pressures.

Since IRIS documentation has only recently been submitted, specific research and code development plans have not been formulated. However, as with the ESBWR and SWR-1000, a close coupling between in-vessel and containment thermal-hydraulics is expected and the coupling of the TRACE and CONTAIN codes will provide benefits to the IRIS review.

GT-MHR: The Gas Turbine - Modular Helium Reactor (GT-MHR) is an advanced gas reactor currently under development that couples a gas cooled reactor with a high efficiency Brayton cycle gas turbine. Use of the direct Brayton cycle results in a net plant efficiency of approximately 48%. Helium flows downward through coolant channels in the fuel and then cross flows to a separate vessel that contains the power conversion system. The TRISO coated particle fuel used in the GT-MHR consists of a spherical kernel of fissile material encapsulated in multiple coating layers.

PBMR: The Pebble Bed Modular Reactor (PBMR) is also an advanced gas reactor which uses helium as the coolant. The PBMR consists of a vertical steel pressure vessel lined with graphite that serves as an outer reflector. Enclosed within the outer reflector is an annular fuel region loaded with over 450000 fuel spheres. Helium flows downward through the porous matrix transferring heat to the direct gas cycle.

For both the GT-MHR and PBMR, an independent audit capability is considered necessary. Because both systems utilize helium as the coolant and only single phase processes are possible, the TRACE code, developed primarily for light water reactors and the two-phase conditions that

occur in a hypothetical loss of coolant accident, is not considered the most suitable analysis tool. Moreover, the distinction between "design basis" and "severe" accidents is not clearly defined for gas reactors such that a new regulatory framework is necessary. Thus, a more suitable starting point for development of a thermal-hydraulic analysis tool for advanced gas reactors is the MELCOR code, which can track multiple gas species and model fission product release and transport. Improvements anticipated for MELCOR to enable it to accurately simulate GT-MHR and PBMR transients include the addition of high temperature graphite material properties, modeling of flow and heat transfer in a packed bed, conduction/radiation modeling in porous media and in spherical fuel geometries, and coupling MELCOR with the PARCS kinetics code.

Conclusions

The advanced reactor designs represent significant advancements in nuclear power technology. These designs offer improved economics and at the same time may provide enhanced safety margins. Verification of improved safety may require new research to investigate the performance of some of the novel design features and to improve the understanding of complex thermal-hydraulic processes. Research needs are expected to evolve and become better defined as these designs are reviewed by the staff.

Cladding Behavior during Dry Cask Handling and Storage

H. Tsai and M. C. Billone

Argonne National Laboratory
Argonne, Illinois 60439 U.S.A.

Abstract

Cladding behavior during dry-cask handling and storage is being studied with irradiated fuel rods from two pressurized water reactors -- Surry at 36 GWd/MTU burnup and H. B. Robinson at 67 GWd/MTU burnup. The Surry rods were stored in a dry cask for 15 years and experienced a range of temperature histories during thermal benchmark tests, some of which emulated vacuum drying. The Robinson cladding, owing to the high burnup, has a significant oxide corrosion layer ($\approx 100 \mu\text{m}$ max.) and hydrogen content (≈ 800 wppm max.). Characterization of post-storage Surry rods showed the effects of storage and thermal benchmark tests were benign, with no evidence of cladding creep, hydride reorientation or hydrogen axial migration in cladding. Thermal creep tests performed on the Robinson and post-storage Surry cladding revealed respectable creep ductility -- in excess of 3-4% in the 400°C and 190-250 MPa hoop stress test regime -- for both cladding types. One Robinson creep sample ruptured during shutdown under internal gas pressure; the cause of this rupture is being investigated. Radiation-induced hardening in cladding was found to be readily removed in annealing tests for the Robinson cladding at 420-500°C. No deleterious hydride radial reorientation was noted in the Robinson annealing tests as the samples were stress-free. Additional annealing tests with samples under hoop stress are being planned to evaluate factors that may result in hydride radial orientation.

1. Introduction

Because of the limited storage capacity in spent-fuel pools, discharged fuel assemblies are increasingly being relocated into dry casks for interim storage until long-term geological repositories are available. Some of the original licenses issued by the U.S. NRC for 20 years of dry-cask storage of spent fuel up to 45 GWd/MTU burnup are coming up for renewal shortly. As the burnup for fuel assemblies discharged from reactors increases, extending the database for high-burnup fuel cladding becomes pressing for dry-storage cask licensing. High-burnup fuel rods are perceived to be more vulnerable because of their greater water-side corrosion, hydrogen uptake, and radiation damage in the cladding.

Cladding behavior during dry cask handling and storage is being studied with irradiated materials from two pressurized water reactors -- Surry at 36 GWd/MTU burnup and H. B. Robinson at 67 GWd/MTU burnup. The scope of our study consists of characterization of the post-storage Surry rods, thermal creep testing of both Robinson and post-storage Surry cladding, and annealing tests of the Robinson cladding.

The Surry rods in our work are unique in that they had been stored in a Castor-V/21 dry cask for 15 years and had experienced a range of temperature conditions as part of thermal benchmark tests while in the cask [1, 2]. The thermal benchmark tests were performed with the cask in horizontal and vertical positions while filled with air, helium, nitrogen, or vacuum. For our study, we retrieved rods from an assembly in the cask with the highest burnup and near-highest temperature. The peak cladding temperature the rods experienced was $\approx 415^{\circ}\text{C}$ when the cask was in vacuum; the duration for this peak temperature condition was ≈ 3 d. The retrieved rods were characterized in detail to determine possible degradation of fuel-rod condition due to the storage/benchmark test history.

During certain phases of cask operation, such as vacuum drying and transfer, temperature of cladding may reach up to $\approx 400\text{-}500^{\circ}\text{C}$ for hours [3]. Thermally-induced processes in Zircaloy at these temperatures may relieve some of the radiation-induced hardening, thereby improving the properties of the material, including creep performance, in dry cask operations. To assess the degree of hardening recovery at elevated temperatures, a series of annealing tests in the range of $420\text{-}500^{\circ}\text{C}$ were conducted with the high-burnup Robinson cladding. A corollary objective of this work is to investigate hydride redistribution and reorientation under stress-free conditions.

Thermal creep of spent-fuel cladding is an important consideration in assessing the viability of extended dry-cask storage, as it is the dominant mechanism of cladding deformation under normal storage conditions [4-8]. It is being investigated with defueled cladding segments from the Surry and Robinson rods in hot cells. For the Surry cladding, in addition to generating creep rate data for predictive modeling, a key objective is to evaluate residual creep ductility of the cladding after the 15-y dry-cask storage. A significant residual creep strain ($>\approx 1\%$) would suggest that the rods may be suitable for further storage in the cask and may survive creep during transportation, reconsolidation and final repository conditions. For the Robinson cladding, of particular importance is the determination of creep strain capacity and the rate of creep deformation as affected by higher fluence and hydrogen content in the cladding. Avoiding extensive cladding creep rupture in casks is important as these ruptures may lead to significant fission-product release, high surface dose rates, and assembly retrievability issues [3].

2. Effect of 15-y Dry-Cask Storage - Surry Rod Characterization

The Surry rods examined were from one of the 15×15 fuel assemblies loaded in a Castor-V/21 dry cask [1, 2]. After the thermal benchmarking tests, the cask was left undisturbed with an inert atmosphere ($\text{He}/<1\%$ air) for 15 years until the rod retrieval for the present work. The retrieved rods have an average burnup of 36 GWd/MTU (40 GWd/MTU peak pellet) and attained near the highest cladding temperatures in the cask ($\approx 415^{\circ}\text{C}$ for ≈ 3 d while the cask was in vacuum). The fuel enrichment is 3.1% and the nominal fuel pellet dimensions are 9.29 mm dia. \times 15.2 mm height, with an active fuel height of 3.66 m. The cladding is a cold-worked and stress-relieved Zircaloy-4, with a dimension of 10.72 mm OD \times 9.50 mm ID. The rods were pressurized with helium to 2.8 MPa during fabrication.

Profilometry of 12 of the post-storage rods shows the cladding creep-down to be $\approx 0.6\%$. As this value is typical of PWR rods at this burnup [9,10], the result suggests no significant outward creep of the cladding during the benchmarking tests or the extended cask storage.

Fission-gas release was measured for four rods and the results show release fractions ranging from 0.4 to 1.1%. These values are within the data band for as-irradiated PWR rods of this type and burnup without a dry-storage history [9,10].

The condition of the post-storage Surry fuel is shown in Fig. 1 for one of the rods. All features appear to be normal with no evidence of degradation from the extended storage. As expected for rods of this burnup, fuel restructuring is only minor. The fuel/cladding gap is open and fuel/cladding chemical interaction and fission product deposit in the gap are both minor.

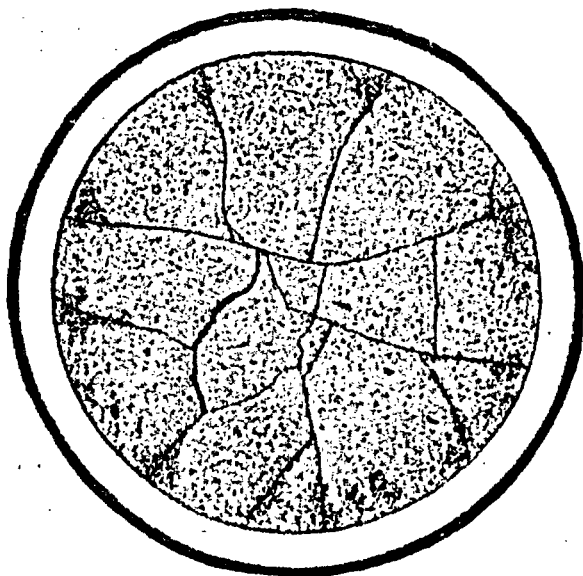


Fig. 1
Cross-sectional photocomposite of a post-storage Surry rod at the fuel axial midplane. No storage-induced effects are apparent in either the fuel or the cladding.

Average cladding oxide thickness in post-storage Surry rods was measured with optical metallography. The thicknesses, ranging from $\approx 25 \mu\text{m}$ at the axial midplane, $\approx 33 \mu\text{m}$ at 0.5 m above the midplane, $\approx 40 \mu\text{m}$ at 1 m above the midplane, $\approx 30 \mu\text{m}$ at 1.5 m above the midplane, and $\approx 12 \mu\text{m}$ at 2.0 m above the midplane (i.e., in the plenum), are within the normal range [9,10] for PWR rods of this burnup and suggest no additional oxidation occurred during cask loading or storage.

Measured hydrogen contents in the cladding are ≈ 250 wppm at the axial midplane and ≈ 300 wppm at 0.5 m above the midplane. These readings are consistent with the observed oxide thickness.

Hydride morphology in the cladding was determined at multiple axial locations. The results at 0.5 m above fuel midplane and in the rod plenum are shown in Fig. 2. In spite of the cyclic temperature during the benchmark tests, the precipitated hydride platelets are aligned mostly in the circumferential direction with no evidence of harmful radial reorientation. (Hoop stress in the Surry cladding was relatively low, $< 65 \text{ MPa}$ at the $\approx 415^\circ\text{C}$ peak temperature.) On the important issue of temperature-driven hydrogen axial migration [7], which has the potential for causing embrittlement of the colder ends of the fuel-rod cladding, there is no evidence that the migration, if any, is significant, as shown in Fig. 2. This observation will be verified with quantitative hydrogen analyses, which will be performed. Probably because of a lack of strong radial temperature gradient while in the cask, the distribution of the precipitated hydrides is fairly uniform across the cladding thickness.

Microhardness of the Surry cladding was measured with a diamond pyramid indentation method at multiple axial and circumferential locations across the cladding thickness. The Vickers hardness

readings, 235-240 DPH, are consistent with as-irradiated values, suggesting little or no annealing of the cladding during the cask storage and thermal benchmark tests.

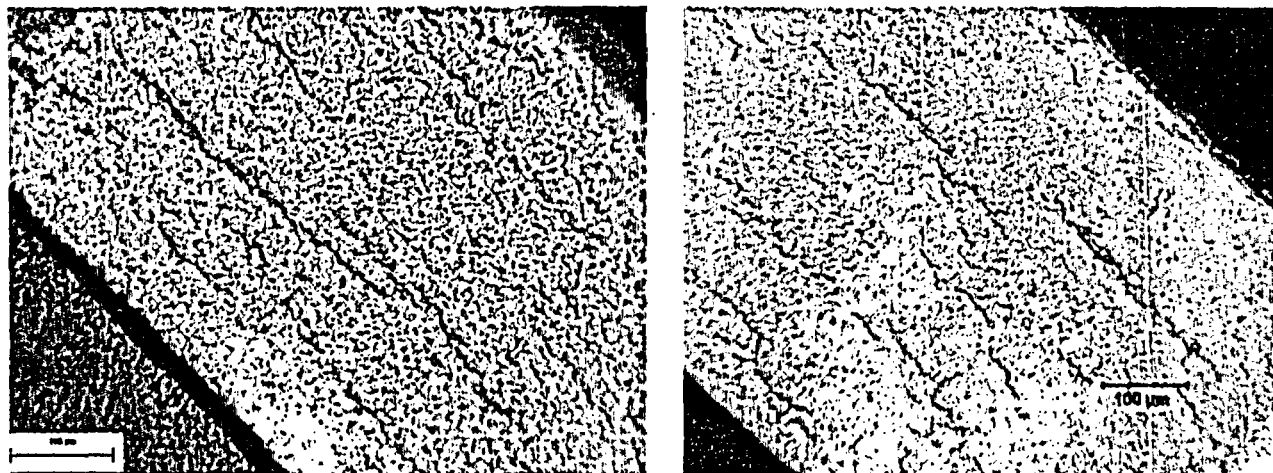


Fig. 2. Distribution of hydride precipitates in post-storage Surry rod in transverse cross-sectional view. The axial elevations are (left) 0.5 m above the midplane and (right) in rod plenum. The gray band on the outer surface of the cladding is the oxide layer from in-reactor corrosion.

3. Effect of Thermal Annealing on Microhardness and Hydride Morphology

During the initial phases of cask operation, including vacuum drying and transfer, cladding temperature of fuel rods may reach $\approx 400\text{-}500^\circ\text{C}$ for several days [3]. These conditions may relieve the radiation-induced hardening of Zircaloy, thereby restoring some of the lost ductility of the cladding [11]. With an implicit objective of generating data to help interpret thermal creep test results, a series of six isothermal annealing tests was performed with the Robinson cladding to investigate this effect. The test temperature range was 420 to 500°C and the test duration was 2 to 72 h.

The annealing tests were performed with short segments of defueled cladding from just above the axial midplane of a Robinson rod. The rod is from a 15×15 assembly with an averaged burnup of 67 GWd/MTU (72 GWd/MTU peak pellet). The cladding is a cold-worked and stress-relieved Zircaloy-4 with an outer diameter of 10.76 mm and a wall thickness of 0.762 mm. The local neutron fluence is 1.4×10^{26} n/m² ($E > 1$ MeV) and the hydrogen content is ≈ 600 wppm at the fuel axial midplane.

The ends of the annealing segments were open and the samples were stress-free. Following the heating tests, the Vickers microhardness of the samples were measured and compared with those of the as-received and as-irradiated controls. Changes of hydride morphology from that in the as-irradiated control sample were also evaluated.

Table 1 shows the measured hardness and the calculated percent recovery defined as

$$\text{Recovery} = \left[1 - \frac{H - H_0}{H_i - H_0} \right]$$

where H is the hardness after annealing, H_0 is hardness before irradiation, and H_i is the hardness after irradiation.

Table 1. Microhardness and percent recovery (in parentheses) after the annealing tests. Microhardness of the as-received and as-irradiated controls are 203 and 252, respectively.

Temp. (°C)	Duration (h)				
	2	10	20	48	72
420	--	--	226 (54%)	--	215 (75%)
450	224 (58%)	217 (71%)	--	--	--
500	218 (69%)	--	--	206 (94%)	--

These results show that at 500°C for 2 days, much of the hardening due to radiation damage could be removed. As expected, at lower temperatures, longer periods would be required to achieve the same degree of recovery. The fact that irradiation-induced hardness can be annealed out for these time-temperature regimes suggests that creep ductility may also be restored.

The morphology of hydride precipitates after the annealing tests is shown in Fig. 3 along with that of the as-irradiated control. In the as-irradiated sibling, there is a pronounced gradient of hydride density from the outer to the inner surfaces of the cladding owing to the radial temperature differential in the reactor shutdown. This gradient of hydride distribution is progressively reduced with time in the annealing tests. This redistribution attests to the high mobility of hydrogen at these temperatures. In the annealing tests, cool-down from temperature was relatively fast (minutes) and without a substantial temperature gradient from the sample inside to outside surfaces.

Because the samples were stress-free, and because the Robinson cladding is cold-worked and stress-relieved with grains elongated predominantly in the circumferential and axial directions, the reprecipitated hydrides after the annealing tests are still mostly circumferentially oriented. Little or no radial hydrides are discernible. This finding is consistent with published data [12], which show a hoop stress of ≈ 90 MPa would be required for reorientation to occur during cooling from these temperatures.

4. Thermal Creep

Thermal creep is the dominant mechanism of cladding deformation under normal cask-storage conditions and is being investigated with Surry and Robinson cladding. For the Surry cladding, in addition to generating creep rate data for predictive modeling, a key objective is to evaluate residual creep ductility of the cladding after the 15-y dry-cask storage. A significant residual creep strain, e.g., $> \approx 1\%$, would

suggest that the rods may be suitable for further storage in the cask and may survive creep during transportation, reconsolidation and final repository conditions. For the Robinson cladding with higher neutron damage, greater waterside corrosion, and higher hydrogen content, the objective is to evaluate, vis-à-vis the Surry results, whether these conditions associated with high fuel burnup significantly degrade the creep performance of Zircaloy. The oxide thickness and hydrogen content for the Surry samples are $\approx 23\text{-}30\ \mu\text{m}$ and 230-265 wppm, respectively. The corresponding values for the high-burnup Robinson samples are $\approx 80\text{-}90\ \mu\text{m}$ and 650-700 wppm.

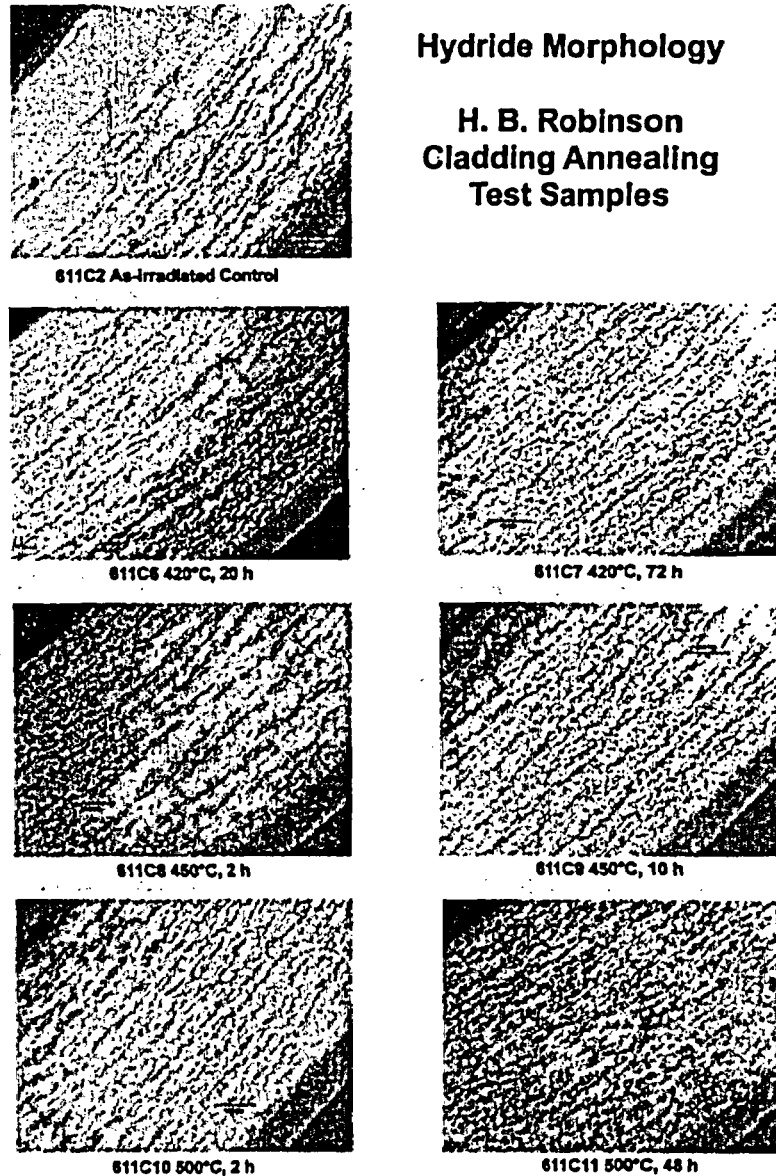


Fig. 3. Changes in hydride morphology in the Robinson cladding due to the annealing.

The thermal creep tests are performed with 76-mm-long sections of defueled cladding from the flat-power region of the rods above the midplane. The end fittings for the samples are welded for reliability. Internal gas pressurization is achieved with a microprocessor-based pressure controller via a line exiting the sample's top end fitting. Very stable pressure is maintained in this manner over extended period of time for each sample. High-purity argon is used for both the sample pressurization and test chamber purge (to protect the samples from oxidation). Periodically, the sample is removed from the test chamber for diametral and length measurements performed at room temperature with a precision laser profilometer. Because of the periodic shutdowns, each test consists of multiple runs. To inhibit possible hydride reorientation [13,14] in the sample, all shutdowns, with the exception of three, were performed with the samples depressurized first before turning down the furnace. The exceptions were for three samples in their final shutdown for the specific purpose of studying hydride reorientation. In these three cases, full pressure was maintained during the sample cool-down to room temperature.

Eight creep tests have been conducted thus far, five on Surry cladding samples and three on Robinson cladding samples, as shown in Table 2.

Table 2. Conditions of Thermal Creep Tests

Test	Temp. (°C)	Hoop Stress (MPa)	Duration (h)
Surry C3 ⁽¹⁾	360	220	3305
Surry C6 ⁽¹⁾	380	190	2348
Surry C8	380	220	2180
Surry C9 ⁽²⁾	400	190/250	1873/693
Surry 2-C9	400	160	286, on-going
Robinson C14	400	190	2427
Robinson C15 ⁽¹⁾	400	190	2439
Robinson C17	380	220	404, on-going

(1) Final shutdown under internal gas pressure to study hydride reorientation.

(2) Same sample but with the stress increased from 190 to 250 MPa at 1873 h.

4a. Surry Creep Test Results

All Surry samples were intact at the end of the tests, including the C3 and C6 samples that were shut down while under internal gas pressure. Measured creep deformations as a function of time for the five completed tests are summarized in Fig. 4. For the C8 sample (380°C, 220 MPa hoop), the measured hoop strain was 1.1% at the end of test at 2180 h. For the 400°C C9 sample, after demonstrating >1% creep strain at the end of 1873 h at 190 MPa hoop stress, the pressure was increased to produce a hoop stress of 250 MPa. The sample remained intact at the end of 693 incremental hours with a measured hoop strain of 5.8%. Significant creep ductility was thus demonstrated for the post-storage Surry cladding in

these tests. (It should be noted that the reported hoop stresses are engineering stresses, not true stresses. No efforts were made during the tests to adjust the gas pressure to keep the hoop stress constant to account for wall thinning and diameter increase. Rather, the internal pressure was maintained constant over the entire test duration.)

Radial plots depicting the cross-sectional profiles of the samples were evaluated after every run. The data are useful to detect localized bulging, which may be a precursor of imminent burst rupture. All results indicate the deformation to be azimuthally uniform, even for the C9 sample, suggesting that the sample may possess creep ductility beyond the measured 5.8%.

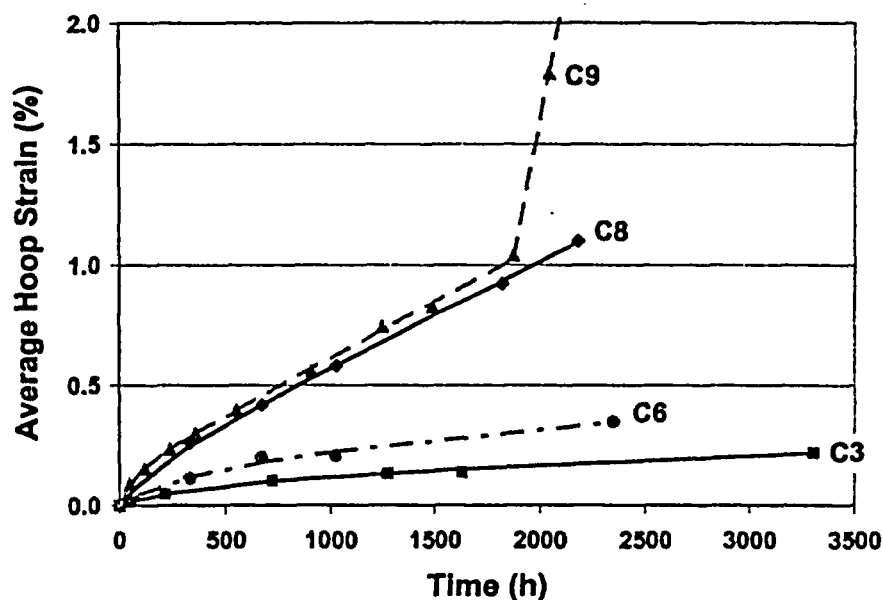


Fig. 4. Creep deformation histories for the Surry tests. For the C9 test, the stress loading was increased from 190 to 250 MPa at 1873 h, resulting in the sharp change of the creep rate. Not shown in this chart is the hoop strain of 5.8% at the conclusion of C9 test at 2566 h. The sample was intact.

As can be seen in Fig. 4, at the time of termination, all Surry samples were in the secondary (steady-state) creep regime. Calculated steady-state creep rates from the straight portion of the curves are shown in Table 3. The data suggests a strong temperature and pressure dependency of steady-state creep rates in the regime tested.

There were no discernible sample length changes in any of the tests, suggesting the creep deformation was isotropic.

Samples C3 and C6 were shut down while under internal gas pressure for the purpose of studying radial reorientation of hydrides. Figure 5 shows the morphology of the hydrides at room temperature in these two samples. In comparison to the pretest sample (see Fig. 2), it is evident that reprecipitation

occurred and that a significant fraction of the hydride platelets now has a radial component. Possibly because of the moderate hydrogen content in the Surry cladding (≈ 250 wppm), no long-range linkage of the radial hydrides is evident.

Table 3. Creep Strain and Secondary Creep Rates of Surry Cladding

Sample	Temp. (°C)	Hoop Stress (MPa)	Duration (h)	Hoop Strain (%)	Secondary Creep Rate (%/h)
Surry C3	360	220	3305	0.22	4.2×10^{-5}
Surry C6	380	190	2348	0.35	8.8×10^{-5}
Surry C8	380	220	2180	1.10	4.5×10^{-4}
Surry C9	400	190	1873	1.04	4.9×10^{-4}
	400	250	693 ⁽¹⁾	5.83	$>4.9 \times 10^{-3}$
Surry 2C9	400	160	286 ⁽²⁾	0.22	-

(1) Incremental hours.

(2) On-going.



Fig. 5. Morphology of reprecipitated hydrides in Surry creep samples C3 (left) and C6 (right) after shutdown under internal gas pressure. There is a significant radial component in the hydrides but not long-range linkage (see Fig. 2 for pretest morphology). Outside surface is to the left.

4b. Robinson Thermal Creep Results

Robinson creep testing is in its initial phase. Three tests have been conducted so far (see Table 2).

In the Robinson C17 test, presently at 404 h, the test conditions, 380°C and 220 MPa hoop, are identical to that of the Surry C8 test. As shown in Fig. 6, creep deformation in the Robinson C17 sample

is only $\approx 1/3$ of that in the sibling Surry C8 sample after ≈ 400 h. The lower creep rate is as anticipated and illustrates the effect of the higher fluence (radiation damage) and greater hydrogen content in the Robinson material.

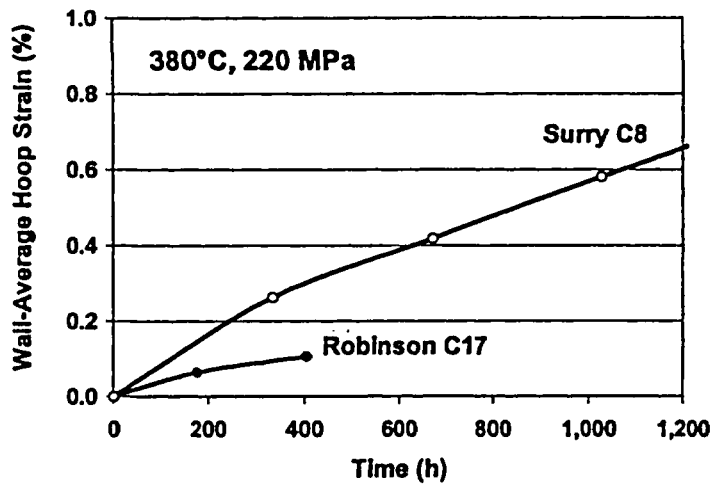


Fig. 6. Comparison of creep strain between high-burnup Robinson and lower-burnup Surry samples tested at 220 MPa hoop and 380°C.

The results of the two completed Robinson tests, C14 and C15, provide a direct comparison with the results of the lower-burnup Surry C9 at 400°C and 190 MPa hoop conditions. This comparison is summarized in Fig. 7. Consistent with the greater irradiation hardening in the higher-fluence Robinson material, the creep rate of the Robinson samples trailed that of the Surry in the first several hundred hours of testing. After this initial period, however, the rate of creep deformation in the Robinson samples surpassed that in the Surry. It is likely that the increased deformation rate in Robinson with time is related to the thermal annealing effect discussed earlier. (It is possible that, over time, some annealing effect may also occur in the lower-temperature Robinson C17 test at 380°C. The extent, to be determined, is expected to be smaller.) The apparent higher steady-state creep rate of the Robinson cladding over that of the Surry cladding may be due to alloy chemistry, grain size, dislocation densities, or other factors; they are not explicitly studied due to the limited cladding types available.

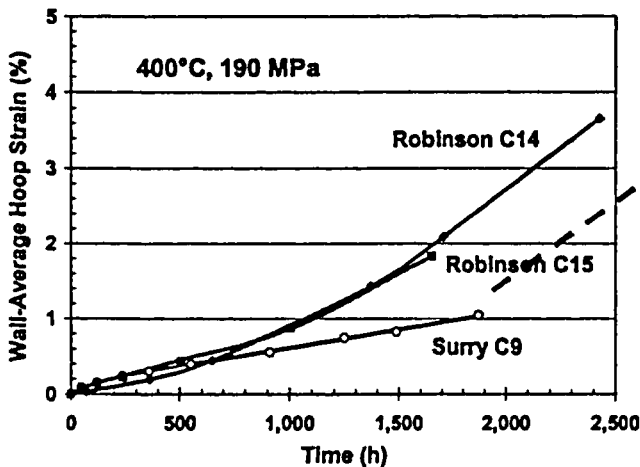


Fig. 7. Comparison of creep strain between high-burnup Robinson and lower-burnup Surry samples tested at 190 MPa hoop and 400°C. The last segment of Robinson C15 deformation, shown in dashed line, is the anticipated result, as actual measurements have not been made yet. See text.

The Robinson C14 sample was intact at the end of test at 2427 h. The measured hoop strain is 3.6%, which is significant for high-burnup fuel cladding. The sample was found to be in good condition with no localized bulging, suggesting that additional ductility is likely in the sample.

The follow-up C15 test behaved similarly to that of the C14 test up to the next to the final shutdown, with $\approx 1.8\%$ creep strain at 1650 h, confirming the good creep ductility of the Robinson material measured in C14. With this confirmation objective satisfied, the final shut down of the C15 test, at 2439 h, was administrated with the sample under internal gas pressure, in a manner comparable to that of the Surry C3 and C6 tests. The objective was to study stress-induced hydride reorientation in the higher-burnup, higher-H-content Robinson material. During the C15 shutdown, however, an abrupt rupture was detected and the ensuing depressurization triggered a system scram. The temperature and pressure history during the C15 shutdown is shown in Fig. 8. Because the internal gas pressure in actual spent fuel rods would decrease as the cladding temperature drops, the C15 shutdown conditions with the pressure held constant represented a significant overtest. The 190 MPa engineering hoop stress (at 4400 psi gas pressure) corresponds to less than 25% of the estimated yield strength of the cladding, indicating the failure was possibly brittle.

The cause of the C15 rupture is under investigation as the sample is still in the enclosed test chamber. It is possible that the rupture is hydride-related. It is also possible that the rupture is an experimental artifact, for instance, caused by end-fitting weld failure. Effort is underway to retrieve this sample to determine the cause of the rupture.

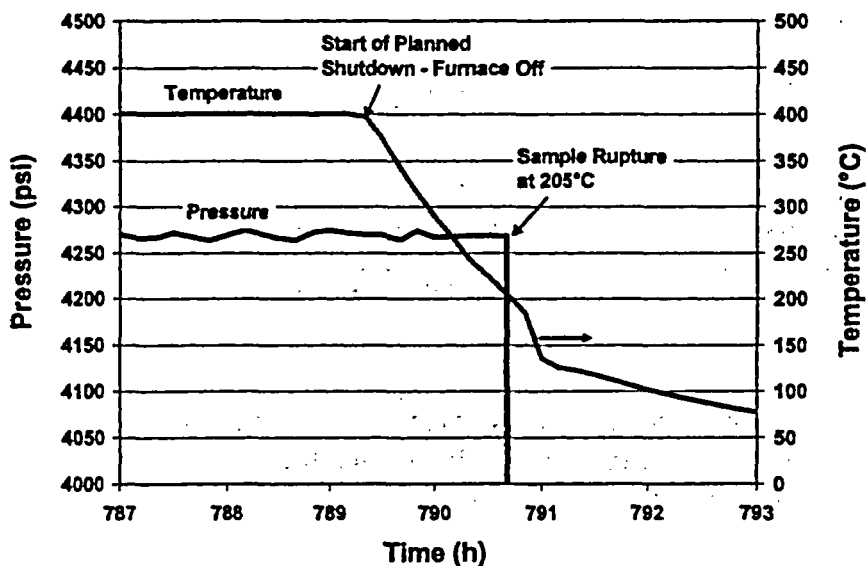


Fig. 8. Robinson C15 sample rupture during the shutdown at 205°C while under internal gas pressure.

5. Conclusions

Medium-burnup Surry fuel rods were characterized in detail after the 15-y storage in a dry cask. Elevated cladding temperature, up to $\approx 415^{\circ}\text{C}$ for several days, resulted from the cask thermal benchmark tests prior to the long-term storage. In the post-storage characterization of the rods, little evidence of deleterious effects, such as additional oxidation, fission gas release, or cladding creep, could be discerned. There is no evidence of hydride reorientation in the cladding. These results bode well for the extended storage of medium-burnup spent fuel rods.

Hardening occurs in Zircaloy cladding during reactor service due to neutron damage, which produces point defects and dislocation loops. In a series of isothermal annealing tests performed with high-burnup Robinson cladding, it was demonstrated that a significant fraction of the radiation-induced defects can be annealed out at temperatures of $420\text{-}500^{\circ}\text{C}$. The hardening recovery during the early phase of cask operation, such as vacuum drying, may benefit subsequent long-term cladding creep behavior. In the same annealing tests, it was found that hydrogen redistributes readily in the radial direction. No deleterious hydride reorientation was experienced, as the annealing samples were stress-free.

Steady-state creep rate and residual ductility in temperature and hoop stress regimes of $360\text{--}400^{\circ}\text{C}$ and $190\text{--}250\text{ MPa}$ have been measured for post-storage Surry cladding. None of the samples ruptured in the tests. Significant residual creep strain was found in the Surry cladding: $>1\%$ at 380°C (220 MPa) and 400°C (190 MPa). A residual strain of $>5.8\%$ was achieved in the 400°C sample after raising the stress level to 250 MPa for $\approx 700\text{ h}$. No localized bulging, a precursor to burst rupture, was observed in this 250 MPa sample, suggesting additional creep capacity is likely. Secondary creep rates spanning two orders of magnitude were measured in the Surry tests. The data, showing strong dependency on both temperature and stress, are valuable for code benchmarking and model improvement. Two of the samples were shutdown under hoop stress. In these two samples, a significant component of radial hydrides can be noted. However, the hydrides did not form long-range linkage as the hydrogen content in the Surry cladding is relatively low ($\approx 250\text{ wppm}$).

In the limited creep tests conducted thus far with the high-burnup Robinson cladding, significant creep ductility, in excess of 3% at 400°C , was demonstrated. One of the samples apparently suffered a rupture during shutdown under pressure. Whether this rupture is related to hydride reorientation or caused by an experimental artifact is being determined. The findings from this investigation will be factored into the future testing of high-burnup cladding materials.

Acknowledgments

The authors appreciate the support provided by NRC, EPRI, and DOE-RW for the projects. The authors would like to acknowledge Dr. B. Hilton and the excellent team at ANL-West for the nondestructive examination of the Surry fuel rods.

References

1. D. Dziadosz, et al. "The Castor-V/21 PWR Spent-Fuel Storage Cask: Testing and Analyses," EPRI Report NP-4887, November 1986.
2. M. A. McKinnon and V. A. Deloach, "Spent Nuclear Fuel Storage - Performance Tests and Demonstration," PNL-8451, Pacific Northwest Laboratory, 1993.

3. K. A. Gruss and M. W. Hodges, "Regulatory Issues Associated with the Dry Storage and Transportation of High Burnup Fuel," 9th ICONE, April 8-12, 2001.
4. US NRC Spent Fuel Project Office Interim Staff Guideline -11, Revision 2, July 2002.
5. J. P. Foster, et al. "Creep, Hydride Orientation, and Oxide Spalling Issues Associated with Fuel Cladding: Impact on High Burnup Fuel Dry Storage," Proc. ICAPP 2002, Hollywood, FL.
6. W. Goll, et al. "Short-time Creep and Rupture Tests on High Burnup Fuel Rod Cladding," J. Nucl. Mater. 289 (2001) 247.
7. C. Cappelaere, et al. "Long Term Behavior of the Spent Fuel Cladding in Dry Storage Conditions," Proc. ICEM 2001 Conference, Brugges, Oct. 2001, pp. 195-200.
8. P. Bouffioux, et al. "Interim Dry Storage of PWR Spent Fuel Assemblies – Development of A Long Term Creep Law to Assess the Fuel Cladding Integrity," Proc. ICEM 2001 Conference, Brugges, Oct. 2001, pp. 201-206.
9. R. B. Davis, "Pretest Nondestructive Examination Data Summary Report on Turkey Point Spent Fuel Assemblies D01, D04, and D06 for the Climax – Spent Fuel Tests," HEDL-TME 80-83, UC-70, Hanford Engineering Development Laboratory, January 1981.
10. S. D. Atkin, "Destructive Examination of 3-Cycle LWR Fuel Rods from Turkey Point Unit 3 for the Climax - Spent Fuel Tests," HEDL-TME 80-89, UC-70, Hanford Engineering Development Laboratory, June 1981.
11. G. J. C. Carpenter and J. F. Watters, "Irradiation Damage Recovery in Some Zirconium Alloys," Zirconium in Nuclear Applications, ASTM STP 551, August 1973.
12. R. E. Einziger and R. Kohli, "Low-Temperature Rupture Behavior of Zircaloy-Clad Pressurized Water Reactor Spent Fuel Rods Under Dry Storage Conditions," Nuclear Technology, V.67, October 1984.
13. M. Leger and A. Donner, "The Effect of Stress on Orientation of Hydrides in Zircaloy Alloy Pressure Tube Materials," Canadian Metallurgical Quarterly 24, 235-243 (1985).
14. R. P. Marshall and M. R. Louthan, Jr., "Tensile Properties of Zircaloy with Oriented Hydrides," Trans. ASM, 56, 693 (1963).

MECHANICAL PROPERTIES OF IRRADIATED ZIRCALOY-4 FOR DRY CASK STORAGE CONDITIONS AND ACCIDENTS

Robert S. Daum, Saurin Majumdar, and Michael C. Billone
Energy Technology Division
Argonne National Laboratory (ANL)
Argonne, IL 60439

Abstract

The mechanical integrity of fuel cladding is essential for mitigating fuel dispersal during pre-storage vacuum drying and transfer, during dry cask storage, and during transfer from the dry cask to a permanent repository site. Rupture may occur during handling or transportation accidents if cladding ductility has been reduced due to the separate or combined effects of pre-existing flaws, hydride concentration and orientation, radiation-induced hardening, and creep strain accumulated during vacuum drying and dry storage. Therefore, it is important to determine the cladding mechanical behavior under a variety of microstructural conditions, temperatures, and strain rates. Axial tensile tests are in progress at ANL to address part of the data needs for dry-cask storage. This paper presents a preliminary database for the temperature-dependent mechanical properties of non-irradiated, low-Sn Zircaloy-4 (Zry-4); irradiated-and-dry-cask-stored Zry-4 at 36 GWd/MTU; and irradiated Zry-4 at 67 GWd/MTU.

Introduction

The mechanical behavior of spent-fuel cladding during postulated transportation and handling accidents is of considerable concern for the licensing of dry-cask-storage systems. Increasing this concern is the need to store assemblies with discharge burnups up to 62 GWd/MTU and for extended periods of time (up to 100 years). For pressurized-water reactors (PWRs) utilizing Zry-4 fuel cladding, this high burnup and extended storage times can result in a degradation of cladding mechanical properties; namely, a loss in ductility such that cladding rupture may occur during cask handling or transport.

After years in dry storage, fuel cladding may undergo permanent plastic strains due to thermal creep (applied stress < yield strength), which may reduce the residual ductility during high stress (> yield strength) loading associated with handling or transportation accidents. Although results from ANL thermal creep tests indicate that cladding rupture does not occur even after 4% hoop strain [1], the increase in defect density (from creep-induced dislocations) may further degrade the strain-hardening properties or ability to plastically deform in a material already hardened by radiation-induced defects. Therefore, it is important to understand the effects of creep deformation on the residual cladding ductility during handling and transportation.

Moreover, the residual ductility after creep deformation may be further reduced due to pre-existing cracks oriented along the radial direction of the cladding. These cracks may initiate within a layer of highly dense, circumferentially oriented hydrides near the outer surface and may result in through-wall cracking or limitation to the load-carrying capacity of the cladding [2,3]. In fact, licensees are required to account for this layer of hydrides in cladding stress calculations for design basis accidents [4]. Furthermore, radially oriented hydrides may precipitate in the cladding under certain temperature-stress history [5,6], increasing the possibility for through-wall crack initiation and propagation under tensile states of stress.

From an environmental standpoint, temperatures of high-burnup spent fuel are currently not to exceed 400°C during vacuum drying, handling, and dry-cask storage [4] and are expected to decrease to about 150-200°C at the end of storage [6]. Furthermore, certain handling operations from storage in a spent fuel pool to a dry cask correspond to temperatures <100°C. Additionally, complex stress states, deformation paths, and strain rates may potentially occur during handling and accident conditions [7]. Therefore, it is important to determine the environmental effects on cladding mechanical properties, covering a temperature range of 25-400°C, a range of strain rates from quasi-static ($\approx 10^{-3}$ per sec) to impact rates, and loading conditions that cover uniaxial and biaxial tension, bending, and impact.

This paper presents the results of an effort to add to the mechanical properties database regarding operating and accident conditions during dry-cask storage and transportation under these ranges of temperature and strain rate. These results come from hydride characterization and uniaxial tensile tests. Additionally, areas of future work concerning the separate and combined (possibly synergistic) effects of radiation-induced damage and hydrides will be discussed.

Test Materials

All of the Zry-4 materials for this study are from 15x15 PWR fuel cladding that has been cold-worked and stress-relieved and irradiated in:

- Surry-2 reactor to a fluence of 7×10^{25} n/m² ($E > 1$ MeV) and an average fuel burnup of 36 GWd/MTU in which the cladding has a ≤ 40 μ m oxide layer and contains 250-300 wppm hydrogen. The clad spent fuel was placed in a dry-storage cask (Castor-V/21) for 15 years with varying environmental and thermal histories during code benchmarking studies conducted prior to storage.
- H.B. Robinson (HBR) reactor to a fluence of 14×10^{25} n/m² ($E > 1$ MeV) and an average fuel burnup of 67 GWd/MTU in which the cladding has a ≤ 100 μ m oxide layer and contains ≤ 300 wppm hydrogen.

The histories of these cladding materials are discussed in more detail elsewhere [8]. It is worth noting that the thermal history of Surry-2 cladding during the code benchmarking studies resulted in temperatures of 350-415°C for several hours and upwards of several days, which may have caused partial annealing of radiation-induced damage. At the time of this paper, tensile specimens fabricated from HBR cladding have yet to be tested so the results and discussion will concentrate on the characterization of HBR cladding and the implications on mechanical properties. Unfortunately, archival cladding materials (both as-manufactured and as-irradiated but prior to dry-cask storage) were not available for comparison to the irradiated Surry from dry-cask storage. Instead, non-irradiated Zry-4 cladding material with similar thermomechanical treatment as the HBR cladding was obtained from the manufacturer and will be used for baseline comparison of the irradiated materials.

Fuel was chemically removed from the cladding by dissolution in a 70% nitric acid-30% water solution in an ultrasonic bath. Additional cleaning steps using fresh solutions were conducted to further remove fuel and fission-product deposits bonded to the inner surface of the cladding. The corrosion-induced oxide layer on the outer surface of the cladding was partially removed by iteratively applying a diamond file to the outer surface for 5 sec while the cladding was rotated at high speeds, followed by checking the electrical continuity across two probes on the outer surface until a resistance was measured. Metallography showed that a 5-10 μm oxide layer remained. Subsequently, the gauge section of the tensile specimen was machined to the dimensions shown in Fig. 1 by using a wire electro-discharge machine with computer control. Endplugs made of Zircadyne-702 alloy were then arc-welded to the specimen for connecting to the experimental load train, as shown in Fig. 2.

A loading analysis of this weld design has been performed. It was based on the fully annealed Zry-4 material properties in the weldment and the high-fluence, irradiated material properties for the gauge section in Fig. 1. The effects of hydrogen on these material properties were ignored. This analysis found a safety factor of 1.5 for the required load to yield the weldment compared to the required load to fail the gauge section given the specimen design tolerances. However, for cladding materials with a high level of hydrogen, like that of HBR cladding, the grip design may have to differ from the welded one of this study. Further details regarding the axial tensile specimen are discussed elsewhere [9].

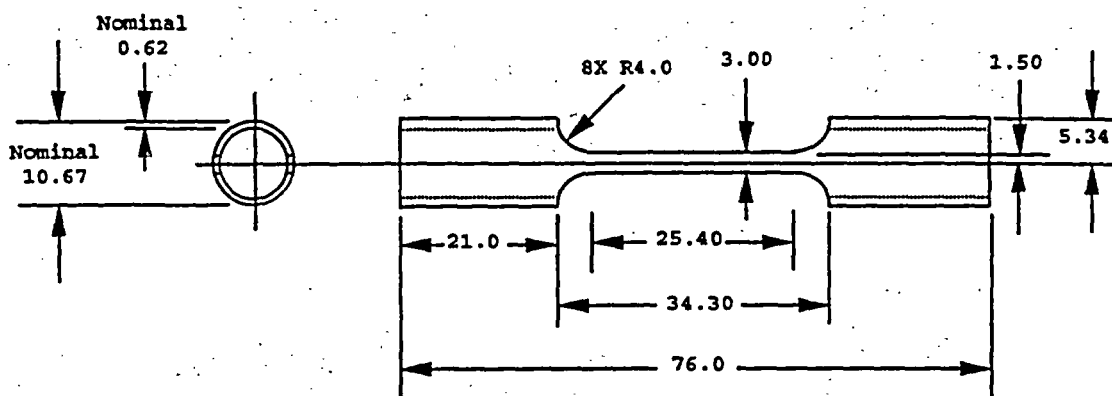


Figure 1 – Dimensions of axial tensile specimen prior to endplug welding (in mm)

Experimental Procedures

The dimensions of the specimen gauge sections were measured at three locations using a video microscope and stereoscope and digital micrometers in order to calculate engineering stress. The length of the gauge section was assumed to be equal to 25.4 mm for calculating engineering strain. The widths and thicknesses of the gauge section at these three locations varied by less than 2% and 5%, respectively. The measured thickness was found to be greater than the cladding thickness (as measured by metallography), suggesting that some oxide remains after the removal process. Therefore, the engineering stress values are a lower bound (assuming the oxide is not load-bearing), including error bars associated with stress values to represent the uncertainties in thickness.

The specimens were then placed in the experimental load train and were tested by using an Instron Model 8511 servo-hydraulic machine located within a radiological glovebox. The Instron permitted strain rates of 0.1-100 %/sec or an actuator displacement of 0.001-1 inch/sec (0.0254-25.4 mm/sec). Load and displacement were monitored with a load cell having a capacity of 2200 lb-force (10 kN) and a linear variable differential transducer (LVDT) with a stroke of 4 inches (10.2 cm), respectively. Two data acquisition programs based on LabVIEW Graphical Programming Language acquired signals from the load cell and LVDT at sampling rates of 1-3000 Hz.

Specimens were tested at room temperature and 400°C (293-673K) in an inert atmosphere (<0.6% oxygen) to mitigate oxidation effects. A Model E4 quad-elliptical, radiant-heating furnace (Research, Inc.) heated the specimen with a Eurotherm Model 1416 temperature controller. A thermocouple-feedback system controlled the heating rate and target temperature. Type K thermocouples were located at fixed positions in the load train, and the temperature of the specimen gauge section was inferred on the basis of previous furnace-calibration measurements. Temperature histories from these thermocouples were recorded by a Cole-Parmer Model 80807-00 digital recorder. Tensile testing started after the target temperature was stable, which was typically within 10 minutes of initiating furnace power.

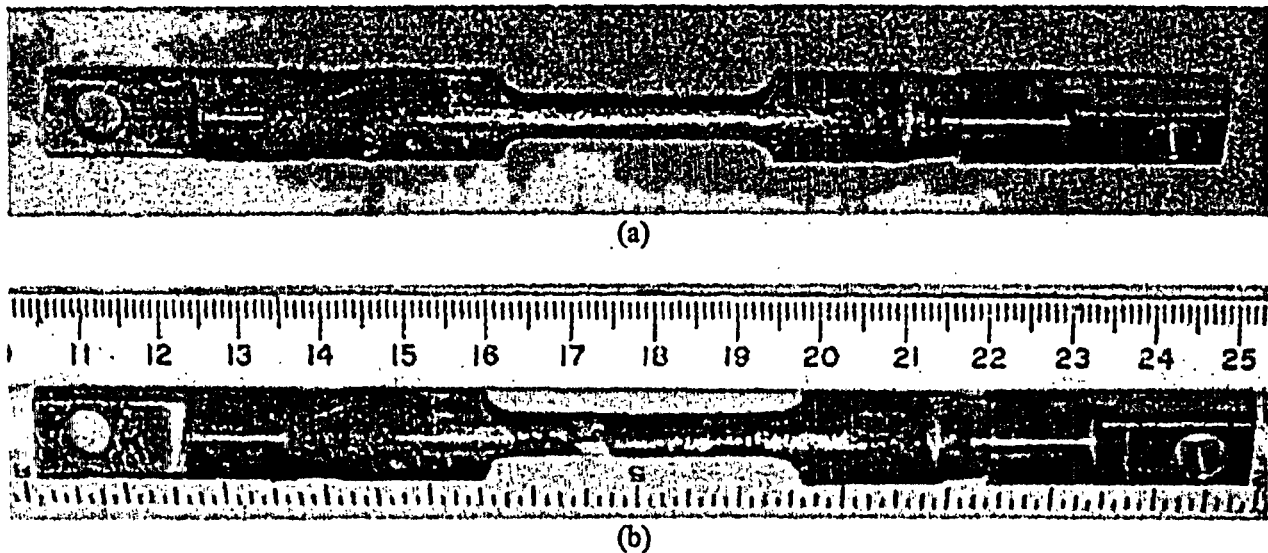


Figure 2 – Image of a Surry axial tensile specimen (a) before and (b) after tensile testing at room temperature and 0.1%/s. Note graphite paint (dark surfaces) was applied to all specimen surfaces, except the gauge sections, for contamination control.

Results

Microstructure

The microstructures of the irradiated cladding were examined using optical microscopy with particular emphasis on hydride orientation and distribution. Figure 3 shows the transverse microstructure in an etched condition of both Surry-2 cladding (36 GWd/MTU) and H.B. Robinson cladding (67 GWd/MTU) at a location above the mid-plane of the fuel column in Grid Span No. 4. Hydrides are predominantly

circumferentially oriented with little or no radial orientation. Hydrides are located more toward the outer or inner surface of the Surry-2 cladding with little hydride precipitation in the interior. The HBR cladding has a higher density of hydrides near the oxide on the outer surface of the cladding. This finding is consistent with the presence of a temperature gradient throughout the discharge history of these materials. Total hydrogen content of Surry-2 and HBR cladding in Grid Span No. 4 was found to be 307 ± 27 and 762 ± 21 wppm, respectively.

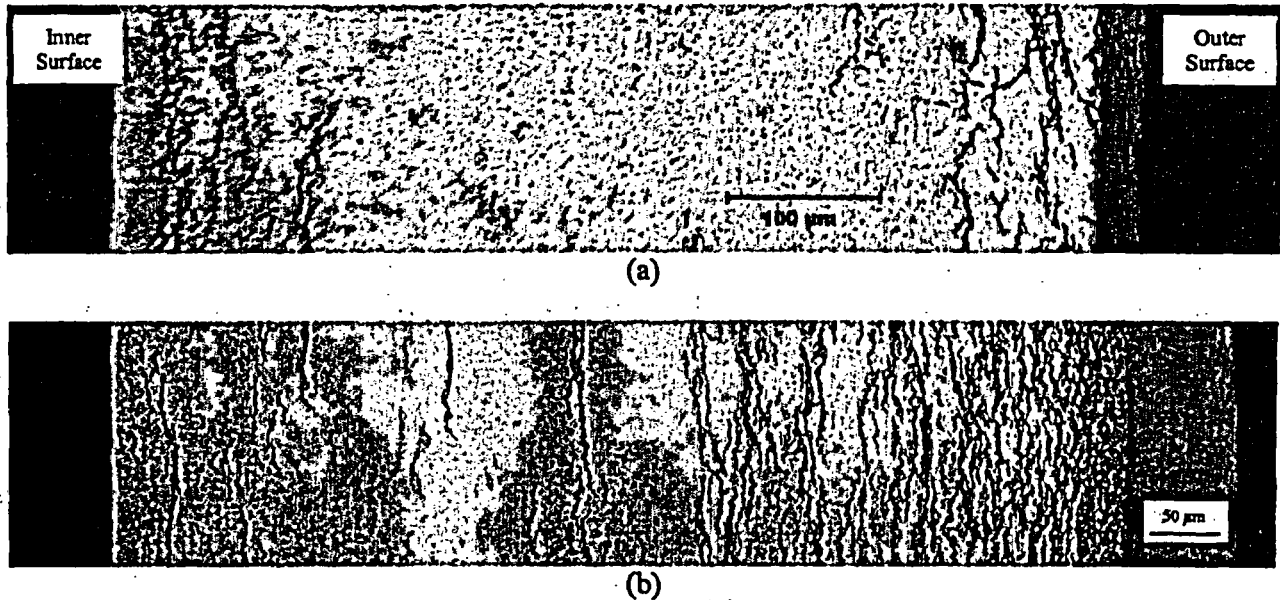


Figure 3 – Transverse metallography in an etched condition showing hydrides in (a) Surry-2 cladding at a location 20 inches (50.8 cm) above the mid-plane of the fuel column and (b) H.B. Robinson cladding at a location 27 inches (68.6 cm) above the mid-plane of the fuel column.

The hydride area fraction (HAF) of H.B. Robinson cladding from Fig. 3b was measured using differential-contrast techniques, and the results are given in Fig. 4; HAF was not measured for Surry-2 cladding. The error bars in Fig. 4 represent the uncertainties associated with the etching process and imaging techniques such that the relative values across the entire thickness are of interest. By area, the cladding within $50 \mu\text{m}$ of the outer surface under the corrosion-induced oxide consists of 50% hydride precipitates and drops below 40% to a depth of $300 \mu\text{m}$. This high-density rim or layer of hydrides may be susceptible to crack initiation during creep deformation and/or the mechanical loading during handling and transportation of spent fuel in dry storage. This point will be discussed further in this paper.

The local hydrogen concentration ($[H]_{local}$) along the radial direction of the cladding is also shown in Fig. 4. $[H]_{local}$ was calculated using HAF with a correction factor to compensate for uncertainties associated with the etching process and imaging techniques and assuming a $\delta\text{-ZrH}_2$ hydride structure. The correction factor was determined by equating the total hydrogen concentration to the numerical

integration of the uncorrected $[H]_{local}$ normalized over the thickness of the cladding. The hydride distributions and calculated hydrogen concentrations are consistent with other studies of Zircaloy-4 irradiated to fuel burnups greater than 44 GWd/MTU [10].

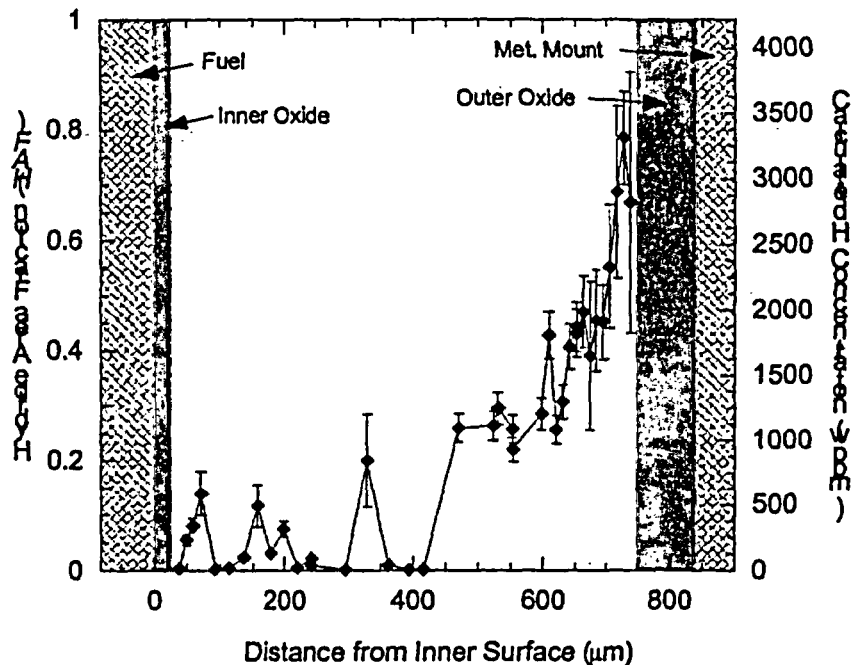


Figure 4 – Hydride Area Fraction (HAF) of the image in Fig. 3b and the corresponding local hydrogen concentration (corrected) for H.B. Robinson cladding with radial average concentration of 762 wppm.

Mechanical Properties

The engineering stress-strain responses for non-irradiated and irradiated cladding materials are shown in Fig. 5. A Surry specimen tested at room temperature and 120%/s resulted in premature deformation and failure due to a flaw in the gauge section produced during specimen fabrication; therefore, the majority of this test was invalid, and the stress-strain response is not presented in Fig. 5. The mechanical properties for non-irradiated and irradiated-and-dry-cask-stored cladding are presented in Fig. 6 and Tables I and II.

Figure 5 shows the radiation-induced hardening of the Surry cladding material as compared to non-irradiated HBR cladding. The data indicate that annealing of radiation-induced defects has not entirely occurred during the thermal-benchmarking studies (see Test Materials). This observation will be discussed later in this paper in light of the fact that the as-manufactured and as-irradiated (but prior to dry-cask storage) properties of Surry cladding are unknown.

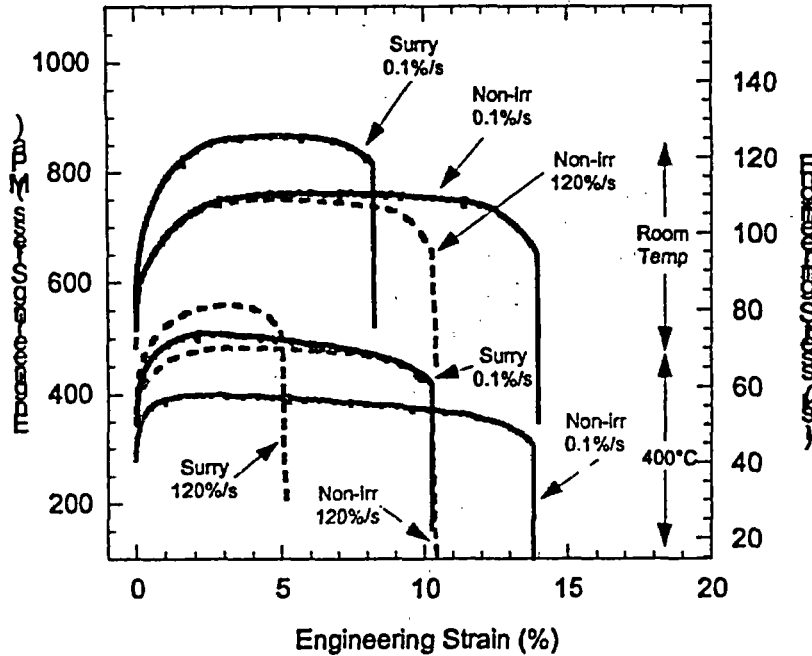


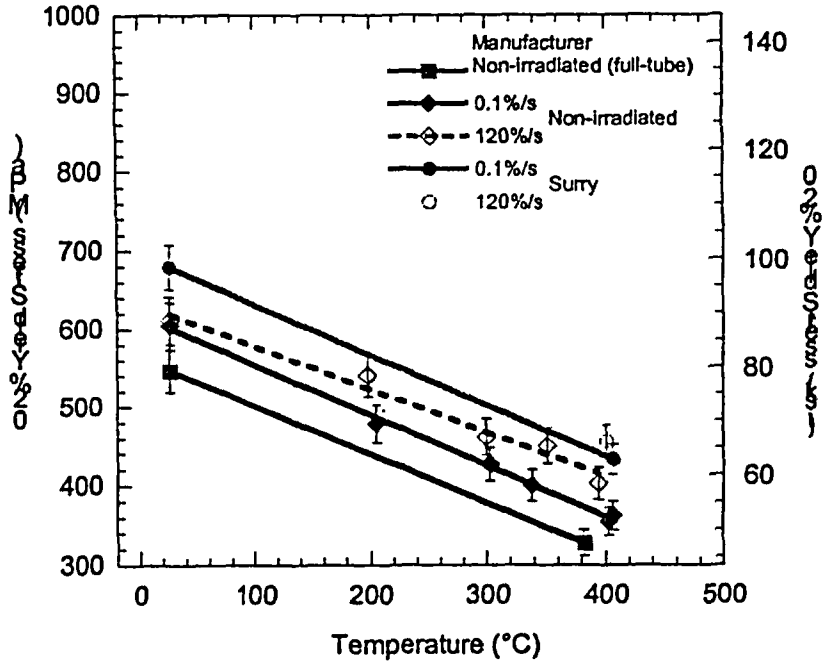
Figure 5 – Engineering stress-strain curves for non-irradiated (Non-irr) and Surry cladding materials for nominal temperatures of 26 and 400°C and nominal strain rates of 0.1 and 120%/s.

The differences of yield and ultimate stress in Figs. 5 and 6 also indicate that Surry cladding has remaining strain-hardening capacity like that of the non-irradiated cladding. However, because of the relatively flat responses (i.e., constant stress over a range of strain in Fig. 5), it is difficult to accurately calculate uniform elongation from Fig. 5 and to model the true stress-true strain curve to the Power Law ($\sigma = K\epsilon^n$) for correlating uniform elongation to the strain-hardening exponent according to the Considère criterion. Figure 6c shows a decrease in uniform elongation with increasing temperature for $\leq 400^\circ\text{C}$. Both the non-irradiated and Surry cladding materials indicate slightly higher uniform elongations at 120%/s compared to 0.1%/s at 400°C and possibly as low as 325°C.

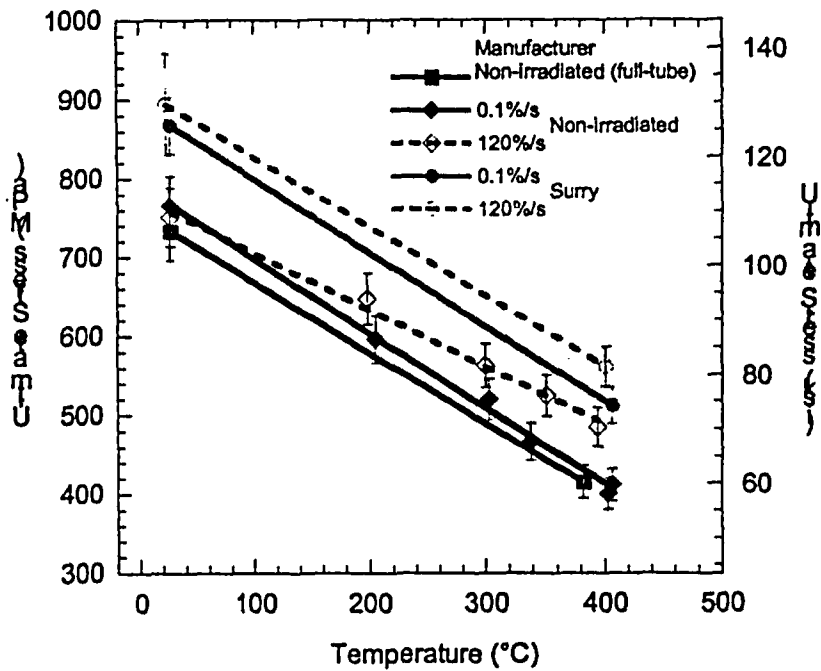
Although more testing is needed, the strain-rate sensitivity at 400°C is found to be 0.01 ± 0.003 for Surry cladding and 0.021 ± 0.004 for non-irradiated cladding. These preliminary results also suggest that strain-rate sensitivity decreases with temperature for both non-irradiated and Surry cladding materials.

Discussion and Future Work

As mentioned earlier, the hydride precipitation in high-burnup fuel cladding may affect the mechanical behavior during severe mechanical stresses caused by handling and transportation accidents. Figure 3b shows the hydride microstructure of HBR cladding after irradiation to a high fuel burnup. Under biaxial

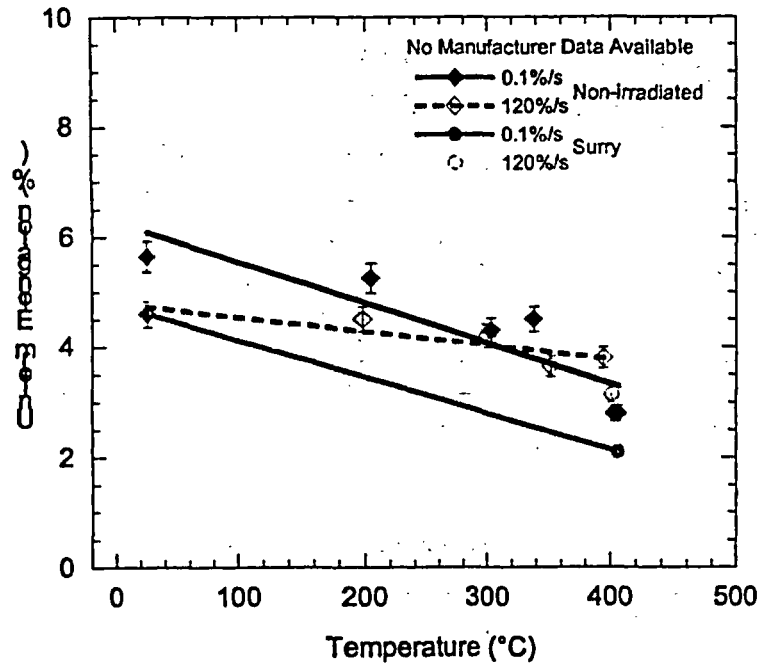


(a)

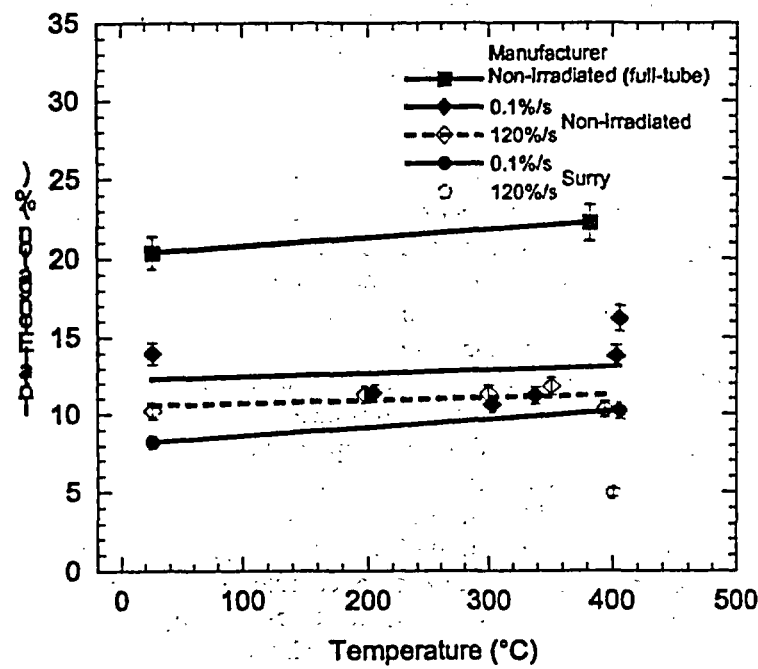


(b)

Figure 6 – Results from axial tensile testing of non-irradiated and irradiated-and-dry-cask-stored Surry cladding materials showing the temperature and strain-rate dependencies of (a) 0.2% yield strength, (b) ultimate tensile strength, (c) uniform elongation, and (d) total elongation.



(c)



(d)

Figure 6 (continued) – Results from axial tensile testing of non-irradiated and irradiated-and-dry-cask-stored Surry cladding materials showing the temperature and strain-rate dependencies of (a) 0.2% yield strength, (b) ultimate tensile strength, (c) uniform elongation, and (d) total elongation.

Table I – Axial tensile properties of non-irradiated Zry-4 cladding

Specimen ID	Temp. (°C)	Strain Rate (%/s)	0.2% Yield Stress (MPa)	Ultimate Stress (MPa)	Uniform Elong. (%)	Total Elong. (%)
ax 1	26±1	0.1	601.8	765.4	5.7	14.0
ax 2	26±1	124	611.2	751.2	4.6	10.4
ax 20	205±7	0.1	471.3	596.0	5.4	11.4
ax 21	198±6	121	530.2	647.2	4.5	11.3
ax 22	303±5	0.1	420.6	519.7	4.4	10.6
ax 23	300±8	121	461.6	562.6	4.3	11.4
ax 24	338±25	0.1	395.3	466.4	4.5	11.1
ax 26	351±5	121	442.6	524.6	3.7	11.8
ax 27	406±5	0.1	359.4	411.7	2.8	16.2
ax 28	394±17	121	403.1	485.0	3.8	10.3

Table II – Axial tensile properties of irradiated-and-dry-cask-stored Zry-4 cladding

Specimen ID	Temp. (°C)	Strain Rate (%/s)	0.2% Yield Stress (MPa)	Ultimate Stress (MPa)	Uniform Elong. (%)	Total Elong. (%)
surry ax 1	26±1	0.1	679.5	868.2	4.6	8.2
surry ax 4*	23±1	119	-	894.8	-	-
surry ax 3	406±6	0.1	432.7	512.2	2.1	10.2
surry ax 5	401±6	124	455.8	561.5	3.5	5.0

* - Denotes majority of test invalidated due to premature failure from fabrication flaw in gauge section.

tension, this localization of hydride precipitates appears to be susceptible to surface crack initiation at small plastic strains. Under more severe states of stress with highly localized deformation, likes those of bending and impact during cask-drop accidents, hydrided cladding may be even more susceptible to cracking. However, after vacuum drying and extended time in dry-cask storage, the distribution of hydrides may evolve from this localization to a more-uniform distribution, which could increase cracking resistance or toughness in high-burnup fuel cladding. Moreover, the potential for precipitation of radially oriented hydrides in cladding like HBR increases the likelihood of low-plasticity cracking. To date, Tsai and Billone [1] have exposed both irradiated-and-dry-cask-stored Surry and irradiated HBR cladding materials to thermal transients with and without an applied hoop stress to investigate the evolution of radial-hydride reorientation and hydride redistribution, respectively. These hydride precipitates may have little effect on the ductility of Zry-4 cladding irradiated to low fuel burnup at the beginning of dry storage, when temperatures may range between 350-400°C and a majority of the hydrogen is in solution. However, as dry-cask-storage temperatures decrease over time, the fraction of hydrogen in the form of hydrides (circumferentially and/or radially oriented) increases, making the cladding more susceptible to low-ductility failure under severe loading. Increased hydrogen contents, like that of Zry-4 cladding irradiated to intermediate and high fuel burnup, further increases this susceptibility over a broader range of storage temperatures. To build upon the results of Tsai and Billone, studies are planned to investigate the mechanical properties of high-burnup fuel cladding with various hydride microstructures (i.e., total hydrogen content and hydride distribution and orientation) under severe loading conditions at temperatures of 25-400°C.

The preliminary tensile results of this study indicate that irradiated-and-dry-cask-stored Surry cladding exhibits higher yield and ultimate strengths and lower elongations as compared to the non-irradiated cladding of this study. Published tensile results of cladding irradiated in HBR to a fast fluence of 4.2×10^{25} n/m² ($E > 1$ MeV) by Bauer and Lowry [11] also show yield and ultimate stresses higher than those of the Surry cladding (7×10^{25} n/m² ($E > 1$ MeV)), which may be the result of different manufacturing treatments. Likewise, MATPRO models [12] indicate that the strength of post-storage Surry is lower than that of the as-irradiated cladding. Although the cold-worked amount of the as-manufactured Surry cladding and the as-irradiated properties are not specified [13], these observations suggest that post-storage Surry exhibits radiation-induced hardening, indicating that partial annealing may have occurred during the thermal benchmarking studies of Surry fuel in dry storage.

As mentioned earlier, the benchmarking exposed the dry-cask-stored Surry cladding to a number of temperature transients with a peak temperature (axially through the cask) of 400–415°C for approximately 144 hours [14]. Tsai and Billone [1] recently found that the microhardness of irradiated HBR cladding (14.0×10^{25} n/m² ($E > 1$ MeV)) was recovered by approximately 54% and 75% compared to that of the as-manufactured HBR cladding after exposure to 420°C for 20 and 72 hours, respectively; the technique of calculating this percentage of recovery is described in detail in [1]. Bauer and Lowry [11] also conducted thermal annealing tests from which, using the technique of [1], we calculate that the recovered yield strength is approximately 54% after exposure to 427°C for 1 hour. Likewise, microhardness measurements of post-storage Surry compared to as-irradiated Turkey Point cladding (5.6×10^{25} n/m² ($E > 1$ MeV)) suggest that slight annealing may have occurred [14]. At any rate, without true baseline properties of as-manufactured and as-irradiated Surry cladding, it is difficult to definitively state whether or not annealing of radiation-induced damage in post-storage Surry has occurred.

Lastly, the effect of creep deformation on the residual mechanical properties is not well understood. Although the tensile results of this study indicate that post-storage Surry cladding (essentially, zero creep strain) show relatively similar strain-hardening capacity as compared to non-irradiated cladding, it is not clear what effect creep strains upwards of 4% would have on this capacity. Additional tests are in the planning stage for performing mechanical tests on cladding that has experienced >1% creep strain.

Conclusions

Preliminary results are presented on the mechanical properties of as-irradiated and dry-cask-stored Zry-4 fuel cladding at intermediate-to-high fuel burnups. At the time of this paper, mechanical properties were limited to Zry-4 cladding irradiated to 36 GWd/MTU in Surry-2 reactor and stored in dry-cask for 15 years. The following observations were made from our study:

1. Uniaxial tensile tests along the longitudinal direction of the cladding tube were conducted at room temperature and 400°C and at strain rates of 0.1 and 120%/s. The properties of dry-cask-stored Surry cladding showed slightly higher strength and reduced elongation as compared to non-irradiated cladding, consistent with radiation-induced hardening. Post-storage Surry cladding exhibited strain hardening comparable to that of non-irradiated cladding.
2. It was not apparent whether thermal annealing of radiation-induced defects in Surry cladding occurred during thermal benchmark tests or dry-cask storage.

Future work is needed to expand the mechanical properties database and to investigate the effect of hydride precipitation (i.e., hydride distribution and orientation and total hydrogen content) and pre-existing creep deformation on the mechanical behavior of Zry-4 irradiated to high fuel burnups for licensing of dry-cask-storage systems.

Acknowledgments

The authors would like to thank H. Scott, R. Meyer, R. Eizinger, and H. Tsai for their technical assistance and J. Dobrzynski, K. Byrne, N. Hins, G. Quick, L. Essenmacher, D.P. McGann, and T. Burtseva for their experimental assistance. This work was supported by the U.S. Nuclear Regulatory Commission, Office of Nuclear Regulatory Research and Spent Fuel Project Office, and the U.S. Department of Energy under Contract Number W-31-109-ENG-28.

References

1. H. Tsai and M.C. Billone, "Cladding Behavior during Dry Cask Handling and Storage," Proceedings of the 2003 Nuclear Safety Research Conference, *to-be-printed*.
2. R.S. Daum et al., "The Influence of a Hydrided Layer on the Fracture of Zircaloy-4 Cladding Tubes," Proceedings of the International Conference on Hydrogen Effects on Material Behavior and Corrosion Deformation Interactions, September 2002, *in-print*.
3. M. Kuroda et al., "Analysis of the Fracture Behavior of Hydrided Fuel Cladding by Fracture Mechanics," Nuclear Engineering and Design, Vol. 203, 2001, pp. 185-194.
4. Interim Staff Guidance – 11, Revision 3, "Cladding Considerations for the Transportation and Storage of Spent Fuel," U.S. Nuclear Regulatory Commission, Spent Fuel Project Office, November 2003.
5. H.M. Chung et al., "Characteristics of Hydride Precipitation and Reorientation in Spent-Fuel Cladding," *Zirconium in the Nuclear Industry: Thirteenth International Symposium*, ASTM STP 1423, G.D. Moan and P. Rudling, Eds., ASTM International, West Conshohocken, PA, 2002, pp. 561-582.
6. E. Siegmann, "Clad Degradation – Summary and Abstraction," DOE Office of Civilian Radioactive Waste Management, ANL-WIS-MD-000008 Rev. 00, December 2000.
7. T.L. Sanders et al., "A Method for Determining the Spent-Fuel Contribution to Transport Cask Containment Requirements," Sandia National Laboratory, SAND90-2406/TTC-1019/UC-820, November 1992.
8. H. Tsai and M.C. Billone, "Characterization of High-Burnup PWR and BWR Rods, and PWR Rods after Extended Dry-Cask Storage," Proceedings of the 2002 Nuclear Safety Research Conference, NUREG/CP-0180, pp. 157-168.
9. R.S. Daum et al., "Mechanical Property Testing of Irradiated Zircaloy Cladding under Reactor Transient Conditions," *Small Specimen Test Techniques: Fourth Volume*, ASTM STP 1418, M.A. Sokolov, J.D. Landes, and G.E. Lucas, Eds., ASTM International, West Conshohocken, PA, 2002, pp. 195-210.
10. F. Nagase and H. Uetsuka, "Hydride Morphology and Hydrogen Embrittlement of Zircaloy Fuel Cladding Used in NSRR/HBO Experiment," Proceedings of the 1997 International Topical Meeting on LWR Fuel Performance, Portland, OR, 1997, pp. 677-684.
11. A.A. Bauer and L.M. Lowry, "Tensile Properties and Annealing Characteristics of H.B. Robinson Spent Fuel Cladding," Nuclear Technology, Vol. 41, 1978, pp. 359-372.
12. D.D. Lanning, C.E. Beyer, and C.L. Painter, "FRAPCON-3: Modifications to Fuel Rod Materials Properties and Performance Models for High-Burnup Applications," U.S. Nuclear Regulatory Commission, NUREG/CR-6534, December 1997.
13. D. Dziadosz et al., "The CASTOR-V/21 PWR Spent-Fuel Storage Cask: Testing and Analysis," Electric Power Research Institute, EPRI NP-4887/PNL-5917, Nov. 1986.
14. R.E. Einziger et al., "Examination of Spent PWR Fuel Rods after 15 Years in Dry Storage," U.S. Nuclear Regulatory Commission, NUREG/CR-6831, September 2003.

LOCA RESULTS FOR ADVANCED-ALLOY AND HIGH-BURNUP ZIRCALOY CLADDING

Y. Yan, T. Burtseva, and M. C. Billone

Argonne National Laboratory (ANL)
Argonne, Illinois, USA

Abstract

LOCA integral test results are reported for high-burnup BWR cladding ramped in steam from 300°C through ballooning-and-burst to 1204°C, oxidized at 1204°C for 5 minutes ($\approx 20\%$ maximum ECR), and slow cooled. The 300-mm fueled LOCA sample was sectioned for fuel and cladding metallographic imaging, as well as hydrogen and oxygen determination. The measured cladding oxide layer thicknesses in the ballooned region were comparable to the ones measured for a nonirradiated Zry-2 sample tested under the same conditions. Thus, the 10- μm corrosion layer, the fuel-cladding bond and the presence of fuel do not protect the cladding from steam oxidation in the ballooned region. However, the hydrogen pickup in the balloon neck region was low (≈ 200 wppm), as compared to measured peak values (≈ 4000 wppm) for the nonirradiated Zry-2 sample. Results are also presented for the oxidation kinetics and post-quench ductility of nonirradiated ZIRLO and M5, as compared to the performance of Zry-4.

Introduction

The LOCA licensing criteria (10 CFR 50.46) limit peak cladding temperature to 2200°F (1204°C) and maximum oxidation (expressed as equivalent cladding reacted, ECR) to 17% to ensure cladding ductility during the emergency-core-cooling-system quench and during possible post-LOCA events (e.g., seismic). In formulating these criteria, it was assumed that the detailed loading modes and magnitudes experienced by the cladding, beyond the thermal stresses induced by rapid cooling, are not well defined. Cladding that retains some plastic ductility has more margin than brittle cladding for surviving quench and post-quench loads without fragmenting. Based on Appendix K of this regulation, the Baker-Just (BJ) correlation is to be used to calculate the metal-water (i.e., steam) reaction. Regulatory Guide 1.157 (1989) allows the use of best-estimate correlations, such as Cathcart-Pawel (CP), to calculate the oxidation rate in steam for $T > 1900^\circ\text{F}$ (1038°C). At 1204°C, the ratio of the BJ-to-CP prediction is ≈ 1.3 . To compensate for the possible effects of high burnup operation (e.g., hydrogen pickup), NRC Information Notice 98-29 (1998) defines total oxidation to include in-reactor corrosion (ECR_{in}), as well as transient steam oxidation (ECR_{t}).

The LOCA integral tests at ANL, using high burnup BWR and PWR fuel-rod segments, are designed to address the adequacy of the embrittlement criteria, of the correlations (CP vs. BJ) used to calculate oxidation, and of the decrease in allowable transient oxidation ($\text{ECR}_{\text{t}} \leq 17\% - \text{ECR}_{\text{in}}$) to compensate for the embrittling effects of hydrogen. In addition to this confirmatory aspect of the research, the fundamental behavior of high-burnup fuel and cladding, exposed to a LOCA transient, is investigated and characterized. For advanced cladding alloys, the post-quench ductility of nonirradiated

samples is characterized vs. ECR and oxidation temperature (1000-1260°C) and compared to the behavior of Zry-4 and Zry-2, for which an extensive database exists in the open literature.

LOCA-relevant research at ANL includes cladding high-temperature steam oxidation studies [1], LOCA integral testing of fueled segments [2], post-quench ductility testing of LOCA integral specimens, and post-quench ductility testing of nonirradiated zirconium-based cladding alloys (Zircaloy-2, Zircaloy-4, ZIRLO, M5, and E110). Two LOCA integral tests with high-burnup BWR samples (from a Limerick fuel rod at 56 GWd/MTU) were completed in 2002: ramp-to-burst in Ar (ICL#1); and ramp through burst in steam to 1204°C followed by 5 minutes of oxidation and slow cooling (ICL#2). Limerick cladding is Zr-lined Zry-2 (GE-11 9x9 assembly design) with $\approx 10 \mu\text{m}$ of in-reactor corrosion, $\approx 0.7 \text{ wt.}\%$ oxygen and $\approx 70 \text{ wppm}$ hydrogen. Burst temperatures and pressures, fuel permeability results, profilometry, and burst-opening characteristics were presented at NSRC-2002 [2]. The full LOCA integral test (ICL#3), including quench from 800°C, is scheduled for early 2004. This sequence is indicated schematically in Fig. 1. After completion of the high-burnup BWR test matrix, high-burnup PWR rods (from the H. B. Robinson reactor) will be subjected to the LOCA test sequence indicated in Fig. 1. In this paper, the results of the destructive examinations of the ICL#2 sample are presented: fuel morphology, cladding inner- and outer-surface oxidation within the ballooned region, and hydrogen pickup near the neck region. Advanced-alloy weight gain data and post-quench ductility data are also presented and compared to the performance of Zry-4 for samples oxidized at 1000°C and 1100°C to CP-calculated ECR values $\leq 20\%$.

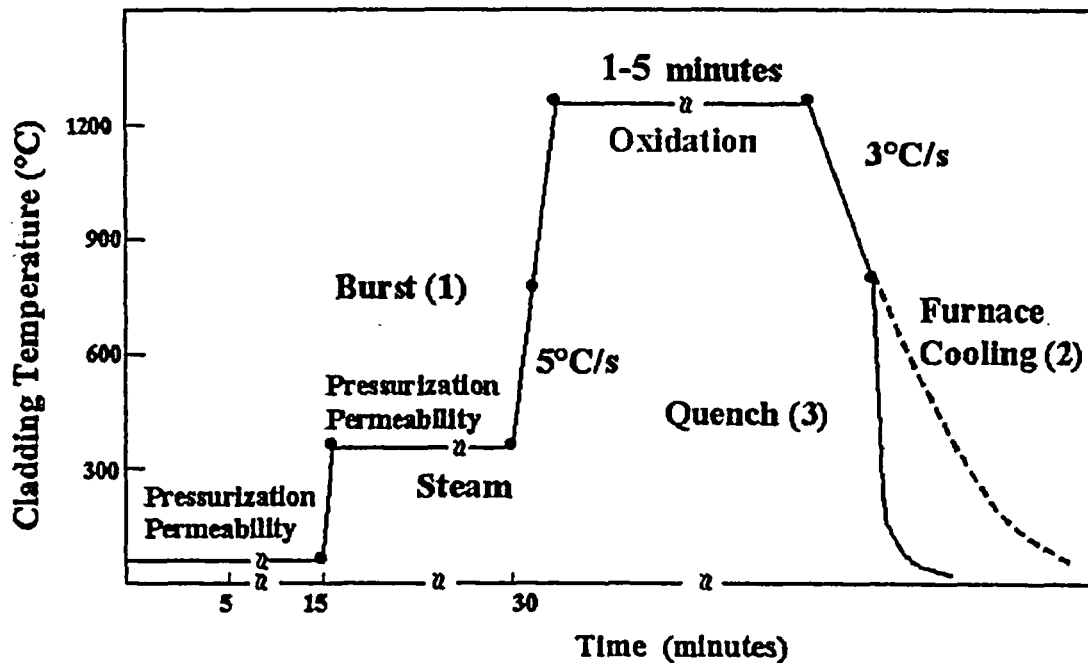


Fig. 1. Temperature histories for the LOCA integral tests: (1) ramp-to-burst test conducted in August 2002; (2) full LOCA sequence up through slow-cooling to 800°C followed by furnace cooling (September 2002); and (3) full LOCA sequence including quench from 800°C to 100°C (2004).

LOCA Out-of-Cell Integral Tests Results: OCL#11 Sample

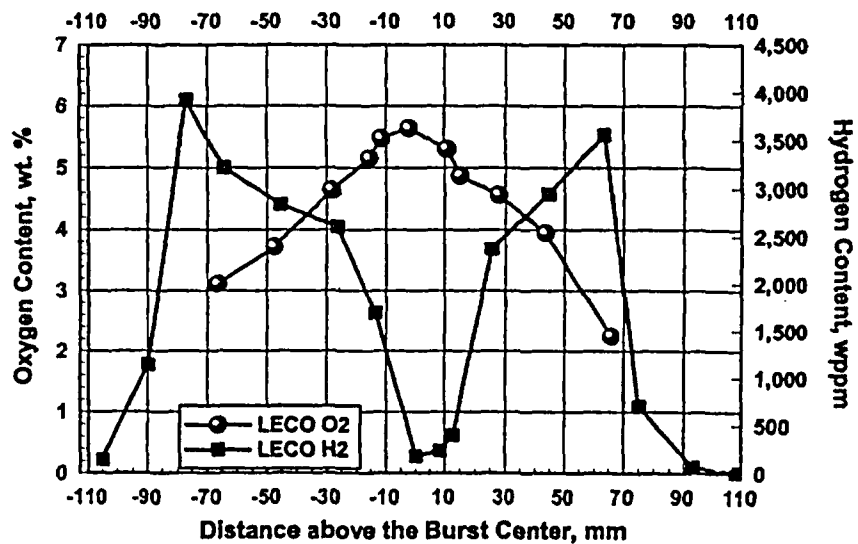
The out-of-cell LOCA integral apparatus contains the same features as the in-cell apparatus: radiant furnace, argon purge system, high-pressure system to internally pressurize the 300-mm-long test sample, steam supply system, and quench system. Both share the same control and data acquisition systems. The out-of-cell apparatus has been used to generate baseline data for nonirradiated Limerick archival cladding: 9×9 Zry-2, 11.18-mm outer diameter (OD), and 0.71-mm wall thickness. Results for the OCL#11 companion test to ICL#2 are discussed here. Figure 1 shows a schematic of the temperature history for this test (5 minutes at 1204°C), with the dashed line indicating furnace cooling at the end of the test from 800°C to room temperature. Nondestructive results and some destructive results for the ICL#11 sample are reported in Ref. 2.

Additional characterization of the axial distribution of oxygen and hydrogen was performed. Figure 2a shows the concentrations of oxygen (L_O) and hydrogen (L_H), measured by the LECO method after the OCL#11 LOCA test. These concentrations are referenced to the weight of the oxidized samples. The data need to be converted to concentrations referenced to the pre-oxidized sample weight in order to determine pickup values during the transient. Following the weight-gain correction, the as-fabricated oxygen ($C_{O_i} = 0.11$ wt.%) and hydrogen ($C_{H_i} = 5$ wppm) contents are subtracted to give oxygen (ΔC_O) and hydrogen (ΔC_H) pickup, referenced to the cladding prior to oxidation. The algorithms for calculating ΔC_O (in wt.%) and ΔC_H (in wppm) from the LECO data (L_O and L_H) are:

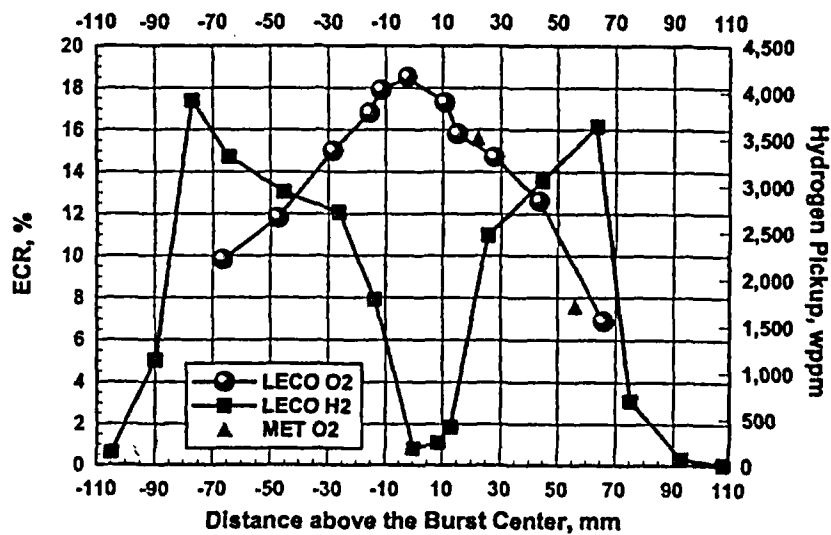
$$\Delta C_O = (L_O - C_{O_i}) / (1 - L_O / 100\%) \quad (1)$$

$$\Delta C_H = (1 + \Delta C_O / 100\%) L_H - C_{H_i} \quad (2)$$

The ECR (in %) is determined from the oxygen pickup: $ECR = 2.85 \Delta C_O$. However, based on benchmarking tests, it has been shown that $\approx 10\%$ of the oxygen is lost during LECO sample preparation. Thus, for the ECR calculation " L_O " is replaced by " $1.1 L_O$ " in Eq. 1. In addition, quantitative metallography, along with the CP models for interface oxygen concentrations and diffusion within the oxide, alpha and beta layers, was used to determine oxygen concentration, weight gain, and the corresponding ECR. The axial distributions of ECR and hydrogen pickup are shown in Fig. 2b. As expected, the oxygen pickup and ECR peak at the center of the burst region where the cladding is thinnest and the oxidation is fully two-sided. The ECR decreases away from the burst center as the cladding wall thickness increases and the degree of inner-surface oxidation decreases. Also, as expected, the hydrogen pickup, due to secondary hydriding, peaks near the balloon neck regions. The magnitude of these hydrogen peaks, however, is larger than previously reported [3] and may depend on the details of ballooning strain profile, burst opening, diameter of pellets (zirconia) inside the cladding, heating method (internal vs. external vs. direct-electrical) and cladding type (lined Zry-2 vs. Zry-4). As these hydrogen peaks, as well as the hydrogen within the balloon region, are potentially embrittling, it is important to determine the magnitude of such effects for high-burnup cladding.



(a)



(b)

Fig. 2. Axial distributions of oxygen, hydrogen and ECR for out-of-cell test OCL#11 sample with nonirradiated Zry-2 cladding: (a) LECO data for concentrations referenced to the weight of the oxidized samples; and (b) data corrected for weight gain and pre-transient concentrations of oxygen and hydrogen. Oxygen concentrations in the oxide and alpha layers are much higher than the measured average value, while hydrogen concentration in the prior-beta layer is much higher than the measured average value.

LOCA In-Cell Integral Test Results: ICL#2 Test Sample

Background

The ICL#2 test was conducted in September 2002. Nondestructive characterization (photography, profilometry, etc.) was completed shortly after the test. The results were reported at NSRC-2002 [2] and are summarized in Table 1. During the post-test handling, some fuel particles (<0.3 mm in size) fell out through the burst opening. The mass of particles collected represents <25% of one fuel pellet. In October 2002, the hot cells were closed for significant maintenance and repair. Movement of radioactive material was required to do the repairs. In preparation for the movement of the ICL#2 sample, the burst area was epoxied. As the epoxy was applied very quickly, some of it spread through much of the balloon region. The consequences of the epoxy are twofold: fuel particles present about a month after post-test sample handling were "frozen" in position; and no hydrogen analyses of the cladding could be performed within the ballooned region because of the high hydrogen content of the epoxy and the difficulty of removing the fuel-embedded epoxy.

Axial Locations of Samples Sectioned for Destructive Evaluation

Figure 3 shows the axial locations from which the fuel and cladding metallography samples and the hydrogen-analysis samples were sectioned relative to the burst opening location and the ballooning strain. Oxygen-analysis samples were also prepared next to the H₁ and H₂ locations.

Fuel Morphology

There is considerable interest in the behavior of high-burnup fuel during a LOCA transient. Prior to the transient, the fuel is tightly bonded to the cladding. During ballooning, the cladding pulls away from the fuel. This allows space for fuel particles (macro-cracked, micro-cracked, and very small particles from the rim layer) to fall into the balloon region. If such movement were to result in a local increase in fuel per unit length, then the higher decay heat per unit length would cause an increase in cladding oxidation temperature and maximum ECR in the burst region. Also, if the fuel-cladding bond material moves with the cladding, such a layer could slow down the initial steam oxidation rate and could protect the cladding from the large hydrogen absorption observed in tests with bare-wall, nonirradiated cladding (see Fig. 2). As methods that could be used to freeze the fuel particles in place (e.g., epoxy) conflict with cladding characterization, the ANL program is more focused on the details of cladding oxidation, hydriding, and ductility than on fuel behavior. This was certainly the case for the ICL#2 sample, as no attempt was made to prevent fuel fallout during handling. In future tests, the burst area will be taped following the test to minimize fuel fallout and the samples will be gamma-scanned – prior to other nondestructive characterization – to determine the axial distribution of fuel in and beyond the balloon region. For ICL#2 axial locations with little-to-no permanent strain, metallographic images of the fuel most likely represent the condition of the fuel at the end of the LOCA test. For the ICL#2 balloon region, it is likely that significant redistribution of fuel particles took place between the end of the LOCA test and the filling of this region with epoxy.

Table 1 Comparison of Results from In-Cell Test ICL#2 and Out-of-Cell Test OCL#11. Samples were ramped from 300°C to 1204°C in steam, held for 5 minutes at 1204°C, cooled at 3°C/s to 800°C and furnace-cooled to room temperature.

Parameter	ICL#2	OCL#11
Environment	Steam	Steam
Hold Temperature, °C	1204	1204
Hold Time, minutes	5	5
$(P_g)_{max}$, MPa	8.87	8.61
T at $(P_g)_{max}$, °C	728	680
Burst Pressure (P_B), MPa	≤ 8.01	≤ 7.93
Burst Temperature (T_B), °C	≥ 750	753±22
Burst Center Relative to Specimen Midplane, mm	+25	+35
Burst Shape	Oval	Dog Bone
Burst Length, mm	14	11
Max. Burst Width, mm	3.5	1
Length of Balloon, mm	90	140
$(\Delta D/D_o)_{max}^a$, %	39±10	43±10
Reference Minimum Wall Thickness for ECR, mm	≈ 0.514	≈ 0.500
Maximum ECR, %		
Calculated	≈ 20	≈ 20
Measured	---	19

^aFrom profilometry at 0° and 90° relative to burst opening

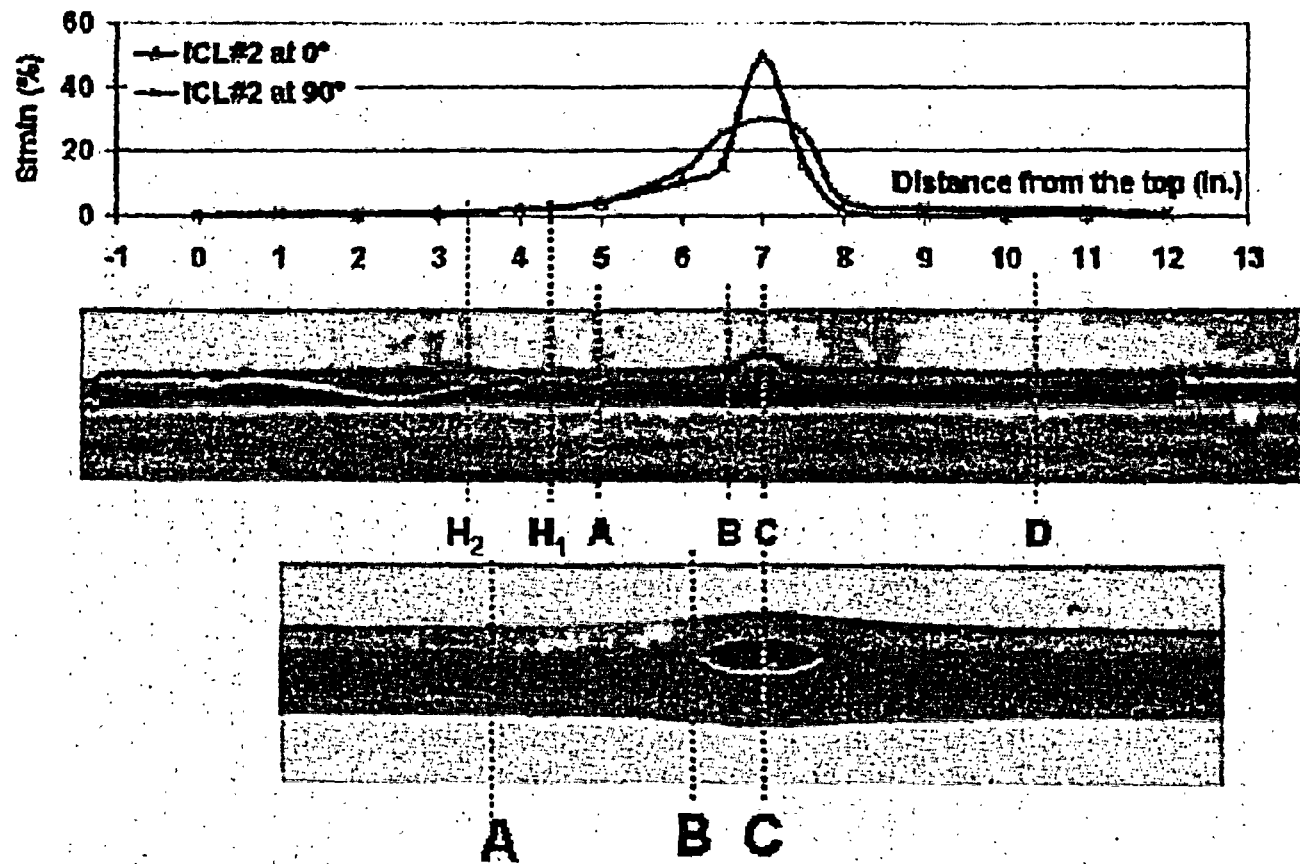


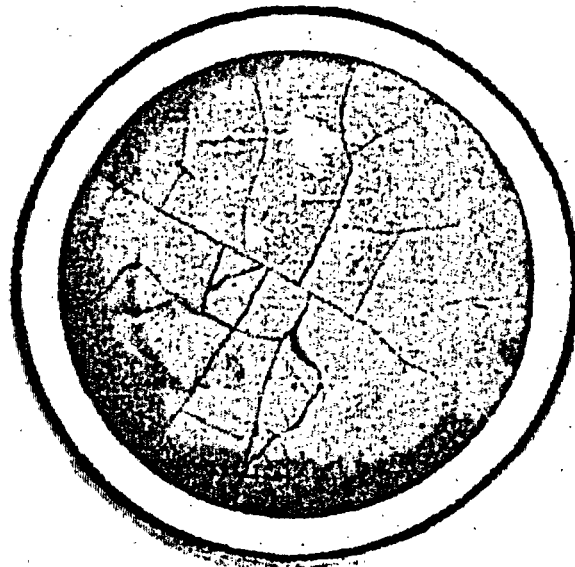
Fig. 3. Sectioning diagram for high-burnup-BWR LOCA sample ICL#2. Hydrogen, as well as oxygen, measurements were taken at locations H₁ and H₂.

Figure 4 shows the fuel structure ≈ 130 mm below the burst center (45 mm above the bottom endcap), as compared to the fuel structure of the as-received Limerick fuel. The structures are similar, except that the post-LOCA fuel shows a ring of circumferential tearing about mid-radius. This tearing may have occurred as the cladding tried to move a small distance (0-0.1 mm) away from the fuel and/or because of the effects of fission-product gases on the fuel (see dark ring near mid-radius for the pre-LOCA fuel in Fig. 4a). Figure 5a shows a high-magnification of a small area of the mid-radius of the Limerick pre-LOCA fuel with the high concentration of fission gas within the grains, as well as some fission gas bubbles on grain boundaries. Figure 5b shows an enlargement of the region of post-LOCA fuel with the circumferential tearing.

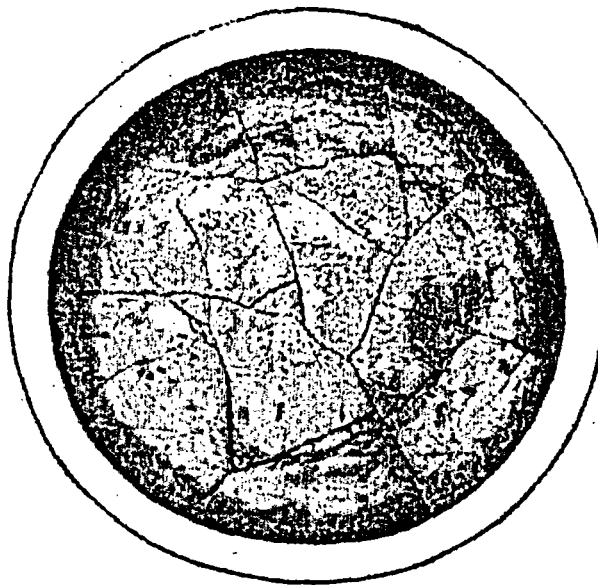
Figure 6 shows low-magnification images of the fuel structure at: (a) ≈ 50 mm above the burst (axial position A in Fig. 3) and (b) ≈ 12 mm above the burst center (axial position B in Fig. 3). At ≈ 50 mm above the burst, the circumferential tearing is enhanced as compared to the ≈ 130 -mm location, most likely due to the larger cladding strain. Some fuel fallout, which may have occurred during cutting is observed, although this region of the fuel column was embedded in a soft epoxy prior to cutting. Smaller fuel particles are also observed. In Fig. 6b, a wide range of fuel-particle sizes is observed, although these particles and fuel chunks are not co-planar. The particles and chunks are held in place by soft epoxy. Because this photograph was taken after extensive handling of the sample, resulting in axial redistribution of particles and fuel fallout through the burst opening, it does not represent the fuel condition near the burst center during the LOCA test or after cooldown. The most that one can glean from such a picture is that the wide range of fuel-particle sizes would allow some fuel to fall from < 50 mm above the burst center to the burst region.

Cladding Metallography

Low-magnification photographs were taken at 10 circumferential locations of the burst midplane and pieced together (see Fig. 7) to obtain an image of the metal (oxygen-stabilized alpha and prior-beta) thickness vs. circumferential location. The inner and outer oxide layers are not visible in Fig. 7. Also, the burst tips, which are very thin and heavily oxidized are likely lost in the cutting process. However, the low-magnification image is consistent with the higher-quality images taken of the companion out-of-cell sample (OCL#11): thin metal wall near the burst opening, which increases in thickness as the circumferential position increases to 180° from the burst opening. High-magnification micrographs were obtained of the inner and outer cladding regions away from the burst tips. These are shown in Figs. 8a (outer surface) and 8b (inner surface). The thickness of the outer-surface oxide layer is consistent with CP-calculated oxide thickness and consistent with the results of oxidation tests conducted on undeformed cladding samples [2]. The results demonstrate that the ≈ 10 - μm -thick corrosion layer is not protective with regard to steam oxidation. The inner-surface oxide layer is wavy in appearance, which may be due to the high hydrogen-to-steam ratio within the burst region. It is comparable in thickness to the outer-surface layer, which suggests that the fuel-cladding bond layer is also non-protective with regard to steam oxidation. Alpha incursions into the prior-beta layer are observed at this location, just as they were observed in the oxidation tests [1,2]. These most likely formed during the 3°C/s cooling from 1200°C to 800°C . They represent regions with higher oxygen content than the remaining prior-beta material and lower oxygen content than the alpha layer formed at 1200°C .

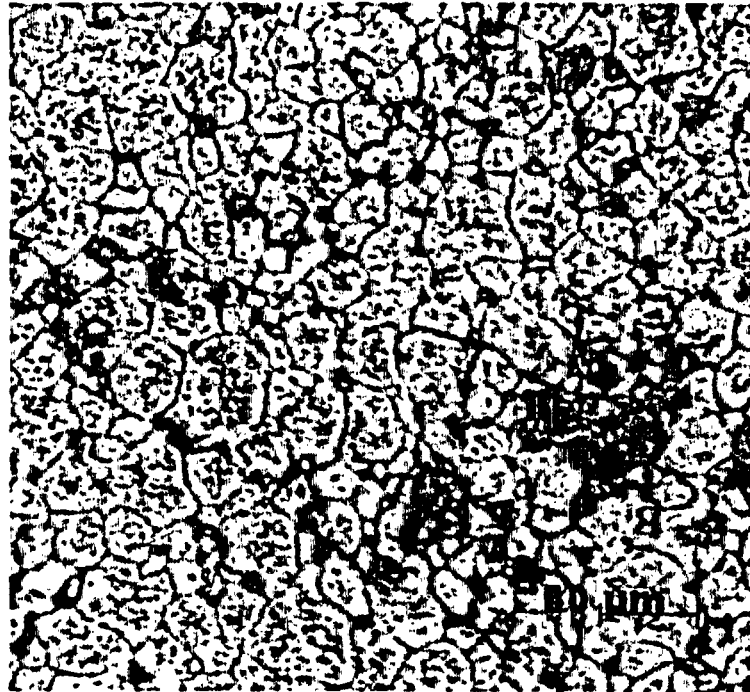


(a)



(b)

Fig. 4. Low-magnification images of the Limerick fuel prior to LOCA testing (a) and after LOCA test ICL#2 (b). The location of the pre-LOCA fuel is 180 mm from the LOCA sample. The post-LOCA fuel is ≈ 130 mm below the ICL#2 burst center and ≈ 45 mm from the lower endcap – axial location D in Fig. 3.

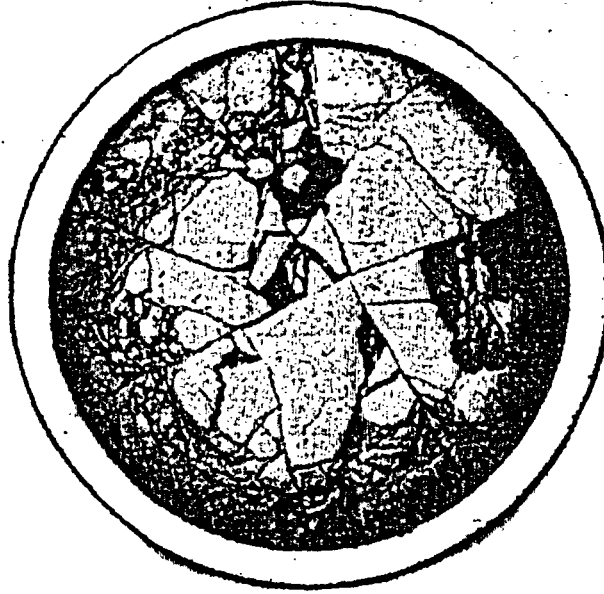


(a)



(b)

Fig. 5. High-magnification of pre-LOCA-fuel mid-radius showing high concentration of fission gas within the grains (a) and enlargement of the post-LOCA fuel mid-radius region showing circumferential tearing (b) – axial location D in Fig. 3.



(a)



(b)

Fig. 6. Fuel morphology of ICL#2 sample at ≈ 50 mm above burst center (a) – axial location A in Fig. 3 – and ≈ 12 mm above burst center (b) – axial location B in Fig. 3. Cladding diametral strains are 2-4% for the Fig. 6a cross-section and 15-25% for the Fig. 6b cross-section.

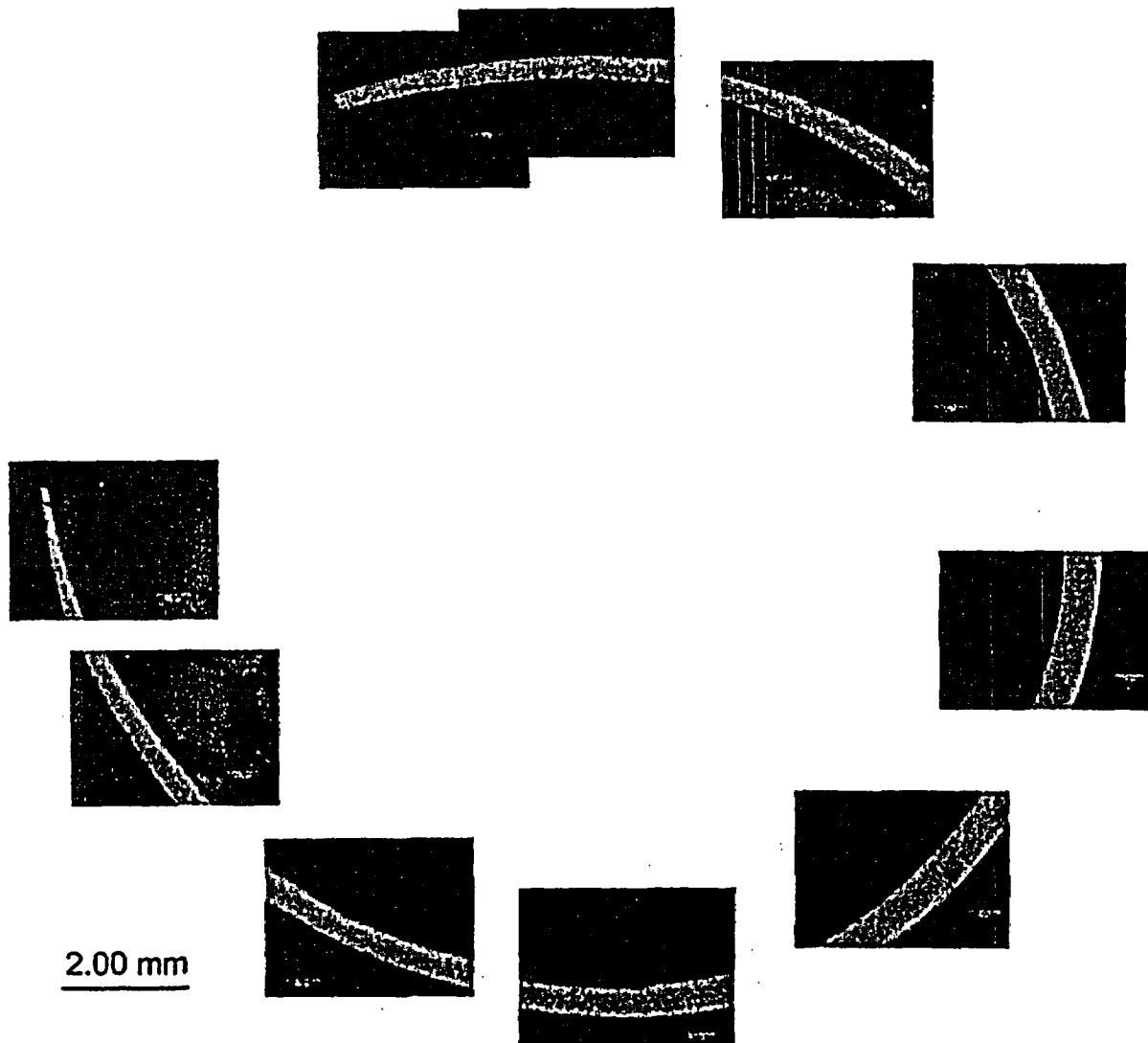
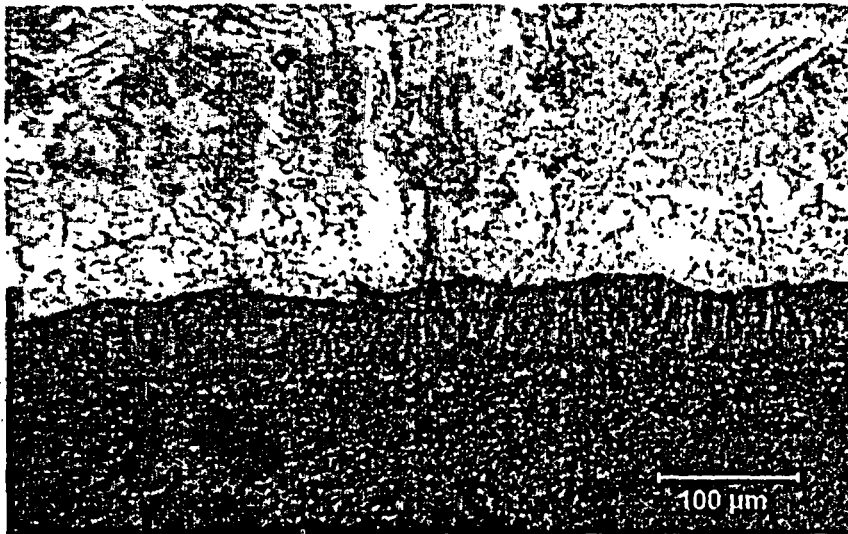


Fig. 7. Low-magnification composite of the cladding metal (alpha and prior-beta) cross-section at the burst midplane of the ICL#2 sample – axial position C in Fig. 3. Cladding diameter increase from burst opening to 180° from burst opening is ≈50%. Diameter increase ±90° from burst opening is ≈30%. Fuel particles embedded in epoxy can also be observed.



(a)



(b)

Fig. 8. Outer (a) and inner (b) cladding oxide layers $\approx 180^\circ$ from burst center – axial position C in Fig. 3. These etched samples show oxygen-stabilized alpha incursions into the prior-beta layer.

More detailed metallography was obtained at axial position B (≈ 12 mm above the burst midplane). Figures 9a-b show the images of the arc segment after etching. Double-sided oxidation is evident at this location, with the inner-surface oxide thickness \geq the outer-surface oxide thickness. Eight such regions were imaged around the cladding at axial location B, and quantitative metallography was performed to determine the distribution of cladding thickness, outer-surface oxide layer thickness and inner-surface oxide layer thickness with respect to circumferential orientation. These results (b) are compared in Fig. 10 to the baseline results obtained for the nonirradiated Zry-2 sample used in the OCL#11 test (a). In order to focus on the transient oxidation of the high-burnup LOCA sample (ICL#2), $10 \mu\text{m}$ was subtracted from the total outer-surface oxide-layer thickness to generate the transient oxidation data. Notice that the oxide layer thicknesses shown in Fig. 10 were multiplied by 7 to allow them to be plotted on the same scale as the wall thickness. For the OCL#11 sample, the oxide layers formed on the inner- and outer-cladding surfaces are consistent with respect to circumferential orientation. Average values for outer- and inner-surface oxide layer thicknesses for OCL#11 are $59 \mu\text{m}$ and $56 \mu\text{m}$, respectively. The weight gain and ECR were determined to be 11.4 mg/cm^2 and 15.7% , respectively, while the prior-beta layer thickness was measured to be $398 \mu\text{m}$. The high-burnup sample differs somewhat in that there is more circumferential variation in the inner-surface oxide-layer thickness. The average outer- and inner-surface oxide layers are $55 \mu\text{m}$ and $57 \mu\text{m}$, respectively. The weight gain and ECR were determined to be 10.5 mg/cm^2 and 14.9% , respectively, while the prior-beta layer thickness was measured to be $435 \mu\text{m}$ for the ICL#2 sample at this location. Although the axial locations with respect to the burst center are slightly different (18 mm above for OCL#11 and 12 mm above for ICL#2), the values for oxide layer thickness, weight gain, ECR, and prior-beta layer thickness are remarkably close. These results indicate that close to the burst region the steam oxidation of nonirradiated and high-burnup Zry-2 samples is essentially the same. No high-burnup effects were observed.

Secondary Hydriding

Hydrogen is released during inner-surface oxidation within the balloon region, particularly near the burst region. Because of the flow resistance of the small burst opening, a relatively high fraction of this hydrogen remains within the sample and migrates up and down the sample towards the balloon neck-and-beyond regions. For the nonirradiated samples, there is little resistance to this migration and the bare cladding inner surface absorbs a large amount of hydrogen (see Fig. 2). Qualitatively, the same behavior would be expected for fresh and low-burnup fuel cladding. For high-burnup fuel, the axial extent of hydrogen that could come in contact with the cladding would be limited by the presence of the fuel, and the local hydrogen absorption would be limited by the fuel-cladding bond layer. Although this layer has been shown to be non-protective with regard to steam oxidation, it is of great interest to determine whether or not it is protective with respect to hydrogen diffusion into the cladding. Hydrogen and oxygen concentrations were measured for ICL#2 samples sectioned from ≈ 70 mm (axial position H_1 in Fig. 3) and ≈ 90 mm (axial position H_2 in Fig. 3) above the burst center. The raw data give oxygen and hydrogen concentrations of $L_O = 2.92 \text{ wt.}\%$ and $L_H = 230 \text{ wppm}$, respectively, at H_1 and $L_O = 2.78 \text{ wt.}\%$ and $L_H = 284 \text{ wppm}$, respectively, at H_2 . Using these data, hydrogen pickup and ECR values were determined to be: $\Delta C_H = 167 \text{ wppm}$ and $\text{ECR} = 7.4\%$ at H_1 , and $\Delta C_H = 220 \text{ wppm}$ and $\text{ECR} = 6.9\%$ at H_2 . These results are compared in Fig. 11 to the peak hydrogen-content locations and values for OCL#11, relative to the average diametral strain. It is clear that the high-burnup-cladding values are significantly lower than the nonirradiated-cladding values at comparable cladding strain values. This shows a significant difference in the behavior of high-burnup-fueled vs. nonirradiated cladding. More data are needed to map out the axial distribution of hydrogen in post-LOCA high-burnup cladding.

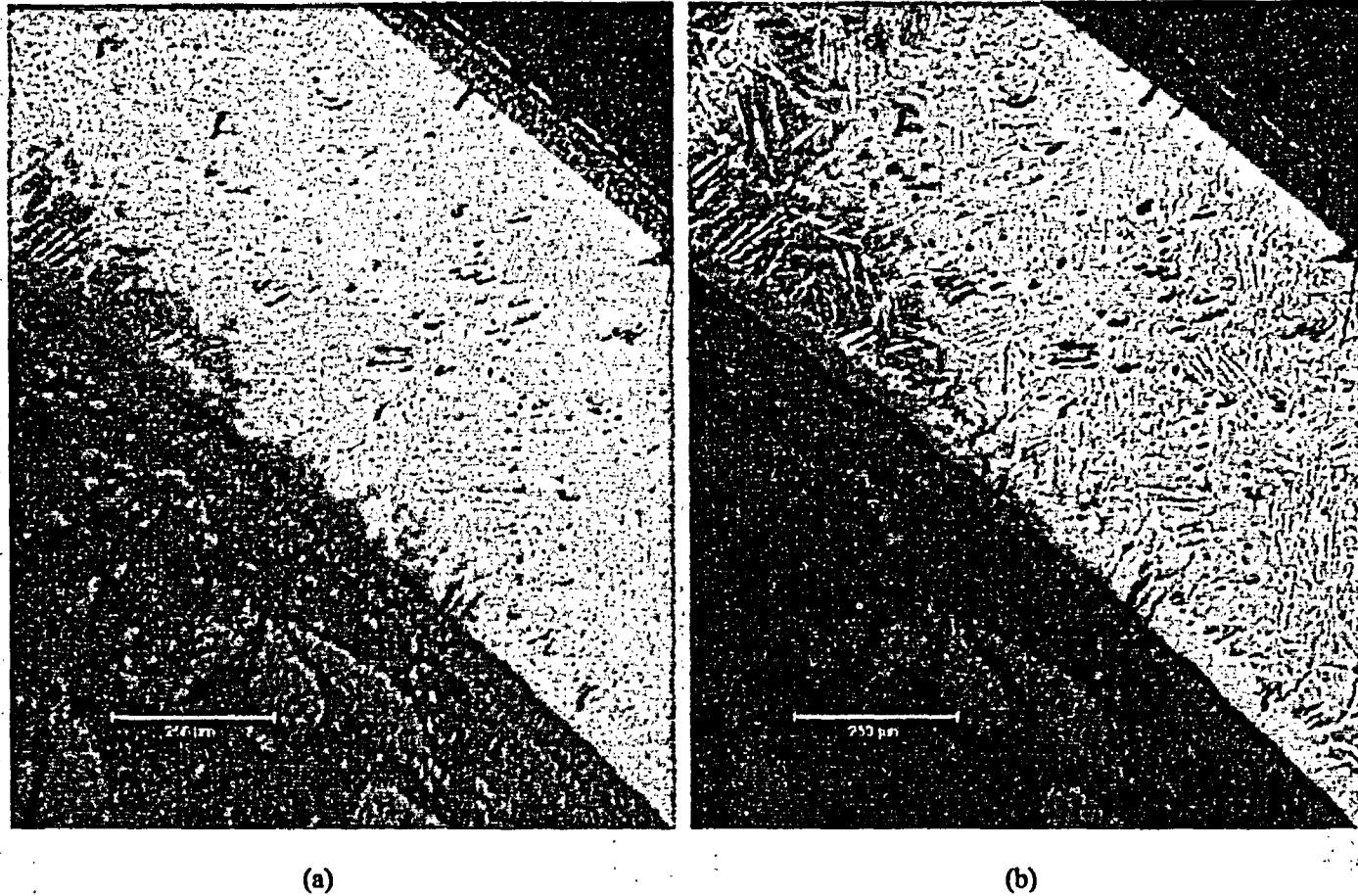


Fig. 9. Metallographic images of the cladding ≈ 12 mm above the burst midplane. The micrograph (a) shows good definition of the inner- and outer-surface oxide layers; and the micrograph (b) shows well-defined alpha layers that formed at 1200°C and large prior-beta grains surrounded by oxygen-stabilized alpha layers formed during slow cooling to 800°C .

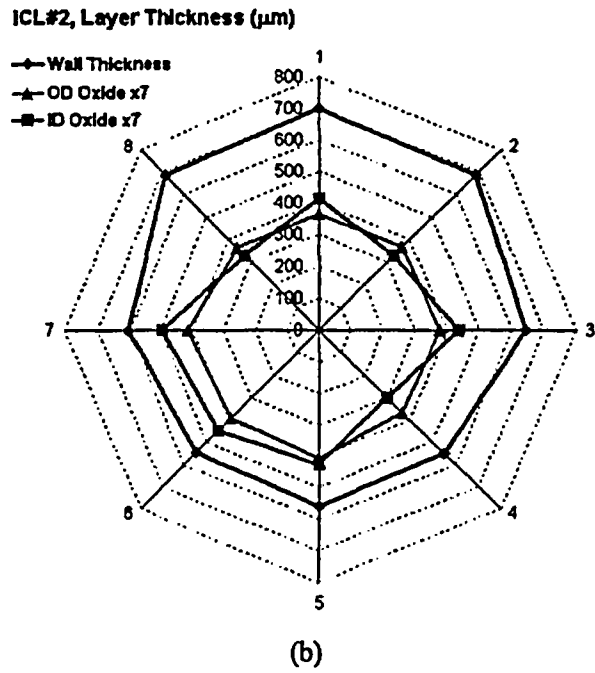
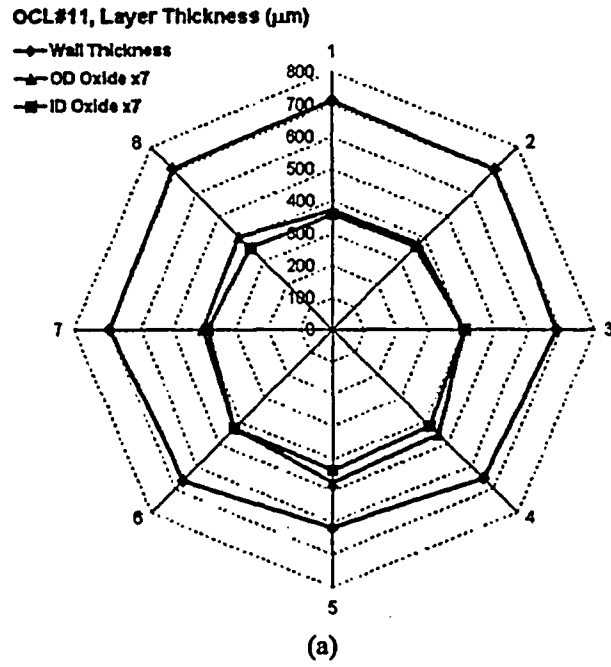


Fig. 10. Circumferential variation in post-LOCA cladding wall thickness, outer-surface (OD) oxide-layer thickness, and inner-surface (ID) oxide layer thickness for : (a) nonirradiated OCL#11 Zry-2 sample 18 mm above burst center; and (b) high-burnup ICL#2 Zry-2 sample 12 mm above burst center.

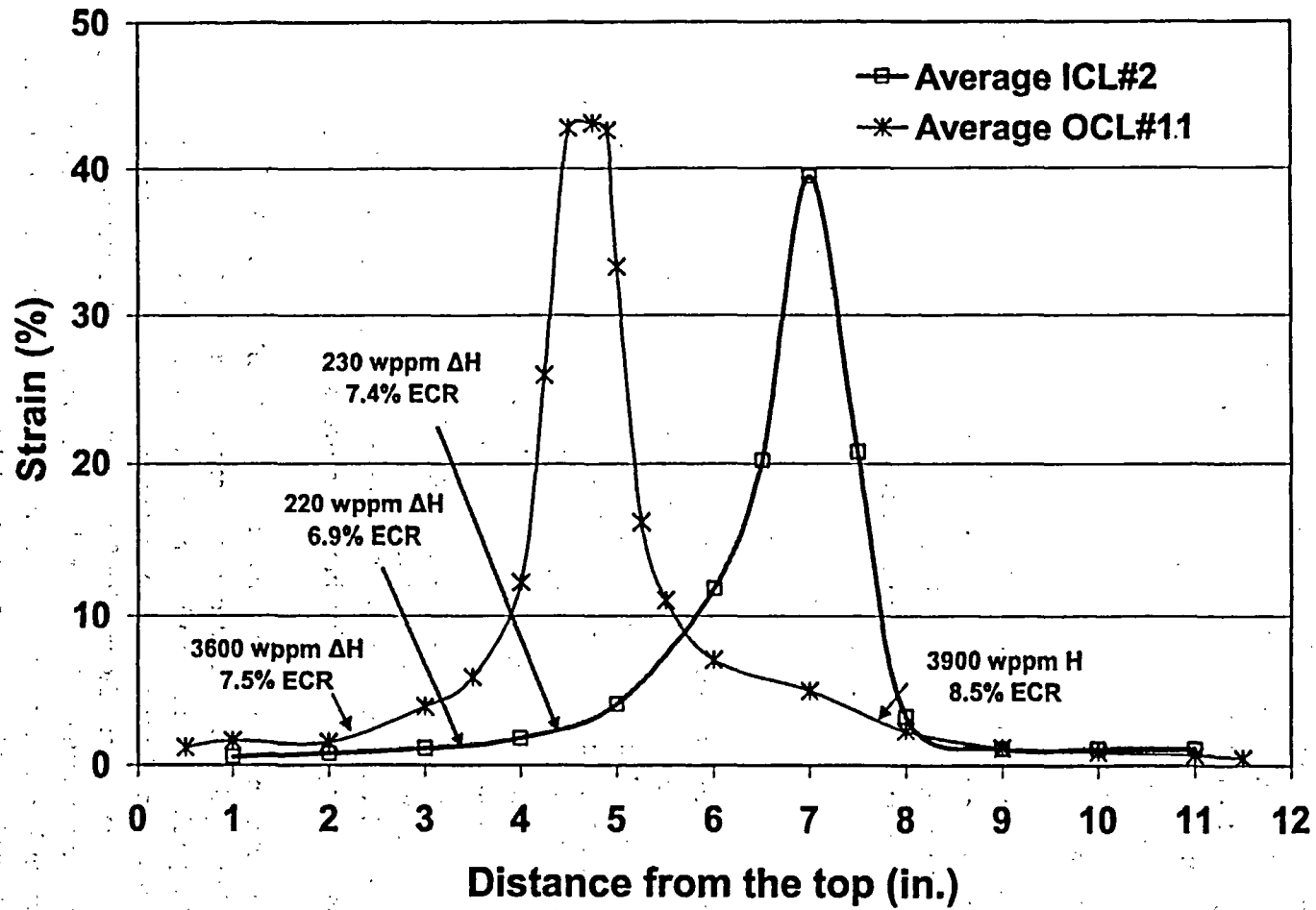


Fig. 11. Hydrogen pickup and ECR distributions for post-LOCA ICL#2 high-burnup-fueled Zry-2 sample as compared to hydrogen peaks in post-LOCA OCL#11 nonirradiated Zry-2 sample (see Fig. 2).

Advanced-Alloy Cladding Post-Quench-Ductility Results

The purpose of this program is to determine the post-quench ductility of advanced cladding alloys ZIRLO and M5, as compared to the post-quench ductility of Zry-4. While extensive literature data are available for traditional Zircaloy claddings (Zry-4 and Zry-2), relatively little data have been published for ZIRLO and M5. Also, the published data [4, 5] for advanced alloys were generated in different laboratories by very different methods. In this program, all samples are oxidized in the same apparatus at the same ramp rates, hold times, and cooling rates (slow-cooled to 800°C and water-quenched). The 25-mm-long samples are exposed to two-sided steam oxidation prior to cooling. Also, the samples are compressed in the same Instron machine, and the load-displacement data are analyzed by a common method to determine ductility.

The Zry-4 and ZIRLO tubing (17×17 PWR) provided by Westinghouse has an outer diameter of 9.50 mm and a wall thickness of 0.57 mm. The M5 tubing (17×17 PWR) provided by Framatome has an outer diameter of 9.50 mm and a wall thickness of 0.61 mm. Table 2 summarizes the test matrix for oxidizing the samples prior to ring-compression, post-quench ductility testing. The times listed are the equivalent isothermal times at the test temperature to give Cathcart-Pawel (CP) calculated ECR values of 5, 10, 15, 17, and 20%, for an assumed wall thickness of 0.57 mm. Actual ECR values vary depending on the measured weight gain and non-oxidized wall thickness for each sample.

Following oxidation and quench, 8-mm rings are cut from near the middle of the 25-mm-long samples. Ring compression tests are performed at room temperature and a cross-head displacement rate of 2 mm/min. The load-displacement curves are analyzed by the traditional offset-displacement method. The offset displacement, which is often used as the measure of permanent displacement, is normalized to the outer diameter (9.50 mm) to give a nominal plastic hoop strain. Samples that exhibit offset strains >2% are considered to be ductile. However, for samples with ≤2% offset strain, another method is used to better determine permanent deformation and ductility. For this second method, the sample is unloaded after the first significant load drop indicating through-wall failure along the length of the sample. The post-test diameters along and normal to the loading direction are measured directly and compared to the pre-test diameter to give a direct measure of permanent strain. For these low-offset-strain samples, the permanent diameter change in the loading direction is used as the direct measure of ductility.

Oxidation and quench have been completed for Zry-4, ZIRLO and M5 samples oxidized at 1000°C and 1100°C. Weight gains were recorded for each sample, normalized to the oxidation surface area, and compared to CP predictions (in mg/cm²). Ring-compression tests have also been completed on 8-mm-long rings cut from the oxidation samples. Metallography, microhardness, and hydrogen-content analyses are in progress for the highest ECR samples for each alloy. This characterization is performed to allow correlation between the ductility observed in the ring compression test and the material structure (e.g., prior-beta-layer thickness, extent of alpha incursions into this layer, etc.) and the hydrogen content. Results for E110 oxidized at 1000°C are reported in Ref. 6.

Table 2 Test Matrix for Oxidation of Samples for Post-Quench Ductility Tests. The times and ECR values listed correspond to those calculated using the Cathcart-Pawel weight gain correlation, a nominal wall thickness of 0.57 mm, and two-sided isothermal oxidation in steam. The relationship between ECR (%) and normalized weight gain (Δw in mg/cm^2) is $\text{ECR} = 1.538 \Delta w$ for 0.57-mm-thick cladding samples.

Temperature °C	ECR %	Equivalent Oxidation Time s
1000	5	210
	10	841
	15	1892
	17	2430
	20	3364
1100	5	67
	10	266
	15	599
	17	769
	20	1065
1200	5	25
	10	99
	15	222
	17	285
	20	394
1260	5	14
	10	58
	15	130
	17	167
	20	231

Weight Gain Kinetics

The weight gain data for Zry-4, ZIRLO and M5, oxidized at 1100°C, were in excellent agreement with each other and the CP-predicted weight gain values. These results are consistent with published data for ZIRLO vs. Zry-4 [4] and M5 vs. Zry-4 [5]. At the highest test time, measured values were 13.2 mg/cm^2 (Zry-4), 13.7 mg/cm^2 (ZIRLO), and 13.3 mg/cm^2 (M5), as compared to the predicted value of 13.0 mg/cm^2 . Using the measured wall thickness for each alloy, these weight-gain values convert to "measured" ECR values of 20.3% (Zry-4), 21.1% (ZIRLO) and 19.1% (M5).

After oxidation at 1000°C, the weight gain of ZIRLO tracks well with the CP-predicted values up through 17% ECR and is low by only 10% at the highest test time (≈3400 s). Beyond ≈10% CP-ECR, the Zry-4 weight-gain values are 9-13% higher than the CP-values. Consistent with previous work [5], the M5 weight gain is ≈30% lower than the CP prediction and ≈36% lower than the Zry-4 data point at the highest test time. The ECR values determined from the weight gains and the as-received cladding wall thicknesses are: 22.4% (Zry-4), 18.0% (ZIRLO) and 13.3% (M5). In order to further explore these differences in weight gain, metallography was performed on as-polished and etched samples oxidized at 1000°C for ≈3400 s. Figure 12 shows a comparison between as-polished samples of Zry-4 and ZIRLO after this long test time. The inner/outer oxide layer thicknesses are 83-μm/82-μm for Zry-4 and 57-μm/66-μm for ZIRLO, based on quantitative analysis of eight arc segments around the circumference of the samples. The ratio of total oxide thickness is ZIRLO/Zry-4 = 0.75, while the ratio of weight gains is 0.80. Thus, the higher weight gain of Zry-4 at 1000°C and ≈3400 s is a direct result of the thicker oxide layers formed on the Zry-4 inner and outer surfaces.

Figure 13 shows a comparison between as-polished Zry-4 and M5 samples oxidized at 1000°C for ≈3400 s. Based on averaging the oxide layer thicknesses for eight circumferential arc segments, the M5 outer/inner oxide layer thicknesses are 36-μm/32-μm. The ratio of total oxide thickness is M5/Zry-4 = 0.41, while the weight gain ratio is 0.64. Thus, the primary reason for the lower weight gain of M5 as compared to Zry-4 is the relatively slow growth of the inner and outer oxide layers. However, these results also suggest that the alpha and prior-beta regions of M5 pick up more oxygen than Zry-4 for long oxidation times at 1000°C. The results are consistent with the observation that thicker oxide layers are more effective diffusion barriers than thin oxide layers.

Post-Quench-Ductility Results

The load-displacement curves from the ring compression tests were analyzed by the offset method. Figure 14 illustrates this method for a Zry-4 ring oxidized at 1100°C to a CP-calculated ECR of 15% and a measured ECR of ≈16%. The sample fractured into four pieces with the first through-wall fracture occurring at the load or support point. The offset displacement (0.516 mm) prior to the first through-wall crack is determined by mathematically by unloading the specimen at the elastic loading-stiffness rate. Normalizing this offset displacement to the as-fabricated outer diameter (9.50 mm) gives an offset strain of 5.4%. For samples oxidized at 1100°C to a CP-calculated ECR value of ≈17% (≈21% BJ-ECR), the ductility determined by offset strain was in the range of 4-5%. For samples oxidized at 1000°C to ≈17% CP-ECR (≈19% BJ-ECR), the offset-strain ductility was 4-5% for Zry-4 and ZIRLO and >5% for M5. It is interesting to note that all three alloys oxidized at 1000°C to ≈20% CP-ECR (≈22% BJ-ECR) had a post-quench ductility of ≈3%, even though their ECR values determined from measured weight gain and sample thickness range from 22.4% for Zry-4 to 18.0% for ZIRLO to 13.3% for M5. Thus, the post-quench ductility of these alloys oxidized at 1000°C correlates better with time-at-temperature or predicted ECR, which varies as the square-root of time, than with measured ECR.

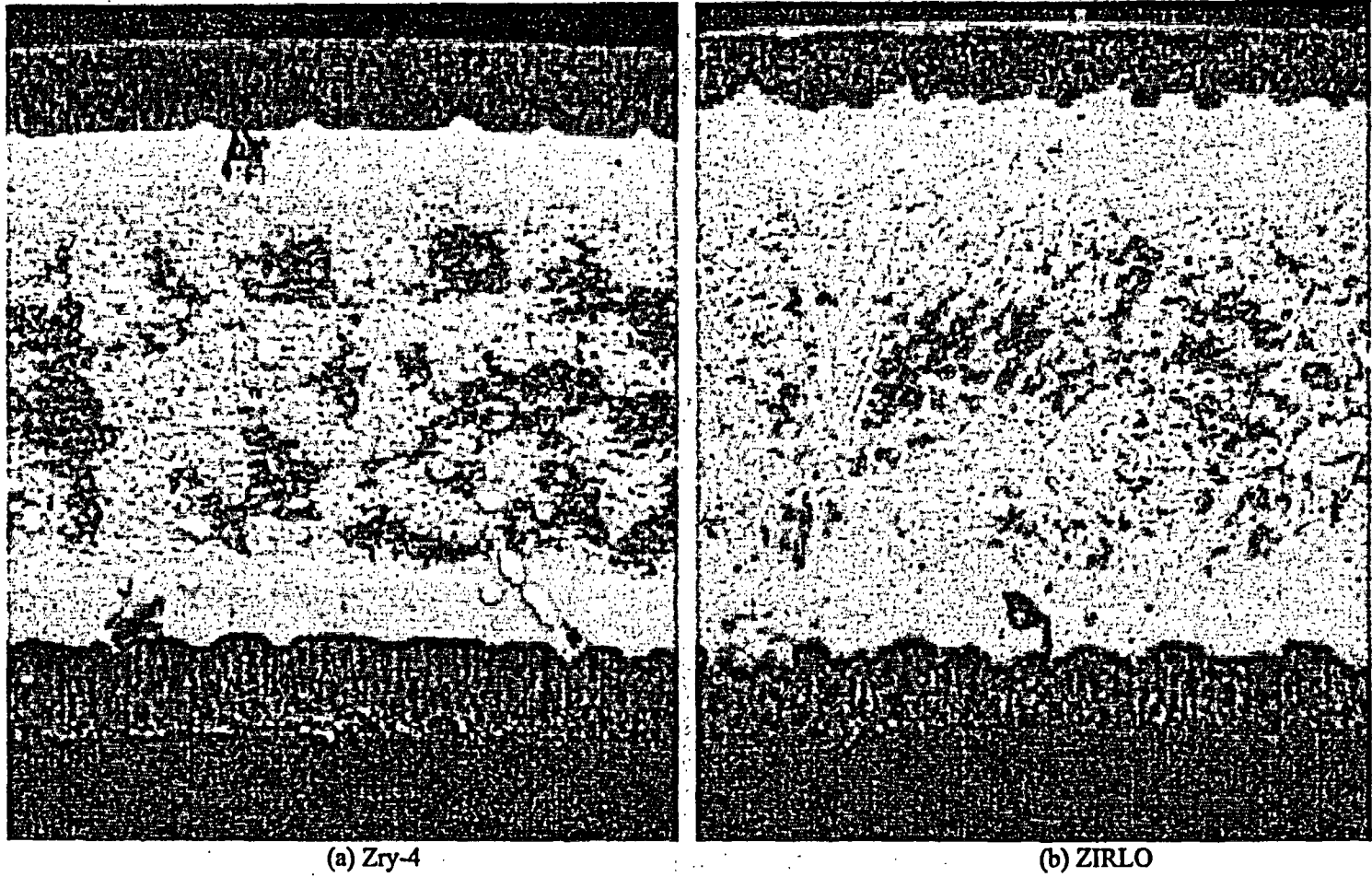


Fig. 12. Metallography of as-polished Zry-4 (a) and ZIRLO (b) oxidized in steam at 1000°C for ≈ 3400 s, slow cooled to 800°C and water quenched. Measured ECR values are 22.4% for Zry-4 and 18.0% for ZIRLO.

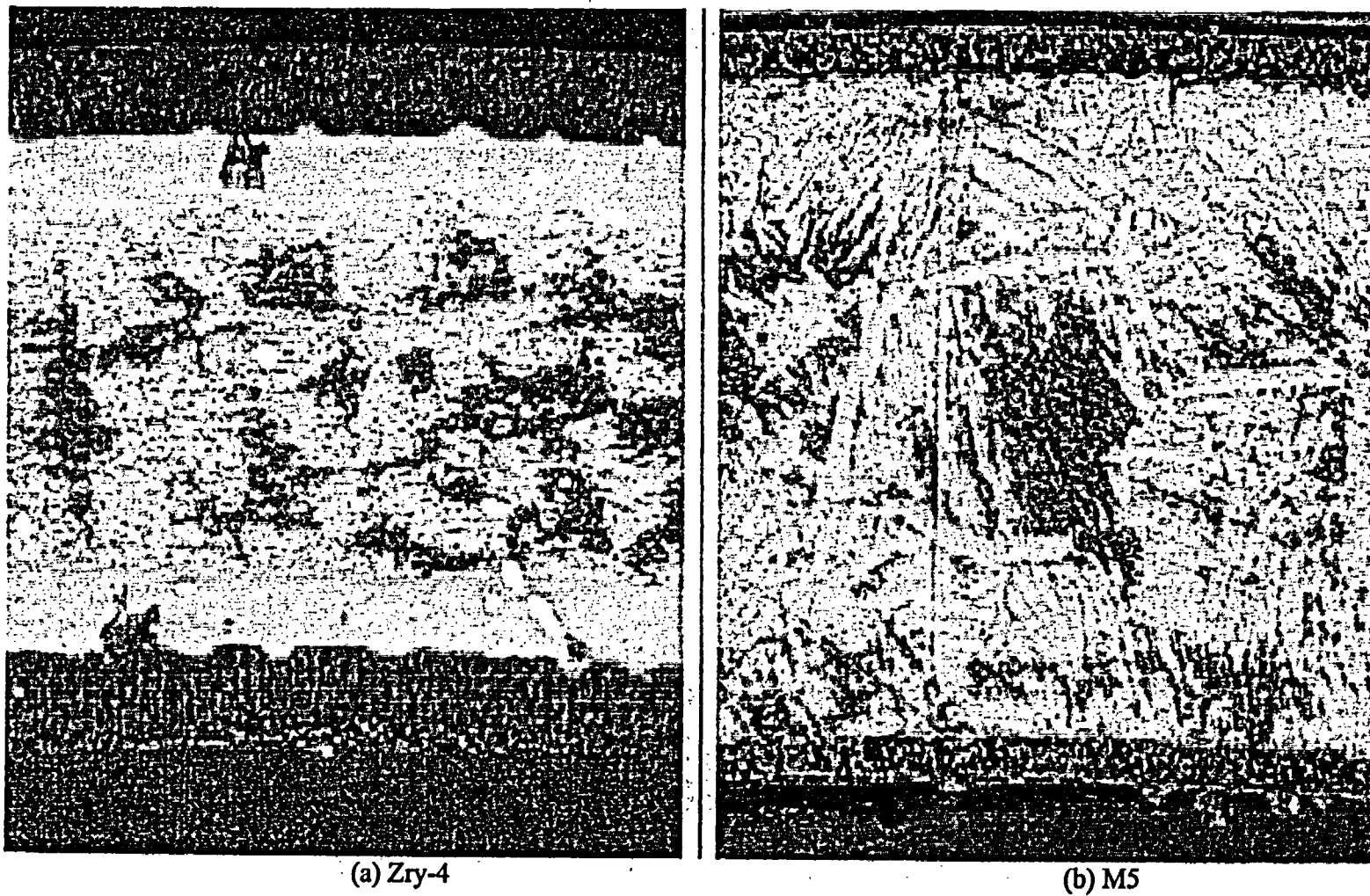


Fig. 13. Metallography of as-polished Zry-4 (a) and M5 (b) oxidized in steam at 1000°C for ≈ 3400 s, slow cooled to 800°C and water quenched. Measured ECR values are 22.4% for Zry-4 and 13.3% for M5.

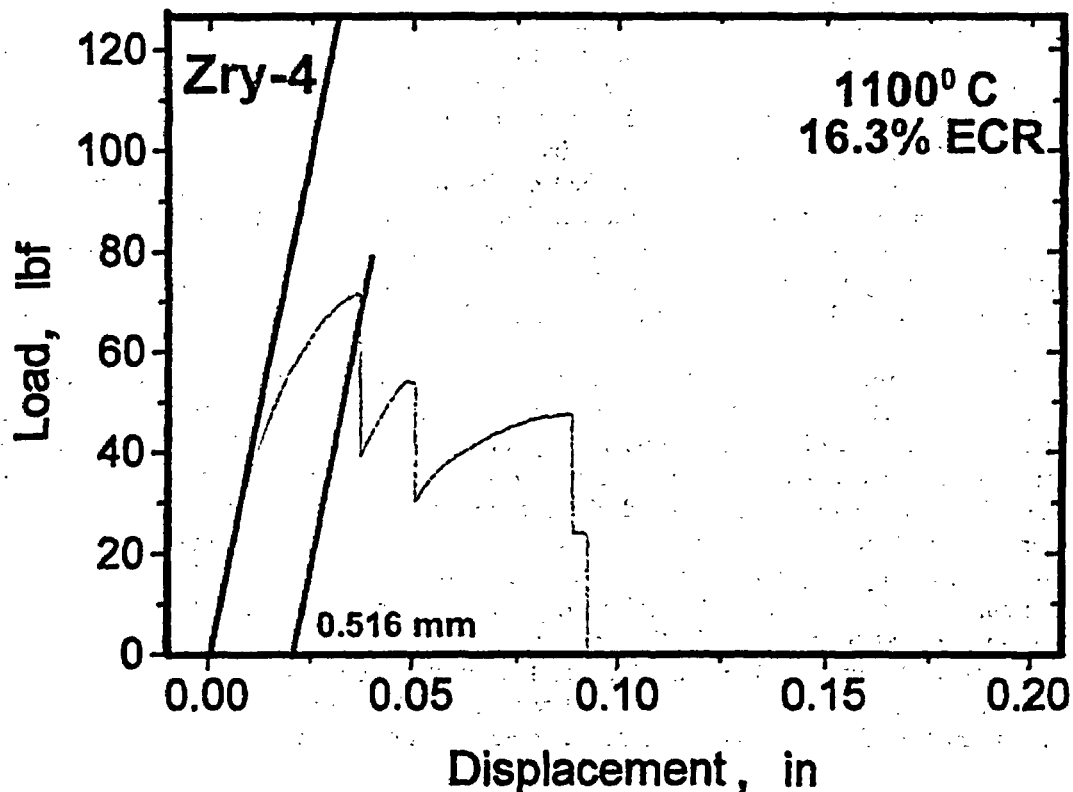


Fig. 14. Load-displacement curve for Zry-4 oxidized at 1100°C to a CP-calculated ECR of 15%, slow-cooled to 800°C and quenched to 100°C. The test was conducted on an 8-mm-long ring at room temperature and a cross-head displacement rate of 2 mm/minute. The offset displacement prior to the first through-wall crack is 0.516 mm.

Conclusions and Future Work

LOCA Integral Test Results for High-Burnup BWR Fuel

Metallography was conducted at several locations of the ICL#2 high-burnup LOCA integral sample to determine fuel morphology and Zry-2 cladding layer (oxide, alpha, and prior-beta) thicknesses. This sample had been pre-pressurized to ≈ 8.4 MPa at 300°C, ramped in flowing steam through ballooning and burst to 1204°C, held at 1204°C for 5 minutes, cooled to 800°C at 3°C/s and furnace-cooled from 800°C to room temperature. These destructive examinations were performed after significant handling of the LOCA specimen during nondestructive examinations and after the ballooned region had been filled with epoxy. Prior to this test, a companion out-of-cell test (OCL#11) had been conducted with nonirradiated Zry-2 (filled with zirconia pellets) to provide baseline data for the in-cell test. The condition of the fuel

below the balloon neck region appeared to be essentially the same as the pre-LOCA fuel structure of a sample sectioned from near the LOCA specimen. Some circumferential tearing of the post-LOCA fuel was observed at mid-radius, which may be due to the behavior of the high concentration of fission gas in this fuel ring and to the small expansion of the cladding away from the fuel. Fuel morphology was also imaged ≈ 50 mm above the burst center, ≈ 12 mm above the burst center and at the burst center. These results are interesting, but they are not necessarily indicative of the fuel morphology during the test. Essentially, these results demonstrate that the fuel cracks into small enough fragments that some axial relocation of fuel may occur during and/or following ballooning and burst. However, there is no evidence from the ICL#2 sample that the fuel mass per unit length increased within the ballooned region. In subsequent LOCA integral tests – with quench – the burst area will be taped prior to movement and handling to prevent fuel fallout. Also, gamma scanning will be performed to assess fuel relocation.

Based on measurements of cladding outer- and inner-surface oxide thickness at several axial locations, it appears that the presence of ≈ 10 μm of corrosion does not inhibit or slow down outer-surface oxidation and the presence of fuel and fuel-cladding bond does not retard inner surface steam oxidation. With regard to steam oxidation, high-burnup-fueled Zry-2 behaved very similar to nonirradiated Zry-2 during the LOCA transient. The major difference observed between post-LOCA high-burnup-fuel cladding and nonirradiated cladding was the degree of secondary hydriding in the balloon neck region: ≈ 4000 wppm hydrogen pickup for both necks of the nonirradiated cladding and ≈ 200 wppm for one neck of the high-burnup sample. A more detailed axial profile of hydrogen concentration and pickup will be obtained from the next high-burnup LOCA integral test (ICL#3) scheduled for December 2003. An additional test (ICL#4) with a high-burnup BWR fuel segment will be conducted – with quench – early in 2004 to generate a sample for post-quench-ductility testing. High-burnup PWR LOCA testing will be initiated following the ICL#4 test and maintenance at the LOCA hot-cell work station.

Advanced-Alloy Cladding Post-Quench Ductility

Zry-4, ZIRLO and M5 samples (25-mm-long) were oxidized at 1000°C and 1100°C to Cathcart-Pawel (CP) ECR values of 5-20%, slow cooled to 800°C and quenched. Rings (8-mm-long) cut from these samples were subjected to ring-compression testing at room temperature and a cross-head displacement rate of 2 mm/minute. All three alloys oxidized at 1100°C exhibited similar weight gains per time, which were consistent with CP-model predictions. At 1000°C, the ZIRLO and Zry-4 weight gains were within $\pm 12\%$ of the CP-predictions, with ZIRLO weight gain $\approx 10\%$ lower and Zry-4 $\approx 12\%$ higher than predicted for the longest test time (≈ 3400 s). These weight-gain differences scaled linearly with total oxide layer thickness for Zry-4 and ZIRLO. At 1000°C oxidation temperature, the M5 weight gain was $\approx 30\%$ lower than predicted and $\approx 36\%$ lower than the Zry-4 weight gain at ≈ 3400 s. The low weight gain of M5 under these conditions is due mostly to the slower growth rate of the inner- and outer-surface oxide layers. However, the M5/Zry-4 total-oxide ratio was less than the weight gain ratio, indicating more oxygen pickup in the M5 alpha and prior-beta regions. The resulting ECR values at 1000°C, based on measured weight gain, were 22% for Zry-4, 18% for ZIRLO and 13% for M5.

The results of the post-quench-ductility tests indicated that the three alloys oxidized at 1100°C had offset strains $\geq 4\%$ at $\leq 17\%$ CP-ECR. It was interesting to observe that all three alloys oxidized at 1000°C had $\approx 3\%$ offset strain at 20% CP-ECR, even though the measured ECR values ranged from 13-22%. These results suggest that, for alloys oxidized at 1000°C, post-quench ductility correlates better with time-at-temperature, CP-calculated ECR and BJ-calculated ECR than with measured ECR. Microhardness and hydrogen analyses of these alloy samples are in progress, along with preparation of samples oxidized at 1200°C and 1260°C.

References

1. Y. Yan, R. V. Strain, T. S. Bray, and M. C. Billone, "High Temperature Oxidation of Irradiated Limerick BWR Cladding," Proceedings of the Nuclear Safety Research Conference (NSRC-2001), Washington, DC, October 22-24, 2001, NUREG/CP-0176 (2002) 353-372.
2. Y. Yan, R. V. Strain, and M. C. Billone, "LOCA Research Results for High-Burnup BWR Fuel," Proc. Nuclear Safety Research Conference (NSRC-2002), Washington, DC, October 28-30, 2002, NUREG/CP-0180 (2003) 127-155.
3. G. Hache and H. M. Chung, "The History of LOCA Embrittlement Criteria," Proc. 28th Water Reactor Safety Meeting, Bethesda, MD, October 23-25, 2000, NUREG/CP-0172 (2001) 205-237
4. W. J. Leech, "Ductility Testing of Zircaloy-4 and ZIRLOTM Cladding after High Temperature Oxidation in Steam," Proceedings of the Topical Meeting on LOCA Fuel Safety Criteria, Aix-en-Provence, 22-23 March, 2001, pp 135-143. <http://www.nea.fr/html/nsd/docs/2001/csni-r2001-18.pdf>
5. A. Le Bourhis, "Justification of the M5TM Behavior in LOCA," Proceedings of the Topical Meeting on LOCA Fuel Safety Criteria, Aix-en-Provence, 22-23 March, 2001, pp 105-133. <http://www.nea.fr/html/nsd/docs/2001/csni-r2001-18.pdf>
6. L. Yegorova, K. Lioutov, V. Smirnov, A. Goryachev, and V. Chesnov, "LOCA Behavior of E110 Alloy," these proceedings.

LOCA BEHAVIOR OF E110 ALLOY

L.Yegorova, K.Lioutov

Nuclear Safety Institute of Russian Research Center "Kurchatov Institute", Moscow, Russian Federation

V.Smirnov, A.Goryachev, V.Chesanov

State Research Center "Research Institute of Atomic Reactors", Dimitrovgrad, Russian Federation

Abstract

Experimental studies of the mechanical behavior of E110 (Zr-1%Nb) oxidized claddings were continued during 2003. The previous investigations performed during 2001–2002 allowed to determine the zero-ductility threshold of the E110 cladding as a function of a large set of LOCA-related parameters. The major goal of the current stage of the research was to evaluate the corrosion resistance and ductility margin from the viewpoint of such selected manufacture factors as the cladding surface treatment, method used to produce the Zr-1%Nb ingot, microstructure of the alloy.

1. Introduction

The Nuclear Safety Institute of the Russian Research Center "Kurchatov Institute" (NSI RRC KI), in cooperation with the Russian State Research Center "Research Institute of Atomic Reactors" (RIAR) with the support of the Joint Stock Company "TVEL" (Russian Federation), the U.S. Nuclear Regulatory Commission (USA), and the Institute for Radiological Protection and Nuclear Safety (France), is conducting a program to further study the mechanical behavior of Russian zirconium-niobium alloys under LOCA conditions. The first part of the program carried out during 2001-2002 was devoted to the experimental study of the LOCA-related ductility in E110 (Zr-1%Nb) cladding on the basis of ring compression mechanical tests [1]. These studies have shown that (Fig. 1):

- the zero ductility threshold of the E110 alloy is lower than that of Zircaloy-4 alloy;
- an earlier initiation of the breakaway effect in nodular corrosion form and the intensive absorption of hydrogen are the most significant differences in the LOCA behavior of these two alloys.

After that additional tests have demonstrated that there is no correlation between the ductility threshold and the alloying elements (O, Fe, Sn) in those alloys examined. This finding prompts more general question: is this oxidation behavior typical of the whole family of zirconium-niobium alloys or only the Russian cladding types?

Several approaches have been proposed to get the answer to this question. The first of them was based on the comparative analysis of two Zr-1%Nb alloys: E110 and M5 (France). The comparison performed with the using of the E110 test results (obtained due to this work) and the M5 published data [2, 3] allowed to note the following:

- unlike that of the E110 cladding, the embrittlement thresholds of M5 and Zircaloy-4 claddings are similar;

- unlike that of the E110 cladding, the embrittlement of the M5 cladding is not accompanied by the nodular corrosion and hydrogen uptake.

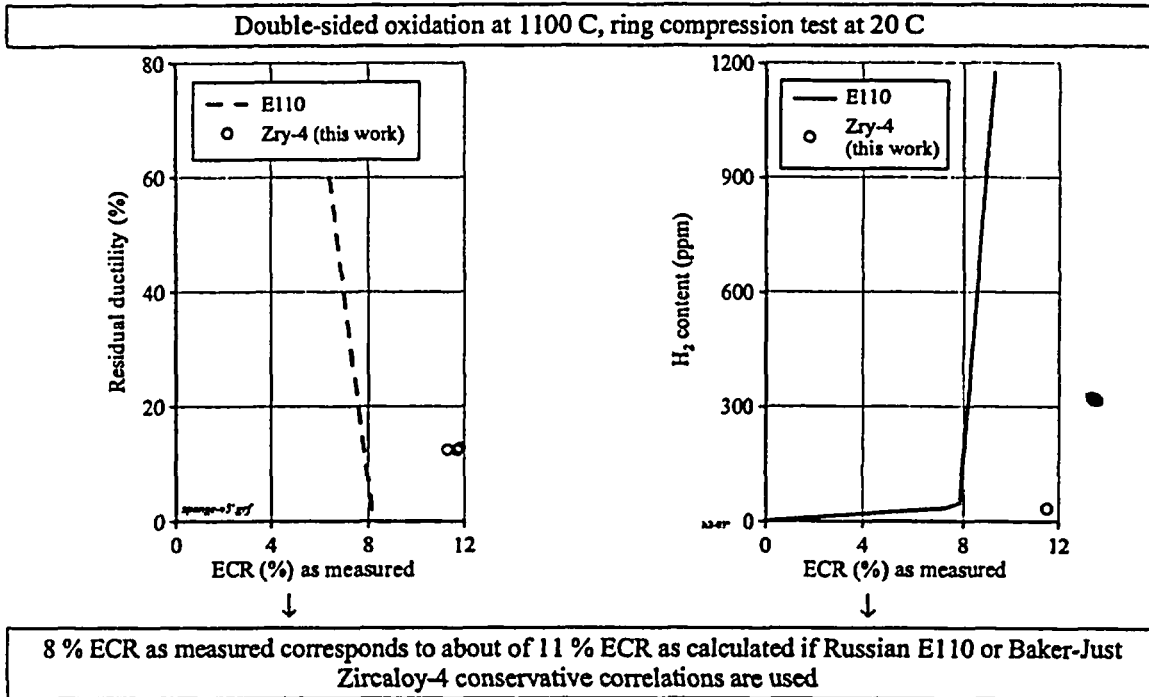


Fig. 1. Comparative data to characterize residual ductility and hydrogen concentration as a function of the ECR for E110 and Zircaloy-4 alloys

However, taking into account: a) the importance of the problem, b) the understanding that the noted differences in the E110 and M5 behavior could be caused by differences in experimental procedures and methods of the processing of test results, c) the assumption (based on the literature data) that the oxidation behavior of zirconium-niobium claddings is very sensitive to fabrication procedures, the participants interested in the research developed a special plan to get a well-defined answer to the above mentioned question. In accordance with the plan, it was decided:

- to perform comparative tests with M5, E110, Zirlo, Zircaloy-2, Zircaloy-4 alloys in Argonne National Laboratory (ANL) in the same apparatus by the same technicians;
- to perform the coordinated RRC KI/ANL test programs to reveal the response of the E110 cladding to the variation of selected manufacture factors.

The development of the coordinated RRC KI/ANL program with the E110 alloy was completed at the beginning of 2003. The major focus of this program was concentrated on the issues listed in Table 1. The experimental parts of this program were performed separately by ANL and by RRC KI (in the cooperation with RIAR) during 2003. This paper contains the preliminary analysis of results obtained by RRC KI/RIAR.

Table 1. Characterization of the Factors Selected for Studies

Type of possible factors	Specification	Approaches to demonstrate the sensitivity of test results to different factors	Involved laboratories	
			RRC KI/RIAR	ANL
1. Surface effects	Surface roughness and surface contamination	To polish, machine, etch the cladding surface	+	+
2. Bulk effects	Chemical composition of Zr-1%Nb ingot	To use the sponge Zr-1%Nb ingot and Zr-1%Nb ingot with low Hf instead of iodide and electrolytic Zr-1%Nb ingots	+	-
	Microstructure effects (grain size, phase composition, secondary precipitates (composition, size, distribution) as a function of the fabrication process	To perform comparative SEM, TEM examinations for different types of cladding specimens	+	+
3. Geometrical sizes	Typical cladding thickness of E110 cladding is 0.69-0.71 mm. Typical cladding thickness of M5 cladding is 0.56-0.6 mm	To machine the E110 cladding to the M5 size	-	+

2. Major Provisions of Test Procedures

The test apparatus and conditions were developed and validated during the previous stage of the research [1]. Table 2 presents the schematic description of the experimental approaches used for the current work.

Table 2. Characterization of test procedures

Position	Characteristics
1. Oxidation type	Double-sided oxidation
2. Oxidation diagram	Cladding sample heating at a rate of 30-40 C/s in a steam flow, isothermal oxidation of a sample, cooling with a rate of 30 C/s
3. Geometrical parameters of cladding samples	Sample length for oxidation tests: 100 mm Sample length for mechanical tests: 8 mm
4. Type of mechanical tests	Ring compression tests at 20 C

Besides the characteristics listed in Table 2, Fig. 2 presents the additional information to understand the procedure for processing of ring compression test results. It should be noted that a large scope of individual effect tests was performed to validate general principles of this procedure.

3. The Analysis of Experimental Results

3.1. Surface Effect Studies

This stage of the work was devoted to the evaluation of the sensitivity of E110 corrosion behavior to such factors as the surface chemistry and roughness. To clarify these effects, two types of E110 claddings were tested:

1. E110 etched and anodized standard claddings.
2. E110 standard as-received tubes after the following special procedure performed by RIAR: one-half length of the inner and outer surfaces of each sample was polished to reduce the surface roughness and surface contaminations.

Fig. 3 demonstrates the results of experiments with the first type of claddings.

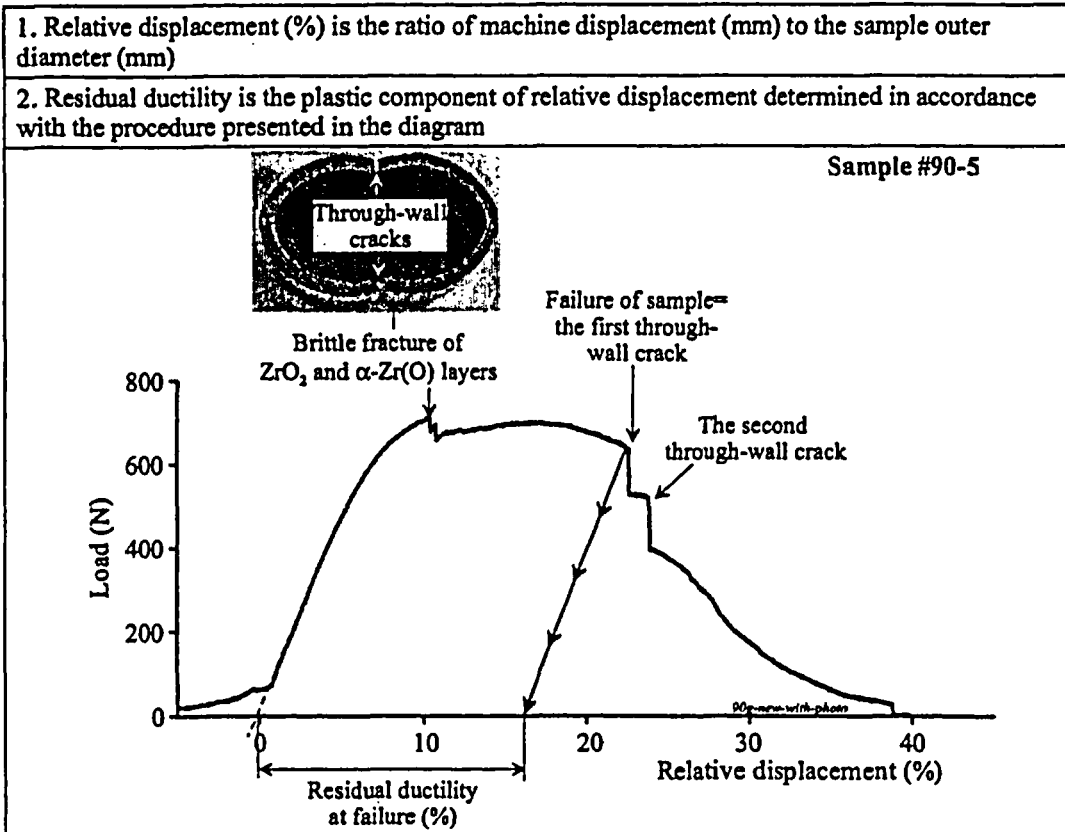


Fig. 2. The appearance of the oxidized sample #90-5 after mechanical tests and interpretation of ring compression test results on the basis of the load-displacement diagram

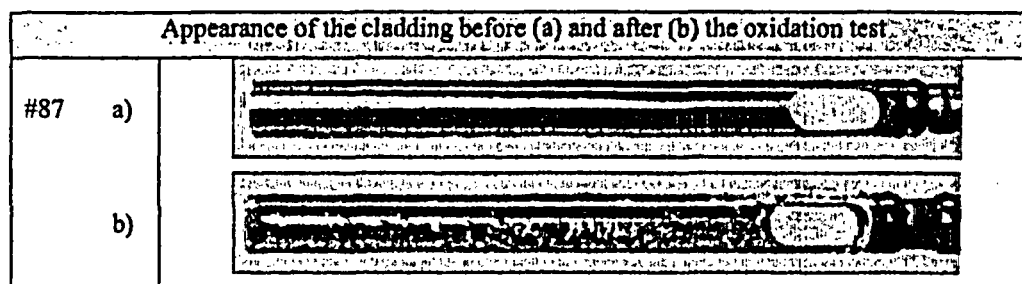


Fig. 3. Demonstration of the oxidation behavior for the etched and anodized cladding after the double-sided oxidation at 1100 C (ECR=9 %)

The obtained results allow to conclude that:

- the breakaway effect is observed on the cladding surface;
- the cladding final chemical treatment of this type does not improve the E110 corrosion resistance.

These conclusions fully agree with results of tests with the etched E110 cladding performed by ANL [4]. The background for the next stage of the surface effect studies was based on the following:

- it is known, that a high level of the surface roughness and surface contaminations are favorable to the generation of the nodular corrosion in zirconium alloys;
- during the previous RRC KI/RIAR tests with E110 as-received tubes it was revealed that the nodular corrosion was a typical component of oxidation;
- E110 as-received tubes have a sufficient surface roughness because in accordance with the traditional approach, the final etching of as-received tubes was employed to reduce a tube roughness and to produce the E110 standard cladding;
- the final polishing instead of etching will be used in the new generation of VVER claddings to reduce the surface roughness.

Taking into account these considerations, it was decided to determine the sensitivity of the E110 corrosion behavior to the surface roughness using specially prepared polished samples. One half of this 100 mm sample was polished and the second one was remained in the as-received condition. This interesting approach proposed by the ANL specialists allowed to test: two cladding types under absolutely the same experimental conditions. Fig. 4 shows some results of the test with polished/as-received samples.

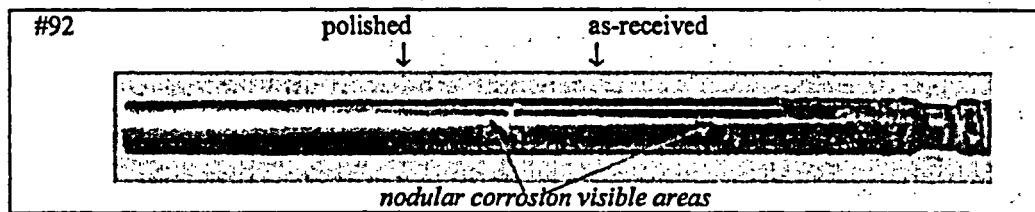


Fig. 4. Appearance of E110 polished/as-received sample after the double-sided oxidation at 1100 C during 555 s

As can be seen from Fig. 4, the as-received half of the sample is covered with local "white spots" which are the typical marker of the nodular corrosion. The surface of the polished half is covered with a more uniform oxide layer. These observations were confirmed by the results of mechanical tests (see Fig. 5a).

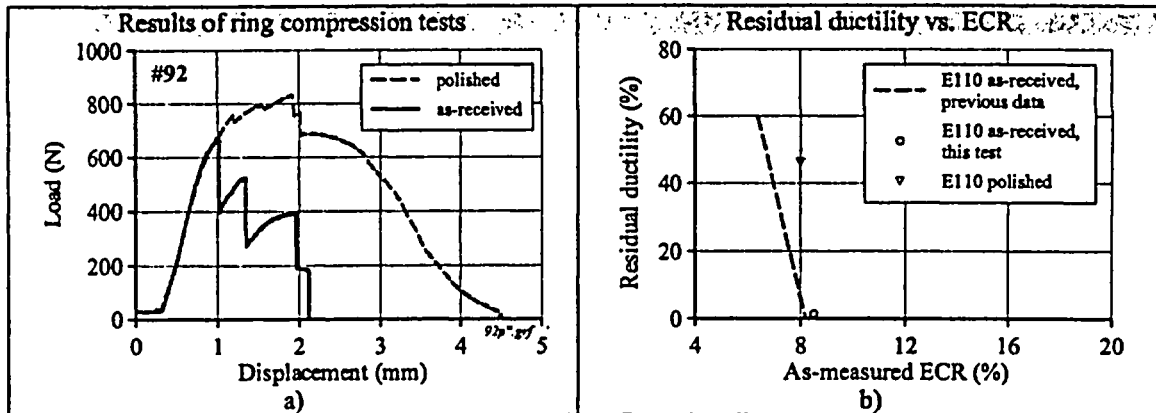


Fig. 5. a) Load-displacement diagrams for polished and as-received rings, b) sensitivity of residual ductility of E110 oxidized samples to roughness/contamination effects

The analysis of obtained load-displacement diagrams and of the data presented in Fig. 5b has shown that polishing of the E110 as-received tubes allows to increase the ductility margin of oxidized claddings. The independent research of the same type performed in ANL confirms this conclusion [4]. But the following question could be formulated on the more precise analysis of this issue: does the E110 cladding polishing allow to eliminate the nodular corrosion effect in the ECR range 0–13 % (as-measured) at the representative range of the oxidation temperature (up to 1200 C)? The first investigations performed to answer this question allowed to reveal that polishing of E110 tubes leads to a significant improvement of the cladding corrosion resistance. This conclusion is based on the following data:

- the hydrogen content in the cladding oxidized to as-measured ECR=8.5 % decreases from 690 ppm in the as-received half down to 30 ppm in the polished half;
- the corrosion rate (weight gain at the same time) is reduced in the polished part of the cladding;
- the residual ductility increases from 1.4 % in the as-received segment up to 46 % in the polished part;
- these effects are manifested most clearly at 1000 C (see Fig. 6).

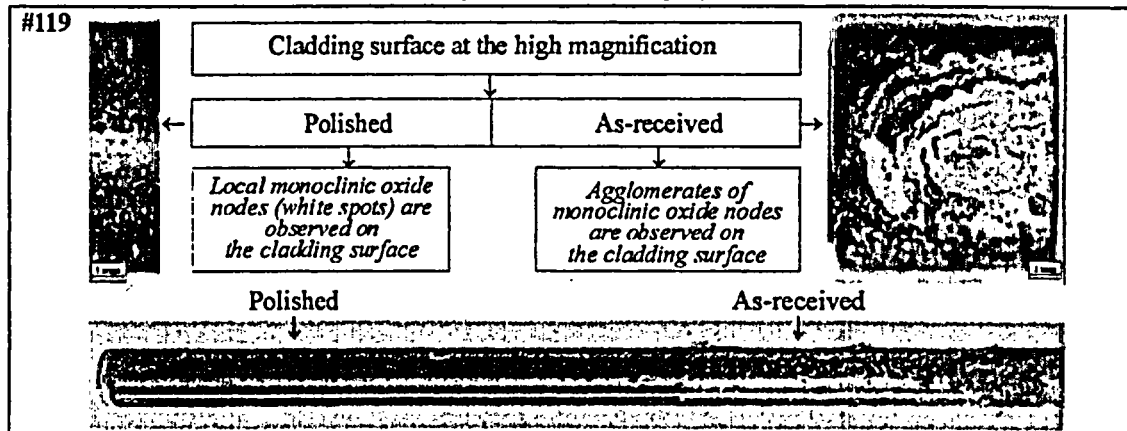


Fig. 6. Appearance of E110 polished/as-received cladding after the double-sided oxidation at 1000 C (ECR=4.3 % for polished part, ECR=5.7 % for as-received part)

These preliminary data have shown that the cladding polishing leads to a significant delay of nodular corrosion in E110 claddings but this procedure does not allow to get the absolute effect. Therefore, the next stage of the program was concentrated on the evaluation of the sensitivity of the E110 corrosion behavior to cladding bulk effects.

3.2. Bulk Effect Studies

3.2.1. Effects of the Bulk Chemistry

The logical principles used while developing this line of the research are formulated in Table 3. The background of the analysis was outlined with the following provisions:

- it was assumed that there is a real difference in the corrosion behavior of such Zr-1%Nb alloys as the E110 and M5;
- a multifactor comparative characterization of these two types of the cladding was performed to reveal possible reasons of their different behavior under the LOCA-relevant conditions.

Table 3. Analysis of E110 and M5 differences

Variant of answers	Comments
1. Different oxygen concentration in these alloys (0.04–0.06% in E110, 0.13% in M5) leads to the different oxidation behavior	Special studies of E110K alloy (oxygen concentration 0.13%) have demonstrated that the increase of oxygen concentration does not change the oxidation behavior of E110 alloy
2. Different conditioning of the cladding surface (polishing for M5, etching for E110) leads to the different oxidation behavior	Surface effect studies of E110 polished specimens have shown that the appropriate manipulation with cladding surface allows to slow down the initiation of the nodular corrosion but this procedure does not allow to avoid this type of the oxidation in the given range of ECRs (especially at 1000 C)
3. Differences in the chemical composition of Zr-1%Nb ingot	1. All types of alloys developed for PWR reactors (including advanced zirconium-niobium alloys) are manufactured on the basis of the sponge Zr. Therefore, the differences in the chemical composition of this family of alloys are determined by differences in the alloying composition
	2. Cladding alloys for the VVER reactor are manufactured on the basis of the mixture of iodide and electrolytic Zr
	3. Thus, the chemical composition of the PWR cladding and VVER cladding with the same alloying components differ in the composition of impurities
	4. To verify the sensitivity of E110 oxidation behavior to the chemical composition of impurities, it was decided to perform the oxidation and mechanical tests with advanced types of E110 claddings manufactured on the basis of the modified process of Zr-1%Nb ingot fabrication

Variant of answers	Comments
4. Differences in the cladding fabrication process	1. It is known that cladding properties (mechanical and oxidation parameters) are a strong function of the fabrication process
	2. Besides, it is known that a strong correlation is observed between the cladding microstructure and cladding oxidation behavior
	3. Thus, if the differences in the oxidation behavior of zirconium-niobium alloys are determined by the cladding fabrication process, the comparison of appropriate microstructures will allow to reveal this effect

In accordance with the analysis results, different pilot samples of new E110 claddings (manufactured by the modified Russian fabrication processes) were selected for this stage of the work. Table 4 presents the specification of these samples.

Table 4. Types of E110 claddings material tested at the bulk effect studies

Notation conventions of cladding types developed for this research	Alloying composition	Input components used for the fabrication of Zr-1%Nb ingot
E110	Zr-1%Nb	Iodide Zr, electrolytic Zr, recycled scrap, Nb
E110 _{C(fr)}	Zr-1%Nb	French sponge Zr (CEZUS standard)
E110 _{C(ru)}	Zr-1%Nb	Russian sponge Zr, iodide Zr, Nb and recycled scrap were used to fabricate the sponge Zr-1%Nb ingot
E110 _{C(fr)}	Zr-1%Nb	French sponge Zr, iodide Zr, Nb and recycled scrap were used to fabricate the sponge Zr-1%Nb ingot
E110 _{lowHf}	Zr-1%Nb	Iodide Zr, electrolytic Zr with low Hf content, recycled scrap, Nb

The first data to evaluate the sensitivity of the E110 oxidation behavior to the bulk chemistry were obtained for the E110_{C(fr)} type of modified claddings in accordance with the following program approach:

- to oxidize E110_{C(fr)} cladding samples to high ECRs (up to 13 % (as-measured));
- to examine the visual oxidation effects (see Fig. 7);
- to measure the hydrogen content (see Fig. 7);
- to perform the ring compression mechanical tests at 20 C (see Fig. 8);
- to compare E110, E110_{C(fr)}, Zircaloy-4 residual ductility as a function of ECR (see Fig. 9).

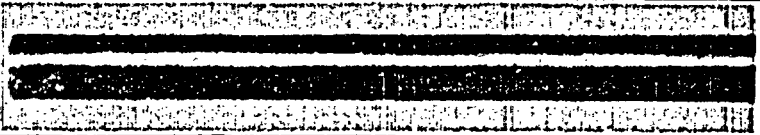
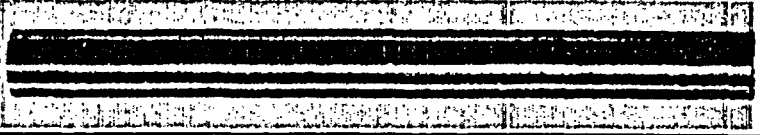
<p>Sample #89:</p> <ul style="list-style-type: none"> • 10.5% ECR • 22 ppm of H content 	
<p>Sample #90</p> <ul style="list-style-type: none"> • 13% ECR • 30 ppm of H content 	

Fig. 7. Appearances of E110_{C(fr)} samples after the double-sided oxidation at 1100 C

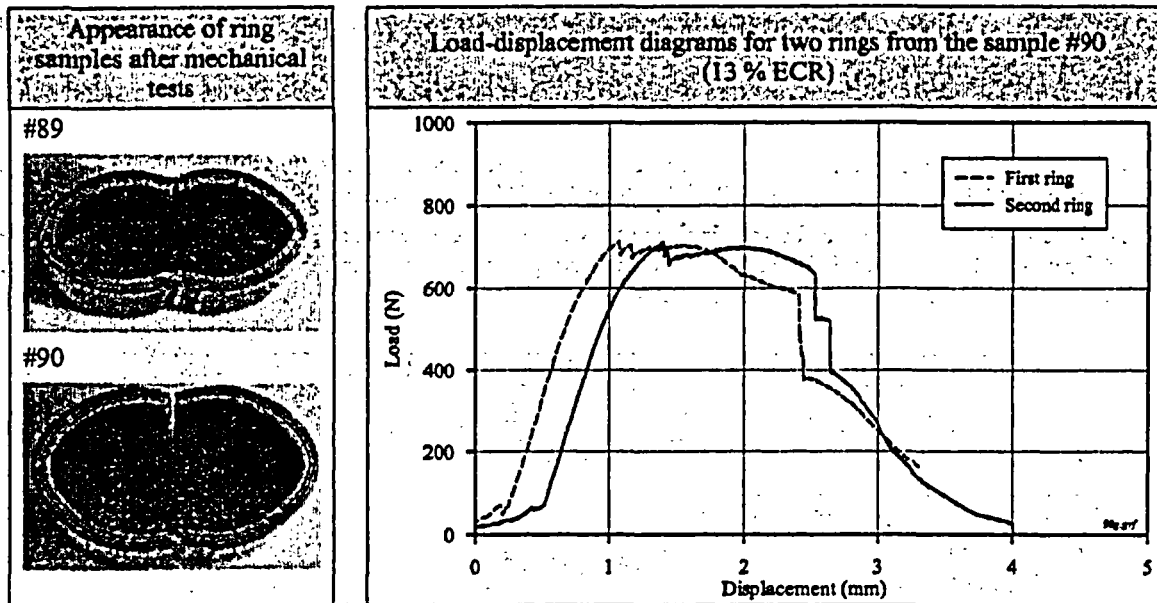


Fig. 8. Results of ring compression tests with E110_{G(tr)} oxidized samples

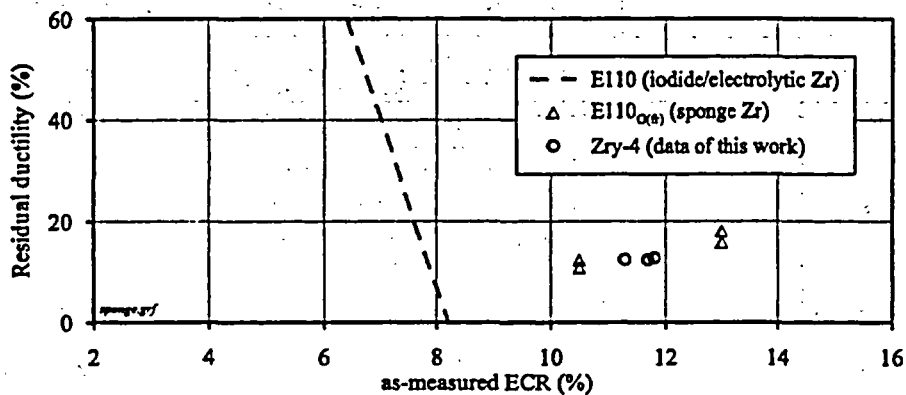


Fig. 9. Residual ductility of E110, E110_{G(tr)}, Zircaloy-4 cladding samples after the double-sided oxidation at 1100 C

The obtained results have shown that:

- E110 oxidized claddings manufactured on the basis of French sponge Zr have a black lustrous protective oxide layer up to ECR=13 % (as-measured);
- hydrogen absorption in prior β -phase is very low (22–30 ppm);
- prior to the oxidized cladding failure during ring compression tests, the plastic deformation was visually observed;
- oxidized claddings retain a significant margin of residual ductility up to 13 % ECR (as-measured).

The comparative analysis of these data with the E110 (standard) and Zircaloy-4 data allows to conclude that:

- the E110 cladding fabricated on the basis of sponge Zr-1%Nb demonstrates the same behavior as the Zircaloy-4 cladding;
- there are general differences in the oxidation and mechanical behavior of this E110 cladding and standard E110 cladding at the ECR higher than 6.5–7 % (as-measured).

To widen the test data base for the final analysis of revealed phenomena, the additional studies were performed with two other E110 claddings of the "sponge" type. Fig. 10 and Fig. 11 present the results of these studies confirmed the above listed conclusions.

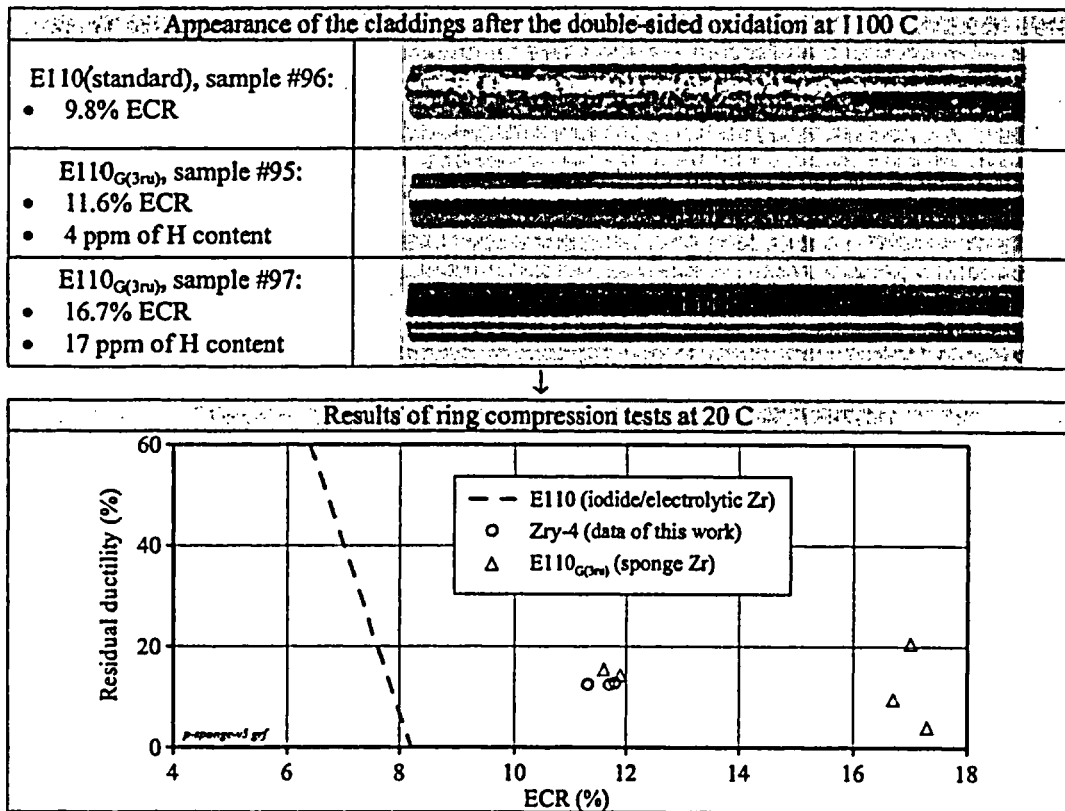


Fig. 10. Comparative data base characterizing the E110_{G(3ru)} oxidation/mechanical behavior

Thus, all E110 "sponge" claddings showed a high resistance to the nodular corrosion at the temperature 1100 C and the ECR up to 17 % (as-measured). But it is known that the most pronounced effects of the nodular corrosion in the E110 standard cladding occur at the temperature about 1000 C. Therefore, several tests with E110 "sponge" claddings were performed at this temperature (see Fig. 12, Fig. 13).

Appearance of the E110 _{G(3tr)} and E110 _{G(3tr)} claddings after the double-sided oxidation at 1100 C	
E110 _{G(3tr)} , sample #99: • 11.5% ECR • 13 ppm of H content	
E110 _{G(3tr)} , sample #95: • 11.6% ECR • 4 ppm of H content	

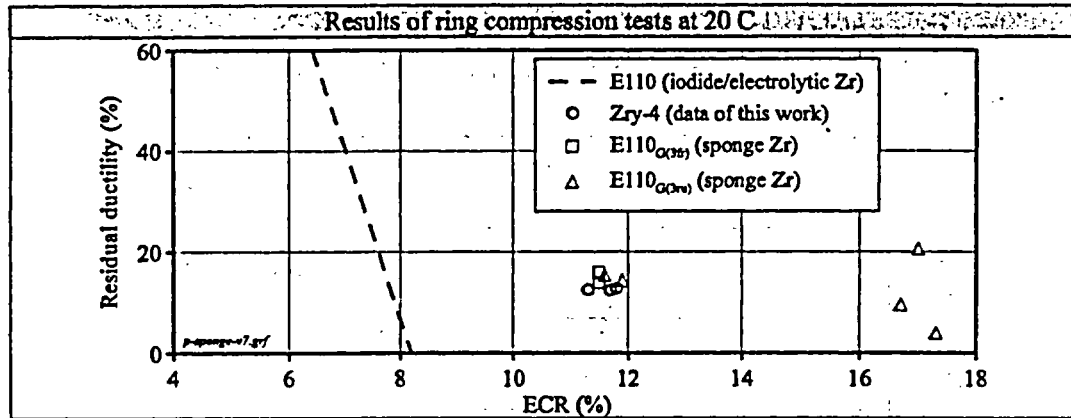


Fig. 11. Comparative data base characterizing the E110_{G(3tr)} and E110_{G(3tr)} oxidation/mechanical behavior

E110 standard; #44 • ECR=7.7%	$t_{ef}=865$ s	
E110 _{G(3tr)} ; #91 • ECR=6.5% • 28 ppm of H content	$t_{ef}=2016$ s	
E110 _{G(3tr)} ; #93 • ECR=8.5% • 12 ppm of H content	$t_{ef}=5013$ s	
E110 _{G(3tr)} ; #98 • ECR=6.9% • 16 ppm of H content	$t_{ef}=2519$ s	
E110 _{G(3tr)} ; #101 • ECR=8.9% • 11 ppm of H content	$t_{ef}=5028$ s	

Fig. 12. Appearances of E110 standard and E110 "sponge" claddings after the double-sided oxidation at 1000 C

The analysis of obtained results allowed to reveal the following new important findings characterizing the general physical differences in the oxidation behavior of the "iodide/electrolytic" and "sponge" E110:

- after 800–900 seconds of the oxidation at 1000 C, the E110 standard "iodide/electrolytic" cladding achieves the zero ductility threshold accompanied by the demonstration of classical break away phenomena;
- after 2500 seconds of the oxidation at 1000 C, the E110 "sponge" claddings have a high margin of residual ductility (more than 40 %); the cladding surface is covered with the black uniform oxide and the hydrogen content in the cladding is very low;
- after the 5013 seconds of the oxidation at 1000 C, the E110_{Q(h)} cladding achieves the zero ductility threshold accompanied by the nodular corrosion but the hydrogen content in the cladding is very low;
- after the 5028 seconds of the oxidation, the E110_{Q(3n)} cladding does not achieve the zero ductility threshold.

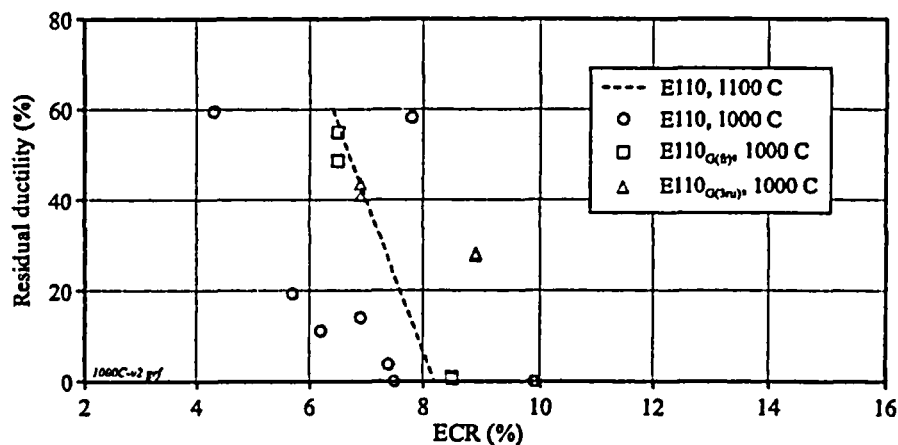


Fig. 13. Comparative data characterizing the residual ductility of claddings as a function of the ECR after the double-sided oxidation at 1000 and 1100 C

These test data have shown that the oxidation rate of "sponge" Zr-1%Nb alloy is much less than that for the Zircaloy-4 cladding. Moreover, the obtained results have demonstrated that E110 "sponge" and M5 claddings have the same oxidation kinetics (see Fig. 14).

The following important conclusions can be formulated on the basis of these data:

- the oxidation duration of 2000, 5000 seconds is outside of the practical interest for the large break LOCA safety analysis;
- general differences in the oxidation kinetics of "sponge" Zr-1%Nb claddings and Zircaloy cladding lead to the development of a global question about the representativity of fixed critical ECR (15–18 %) as the universal safety criterion for the LOCA-relevant conditions.

To summarize the knowledge base obtained due to this stage of bulk effect studies, several preliminary considerations can be formulated:

- it has been revealed that the oxidation behavior of Zr-1%Nb alloy is strongly determined by the method of Zr-1%Nb ingot fabrication;

- experiments with the E110 alloy have shown that:
 - a traditional method of the fabrication based on the mixture of iodide and electrolytic zirconium is accompanied with the tendency to the nodular corrosion;
 - the alloy fabrication on the basis of the sponge zirconium allows to provide the uniform type of the cladding oxidation;
- a high sensitivity of the Zr-1%Nb oxidation behavior to the alloy impurity composition is the most probable explanation of fixed phenomena;
- it is of interest to note that the iodide/electrolytic alloy contains less impurities than the sponge alloy; therefore the problem must not be outlined as "to free the alloy from impurities". The real formulation of the problem is as follows: to reveal (from the impurity compositions) chemical elements responsible for the change of the oxidation mechanism (nodular/uniform) and to provide the given concentration of these elements in the alloy (may be as the alloying components).

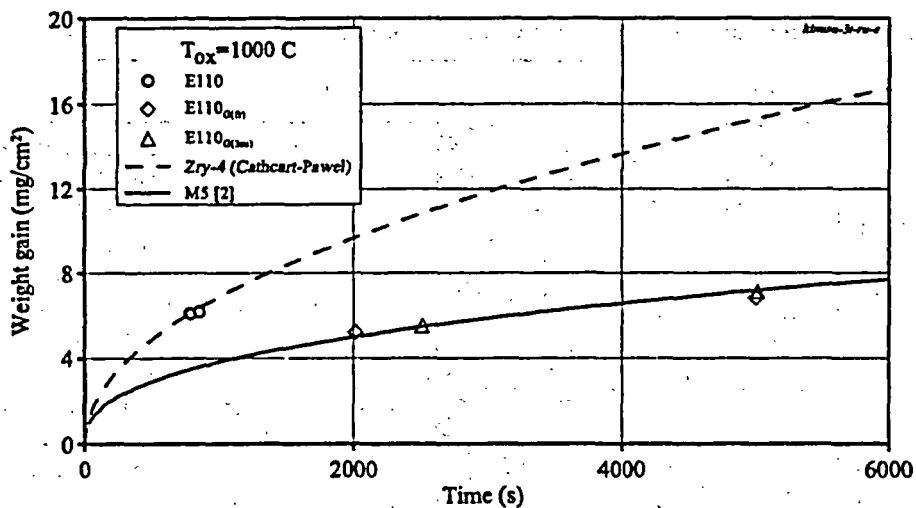


Fig. 14. Comparative data to characterize Zircaloy-4, E110, M5 oxidation kinetics at 1000 C

The first attempts to implement this approach were initiated by Russian specialists from the Institute of Inorganic Materials (VNINM, "Bochvar Institute", A. Nikulina et.al.). After that the appropriate investigations were continued up to now. Taking into account the results of this RRC KI/RIAR research and ANL research with E110 and M5 alloys, Dr. H. Chung from ANL proposed the theory of influence impurities based on the effect of aliovalent elements [5]. But it is obvious that a more fundamental research should be performed in the future to understand the nature of revealed differences in the behavior of zirconium-niobium alloys.

3.2.2. Effects of other fabrication processes

The analysis performed in the section 3.2.1 of the paper was based on the following assumption: the only parameter (Zr-1%Nb ingot composition) was varied in these bulk effect studies. Nevertheless, numerous investigations carried out during the recent thirty years have shown that other fabrication processes such as hot work, cold work, heat treatment etc. affect the cladding oxidation behavior also. Moreover, these investigations allow to establish the fact that the cladding material microstructure accumulates the whole

run of the fabrication process. In particular, the experience of the M5 alloy development allowed to formulate several requirements to the optimized microstructure of Zr-1%Nb alloy [6]:

- maximum degree of recrystallization;
- small size of α -Zr grain;
- fine size of β -Nb precipitates;
- uniform distribution of β -Nb precipitates inside the Zr matrix.

It should be noted that the similar requirements were developed earlier for E110 alloy. Taking into account this approach to the cladding microstructure characterization, the tested types of E110 claddings (standard E110, E110_{G(fr)}, E110_{G(3)}, E110 low Hf) were compared, using the results of TEM examinations. The analysis of the obtained data has shown that there are no general differences in the microstructure parameters for these types of cladding. Table 5 illustrates the comparison of E110 and M5 results of TEM examinations.

Table 5. Comparative data on the microstructure parameters for E110, E110_{G(fr)}, M5 claddings

Type of cladding	The microstructure appearance	Characterization of the microstructure
E110 standard Russian as-received tubing		<ul style="list-style-type: none"> • fully recrystallized structure (αZr matrix with βNb globular precipitates) <ul style="list-style-type: none"> • grain size 2.8 μm • a high level of dispersion of β-Nb precipitates: D = 45, 60 nm (results of measurements in two laboratories) N = $1.84 \times 10^{14} \text{ cm}^{-3}$
E110 _{G(fr)} as-received tubing fabricated with French sponge Zr by the Russian procedure		<ul style="list-style-type: none"> • fully recrystallized structure (αZr matrix with βNb globular precipitates and Zr(Nb, Fe)₂ precipitates) <ul style="list-style-type: none"> • grain size 3.2 μm • a high level of dispersion of precipitates • parameters of β-Nb precipitates: D = 41–43 nm (results of measurements in two laboratories) N = $1.8 \times 10^{14} \text{ cm}^{-3}$
M5 as-received tubing (All presented data were taken from [6])		<p>"Thermodynamically stable microstructure is characterized by a highly refined dispersion of β-Nb precipitates (D = 45 nm, N = $1.5 \times 10^{14} \text{ cm}^{-3}$) with no alignment of particles"</p>

The performed research allows to conclude that:

- appearances and parameters of microstructures "iodide/electrolytic" and "sponge" E110 alloy are the similar, moreover, the microstructure of the E110 cladding material is similar to that of the M5 cladding material;
- it can be assumed that differences in the oxidation behavior and embrittlement threshold of all tested alloys are not a direct function of the cladding fabrication process.

It should be also noted that many attempts were made to explain general differences in the oxidation behavior of iodide/electrolytic and sponge Zr-1%Nb alloys by the differences in the iron content in the ingots (the iron content in the iodide/electrolytic ingot is much less than the iron content in the sponge ingot). In this context, it is interest to note that considered types of E110 "sponge" claddings contained different contents of iron. The maximum iron content was in E110_(G) cladding. The iron in this cladding was present in the form of intermetallic Zr(Nb,Fe)₂ precipitates. The similar intermetallic phase was not revealed in other "sponge" E110 claddings. But the oxidation behavior of all types of the "sponge" E110 claddings was similar. Therefore, this issue (iron influence) is left open till to the future research.

4. Summary

1. Experimental studies performed during 2001–2002 with the Russian Zr-1%Nb cladding manufactured from the E110 alloy allowed to reveal that the nodular corrosion accompanied by hydrogen absorption is responsible for the earlier embrittlement of the E110 cladding in comparison with the Zircaloy-4 cladding under LOCA relevant conditions.
2. A thorough physical analysis of obtained results performed with the participation of JSC "TVEL", VNIINM (Russia), ANL, NRC (USA), IRSN (France) was used as the basis for the development of coordinated programs of investigations of the E110 alloy carried out by RRC KI/RIAR and ANL during 2003.
3. The following phenomena were selected for these studies:
 - surface effects;
 - bulk effects associated with the chemical composition of impurities in the cladding material;
 - bulk effects associated with variations in the fabrication process.
4. The research performed by RRC KI/RIAR allows to conclude the following:
 - 4.1. Different methods of the cladding surface conditioning lead to the different oxidation behavior of the E110 cladding:
 - etching accelerates the nodular corrosion effects;
 - polishing slows down the nodular corrosion and increases the critical ECR (embrittlement threshold).

It should be noted that in accordance with the numerous Russian experience in this area, the Russian vendor of VVER fuel (JSC "TVEL") eliminated the final etching of the E110 cladding from the current standard conditioning procedures. Coincidentally with this action, the polishing of the external cladding surface was introduced as a final conditioning procedure.

- 4.2. The analysis of the TEM microstructure data base obtained to determine the post-LOCA ductility as a function of current E110 cladding fabrication processes has shown that these

procedures (hot work, cold work, heat treatment) are not responsible for the different behavior of such zirconium-niobium alloys as E110 and M5.

- 4.3. Several advanced types of E110 claddings manufactured on the basis of sponge Zr ($E110_{G(H)}$, $E110_{G(Nb)}$, $E110_{G(3Nb)}$) were tested to evaluate the sensitivity of the oxidation phenomena to the bulk chemistry of the cladding material (chemical composition of impurities in the alloy). A direct comparison of E110 advanced claddings with the traditional one manufactured on the basis of iodide/electrolytic Zr has shown that the embrittlement threshold and hydrogen absorption of E110 advanced claddings are the same as those for Zircaloy-4 and M5 claddings (see Fig. 15).

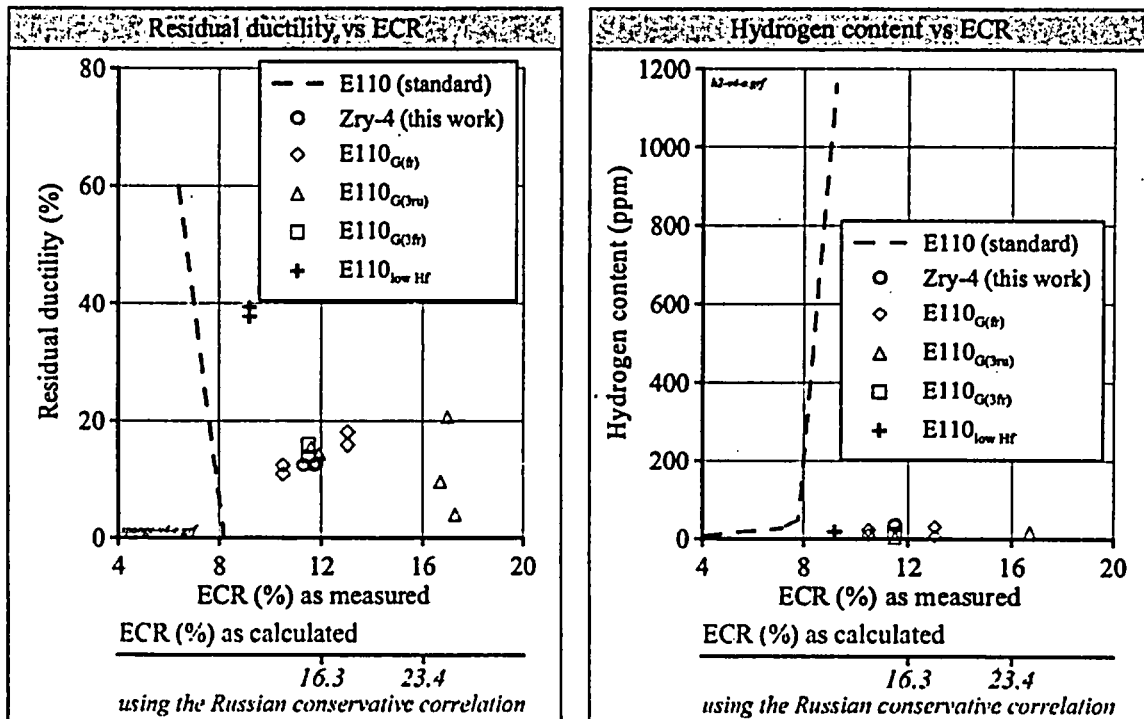


Fig. 15. Comparative data to characterize the bulk chemistry effects

- 4.4. In accordance with the obtained data, the chemical composition of impurities in the cladding material is considered as a key factor responsible for the different oxidation behavior of different zirconium-niobium alloys.
- 4.5. An additional confirmation of the importance of the bulk chemistry was obtained due to the tests with $E110_{low Hf}$ cladding. The traditional iodide/electrolytic Zr mixture was used to fabricate the Zr-1%Nb ingot for this cladding. But a special procedure was applied to decrease the Hf content in the electrolytic Zr. Oxidation and mechanical tests demonstrated that the corrosion resistance of $E110_{low Hf}$ cladding was better than that for the standard E110 cladding (Fig. 15). However, it is known that hafnium is the neutral element in the context of the cladding oxidation behavior.

Therefore, it can be assumed that purifying of electrolytic Zr from hafnium was accompanied by the change in the content of other impurities also.

- 4.6. It was revealed that the oxidation rate of the "sponge" E110 cladding at 1000 C is much less than that for the zircaloy cladding. After 5000 seconds of oxidation, the ECR in Zr-1%Nb cladding was about 11.5 % (as-calculated) only. These data allow to formulate the problem of the representativity for the current safety criteria (18 %) under LOCA conditions. Moreover, these data show that zircaloy oxidation kinetics correlations should not be applied for the zirconium-niobium cladding manufactured from the sponge material.
- 4.7. The integral analysis of this work results allows to conclude that the best way for the improvement of the corrosion resistance of E110 claddings is as follows:
 - sponge Zr should be used for the fabrication of Zr-1%Nb alloy;
 - polishing of the internal and external surfaces of the E110 cladding could be recommended as the final conditioning.

References

- [1] V. Asmolov, L. Yegorova, K. Lioutov, V. Smirnov, A. Goryachev, V. Chesanov, V. Prokhorov "Understanding LOCA-Related Ductility in E110 Cladding", *Proceedings of the 2002 Nuclear Safety Research Conference*, NUREG/CP-0180, March 2003, pp.109–125.
- [2] Brachet J., Pelchat J., Hamon D., Maury R., Jaques P., Mardon J. "Mechanical Behavior at Room Temperature and Metallurgical Study of Low-Tin Zry-4 and M5™ (Zr-NbO) Alloys after Oxidation at 1100°C and Quenching", *Proceedings of IAEA Technical Committee Meeting on "Fuel Behavior under Transient and LOCA Conditions"*, Halden, Norway, September 10–14, 2001.
- [3] Mardon J., Frichet A., Bourhis A. "Behavior of M5™ Alloy under Normal and Accident Conditions", *Proceedings of Top Fuel-2001 Meeting*, Stockholm, May 27–30, 2001.
- [4] M. Billone "Overview of Advanced Alloy Post-Quench Ductility Program", *Proceedings of ANL High-Burnup Cladding Performance Review Meeting*, July 16–17, 2003, ANL.
- [5] H.M. Chung "The Effects of Aliovalent Elements on Nodular Oxidation of Zr-1%NbBase Alloys", *Proceedings of Nuclear Safety Research Conference*, Washington DC USA, October 20–22, 2003, to be published.
- [6] D.Gilbon et.al. "Irradiation Creep and Growth Behavior, and Microstructural Evolution of Advanced Zr-Base Alloys", *Zirconium in the Nuclear Industry: Twelfth International Symposium, ASTM STP 1354*, 2000, pp.51–73.

RECENT DATA ON M5™ ALLOY UNDER LOCA CONDITIONS

J.P.Mardon¹ - N.Waeckel²

1-Framatome ANP SAS,France

2- EDF-SEPTEN,France

Abstract

Experience feedback from irradiation in PWRs has confirmed that M5™ possesses all the properties required for upgraded reactor operation under normal conditions. Several papers recently reported Nb based alloys may have worse behavior under LOCA conditions than Zircaloy-4. To address this issue, Framatome-ANP and EDF started in CEA labs a number of full-scale tests and comprehensive analyses on both M5™ and SRA low-tin Zircaloy-4.

We will focus hereafter on the behavior of pre-hydrided M5™ cladding in LOCA conditions as compared to the Zircaloy-4 behavior.

We first present the recent research on phase transformation kinetics, mechanical behavior (creep and temperature ramp tests), oxidation kinetics and quench behavior of pre-hydrided samples as compared to as-received material.

It is noticed that the phase transformation kinetics and mechanical behavior of both virgin alloys are very similar and are not affected by pre-hydridding for a hydrogen content (150 ppm) greater than the value obtained at EOL for elevated burnups for M5™.

At high-temperature the M5™ cladding exhibits oxidation kinetics and quench behavior at least equivalent to Zircaloy-4.

The oxidation kinetics fits well with the Cathcart-Pawel correlation and the Baker-Just correlation is still overly conservative. No breakaway of the oxidation reaction has been detected up to 1400°C for LOCA prototypical time ranges. No effect of hydridding on the oxidation kinetics of the two alloys is noted, in particular the Baker-Just correlation remains conservative up to an hydrogen content of 450 ppm.

The M5™ cladding failure threshold upon quench doesn't vary much from 1100 to 1300°C: the physical failure limit upon quench is greater than 27% ECR or 38% ECR when calculated with the Baker-Just correlation. To take into account the influence of high- burnup conditions, quench tests were performed on pre-hydrided samples for a testing temperature of 1200°C. Hydrogen content has only a little influence on their resistance to quenching after oxidation at 1200°C.

The post-quench mechanical properties, for different high temperature oxidation levels, between 1000 and 1200°C, were then investigated for both M5™ and Zircaloy-4 alloys. The residual ductility properties at RT were determined using impact, bending and compression tests.

After single face oxidations giving weight gains ranging from ~4 mg/cm² up to ~38 mg/cm² and according to the measured residual ductility/toughness properties at RT, we can observe that the M5™ and Zy-4 alloys have comparable properties. Also, it is worth noticing that, even for the M5™ alloy, no hydrogen pick-up is observed after oxidation at 1100°C and 1200°C. We only measured hydrogen pick-up at 1000°C for both alloys (Zy4 and M5™), after the beginning of the break-away phenomenon occurring for times much higher than the prototypical LOCA time range (less than 30 min). In addition, it was found that there is a residual ductility for both alloys even at the maximum oxidation within the range of the tested conditions. All these results are different from previously published data on Zr-1%Nb alloy.

For Nb-containing alloys, recent studies suggest that the impurity content in the metal (Ca, Hf), the SPP (Secondary Phase Particle) size and distribution and the surface finish

(chemistry and roughness) may play a significant role in the oxidation and the quench performance.

In the second part of this paper, we present the study performed before 1996 by Framatome-ANP within the scope of the optimization of the M5™ cladding tubes. The various possible factors and potential causes of variability have been thoroughly analyzed from the point of view of their impact on the finished product properties (corrosion, phase transformation kinetics).

In this way, all the chemical composition variabilities of the alloying elements and impurities (Fe, O, S, Hf, Al, N, C, Ca, ...) have been investigated. Also, a number of manufacturing process variants (Zircon, ore, Zr sponge, β -quench, heat treatments, ID and OD surface preparations) have been studied. Finally, the impact of the microstructure (SPPs chemical composition size and distribution) on the heterogeneous corrosion has been investigated.

It has been shown that most of these parameters have little or no impact on the high temperature oxidation and quench behavior of the Nb based alloys tested and selected.

Key words: Nuclear fuel, M5, LOCA, experience

1. Introduction

Framatome ANP's products and services are targeted to meet the requirements for lower operating costs and higher safety margins demanded by today's nuclear market. Low fuel cycle costs help to ensure the competitiveness of nuclear power generation.

The opportunities for cost reduction, i.e.:

- burnup extension up to 70 GWd/tU and,
- the use of high duty fuel management schemes

are currently reviewed and analyzed by the utilities and implemented depending on licensing requirements and conditions which vary in the different countries. Depending on their market needs, some utilities require additional operational flexibility, i.e. for load follow operation [1].

For the fuel supplier, the demands and expectations of the customer translate into product requirements as follows:

- High reliability within a wide range of normal and hypothetical accident operating conditions and, more specifically, with respect to fuel assembly design and cladding material
- Dimensional stability
- High corrosion resistance and low hydrogen pickup
- Improved PCI (pellet-cladding-interaction) behavior
- Compliance with RIA and LOCA criteria.

Based on an extensive program of optimisation and industrial development, Framatome ANP is now offering utilities its M5™ alloy exhibiting the aforementioned properties for the increasingly challenging operating conditions.

Within the scope of the optimisation of M5™ as an industrial product, the chemical composition including so-called impurities as well as the fabrication process were varied in a broad range [2]. Based on out-of-pile and in-pile results it can be stated that M5™ - α -processed, fully recrystallized and containing a well-balanced amount of S, O, Fe and C besides the main elements Zr and Nb - exhibits low corrosion, low hydrogen pickup, low growth and low creep required for burnup extension to values that are achievable with today's licensed enrichment of 5% U235.

2. PWR performance of M5™ under normal operating conditions

To date, more than 550,000 fuel rods with M5™ cladding are under irradiation or discharged in 37 PWRs worldwide including 44 full reloads [3,5].

Oxide data from fuel rods with M5™ cladding clearly demonstrate the excellent corrosion behavior up to a burnup of 71 GWd/tU (Fig.1). The irradiation in reactors worldwide covers a wide range of different operating conditions: all fuel assembly arrays used in PWRs, i.e. 14x4

through 18x18, incorporating cladding with different wall thicknesses and UO₂ as well as MOX pellets, different coolant chemistry regimes including high LI, different cycle lengths, different fuel duties.

At the highest burnup achieved with M5TM in commercial PWRs, the hydrogen content is still below 100 ppm (Fig.2). The very low hydrogen level positively influences the dimensional stability, the behavior under accident conditions, and the stability in long term storage.

Compared to Zircaloy-4, M5TM exhibits a higher creep resistance and lower growth. Even for burnups as high as 71GWd/tU, no acceleration in fuel rod growth was observed with M5TM [3,5].

Ramp tests indicate a better performance of M5TM with respect to power transients as compared to Zircaloy-4, giving rise to additional margins in fuel manoeuvrability [3,5].

3. Performance of M5TM under LOCA conditions

Full-scale-testing and comprehensive analyses were performed on M5TM for comparison with SRA Low-tin Zircaloy-4 in LOCA conditions [5,10].

3.1 - Approach adopted

The LOCA criteria adopted in the wake of the ECCS (Emergency Core Cooling System) Rule-making Hearing in 1973 had the overall objective of guaranteeing core coolability. The criteria for peak cladding temperature (PCT=1204°C/2200F) and maximum equivalent oxidation (17% ECR) are the physical and quantitative translation of this objective. These two criteria were established on the basis of:

- oxidation and quench tests on single rods by Hesson-ANL and by GE, which led to the rupture limits being defined as 18.4 and 17.6% ECR respectively,
- 315°C compression tests on rings sampled from oxidized tubes at high temperature (1700 to 2400°F) by Hobson and Rittenhouse of ANL, which led to a "zero ductility" limit being located at 24% ECR (Baker-Just) and at 2200°F. This limit, based on the very abstract notion of "ductility", does not provide evidence that the geometrical integrity of the cladding is preserved, as required by the aforementioned overall objective.

To sum up, the Commission:

- considered the cladding residual ductility after a LOCA transient as an important factor for quench and not for post-quench loadings. Further, it cites neither a scenario generating post-quench mechanical loadings nor a stress/strain value that the oxidized cladding would have to withstand before or after quench; the only explicit loading is therefore the thermal shock related to the quench phase.
- preferred out of pragmatism and for the sake of conservatism to avoid any threshold effect by retaining only the worst-case points in the database, by requiring compliance with the criteria throughout the core (and therefore locally at the hottest spot) and by retaining an overall parameter (ECR) rather than a metallurgical parameter (the β phase fraction proposed by Hobson).

The experimental approach we have adopted relies upon oxidation tests with steam sweeping and instantaneous quench on empty cladding sections, tests which are more severe and performed more thoroughly and analytically than those of 1973. Direct quench performed from the oxidation temperature is a worse-case procedure with respect to the reactor case of slow cooldown (1 to 10°C/s) preceding quench. To define the rupture, we have opted for loss of integrity of the cladding tube subjected to a slight argon overpressure; this interpretation leads to an oxidation threshold equivalent to the one deduced from post-quench mechanical tests such as those of Hobson. This approach, in which the threshold is defined by loss of integrity, introduces a large conservatism with respect to material collapse, which must be avoided to guarantee core coolability.

We have adopted a broad experimental approach for differential analysis of M5TM behavior compared with Zircaloy-4 in fresh and pre-hydrided states, which relies upon :

- high temperature oxidation tests to verify the conservatism of the Baker-Just correlation
- post-oxidation quench behavior tests to justify the ECCS criteria (PCT and ECR)
- post-oxidation and quench mechanical tests to confirm the quench behavior results.

To guarantee core coolability, it has to be shown that the cladding can be raised to high temperature during a given period, which causes its oxidation and therefore embrittlement, without it leading to collapse under the effect of the mechanical loadings associated with cooldown and quench. This is the time needed at a given temperature to reach 17%ECR. The LOCA safety studies, irrespective of the type of reactor, management or transient under consideration, show that the maximum duration during which the bounding cladding temperature is beyond 600°C does not exceed 30 minutes, conservatively taking a factor 2. Of the phenomena resulting from irradiation (mechanical stresses, irradiation defects, waterside corrosion and relative hydriding), only hydriding does not disappear during the LOCA transient. The high temperatures reached during a LOCA clear all memory of irradiation in terms of annealing of defects, changes in precipitation and mechanical stresses. A cladding hydrided to a content bounding the one obtained in service will therefore accurately simulate the behavior of an irradiated cladding.

3.2 – Phase transformation and mechanical behaviour

Figure 3 shows the effect of hydrogen content on the $\alpha \leftrightarrow \beta$ phase change temperatures of M5™ measured at 10°C/min by calorimetry [11]. This figure shows that the β -gene effect of the hydrogen is clearly evidenced by the significant drop in the transus temperatures, particularly that of the low transus $T_{\alpha/\alpha+\beta}$, with an increase in hydrogen content. This effect is also observed, with the same acuity, for Zircaloy-4 both at equilibrium and in dynamic conditions. Nevertheless, since the end of life (EOL) hydrogen content of M5™ is always lower than 150ppm the effective impact of in-reactor hydrogen is less than about 30°C on the $T_{\alpha/\alpha+\beta}$ low transus at equilibrium for M5™.

Moreover, the effect of a hydrogen content of 150 ppm by weight on the mechanical behavior of alloy M5™ both in creep between 600 and 950°C (Fig 4: time to rupture and Fig 5: ductility) and in temperature ramps remains within the scatter band intrinsic to the material. As a result, at least for M5™, the phase change kinetics and the swelling – rupture models, built out of the virgin material, are applicable to the hydrided state, representative of the end of life (EOL) in-reactor conditions.

3.3 - High temperature oxidation kinetics

The double-face steam oxidation tests carried out between 700 and 1400°C on fresh M5™ and low-tin Zircaloy-4 and at 1000 and 1200°C on pre-hydrided samples up to 200 ppm (envelope value of the EOL H content for elevated burnups for M5™) and 450 ppm show that

- the oxidation kinetics of M5™ and low-tin Zircaloy-4, measured with an uncertainty of 10%, are parabolic in form between 700 and 1400°C for LOCA prototypical time ranges (Fig.6a-b) [6]. For both materials the oxidation process, combined with a dense oxide, is controlled by the same mechanism of oxygen diffusion through the oxide layer and in the metal.
- M5™ and Zircaloy-4 exhibit similar oxidation kinetics except in the 950-1050°C range, where M5™ exhibits an oxidation kinetics significantly lower (about 30%) than for Zy4 (Fig 6c)
- the Leistikow and Cathcart-Pawel laws appear to be "best-estimate" in the 1100-1400°C range and are bounding below 1050°C (Fig 7)
- the Baker-Just correlation is bounding throughout the temperature range (with a 50% margin) and especially between 950 and 1050°C (factor 2) and beyond 1200°C (Fig 7).
- no effect of hydriding on the oxidation kinetics of the two alloys has been observed, in particular the Baker-Just correlation remains conservative (Fig 8).

Given the actual oxidation kinetics of M5™ and the prototypical LOCA time frame, the time-temperature range of interest to reach 17% ECR is restricted to [t<30min and T=1000-1204°C] (Fig 9).

3.4 - Behavior upon quench

The water quench tests carried out after double-face oxidation between 1000 and 1300°C on fresh M5™ and low-tin Zircaloy-4, show that (Table.1) :

- the times to rupture, corresponding to the value of the last specimen found leak-tight, largely decrease with temperature showing embrittlement is directly related to the quantity of oxygen that penetrates into the metal
- the times to rupture at 1000°C are far higher than the prototypical times to consider for LOCA. This demonstrates, for M5™ in particular, there is no specific embrittlement issue at 1000°C.
- the quench behavior thresholds between 1100 and 1300°C are relatively insensitive to the oxidation temperature (Fig 10). They are similar for both alloys (27 %ECR realistic and 38% ECR with the Baker-Just correlation) : using the Baker-Just correlation in the design studies implies an effective 100°C margin with respect to 1204°C temperature criterion.
- no transient hydriding has been observed after the high temperature oxidation and quench (less than 17 to 25 ppm have been measured)

Quench tests carried out after double-face oxidation at 1000 and 1200°C on M5™ and low-tin Zircaloy-4 pre-hydrided up to 450ppm, show that the rupture thresholds of both alloys are similar and no significant effect of hydriding on quench behavior is observed (Table 1).

However the quench failure threshold of Zircaloy-4 at 1200°C, which is not affected by a hydrogen content up to 450 ppm (26 to 38 % ECR) tends to decrease beyond this level when the hydrogen content reaches 600 ppm.

This failure upon quench threshold drop could be related to an increase of the transient oxygen in the prior-β phase and to a higher initial and transient hydrogen contents combined with an effect of the stress state in the cladding.

Temperature (°C)	1000	1100	1200	1300	1000	1200
As-received (A)	A	A	A	A		
Pre-hydrided (ppm)					150 to 250	150 to 250
Time to failure ¹ (s) Zy4	6540	2970	950	390	4980	860
Time to failure ¹ (s) M5™	13500	2950	1200	495	4980	836
ECR-BE limit ² (%ECR) Zy4	-	30	28	28	28	26
ECR-BE limit ² (%ECR) M5™	-	28	30	31	30	26
ECR-BJ limit ² (%ECR) Zy4	-	41	41	43	41	39
ECR-BJ limit ² (%ECR) M5™	-	39	43	46	43	38

With: 1-Time to failure is corresponding to the shortest time before any of the samples failed (conservative approach)

2-ECR-BE (Best-Estimate) and ECR-BJ (Baker-Just) limit corresponding to the last non failed sample.

Table 1- Quench test results on as-received and pre-hydrided M5™ and low-tin Zircaloy-4 claddings.

3.4 - Post-quench mechanical behavior

3.4.1-As-received material

With the aim of acquiring additional data, we performed, with specimens made of fresh M5™ and Zircaloy-4, single-face oxidized at 1000, 1100 and 1200°C for several realistic ECR values, three types of post quench mechanical tests at ambient temperature :

- ring compression tests, for the sake of consistency with the 1973 Hobson tests,
- 3-point bending tests which are more rigorous,
- impact tests.

Even for test times longer than that of interest for LOCA transients ($t < 30$ min) no breakaway of the oxidation kinetics was detected (Fig 11) and no spalling was observed as mentioned by Yegorova et al. for E110 alloy [12].

For test time range of interest for typical LOCA transients, no failure upon quench has been observed, in keeping with the quench test results previously mentioned, and no transient hydriding has been observed after oxidation and quench (less than 100 ppm H typically).

Figure 12 shows the ring compression load trend versus weight gain. On this figure we can notice that the mechanical properties:

- decrease according to a $1/x$ power law with the weight gain, which confirms the embrittling effect of oxygen and the relevance of the ECR parameter,
- are equivalent for both alloys and the different types of test
- are combined with a residual ductility consistent with Hobson 1973,
- are only slightly diminished by the temperature rise from 1000 to 1200°C, particularly at high ECR.

Also, it is worth noticing that, for both alloys, no hydrogen pick-up has been observed after oxidation at 1100°C and 1200°C. We have only measured large hydrogen and nitrogen pick-up at 1000°C for both alloys Zircaloy-4 and M5™ (Fig 13), after the beginning of the break-away phenomenon occurring for times much higher than the prototypical LOCA times range known to be lower than 30 mn (Fig 14).

After single face oxidations giving weight gains ranging from ~ 4 mg/cm² up to ~ 38 mg/cm² and according to the measured residual ductility properties at room temperature (R.T), we can observe that the M5™ and Zy-4 alloys have comparable properties.

3.4.2- Pre-hydrided material

Using specimens made of M5™ pre-hydrided at 200 ppm (conservatively bounding the in-reactor EOL cladding H content) then single-face oxidized at 1200°C at several realistic ECR values, the following mechanical tests have been performed :

- ring compression tests at room temperature and 315°C
- 3-point bending tests at room temperature

At room temperature the compression tests show, for a given weight gain, that the M5™ residual ductility slightly decreases with H content but is still comparable to the one observed on the as-received Zircaloy-4 (Fig 15a).

At room temperature the bending tests show that the ductility of the M5™ pre-hydrided up to 200 ppm is almost similar to the one observed on the as-received M5™ and Zircaloy-4 materials (Fig 16).

At 135°C the compression tests show that the ductility of the M5™ pre-hydrided at 200 ppm is restored to the level of the as-received material (Fig 15b).

It is worth noticing that the pre-hydrided M5™ samples still exhibited some residual ductility even at the maximum oxidation levels that has been investigated.

3.5 - Conclusions on the cladding behaviors under LOCA conditions

The phase transformation kinetics and the thermal-mechanical models developed for fresh M5™ can be used to predict the behavior of the material with a hydrogen content greater than the value expected at 75 GWj/T.

M5™ exhibits high-temperature oxidation kinetics similar or lower than those observed with Zircaloy-4. The Baker-Just correlation is always very conservative and no runaway of the oxidation reaction has been detected up to 1400°C.

The M5™ failure threshold upon quench is almost constant in the 1100-1300°C temperature range ; it is greater than 27 % ECR realistic or 38 % ECR Baker-Just.

There is no evidence of any hydrogen effect (stemming from in-service corrosion) on the high-temperature corrosion kinetics or on the quench behavior. These results justify the validity of the 1204°C temperature criterion with a margin of at least 100°C.

The post-quench mechanical properties at 1000, 1100 and 1200°C of fresh M5™ are similar to those of fresh Zircaloy-4, in contradiction with the results obtained with the E110 alloy [12]. After oxidation at 1200°C, the post-quench residual ductility at room temperature of pre-hydrated M5™ is slightly reduced to a level almost similar to the one observed on as-received Zircaloy-4.

At 135°C, the post-quench ductility of M5™ pre-hydrated to 200 ppm (i.e. almost 2 times the H content level expected at 75 GWd/T) is similar to the one obtained on the as-received cladding.

The LOCA criteria ($T_{max} \text{ cladding} < 1204^\circ\text{C}$ and $\text{ECR} < 17\%$) are therefore fully justified and can be used for M5™ with a substantial margin of a factor 2 on the ECR threshold.

4. Optimisation of M5™ cladding tube vs. corrosion behaviour

Recent studies suggest that the impurity content in the metal (Ca, Hf), the Single Phase Precipitates (SPP) size and distribution or the surface finish (chemistry and roughness) may play a significant role on the oxidation and the quench performances of the Nb-based alloys. Before 1996 Framatome-ANP conducted an extensive optimization program of the M5™ alloy. The various possible factors and potential causes of variability were thoroughly analyzed from the point of view of their impact on the finished product properties.

In this way, all the chemical composition variabilities of the alloying elements and impurities (Fe, O, S, Hf, Al, N, C, Ca) have been investigated. Also, a number of manufacturing process variants (Zircon ore, Zr sponge, β -quench, heat treatments, ID and OD surface preparations) were studied.

4.1- Influence of chemical composition

Although Zirconium alloys are always fairly lean, they rarely contain more than 3 weight % of alloying additions.

A large number of different elements can be used to improve the properties of the pure metal. The choice of what is considered as the major alloying elements is, to some extent, arbitrary. However, only iron, chromium, nickel, vanadium, tin, niobium and oxygen are added in significant amounts in industrial alloys. In contrast, elements such as carbon, silicon, nitrogen, hydrogen, sulphur, chlorine, aluminium, etc., are usually present at levels of no more than 100 ppm by weight.

In general, alpha-stabilizing elements are relatively soluble in alpha zirconium when they produce little distortion in the hexagonal lattice. This is true for tin, oxygen and nitrogen. Conversely, beta-stabilizing elements are often poorly soluble in the alpha phase (they induce a strong lattice distortion), but are relatively soluble in the beta phase. Elements of this type include transition metals such as iron, chromium, nickel, etc. Thus, niobium is a beta-stabilizer, with a solubility in the alpha phase close to 0.6% in weight or atomic %, whereas it forms a continuous series of solid solutions with beta zirconium.

The influence of addition elements around the M5 composition is summarized below.

In the range 0.8% - 1.5%, **Niobium** seems to have little effect on the corrosion, both in steam and in lithiated water. For very low Nb contents (Nb < 0.4 wt%, but depending on other parameters like the iron content), there is a dramatic increase in the corrosion rate at 415 °C or 500 °C in autoclave .

The role of **Iron** is not totally clarified. However, it does not seem to be very important in autoclave under steam conditions. Its influence on corrosion in autoclave under steam conditions (400, 415 and 500°C) is negligible up to 0.29 %. Iron reduces the sensitivity to oxygen in 360 °C water conditions.

Up to 40 ppm, **Sulphur** has no impact on corrosion in autoclave (400°C, and 360°C 70 ppm Li) .

Carbon has a strong deleterious influence on steam corrosion in autoclave at 400 and 415 °C, much more pronounced than for Zircaloy-4 or Zircaloy-2. An increase of 100 ppm in the carbon content leads to 35 to 55% increase of the weight gain.

Aluminum between 20 and 150 ppm has a detrimental influence on corrosion in autoclave at 400 and 415 °C and in lithiated 360 °C water where the effect is very pronounced.

Nitrogen has a detrimental influence on corrosion in autoclave at 400 and 415 °C.

A good correlation between corrosion results and the sum **N+C+Al** has been observed (Figure17).

Tin has a detrimental influence on the corrosion in autoclave under steam conditions (500°C, 415 and 400°C), which can be neglected below 100 ppm Sn. Tin is undoubtedly detrimental for in-pile corrosion, at least for contents > 0.5%. However, for low levels up to a few 0.1%, it does not seem to have a big influence.

Silicon is detrimental for the corrosion resistance in autoclave in steam at 400 and 415 °C and in lithiated water at 360 °C from 80 to 110 ppm. For lower contents, its effect is negligible. The existence of a threshold at about 80 ppm Si is confirmed after 400°C steam corrosion test.

The influence of **Oxygen** on corrosion in steam in autoclave at 400 and 415 °C can be neglected in the range 900 – 1800 ppm.

Hafnium possible impact is going to be investigated.

It appears that the M5™, with its well-mastered chemical composition, has a rather stable behavior as regards to usual conditions. Variations of the main addition elements (Nb, Fe, O, S) in the specified ranges have little influence on the standard corrosion behavior. However, some impurities such as Al, N, C must be carefully controlled. Improvements in oxidizing or galvanic coupling conditions could be obtained by addition of iron.

4.2- Influence of the manufacturing process

The M5 manufacturing process was subjected to extensive investigations relatively to the corrosion behavior. Number of variants has been tested beside the M5 low-temperature process, with a fully recrystallised final state. We will try to identify the potential impact of each process parameter, remembering, however, that interactions may exist.

The **impurity content** in sponge Zr, coming from ore reduction by Kroll process (Carbochloration of Zircon + Dehafniation + Carbochloration of Zirconia + Mg reduction) is very low. Typically we obtain less than 1 ppm for Ca, Mg, Sn, S and a few ppm for Si, Zn, Al.

The number of **melting** (2 and 3) has no influence on 400°C steam autoclave corrosion.

The two usual **quenching modes** (log quench after heating in an electric furnace, and solid billet quench after induction heating) have no influence on steam autoclave corrosion (400, 415 and 500 °C).

The extrusion temperature, as well as the change in the billet dimensions has no impact on the corrosion in autoclave at 415°C and at 360°C 70 ppm Li.

The number of pilgering steps has no influence on the autoclave steam corrosion.

As a general rule, the mixed and high temperature processes lead to a very poor corrosion resistance in water, and to a very high sensitivity to oxygen dissolved in water. This bad behavior, due to non-optimized microstructure (Fig 18a), is observed also in 400 and 415°C steam medium. The low temperature process produces an optimized and stable microstructure (Fig 18b) with excellent corrosion behavior in all test conditions.

When the last heat treatment temperature is raised from 580 °C to 625 °C, there is a pronounced degradation of the corrosion resistance. Increasing the temperature of the last heat treatment from 580 °C to 700-1000°C degrades strongly the corrosion resistance in steam in autoclave at 415 °C.

Several OD surface preparations have been investigated (pickling, blasting, mechanical polishing). This operation strongly influences the corrosion behavior. We have selected the OD polishing with grinding and scotch-brite wheels. This specific surface preparation exhibits a low surface roughness with a Ra value of 0.15 µm (Fig 19 b), a low fluorine contamination of 0.02 at% [Zr] at % and excellent corrosion behavior. A higher OD roughness of 0.35 µm (Fig 19 a) is associated with a poor high temperature corrosion behavior.

Etching the low-roughness outer surface with hydrofluoric acid removes a few µm layer of the final cladding but does not affect the weight gain after corrosion test. However, the visual aspect of the oxide layer is more uniform for the etched samples.

The same etching, followed with a poor rinsing will lead to a non-uniform oxide layer after oxidation, due to surface fluoride contamination. A soft brush eliminates these fluorides. This last operation is very efficient to eliminate the possible residual fluorides.

4.3- Conclusion

The M5 corrosion behavior is fairly robust regarding:

- the variation of chemical composition, except the Al+C+N content that must be lowered as much as possible,
- the manufacturing process variation, with the major exception of the annealing temperature that must be carefully controlled below the eutectoid temperature. All the processes leading to the presence of β-Zr (high temperature process, quenching as a final step) must be avoided.

5. General conclusion

Alloy M5™ is fully optimised and industrially mastered, its properties are stable and its stability is maintained under irradiation.

Experience feedback from irradiation in PWRs clearly demonstrated that M5™ possesses all the properties required for upgraded reactor operation under normal conditions.

Tests under LOCA conditions demonstrate that M5™ complies with all the design requirements, including all the accident phases.

It has been shown that most of the M5™ chemical composition variabilities and process parameters have little or no impact on the high temperature oxidation and quench behavior of the Nb- based alloys tested and selected.

The authors thank Jean-Christophe BRACHET, Laurence PORTIER and Valérie MAILLOT from CEA for their experimental works.

M5 is a trade mark of Framatome ANP

References:

- [1] J.P. West et al., "Challenges for the Nuclear Fuel – A Utility Perspective", Proceedings of the International Topical Meeting on LWR Fuel Performance, Park City, Utah, April 10-13, 2000, p. 745.
- [2] J.P. Mardon et al., "Influence of composition and Fabrication Process on Out-of-Pile and In-Pile Properties of M5 Alloy", Twelfth International Symposium on Zirconium in the Nuclear Industry, ASTM STP 1354, Jan. 2000, p. 505
- [3] A.Seibold and J.P.Mardon., "M5™ cladding experience in European PWRs", JTK'2002; Stuttgart, May 14-16,2002, pp292-298.
- [4] G.L.Garner and J.P.Mardon, "Performance of alloy M5™ in a high duty US reactor" Nuclear Engineering International, September, 2002.
- [5] J.P.Mardon, G.L.Garner and A.Seibold, "Performance of M5™ alloy under normal and accident conditions", PBNC'2002, Shenzhen, China, October 21-25, 2002.
- [6] J.P. Mardon et al., "Behavior of M5™ alloy under Normal and Accident Conditions", TopFuel Stockholm, May 27-30, 2001, p. 2.7
- [7] J.P. Mardon et al., "Justification of M5™ Alloy Behavior under Accident Conditions", Annual Meeting Nuclear Technology Dresden, May 15-17, 2001, p. 389.
- [8] A. Le Bourhis "Ring compression tests results on M5 LOCA embrittlement", LOCA topical meeting on fuel safety criteria, Aix en Provence, 22-23 March 2002.
- [9] J.P.Mardon ,N.Waeckel "Behavior of M5™ alloy under LOCA conditions" ANS-Top-Fuel, Wurzburg, March 17-19,2003
- [10] J.P.Mardon et al. "Performance of M5™ alloy as cladding tube and structural component material" 18th KAIF-KINS, Séoul, April 9-11, 2003
- [11] J.C.Brachet et al. "Influence of hydrogen content on the α/β phase transformation temperatures and on the thermal-mechanical behavior of Zy4, M4(ZrSnFeV) and M5™ (ZrNbO) alloys during he first phase of LOCA transient" ASTM STP 1423, Annecy, June 10-14,2001, pp 673-701.
- [12] L.Yegorova et al. "Understanding LOCA-related ductility in E110 cladding", NSRC 2002, Washington, October 29th, 2002.

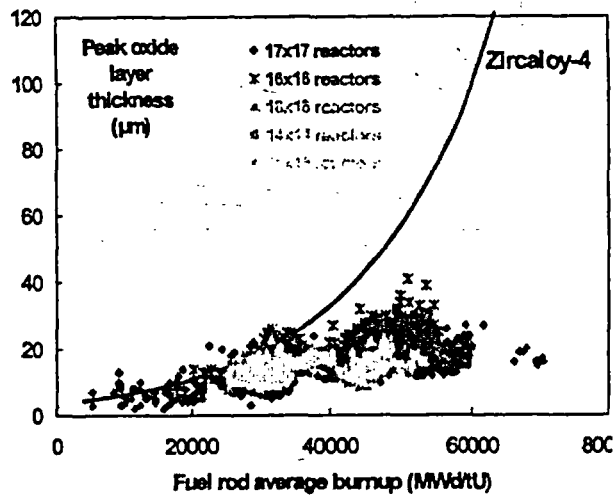


FIGURE 1 - Corrosion performance of M5™ in PWRs

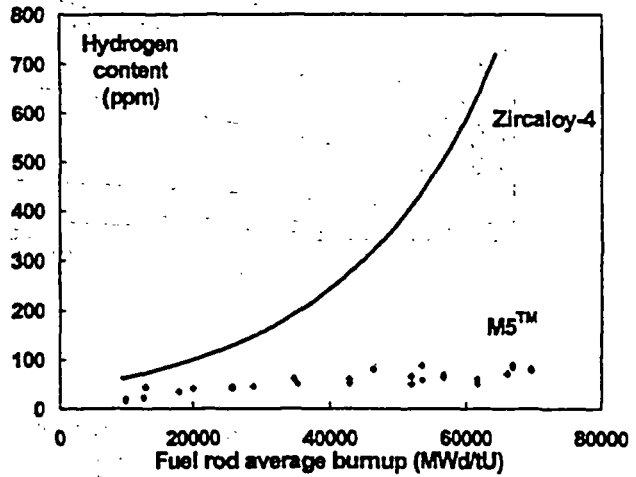


FIGURE 2- Hydrogen performance of M5™ in PWRs

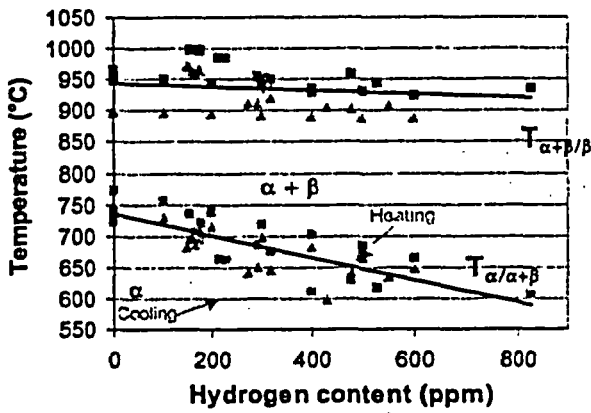


FIGURE 3 – Phase transformation temperature of M5™ vs. hydrogen content

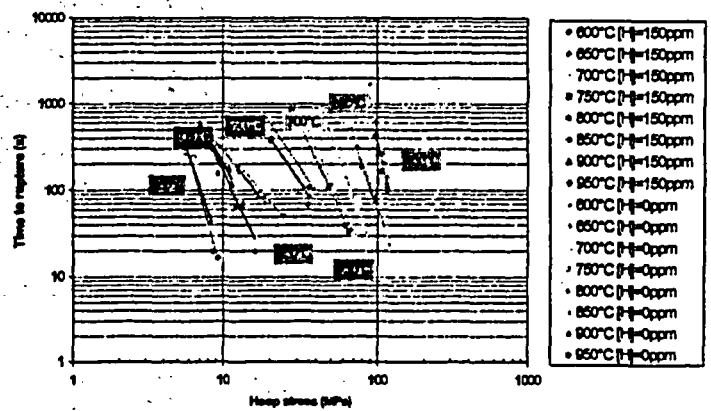


FIGURE 4 – Time to rupture vs. hoop stress for as-received and pre-hydrated M5™ - Creep test.

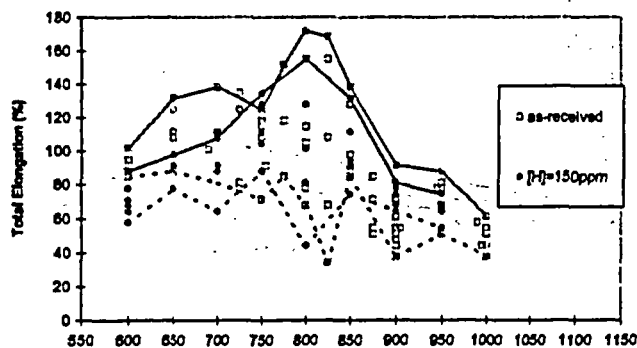
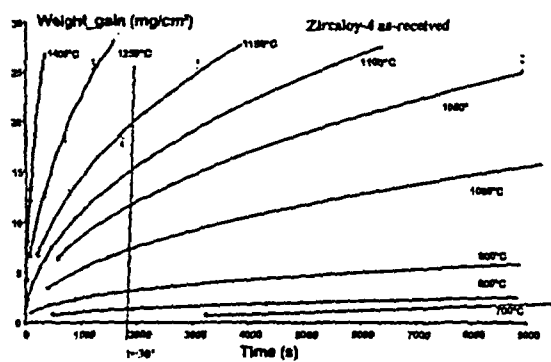
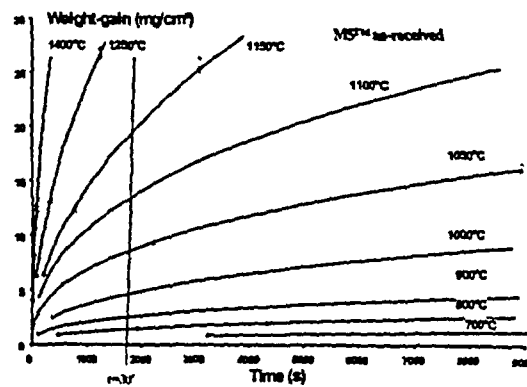


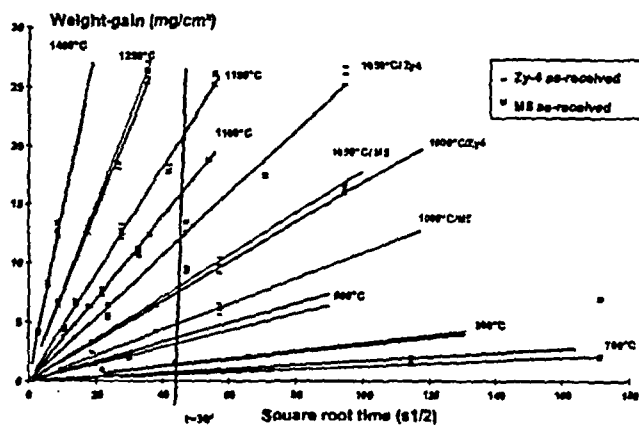
FIGURE 5 – Total elongation vs. test temperature for as-received and pre-hydrated M5™ - Creep test



6a



6b



6c

FIGURE 6- High temperature oxidation kinetics for M5™ and low tin Zircaloy-4

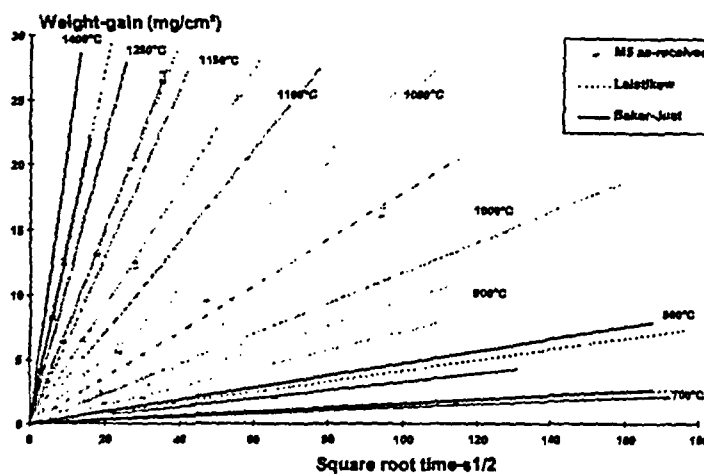
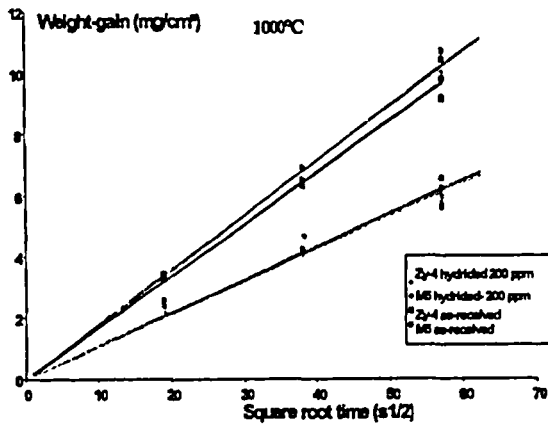
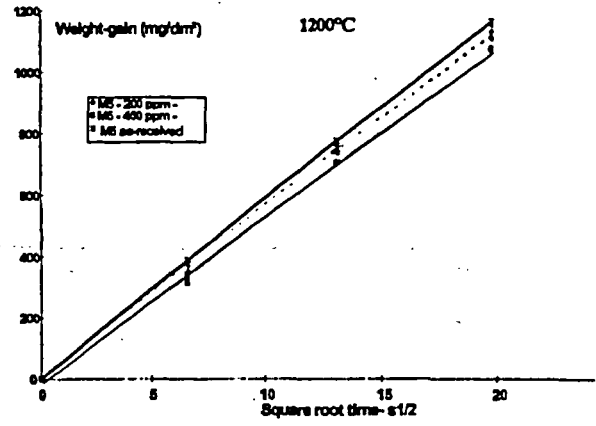


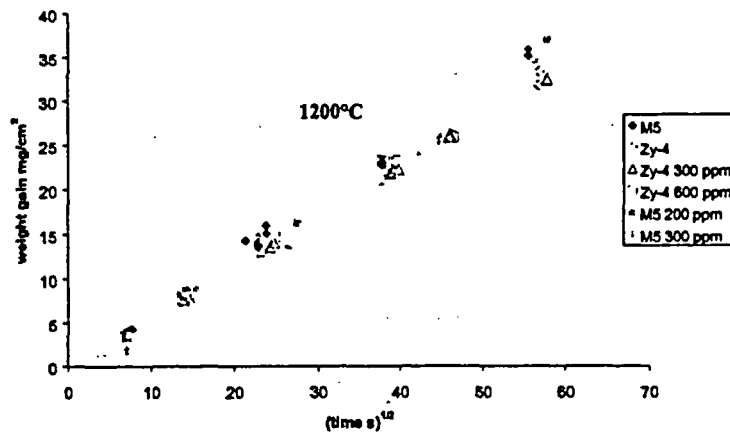
FIGURE 7 - M5 corrosion kinetics, comparison with Baker-Just and Lestikow correlations



8a



8b



8c

FIGURE 8 -Effect of hydrogen content on M5 and Zircaloy-4 corrosion kinetics at 1000°C (a) and at 1200°C (b and c).

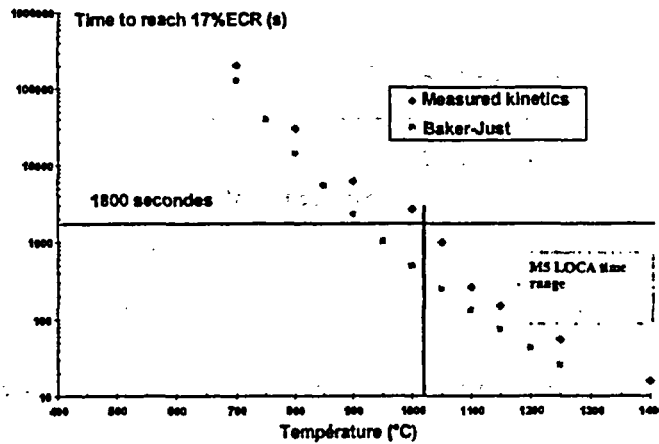
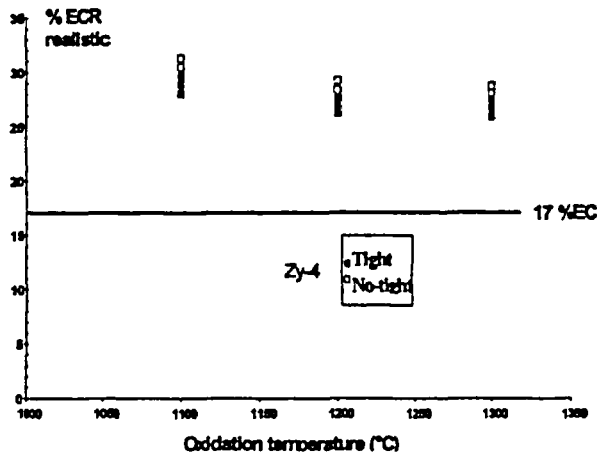
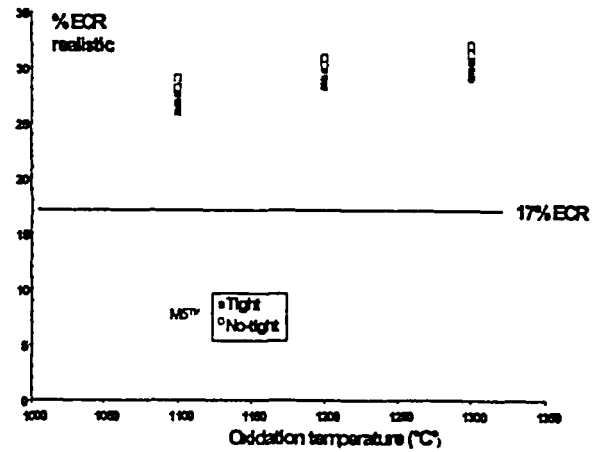


FIGURE 9- LOCA time-temperature range of interest for M5™



10a



10b

FIGURE 10 - Quench behavior thresholds for Zircaloy-4 (a) and M5 (b)

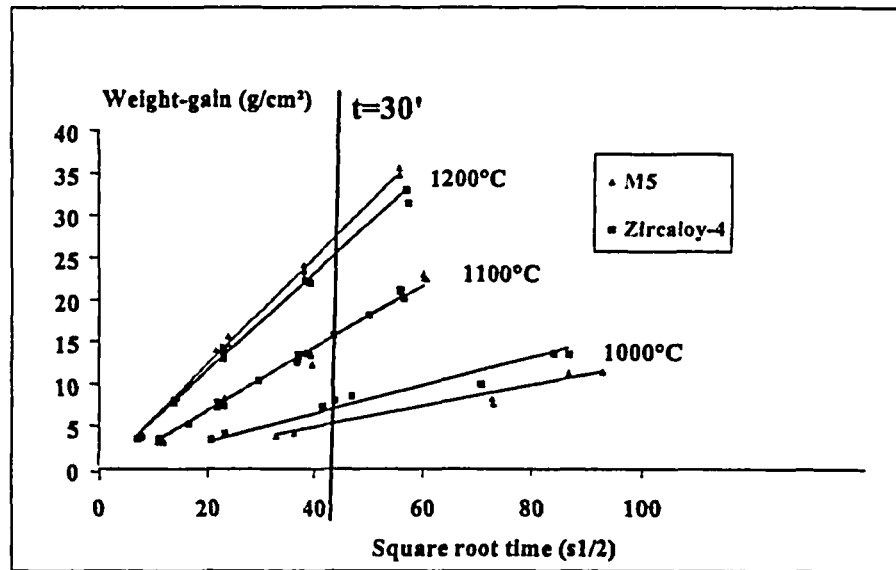
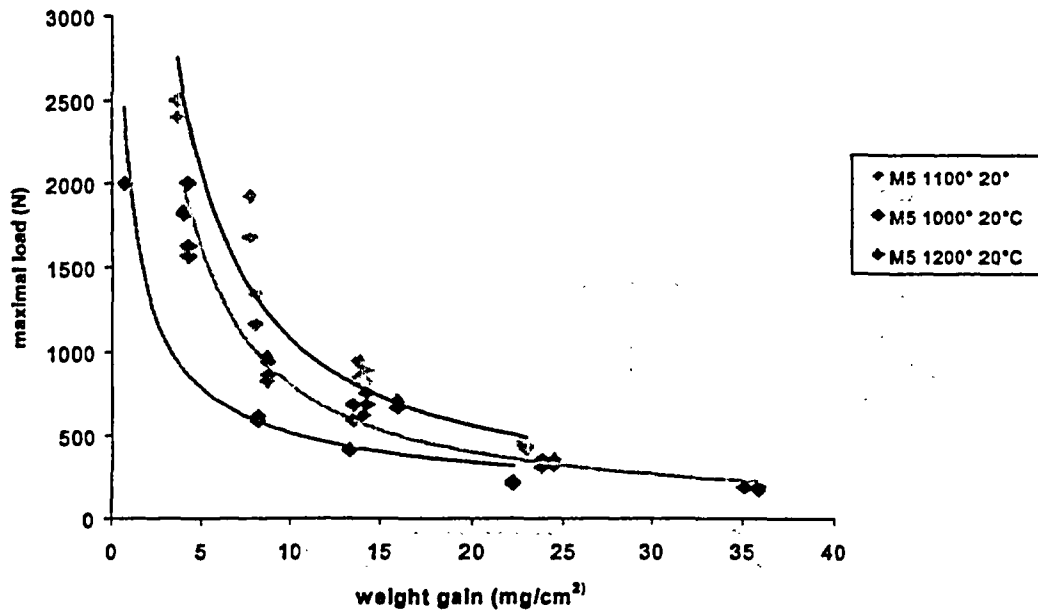
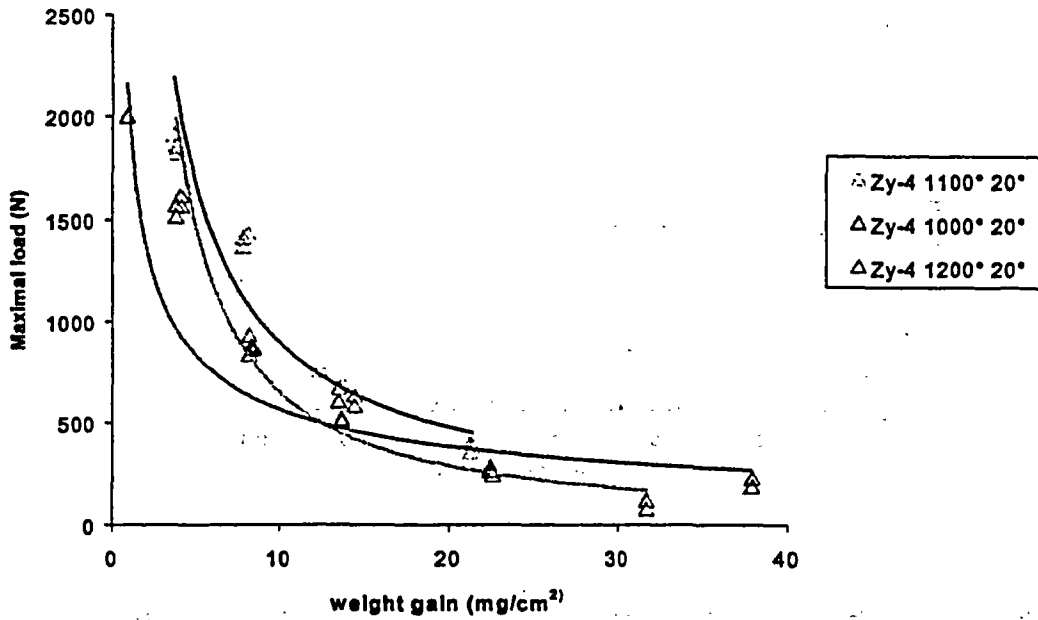


FIGURE 11- M5 and Zircaloy-4 single face oxidation kinetics at 1000,1100 and 1200°C

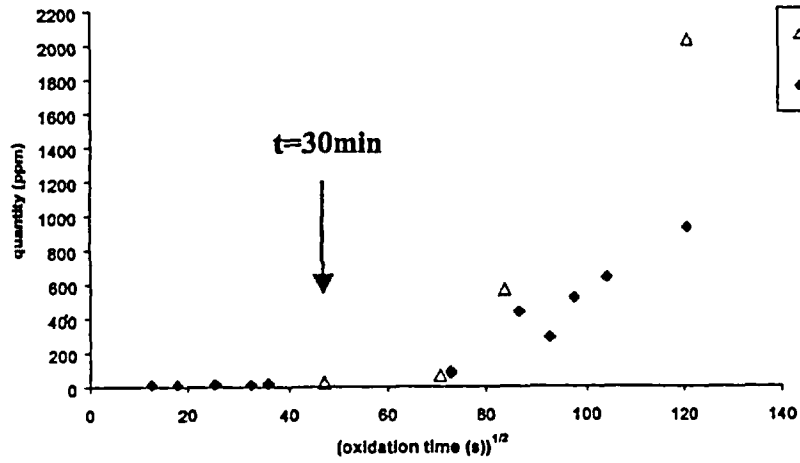


12a

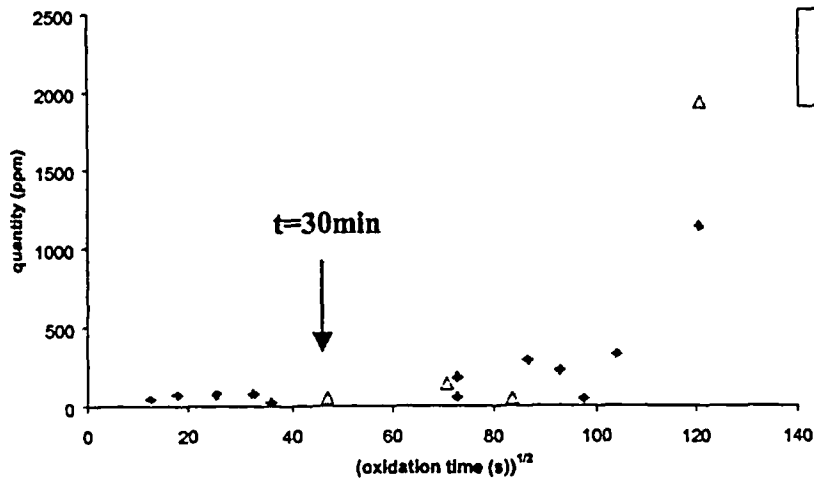


12b

FIGURE 12- Room temperature ring compression test on M5™ (a) and low-tin Zircaloy-4 (b) at 1000, 1100 and 1200°C



13 a



13 b

FIGURE 13 – Hydrogen (a) and Nitrogen (b) pick-up on M5 and Zircaloy-4 after single face oxidation kinetics at 1000 °C

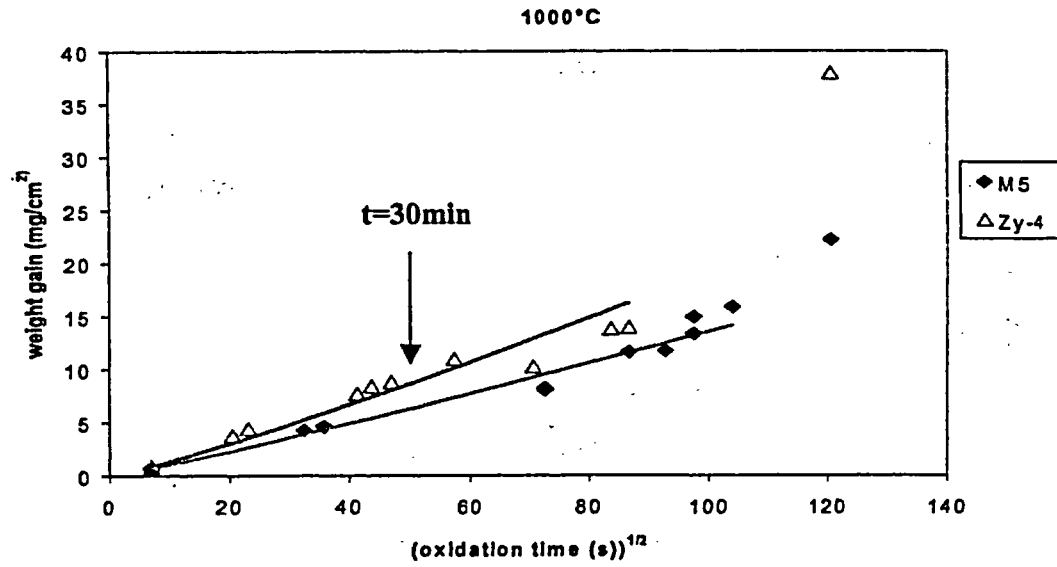
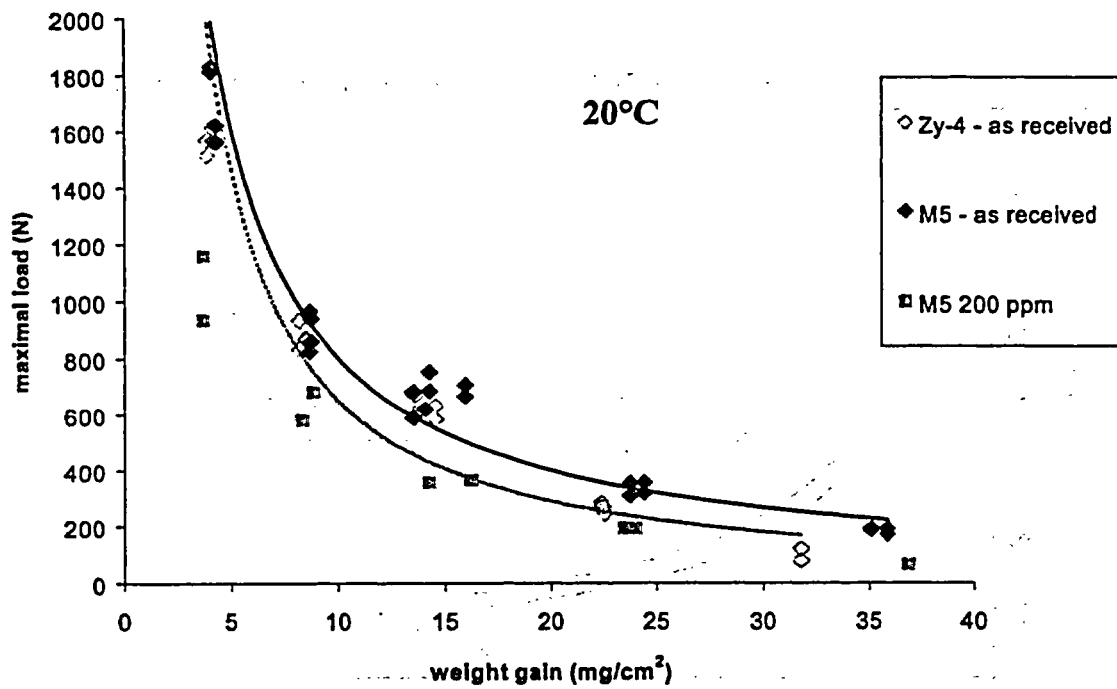
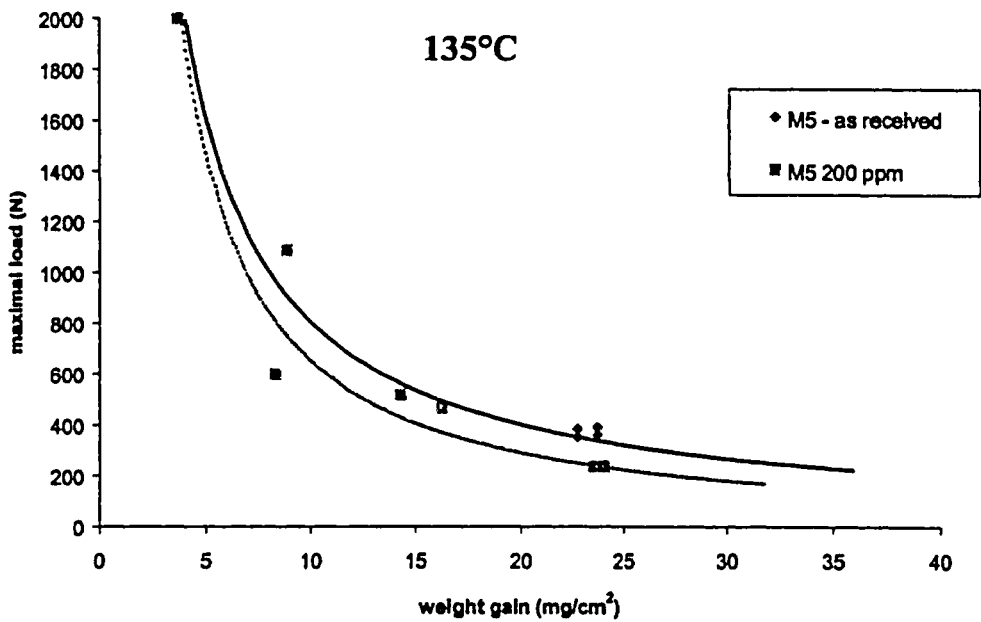


FIGURE 14 - M5 and Zircaloy-4 single face oxidation at 1000°C



15 a



15 b

FIGURE 15- Room temperature (a) and 135°C (b) ring compression test on as-received and pre-hydrated M5™ after oxidation and quench at 1200°C

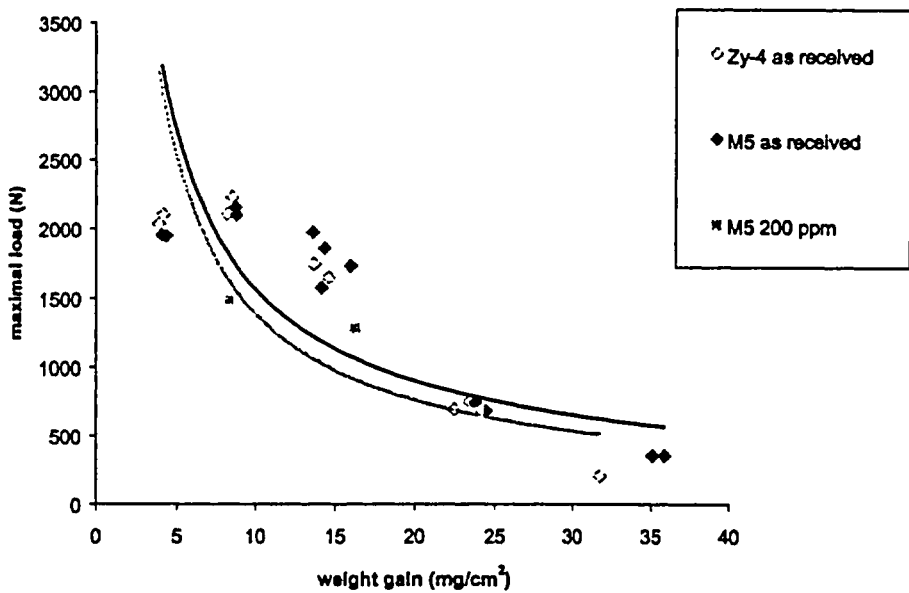


FIGURE 16- Room temperature 3-point bending test on as-received and pre-hydrated M5™ after oxidation and quench at 1200°C

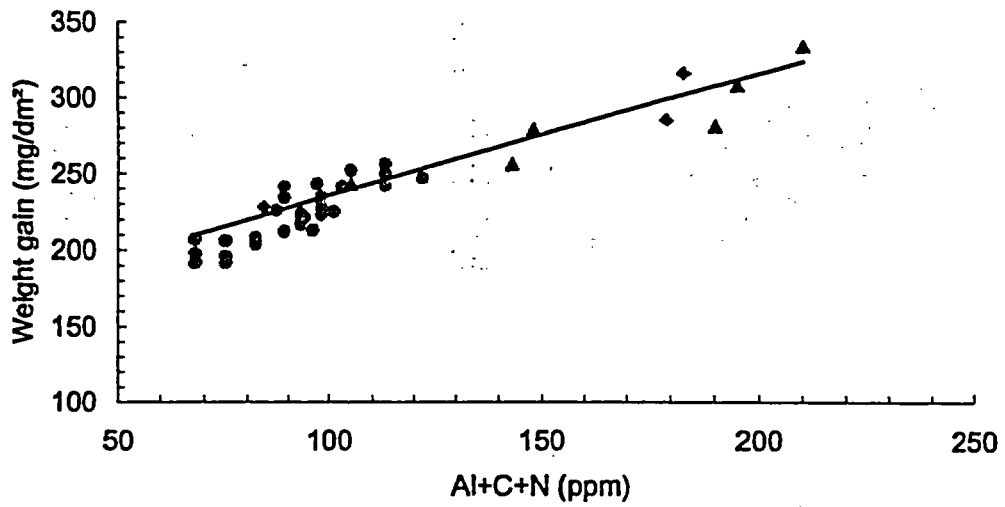
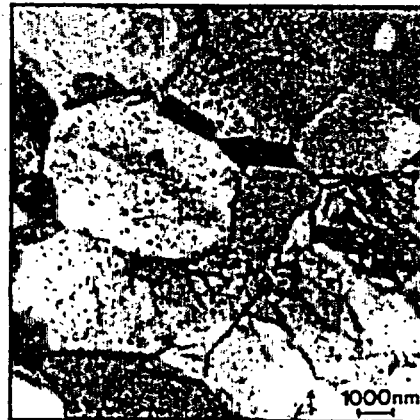


FIGURE 17- Influence of C+Al+N on the weight gain after 415°C autoclave steam test after 250 days

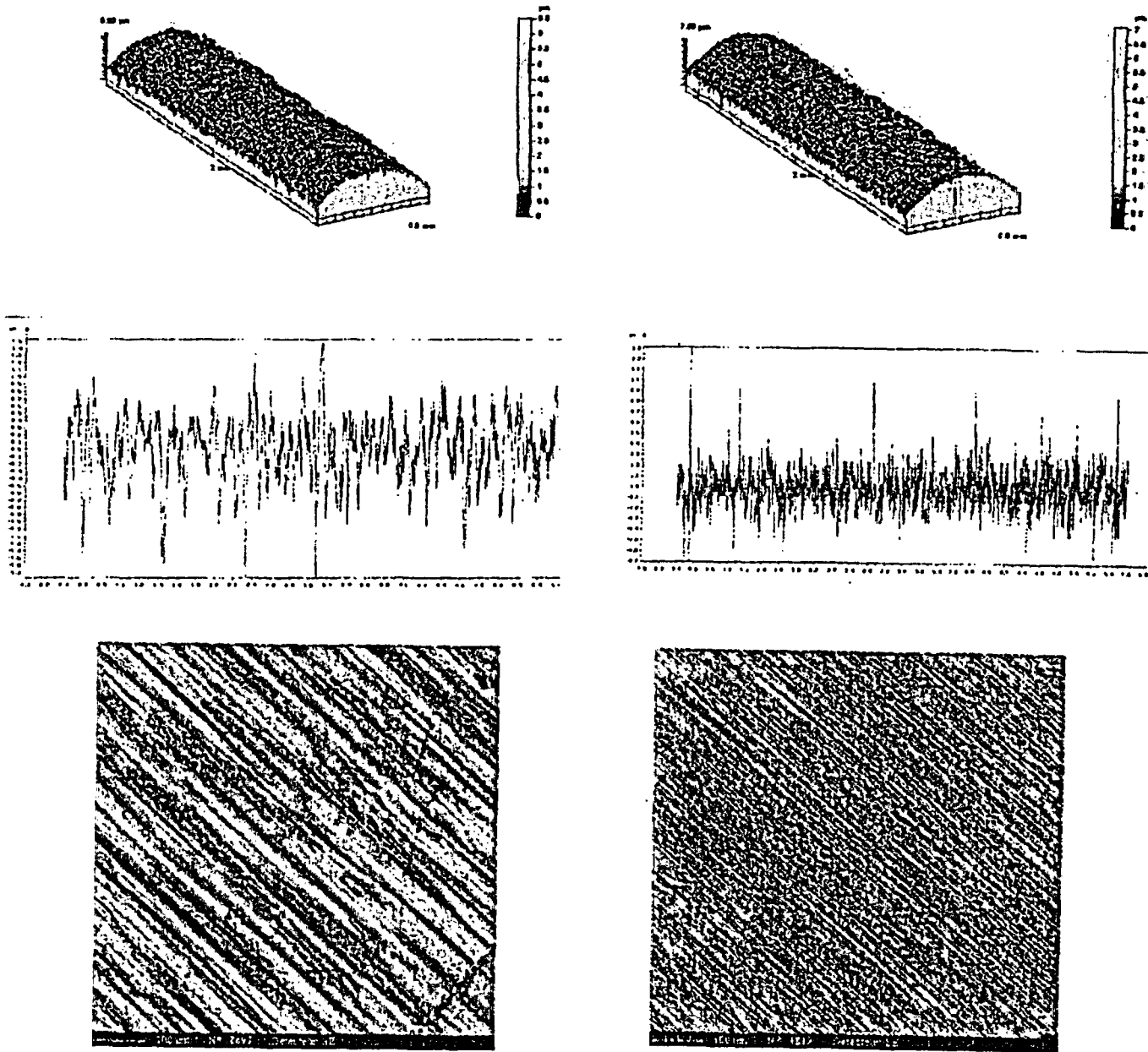


(β -Zr, β -Nb) alignments // rolling direction



M5™ "low temperature" process

FIGURE 18- Microstructure of mixed process (a) and M5 low temperature process (b)



a- Non optimized OD surface preparation

b- OD standard M5™ process

FIGURE 19- Cladding tube OD surface: 3D-roughness - Ra chart - MEB surface examination

EFFECTS OF PELLETS EXPANSION AND CLADDING HYDRIDES ON PCMI FAILURE OF HIGH BURNUP LWR FUEL DURING REACTIVITY TRANSIENTS

Toyoshi FUKETA, Tomoyuki SUGIYAMA, Takehiko NAKAMURA,

Hideo SASAJIMA and Fumihisa NAGASE

Department of Reactor Safety Research

Japan Atomic Energy Research Institute

Tokai-mura, Ibaraki-ken, 319-1195 Japan

To provide a data base for the regulatory guide of light water reactors, behavior of reactor fuels during off-normal and postulated accident conditions such as reactivity-initiated accident (RIA) is being studied in the Nuclear Safety Research Reactor (NSRR) program of the Japan Atomic Energy Research Institute (JAERI). A series of experiments with high burnup fuel rods are being performed by using pulse irradiation capability of the NSRR. This paper presents recent results obtained from the NSRR power burst experiments with irradiated PWR fuels with ZIRLO™ and MDA claddings, and discusses effects of pellet expansion as PCMI (Pellet-Cladding Mechanical Interaction) loading and cladding embrittlement primarily due to hydrogen absorption. Separate-effect studies including tube-burst and ring-tensile tests on artificially hydrided Zircaloy cladding are also described.

I. INTRODUCTION

To promote a better understanding on fuel behavior under reactivity-initiated accident (RIA) conditions, more than sixty experiments have been performed with irradiated LWR fuel rods by using a pulse-irradiation capability of the Nuclear Safety Research Reactor (NSRR). Among twenty-four PWR fuel experiments⁽¹⁾ with Zircaloy claddings, four tests at burnups of 48 to 50 MWd/kgU resulted in fuel failure and provided key information regarding hydride-assisted PCMI (pellet-cladding mechanical interaction) failure, fuel dispersal and mechanical energy generation. Fuel failures and fuel fragmentation have been observed also in BWR fuel experiments⁽²⁾ at burnups above 61 MWd/kgU.

II. NSRR EXPERIMENTS

Pulse-irradiation experiments in Nuclear Safety Research Reactor (NSRR)

The NSRR is a modified TRIGA-ACPR (Annular Core Pulse Reactor) of which salient features are the large pulsing power capability which allows the 10% enriched fuel to be heated by nuclear fission to temperature above the melting point of UO₂; and large (22 cm in diameter) dry irradiation space located in the center of the reactor core which can accommodate a sizable experiment. The core structure is mounted at the bottom of a 9 m deep open-top water pool, and cooled by natural circulation of the pool water. The NSRR core consists of 149 driver uranium-zirconium hydride (U-ZrH) fuel/moderator

elements, six fuel follower regulating rods and two fuel follower safety rods. The pulsing operation is made by quick withdrawal of enriched boron carbide transient rods by pressurized air. The pulsing power escalation is controlled by spectrum hardening caused by the moderator temperature increase, and the Doppler effect in the NSRR. During the maximum reactivity insertion of $3.4\% \Delta k/k$ ($\$4.67$), the pulse power reaches 21.1 GW with a corresponding core energy release (integrated reactor power) of 117 MJ with a minimum reactor period of 1.17 ms. The energy deposition in a test fuel rod is controlled by the amount of reactor power and by the fissile content of the fuel. With the maximum pulse, approximately 2100 J/g fuel (500 cal/g fuel) can be deposited in a 10% enriched fresh fuel rod contained in a single-wall test capsule. Shape of reactor power history depends on the inserted reactivity, and the smaller pulse becomes broader. While the full width at half maximum (FWHM) in $\$4.6$ pulse is 4.4 ms, that in $\$3.0$ pulse is 6.9 ms.

The energy deposited to a test fuel during pulse irradiation, is a key attribute among test conditions, which represents magnitude of power burst. To evaluate the energy deposition, the number of fissions generated during the pulse irradiation is obtained from gamma-ray measurement of sample solution from post-pulse fuel pellet. Because additional burnup during the pulse irradiation is much smaller than that accumulated during irradiation in a commercial reactor, only short life fission products are used for evaluating the number of fissions during the pulse irradiation. Fission product Ba-140, with a half life of 12.75 days, is selected for the evaluation. In order to reduce high gamma ray background from Cs-137 and other fission products, chemical separation scheme is applied to the sample solution. A ratio between the number of fissions in unit mass of a test fuel and the integrated reactor power including power during runout phase is constant in different experiments as far as the test fuel specifications, e.g. fuel burnup, initial enrichment, dimension, etc., and test setup, e.g. irradiation capsule, coolant subcooling, etc., are identical. Since the energy deposition includes an energy released during runout phase, one should know an amount of energy promptly generated at pulse for assessment of fuel behavior. The prompt energy deposition, can be calculated by using a ratio which is provided from the EUREKA analysis⁽³⁾ as a function of an inserted reactivity. Since the NSRR transient is extremely fast, the prompt energy deposition becomes identical to peak fuel enthalpy under adiabatic assumption.

Test capsule and instrumentation

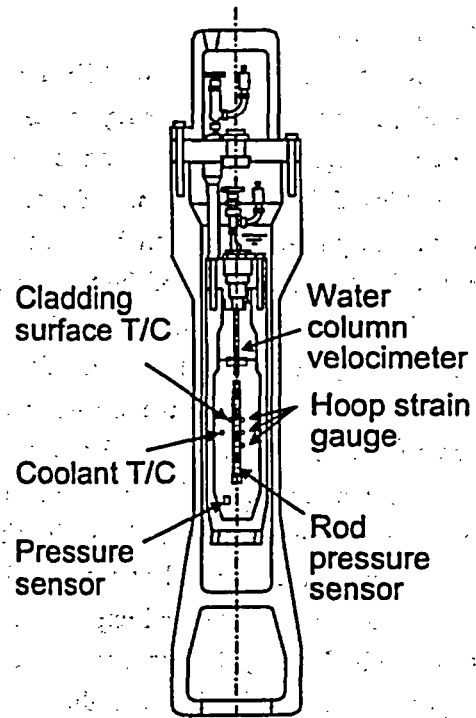
The experimental capsule used in the pulse irradiation is a double container system for the irradiated fuel rod test in the NSRR. The outer capsule is a sealed container of 130 mm in inner diameter and 1,250 mm in height, and the inner capsule is a sealed pressure vessel of 72 mm in inner diameter and 680 mm in height. The outer and inner capsules are illustrated in Fig. 1. In terms of the design of the capsule, the easiness of assembling and disassembling works by the remote handling system is one of primary concern as well as the structural strength. The capsule contains an instrumented test fuel rod with stagnant water at atmospheric pressure and ambient temperature.

Cladding surface temperatures are measured by 0.2 mm bare-wire R type (Pt/Pt 13%Rh) thermocouples (T/Cs) spot-welded to the cladding. Coolant water temperature is measured by sheathed K type (CA) thermocouples (1 mm in diameter) near the cladding surface at top of the test fuel rod and/or

center of the fuel stack. A strain gauge type pressure sensor is installed at the bottom of the inner capsule to measure the increase of capsule internal pressure. A foil type strain gauge was attached at axial center on the outer surface of the inner capsule wall to measure the deformation of capsule. In some experiments, a float-type water column velocity sensor is instrumented in order to evaluate mechanical energy caused by post-failure events.

III. TESTS OI-10 AND OI-11

PWR 55 GWd/t lead-use fuels were subjected to the Tests OI-10 and -11. The fuels had been irradiated in Ohi Unit 4 reactor for four cycles from March, 1997 to March, 2002. A fuel of the Test OI-10 has an MDA cladding and that of the Test OI-11 has a ZIRLO™ cladding. Specifications of the tested rods and conditions in power reactor operations are listed in Table 1. The both tests were performed with a cooling condition of room temperature and ambient pressure with stagnant water.



Instrumentation

Fig. 1 NSRR test capsule

Table 1 Test fuel rods in the OI-10 and OI-11

Test ID	OI-10	OI-11
Fuel type	PWR 17 x 17	
Cladding material	MDA	ZIRLO
Initial enrichment (%)	4.5	4.5
Pellet grain size (μm)	~25	~8
Operation period	4 cycles from Mar. 97 to Mar. 02	
Test rod sampling position	2nd span from the top	
Test rod burnup (MWd/kgU)	60	58
Average / Max. heat rates in PWR (kW/m)	15.6 / 19.5	15.2 / 20.3
Heat rate in last cycle (kW/m)	13.0	13.2
Cladding oxide thickness (μm)	~30	~30

Tests OI-10

MDA is an acronym of Mitsubishi Developed Alloy, and is a zirconium-based cladding alloy⁽⁴⁾ developed by Mitsubishi Heavy Industries, Ltd. for high burnup application. The alloy is designed for a better performance in terms of corrosion resistance, and has a composition of Zr-0.8Sn-0.2Fe-0.1Cr-0.5Nb. A fuel rod of the OI-10 has the MDA cladding, has pellets with the larger grain size of ~25 μm , and has been sampled from the 2nd span from the top. The burnup is 60 MWd/kgU in an average of the test segment, and the cladding oxide thickness is ~30 μm .

The test fuel rod was subjected to the pulse-irradiation in the NSRR on July 11, 2003 with conditions of 0.44 kJ/g (104 cal/g) for a peak fuel enthalpy and 5.6 ms for a pulse-width. The fuel remained intact in the Test OI-10, and the post-test rod deformation is significantly smaller than those observed in previous tests in the NSRR. The cladding residual hoop strain in the OI-10 remained only 0.7% even at a maximum location. On the other hand, approximately 5% is measured for the residual hoop strain in high burnup PWR fuel rods with Zircaloy-4 cladding after pulses with similar peak fuel enthalpy conditions. The residual strain of ~5% cannot be generated only by solid thermal expansion of fuel pellets, because the thermal expansion is only ~1.6%⁽⁵⁾ at the present fuel enthalpy condition. Previous tests with Zircaloy-4 rods suggested that the large strain was caused by fission-gas-induced pellet expansion in combination with thermal expansion during the post-DNB (departure from nucleate boiling) phase (a stable film boiling) of transients with an elevated cladding temperature⁽¹⁾. The cladding surface temperature was not measured in the OI-10 because of unsuccessful attachment of thermocouples. Although the previous experiments showed that the DNB could occur under the fuel enthalpy condition, Vickers hardness measurements indicated that the cladding is not annealed in the OI-10. This suggested that a duration of high temperature was very limited in the OI-10 even the cladding surface temperature reached several hundreds degree C. The large grain size of the OI-10 pellets may affect fission gas accumulation in grain boundaries during power-reactor irradiation (base-irradiation) and accordingly on fission-gas-induced expansion during a transient (pulse-irradiation), but the effect is not cleared at this stage.

Tests OI-11

A fuel rod of the subsequently performed OI-11 has a ZIRLOTM cladding and pellets with a conventional grain size of ~8 μm . The rod has been sampled also from the 2nd span, and has a burnup of 58 MWd/kgU and cladding oxide thickness of ~30 μm .

The test fuel rod was subjected to the pulse-irradiation on July 28, 2003. The largest pulse available in the NSRR with a width of 4.4 ms was used in this experiment. A combination of the OI-11 test rod and the largest pulse gives a condition of 0.66 kJ/g (157 cal/g) for a peak fuel enthalpy. The peak fuel enthalpy of 0.66 kJ/g is the highest among the NSRR experiments with LWR fuels irradiated in commercial reactors. The Test OI-11 resulted in fuel failure, pellets fragmentation and mechanical energy generation. Transient histories of the NSRR power, cladding surface temperature and capsule internal pressure are shown in Fig. 2. The cladding failed due to the pellet-cladding mechanical interaction (PCMI) when the fuel enthalpy reached 0.50 kJ/g (120 cal/g). The fuel enthalpy at a time of

failure was much higher than those observed in previously tested fuels with Zircaloy-4 cladding. As shown in Fig. 3, a long axial crack was observed in the post-test cladding over the active fuel length and the crack reached to the bottom end fitting resulting in separation. The cracking occurred along a position where thermocouples were welded at surface of the cladding. This fact indicated that the crack initiated from the welding position and a threshold of cladding failure in terms of a fuel enthalpy could exceed 0.50 kJ/g in the fuel rod.

Although mechanical energy generation was detected immediately after the cladding failure, and all of fuel pellets were collected from capsule water as finely fragmented particles, it is premature to discuss these in this paper.

The next experiment in the OI test series, OI-12, will be performed year 2005

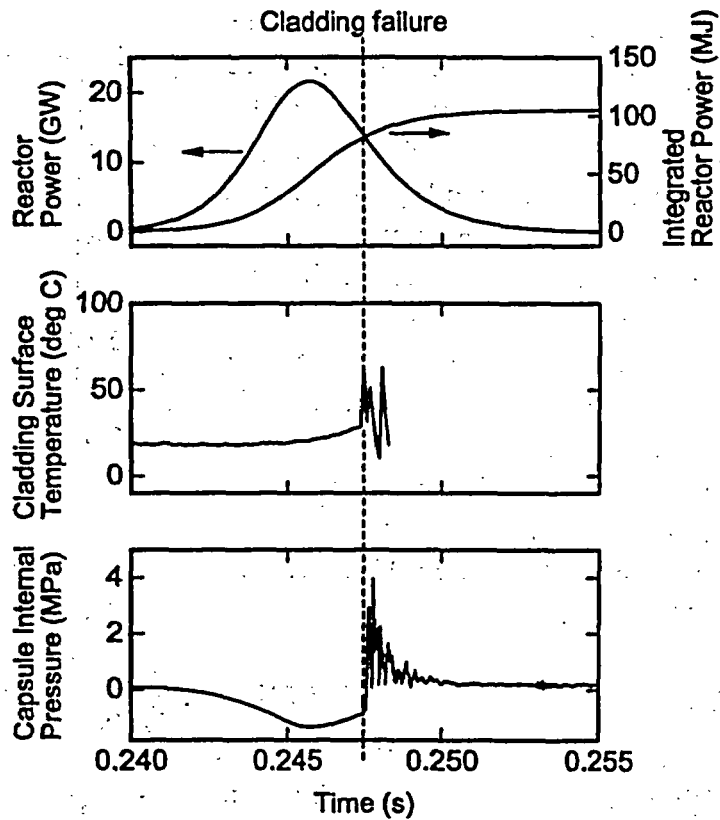


Fig. 2 Transient records in the OI-11

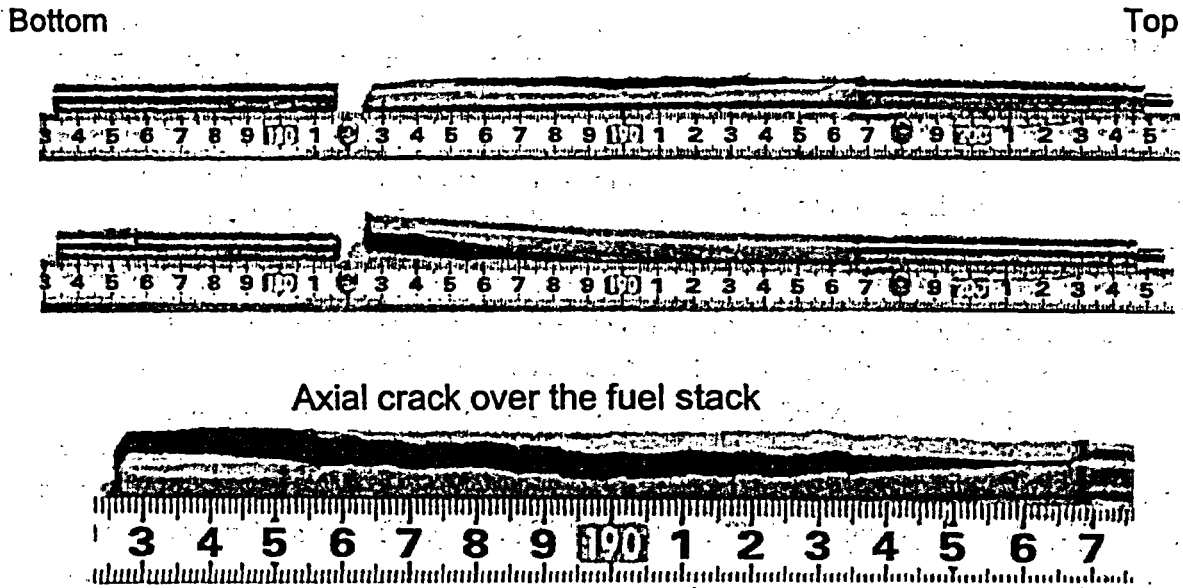


Fig. 3 Post-test appearance of the OI-11rod

with test fuel rod with an NDA cladding. The long interval between the OI-11 and OI-12 is due to conversion work of the NSRR facility for handling of higher burnup MOX fuels and high temperature capsules. NDA is an acronym of New Developed corrosion resistance Alloy, and is a zirconium-based cladding alloy⁽⁶⁾ developed by Nuclear Fuel Industries, Ltd. and Sumitomo Metal Industries, Ltd. for high burnup application. The alloy is designed also for a better performance in terms of corrosion resistance, and has a composition of Zr-1.0Sn-0.27Fe-0.16Cr-0.1Nb-0.01Ni.

III. PELLET EXPANSION IN PCMI

Transient cladding deformation of high burnup fuel was measured by strain gages in NSRR tests. The tests revealed that brittle cladding fracture occurred at a small cladding strain of ~0.4% during an early phase of the transients. The transient measurement was made in two BWR fuel tests, FK-10 and -12, and in a PWR fuel test, TK-10. Figure 4 shows the data obtained in the FK-10 and TK-10, respectively. Hoop strain at a time of cladding failure was 0.33% and 0.37% during the transients of the BWR fuel tests.

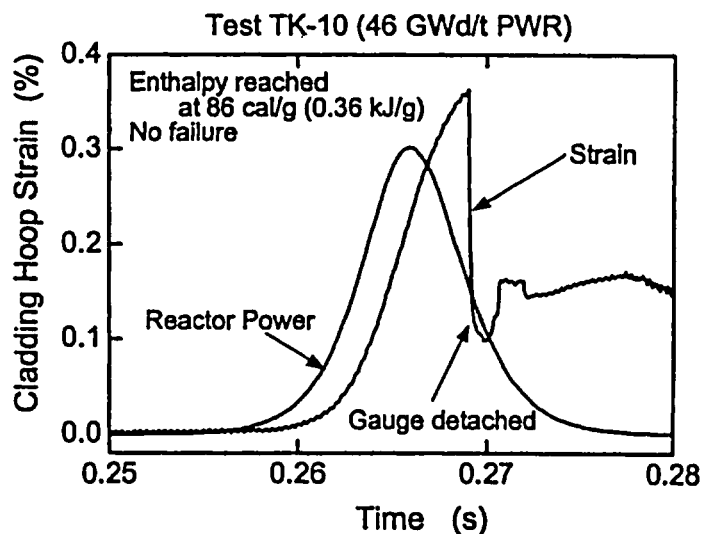
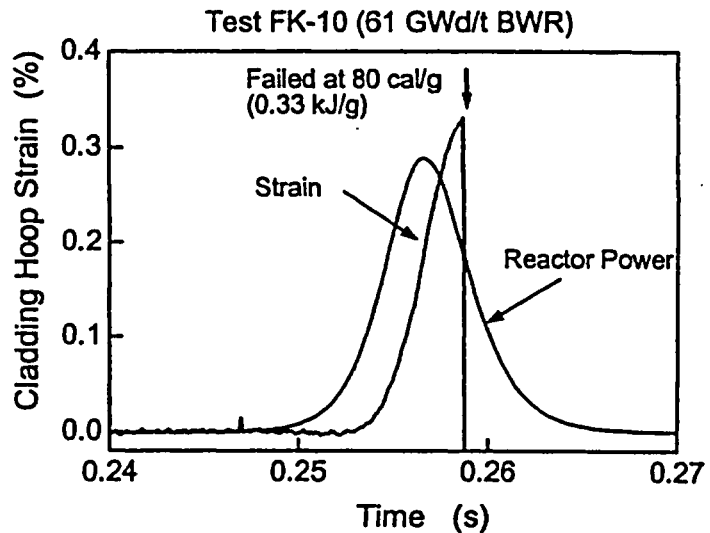


Fig. 4 Transient records of cladding hoop strain during the FK-10 and TK-10

Post test examination of the BWR cladding in earlier BWR fuel tests indicated residual hoop strains below 0.1% at an enthalpy level of about 0.25 to 0.29 kJ/g (60 to 70 cal/g). The maximum elastic strain level was estimated to be about 0.5% from the residual strain using cladding properties of MATPRO package⁽⁵⁾. The elastic strain level is consistent with the measured peak strains. A PWR fuel test indicated consistent peak strain of 0.37% at a fuel enthalpy of 0.29 kJ/g. Although cladding deformation due to thermal expansion of the pellets could vary depending on the pellet-cladding gap condition and constraint by the cladding, the deformation would be ~0.5% at fuel enthalpy of 0.29 kJ/g according to the MATPRO. These results shown in Fig. 5 suggested that the cladding deformation was caused primarily due to thermal expansion of pellets and fission-gas-induced

pellet expansion was negligible in the early phase of transients.

IV. MECHANICAL TESTS WITH ARTIFICIALLY HYDRIDED CLADDING

In order to promote a better understanding on hydrides effect on cladding integrity, artificially hydrided Zircaloy-4 samples are being subjected to several mechanical tests, including tube burst and ring-tensile tests, at JAERI. Three types of specimens consist of as-received sample (non-hydrided); uniformly hydrided sample; and sample with hydride rim. Hydrogenation was performed in mixture gas of hydrogen and argon at about 600 K, and samples with hydrogen concentrations of 100 to 1100 ppm were produced. Variation in hydrogen concentration throughout a sample was estimated to be within $\pm 30\%$ from the analysis of reference sample. In the sample with hydride rim, hydrides are localized in 50 to 150 μm of sample periphery. Hydrogen concentration inside the rim increases with increase of average concentration of sample, and varies from 2000 to 3000 ppm. The concentration outside the rim is 100 to 200 ppm. The hydrogen concentration inside the rim is about three times higher than the average of the sample.

Tube burst test

Transient tube burst test has been performed simulating PCMI loading in the high burnup PWR fuel rod during an RIA. The objective of the test is to understand failure behavior of embrittled cladding, in particular, effect of hydride rim (radially-localized hydride layer). Uniformly hydrided specimens and samples with hydride rim were tested at room temperature and at 620 K. The test set-up and results from the test were already described in previous documents⁽⁷⁻⁹⁾, but data at an elevated temperature were newly obtained. In tests at high temperature the cladding sample was heated to 620 K at a rate of 1 K/s with an infrared furnace and pressurization was initiated after 900 s duration. Sample temperature is measured with K type thermocouple attached to the surface. Radial temperature in the sample is nearly uniform. On the other hand, the cladding temperature has an axial profile, and the profile has a peak at 60 mm below the top end. The temperature difference between the peak position and the top end is within 10 K, while the temperature decreases continuously to the bottom end and the temperature difference between the peak position and the bottom end is about 50 K. The temperature at the peak position is maintained at 620 K during the experiment. Test specimens are low-tin (1.3wt%Sn) Zircaloy-4 cladding tubes. The inner and outer diameters of the sample are 9.50 mm and 8.36 mm, respectively, and the length is 160 mm.

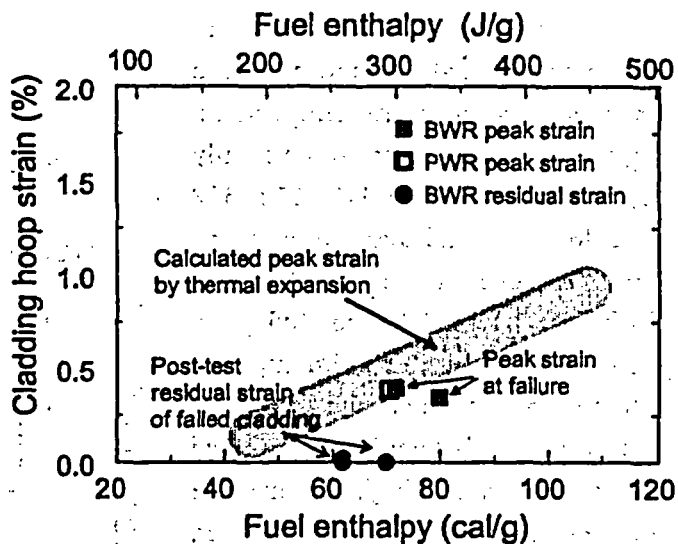


Fig. 5 Cladding strain at failure

Figure 6 shows transient histories of sample internal pressure measured in the tests at room temperature. Hydrogen concentrations of uniformly hydrided samples are 148, 172, 312 and 461 ppm, and average hydrogen concentrations of the samples with hydride rim are 302 and 305 ppm. Samples with hydrided rim ruptured 18 to 25 ms after the onset of pressurization, but uniformly hydrided samples with higher average concentrations were ruptured at later, about 70 ms. Burst pressure of the samples with hydride rim is slightly lower than that of the uniformly hydrided samples.

Residual hoop strain was evaluated after burst at both the inner and the outer surfaces through photo-image analysis on radial cross-section at the axial position where the maximum deformation occurred in post-test sample. The residual hoop strain is shown in Figs. 7 and 8 as a function of hydrogen concentration. Data obtained at room temperature are shown in Fig. 7

and those at 620 K are in Fig. 8. The maximum and the minimum values of the error bar correspond to hoop strains at the inner and the outer surfaces, respectively. Larger hoop strain was always seen at the inner surface. Hydrogen concentration was measured with hot extraction method for the sliced piece sampled from the vicinity of the position where the hoop strain was evaluated. In the tests at room temperature, as shown in Fig. 7, the hoop strain decreases with the increase of hydrogen concentration, and the reduction becomes remarkable in hydrogen concentration of 300 ppm or higher. The samples with hydride rim failed with significantly low hoop strain, less than 1% in average between the inner and outer surfaces. Figure 8 shows the residual hoop strain of the samples tested at 620 K. Non-hydrated and uniformly hydrided samples ruptured with the strain of ~7% or higher at the high temperature, and an uniformly hydrided sample with 606 ppm hydrogen showed the strain of 12.5%. On the other hand, the residual hoop strain decreased significantly in samples with hydride rim thicker than ~100 μm .

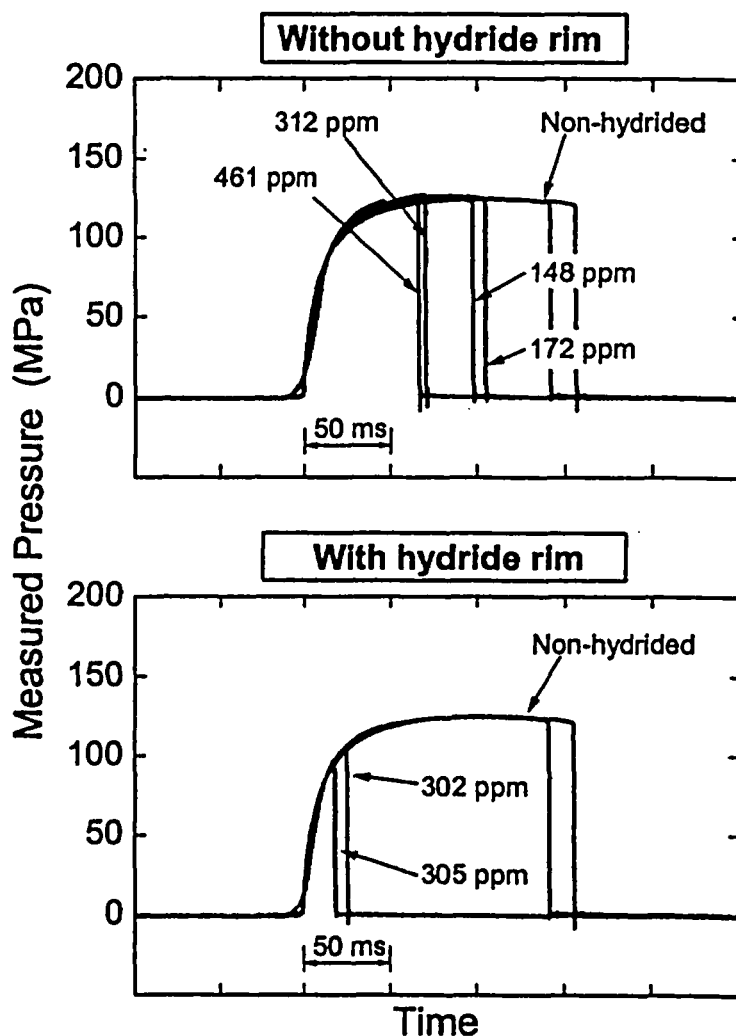


Fig. 6 Transient histories of sample internal pressure during tube burst tests at room temperature

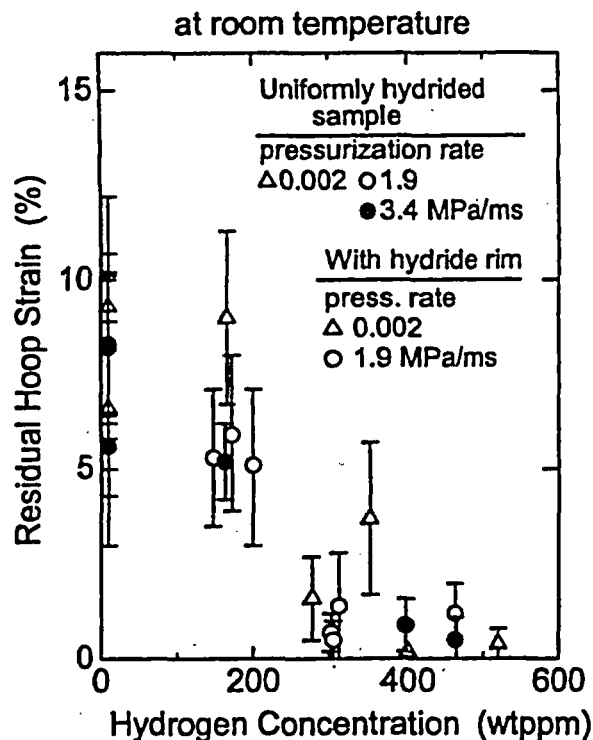


Fig. 7 Residual hoop strain as a function of hydrogen concentration (Burst tests at room temperature)

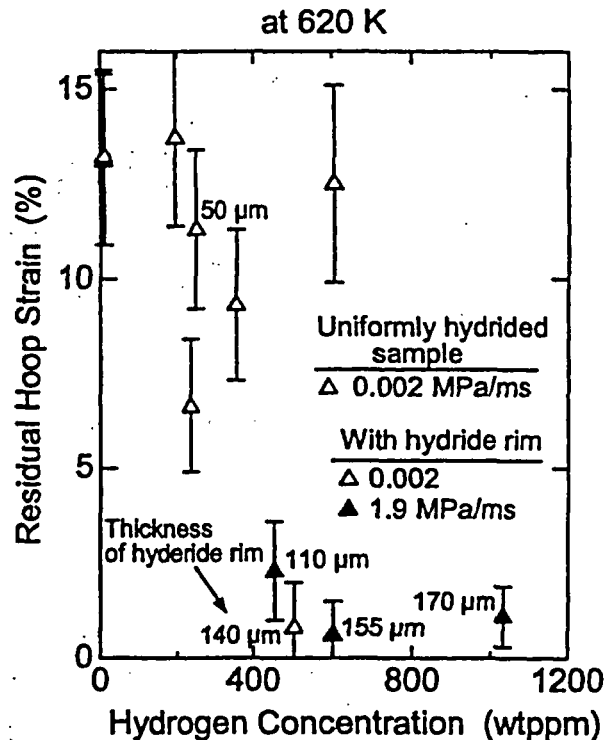


Fig. 8 Residual hoop strain as a function of hydrogen concentration (Burst tests at 620 K)

Thickness of hydride rim of each sample is indicated in the figure. The residual hoop strain is more than 10% in the cladding containing 250 ppm of hydrogen (50 μm hydride rim), but is significantly reduced in samples with hydrogen concentration above 400 ppm (with hydride rim thicker than $\sim 100 \mu\text{m}$). Even at 620 K, the residual hoop strain becomes less than 1% in samples with hydrogen concentration above 500 ppm (with hydride rim thicker than 140 μm). The results from the tube burst test indicate an important role of the thicker hydride rim in the process of PCMI failure of the high burnup PWR fuels.

The recent results from tube burst test on BWR, Zircaloy-2 claddings showed evidently different nature from the PWR tests described here. The BWR test indicates that a combination of hydriding and irradiation hardening has a particular importance in the PCMI failure of BWR fuels. The tube burst test on BWR samples will be presented separately.

Ring tensile test

The artificially hydrided Zircaloy-4 claddings were subjected also to a modified ring-tensile test. Specimens have a one-sided gauge section as shown in Fig. 9. The ring-tensile test was conducted with non-hydrided and uniformly hydrided samples with different hydrogen concentrations at room and elevated temperatures. Figure 10 shows plastic strain at fracture as a function of hydrogen concentration.

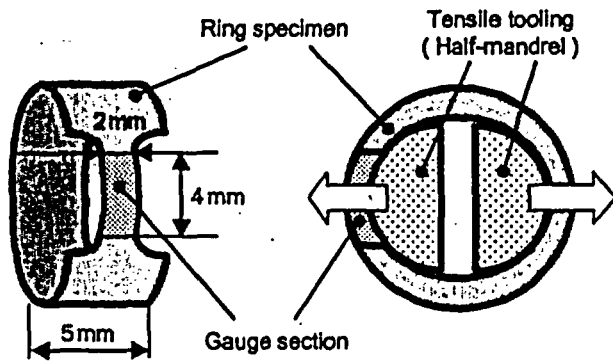


Fig. 9 Ring specimen with a one-sided gauge section

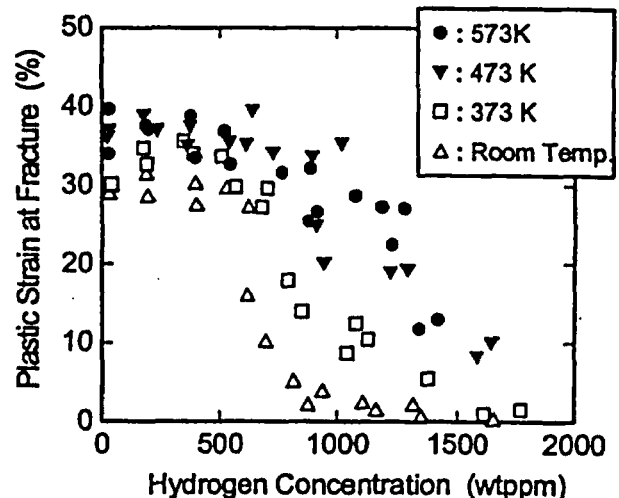


Fig. 10 Plastic strain at fracture as a function of hydrogen concentration

The strain represents ductility, and decreases significantly at higher hydrogen concentration in each temperature. The higher temperature results in the reduction of the strain at the higher hydrogen concentration. The temperature effect can be more clearly seen in Fig. 11, which shows the strain as a function of temperature. The strain increases at elevated temperatures, and the increase becomes negligible at above 473 K in samples with hydrogen concentration of ~700 ppm or lower.

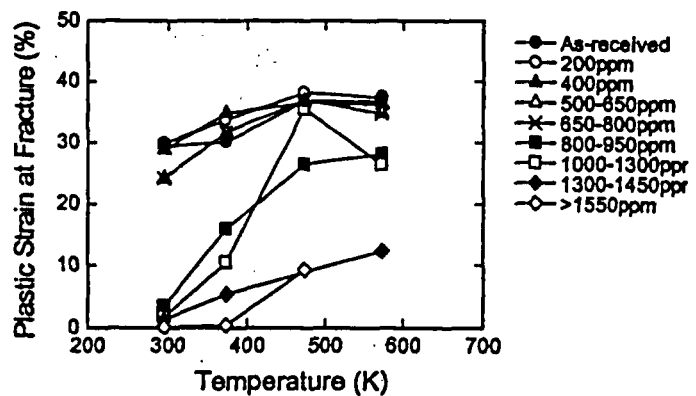


Fig. 11 Plastic strain at fracture as a function of temperature

V. HIGH TEMPERATURE CAPSULE AND FUTURE TESTS IN THE NSRR

As indicated by the results from the ring-tensile test shown in Fig. 11, the effect of temperature on cladding ductility is significant, in particular, at below 473 K. In order to perform the NSRR experiment at an elevated temperature, a high temperature capsule is being developed. Figure 12 illustrates the high temperature capsule. A design of the capsule was licensed last year, and out-of-pile tests with chemical explosive were performed to confirm integrity of the capsule. Test conditions achieved with the capsule are coolant temperature of 560 K and coolant pressure of 7 MPa. Due to the limitation of capsule internal space, the size of test fuel rod is limited to ~120 mm for total length, i.e. ~50 mm for pellet stack length. Cladding surface temperature, coolant temperature and capsule internal pressure will be measured in tests with the high temperature capsule.

Table 2 lists fuel rods to be tested in the NSRR from Japanese fiscal year 2004 to 2007. Segment averaged burnups for OI, Fugen and R2 and rod averaged burnups for others are listed in the table. RTP and HTP denote tests with room temperature/pressure capsules and tests with high temperature/pressure capsules, respectively. From these experiments, data for ~80 MWd/kgU PWR/ UO_2 and 66 MWd/kgU BWR/ UO_2 fuels become available until FY2005. Those of 62 MWd/kgHM PWR/MOX will be also obtained by FY2006.

VI. SUMMARY

The results from two NSRR RIA-simulating experiments, no failure in the test OI-10 and the higher failure energy in the test OI-11, reflect the better performance of the new cladding materials in terms of corrosion, the thinner oxides and accordingly lower hydrogen content generated during irradiation in the PWR. It can be accordingly concluded that these rods with improved corrosion resistance have larger safety margin against the PCMI failure than conventional Zircaloy-4 rods. The NSRR experiments and related separate-effect tests will be continued for higher burnup fuels and MOX fuels.

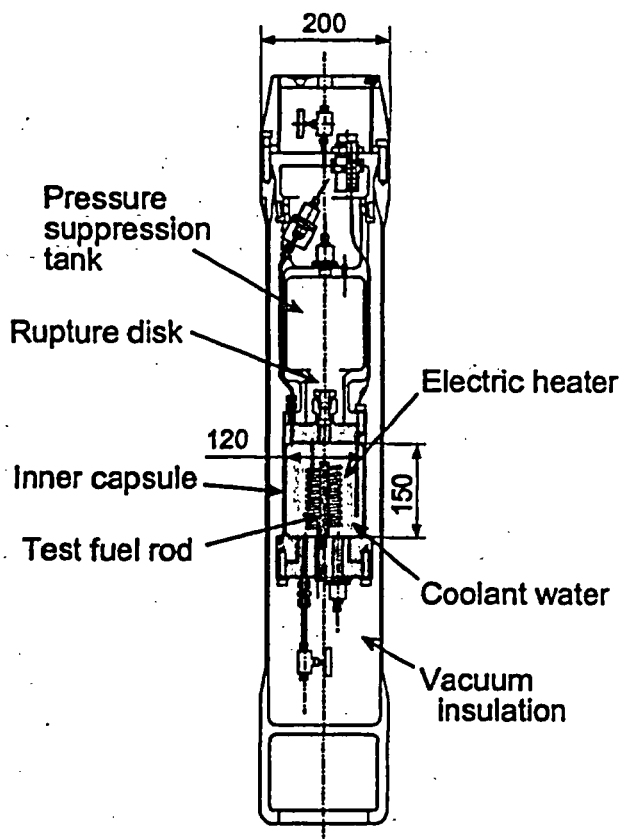


Fig. 12 High temperature capsule

Table 2 Fuel rods to be tested in the NSRR from FY2004 to FY2007

Specifications			Power reactor (Country)	Burnup MWd/kg	Cladding	Number of tests	
Fuel	Reactor	Type				RTP	HTP
UO_2	PWR	17x17	Oi (Japan)	~60	NDA	1	0
			Vandellos (Spain)	74	MDA	2	1
			McGuire (US), R2 (Sweden)	71	ZIRLO	1	0
			Gravelines (France)	66 - 69	M5	1	1
			Leibstadt (Switzerland)	63	Zry-2	1	1
			Fugen (JPN)	43	Zry-2	1	0
MOX	PWR	14x14	Beznau (Switzerland)	59	Zry-4	1	1
				44		1	0
			Dodewaard (Netherlands)	46	Zry-2	1	0

Acknowledgements

The tests OI-10 and OI-11 have been performed as a collaboration program between Japan Atomic Energy Research Institute (JAERI) and Mitsubishi Heavy Industries, LTD. by using fuel rods transferred from Kansai Electric Power Company, Inc. The authors would like to acknowledge and express their appreciation for the time and effort devoted by numerous engineers and technicians in Reactivity Accident Research Laboratory, NSRR Operation Division, Department of Hot Laboratories, Department of JMTR Project and Analytical Chemistry Laboratory, JAERI.

REFERENCES

- (1) Fuketa, T., Sasajima, H. and Sugiyama, T., "Behavior of High Burnup PWR Fuels with Low-Tin Zircaloy-4 Cladding Under Reactivity-Initiated-Accident Conditions", *Nucl. Technol.*, Vol.133, No.1, pp.50-62, (2001).
- (2) Nakamura, T., Kusagaya, K., Fuketa, T. and Uetsuka, H., "High Burnup BWR Fuel Behavior under Simulated Reactivity-Initiated Accident Conditions", *Nucl. Technol.*, Vol.138, pp.246-259, (2002).
- (3) Ishikawa, M., Ohnishi, N., Kanbayashi, Y., Kuge, Y. and Takeuchi, E., "EUREKA: A Computer Code for Uranium-Oxide Fueled Water Cooled Reactor Kinetics", JAERI 1235, (1974).
- (4) Doi, S., Suzuki, S., Mori, M. and Takahashi, T., "Advanced Fuel Design and Performance for Burnup Extension", *Proc. Int. Top. Mtg. on Light Water Reactor Fuel Performance*, Apr. 10-13, Park City, Utah, U.S.A., CD-ROM, (2000).
- (5) Hagrman, D. T. (Ed.), "SCDAP/RELAP5/MOD 3.1 Code Manual; MATPRO – A Library of Materials Properties for Light-Water-Reactor Accident Analysis", NUREG/CR-6150, EGG-2720, Vol.4, (1995).
- (6) Goto, K., Matsumoto, S., Murata, T., Miyashita, T., Anada, H. and Abe, H., "Update on the Development of Japanese Advanced PWR Fuels", *Proc. Int. Top. Mtg. on Light Water Reactor Fuel Performance*, Apr. 10-13, Park City, Utah, U.S.A., CD-ROM, (2000).
- (7) Fuketa, T., Nagase, F., Nakamura, T., Uetsuka, H. and Ishijima, K., "NSRR Pulse Irradiation Experiments and Tube Burst Tests", *Proc. 26th Water Reactor Safety Information Mtg.*, Bethesda, Maryland, October 26-28, 1998, NUREG /CP-0166, Vol.3, pp.223-241, (1999).
- (8) Fuketa, T., Nagase, F., Nakamura, T., Sasajima, H. and Uetsuka, H., "JAERI Research on Fuel Rod Behavior during Accident Conditions", *Proc. 27th Water Reactor Safety Information Mtg.*, Bethesda, Maryland, October 25-27, 1999, NUREG /CP-0169, pp.341-354, (2000).
- (9) Fuketa, T., Nakamura, T., Sasajima, H., Nagase, F., Uetsuka, H., Kikuchi, K. and Abe, T., "Behavior of PWR and BWR Fuels During Reactivity-Initiated Accident Conditions", *Proc. Int. Top. Mtg. on Light Water Reactor Fuel Performance*, Apr. 10-13, Park City, Utah, U.S.A., CD-ROM, (2000).

CABRI CIP0-1 preliminary test results

J-C Mélis, M. Faury, C. Marqué, J. Papin
IRSN

Introduction

Economic considerations lead most of the electricians in the world to wish to increase of the burn-up values of the nuclear fuel they use in their power plants.

For the future, maximum burn-up values of 60,000 MWd/tM or more are foreseen.

Some electric companies for more than 10 years, have also used the MOX fuel concept (mixture of uranium and plutonium oxides, UO_2 , PuO_2). The average burn-up fraction of the MOX fuel is currently limited to 45,000 MWd/tM according to its use instructions. The increase of the MOX burn-up fraction is also a short-term industrial objective. In order to determine the behaviour of even higher burn-up fraction-fuels, IRSN has launched in 2000 a new international program called CABRI Water Loop, mainly conducted within the framework of the NEA of the OECD.

The tests in the CABRI reactor will be performed in a pressurised water loop, more representative of the thermohydraulic conditions characterizing the PWRs than the sodium loop which has equipped this reactor until now.

In November 2002, the two first tests of the CABRI-Water loop program were performed. These are reference tests, performed in the existing loop cooled by liquid sodium, before the replacement by the water loop and the reactor upgrading. The first test (CIP0-2) using EDF fuel with M5 cladding showed no sign of clad failure: the analysis of the experimental results is in progress.

The second test (CIP0-1) using ENUSA fuel with Zirlo cladding is the subject of this paper.

Pre-test Examinations

The CIP0-1 rodlet was re-fabricated in Studsvik facility (Sweden) according to the Studsvik FAB process from the fifth span of the A06 ENUSA rod (mother rod).

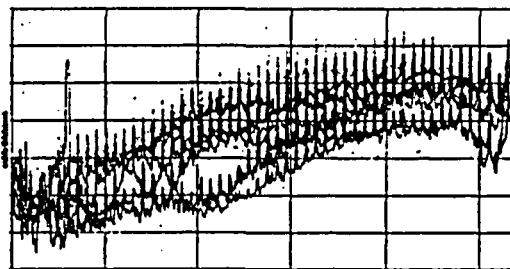
The A06 rod was irradiated in Vandellós reactor (Spain) up to 68 GWd/tM (rod average) and the mean burn-up of the CIP0-1 rodlet is 74.75 GWd/tM, according to Studsvik measurements. The CIP0-1 mother rod and, after re-fabrication, the CIP0-1 rodlet were submitted to several examinations: puncturing and fission gas analysis, metrology, neutron radiographies, visual

examinations, oxide thickness measurements, Eddy current defect examinations, and gamma scanning.

The main observations related to cladding concerned:

- An important oxide layer thickness (75 μm average),
- The absence of oxide spalling,
- The presence of significant hydride concentration at the pellet-pellet interface and a high level of mean hydrogen content,

Oxide thickness



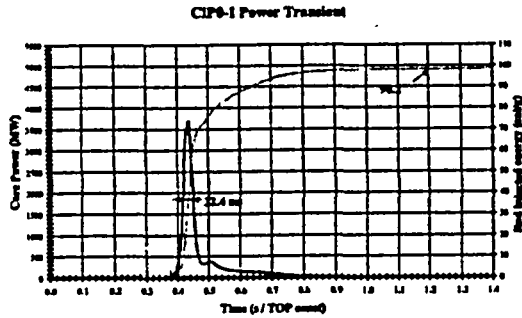
After transportation to France and before loading in the CABRI facility, the satisfying state of the rodlet was checked through: visual examination, metrology and gamma scanning. The results were consistent with the Studsvik measurements.

The CIP0-1 rodlet was then loaded in the test device and sent to the CABRI facility. There, X-ray radiography, tomography and gamma scanning were performed (IRIS facility).

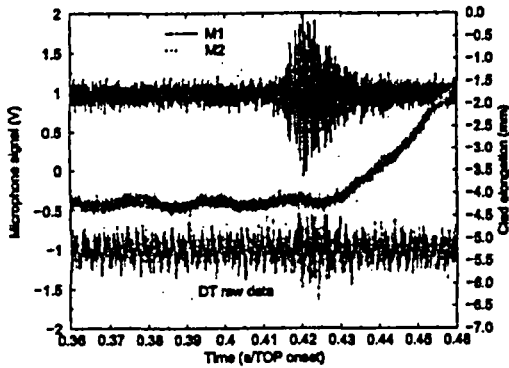
CIP0-1 test: conditions and first results

The CIP0-1 was performed in the CABRI facility on November 29th 2002. During this test, the CIP0-1 rodlet was submitted to a 32.4-ms half width power transient starting from representative hot shutdown conditions (zero power, about 4m/s fluid velocity and coolant temperature of 280°C). The total energy deposit at PPN¹ was 98.2 cal/g at the end of the transient.

¹ PPN: Peak Power Node



The microphones recorded a first event at an energy deposit about 8.5 cal/g at PPN. This signal is correlated to the clad elongation. This kind of signal, with a characteristic signature, is usually seen in all the previous sodium tests (REP Na).



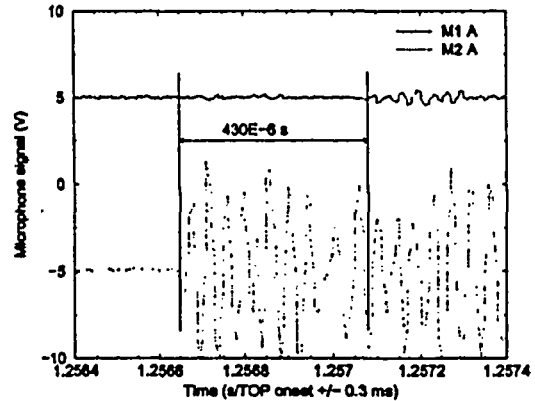
First microphone event

No other event has been evidenced during the transient. The rod elongation and swelling is similar to other REP-Na tests results under similar conditions.

After SCRAM, at TOP onset + 1.26 s, an unusual event is recorded on the microphones, pressure sensors, flowmeters and void detectors.

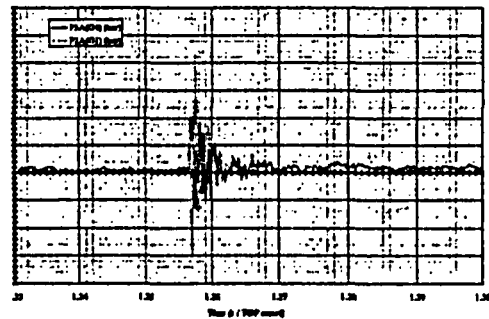
These signals exclude the possibility of significant fuel ejection. But, those signals raised the question of a possible clad failure.

The acoustic event is mainly evidenced by the upper microphone (M2). The M2 signal is similar to usual "failure event". But the M1 signal is barely noticeable. Moreover, the tentative location led to identify an event occurring well above the tested rod.



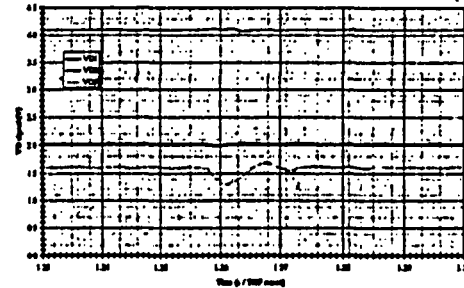
Late microphone event

The pressure transducers recorded strong oscillations with unusual behaviour. At the same time, small oscillations are recorded by the upper flowmeter. These signals occurred before the microphone event (about 150 μ s), which is the reverse order of expected phenomenology in case of failure: first clad failure (acoustic event), and then gas ejection (pressure / flow event).



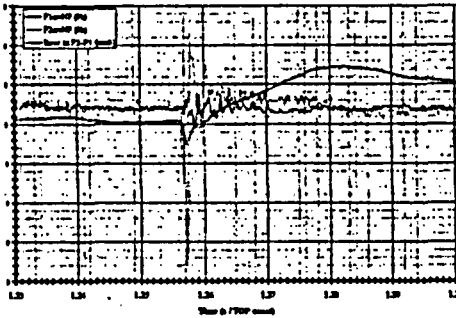
Pressure event

About 3 ms later, it is possible to see very small perturbations on the upper void detectors,



Void detectors

and a sodium ejection (0.15 cm^3) is measured by flowmeters.

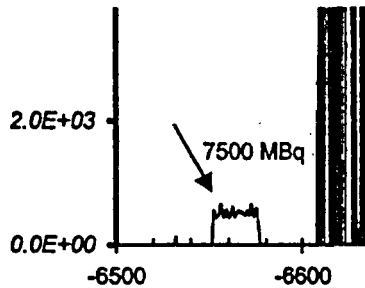


Flow event

The origin of this late event recorded by the instrumentation is still under investigation.

After the test, a measurement of the activity of the Argon cover gas was performed. There was no ^{85}Kr inside, as we usually observed with a test leading to failure, even without fuel ejection as in REPNa-10. The DND (Delayed Neutron Detector) signal, which measures the neutron emission in the channel just after the test section, gave no evidence of clad failure.

After the test, it was possible to precisely measure the amount of ^{85}Kr in the upper plenum by spectrometry in the IRIS facility. This amount is of the same order of magnitude as the expected value for a tight cladding (based on calculations).

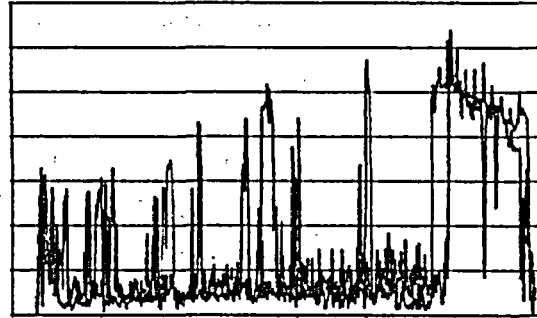


The visual examinations performed in hot cell showed an extended clad spalling but did not evidence any clad failure.

The CIP0-1 was submitted also to non-destructive examinations : gamma-scanning, profilometry and zirconia layer measurements.

The profilometry showed a slight clad deformation as expected from precalculations.

The zirconia measurements confirmed the extended spalling due to the transient, with a remaining oxide layer thickness as low as 10 μm .



Zirconia layer after test

In conclusion, from the set of examinations already performed, there is an important presumption that the clad did not fail. The next examinations in hot cells (pin piercing) planned in fall 2003, will allow to confirm this assertion.

The throughout analysis of the test signals should be completed by January 2004.

The destructive examinations are scheduled before the end of 2003.

Mechanical characterisation of the Zirlo cladding : the PROMETRA tests

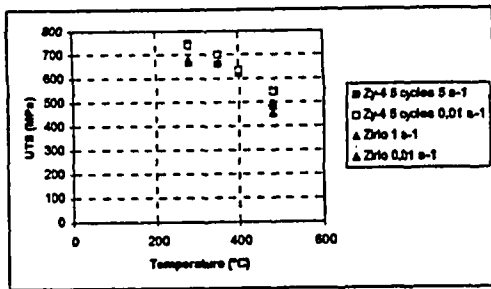
In association with the CIP tests, a mechanical characterisation program of the advanced claddings has been defined (PROMETRA program). It presently concerns the Zirlo and M5-6cycles cladding materials related to the CIP0-1 and CIP0-2 rods respectively.

The main objectives are to determine the stress-strain laws based on hoop tensile tests and their interpretation and failure data based on plain strain and burst tests. For each tested material, the test matrix is the following, using doubled tests:

	$\dot{\epsilon} = 1 \text{ s}^{-1}$				$\dot{\epsilon} = 0.01 \text{ s}^{-1}$
	T (°C)				
	280	480	600	800	480
Hoop tensile (5x2)	x	x	x	x	x
Penn-State (4x2)	x	x	x	x	
Burst tests (2)	x				

For the Zirlo material related to CIP0-1, samples from the zones close to the 5th span of the ENUSA rods A06 and A12, have been defueled at Studsvik. The first six ring tensile tests have been performed using samples from the 6th span of the A12 rod exhibiting 80 μm corrosion thickness.

The following figure shows the ultimate tensile strength versus temperature, compared to the standard Zr4-5 cycles values.



Compared UTS of Zirlo 75 GWd/tM and Zr4-5cycles

These results underline a similar behavior of the Zirlo and Zr4 5cycles in the temperature domain of 280 to 480 °C. The other hoop tensile tests at higher temperature have been realised and results will be

available soon. The following part of the programme is planned in 2004.

Conclusions

The CIP0-1 test has been successfully performed in the Na loop of the CABRI reactor. A careful analysis of the experimental signals and non-destructive examinations lead to the conclusion that the rod survived the transient overpower. A final confirmation of the rod tightness will be obtained after the rod piercing and gas analysis.

This test was the very last one performed in the 25 years old CABRI Na loop. The reactor is now shut down to allow the upgrading and the pressurized water loop instalment. The first test in the new configuration is scheduled in 2006.

Overview of Research Findings on the Mitigating Systems Performance Index (MSPI)

D.A. Dube

Operating Experience Risk Analysis Branch
Division of Risk Analysis and Applications
Office of Nuclear Regulatory Research
U.S. Nuclear Regulatory Commission

Abstract

The Reactor Oversight Process currently uses performance indicators that quantify system unavailability for four important nuclear power plant systems. A number of issues have been identified with these indicators, including the fact that they do not account for component unreliability. Also, the indicators use generic thresholds irrespective of the relative risk importance of the particular systems at each nuclear plant. A more risk informed performance indicator, the Mitigating Systems Performance Index (MSPI), has been proposed that addresses most of the concerns with the current indicators. A twelve-month pilot program to assess the feasibility of the MSPI was completed in September, 2003. The Office of Research substantially verified the results of that effort, while identifying a number of technical issues that needed further evaluation. Recommendations to address all major technical issues have been proposed.

Background

The Reactor Oversight Process (ROP) currently uses performance indicators that quantify system unavailability. There are certain issues associated with these indicators, including (a) the use of generic thresholds, (b) the way in which fault exposure time associated with failure events affects the values of the current indicators, and (c) the method of cascading failures of cooling water support systems.

Phase 1 of the Risk-Based Performance Indicator (RBPI) Development program (Ref. 1) explored several possible enhancements to the ROP performance indicators. A key aspect of the Ref. 1 approach was the use of plant-specific models (the Standardized Plant Analysis Risk or SPAR models) to assess the risk significance of changes in unreliability (UR) and unavailability (UA). Based on these models, it was possible to develop candidate RBPIs that separately quantify UR and UA within a common model framework. It was also possible to determine plant-specific thresholds for these indicators. These enhancements help to address the issues mentioned above for current ROP indicators. In the Phase 1 RBPI effort, these enhancements were shown to be generally feasible, although for some UR indicators, statistical uncertainty is an issue.

Although these candidate indicators have certain benefits compared to the performance indicators (PIs) currently in use, they also have certain drawbacks. In particular, implementing separate train-level UR and UA indicators leads to a substantial increase in the number of indicators. This increase in the number of indicators raises concerns regarding their effect on the action matrix. In addition, including a larger number of indicators increases the likelihood that at least one indicator will give a false indication.

The MSPIs are intended to reap the benefits of the improved treatment developed in the RBPI program (improved quantification of UR, using plant-specific thresholds) while resolving the issues associated with proliferation of indicators. The MSPI approach separately quantifies the significance of changes in UR and UA, but then rolls up these contributions into a single system-level indicator. The MSPI approach does this using a simplified calculational approach based on importance measures, thereby avoiding the need for ongoing manipulations of the entire probabilistic risk assessment (PRA) model. This approach is quantitatively adequate until changes in UR and UA become very large, at which point the numerical inaccuracy does not matter, because licensee and regulatory attention has already become focused on these contributions.

Formulation of the MSPI

The purpose of MSPI's (Ref. 2) is to "monitor the performance of selected systems based on their ability to perform risk-significant functions..." If implemented, the MSPI would replace some or all of the existing Safety System Unavailability Performance Indicators in the ROP, and would continue to complement the Significance Determination Process (SDP). In so doing, the MSPI would address many of the known issues with the current indicators including: the use of fault exposure hours in the SSU, the omission of unreliability elements in the indicator, the use of mostly one-size-fits-all performance thresholds irrespective of risk-significance of the system, and the cascading of support system failures onto mitigating system unavailability.

The systems to be monitored under the MSPI include emergency AC power, residual heat removal, and safety-related support system cooling such as service water and component cooling water. Furthermore, for Boiling Water Reactors, high pressure coolant injection and/or core spray are included, along with reactor core isolation cooling. (There were no Pilot plants with isolation condensers, but these would be included as well). For Pressurized Water Reactors, the additional systems to be monitored consist of high pressure safety injection including Chemical and Volume Control System valves and centrifugal pumps, along with auxiliary (or emergency) feedwater.

As currently formulated, the MSPI of a system is a simplified and linearized approximation to the change in core damage frequency (*CDF*) due to changes in reliability and availability of risk-significant elements of that system. The calculation focuses on key components, and quantifies the change in *CDF* using a simple formula based on importance measures.

The MSPI is formulated as a sum of changes related to UA and changes related to UR:

$$MSPI = UAI + URI$$

Unavailability-Related Contributions

UAI , the UA-related contribution, is a sum of contributions from different trains:

$$UAI = \sum_{j=1}^n UAI_j \quad (\text{Equation 1})$$

The summation runs over trains, and UAI_j is the contribution of the j th train to the change in CDF due to changes in unavailability of this train.

If contributions to a given train's unavailability can be collected into a single PRA basic event having unavailability UA_t , then the change in CDF associated with a change in train UA can be written as (Ref. 2):

$$\begin{aligned} UAI_t &= B(UA) * \Delta UA \\ UAI_t &= B(UA) * (UA_t - UA_{BL}) \\ UAI_t &= CDF_p \left[\frac{FV_{UA_p}}{UA_p} \right] (UA_t - UA_{BL}), \end{aligned}$$

where $B(UA)$ is the Birnbaum importance for UA, FV_{UA} is the Fussell-Vesely importance for UA, and UA_{BL} is the baseline unavailability. Items carrying a "p" subscript are understood to be calculated using the "P"RA values, while items on the right-hand side *not* carrying a "p" subscript (carrying instead a "t" subscript) are derived either from current operating data or from baseline data. In the NEI formulation, the "t" subscript just refers to "train." This formulation divorces the calculation of $B(UA)$ from the calculation of ΔUA . In other words, $B(UA)$ is independent of the value of UA. Given $B(UA)$, the terms whose difference yields ΔUA need only to be calculated on a mutually consistent basis – not necessarily consistently with the PRA – in order for the formula to yield a good estimate of the change in CDF . Of course, if CDF and FV are calculated and combined as above, then in order to yield $B(UA)$ as desired, CDF and FV both need to be based on the same value of UA that appears in the denominator of the formula.

In practice, UA data are collected on a train basis. This avoids the potential for the overestimation of train unavailability that could result if individual components' unavailabilities were collected and summed as if they were independent. If one has separate terms in Equation 1 that cannot be collected into a single basic event, then each element of the sum can still be calculated using the above approach.

The Unreliability-Related Contribution

The treatment of the UR-related contribution generally follows the above treatment of UAI. However, the elemental contributions to train unreliability need to be assessed separately, and partly as a result of this, there are additional considerations in URI.

The following quantity is used for the UR-related contribution:

$$URI = CDF_p \sum_{j=1}^m \left[\frac{FV_{URcj}}{UR_{pcj}} \right]_{\max} (UR_{Bcj} - UR_{BLcj}),$$

where

the summation is over those active components and failure modes in the system that can by themselves fail a "train,"

CDF_p is the plant-specific internal events, at-power core damage frequency,

FV_{URc} is the component-specific Fussell-Vesely value for unreliability,

UR_{pc} is the plant-specific PRA value of component unreliability,

UR_{Bc} is the current estimate of ("Bayesian corrected") component unreliability for the previous 12 quarters,

UR_{BLc} is the historical baseline unreliability for the component.

Max refers to using the highest FV/UR from all the basic events (i.e. failure modes) for a given component (see Ref. 2). Note also that the current formulation considers only the internal events initiators, and does not include internal flooding events or external events initiators.

MSPI values below 1E-6/yr would be designated as a GREEN indication, consistent with the current ROP guidance. Values between 1E-6/yr and 1E-5/yr would be designated WHITE; between 1E-5/yr and 1E-4/yr would be YELLOW; and above 1E-4/yr would be considered RED.

Description of the Pilot Program

The MSPI Pilot Program was initiated in the summer of 2002. The Pilot consisted of a six-month data collection phase by twenty nuclear power plant units, followed by a six-month analysis phase. At the onset of the Pilot Program, there were three primary objectives:

- 1) Exercise the MSPI Guidance
- 2) Perform Validation and Verification
- 3) Perform Temporary Instruction Inspections.

The first objective was performed primarily by the licensees of the twenty nuclear power plant units in the Pilot. With Reference 2 as guidance, this activity included:

- Identifying risk significant functions for the six systems of interest
- Identifying success criteria
- Identifying data sources
- Identifying system boundaries
- Identifying active components to be monitored
- Tabulating Fussell-Vesely importance measures and basic event probabilities for all components to be monitored
- Collecting relevant unavailability and unreliability data

- Providing input to the pre-formatted NEI electronic worksheets
- Computing UAI, URI, and MSPI results on a quarterly basis, and submitting on-going results to the NRC on a monthly basis (for this Pilot only)
- Identifying possible "Invalid Indicators"
- Assessing the reasonableness of results.

The second objective was carried out by the NRC Office of Research. It included a plant-by-plant performance data cross-comparison, use of SPAR models to validate importance measures, and identification and resolution of significant issues with the MSPI methodology. In order to reconcile differences between the Plant PRA and the SPAR models, a major effort was undertaken to make further enhancements to the SPAR models to make these models compatible for MSPI applications.

Finally, the third major objective was to exercise Temporary Instruction inspections via TI 2515/149 (Ref. 3). This task was undertaken by the site Resident Inspectors/Senior Resident Inspectors and Region Senior Reactor Analysts. This activity included an item-by-item verification of many of the tasks performed by the licensees. The reader is referred to Reference 4 for a full description of inspection activities and findings.

As noted above, twenty nuclear power plant units participated in the Pilot Program. The list below identifies the Regions and plants in the Pilot. The plants represent a reasonable cross-section of U.S. plant type, age and design, and reactor manufacturers. No Babcock & Wilcox reactors were in the Pilot. However, of perhaps equal if not greater importance to the program demonstration was the availability of internal events, level-1 at-power plant PRAs and the varied experience of the licensees' staffs to exercise the models. NEI has stated that, in this regard, the Pilot participants were a reasonable representation of industry capabilities.

<u>Region I</u>	<u>Region II</u>	<u>Region III</u>	<u>Region IV</u>
Hope Creek	Surry 1 & 2	Braidwood 1 & 2	Palo Verde 1, 2 & 3
Limerick 1 & 2		Prairie Island 1 & 2	San Onofre 2 & 3
Millstone 2 & 3			South Texas 1 & 2
Salem 1 & 2			

The data collection phase ended in February, 2003. The NRC and its contractors analyzed the results over the following six months, resulting in a preliminary draft report on the MSPI verification effort in September, 2003. After internal review, the draft report will be issued for public review and comment in early 2004. Additional issues mostly related to MSPI implementation continue to be addressed as well.

Overall MSPI Results

The purpose of the MSPI verification effort was to obtain reasonable assurance of the adequacy of the inputs into the MSPI calculation, and reasonableness of Pilot Plant results. This was accomplished by assessing the individual inputs to the MSPI calculation on a plant-by-plant, system-by-system, and in many instances component-by-component basis. In addition, a comparison of MSPI results using the plant PRA models and the SPAR resolution models was performed. The detailed tasks performed in this activity included:

- Baseline data verification
- Current performance data verification
- Verification of FV/UA and FV/UR importance measures
- Electronic spreadsheet calculation verification
- Overall MSPI results verification.

The major findings of the verification effort are as follows:

1. The generic failure rate values in Table 2 of Appendix F of Reference 2 are not truly representative of 1995-1997 performance as originally assumed, and are not appropriate for use in the MSPI.
2. The verification effort generally showed the Pilot Plant submittals for train-specific Unavailability baselines to be reasonable. However, the verification did identify several baseline UAs that were lower than the unplanned UA values, which is erroneous. More guidance and perhaps internal software checks need to be provided by the licensees. Current UA results for the three-year period were tabulated and compared across plants and with baselines. No current UA entries were identified as outliers.
3. The verification effort did identify Pilot Plant data entry issues. These included cases of double or "multiple counting" of failures or demands. The discovered issues were brought to the attention of the licensees, and most were corrected by the final data submittals in March 2003.
4. In general, it was found that the existing SPAR Rev. 3 models were not adequate to verify risk model importances at the component level for MSPI purposes. A major effort to enhance the SPAR models was successful in identifying and resolving many issues related to component FVs. Using the geometric mean as the figure-of-merit, the SPAR resolution models agreed with the eleven unique plant PRA FV/URs within a factor of two on average.
5. The MSPI calculations performed within the NEI spreadsheet were verified by comparing results from an independently developed spreadsheet. Results from both sets of spreadsheets agreed.

Overall, the MSPI results from the Pilot Plant models and from the SPAR resolution models were found to be in very good agreement. The Pilot Plant model and SPAR resolution model results for the 4th Quarter 2002 matched color indication for all one hundred systems using a consistent set of assumptions such as Year 2000 industry baseline failure rates. Both models identified WHITE conditions for two systems at two pilot plants. Numerical results for MSPI values above 1E-7 (the practical limit of significance) generally agreed within a factor of three.

Key Technical Issues

In the course of the Pilot Program, a number of significant issues arose regarding the fundamental methodology of the MSPI as described in Reference 2. Resolution of these items first required a thorough understanding of how the issue affected MSPI results plant-by-plant, within the group of Pilot Plants, and across the industry as a whole. These issues relate to:

- The appropriateness of generic baseline reliability data.
- Invalid Indicators whereby one failure beyond baseline performance results in exceeding the WHITE threshold.
- Insensitive Indicators whereby a very large number of similar component failures within a system would be necessary to reach the WHITE threshold.
- The recognition that an increase in Unreliability increases delta CDF both through the independent failure contribution and through a common cause failure contribution.
- The concern that because of the deterministic nature for inclusion of components within the program, some plants may need to monitor an inordinately large number of low risk significance valves.
- The concern that there is an inconsistency in the treatment of support system initiators for safety-related service water and component cooling water from plant-to-plant.

Six major recommendations to improve the MSPI as currently formulated in the Reference 2 guidance have been made to address the above issues.

- (1) The proposed generic failure rate data (Ref. 2) should be revised to use industry failure rates derived for the period 1999-2001. The 1999-2001 data sources have a higher degree of quality, and are representative of 1995-1997 industry performance.
- (2) A "frontstop" should be used as the means of addressing the Invalid Indicator issue. The frontstop would take the form of a limit on the delta URI associated with the single most risk significant failure, so long as the delta URI is less than $1E-5$. The frontstop would only be applied to the GREEN/WHITE threshold.
- (3) The variable backstop should be employed as the means of addressing the Insensitive Indicator issue. The backstop is a performance and statistically-based limit to the number of failures of a component type within a system before indication is declared "WHITE."
- (4) The Common Cause Failure contribution to Fussell-Vesely Importance should be included in the MSPI formulation. The preferred approach would be to add the FV owing to common cause directly to the FVs for the independent basic events. Several alternatives to this approach continue to be investigated.
- (5) Licensees may opt to exclude low risk valves from the list of monitored components based on Birnbaum importance measures less than $1E-6$ /yr.
- (6) The contribution of cooling water support system initiators to Fussell-Vesely importance must be included. The preferred approach is to add cooling water support system initiator fault trees to the linked PRA models. A simpler although slightly more conservative approach also would be allowed.

Additional issues mostly related to the *implementation* of the MSPI, such as the relationship to the Significance Determination Process and the possible extension of the treatment to external events, continue to be addressed.

Conclusions

The Mitigating Systems Performance Index is a risk-informed indicator using plant-specific design configuration and equipment performance data. Both equipment unreliability and system unavailability are factored into the index. Risk importance measures are used to weight the importances of the components in the six monitored systems.

A twelve-month pilot program to assess the feasibility of the MSPI was completed in September, 2003. The Office of Research substantially verified the results of that effort. As part of this verification, a major effort to enhance the eleven unique SPAR models for the twenty pilot plants was undertaken to update the models for MSPI application. In addition, the verification effort identified a number of major technical issues with the originally proposed approach to the MSPI. Based on analysis and simulation, recommendations to resolve all major technical issues have been proposed. This includes a "frontstop" and "backstop" that essentially provide minimum and maximum limits to the number of component failures before the system is deemed degraded (i.e. performance is assessed non-GREEN). Additional research will continue through early 2004 to address implementation issues with the MSPI.

References

1. H. G. Hamzehee, et. al., U.S. Nuclear Regulatory Commission (NRC), NUREG-1753, "Risk-Based Performance Indicators: Results of Phase 1 Development," Washington, D.C. April 2002.
2. U. S. Nuclear Regulatory Commission, "NRC Regulatory Issue Summary 2002-14, Supplement 1 Proposed Changes to the Safety System Unavailability Performance Indicators," Attachments 1 and 2, draft NEI 99-02, Rev. 0, "Regulatory Assessment Performance Indicator Guideline," Section 2.2 "Mitigating Systems Performance Index" and Appendix F "Methodologies for Computing the Unavailability Index, the Unreliability Index, and Determining Performance Index Validity", Adams Accession Number ML022740008, Issue Date September 30, 2002.
3. U.S. NRC Inspection Manual, Temporary Instruction 2515/149, Mitigating Systems Performance Index Pilot Verification, Issue Date September 24, 2002.
4. U.S. NRC TI 2525/149, "Mitigating Systems Performance Index Pilot Verification," Adams Accession Number ML030840341, March 25, 2003.

Acknowledgments

The author notes the significant contributions to the MSPI Research Program made by B. Mrowca and R. Youngblood of ISL, Inc., S. Eide and D. Zeek of Idaho National Engineering and Environmental Laboratory, and C. Atwood of Statwood Consulting.

Boron Dilution Tests / PKL

**Klaus Umminger, Bernhard Brand
Framatome ANP, Germany**

Abstract

For many years the integral test facility PKL has been used for extensive experimental investigations to study the thermal hydraulic system behavior of pressurized water reactor plants under accident conditions. Since April 2001 the PKL project has been included in an international program set up by the OECD. PKL replicates the entire primary system and most of the secondary system of a 1300-MW PWR plant with elevations scaled 1:1 and diameters reduced by a factor of 12.

The current test series PKL III E is focused on boron dilution events following small break loss of coolant accidents and on accidents occurring during shut-down conditions at mid-loop-operation. All these tests have been performed with original boric acid and suitable measurement devices for the detection of the boron concentration in the primary system.

This presentation will summarize the most important findings from the current PKL test program and the topics of further investigations of a planned new PKL/OECD program will be outlined.

1 Introduction

The integral test facility PKL (Fig. 1) is a mock-up of a pressurized water reactor (PWR) of the 1300 MW class and is operated in the Technical Center of Framatome ANP in Erlangen/-Germany. It replicates the entire primary system and most of the secondary system with a volume and power scaling of 1:145 (elevations 1:1). Modeling of the primary system with 4 identical reactor coolant loops arranged symmetrically around the reactor pressure vessel permits accidents to be investigated under realistic conditions, including those accidents characterized by non-symmetrical boundary conditions. Modeling of a 3-loop or 2-loop plant is possible by simply isolating one or two loop(s). As the functions of all major primary and secondary operational and safety systems are also modeled in the test facility, integral system behavior as well as the interaction between individual systems can be investigated under a wide variety of different accident conditions and the effectiveness of either automatically or manually initiated actions can be examined. With its total of around 1300 measuring points, the PKL facility is extensively instrumented, a feature that allows detailed analysis and interpretation of the phenomena observed in the tests.

The experiments conducted at the PKL test facility, which has now been in operation for about 25 years, cover a broad spectrum of topics, ranging from the tests performed to study large-break loss-of-coolant accidents (LB-LOCAs) when the facility was first built, up to the simulation of transients, including, especially, the effects of beyond-design-basis events and the measures to prevent a severe accident situation.

The PKL III tests performed to date have altogether contributed to a better understanding of the sometimes highly complex thermal-hydraulic processes involved in various accident scenarios and to a better assessment of the countermeasures implemented for accident control. In addition,

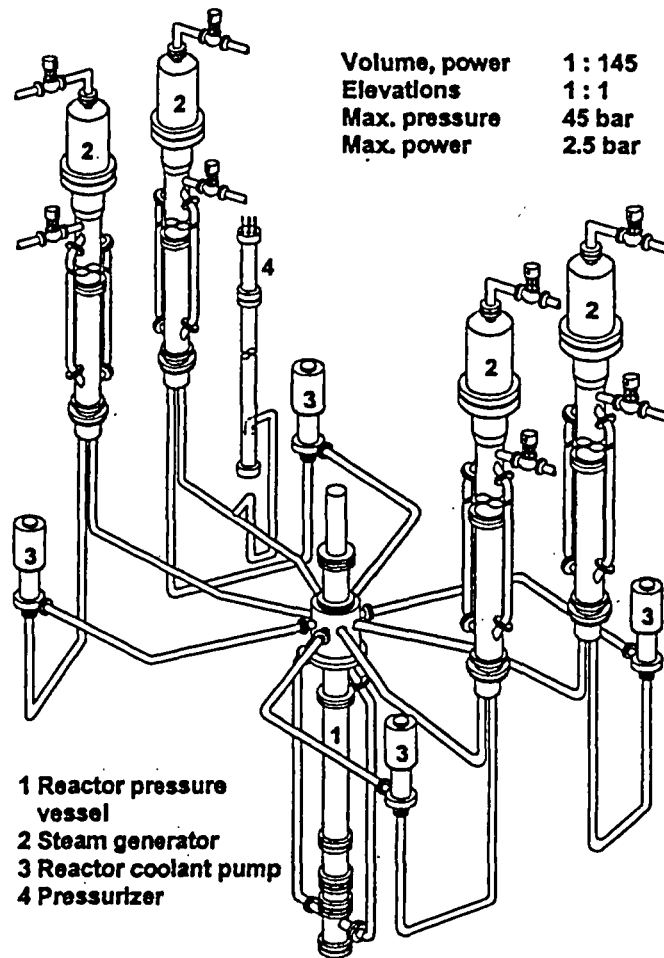


Fig. 1: PKL III Test facility

they have supplied valuable information regarding safety margins available in the plants in the event of beyond-design-basis accidents and have experimentally verified the emergency operating procedures specified for such accidents. Another important benefit of the PKL tests is that they provide an extensive database for use in the further development and validation of thermal-hydraulic computer codes, so-called system codes. These codes employed in designing and licensing nuclear power plants have to be validated beforehand.

Since the early 90s interest has increasingly been focused in reactor safety research on the topic of boron dilution. The importance to safety of boron dilution scenarios lies in the possibility of unborated or boron-depleted water entering the core region, thus leading to recriticality and consequently to a power excursion. A number of experimental and analytical investigations have

been performed by different organizations, and joint international programs (OECD/NEA; EURATOM) have been initiated to address this issue /2/. To evaluate the consequences of boron dilution events, different initiating scenarios have to be taken into account. Several investigations performed up to now have been dealing with the restart of a reactor coolant pump in presence of a low or unborated water slug in the primary system /3/.

The assessment of various accident scenarios that might give rise to boron dilution shows that, in particular, small-break loss-of-coolant accidents (SB-LOCAs) should be investigated in this respect. Such events combined with limited availability of the emergency core cooling system (ECCS) can lead to a temporary reduction of the coolant inventory, resulting in reflux-condenser conditions and hence in inherent boron dilution /4/. When the reactor coolant system (RCS) is refilled later on during the course of the accident, low borated masses of water may be transported into the core with the restart of natural circulation. Inherent boron dilution after SB-LOCA is a main topic in the current test series PKL III E. The tests are conducted utilizing boric acid and boron measuring instrumentation technique. They provide an important contribution for the evaluation of boron dilution events and represent a valuable data source for the validation of computer codes used for the analytical handling of this subject.

Besides inherent boron dilution, accidents in shutdown states are also investigated in PKL III E. In recent years, increasing attention has been devoted to such incidents as various probabilistic safety assessments have shown that the contribution of these accidents to core damage frequencies is much larger than would be commensurate with the outage times. In addition, accidents under shutdown conditions can also lead to situations similar to reflux-condenser and thus in principle to local boron dilution.

2 Current PKL / OECD Project

In 1997, the Committee on the Safety of Nuclear Installations (CSNI) of the OECD's Nuclear Energy Agency (NEA) set up an international working group whose aim was to identify how existing expertise in the field of reactor safety and an appropriate experimental infrastructure could be sustained in the future. One of the main tasks of this Senior Group of Experts on Nuclear Safety Research Facilities and Programmes (SESAR/FAP) was to identify those test facilities and research programs which were threatened by closure in the next two to three years and to select facilities and programs which, if they were able to continue through involvement in OECD projects, would be of particular benefit to the member countries. In selecting these experimental facilities, the group not only based their decisions on the technical capabilities provided by a specific facility but also assessed the competence of the team working there, including the way in which use was made of test results for analytical applications; e.g. for code validation.

At its annual meeting in December 1999, CSNI issued the recommendation that an international collaborative project be set up in the field of thermal hydraulics to implement the recommendation made by SESAR/FAP. A proposal for a project called SETH (SESAR Thermal-Hydraulics) was elaborated in consultation with the NEA Secretariat and was submitted to the member countries in mid-2000. This proposal was based on experiments to be conducted in the PANDA and PKL test facilities. In the large tanks of the PANDA facility, for example, mixing and stratification of steam and air – such as can occur in a containment atmosphere under accident conditions – were to be investigated. For the PKL facility, integral system tests for studying boron dilution

events as well as accidents occurring when the reactor has been shut down were proposed. The SETH project started in April 2001.

As is customary with OECD projects, half of the funds necessary for financing the project are to be provided by the host country in which the tests are performed. The other half is to be provided by those OECD/NEA member countries participating in the project (Belgium, Czech Republic, Finland, France, Hungary, Italy, Japan, Korea, Spain, Sweden, Switzerland, Turkey, United Kingdom, USA).

3 PKL Tests on Boron Dilution

3.1 General Background

Boron-10 is added to the reactor coolant of a PWR to control reactivity. The forced coolant circulation during normal operation or natural circulation ensures that the boric acid is homogeneously distributed in the reactor coolant system so that the boron concentration is practically uniform. Under certain accident conditions there is a potential risk that low borated water can enter the reactor core leading to a local recriticality and thereby to a power excursion. A necessary prerequisite for this to happen is the formation of low borated water slugs and their transport to the core without sufficient mixing.

The possibility of coolant with a relatively low concentration collecting in localized areas of the RCS has been under discussion for several years now. Causes might be injection of coolant with less boron content from interfacing systems (external dilution) or separation of the borated reactor coolant into highly concentrated and diluted fractions (inherent dilution). Examples of external dilution are the injection of coolant of reduced boron concentration by the makeup system, and injection of low-boron pump sealing water into the primary system. Inherent dilution can occur after reflux-condenser heat transfer or back flow from the secondary system in case of primary-to-secondary leakage accidents.

The PKL experiments, which are discussed in the following, are exclusively dealing with inherent boron dilution events after reflux-condenser heat transfer. Operation in the reflux condenser mode over a lengthy period of time could occur in the event of SB-LOCAs concurrent with limited operability of the emergency core cooling systems. It is also conceivable that operation in the reflux condenser mode could occur in the event of a complete loss of residual heat removal (RHR) via the redundant RHR system during the period of time that the RCS is at $\frac{1}{4}$ level and still closed.

3.2 Small Break Loss of Coolant Accident

Background and Topics of Investigation

If, in the event of an SB-LOCA, the primary system contains different water inventories at different times (these depending on the size of the break and the number of available emergency coolant injection systems), then different heat transfer mechanisms will be encountered according to the

water inventory present at that time. If the primary system is nearly "full" and the water is in a subcooled condition, heat transfer to the secondary system occurs through single-phase natural circulation. As soon as saturation conditions have been attained, steam starts to be produced in the core and two-phase natural circulation becomes established. As more and more coolant is lost via the break, phase separation occurs at the apexes of the steam generator U-tubes,

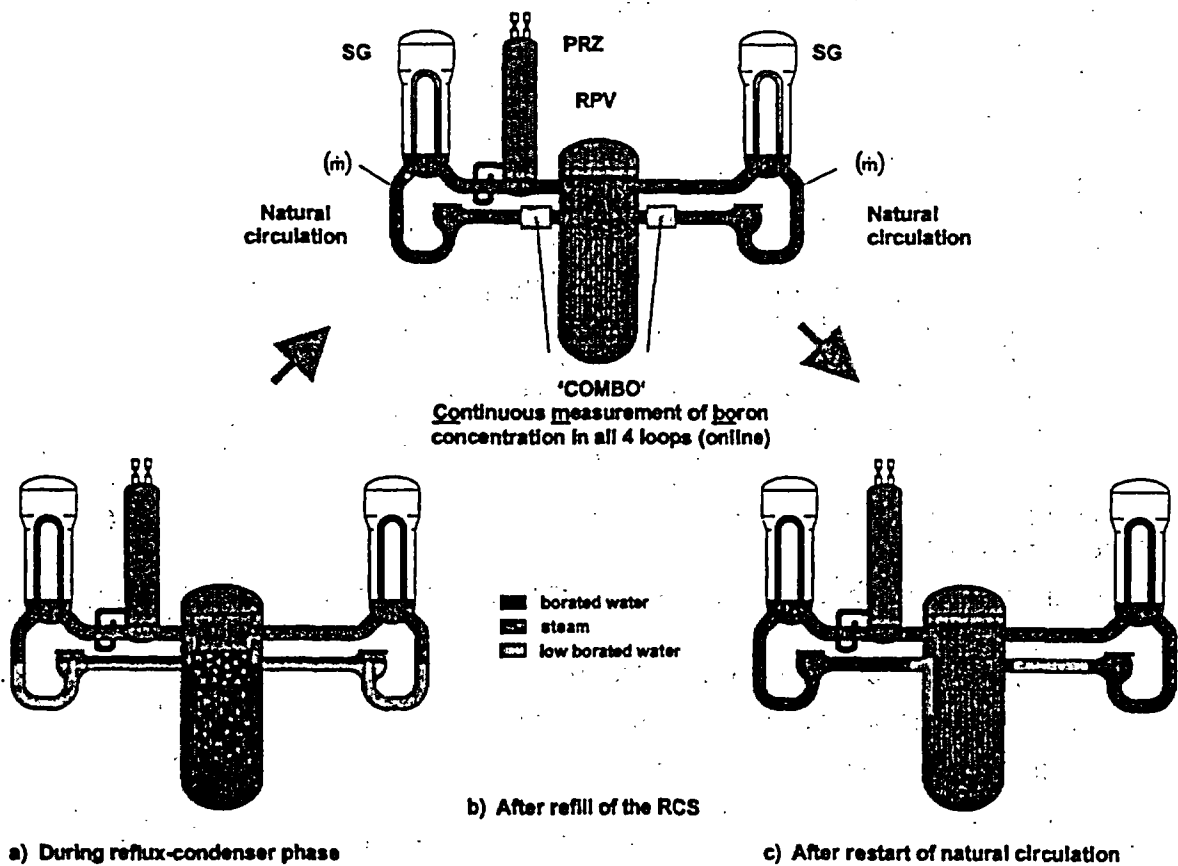


Fig. 2: Transport of Low Borated Slugs of Water after SB-LOCA (Schematically, Without Taking Credit from Mixing)

causing natural circulation to stop. Heat transfer from the core then takes place – presuming that one or more steam generators are still available as primary heat sinks – through operation in the so-called reflux-condenser mode (see schematic illustration in Fig. 2a).

The steam produced in the core flows to the steam generators where it is condensed. The condensate flows back to the reactor pressure vessel (RPV) through both the hot legs and the cold legs of the loops. During this operating mode, removal of decay heat to the secondary system is assured as long as the two-phase mixture in the RPV can be kept at least at the level of the top edge of the core. It must, however, be noted that the steam produced in the core and therefore also the condensate arising in the steam generators will be largely boron-free. If this phase continues for a prolonged period of time, the condensate arising in the steam generators

could lead to large quantities of low-boron water accumulating in the so-called "loop seals" (suction elbows of reactor coolant pumps) and, if water levels are above the elevations of the reactor coolant lines, also in the steam generator inlet plena. If the water level drops during the reflux-condenser phase down to or below the elevations of the reactor coolant lines (as illustrated in Fig. 2a), the condensate arising in the hot legs of the steam generator tubes will flow out through the hot legs of the loops – i.e. in a direction opposite to that of the steam – and back to the RPV where it will mix in the upper plenum of the RPV with water that has a higher boron content.

For operation in the reflux-condenser mode to start, the two-phase mixture must drop below the apex of the steam generator U-tubes by a substantial amount. Furthermore, prolonged operation in the reflux-condenser mode, which is a prerequisite for any accumulation of significant quantities of condensate, would only be possible if parts of the emergency core cooling systems were not available.

If, as primary system pressure continues to drop, the amount of coolant being discharged through the break becomes smaller than the makeup coolant being injected by the emergency core cooling systems, the primary system will refill and natural circulation may, under certain circumstances, restart. While refilling of the primary system is in progress, first the condensate contained in the loop seals will be transported (in a direction opposite to that of "normal" flow) towards the cold legs of the steam generator U-tubes (see schematic illustration in Fig. 2b). Together with any (unmixed) condensate present in the hot legs of the tubes, slugs of condensate are then transported in the direction of the RPV when natural circulation begins (see schematic illustration in Fig. 2c).

Whether and how much low-boron water actually reaches the reactor core is determined by the following factors:

- Quantity of condensate formed and stored during the reflux-condenser phase
- Characteristics of onset of natural circulation (e.g. simultaneously in all four loops)
- Mixing of borated emergency coolant and low-boron condensate on its way to the core.

The PKL experiments are focused on the transport of low borated water slugs within the primary system and their displacement into the RPV. Of special interest are the amount of low borated water entering the RPV from the individual loops, the minimum boron concentration and the velocities of such low borated water slugs as well as the differences between the loops. The mixing of differently borated water flows in the annular gap of the RPV downcomer is not subject of the PKL experiments. To realistically simulate the mixing processes taking place in the RPV downcomer and lower plenum, test facilities that are especially designed for the investigation of phenomena in these components are more suitable. Mixing experiments of this kind have been performed as part of the UPTF TRAM project using a full-scale mock-up of the RPV downcomer and the connected primary system piping and in the scaled test facility ROCOM /5, 6/.

Overall Test Conditions

In the case of the SB-LOCAs concerned here, the above mentioned factors, i.e. the question, if and to what extent minor boronized water would enter the RPV, depends on the boundary conditions such as:

- Size and location (hot or cold leg) of the break
- Availability of the emergency coolant injection systems and location of injection
- Rate of cooldown of the steam generators (secondary sides).

Experiments to investigate all possible break and injection configurations while at the same time using various break sizes and also taking other parameters of influence into account are not justifiable for cost reasons. However, in order that a good idea can nevertheless be obtained regarding the relevant break spectrum, generic tests covering the following aspects have been defined:

- *Maximum possible symmetry*
- *Maximum amount of condensate*

With respect to a possible reduction in boron concentration at the core inlet, an important point is whether the natural circulation starts simultaneously in all loops or with some delay between the loops. In the latter case the condensate slugs from the individual loops would reach the RPV at different times that in turn would promote the mixing of condensate and highly borated water in the downcomer annulus of the RPV. On the other side a simultaneous restart of natural circulation would increase the likelihood of a decrease in boron concentration at the core inlet. A simultaneous restart of natural circulation again can more likely be expected under symmetrical boundary conditions, e.g. when all loops are evenly supplied with ECC water. All tests with symmetrical ECC injection into all four loops (hot leg or cold leg) showed a very effective mixing of differently borated water during the refilling of the RCS and after restart of natural circulation. Consequently only a slight decrease in boron concentration was observed at the RPV inlet.

The test results described in the following concern experiments performed under boundary conditions that lead to maximum amounts of condensate. RELAP calculations for the complete size spectrum of small break LOCAs indicated that the largest condensate inventories in the event of a cold-leg break are to be expected if emergency core coolant injection takes place by two SIPs into the cold-leg piping and, on the one hand, the break is just large enough for a lengthy reflux-condenser phase but, on the other, not so large that the primary-side water/steam mixture falls below the top of the (hot-leg) piping at any time during the reflux-condenser phase. Because of the high liquid level the calculations and estimates predict that low-boron water will collect not only in the loop seals but also in the hot-leg piping and SG plena. Precisely this scenario was modeled in experiment E2.2, which will be described in the following.

Test Initial Conditions

Since the maximum operating pressure of the PKL facility is 45 bar, it is not possible to simulate the high-pressure portion of such accident sequences starting from a PWR's actual operating pressure (160 bar). Hence, in the tests, the accident "starts" at a primary system pressure of less than 45 bar and with initial conditions corresponding to those that would prevail in a real plant at this time (i.e. when the primary system pressure is at this level). These initial conditions were obtained from analyses conducted using the computer code S-RELAP5 for a real PWR geometry and corresponding boundary conditions. The remainder of the accident sequence was then simulated in the tests using real PWR pressures. That the high-pressure portion of these accidents cannot be simulated has no significant effect on the meaningfulness of the test results since the processes that are relevant with respect to boron dilution (refilling, onset of natural

circulation and transport of low-boron water in the direction of the RPV) also take place in a real PWR in the low-pressure range.

The initial conditions for experiment E2.2 in respect of RCS inventory, flow conditions and spatial variation in boron concentration were specified in such a way as to maximize condensate pockets at the (later) start of natural circulation. Since the RELAP analyses performed show that the reflux-condenser phase starts at RCS pressures above 40 bar, condensate would start to accumulate in the real-life PWR transient before 40 bar is reached. In an experiment, which starts

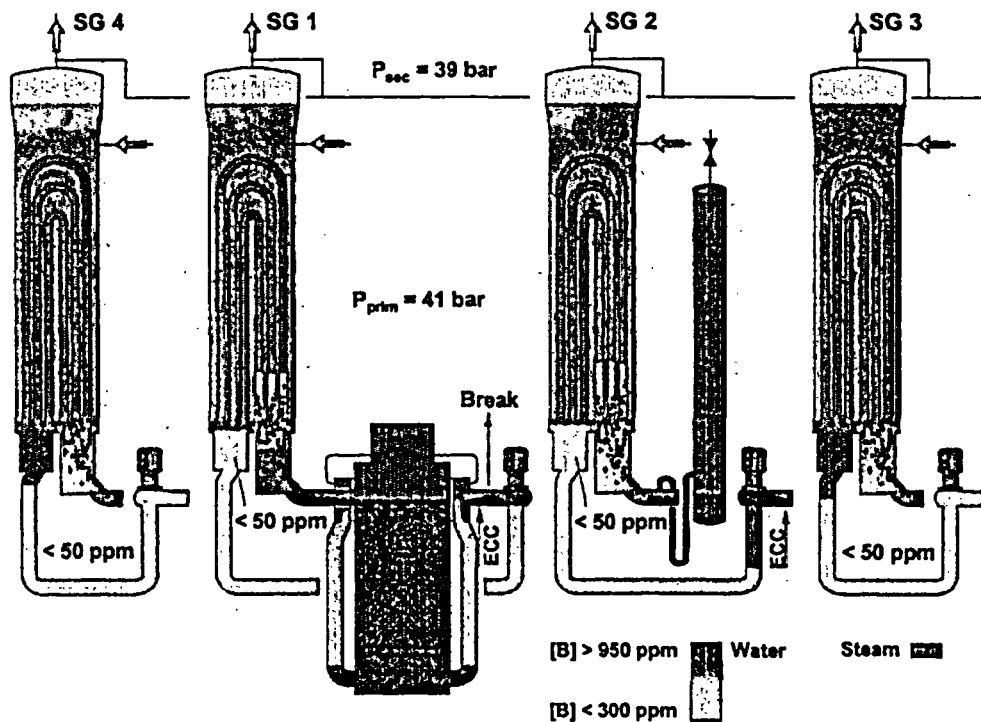


Fig. 3: PKL III E2.2 – Initial Conditions of Test E2.2

at 40 bar, the appropriate quantity of condensate has to be produced in a conditioning phase before the start of the test.

In this conditioning phase, after establishing reflux-condenser conditions, proportionately at least as much (or more) condensate was to be produced in the SGs as would be expected in the PWR on reaching 40 bar. In order to ensure that the experiment would envelop the adverse case that a particularly large proportion of the produced condensate would collect unmixed, the primary-side levels were set as high as possible. In the initial condition of experiment PKL III E2.2, the RCS coolant inventory was partly depleted (Fig. 3) with energy being removed symmetrically via the SGs in the reflux-condenser mode at a primary pressure of 40 bar. The coolant in the loop seals was largely deborated, that in the SG inlet plena partially deborated. The SIPs injecting into loops 1 and 2 had already been cut in shortly before the start of test. From this condition the test

was initiated by opening the break in cold leg 1 and starting 100 K/h cooldown via the SGs. For the subsequent course of the experiment E2.2 it had been postulated that the accumulators (ACC) were inoperable. The accumulators were therefore not used in this experiment.

Boron Concentration Measurement

A system operating according to the principle of neutron absorption – COMBO (Continuous Measurement of Boron Concentration) – was installed at the RPV inlet of all four loops to continuously measure the boron concentration of the water. This system, developed by Siemens (now Framatome ANP), is also successfully used as a process monitoring system in nuclear power plants for measuring the boron concentration in systems conveying reactor coolant. The measuring principle is based on the absorption of neutrons by the isotope boron-10, which varies according to the boron content of the coolant. The COMBO system, which basically consists of a neutron source (positioned underneath the reactor coolant line) and two counter tubes (installed close together above the line), is mounted on the outer wall of the reactor coolant pipe so that it has no effect on the fluid being measured. As a result of using this irradiation method, the measurements covered the entire flow cross section in the pipe.

The test facility was not only equipped with the COMBO system for continuous on-line measurement of the boron concentration, but sampling points for removing grab samples of the water were also provided at several locations in the primary system, such as in the loop seals, in

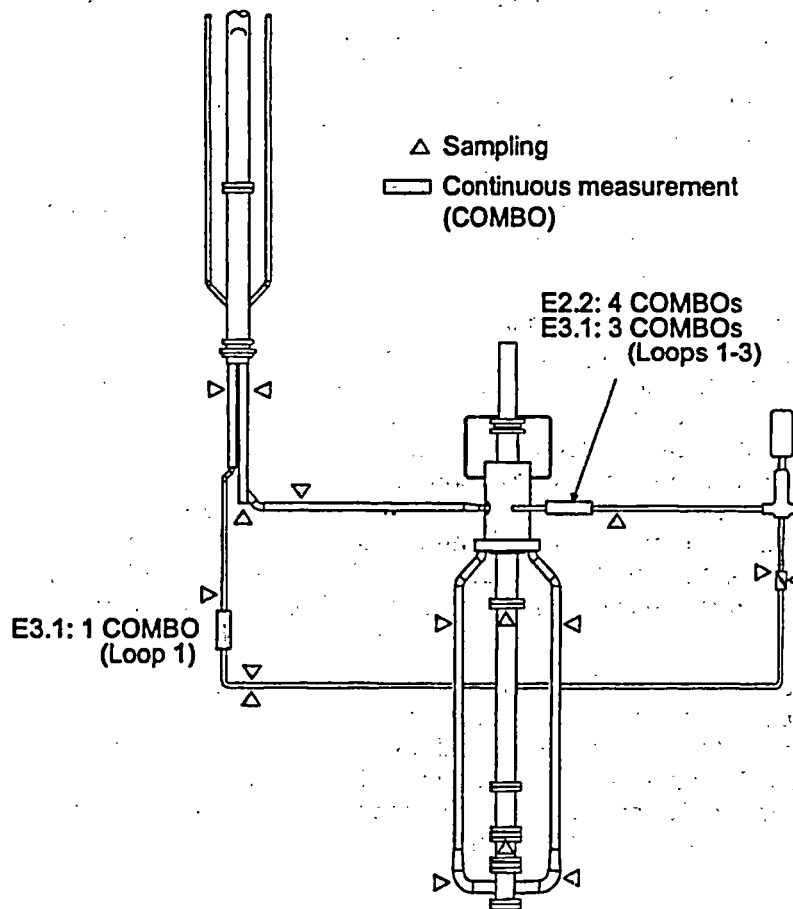


Figure 4. PKL III E - Equipment for Boron Concentration Measurement

the SG inlet and outlet plena, in the RPV downcomer and in the region of the core. The instrument locations for the boron concentration measurements are shown in Fig. 4 exemplarily for test E2.2 and test E 3.1 (see chapt. 3.3).

Test Results

Experiment E2.2 was performed in order to determine empirically the worst-case condensate slug in terms of size in the event of cold-leg ECC injection. The most important results relating to this specific aspect can be formulated as follows:

The condensate slugs which could accumulate were smaller than those which were to be postulated on the basis of conservative thermal hydraulic analyses (RELAP, etc.), namely for two reasons:

- As a result of mixing processes due to the steam flow from the core to the SGs it is not possible for pockets of water to remain diluted during the refilling of the SG inlet plena and the hot-leg piping.
- In contrast to the conditions in the thermal hydraulic analyses, mechanisms occur in the steam generators that cause flow through individual SG tubes as soon as the SG outlet plena are filled as far as the tube sheets with coolant. These flow mechanisms prevent or disrupt the accumulation of low-boron water pockets in the outlet plena and loop seals. Consequently condensate can only accumulate in the cold-leg piping when the SG tubing on the outlet side has emptied. This constitutes a significant restriction of the volume in which condensate could possibly accumulate. This is all the more true of the partly filled reactor coolant system in which level fluctuations repeatedly occur in the SG outlet plena during refilling. Because of these level fluctuations a stable accumulation of condensate can only occur in the cold leg if the time-averaged level is a certain distance from the tube sheet.

Fig. 5 shows for the first and most relevant part of the test, which includes the refilling process, the primary and secondary side pressures as well as the levels in the steam generators. The levels on the SG inlet are always – even when the water inventory is at its minimum – significantly above the elevation of the hot legs.

The coolant and condensate distribution in the RCS short time before natural circulation start up ($t=2900$ s) makes apparent that high-boron water had already reached the SG outlet plenum in some of the SGs. Evidently entrainment (water carryover in a high-velocity flow of steam through individual SG tubes) had caused this transport of water with a relative high boron content from the SG inlet side to the outlet before natural circulation set in. For this to happen, highly borated water must have been previously transported from the core to inside the SG inlet channels. Therefore it may be considered proven on the basis of the measurement results that mixing of low-boron water potentially present in the SG inlet channels with higher-boron water from the core region takes place in the SG inlet channels. At least in the refill phase the two-phase flow in which steam passes from the core to the SGs evidently entrains highly borated water from the core to the SG inlet plena.

In all SGs the short tubes were refilled before the long ones. Refilling of the short tubes occurred more quickly in loops 3 and 4 that were without injection than in loops 1 and 2 with injection. The steam still being generated and flowing from the core to the SG tubes caused the levels in the SGs to rise. At $t = 3020$ s the mixture levels reached the apexes of the short tubes of SG 4 so that coolant transport from the SG inlet to outlet sides took place in loop 4 and therefore – initially two-phase – circulation set in. The initiation of natural circulation and the effects on the boron

concentration at the RPV inlet are presented in Fig. 6. Natural circulation commenced in loop 3 at $t = 3180$ s (somewhat later than in loop 4). At this time steam production in the core was

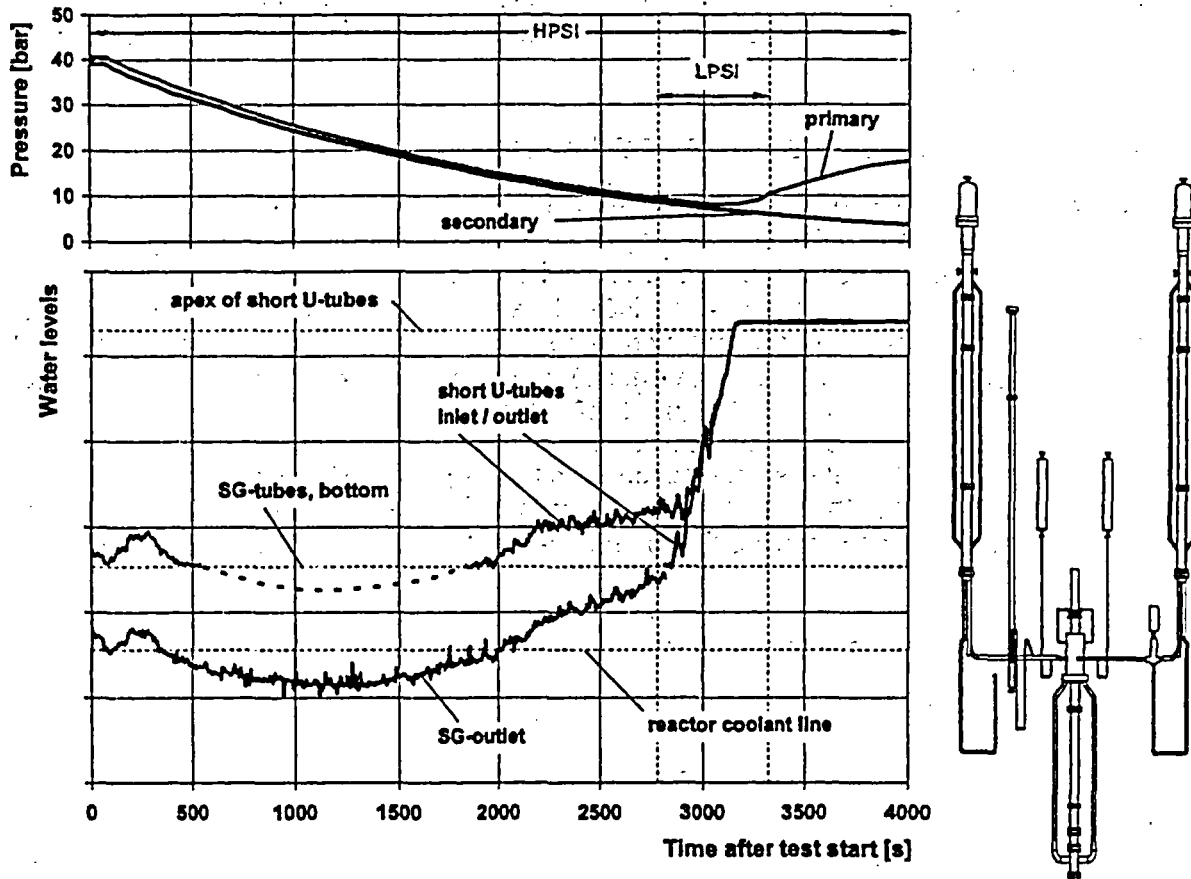


Fig. 5: PKL III E2.2 – Cooldown and Refill

terminated and circulation in loop 3 started under single-phase conditions. The natural circulation beginning at $t = 3180$ s in loop 3 and its effects on the boron concentration at the RPV inlet are also apparent from Fig. 6.

Circulation begins at a later point in loops 1 and 2. It did not result in a decrease in boron concentration at the RPV inlet. In loop 1 circulation began at different times in different SG tubes with ECC being injected into the cold leg. Furthermore the circulation rate was at first so slow that the water that had accumulated in the loop seal and in SG 1 was discharged through the break. In loop 2 alternating forward and reverse flow occurred before a definite circulation set in so that the low-boron water previously in the SG was already well mixed with highly borated water that had penetrated into the SG inlet channels during the refill phase.

A further important result is that the condensate slugs in the loops without ECC injection were located at the start of natural circulation not in the SGs but in the loop seals and SG outlet channels. The slugs were not displaced upwards into the SGs before being transported towards the RPV and therefore the supposed prior mixing with more highly borated water did not take

place. Nevertheless the boron concentration at the RPV inlet did not fall on initiation of natural circulation to the levels previously measured in the loop seals. As the condensate slugs were considerably smaller than the produced ones, mixing with high-boron coolant during refilling and during transport from the loop seals to the RPV caused the minimum boron concentration in the two slugs to increase.

Conclusive Findings up to now and further Investigations

The formation of low borated water slugs under reflux condenser conditions following SB-LOCAs has been experimentally confirmed. Hereby, it could be demonstrated that any condensate slugs are limited to the volume of the loop seal and part of the SG outlet channel. This maximum slug volume is therefore significantly smaller than the magnitude that would have had to be postulated for safety-related considerations for PWRs prior to the performance of the PKL III E experiments. A significant but short term reduction in boron concentration in case of ECC injection into 2 of 4 loops (cold leg) in the loops which are not supplied with ECC-water has been observed. However, no pronounced decrease in boron concentration at the RPV inlet has been observed in the loops with ECC injection. Another important fact is that all PKL experiments performed up to now have in common, that the various mixing mechanisms resulted in the measured minimum boron

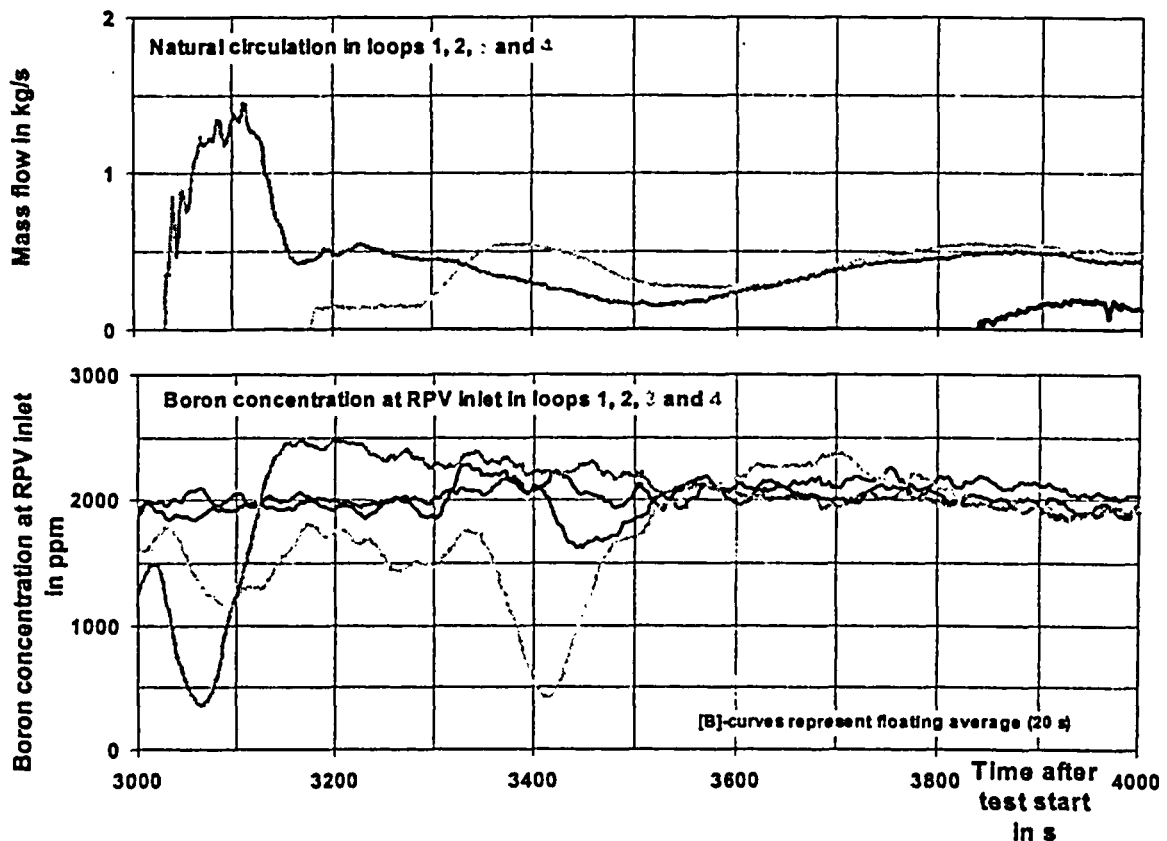


Fig. 6: PKL III E2.2 – Transport of Condensate Slugs due to Restart of Natural Circulation

concentration at the RPV inlet always being higher than the minimum present, originally in the condensate slugs formed in the loops.

In so far the PKL tests performed within the OECD/SETH program have already provided valuable findings on boron dilution events after SB-LOCAs. In order to complete these experimental investigations and to answer some still open questions mainly on the effect of different plant configurations, further tests on this topic are planned within a new PKL program. One important question here is how far the observed phenomena can be applied and extrapolated to other plant configurations (e.g. ECC injection location and rates, cooldown rates). Another important point is to better understand and analyze the physical phenomena when the SG levels are maintained in the SG U-tubes. The key output is there which maximum condensate accumulation is possible in this situation considering that the minimum boron concentration may be higher than 50 ppm.

3.3 Loss of Residual Heat Removal System

Background and General Topics of Investigations

The PKL test E 3.1 which was dealing with loss of residual heat removal was based on the following accident scenario: The PWR has already been shut down ($p = 1$ bar, $T = 60$ °C), e.g. in preparation for refueling and the reactor coolant inventory (boron concentration 2200 ppm) has been reduced to the level for $\frac{3}{4}$ loop operation. The space above the water inventory is filled with nitrogen that was injected into the reactor coolant system as the level was being reduced. The reactor coolant system is still closed and decay heat is initially still being removed through the residual heat removal system. With the reactor coolant system in this condition, complete failure of the residual heat removal system is now postulated.

Loss of the heat sink causes core temperatures to rise with resultant void formation once saturation conditions have been reached; void formation is in turn associated with an increase in primary-side pressure. For the purpose of the present test it was postulated that two SGs are filled with water on their secondary sides ($H = 12$ m with air above) at onset of accident conditions (loss of residual heat removal). The other two SGs were completely filled with air. All four SGs were initially depressurized and isolated on their main steam sides. It was also postulated that one of the two water-filled SGs (SG 1) was maintained at a constant pressure of 2 bar and a constant level of 12 m by the main steam pressure and feedwater control system following a rise in secondary-side pressure as heat is absorbed from the reactor coolant system (RCS). The other water-filled SG (SG 2) and SGs 3 and 4 likewise were isolated on their main steam (MS) and feedwater sides for the entire duration of the incident.

The test was designed to investigate the following main questions:

- To what extent the water-filled SGs assume the task of removing heat from the core following failure of the residual heat removal system and what heat transfer mechanisms become established when nitrogen is present in the SGs.
- At what pressure on the primary side do stable equilibrium conditions result with secured heat removal to the secondary side.

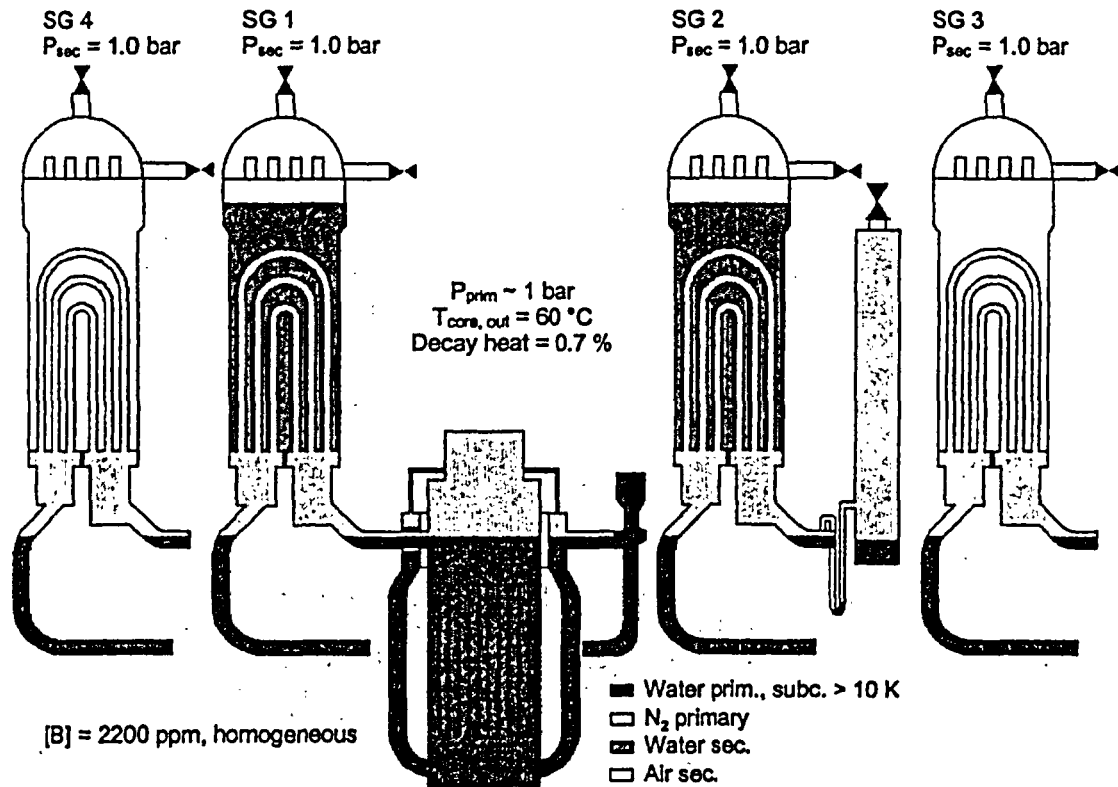


Fig. 7: PKL III E3.1 – Initial Conditions

- Given that the anticipated void formation in the core and condensation processes in the SG(s) are invariably linked with the production of weakly borated water (condensate) other questions related to possible deboration processes, i.e. in which components and to what extent is the boron concentration reduced. To this end, the test was performed with borated reactor coolant and special test instrumentation to measure boron content.

Test Conditions

In order to simulate the described accident scenario the main test boundary conditions were specified as follows:

- PWR has been cooled down for refueling
- Reactor coolant system is still closed and filled with water ([B] = 2200 ppm) up to ¾ loop level, with nitrogen above
- Failure of the residual heat removal system (RHRS)
- The secondary side of one SG is available to take over residual heat removal (two SGs are filled with water on the secondary side).

The initial conditions specified for the test (Fig. 7) were set during a preliminary test phase before the start of the test. At the start of the test reactor coolant system pressure was approx. 1 bar and

core power (decay heat) was 217 kW (equivalent to 0.7 %), with a core outlet temperature of 61 °C. The reactor coolant system inventory had been reduced to ¾ loop level with nitrogen (N₂) above. The water in the pressurizer (PRZ) was at the level of the surge line connection. For the purpose of this test it was postulated that the pressurizer had already been largely cooled down when "Loss of residual heat removal in ¾ loop operation" occurred (about 50°C).

The start of the test, which also represented onset of accident conditions, was initiated by shutting down the residual heat removal system causing a rise in core temperatures and void formation in the core with an associated increase in primary-side pressure. The transfer of heat from the primary to the secondary side heats the water inventory on the secondary side of SGs 1 and 2 to saturation conditions causing a concomitant rise in pressure on these secondary sides. Once pressure on the secondary side of standby SG 1 had reached 2 bar it was controlled at that level so that the heat generated in the core was transferred to the secondary side. As the test proceeded with quasi-steady-state conditions established on the primary side, a series of passive injections was performed from the accumulators (ACC). After the accumulator injections the residual heat removal system was postulated to be available again and was switched on in one loop; the test ended with a core outlet temperature of < 100 °C.

Boron Concentration Measurement

Especially for test E3.1 one of the four COMBOs, which are usually located in the cold legs at the RPV inlet (see chapt. 2.2), has been displaced into the loop seal 1 below the steam generator outlet channel. The reason for this was to detect the spill over of almost boron-free condensate from the inlet to the outlet side of this steam generator and to register the accumulation of a low borated slug in the pump seal. The additional grab sampling systems allowed to keep track of the locally different boron concentration throughout the RCS during the test (see Fig. 4).

Test Results

Due to the postulated failure of the residual heat removal system at the start of the test the core temperatures rose leading to void formation in the core after approx. 12 min. This led to raised pressure in the reactor coolant system resulting in compression of the nitrogen volumes.

Reflux-condenser conditions became established in SGs 1 and 2 (filled with water on their secondary sides to a level of 12.2 m) with condensation of steam on the SG inlet side in the lower areas of the U-tubes. The steam produced in the core and consequently the condensate accumulating in the lower areas of the SG U-tubes and also in the upper area of the SG inlet channels was almost boron-free. With secondary pressure in SG 1 constantly controlled at 2 bar and with primary-side pressure continuing to rise in the first instance, this SG became the main heat sink. The following heat removal conditions became established during this heating phase with the reactor coolant system pressure still rising: The steam generated in the core flowed mainly into SG 1 where it condensed on the inlet side in the lower U-tube areas. Above this the U-tubes contained a stable column of cold water at secondary-side temperature. The remaining U-tube area was filled with nitrogen also at secondary-side temperature.

A continuous increase in the volume of steam entering SG 1 from the core was observed in comparison with that entering SG 2. The swell level in the U-tubes of SG 1 continued to rise as a result of this and eventually reached the top of individual U-tubes. This caused the reactor coolant to spill over from the inlet to the outlet side, displacing the nitrogen contained in these U-tubes into the outlet channel. The almost boron-free condensate that had formed in the U-tubes and in the upper area of the SG inlet chamber was then transported to the SG outlet side and onward

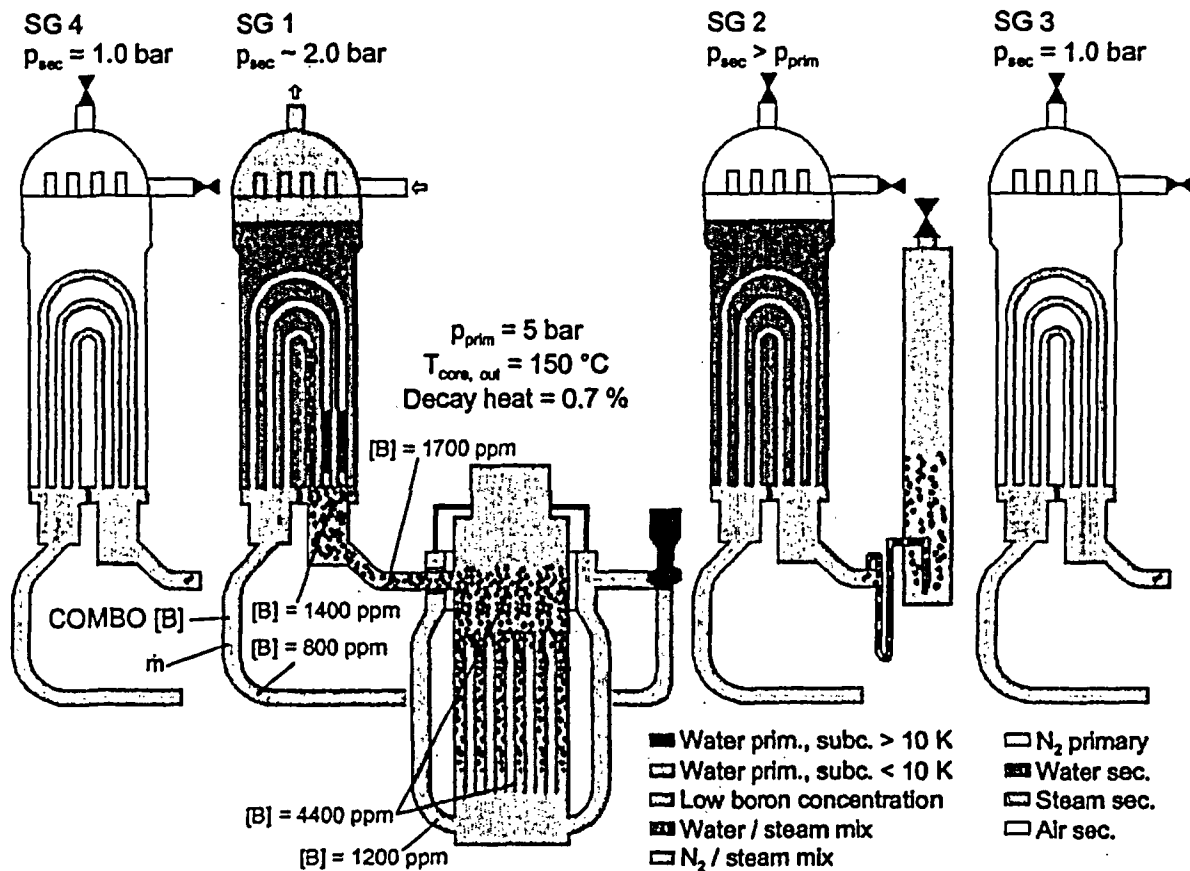


Fig. 8: PKL III E3.1 – Situation after 7 – 8 hours

through the loop seal in the direction of the reactor pressure vessel (RPV) inlet. Figure 8 shows the distribution of inventory after 7-8 hours. With respect to both the distribution of inventory and the flow pattern it is the same situation like after the first spill over of reactor coolant from the inlet to the outlet side in U-tubes of SG 1 (approx. 3.5 h after the failure of the RHRS).

As the test proceeds to the time of the first accumulator injection steady-state conditions prevail with two-phase circulation in individual U-tubes and reflux condenser conditions in the remaining U-tubes in SG 1; reactor coolant system pressure becomes stabilized at around 5 bar (Fig. 9b). During this period most of the heat is removed to the secondary side from the U-tubes with two-phase circulation. SG 1, in which secondary-side pressure is controlled at 2.0 bar, continues to act as the main heat sink with a primary to secondary-side temperature gradient of 30 K under steady-state conditions.

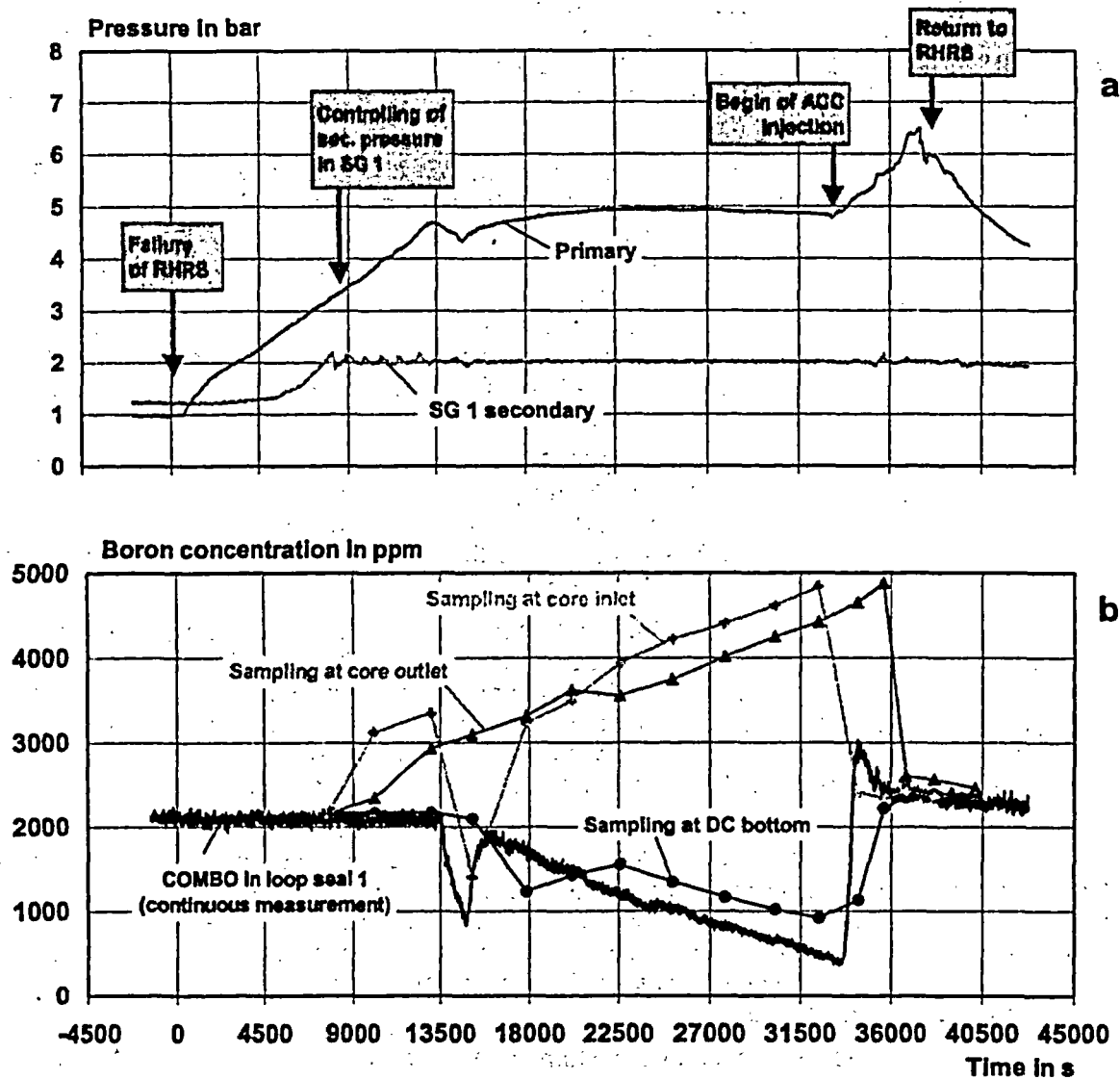


Fig. 9: PKL III E3.1 – Pressures and Boron Concentrations

As regards the boron distribution in the reactor coolant system, the boron concentration in the reactor coolant in the inlet channel of SGs 1 and 2 decreased on attainment of reflux condenser conditions and increased in the reactor coolant in the core.

Low borated water was also accumulated in the upper downcomer region and in the pump seal under the reactor coolant pump because steam flowed out of the upper plenum and through the closure head bypass onto the cold side and small amounts of steam condensed in the area of the cold legs as a result of heat losses.

A significant change in the reactor coolant boron concentration in loop 1 was observed 13500 s after start of the test. As indicated in Fig. 9b, there was a rapid reduction in the boron concentration readings obtained from loop seal 1 under the SG outlet channel using the continuous COMBO measuring instrument. The boron concentration drops from an initial value of approx. 2150 ppm to approx. 830 ppm.

The rapid, transient reduction in the reactor coolant boron concentration under the SG outlet channel occurred because the entrainment of reactor coolant from the inlet to the outlet side of SG 1 allowed water with a low boron concentration to be transported from the inlet area of the U-tubes and subsequently from the Inlet channel to the outlet side of this SG where it became mixed with the water already there, so reducing the boron concentration of the reactor coolant. Reactor coolant continued to be transferred from the inlet to the outlet side of SG 1 so that coolant with a low boron content was consequently transported through the loop seal and onward in the direction of the RPV inlet. The samples taken from the whole of loop 1 and at the core inlet also revealed certain changes in the boron concentration relative to the samples taken previously.

The boron concentration recorded by the COMBO measuring instrument then started to rise just as rapidly as it previously dropped, finally attaining a value of approx. 1900 ppm. This is because water with a low boron content had been replaced with more highly borated water from the lower part of the SG inlet channel or from the hot leg and the upper plenum. This more highly borated water was likewise transported to the outlet side of the SG.

During the further course of the test until the first accumulator injection the boron concentration decreased slowly but continuously with a gradient of approx. 400 ppm/h (Fig. 9b). Water was still being transported intermittently from the inlet to the outlet side of individual U-tubes in SG 1 but at a slower rate than the initial overspill. As a consequence low borated water was also continuously transported from the outlet side of SG 1 onward through the loop seal in the direction of the RPV inlet. This process continued until completion of the first accumulator injection.

During the accumulator injections (into the cold legs) mass flow increased in those U-tubes, which previously exhibited positive, flow conditions and from which the nitrogen had been displaced. This allowed slow continuous natural circulation to become established in loop 1. As a result of this, reactor coolant with an initially low boron concentration entered the core from the RPV downcomer. Reactor coolant boron concentrations in the whole of loop 1 and in the RPV then leveled out at around 2400 ppm. Forward flow conditions through the N₂-free U-tubes were maintained and even increased.

Reactivation of the residual heat removal system in one loop returns the reactor coolant system to a subcooled condition and the test is ended at a core outlet temperature of < 100 °C.

Conclusive Findings up to now and further Investigations

The test described above can be stated to have produced two important findings. Under the selected boundary conditions, controlling secondary-side pressure in one SG at 2 bar limited the increase in RCS pressure following loss of the residual heat removal system to around 5 bar: A quasi-steady-state condition became established although there was a continuous reduction in the boron concentration in the reactor coolant on the cold side of the loop with the active SG. If the ACC injection is very delayed while the plant is in this condition, i.e. as in the test approx. 9 hours after loss of the residual heat removal system, the boron concentration on the cold side including the RPV downcomer was reduced. An ACC injection then has the effect of transporting water with a low boron concentration, particularly from the RPV downcomer, to the

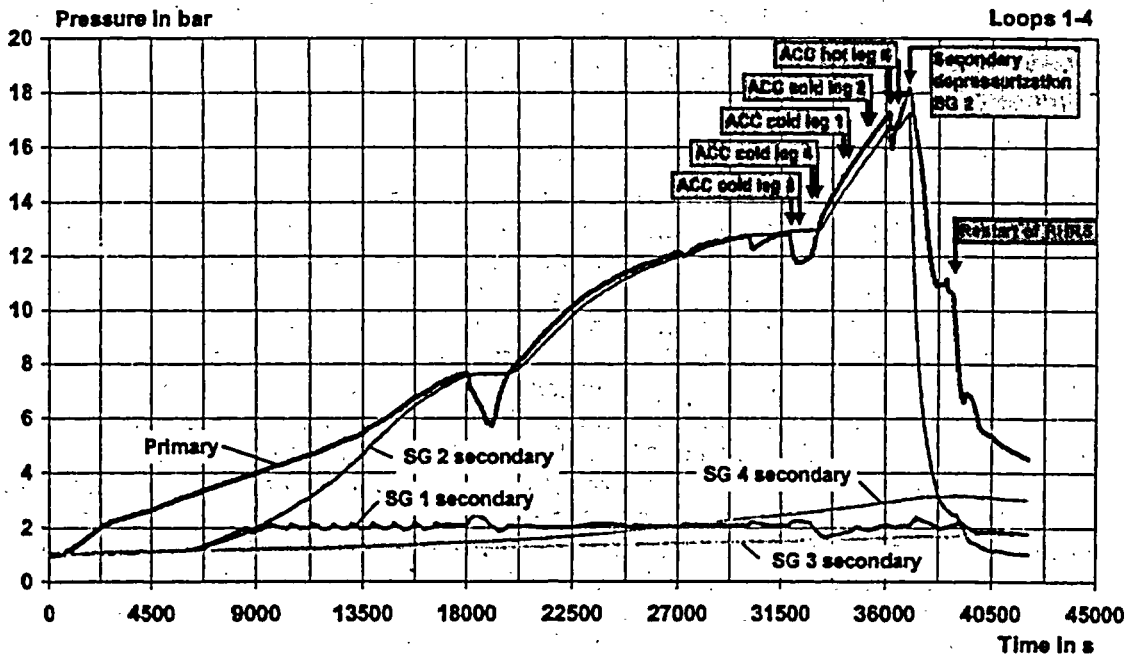


Fig. 10: E3.1 (Commissioning Test): Pressures on primary and secondary sides

core. An early accumulator injection is therefore preferable to a delayed one because a reduction in the boron concentration on the cold side of the loop with active SG is avoided in this case.

In connection with a commissioning test, it became apparent that the heat transfer mechanisms, i.e. primary-to-secondary energy removal, and the mechanisms that cause boron dilution are highly sensitive to the distribution of the primary inventory. In this commissioning test, the assumption of a hot pressurizer at the occurrence of the accident led – due to lower amount of water displaced into the pressurizer – to a situation with higher water inventory in the primary system compared to the above described experiment E 3.1. This again resulted in significant differences with respect to the evolution of the primary pressure and boron dilution phenomena, e.g.:

- Primary pressure stabilization at about 5 bar, however significant reduction of the boron concentration on the 'cold side' in tests E3.1
- No significant reduction of the boron concentration, however increase of the primary side pressure over 10 bar in the commissioning test (Fig. 10).

It is also evident that the above-mentioned phenomena are also dependent on the number of operable steam generators. Systematic investigations concerning the influence of the primary side inventory (e.g. influenced by state of the pressurizer) and the number of available steam generators on primary pressure and boron concentration are planned to be performed within a new PKL program. The objective of these investigations is to generate a sound basis for the evaluation of such events with respect to heat removal in the SGs and boron dilution processes. It is of special interest to analyze those boundary conditions that will secure decay heat removal

and rule out the possibility of primary-side over - pressurization after loss of RHR and also to rule out unacceptable decreases in boron concentration due to boron dilution as a result of the associated energy and material transport mechanisms.

3.4 Extrapolation of Test Results to PWR Plants

Because of its design (all elevations are scaled 1:1 and the four reactor coolant loops are arranged symmetrically), the PKL integral test facility is well suitable for resolving questions related to natural circulation. Due to its exact replication of the steam generators as a whole and especially of the steam generator tubes (including, for example, their differing heights) the processes observed in these regions can be well applied to real power plant configurations. Hence, heterogeneous behavior in the steam generator U-tubes can likewise be assumed for an actual PWR plant under similar boundary conditions. Therefore, important considerations regarding the formation, the maximum volume, the displacement, the dilution and dynamics of low borated water slugs can be extrapolated to real plants, at least in qualitative terms.

The quantitative extrapolation of specific test results such as the minimum boron concentration at the reactor pressure vessel inlet or the rate of the local boron dilution after the loss of residual heat removal system is only possible with the help of validated thermal hydraulic system codes. In this respect the PKL results represent an important database for validating the models employed in thermal-hydraulics codes, thus enabling these validated codes to extrapolate the experimental results for application to the full-scale geometry of a real PWR.

Concerning the mixing processes taking place in the RPV downcomer and lower plenum, test facilities that are especially designed for the investigation of phenomena in these components are more suitable. Mixing experiments of this kind have been performed as part of the UPTF TRAM project using a full-scale mock-up of the RPV downcomer and the connected primary system piping and in the scaled test facility ROCOM /5, 6/. The mixing of differently borated water flows in the RPV downcomer and in the lower plenum is likewise analyzed by 3-D computational fluid dynamics (CFD) codes. In this context, the PKL test results also constitute an important source of data for supplying boundary conditions for these codes.

4 Conclusions and Outlook

Within the international project SETH, set-up by the OECD with 15 participating countries Framatome ANP has conducted system experiments at the PKL Test Facility to look into issues including inherent boron dilution during small-break loss-of-coolant accidents and after loss of residual heat removal under shutdown conditions. Borated coolant and instrumentation for detecting boron concentration has been being used in these experiments.

The formation of the condensate slugs in the reactor coolant system of a PWR under reflux-condenser conditions was empirically confirmed in the experiments. The tests on SB-LOCA demonstrated that the maximum slug volume is significantly smaller than the magnitude that would have had to be postulated for safety-related considerations for PWRs prior to the performance of the experiments. Another important fact derived from the experiments is that the various mixing mechanisms results in the measured minimum boron concentration at the RPV inlet always being higher than the minimum present, originally in the condensate slugs formed in the loops.

A test on loss of residual heat removal under shutdown conditions showed that with closed primary system and at least one steam generator available, the increase in primary pressure is

limited. Quasi steady state conditions with secured heat transfer to the secondary side under reflux condenser conditions are established. However a slow but continuous reduction in the boron concentration on the 'cold side' can occur.

In so far the PKL experiments provide a valuable database for the validation of thermal hydraulic system codes and an important contribution to the resolution of safety issues of PWRs in context with boron dilution events. To perform a final evaluation on this issue further integral tests are needed in which the boundary conditions will vary. These complementary investigations, together with new topics such as loss of residual heat removal with open RCS and boron dilution after steam generator tube rupture are planned to be performed in the course of a new PKL project starting at the beginning of 2004. Thereby it is foreseen to continue the approved and very efficient co-operation in an international frame within a new OECD program.

Nomenclature

ACC	Accumulator
COMBO	Continuous Measurement of Boron Concentration
CSNI	Committee on the Safety of Nuclear Installations
ECC	Emergency core coolant
HP	High pressure
LB	Large break
LOCA	Loss of coolant accident
LP	Low pressure
NEA	Nuclear Energy Agency
OECD	Organization for Economic Co-operation and Development
PKL	Primärkreisläufe-Versuchsanlage (Integral test facility, Germany)
PWR	Pressurized water reactor
RCS	Reactor coolant system
RELAP	Reactor excursion leak analysis program (computer code)
RHRS	Residual Heat Removal System
RPV	Reactor pressure vessel
ROCOM	Rosendorf Mixing Model
SB	Small break
SESAR	Senior Group of Experts on Nuclear Safety Research
SETH	SESAR Thermal Hydraulics
SG	Steam generator
SIP	Safety Injection pump
UPTF	Upper Plenum Test Facility

Acknowledgments

The authors gratefully acknowledge the support of all international organizations participating in the OECD/SETH project. The members of the Management Board and the Program Review Group have substantially contributed to work out the test specifications and their valuable feedback on test results has helpfully supported the interpretation and final evaluation of the tests.

References

1. K. Umminger, B. Brand, V. Teschendorff, 2001, Integral Tests Conducted at the PKL Test Facility on Topical PWR Safety Issues, Topical Session Paper of Annual Meeting on Nuclear Technology, Dresden, Germany, May 15 - 17, 2001.
2. Proceedings of the OECD/CSNI Specialist Meeting on Boron Dilution Transients, Pennsylvania State College, Penn., USA, 18 - 20 October 1995, NUREG/CP-0158, NEA/CSNI/R(96)3, 1997.
3. G. Gavrilas, B. Woods, M. Antkowiak, V. Palazov, G. Pertner, M. Salay, 1999, Rapid Boron-Dilution Transient Investigations in a PWR Integral Test Facility, Proceeding of Ninth International Topical Meeting on Nuclear Reactor Thermal Hydraulics (NURETH-9), San Francisco, California, USA, October 3 - 8, 1999.
4. J. Hyvärinen, 1993, The Inherent Boron Dilution Mechanism in Pressurized Water Reactors, Nuclear Engineering and Design, Vol. 145, pp. 227 - 340, 1993.
5. R. J. Hertlein, K. Umminger, S. Klem, H.-M. Prasser, T. Höhne, F.-P. Weiss, 2003, Experimental and Numerical Investigation of Boron Dilution Transients in Pressurized Water Reactors, Nuclear Technology, Vol. 141, pp. 88 - 107, 2003.
6. K. Umminger, W. Kastner, J. Liebert, T. Mull, 1999, Thermal Hydraulics of PWRs with Respect to Boron Dilution Phenomena - Experimental Results from the Test Facilities PKL and UPTF, Proceeding of Ninth International Topical Meeting on Nuclear Reactor Thermal Hydraulics (NURETH-9), San Francisco, California, USA, October 3 - 8, 1999.

NDE for Reactor Pressure Vessel Head Replacements¹
Steven R. Doctor and George J. Schuster
Pacific Northwest National Laboratory
Richland, WA

ABSTRACT

The recent experience of cracking in control rod drive mechanism (CRDM) penetration tubes and the associated J-groove welds has led to several utilities replacing their vessel heads and many other reactor owners are considering replacement of their vessel heads in the near future. The bulk of evidence supports the position that Primary Water Stress Corrosion Cracking (PWSCC) is causing the observed degradation. But further work is being conducted on CRDMs that have been cut from vessel heads that have been removed from service. The work will investigate the effectiveness of the NDE and further an understanding of the degradation process. In trying to prevent future degradation, the industry has chosen to have replacement heads fabricated using alloys more resistant to PWSCC. There remain many questions concerning how to put in service the highest integrity components, which would then hopefully have the longest service life. What NDE should be employed during construction, what construction activities need to be fully documented and what pre-service NDE should be performed for the baseline are all questions that need to be addressed. This paper will examine these questions based on related research and what insights this research provides.

INTRODUCTION

Inconel Alloy 600 along with weld Alloys 182 and 82 were selected and employed in a variety of nuclear power plant components because of their attractive properties which include high strength, ductility and corrosion resistance. In pressurized water reactors (PWRs) these applications include the steam generators, pressurizer heater sleeves, instrumentation and sampling nozzles, control rod drive mechanism (CRDM) vessel head penetrations, and dissimilar metal piping weldments. Unfortunately these Inconel materials have been found to be susceptible to degradation by a mechanism known as primary water stress corrosion cracking (PWSCC). PWSCC has breached the reactor coolant pressure boundary resulting in degrading plant safety. Because of costs and radiation exposure to personnel, the industry has decided in a number of cases that the best solution is to replace the reactor pressure vessel head using materials more resistant to PWSCC. This paper examines the nondestructive examination (NDE) programs being employed to reliably inspect the replacement reactor vessel heads with the major emphasis on their penetrations.

¹ This work was conducted for the U. S. Nuclear Regulatory Commission under DOE Contract DE-AC06-76RLO 1830: for JCN Y6534 with Carol Moyer, NRC program manager, JCN Y6604 with Debbie Jackson, NRC program manager and JCN Y6909 with Bill Cullen, NRC program manager.

DEGRADATION in INCONEL

The first significant leak in a CRDM occurred in September 1991 at the French plant Bugey 3 (Shah et al 1994, Buisine et al 1993). This was detected during a 10 year hydrotest and was detected with an acoustic emission technique. The leak rate was 0.003 gpm (0.7 l/h). There were two through wall ID axial cracks confirmed by destructive testing (DT) and found to be PWSCC. There were also two circumferential cracks on the outside diameter (OD) of the penetration tube that were confirmed by DT. One crack was a hot crack located in the weld that had been created during fabrication. The other was in the base metal and connected to the through wall axial crack on the down hill side of the nozzle and just above the J-groove weld. As a result the French made the decision to replace all of their reactor heads using more resistant materials. The French have conducted dye penetrant tests (PT) of the J-groove weld crowns and buttering from 11 replaced vessel heads. Of the 754 PT inspections reported by Amzallag et al 2002 no cracks have been found.

The vessel head penetration degradation became a significant problem in the U. S. with the PWSCC degradation detected at Oconee. From 11/2000 to 2/2003 there have been ten plants that have detected PWSCC requiring repair. There were 79 CRDMs that required repair and 13 thermocouple nozzles. Twelve had circumferential cracking and this is of concern because this cracking is above the J-groove weld where the potential of a CRDM ejection is increased. Of course, the worst problem was the severe wastage that was found in the vessel head at Davis Besse.

In April 2003, boric acid deposits were detected on the lower head of the reactor pressure vessel at the South Texas Project (STP) Unit 1. Two bottom mounted instrumentation penetrations had small boric acid deposits (3 mg and 150 mg) that was estimated to be 3 to 5 years old. NDE tests were conducted and confirmed the presence of axial cracking along the weld fusion zone between the penetration tube and the J-groove weld and extending into the penetration tube wall. The cracking was confirmed by ultrasonic tests (UTs), eddy current tests (ETs) and a helium bubble test. A boat sample was taken and documented the cracking with the DT results reported in a supplement to the LER 03-003. The surprising thing about this PWSCC was that it occurred in a zone where the temperature is low and was not expected to crack. The DT results show that a contributing factor was the presence of a lack of fusion flaw at this location.

Based on the preponderance of PWSCC occurrences in these Inconel materials, it has been concluded that this is a generic problem. A recent review paper by Bamford and Hall 2003 documents the history of cracking in these alloys. In addition, the NRC Davis Besse Lessons Learned Task Force Report 2002 has analyzed the licensee event reports (LERs) from 1986 through 2002 in Appendix E. There were a total of 89 LERs and leaks were found to occur in most locations where Inconel had been employed. Seventeen percent of the leaks were associated with CRDMs and most of these had taken place since 2000.

OVERVIEW of NRC FUNDED NDE RESEARCH ACTIVITIES for VESSEL HEADS

There are a number of research activities being conducted by the NRC that relate to the NDE of replacement reactor pressure vessel heads. The efforts are identified in the following by the NRC job code number (JCN) and a brief overview of each is provided.

JCN Y6604

The objective of this work was to address the issue of volumetrically inspecting the J-groove weld and all of the buttering. A CRDM specimen was obtained that had been cut out of a head from the

cancelled Midland nuclear power plant. This specimen was received from Oak Ridge National Laboratory who originally obtained it from Framatome. The specimen which was received had been flame cut from the head. PNNL chose to machine the ferritic material to obtain the largest cylinder of ferritic steel that could be machined and be concentric with the centerline of the penetration tube as shown in Figure 1. A typical result that was obtained by UT from the outside ferritic machined surface at 10 MHz using synthetic aperture focusing technique (SAFT) is shown in Figure 2. Four product forms are being imaged. The goal was to look for the presence of welding flaws and of course all welds are imperfect and contain fabrication flaws. Based on previous studies most of the welding flaws are located along the fusion zones and these have most often been found to be lack of fusion. In this case there were a number of 1 to 2 mm flaws detected. The response of these weld flaws was about -35 dB while the response from the weld grains was typically -42 dB while that from the ferritic base metal was -57 dB when compared to the reference standard. Figure 3 shows a typical example of a fabrication flaw that is along the fusion zone between the buttering and the J-groove weld metal.

What we found in this study was that fusion zone fabrication flaws could be detected using normal incidence. However, these could only be detected for the near fusion zone. If the sound field had to pass through the weld, then it was not successful in detecting these small fabrication flaws on the far side fusion zone. Future work will evaluate the capability of UT to detect and to characterize fabrication flaws on all of the fusion zones as a function of the flaw size.

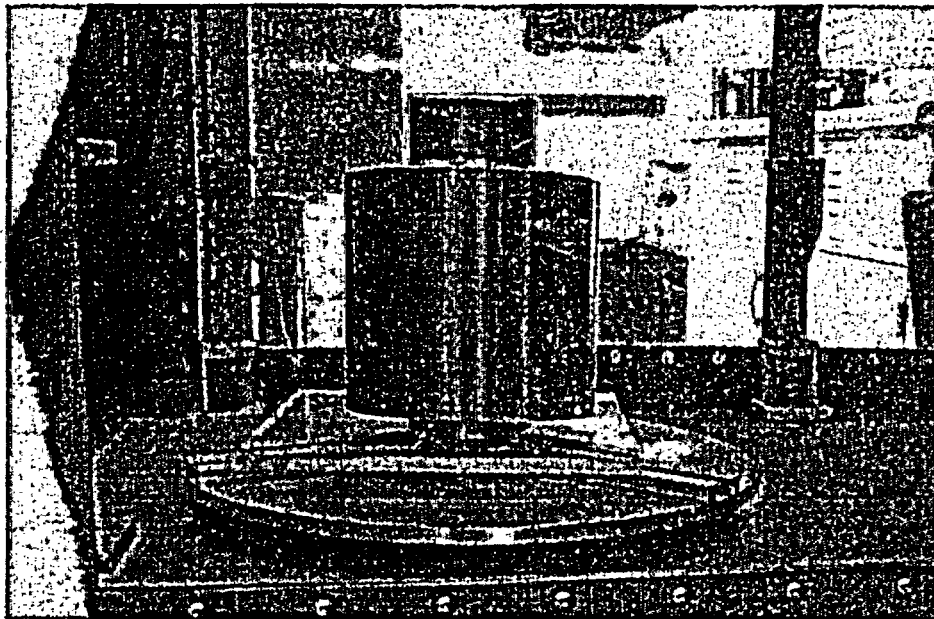


Figure 1. Midland CRDM after machining and located in water immersion tank prepared for inspection.

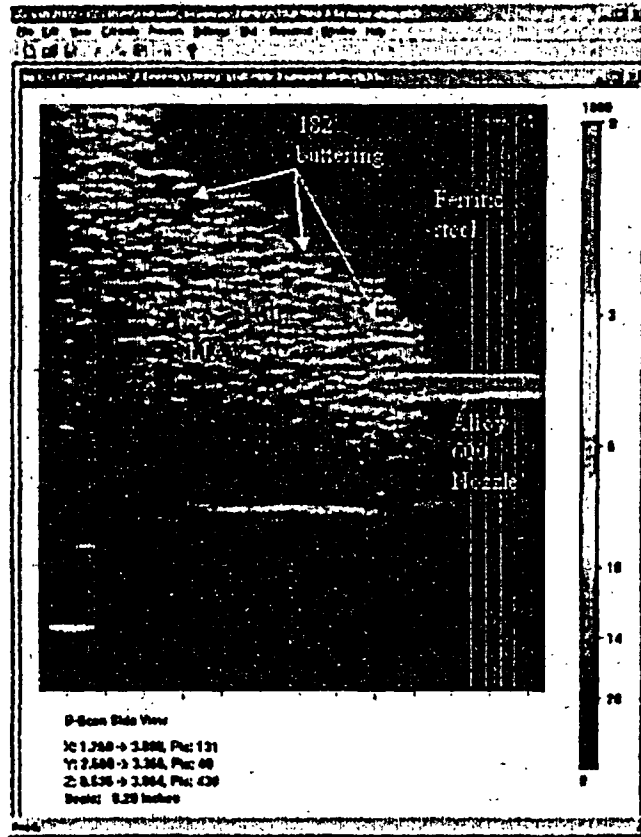


Figure 2. UT results using normal incidence at 10 MHz spherically focused insonification showing the four product forms.

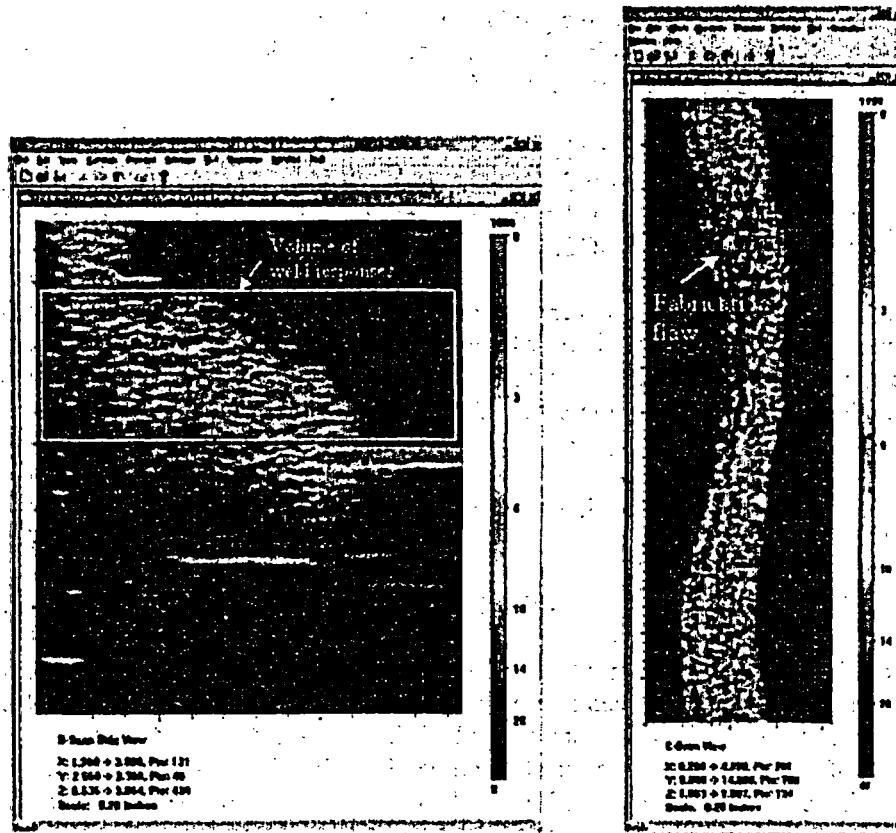


Figure 3. Shows a fabrication flaw at the fusion zone between the buttering and the J-groove weld metal.

JCN Y6534

One of the main objectives of this program is to develop an international cooperative to address the issues of PWSCC and NDE reliability of dissimilar metal welds (DMWs) and nickel based alloys. PNNL is providing support to the NRC in this effort. All interested parties both nationally and internationally are being contacted and offered the opportunity to participate. A presentation on this cooperative was made during the conference. An evening meeting was held to go into more details regarding ideas about the activities that might be addressed during this cooperative. A follow-up was proposed with a mailing to all interested parties to solicit interest and suggested priorities so that a proposed program could be developed based on this input for the cooperative. There are so many issues related to PWSCC in all of the Inconel applications that are not understood, thus, it is important to identify those of highest interest to the participants in the cooperative so that a program can be planned to address them.

One task that was proposed would involve producing an atlas of metallography documentation on PWSCC cracks and NDE responses. This information is needed to understand the variability as well as to understand how one might be able to simulate PWSCC with other flaws.

Another proposed task would be to organize and conduct a round robin study to assess NDE techniques for their reliability in detecting and characterizing PWSCC. The challenge here is identifying which of the many Inconel applications that should be studied so that appropriate mock ups can be designed and fabricated with realistic PWSCC.

Other activities that have been suggested for the cooperative include the assessment of NDE modeling for Inconel applications. This might be one way of extending the studies that are being proposed to those applications that were not studied. There are a number of conditions such as surface preparation that can impact NDE effectiveness and laboratory parametric studies that might be performed to address these issues.

The plan is to have the parties identified, agreements in place, and a plan refined to begin conducting the work by mid 2004.

JCN Y6909

Part of this work is a joint program with EPRI/MRP to decontaminate CRDMs that have been cut from the North Anna 2 head which has been removed from service. These CRDM nozzles were cut and shipped to PNNL where they are being decontaminated while maintaining as best we can, their pristine condition both for NDE studies and destructive characterization of the PWSCC including chemical analysis over the entire crack depth. The CRDMs will be decontaminated in early December 2003 in preparation for NDE vendor inspections. There will be four vendors that will conduct NDE inspections during December and January. Two of the CRDMs are scheduled for destructive testing.

Figure 3 shows a CRDM that has been decontaminated and is being readied for transit to a stand where it will reside during NDE inspections. Four CRDMs will be inspected by the commercial NDE vendors. The really fantastic opportunity that the North Anna 2 CRDMs offer is realistic NDE studies on service induced PWSCC coupled with flaw validation. This will allow us to fully understand how effective the NDE is in detecting PWSCC at all of the locations found in these samples. For the first time, we will also know what was found and what was not found. In addition we will for the first time understand how accurate the NDE techniques are in sizing the PWSCC.

PNNL plans to fabricate some research grade scanners and conduct NDE studies on the remaining North Anna 2 CRDMs that are not sent off for DT. The remaining NRC activity that is now in the planning stage is to conduct studies on material that was received at PNNL from Davis Besse. It is expected that there will probably be both NDE studies and DT studies conducted on this material over the next two years.

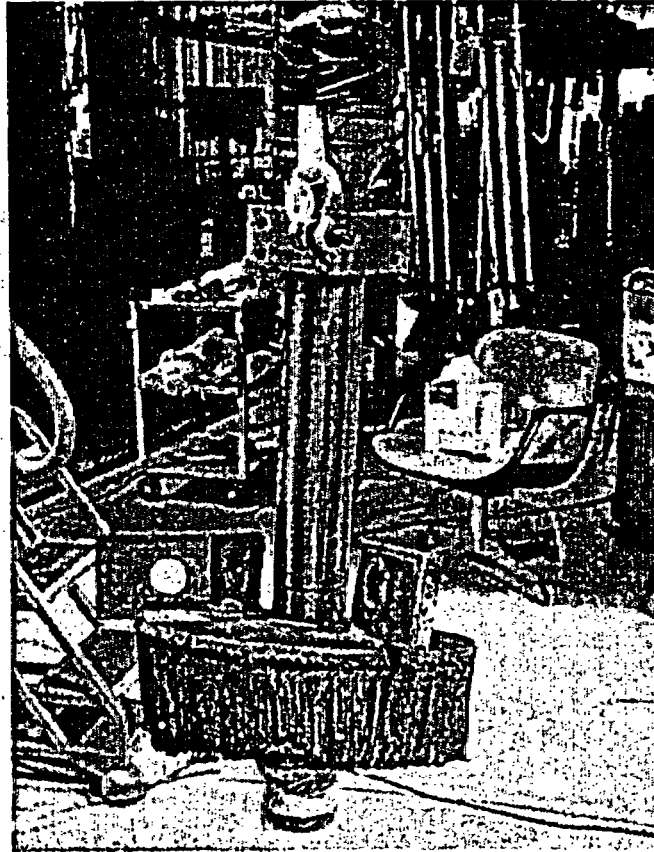


Figure 4. North Anna 2 CRDM that has been decontaminated and is ready for moving to a stand for NDE inspections.

IDENTIFIED FACTORS in DEGRADATION of INCONEL

The degradation of Inconel by PWSCC is a very complex process. There are many factors that appear to influence the initiation and growth rate of PWSCC. There appears to be a correlation between the number of years of operation and the temperature that the Inconel sees during service. But then the failure at STP of the lower head penetrations where they see a much lower temperature was a total surprise. The failure of the dissimilar metal weld at V C Summers has been determined to be caused in part by the extensive weld repairs that were made. Review of construction records on Oconee CRDMs has found no correlation between the locations where PWSCC was found as a function of whether there were repairs to the J-groove weld or straightening of the CRDMs. CRDMs and BMIs are welded into the heads via J-groove welds. The only NDE that is performed is PT after the root pass, when the weld is $\frac{1}{2}$ completed and after full completion of the weld. The PT test only assures that there are no surface breaking flaws but may allow subsurface fabrication flaws to go into service. This was the case for STP where a lack of fusion flaw was found to be a contributor to the BMI failure.

Clearly, PWSCC is a very complex process and the data is sparse regarding all of the factors that appear to influence it. This is part of the problem and is the reason why more research is needed in order to understand the significance of each factor so that these conditions can be assessed for each application and failure predictions can be made.

FABRICATION FLAWS

PNNL has conducted studies to develop engineering databases on fabrication flaws that were created at the time of fabrication. These databases provide valuable data on the density and distribution functions as a function of the product forms. A number of reports have already been published concerning reactor pressure vessel materials (Schuster et al., 1998, 1999, 2000) and work is in progress for similar studies on austenitic stainless steel, cast stainless steel and dissimilar metal piping welds.

PNNL found that for welding processes in ferritic steel, 95% of the fabrication flaws were found to be located along the fusion zones of the welds. Most of these fabrication flaws were lack of fusion and thus are "crack like." All of the largest flaws were associated with repairs. These repair flaws tended to be clustered at the ends of the repair areas and the flaws were very complex and had 3-D properties. The flaws were uniformly distributed as a function of depth.

PNNL has underway a similar study on piping materials where very sensitive NDE inspections have been conducted and flaw validation is in progress. Preliminary results for some dissimilar metal piping welds have found that 398 fabrication flaws have been detected with 96 of these along the fusion zone of the buttering to carbon steel, 34 are in the buttering, 139 are along the fusion zone of the buttering to the SMAW structural weld, 122 are along the fusion zone of the SMAW structural weld to the safe end and 7 are in weld repairs. These three dissimilar metal welds are in 91.5 cm (36 inch) diameter pipe with an 8.9 cm (3.5 inch) wall thickness. The buttering has a volume of 8000 cm³, the volume of the SMAW structural weld is 13,000 cm³ and the volume of the repairs is 150 cm³.

Figure 5 is an example of ultrasonic inspections results conducted using a weld normal inspection with a high resolution ultrasonic transducer and synthetic aperture focusing technique (SAFT) processing. There is a weld repair shown at the pipe ID and there is also a weld repair on the pipe OD. These repair zones are defined by a large number of fabrication flaws in the form of a "boat" shape in the figure. Figure 6 is a typical UT image showing fabrication flaws along the buttering to SMAW fusion zone.

Figure 7 is an example of the fabrication flaws in the bottom mounted instrumentation nozzle penetration #46 that leaked at the South Texas Project Unit 1 (STP presentation to the NRC on 6/5/03 can be found at NRC website <http://www.nrc.gov/reactors/operating/ops-experience/bottom-head-penetration-leakage.html>). These fabrication flaws are along the fusion zone between the OD of the penetration tube and the J-groove weld. Based on the work at PNNL it is expected that these are lack of fusion flaws. There are two lines traversing across the J-groove weld in this figure and these are the locations of the two PWSCC that were detected with TOFD UT. A boat sample was removed from BMI penetration #1 and a cross section through this sample is shown in Figure 8 (LER 03-003 Supplement). There is clearly a tight crack that exists at the surface of the J-groove weld crown and there is a large lack of fusion fabrication flaw along the fusion line between the J-groove weld and the OD of the penetration tube.

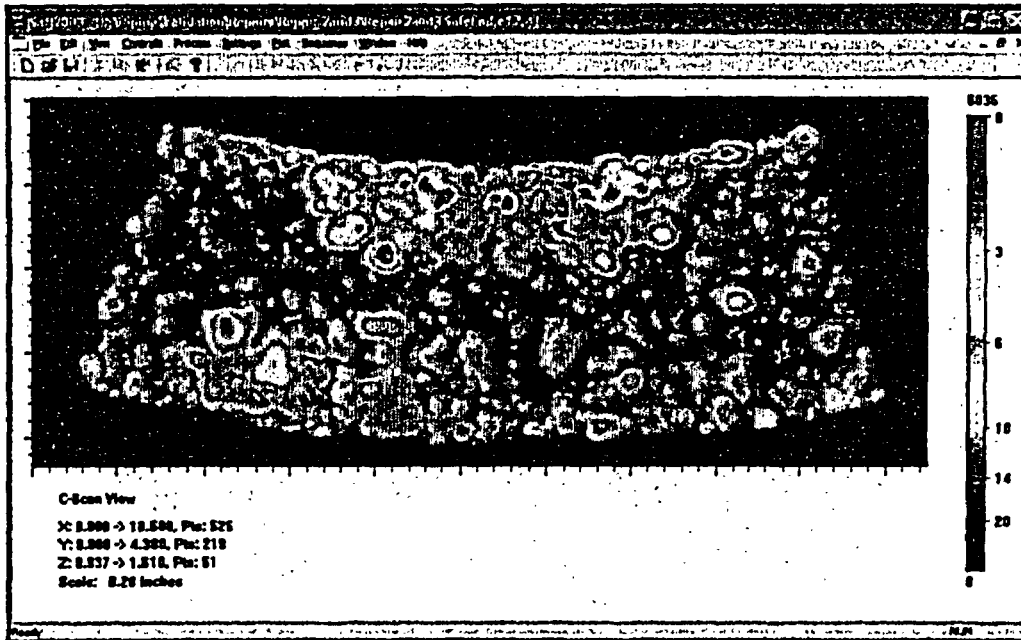


Figure 5. UT C-scan image of a pipe segment containing a repair on the pipe ID and a repair on the pipe OD.

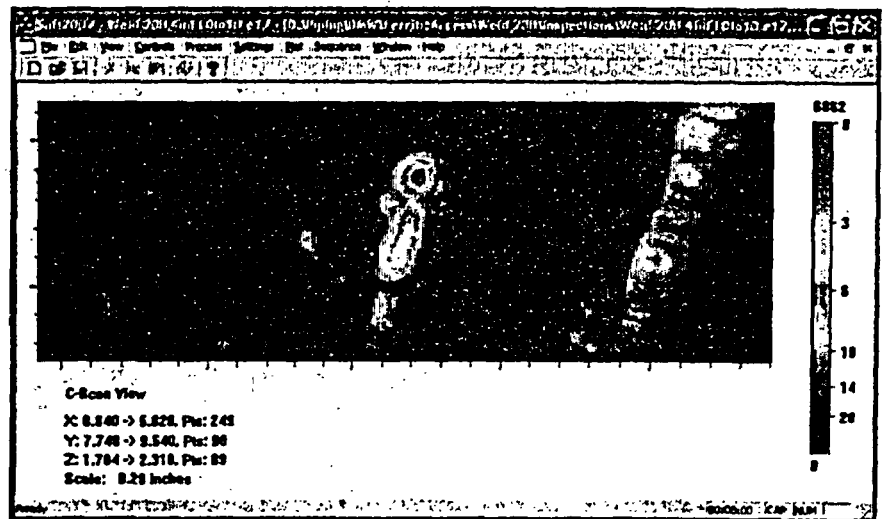
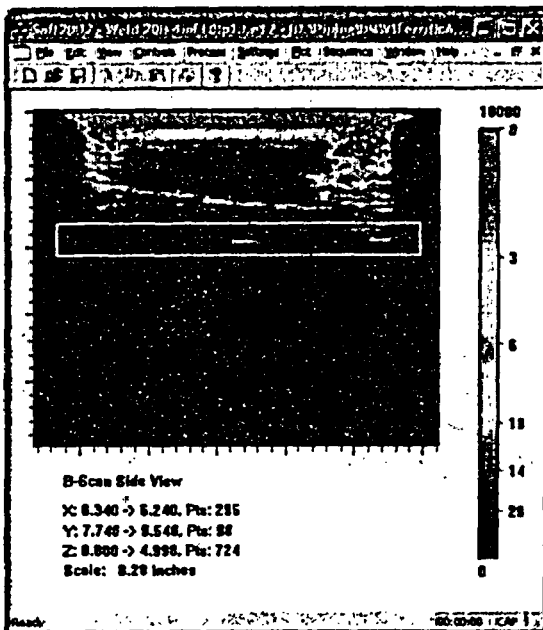


Figure 6. Lack of fusion fabrication flaw in middle of image along the fusion zone between the buttering and the SMAW structural weld.

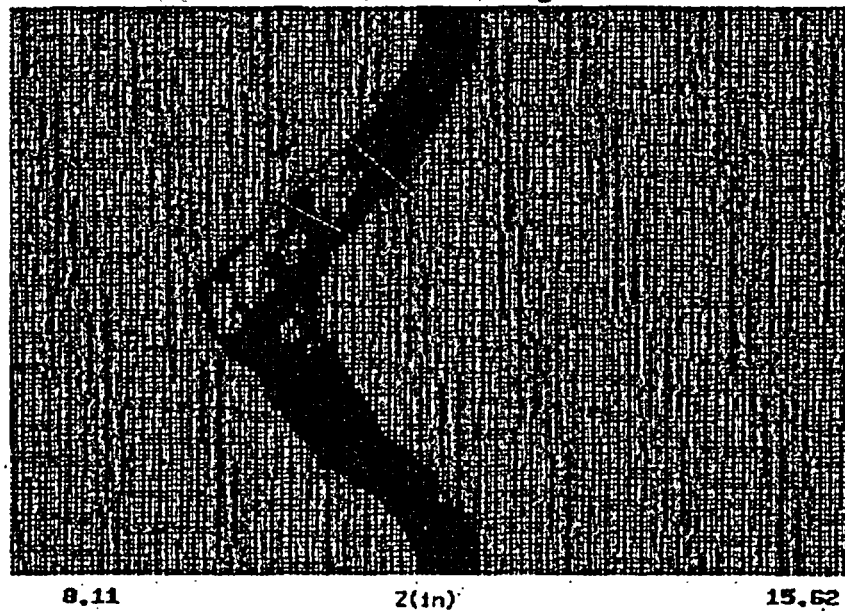


Figure 7. UT weld normal inspection results on BMI nozzle penetration #46 from STP Unit 1 and TOFD PWSCC superimposed (two lines traversing the J-groove weld).

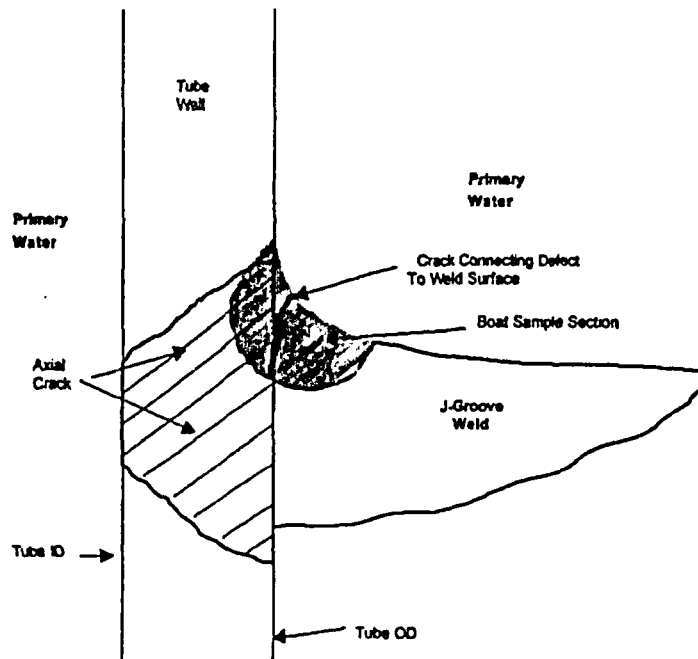


Figure 8. STP boat sample from BMI nozzle #1 showing the crack and fabrication flaw along the fusion line between the J-groove weld and the OD of the penetration tube.

NDE of REPLACEMENT HEADS

The new replacement heads have been improved through designs which reduce the number of welds in the head and the selection of less susceptible materials - Alloys 690/152/52. The heads should be designed to provide good access for VT examinations that will be conducted during service and this involves getting VT equipment onto the head and adequate annulus clearance between the head and the thermal insulation. This access has been improved. The crown of the J-groove weld and the buttering should be prepared to provide optimum inspection surfaces for NDE (at a minimum smooth and regular). It is not clear that this has been done since these surface preparations are performed manually and there are no standards that can be referenced for the surface conditions needed. Welding with weld alloy 152/52 is not easy as has been experienced by the replacement spool piece at V C Summer where it took several months and many weld repairs in order to get a weld that would pass ASME Section III Code requirements.

Because of the complex nature of PWSCC failures in Inconel, it is important to fully document all of the important fabrication processes including all repairs (drawings of all repair cavities, their location, description of flaws removed and the NDE performed to assure that an effective repair had been made) and full details of any straightening of the penetration tubes.

As the majority of the failure problems have been associated with CRDMs, the inspection of these will be the focus of this section. Construction practice is based on ASME Section III Code. This involves the application of PT of the root pass, PT every two weld passes or every 12 mm. A final PT is performed of the ground crown of the J-groove weld and buttering. This final PT is either being documented with camera pictures of every indication to form a permanent record or to work to achieve a "PT White" (no surface breaking flaws) result. Care must be exercised if the PT white condition was achieved by using weld repair and remembering the above cited work by PNNL. This work showed that all of the largest flaws in reactor pressure vessel welds were associated with repairs. The repaired weld may not have surface breaking flaws, but may contain subsurface flaws of importance to component integrity. The pre-service NDE is based on ASME Section XI Code and normally involves the use of ET of the penetration tube ID, UT of the penetration tube (2-5 MHz) using TOFD longitudinal mode and pulse echo shear mode and if there is no thermal sleeve a 0° inspection of the penetration tube.

Since fabrication flaws tend to form along the fusion zones, there is a need to detect, characterize and assess these flaws before service so that appropriate repairs can be made. Currently, only surface breaking flaws are addressed and as the events of the BMIs at STP have shown, these fabrication flaws can be important to their integrity during service. There is a need to reliably inspect the fusion zones of the J-groove welds and buttering. This should be done for all replacement heads and for all current heads that are in service. This is not an easy inspection - it is the classic far side coarse grained inspection problem. Research is needed to assess various NDE technologies for determining how effectively they can detect and characterize flaws with each of the three fusion zones of the J-groove weld and buttering.

Eddy current (ET) technology needs to be assessed for conducting effective surface examinations for the crowns of the J-groove welds and buttering. Surface condition standards need to be developed in order to insure that effective ET examinations can be conducted. This standard needs to be developed now so that ET inspections of high quality can be conducted to form a baseline for comparison with inservice inspection data.

CONCLUSIONS

There are a number of changes to replacement heads that should lead to putting a higher quality component into service. Many of these improvements were placed in service beginning with the replacement heads that the French started using in the early 1990s. Thus, there is only 10 years of service experience and since the degradation of Inconel by PWSCC has a long incubation time, it is unknown if the improvements are really long term solutions. PWSCC is a complex process and many factors affect the initiation time and the growth rate. NDE is used to assure that a high quality product is being produced and placed into service and that it is being monitored to insure that if any degradation occurs during service, it will be detected before component failure occurs.

The biggest shortcoming in the NDE being conducted during fabrication and pre-service is that the NDE program is not designed to detect fabrication flaws in the fusion zones of the J-groove welds and the buttering. Clearly this is important because of the failure that has occurred at STP. The use of PT to inspect the J-groove weld and buttering is necessary but not adequate. The other problem is that there are many important factors that may influence the initiation and growth of PWSCC but they are not being documented. In addition, standards for surface finish conditions are needed to insure that ET examination can be reliably performed. Considering the vessel heads are being replaced, it would be beneficial to examine the vessel head design to determine if they could be designed to enhance the NDE inspections. Reducing the number of the welds is a start but what else can be done to improve the J-groove weld and buttering design to improve the inspection of them? That is a challenge that is not be addressed.

REFERENCES

Amzallag, C., Boursier, J.M., Pages, C., and Gimond, C., "Stress Corrosion Life Experience of 182 and 82 Welds in French PWRs, in Proceedings Fontevraud International Symposium Number 5," September 2002.

Bamford, W. and Hall, J., "A Review of Alloy 600 Cracking in Operating Nuclear Plants: Historical Experience and Future Trends", presented at 10th International Symposium on Environmental Degradation of Materials in Nuclear Power Systems-Water Reactors, August 2003.

Buisine, D., Cattant, F., Champredonde, J., Pichon, C., Benhamou, C., Gelpi, A., and Vaindirilis, M., "Stress Corrosion Cracking in the Vessel Closure Head Penetrations of French PWRs", Sixth International Symposium on Environmental Degradation of Materials in Nuclear Power Systems-Water Reactors, 1993.

Schuster, G.J., Doctor, S.R., and Heasler, P.G., "Characterization of Flaws in U.S. Reactor Pressure Vessels", subheading 'Density and Distribution of Flaw Indications in PVRUF', prepared for U.S. Nuclear Regulatory Commission, NUREG/CR-6741, Vol. 1, PNNL-11143, published 1998.

Schuster, G.J., Doctor, S.R., Crawford, S.L. and Pardini, A.F., "Characterization of Flaws in U. S. Reactor Pressure Vessels", subheading 'Density and Distribution of Flaw Indications in the Shoreham Vessel', prepared for U.S. Nuclear Regulatory Commission, Division of Engineering Technology, NUREG/CR-6471, Vol. 3, PNNL-11143, published November 1999.

Schuster, G.J., Doctor, S.R., Crawford, S.L. and Pardini, A.F., "Characterization of Flaws in U. S. Reactor Pressure Vessels", subheading 'Validation of Flaw Density and Distribution in the Weld Metal of the PVRUF Vessel', prepared for U.S. Nuclear Regulatory Commission, NUREG/CR-6741, Vol. 2, PNNL-11143B, published August 2000.

Shah, V.N., Ware, A.G., and Porter, A.M., "Assessment of Pressurized Water Reactor Control Rod Drive Mechanism Nozzle Cracking", prepared for U.S. Nuclear Regulatory Commission, Safety Programs Division, NUREG/CR-6245, EGG-2715, published October 1994.

Supplement to "Bottom Mounted Instrumentation Indications STP Unit 1 Licensee Event Report (LER) 03-003", dated October 15, 2003, (NOC-AE-03001610)

Predicting the Occurrence of Corrosion Failures in Nuclear Power Components with Emphasis on Applications of Alloy 690

Roger W. Staehle
Adjunct Professor, University of Minnesota

Jeffrey A. Gorman
Dominion Engineering

Abstract

The importance of pro-active research to predict corrosion-related failures in nuclear power plants is emphasized in view of plants now extending their lives through license renewal and of increasing their power capacity. The probability of future failures and reasons for considering them to be highly probable are discussed. The fact that failures of some advanced designs and materials have yet to occur does not provide any certainty that such failures cannot occur in the near future. Possible failures and the need for specific pro-active research on Alloy 690TT is discussed.

Introduction

The purpose of this discussion is to emphasize the importance of pro-active prediction of performance of materials and components used in nuclear power components and uses Alloy 690TT as an example. Such predictions are now increasingly important in view of the longer life times expected of nuclear power plants through the license renewal processes that are now underway. Further, electric utilities are interested in increasing the performance of existing plants. The combination of increased life and increased performance challenge the materials and components now being used.

Achieving goals of increased life and performance requires careful attention at least for the following reasons:

1. The number of experienced professionals and the resources to support programs of prediction is greatly diminished.
2. Deregulation continues to press engineers at utilities to place production of power at the highest priority.
3. While the capacity factor of plants has increased, the occurrence and seriousness of major failures or "almost failures" has not diminished. A recent example is the Davis Besse (a PWR) incident involving the extensive corrosion at the head of the vessel and the extensive stress corrosion cracking of core shrouds (BWR).

While there is great concern about whether potential failures can be pro-actively predicted as well as concerns with the capacity to do so, the nuclear industry has achieved major progress:

1. There is effective and extensive cooperation internationally.
2. Water chemistry in plants has been improved.
3. Methods of inspection have been improved.
4. Methods of mitigation have been improved including zinc inhibition, hydrogen water treatment, improved materials, and improved designs.

This discussion first reviews some of the major failure patterns of the past. Next, obstacles to developing programs to pro-actively predict failures are identified and discussed. Then, the essence of a program to predict future failures pro-actively is described. Finally, the already existing warnings of possible problems with Alloy 690 are discussed and approaches to evaluating these failures are discussed.

Patterns of Major Failures in the Past

Extensive failures have occurred since the middle 1960s in both BWR and PWR plants:

1. BWR plants

The most significant corrosion problems in BWR plants have been related to the radiolytically induced oxidizing nature of their environments and the sensitization of stainless steel either as a furnace sensitization or weld sensitization with accompanying residual stresses. This has led to the more recent problems with shrouds.

The earliest observation of SCC in BWR applications occurred in about 1966 in a cold leg of the Dresden plant. At the time, conventional "wisdom" attributed the SCC to a "bad heat," which is the usual response to early failures—and almost always in error. This early observation was the precursor to observations of extensive SCC in small and large diameter pipes, stub tubes for control rods, and then in reactor internal components such as the shrouds. Over these years, extensive SCC occurred in both furnace and weld sensitized materials.

In response to the oxidizing/sensitizing problem, BWR technology has developed water chemistries that lower the oxidizing potential, alloys that are minimally prone to sensitizing, and mechanical design improvements that reduce the tensile stresses that cause SCC to progress.

2. PWR plants

The most significant corrosion problems in PWR plants have been related to steam generators on both the primary and secondary sides in connection with the Alloy 600MA. On the primary side, LPSCC has occurred especially at locations of high stresses at U bends, denting, and tube expansion at the tubesheet. (Note that the term "LPSCC"—low potential stress corrosion cracking is used in place of the misleading term, "PWSCC," since the latter implies that the phenomenon can occur only in primary systems; whereas "low potential" correctly describes the chemical region of SCC as does "alkaline SCC.") On the secondary side a variety of SCC processes has occurred mainly in heat transfer crevices, as they exist at tube supports and the top of the tubesheet. This array of failures by various modes and at various locations is shown in Figure 1.

The LPSCC in Alloy 600MA first occurred in SG tubes. With time, LPSCC began to occur in instrument nozzles in pressurizer and the RCS piping, in pressurizer heater sleeves, and in reactor vessel head CRDM nozzles and instrument penetrations. With the occurrence of complete perforation to the outside of the primary boundary, deposits of boric acid were observed. These actually served as good indicators of the perforations.

However, if the leak was not corrected shortly after visible accumulations of boric acid at the OD surface began to accumulate, it was possible that rapid general corrosion or wastage could occur of carbon or low alloy steel parts that were impinged by the steam from the leak. This accelerated general corrosion reached its peak in the Davis Besse incident where the entire thickness of the RPV head was corroded over an area of 20-30 in².

In response to the SCC on both primary and secondary sides, the PWR technology has improved water chemistry, improved designs, and changed materials, e.g. from Alloy 600MA to Alloy 690TT.

Thus, in both BWR and PWR technologies, the failures occurred more frequently and in more components as time progressed until very serious failures occurred. In no case were the more serious failures "surprises"—they were predictable based on previous research and occurrences of early failures in the industry.

Problems in Pro-Active Prediction

Probably the biggest deterrent to pro-active research directed toward predicting failures is the inclination that such work is not necessary because "it has not been observed in the field." On the contrary, there are many social aphorisms in common knowledge that such a position is erroneous, e.g. "closing the barn door after the horses are out." Nonetheless, the resistance to pro-active work persists. Other deterrents to proactive predictive research include:

1. Alloy 690TT resists LPSCC and is therefore considered resistant to all SCC. (However, in fact, Alloy 690TT has exhibited extensive SCC in laboratory tests using aggressive caustic and mildly acidic environments.)
2. Early failures result from "bad heats." (In virtually all cases, such early failures have been shown to be the early failures in statistical distributions.)
3. Very pure water maximizes corrosion resistance on the secondary side of SGs. (However, the presence of very pure water could possibly dissolve compounds that immobilize lead and low valence sulfur, thus making local environments more aggressive.)
4. Leak before break is a reliable assumption. (There are important exceptions, including the Duane Arnold safe end event where SCC had progressed around the full circumference of the safe end, raising the possibility of a guillotine break.)
5. If experiments were conducted properly, they would all produce the same results. (Not correct. There is high inherent variability in corrosion.)

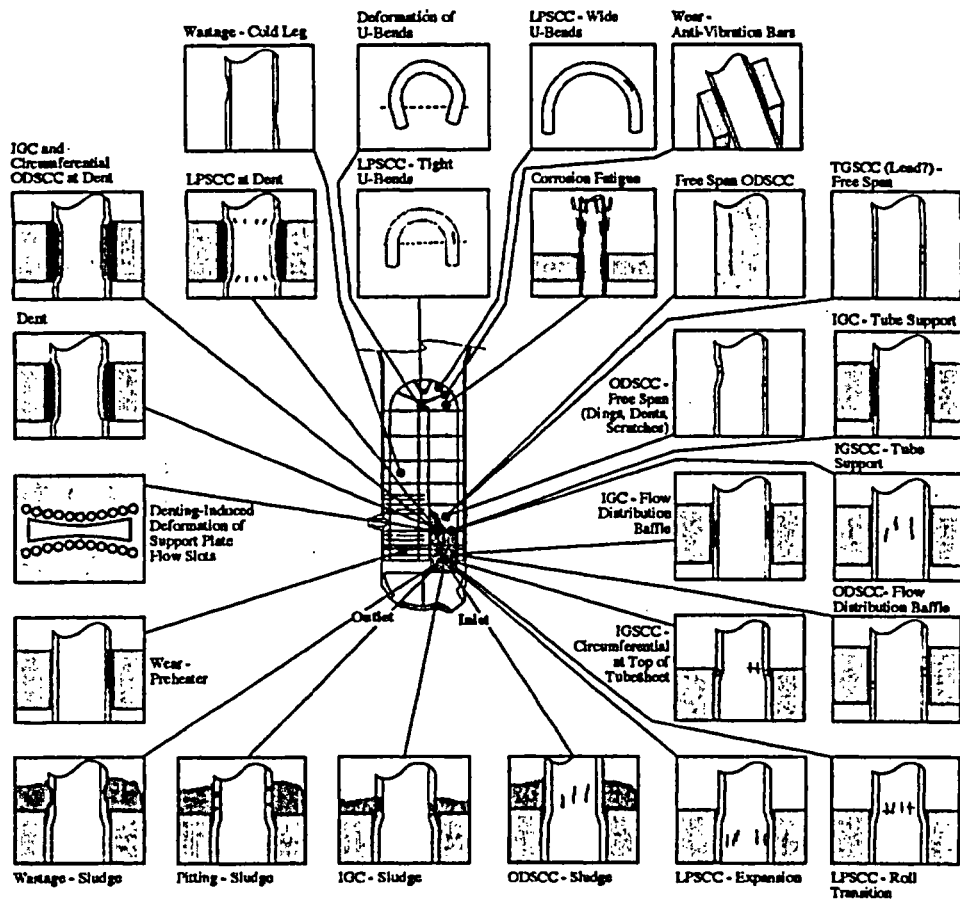


Figure 1 Array of modes of corrosion and locations where failures have occurred in PWR steam generators using Alloy 600MA. From Staehle and Gorman.¹

The claim that “it has not been observed in the field” does not recognize that some failures have required long times before they have been observed:

1. The LPSCC in CRDMs required a mean time of about 20 years before occurring.
2. The SCC in the upper bundle of OTSGs required about 15 years before being significant as shown in Figure 2.
3. The SCC at Duane Arnold required about 10 years.
4. Flow assisted corrosion requires 10 to 20 years to become significant.
5. The SCC of bolting, such as 17-4PH and X750 has often required 10 to 20 years.
6. SCC of girth welds in SGs required 10 to 15 years.

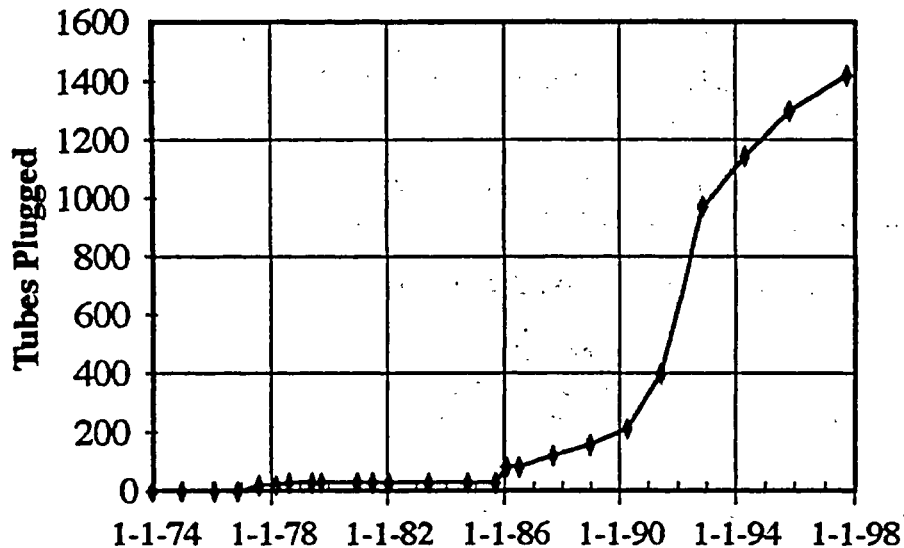


Figure 2 Tubes plugged in upper bundle of steam generator vs. time for Oconee-1B. As presented in Staehle and Gorman¹; Original from Rochester and Eaker.²

These long times for the occurrence of corrosion failures result from many different influences such as:

1. The rate of initiation (increase in depth per unit time) for SCC is in the range of 100 times slower than the propagation phase.
2. Deposits on surfaces that are necessary to produce corrosion require significant times to accumulate and to produce chemistries that are aggressive, especially as the water in the plant systems becomes more pure.
3. Accumulation of the number of stress cycles, which are required to cause initiation requires long times especially for the low cyclic frequencies that are the most aggressive.
4. Changes in the local metallurgy of metal surfaces, such as alloy enrichment/depletion, require long times.

The failures that have occurred have never been “unannounced.” They have not been real surprises. Examples of warnings that could and should have been heeded include the following:

1. LPSCC was first identified and published by Coriou of CEA in 1959.
2. PbSCC was first identified in a paper by Copson and Dean in 1965.
3. Effects of reduced sulfur species on the SCC of Fe-Cr-Ni alloys had been studied extensively since the 1950s.
4. The intergranular corrosion of Fe-Cr-Ni alloys in oxidizing environments had been studied extensively since the 1950s.

5. Processes involved in denting had been studied by Pickering and Fontana of The Ohio State University in 1959.
6. Bases for the concentration of chemicals in heat transfer crevices of PWR SGs were clearly identified by Lindsay of Westinghouse in 1968.

General Characteristics of Pro-Active Prediction

The general approach to pro-active prediction has been described by Staehle³ in terms of the "corrosion based design approach (CBDA)" combined with the "locations for analysis approach." These combined approaches provide an organized stepwise approach to predicting corrosion failures.

The significant steps in the CBDA are the following:

1. Environmental definition—Includes local chemical species and concentrations, stresses, thermal, radiation, and flow. The local chemical conditions on the surfaces are the most important.
2. Materials definition—Includes grain boundary composition, cold work, anisotropy, surface treatments, alloy composition, impurities, second phases and their distribution.
3. Mode definition—Includes the modes and submodes of corrosion and their dependencies on the seven primary variables of pH, potential, species, alloy composition, alloy structure, temperature, and stress.
4. Superposition—Includes the intersection of steps 1-3 to assess possible occurrences of accelerated corrosion.
5. Failure definition—Includes the conditions or circumstances that define when failure occurs and what constitutes failure. The incentive for developing a statistically based description of failure is illustrated by Figure 3 from the work of Scott where the fraction of failures from sequentially prepared heats is shown to be highly variable for both primary and secondary sides.
6. Statistical definition—Includes the statistical definition of the environments, modes, and materials.
7. Accelerated testing—Includes testing that uses stressors such as stress, temperature, pH, potential, and metallurgical conditions in testing to estimate the performance under design conditions.
8. Prediction—Includes steps 1 through 7 to predict the probability of failure as a function of time in operation.
9. Feedback—includes results from monitoring and inspection to identify unexpected failures.
10. Fix—responds to the combination of feedback and prediction to mitigate failures through changes in design, water chemistry, materials, and/or operations.

In addition to the rigorous implementation of these steps, pro-active prediction considers warnings that have already been observed in the data from laboratories and operating plants.

Example of Alloy 690 for predicting failure

Warnings for the possible failures of Alloy 690TT in some circumstances of field applications are implicit in the past patterns of warnings relative to subsequent failures that these other warnings predicted. Alloy 690TT has already exhibited failures in the laboratories in circumstances that can occur in the field. Such warnings make it clear that lack of a well-defined program of prediction of the behavior of Alloy 690TT is unwise.

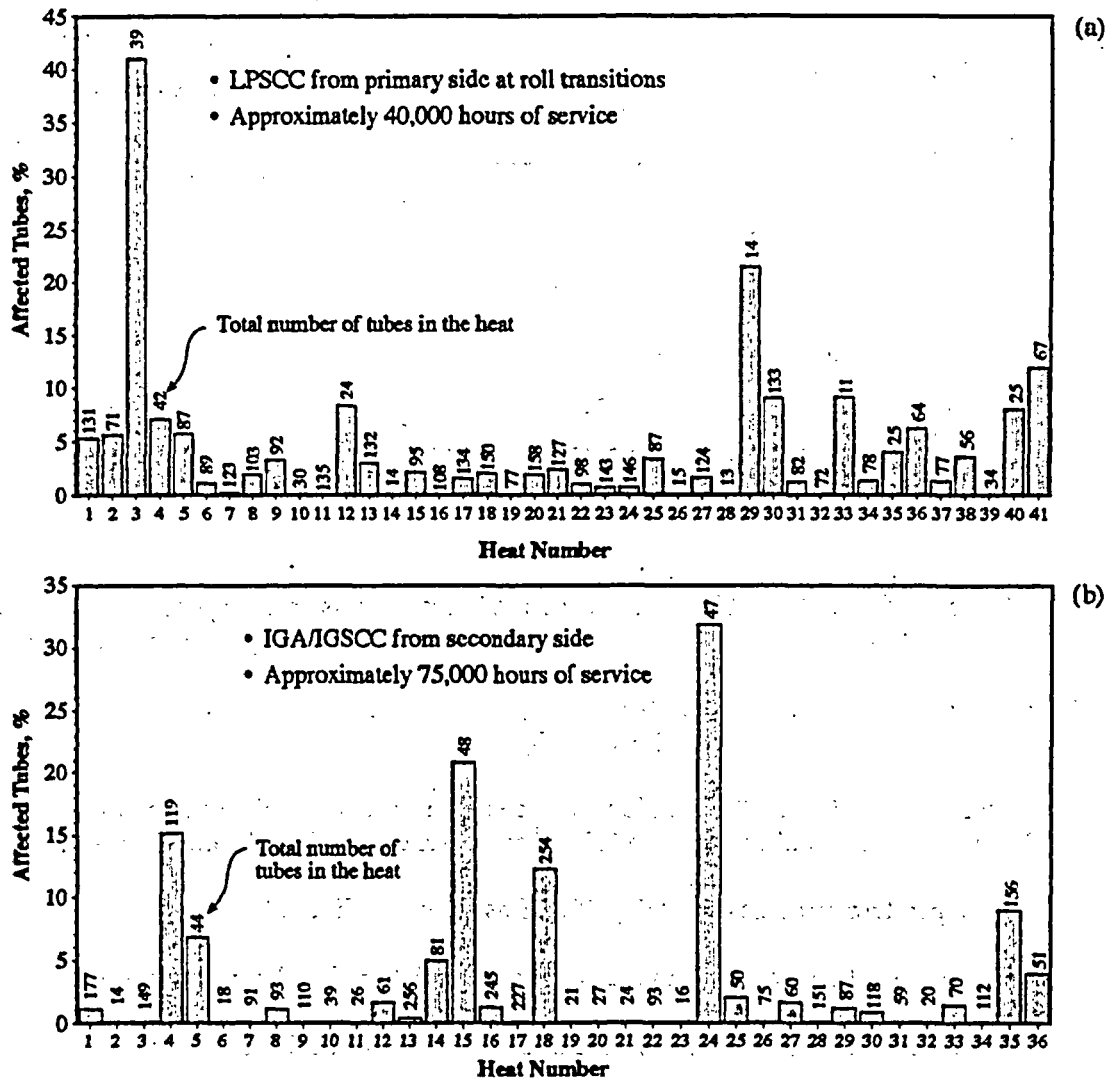


Figure 3 Affected tubes vs. heat number for heats that were manufactured by the same manufacturer for sequential times. Numbers at the top of each bar indicate number of tubes in each heat. (a) Primary side LPSCC. (b) Secondary side IGA/IGSCC. From Scott⁴ as modified by Staehle and Gorman¹.

Specific laboratory data that indicate the potential failure of Alloy 690TT are the following:

1. SCC at low concentrations of Pb in strongly alkaline conditions at operating temperatures and low stresses as shown in Figure 4.
2. SCC and corrosion scaling at mildly acidic chloride conditions at 340°C as shown in Figure 5.

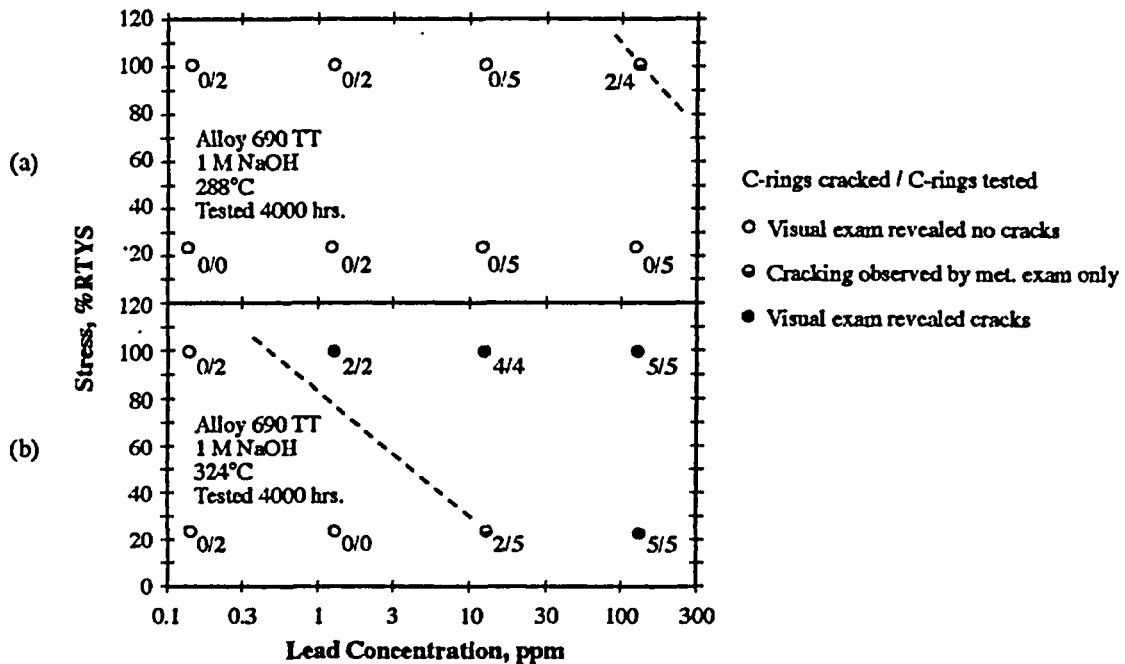


Figure 4 SCC of Alloy 690TT as a function of lead, stress and temperature exposed to 1 M NaOH for 4000 hours. From Sarver⁵ as modified by Staehle and Gorman¹.

3. SCC in the range of low potentials for Alloy 800 and scaling at high potentials of Alloy 690TT in alkaline solutions as shown in Figure 6.
4. SCC of Alloys 690 and 690TT in low valence sulfur in strongly alkaline solutions as shown by Briceno and Castano⁸ and King⁹ as referenced by Staehle and Gorman¹.
5. Low temperature brittleness of Alloy 690TT as shown in Figure 7.
6. Intensive SCC of Alloy 690TT in the steam phase of strongly alkaline bulk solution.
7. There are unpublished data for the SCC of 690TT in neutral solutions.
8. The use of hydrazine on the secondary side produces low valence sulfur from sulfates. Such low valence sulfur would be aggressive to Alloy 690TT.

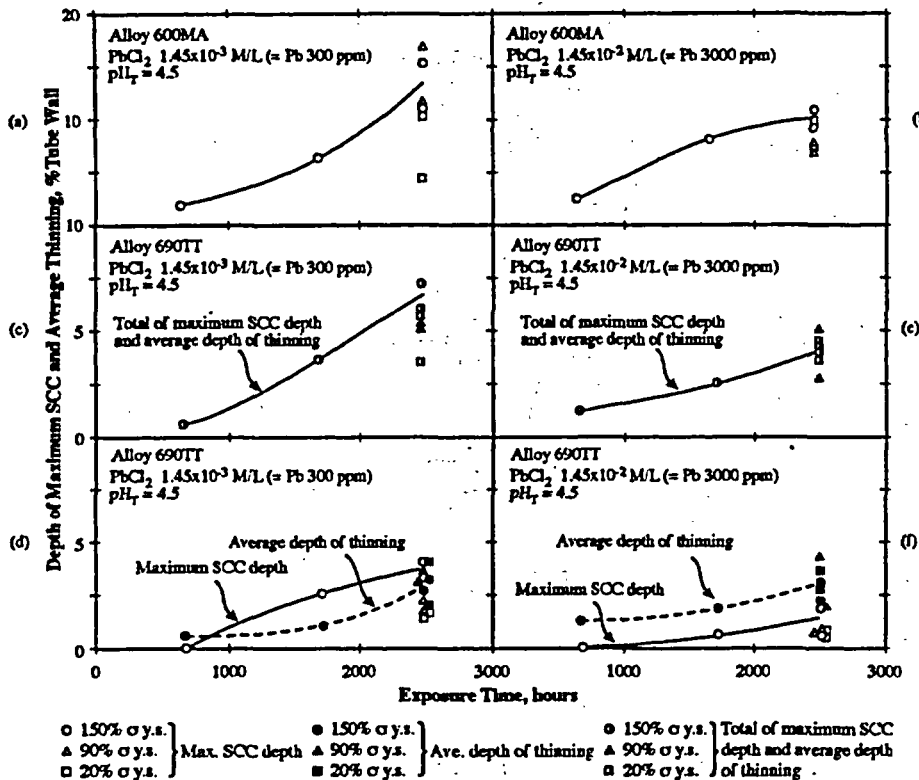


Figure 5 SCC of Alloy 600MA and Alloy 690TT in chloride solutions at 340°C. From Sakai et al.⁶ as modified by Staehle and Gorman¹.

Work that should be undertaken to assess the future behavior of Alloy 690TT includes at least the following:

1. Develop a model boiler program for studying the corrosion of Alloy 690TT in lead and sulfur environments separately and together.
2. Assess the properties of crevices formed by deposits in line-contact crevices on the secondary side.
3. Determine the dependencies for Alloy 690TT in lead and sulfur environments in terms of pH, potential, species, alloy composition, alloy structure, temperature and stress.

Conclusions

1. A pro-active approach for predicting failure is necessary as plants age and as they are pressed to increase performance. In view of the periodic occurrence of serious failures over time, there is no basis for assuming the absence of similar unexpected events in the future. A safety net is required in case failures are observed.

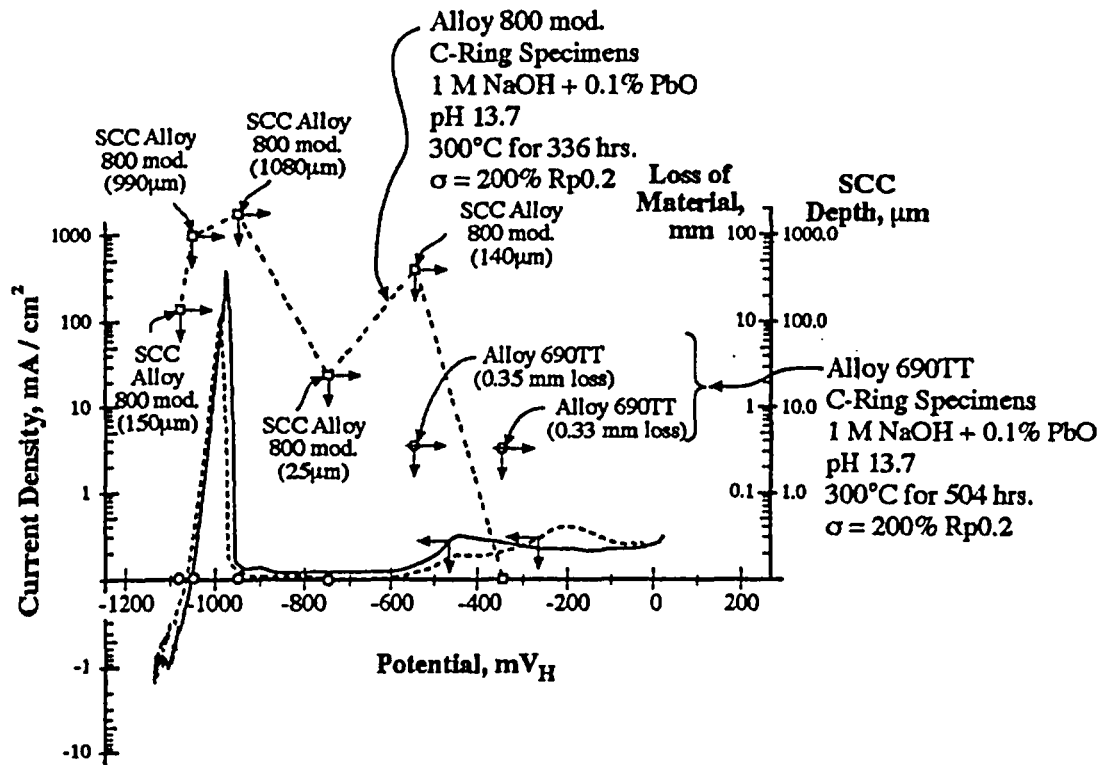


Figure 6 Current density and corrosion vs. potential for Alloys 800 and 690TT exposed in 1 M NaOH + 0.1%PbO and stressed. From Kilian⁷ as modified by Staehle and Gorman¹.

2. Past research has been mostly re-active. Taking a pro-active approach is necessary to provide margins for safe operation.
3. The absence of early service failures in modern plants does not imply lack of degradation; history based on relevant laboratory research indicates that failures eventually occur.
4. Most of the warnings that have developed from laboratory work have subsequently occurred in the field.
5. Economic pressures especially mitigate against pro-active research, and such pressures engender numerous rationalizations to justify avoiding predictive work; such rationalizations are generally incorrect and are evidence of bad judgment.
6. With time, the number of experienced professionals at utilities, vendors, EPRI, national and university laboratories, other international programs and NRC and the resources for their support are decreasing. With such continuous decreases in capacity, it is inevitable that the subtle events that lead to serious problems can be missed.
7. Numerous physical processes cause degradation to be slow and cause failures to occur later rather than earlier. Extensive evidence, even now, indicates that some failures do not occur until times of 10-20 years.

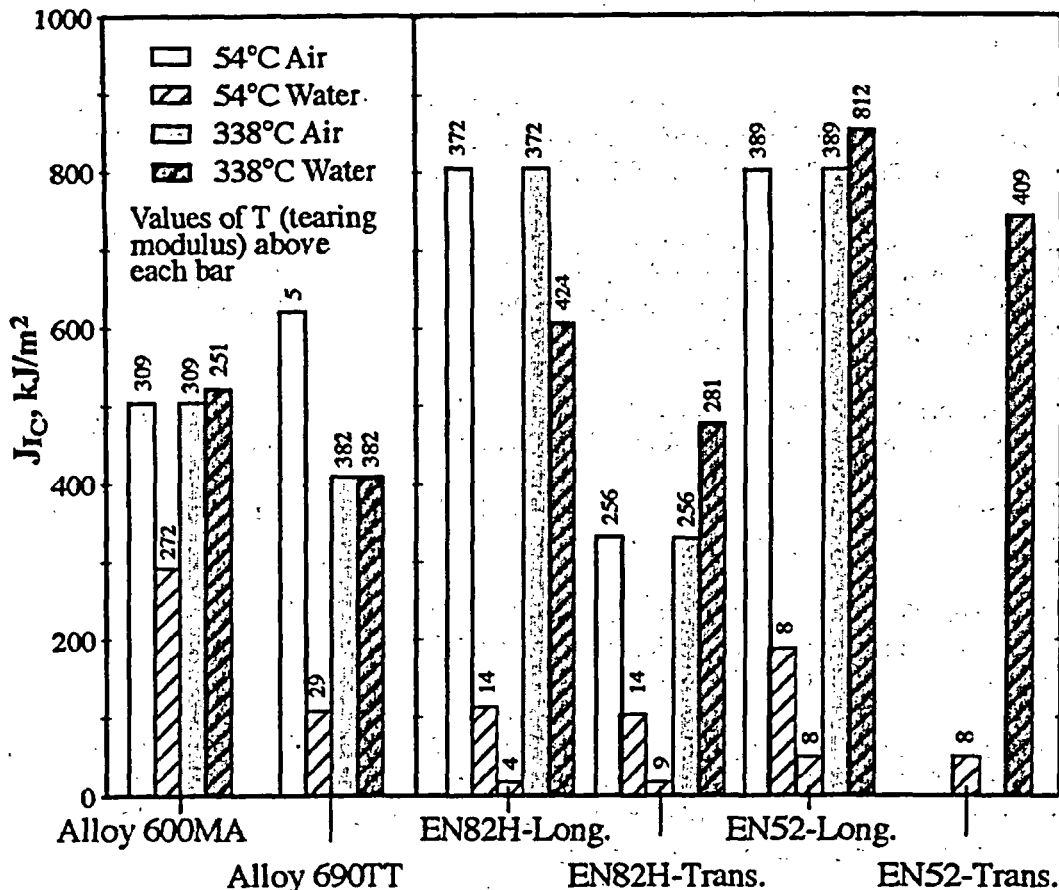


Figure 7 J_{IC} results for Ni base wrought and weld alloys exposed in pH 10.1 to 10.3 at low and high temperatures in water and air. From Mills¹⁰ as modified by Staehle and Gorman.¹

8. Pro-active prediction of failures can be confidently pursued by using collaborative and interdisciplinary interactions to organize hypotheses and to organize and conduct experiments and analyses. Such a program can be expected to provide useful predictions of expected failures.
9. There is a rigorous method to prediction in the corrosion based design approach (CBDA).
10. There are sufficient data already to indicate that Alloy 690TT can fail in service. Work to evaluate and refine the implications of the present data needs to be undertaken in order to assess the conditions under which such failures can occur.

Acknowledgements

We appreciate the invitation from Drs. Muscara and Cullen to participate in this conference as well as their comments on this paper.

We appreciate also the RWS staff for their energetic and professional contributions including Julie L. Daugherty, Erin Kate Rediger, Mary Elizabeth Ilg, and John Ilg.

References

1. R.W. Staehle & J.A. Gorman, "Quantitative Assessment of Submodes of Stress Corrosion Cracking on the Secondary Side of Steam Generator Tubing in Pressurized Water Reactors," *Corrosion* 59, 2003, *Corrosion* 60, 2004, NACE, Houston, TX.
2. D.P. Rochester & R.W. Eaker, "Laboratory Examination Results from Oconee Nuclear Station Once-Through Steam Generator Tubes," Proc. 9th Int. Conf. On Environmental Degradation of Materials in Nuclear Power Systems – Water Reactors, eds. S.M. Bruemmer, F.P. Ford, G.S. Was, TMS, Warrendale, PA, 1999.
3. R.W. Staehle, "Lifetime Prediction of Materials in Environments," Uhlig's Corrosion Handbook, 2nd edition, Ed. R.W. Revie, John Wiley & Sons, New York, NY, 2000.
4. P.M. Scott, "Stress Corrosion Cracking in Pressurized Water Reactors – Interpretation, Modeling, and Remedies," *Corrosion* 56, 2000.
5. J.M. Sarver, "IGSCC of Nickel Alloys in Lead-Contaminated High-Purity Water," EPRI Workshop on Intergranular Corrosion and Primary Water Stress Corrosion Cracking Mechanisms, NP-5971, EPRI, Palo Alto, CA, 1987.
6. T. Sakai, T. Senjuh, K. Aoki, T. Shigemitsu, & Y. Kishi, "Lead-Induced Stress Corrosion Cracking of Alloy 600 and 690 in High-Temperature Water," Proc. 5th Int. Symp. on Environmental Degradation of Materials in Nuclear Power Systems – Water Reactors, American Nuclear Society, LaGrange Park, IL, 1992.
7. R. Kilian, "Influence of Lead on the SCC Behavior of SG Tubing Materials," IAEA Specialists Meeting on Steam Generator Problems and Replacement, International Atomic Energy Agency, Madrid, Spain, 1993.
8. D.G. Briceno & L. Castano, "Inconel 690TT and Incoloy 800 in S, Cu and Pb Environments," EPRI Workshop on Steam Generator Secondary Side IGA/SCC, Reston, VA, 1991.
9. Courtesy of P. King, Babcock and Wilcox, Alliance, OH, September, 2001. Private communication.
10. W.J. Mills, C.M. Brown, & M.G. Burke, "Fracture Behavior of Alloy 600, Alloy 690, EN82H Welds, and EN52 Welds in Water," EPRI 2000 Workshop on PWSCC of Alloy 600 in PWRs, EPRI, Palo Alto, CA, February 14-16, 2000.

Anticipating materials problems; field experience and laboratory studies

W. J. Shack, O. K. Chopra, and H. M. Chung

Argonne National Laboratory

Argonne, IL 60439

This paper reviews some aspects of ongoing USNRC Office of Nuclear Regulatory Research sponsored work on materials degradation at Argonne National Laboratory. Three topics will be presented. The first is concerned with environmental effects on fatigue life of reactor pressure boundary materials such as austenitic stainless steels and carbon and low-alloy steels, and the potential implication of the results for the fatigue design rules of the ASME Boiler and Pressure Vessel Code. The second topic relates to some aspects of the probabilistic model that is being developed to describe the cracking of control rod drive mechanism (CRDM) nozzles. In particular the use of Bayesian updating to reduce some of the uncertainties associated with the prediction of CRDM cracking in individual plants or in groups of plants from the same fabricator or material supplier is considered. The third topic relates to studies on irradiation assisted stress corrosion cracking and some of the open issues that can affect understanding and management of irradiation assisted stress corrosion cracking (IASCC).

Environmental effects on fatigue life

Fatigue strain life (ϵ - N) data developed in laboratories in Japan and the US demonstrate that under some conditions there can be significant effects of LWR coolant environments on the fatigue life of reactor coolant system structural materials.²⁻¹² The degree of degradation in fatigue life depends on the values of a number of critical parameters: strain amplitude and rate, temperature and dissolved oxygen, and flow rates and sulfur content for carbon and low alloy steels. The conditions that produce significant environmental enhancement are reasonably well defined in laboratory situations. However, evaluating the corresponding conditions in the field for some of the parameters such as strain rate can be challenging.

The ASME Code fatigue design curves, given in Appendix I of Section III, are based on strain-controlled tests of small polished specimens at room temperature in air. The design curves have been developed from fits of the experimental ϵ - N data expressed in terms of the Langer equation¹³

$$\epsilon_a = A_1(N)^{-n_1} + A_2, \quad (1)$$

where ϵ_a is the applied strain amplitude, N is the fatigue life, and A_1 , A_2 , and n_1 are coefficients determined by the curve-fit. Equation 1 may be written in terms of stress amplitude S_a instead of ϵ_a . The stress amplitude is the product of ϵ_a and elastic modulus E , i.e., $S_a = E \cdot \epsilon_a$. The Code fatigue design curves are obtained from the best-fit curves to the experimental data by first adjusting for the effects of mean stress on fatigue life, and then reducing the fatigue life at each point on the adjusted curve by a factor of 2 on strain (or stress) or 20 on cycles, whichever is more conservative.

As discussed in the Section III criteria document,¹⁴ the factors of 2 and 20 were intended to account for data scatter (including material variability) and differences in surface condition and size between the test specimens and actual components. The factors are not safety margins but rather adjustment factors that must be applied to the small specimen data to obtain reasonable estimates of the lives of actual reactor components. Although the Section III criteria document¹⁴ states that these factors were intended to cover such effects as environment, Cooper,¹⁵ in his comments regarding the initial scope and intent of the Section III fatigue design procedures, states that the term "atmosphere" was intended to reflect the effects of an industrial atmosphere in comparison with an air-conditioned laboratory not a reactor coolant environment. Subsection NB-3121 of Section III of the Code explicitly notes that the data used to develop the fatigue design curves did not include tests in the presence of corrosive environments that might accelerate fatigue failure. Article B-2131 in Appendix B to Section III states that the owner's design specifications should provide information about any reduction to fatigue design curves that is necessitated by environmental conditions.

Recent work on fatigue at Argonne National Laboratory has focused on reassessment of the margins in the ASME code curves.¹ This work tries to address the question of whether there some "spare" conservatism in the current Code margins that can be used to account for environmental effects.

Effect of Surface Roughness

Fatigue tests have been conducted to establish the effects of surface finish on the fatigue life of austenitic SSs and carbon and low-alloy steels in LWR environments. Tests were conducted on Types 304 and 316NG SS, A106-Gr B carbon steel, and A533-Gr B low-alloy steel; the chemical composition and heat treatments of the steels are given in Table 1.

Table 1. Chemical composition (wt.%) of austenitic and ferritic steels for fatigue tests

Material	Source	C	P	S	Si	Cr	Ni	Mn	Mo
<u>Carbon Steel</u>									
A106-Gr B ^a	ANL	0.290	0.013	0.015	0.25	0.19	0.09	0.88	0.05
	Supplier	0.290	0.016	0.015	0.24	-	-	0.93	-
<u>Low-Alloy Steel</u>									
A533-Gr B ^b	ANL	0.220	0.010	0.012	0.19	0.18	0.51	1.30	0.48
	Supplier	0.200	0.014	0.016	0.17	0.19	0.50	1.28	0.47
<u>Austenitic Stainless Steel</u>									
Type 304 ^c	Supplier	0.060	0.019	0.007	0.42	18.99	8.00	1.54	0.44
Type 316NG ^d	Supplier	0.015	0.020	0.010	0.42	16.42	10.95	1.63	2.14

^a 508-mm O.D. schedule 140 pipe fabricated by Cameron Iron Works, Heat J-7201. Actual heat treatment not known.

^b 162-mm thick hot-pressed plate from Midland reactor lower head. Austenitized at 871-899°C for 5.5 h and brine quenched; then tempered at 649-663°C for 5.5 h and brine quenched. The plate was machined to a final thickness of 127 mm. The inside surface was inlaid with 4.8-mm weld cladding and stress relieved at 607°C for 23.8 h.

^c 76 x 25 mm bar stock, Heat 30956. Solution annealed at 1050°C for 0.5 h.

^d 25-mm-thick plate, Heat P91576. Solution annealed at 1050°C for 0.5 h.

The gauge length of all specimens was given a 1- μ m surface finish in the axial direction to prevent circumferential scratches that might act as sites for crack initiation. Some specimens were intentionally roughened under controlled conditions, in a lathe, with 50-grit sandpaper to produce circumferential scratches. The average surface roughness (R_a) was 1.2 μ m, and the RMS value of surface roughness (R_q) was 1.6 μ m (61.5 micro-inch).

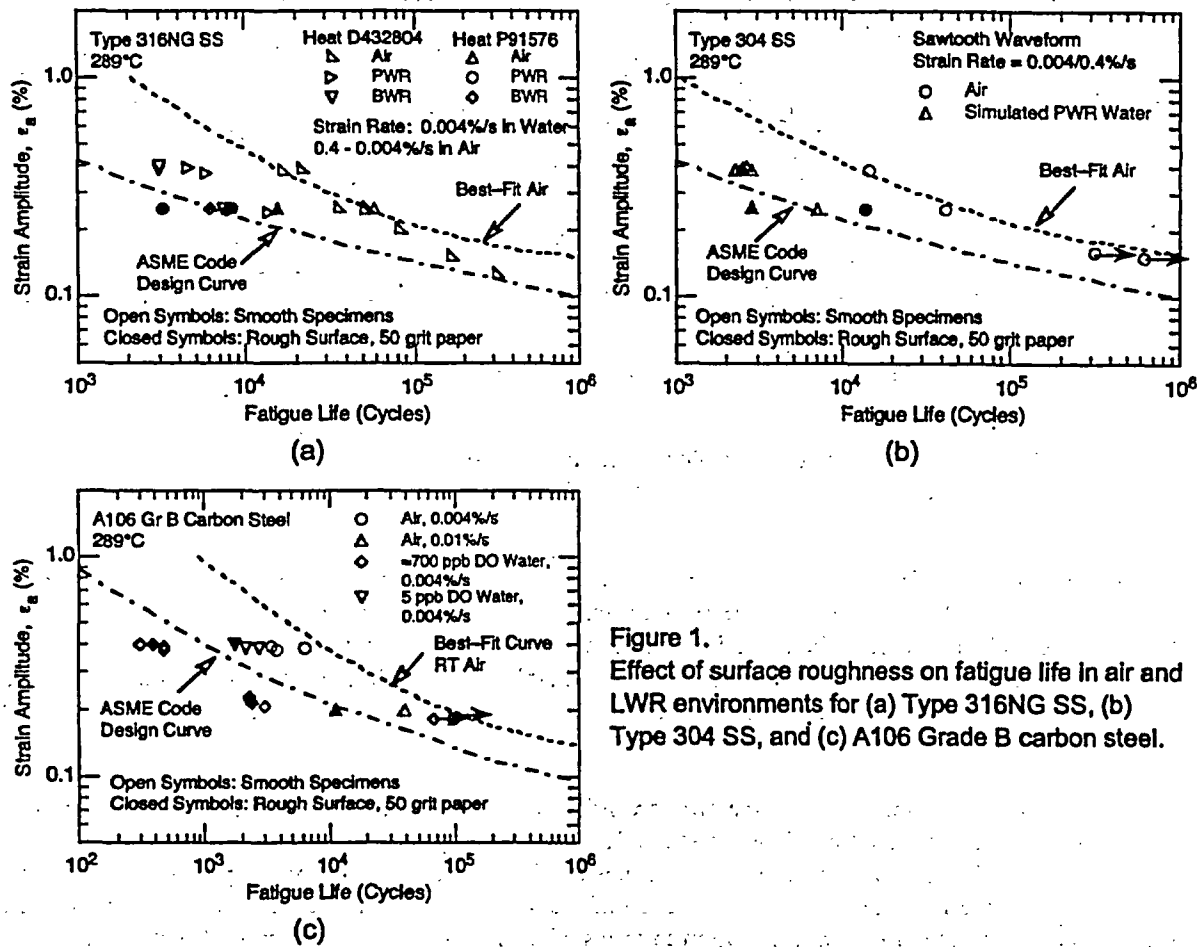


Figure 1. Effect of surface roughness on fatigue life in air and LWR environments for (a) Type 316NG SS, (b) Type 304 SS, and (c) A106 Grade B carbon steel.

The results of the tests are shown in Fig. 1. For both Types 316NG and 304 SS the fatigue life of roughened specimens is lower than that of the smooth specimens in air and low dissolved oxygen (DO) water environments. In high DO water, the fatigue life is the same for rough and smooth specimens. For Type 304 SS, fatigue life of rough specimen is factor of 3 lower than that of smooth specimen both in air and low DO water.

The fatigue life of roughened A106-Gr B specimens is a factor of 3 lower in air, but in high DO water it is the same as that of smooth specimens. In low DO water, the fatigue life of the roughened A106-Gr B specimen is slightly lower than that of smooth specimens.

Effect of Material Variability & Data Scatter

The effects of material variability and data scatter must be included to ensure that the design curves not only describe the available test data well, but also adequately describe the fatigue lives of the much larger number of heats of material that are found in the field.

The effect of material variability and data scatter has been determined by considering the results from tests on individual heats of materials or loading conditions as samples of the much larger population of heats of materials and service conditions of interest. The fatigue behavior of each heat or loading

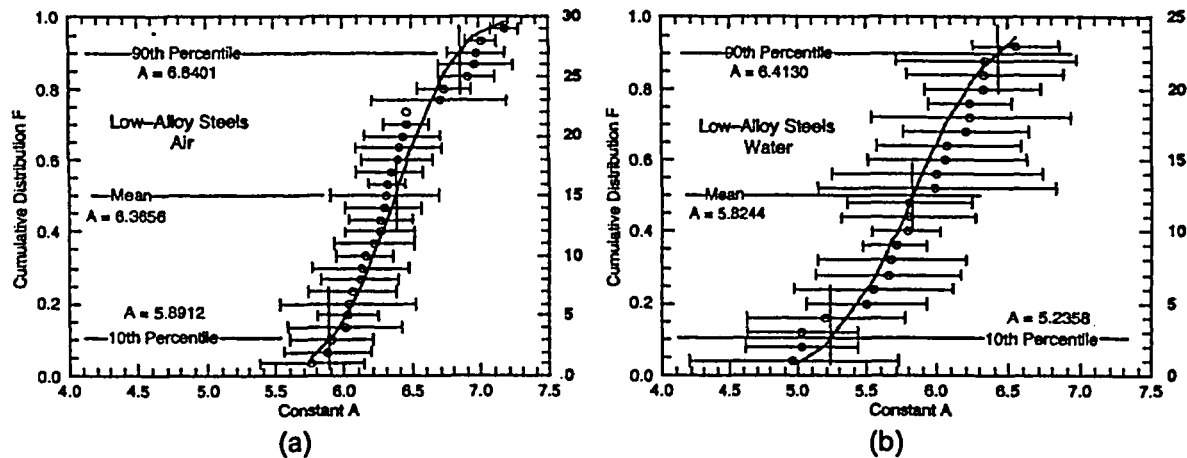


Figure 2. Estimated cumulative distribution of the parameter A in the statistical models for fatigue life for heats of low-alloy steels in (a) air and (b) water environments.

conditions is characterized in terms of a statistical model that includes the effect of strain rate, oxygen, and temperature and by the value of the constant term in the model, denoted as A.^{16,17} The values of A for the various data sets are ordered, and median ranks are used to estimate the cumulative distribution of A for the population. This distribution can be fit reasonably well by a lognormal distribution. Results for low-alloy steels in air and water environments are shown in Fig. 2. The error bars in Fig. 2 denoted the uncertainty in the value of A for a specific heat.

The values of A that describe the 5th percentile of these distributions give fatigue ϵ -N curves that are expected to bound the fatigue lives of 95% of the heats of the specific steel. There are two sources of error in the distributions shown in Fig. 2. The mean and standard deviation of the population have to be estimated from the mean and standard deviation of the sample. Confidence bounds can be obtained on the population mean and standard deviation in terms of the sample mean and standard deviation.¹⁸ Even this, however, does not fully address the uncertainty in the distribution, because of the large uncertainties in the values of A for individual heats themselves as indicated by the error bars in Fig. 2.

Monte Carlo analysis was used to address both sources of uncertainty. The results of the Monte Carlo analysis are values for A that provide bounds for the portion of the population and the confidence that is desired in the estimates of the bounds. For low-alloy steels, the 5th percentile value of parameter A at a 75% confidence level, is 5.6 in air and 4.7 in LWR environments. The mean value of A for the sample is 6.4 and 5.8, respectively, in the two environments. Thus, for low-alloy steels, the 95/75 value of the margin to account for material variability and data scatter is 2.1 and 3.1 on life in air and water environments, respectively. The corresponding margins in air and water environments for carbon steels, and SSs are 2.3 and 2.9 and 2.5 and 3.5, respectively. Thus, average values of 2 and 3 on life in air and water environments, respectively, may be used to account for uncertainties due to material variability and data scatter. These margins are needed to provide reasonable confidence that the resulting life will be greater than that observed for 95% of the materials of interest.

Other Factors

The effect of specimen size on the fatigue life has been investigated for smooth specimens of various diameters in the range of 2–60 mm.¹⁹ The results indicate that the number of cycles to form a 3-mm-deep crack in a 19-mm-thick shell may be 30–50% lower than those in a small test specimen. Thus, a factor of ≈ 1.4 on cycles and a factor of ≈ 1.25 on strain can be used to account for size and geometry.

The effects of variable amplitude loading of smooth specimens are well known.^{20, 21} The presence of a few cycles at high strain amplitude in a loading sequence causes the fatigue life at smaller strain amplitude to be significantly lower than that at constant amplitude loading. In general, the mean fatigue ϵ - N curves are lowered to account for damaging cycles that occur below the constant-amplitude fatigue limit of the material. A factor of 1.5–2.5 on cycles and 1.3–1.6 on strain may be used to incorporate the effects of load histories on fatigue life.

Fatigue Design Curve Margins

The subfactors that are needed to account for the effects of various material, loading, and environmental, variables on fatigue life are summarized in Table 2. As shown by the "total adjustment," a factor of at least 12.5 on cycles with respect to the mean ϵ - N curve for laboratory test specimens in air is needed to account for the effects of data scatter, material variability, component size, surface finish, and loading history. In LWR environments, a factor of at least 19 on cycles with respect to the mean ϵ - N curve for laboratory test specimens is needed for austenitic SSs and at least 10 on cycles for carbon and low-alloy steels.

The factors on strain are needed primarily to account for the variation in the fatigue limit of the material caused by material variability, component size and surface finish, and load history. Because these variables affect life through their influence on the growth of short cracks ($<100 \mu\text{m}$), the adjustment on strain to account for such variations is typically not cumulative but is controlled by the variable that has the largest effect on life. Thus, in relating the fatigue lives of laboratory test specimens to those of actual reactor components, a factor of ≈ 1.7 on strain with respect to the mean ϵ - N curve for laboratory test specimens is needed to account for the uncertainties associated with material variability, component size, surface finish, and load history.

These results suggest that the current ASME Code requirements of a factor of 2 on stress and 20 on cycle to account for differences and uncertainties in fatigue life that are associated with material and

Table 2. Factors on cycles and strain or stress to be applied to mean ϵ - N curve

Parameter	Factor on Life (Air)		Factor on Life (Water)	
	SS	CS/LAS	SS	CS/LAS
Material Variability & Experimental Scatter	2.0	3.0	3.0	3.0
Size Effect	1.4	1.4	1.4	1.4
Surface Finish	3.0	3.0	1.6	1.6
Loading History	1.5–2.5	1.5–2.5	1.5–2.5	1.5–2.5
Total Adjustment:	12.5–21.0	19.0–31.0	10.0–17.0	1.6–1.7

loading conditions are quite reasonable and do not contain excess conservatism that can be assumed to account for the effects of LWR environments. They provide appropriate design margins for the development of design curves from mean data curves for small specimens in LWR environments.

Models for Cracking of CRDM Nozzles

The industry and the USNRC have developed probabilistic models to describe cracking and failure of CRDM nozzles. In these models, the initiation of leaks and cracks are described in terms of Weibull statistics. The Weibull parameters are determined from laboratory and field experience with SCC steam generator tubing (the Weibull slope) and empirical fitting of inspection and failure data for CRDM nozzles. (the Weibull scale factor).

Once a crack has initiated the growth of the crack is described by linear elastic fracture mechanics. Until a crack becomes large ($> 180^\circ$), the stress intensity K , which drives circumferential crack growth, is dominated by the residual stresses due to welding, and the axial load on the nozzle due to the pressure load is relatively unimportant. Solutions for K have been developed by Engineering Mechanics Corporation of Columbus (EMC²) under USNRC sponsorship. Data on the CGR of Alloy 600 materials relevant to CRDM nozzles (i.e. not SG tubes) have been collected and analyzed.²² This data represents a substantial database, although there is, for example, significant uncertainty in the dependence of the crack growth rate on K for $K < 20 \text{ Mpa}\cdot\text{m}^{1/2}$.

The largest uncertainties in the models are associated with the initiation parameters and the correlation of the initiation parameters with the crack growth rates.^a The most substantial changes in the models are likely to arise due to changes in these parameters due to additional information from ongoing inspection programs. It is also apparent from inspection data that there are significant differences in susceptibility between vessel heads from different fabricators.^b

A generic distribution for the Weibull scale factor for initiation has been determined by maximizing the likelihood of the observed numbers of leaking nozzles for the whole fleet of plants for which reliable inspection data are available.^a The resulting distribution is shown in Fig. 3 along with an estimate of the uncertainty in the distributions due to the broad nature of the maximum of the likelihood function.

With these distributions of the Weibull scale factor, the resulting distributions of the probability of failure for a vessel head can be calculated. Some typical results are presented in Figs. 4a and b. The distributions for the probability of failure shown in Figs. 4a and b can be interpreted as describing the range of behavior expected in the whole population of nozzles or heads or as the uncertainty in the prediction of the failure of a specific nozzle or head assuming that we know only its operating temperature and the number of years of operation. The results are believed to be conservative — e.g., the true 95th percentile of probability of failure is lower than the estimates presented here.

^a W. J. Shack, "Parametric Studies of the Probability of Failure of CRDM Nozzles." in *Proceedings of the Vessel Penetration Inspection, Crack Growth and Repair Conference*, Gaithersburg MD, Sept 29-Oct 2003, to appear.

^b G. White, N. Nordmann, L. Mathews, and C. King, "Summary of U.S. PWR Reactor Vessel Head Nozzle Inspection Results" in *Proceedings of the Vessel Penetration Inspection, Crack Growth and Repair Conference*, Gaithersburg MD, Sept 29-Oct 2003, to appear.

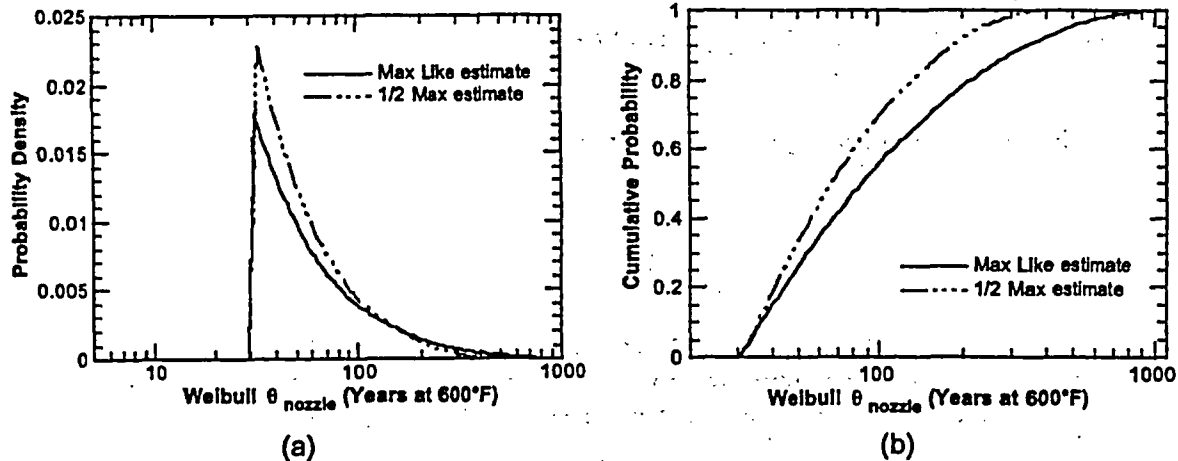


Figure 3. Comparison of the probability density functions (a) and cumulative probability functions (b) for the Weibull scale factor for CRDM nozzles, θ_{nozzle} , and a sensitivity calculation for the case where the upper end of the distribution has been varied to get an estimate that is one half the value of the maximum.

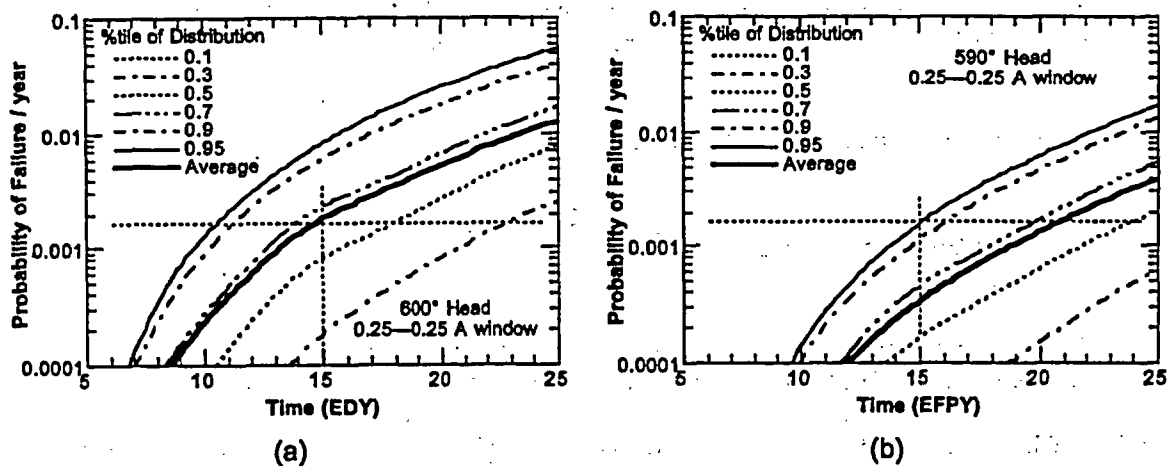


Figure 4. Distribution of the probability of failure for vessel heads operating at (a) 600°F (316°C) and (b) 590°F (310°C).

The distributions are broad, spanning about 3 orders of magnitude at any given time. However, in practice, for the analysis of a specific plant, we would expect to have additional knowledge, e.g., the plant has operated n years without nozzle leaks or that it had m leaks after n years of operation. We would also know the fabricator of the head. Methods are needed to best incorporate ongoing inspection results in models. Because of the limited amount of failure data available, the most effective means of updating the distributions for the initiation parameters may be through the use of Bayes theorem.

If we assume a prior distribution for θ , $p(\theta)$ and if there are M heats of material in a head that has been operating for t years when it is inspected and found to have n leaking nozzles, then Bayes theorem says that a posterior distribution for θ , $\hat{p}(\theta)$ is given by:

$$\hat{p}(\theta_1)\hat{p}(\theta_2)\dots\hat{p}(\theta_M) \propto \left\{ \prod_{m=1}^M W(t, \theta_m)^{n_m} (1 - W(t, \theta_m))^{(N_m - n_m)} \right\} p(\theta_1)p(\theta_2)\dots p(\theta_M) \quad (2)$$

where n_m is the number of leaking nozzles in heat m and N_m is the total number of leaking nozzles from heat m . For the case where $\theta_1 = \theta_2 = \dots = \theta_M$

$$\hat{p}(\theta) \propto \left\{ W(t, \theta)^n (1 - W(t, \theta))^{(N - n)} \right\}^{\frac{1}{M}} p(\theta) \quad (3)$$

In Eqs (2) and (3), it has been assumed that all the nozzles come from the same distribution, i.e., we are updating the generic distribution for nozzles. Alternatively we could seek to find an updated distribution for a particular heat by considering only the nozzles belonging to that heat:

$$\hat{p}_m(\theta) \propto \left\{ W(t, \theta)^{n_m} (1 - W(t, \theta))^{(N_m - n_m)} \right\} p(\theta) \quad (4)$$

This second viewpoint [Eq. (4)] would be appropriate for example when considering the case of a head which has all its nozzles from a single heat and has operated for time T with no failures. The first viewpoint [Eq. (1)] is more appropriate when considering a collection of heads with a large number of heats or when dealing with a plant for which the number of heats and the number of nozzles per heat is not known.

Eq. (3) can be generalized to a collection of K heads:

$$\hat{p}(\theta) \propto \left\{ \prod_{k=1}^K W(t, \theta)^{n_k} (1 - W(t, \theta))^{(N_k - n_k)} \right\}^{\frac{1}{m_1 + m_2 + \dots + m_M}} p(\theta) \quad (5)$$

where N_k is the total number of nozzles and n_k is the number of leaking nozzles in the k th head and m_1, m_2, \dots are the numbers of nozzles from heats 1, 2, ... Because we often do not know the actual numbers of nozzles per heat in a head, it is convenient to write $m_1 + m_2 + \dots + m_M$ as $K \cdot m_{av}$ where m_{av} is the average number of heats in a head which can be estimated. Introducing a normalization to ensure that $\hat{p}(\theta)$ integrates to 1, we get

$$\hat{p}(\theta) = \frac{\left\{ \prod_{k=1}^K W(t, \theta)^{n_k} (1 - W(t, \theta))^{(N_k - n_k)} \right\}^{\frac{1}{K m_{av}}}}{\int_0^{\infty} \left\{ \prod_{k=1}^K W(t, \theta)^{n_k} (1 - W(t, \theta))^{(N_k - n_k)} \right\}^{\frac{1}{K m_{av}}}} p(\theta) \quad (6)$$

In Fig. 5 the generic distribution of the Weibull scale factor calculated from the data from all inspections at all plants is compared with the updated distribution for a plant that has operated for 20 years at 316°C (600°F). Results are given both for the case when nozzles are from a single heat and for the case when the head contains equal numbers of nozzles from five different heats.

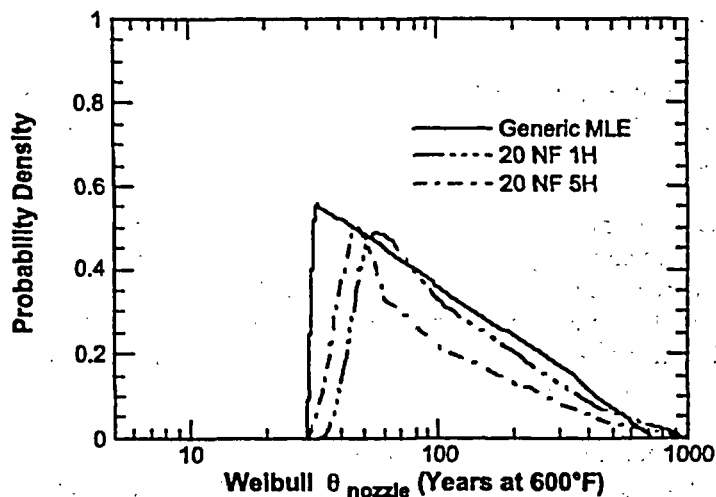


Figure 5. Updated distributions for the Weibull scale factor for initiation for a head that has operated for 20 years at 316°C (600°F). Results are given for the case when nozzles are from a single heat or from five different heats.

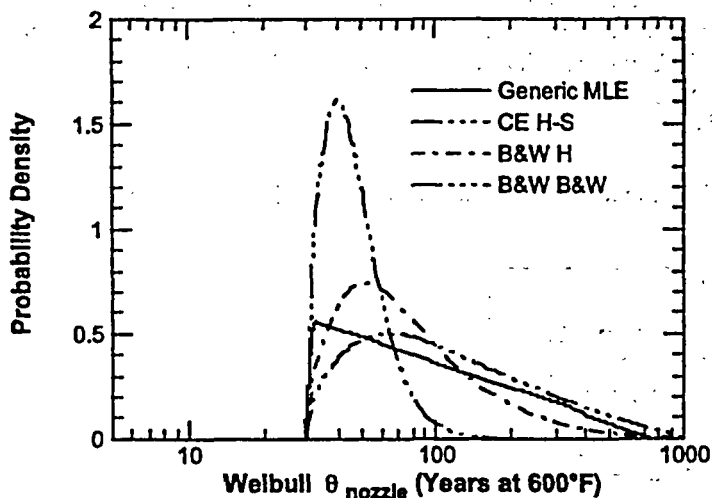


Figure 6. Updated distributions for the Weibull scale factor for initiation for heads fabricated by Combustion Engineering with Huntington or Sandvik nozzle materials, heads fabricated by Sandvik with Huntington nozzle materials, heads fabricated by B&W with Huntington nozzle materials, or heads fabricated by B&W with B&W nozzle materials. It is assumed that the heads contain nozzles from five different heats of material.

In Fig. 6 the generic distribution is compared with distributions for plants from different fabricators. The least susceptible heads seem to be those fabricated by Combustion Engineering with nozzle materials from Huntington or Sandvik. The most susceptible heads seem to be those fabricated by B&W with nozzle materials from B&W. The heads fabricated by B&W with nozzle materials from Huntington are intermediate in susceptibility.

Irradiation assisted stress corrosion cracking (IASCC)

Exposure to high levels of neutron irradiation produces changes microstructure (radiation hardening) and material microchemistry (radiation induced segregation).^{23, 24} These microstructural changes result in increases in yield strength, reductions in ductility and fracture toughness, and susceptibility to stress corrosion cracking.²⁴⁻²⁶ At low fluence susceptibility is apparent in environments with high dissolved oxygen levels; at higher fluence susceptibility can occur at both high and low dissolved oxygen levels.^{23, 28, 29}

Crack Growth of Irradiated Austenitic SSs

The crack growth test program for irradiated austenitic SS is carried out on specimens irradiated in the Halden boiling heavy water reactor at 288°C in a helium environment. Both base metal and heat affected zone (HAZ) materials are being tested.

The results indicate significant enhancement of crack growth rates of irradiated steel in a high dissolved oxygen BWR environment corresponding to operation without hydrogen additions. The crack growth rates of irradiated steels in these environments are a factor of ≈ 5 higher than the disposition curve proposed in NUREG-0313 for sensitized austenitic SSs as shown in Fig. 7. The crack growth rates of Type 304 SS irradiated to 0.9 and 2.0×10^{21} n·cm⁻² ($E > 1$ MeV) [≈ 1.35 , and 3.0 dpa] and of Types 304 and 316 SS irradiated to 2.0×10^{21} n·cm⁻², are comparable.

In low DO BWR environments corresponding to operation with hydrogen additions, the crack growth rates of the irradiated steels decreased by an order of magnitude in some tests, e.g., Heat C3 of Type 304 SS irradiated to 0.9×10^{21} n·cm⁻² and Heat C16 of Type 316 SS irradiated to 2×10^{21} n·cm⁻² (Fig. 7). The beneficial effect of decreased DO was not observed for Heat C3 of Type 304 SS irradiated to 2×10^{21} n·cm⁻². It is possible that this different behavior is associated with the loss of constraint in the specimen due to the high applied load, although it is known that the beneficial effects of lower potential are lost at sufficiently high fluence levels.³⁰

Although it is now well established that crack growth rates can be very high in irradiated stainless

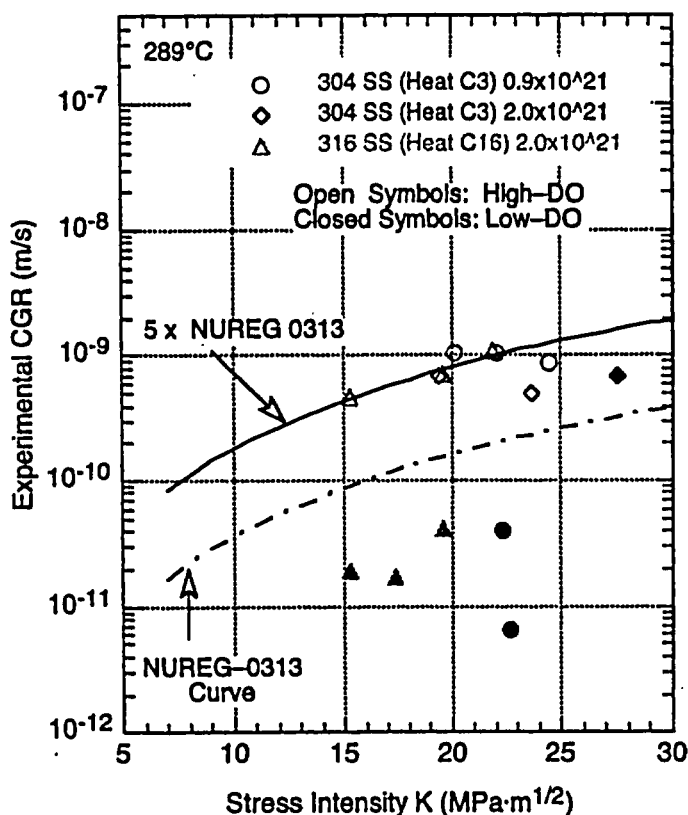


Figure 7.
In NWC BWR environment, CGRs are a factor of ≈ 5 higher than NUREG 0313 curve for sensitized SSs in 8 ppm DO

steels, there are a number of open issues that need to be addressed. Our recent data confirm that at fluence levels less than $2.0 \times 10^{21} \text{ n}\cdot\text{cm}^{-2}$ lower potentials result in substantial reductions in crack growth rates, but the high fluence threshold at which the beneficial effects of lower potential are lost is not well defined. It is not clear, for example, whether the threshold will be high enough to ensure that lower potentials will be an effective method to mitigate cracking in irradiated stainless steels through the operating life of current BWRs. Conversely, it is not clear, that there can not be significant enhancement of crack growth rates in some cases at fluences below the $0.5 \times 10^{21} \text{ n}\cdot\text{cm}^{-2}$ conventionally used as a threshold for IASCC.

Effects of composition on IASCC susceptibility

Although it is possible to mitigate IASCC by control of water chemistry and electrochemical potential, it is desirable to find materials that are more inherently resistant to IASCC. In the early 1990s, high-purity heats of Type 304L SS were actively investigated in the hope of developing a more IASCC-resistant material than commercial-purity Type 304 SS. However, contrary to initial expectations, results from laboratory tests and in-BWR experience showed that IASCC resistance of many high purity heats was worse or no better than that of commercial purity heats of Type 304 SS.

As part of the research program on IASCC being carried out for the USNRC, irradiations of a wide variety of SS compositions in the Halden boiling heavy water reactor were undertaken to try to identify critical material chemistry variables that can affect IASCC.

A major finding of this work is the identification of the deleterious effect of sulfur even at what would normally be considered low levels. As shown in Fig. 8, even sulfur levels as low as 0.003 wt.%, have a strongly deleterious effect at fluences of $2.0 \times 10^{21} \text{ n}\cdot\text{cm}^{-2}$. Higher sulfur levels result in susceptibility at even lower fluence levels. Such effects are also seen in the work of other investigators as shown in Fig. 9.³¹⁻³⁴

A related result is the effect of carbon concentration on IASCC susceptibility of low-S SSs. Figure 10 shows a summary comparison of IASCC susceptibility (i.e., percent IGSCC from SSRT test) of low-S ($S \leq 0.002 \text{ wt.}\%$) high-C heats of Type 304 SS relative to those of their low-S low-C counterparts of Type 304L SS. A similar plot for low-S heats of Types 316 and 316L SSs is shown in Fig. 11.^{31,32,35}

A similar trend was also observed for Type 348 and 348L SS tested under PWR conditions as shown in Figs. 12 and 13 in a series of swelling-tube-failure tests^{36,37} where the resistance to IASCC is expressed in terms of the maximum average diametral strain. In the results shown in Fig. 12, the diametral strain was measured in intact tubes and cracked tubes of the same heat following one-cycle irradiation ($2.3 \times 10^{21} \text{ n}\cdot\text{cm}^{-2}$, $E > 1 \text{ MeV}$). This data for materials irradiated to the same fluence in the same reactor is considered to provide a more direct comparison of the effect of C in low-S heats (see Fig. 12). Examination of the data indicates that Type 348 SS heats containing 0.005-0.007 wt.% S and 0.027-0.031 wt.% C were more resistant to IASCC than lower sulfur Type 348L SS heats containing 0.002-0.004 wt.% S and 0.003-0.015 wt.% C even though the fluence of the former was significantly higher than that of the latter. Figure 13 shows an essentially similar trend when additional data obtained for a wider range of fluence are compared.

It appears that the beneficial effect of carbon is manifested more strongly at very low concentrations of S. At high S concentrations, the deleterious effect of S seems to be so dominant at

about 2 dpa or higher that IASCC susceptibility is high anyway regardless of high or low carbon concentration.

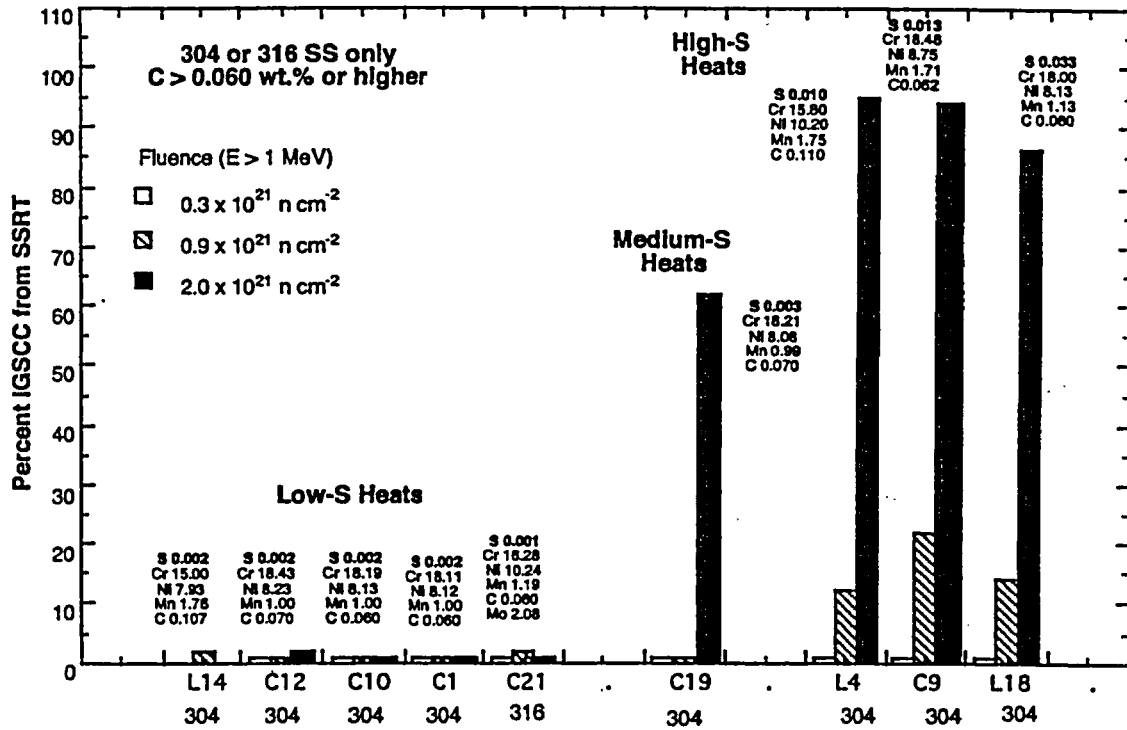


Figure 8. Effect of bulk S content on percent IGSCC of Type 304 and 316 SSs irradiated to three fluence levels.

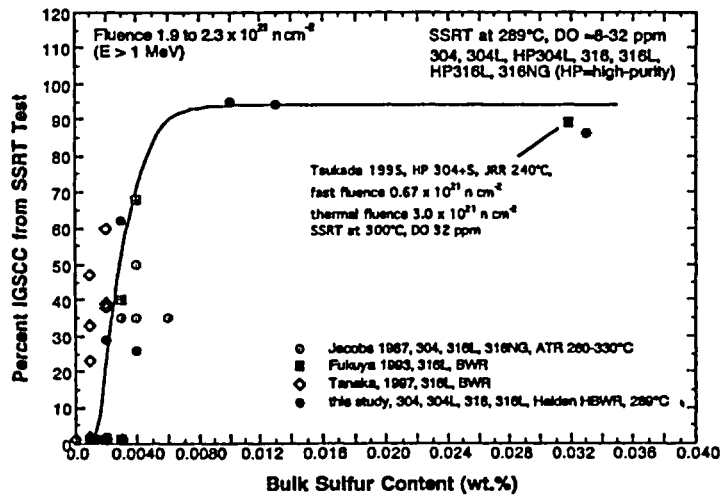


Figure 9. Effect of bulk sulfur content on the Percent IGSCC on the fracture surface.

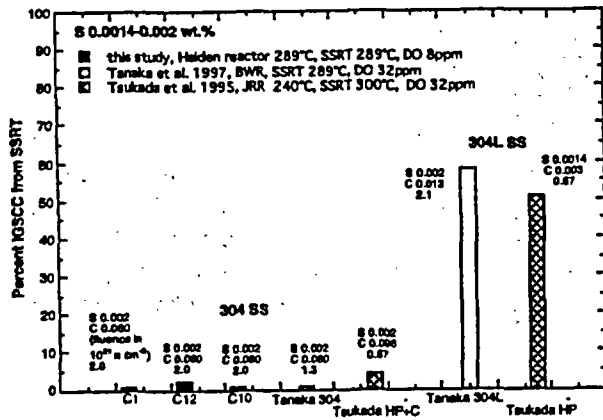


Figure 10. IASCC susceptibility (percent IGSCC from SSRT test) of low-sulfur heats of high- and low-carbon Types 304 and 304L steels.

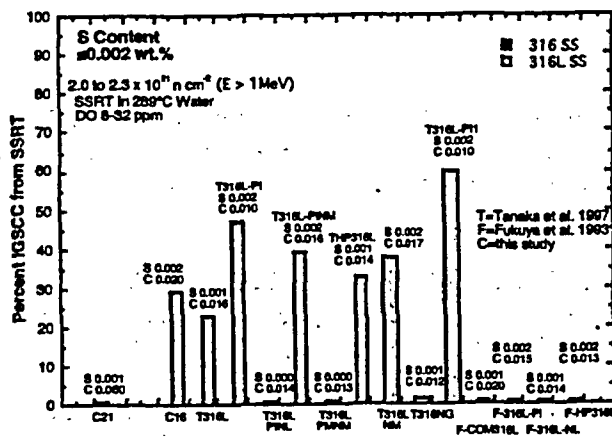


Figure 11. IASCC susceptibility (percent IGSCC from SSRT test) of low-sulfur heats of high- and low-carbon Types 316 and 316L steels.

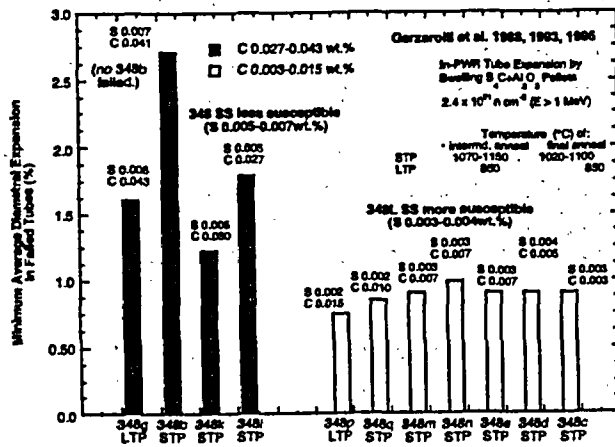


Figure 12. IASCC susceptibility (minimum average diametral strain among failed tubes) of low-S high-C Type 348 SS and low-S low-C Type 348L SSs, one-cycle irradiation to 2.3 x 10²¹ n cm⁻², E > 1 MeV.

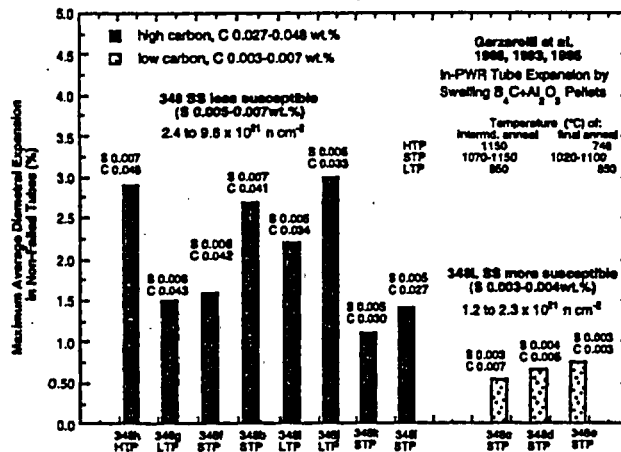


Figure 13. IASCC susceptibility (minimum average diametral strain among failed tubes) of low-S high-C Type 348 SS (high fluence) and low-S low-C Type 348L SSs (low fluence). Note high-fluence high-C heats are more resistant than low-fluence low-C heats.

References

1. O. K. Chopra and W. J. Shack, "ASME Code Fatigue Design Curve Margins - Effects of Surface Finish and Material Variability", *Pressure Vessel and Piping Codes and Standards - 2003, PVP Vol. 453*, G. S. Chakrabarti, ed., American Society of Mechanical Engineers, New York, pp. 71-85 (2203).
2. S. Ranganath, J. N. Kass, and J. D. Heald, "Fatigue Behavior of Carbon Steel Components in High-Temperature Water Environments," *BWR Environmental Cracking Margins for Carbon Steel Piping*, EPRI NP-2406, Electric Power Research Institute, Palo Alto, CA, Appendix 3 (1982).
3. M. Higuchi and K. Iida, "Fatigue Strength Correction Factors for Carbon and Low-Alloy Steels in Oxygen-Containing High-Temperature Water," *Nucl. Eng. Des.* **129**, 293-306 (1991).
4. Y. Katada, N. Nagata, and S. Sato, "Effect of Dissolved Oxygen Concentration on Fatigue Crack Growth Behavior of A533 B Steel in High-Temperature Water," *ISIJ Intl.* **33** (8), 877-883 (1993).
5. G. Nakao, H. Kanasaki, M. Higuchi, K. Iida, and Y. Asada, "Effects of Temperature and Dissolved Oxygen Content on Fatigue Life of Carbon and Low-Alloy Steels in LWR Water Environment," in *Fatigue and Crack Growth: Environmental Effects, Modeling Studies, and Design Considerations*, PVP Vol. 306, S. Yukawa, ed., American Society of Mechanical Engineers, New York, pp. 123-128 (1995).
6. M. Higuchi, K. Iida, and Y. Asada, "Effects of Strain Rate Change on Fatigue Life of Carbon Steel in High-Temperature Water," in *Effects of the Environment on the Initiation of Crack Growth*, ASTM STP 1298, W. A. Van Der Sluys, R. S. Piascik, and R. Zawierucha, eds., American Society for Testing and Materials, Philadelphia, pp. 216-231 (1997).
7. O. K. Chopra and W. J. Shack, "Evaluation of Effects of LWR Coolant Environments on Fatigue Life of Carbon and Low-Alloy Steels," in *Effects of the Environment on the Initiation of Crack Growth*, ASTM STP 1298, W. A. Van Der Sluys, R. S. Piascik, and R. Zawierucha, eds., American Society for Testing and Materials, Philadelphia, pp. 247-266 (1997).

8. O. K. Chopra and W. J. Shack, "Low-Cycle Fatigue of Piping and Pressure Vessel Steels in LWR Environments," *Nucl. Eng. Des.* 184, 49-76 (1998).
9. K. Tsutsumi, H. Kanasaki, T. Umakoshi, T. Nakamura, S. Urata, H. Mizuta, and S. Nomoto, "Fatigue Life Reduction in PWR Water Environment for Stainless Steels," in *Assessment Methodologies for Preventing Failure: Service Experience and Environmental Considerations*, PVP Vol. 410-2, R. Mohan, ed., American Society of Mechanical Engineers, New York, pp. 23-34 (2000).
10. K. Tsutsumi, T. Dodo, H. Kanasaki, S. Nomoto, Y. Minami, and T. Nakamura, "Fatigue Behavior of Stainless Steel under Conditions of Changing Strain Rate in PWR Primary Water," in *Pressure Vessel and Piping Codes and Standards*, PVP Vol. 419, M. D. Rana, ed., American Society of Mechanical Engineers, New York, pp. 135-141 (2001).
11. O. K. Chopra and D. J. Gavenda, "Effects of LWR Coolant Environments on Fatigue Lives of Austenitic Stainless Steels," *J. Pressure Vessel Technol.* 120, 116-121 (1998).
12. O. K. Chopra, "Development of Fatigue Design Curve for Austenitic Stainless Steels in LWR Environments: A Review," in *Pressure Vessel and Piping Codes and Standards - 2002*, PVP Vol. 439, R. D. Rana, ed., American Society of Mechanical Engineers, New York, pp. 119-132 (2002).
13. B. F. Langer, "Design of Pressure Vessels for Low-Cycle Fatigue," *ASME J. Basic Eng.* 84, 389-402 (1962).
14. *Criteria of the ASME Boiler and Pressure Vessel Code for Design by Analysis in Sections III and VIII, Division 2*, The American Society of Mechanical Engineers, New York (1969).
15. W. E. Cooper, "The Initial Scope and Intent of the Section III Fatigue Design Procedure," in *Welding Research Council, Inc., Technical Information from Workshop on Cyclic Life and Environmental Effects in Nuclear Applications*, Clearwater, Florida, January 20-21, 1992.
16. O. K. Chopra and J. L. Smith, "Estimation of Fatigue Strain-Life Curves for Austenitic Stainless Steels in Light Water Reactor Environments," in *Fatigue, Environmental Factors, and New Materials*, PVP Vol. 374, H. S. Mehta, R. W. Swindeman, J. A. Todd, S. Yukawa, M. Zako, W. H. Bamford, M. Higuchi, E. Jones, H. Nickel, and S. Rahman, eds., American Society of Mechanical Engineers, New York, pp. 249-259 (1998).
17. O. K. Chopra, "Development of Fatigue Design Curve for Austenitic Stainless Steels in LWR Environments: A Review," in *Pressure Vessel and Piping Codes and Standards - 2002*, PVP Vol. 439, R. D. Rana, ed., American Society of Mechanical Engineers, New York, pp. 119-132 (2002).
18. J. Beck and K. Arnold, *Parameter Estimation in Engineering and Science*, J. Wiley, New York (1977).
19. O. K. Chopra, *Mechanism and Estimation of Fatigue Crack Initiation in Austenitic Stainless Steels in LWR Environments*, NUREG/CR-6787, ANL-01/25 (2002).

20. A. Conle and T. H. Topper, "Overstrain Effects During Variable Amplitude Service History Testing," *Int. J. Fatigue* 2, 130-136 (1980).
21. M. A. Pompetzki, T. H. Topper, and D. L. DuQuesnay, "The Effect of Compressive Underloads and Tensile Overloads on Fatigue Damage Accumulation in SAE 1045 Steel," *Int. J. Fatigue* 12 (3), 207-213 (1990).
22. *Materials Reliability Program (MRP) Crack Growth Rates for Evaluating Primary Water Stress Corrosion Cracking (PWSCC) of Thick-Wall Alloy 600 Materials (MRP-55) Revision 1*, EPRI, Palo Alto, CA, TR-1006695, 2002.
23. S. M. Bruemmer et al., *Critical Issue Reviews for the Understanding and Evaluation of Irradiation-Assisted Stress Corrosion Cracking*, EPRI TR-107159, Electric Power Research Institute, Palo Alto, CA (1996).
24. P. L. Andresen, F. P. Ford, S. M. Murphy, and J. M. Perks, "State of Knowledge of Radiation Effects on Environmental Cracking in Light Water Reactor Core Materials, Proc. 4th Intl. Symp. On Environmental Degradation of Materials in Nuclear Power Systems - Water Reactors, NACE, pp. 1.83-1.121 (1990).
25. M. L. Herrera, et al., *Evaluation of the Effects of Irradiation on the Fracture Toughness of BWR Internal Components*, in Proc. ASME/JSME 4th Intl. Conf. on Nucl. Eng. (ICONE-4) Vol. 5, A. S. Rao, R. M. Duffey, and D. Elias, eds., American Society of Mechanical Engineers, New York, pp. 245-251 (1996).
26. W. J. Mills, *Fracture Toughness of Type 304 and 316 Stainless Steels and their Welds*, Intl. Mater. Rev. 42, 45-82 (1997).
27. O. K. Chopra, E. E. Gruber, and W. J. Shack, *Fracture Toughness and Crack Growth Rates of Irradiated Austenitic Stainless Steels*, NUREG/CR- 6826, ANL-03/22 (2003).
28. A. Jenssen and L. G. Ljungberg, "Irradiation Assisted Stress Corrosion Cracking of Stainless Alloys in BWR Normal Water Chemistry and Hydrogen Water Chemistry," *Proc. Sixth Intl. Symp. on Environmental Degradation of Materials in Nuclear Power Systems - Water Reactor*, p. 547, Eds., R. E. Gold and E. P. Simonen, The Minerals, Metals & Materials Society, Warrendale, PA (1993).
29. A. Jenssen and L. G. Ljungberg, "Irradiation Assisted Stress Corrosion Cracking: Post Irradiation CERT Tests of Stainless Steels in a BWR Test Loop," *Proc. Seventh Intl. Symp. on Environmental Degradation of Materials in Nuclear Power Systems - Water Reactor*, p. 1043, Eds., G. Airey et al., NACE, Houston, TX (1995).
30. M. Kodama et al., "IASCC Susceptibility of Austenitic Stainless Steels Irradiated to High Neutron Fluence," *Proc. Sixth Intl. Symp. on Environmental Degradation of Materials in Nuclear Power Systems - Water Reactor*, R. E. Gold and E. P. Simonen eds., The Minerals, Metals & Materials Society, pp. 583-588 (1993).

31. Y. Tanaka, S. Suzuki, K. Fukuya, H. Sakamoto, M. Kodama, S. Nishimura, K. Nakata, and T. Kato, "IASCC Susceptibility of Type 304, 304L, and 316 Stainless Steels," in Proc. 8th Int. Symp. on Environmental Degradation of Materials in Nuclear Power Systems - Water Reactors, S. M. Bruemmer, ed., American Nuclear Society, La Grange Park, IL, 1997, pp. 803-811.
32. K. Fukuya, S. Shima, K. Nakata, S. Kasahara, A. J. Jacobs, G. P. Wozadlo, S. Suzuki, and M. Kitamura, *Mechanical Properties and IASCC Susceptibility in Irradiated Stainless Steels*, in Proc. 6th Int. Symp. on Environmental Degradation of Materials in Nuclear Power Systems - Water Reactors, R. E. Gold and E. P. Simonen, eds., The Minerals, Metals, and Materials Society, Warrendale, PA, pp. 564-572 (1993).
33. A. J. Jacobs, G. P. Wozadlo, K. Nakata, T. Yoshida, and I. Masaoka, "Radiation Effects on the Stress Corrosion and Other Selected Properties of Type-304 and Type-316 Stainless Steels," in Proc. 3rd Intl. Symp. Environmental Degradation of Materials in Nuclear Power Systems - Water Reactors, G. J. Theus and J. R. Weeks, eds., The Metallurgical Society, Warrendale, PA, pp. 673-680 (1988).
34. A. J. Jacobs, G. E. C. Bell, C. M. Shepherd, and G. P. Wozadlo, *High-Temperature Solution Annealing as an IASCC Mitigating Technique*, in Proc. 5th Int. Symp. on Environmental Degradation of Materials in Nuclear Power Systems - Water Reactors, D. Cubicciotti, E. P. Simonen, and R. Gold, eds., American Nuclear Society, La Grange Park, IL, pp. 917-934 (1992).
35. T. Tsukada and Y. Miwa, "Stress Corrosion Cracking of Neutron Irradiated Stainless Steels," in Proc. 7th Int. Symp. on Environmental Degradation of Materials in Nuclear Power Systems - Water Reactors, NACE International, Houston, pp. 1009-1018 (1995).
36. F. Garzarolli, P. Dewes, R. Hahn, and J. L. Nelson, "Deformability of High-Purity Stainless Steels and Ni-Base Alloys in the Core of a PWR," in Proc. 6th Intl. Symp. on Environmental Degradation of Materials in Nuclear Power Systems - Water Reactors, R. E. Gold and E. P. Simonen, eds., The Minerals, Metals, and Materials Society, Warrendale, PA, pp. 607-613 (1993).
37. F. Garzarolli, P. Dewes, R. Hahn, and J. L. Nelson, "In-Reactor Testing of IASCC Resistant Stainless Steels," *ibid.*, 1055-1065 (1995).

Strategic Planning for RPV Head Nozzle PWSCC

Glenn White and Steve Hunt
Dominion Engineering, Inc., Reston, VA

Abstract: Utilities are faced with difficult economic choices in managing PWSCC of RPV head penetrations. Inspections are expensive, especially if required on a frequent basis; if leaks are discovered during an outage when no inspections are performed, and no provision to perform repairs has been made, repairs can lead to significant lost production; repairs and remedial measures are expensive and, depending upon conditions, may result in future cracks or leaks; and head replacements are expensive. Life cycle management planning has been performed for a moderate susceptibility plant to determine the most attractive long-term strategy. This work has been based on predictive modeling and net present value economic analysis. The approach described can help a utility determine the best management strategy for its plant.

BACKGROUND

Nickel-chromium-iron Alloy 600 material has been used in all PWR plants in the United States. The main reasons for originally selecting this material were its corrosion resistance and close match in coefficient of thermal expansion to the low-alloy steel pressure vessel materials. Figure 1 shows typical locations of thick-section Alloy 600 materials. The exact locations vary between the plants and are primarily a function of the designer of the nuclear steam supply system (NSSS). While Alloy 600 material has good general corrosion resistance to PWR plant primary and secondary water chemistry, experience has shown that the material is susceptible to primary water stress corrosion cracking (PWSCC) given the operating environments and stresses in PWR applications.

The most significant consequences of Alloy 600 PWSCC to date have involved the reactor pressure vessel (RPV) closure head nozzles which are attached to the inside surface of the head by J-groove welds. Shrinkage of the J-groove welds during cooling applies strains and resultant high stresses to the nozzles and welds. As shown in Figure 2, the resulting cracks have been both axial and circumferential with some of the cracks propagating through the nozzle wall and J-groove welds to produce leaks.

The economic consequences of managing RPV head nozzle PWSCC can be significant. For example:

- The French nuclear utility EDF is replacing all of its RPV heads.
- Cracks and leaks in nozzles in several domestic plants have resulted in significant outage extensions and repair costs.
- Boric acid corrosion resulting from a PWSCC leak at the Davis-Besse plant has led to over a 22 month outage.
- Cracks in large numbers of welds at North Anna 2 led to about a four month outage while the head was replaced.

- Industry findings and NRC guidelines/requirements have led to many expensive inspections.
- 31 of 69 plants in the US have announced plans to replace heads as of December 2003.

PURPOSE

The purpose of this paper is to review issues associated with developing a strategic plan for managing RPV head nozzle PWSCC including the basis for setting the re-inspection interval for nonvisual examinations. The strategic plan must:

- Ensure a low risk of leakage.
- Ensure an extremely low risk of core damage. For purposes of this paper, it is assumed that this objective can be met by meeting the core damage risk criterion of NRC Regulatory Guide 1.174.
- Result in the lowest net present value (NPV) cost consistent with the above criteria.

Three types of analyses will be described. First is a deterministic approach to demonstrate that nozzle ejection and significant head wastage are unlikely to occur given the assumed re-inspection interval. Second, a probabilistic approach is described where Monte Carlo analyses are performed to demonstrate that the calculated increase in core damage frequency (CDF) due to potential nozzle ejection and boric acid wastage is within acceptable limits. Acceptable limits for the probabilistic analysis are defined based on the criterion of NRC Reg. Guide 1.174, which sets an acceptable increase in core damage frequency as 1×10^{-6} per year. The probabilistic assessments are also used to verify that the inspection strategy used results in a low probability of penetration leakage. Third, an example net present value economic analysis is presented for a typical moderate susceptibility plant.

TIME TO PWSCC

Many factors are believed to contribute to PWSCC, including:

- Material chemistry (primarily carbon content)
- Material thermal/mechanical processing (annealing)
- Cold work prior to and after welding (straightening, machining, grinding, reaming, etc.)
- Operating stresses including welding residual stresses
- Water chemistry and operating temperature

Unfortunately, there is no proven model for predicting the time to PWSCC for a given nozzle based on these parameters. In some cases, important details such as the annealing conditions, welding details, repairs, etc. are not known. Given these uncertainties, recent work in the industry has focused on ranking plants based on their operating time and temperature. The measure used is effective degradation years (EDYs), which represents the plant operating time adjusted to a common reference temperature of 600°F based on an activation energy of 50 kcal/mole for crack initiation. For plants that operate with a head temperature of 600°F, the EDYs is equal to the effective full power years (EFPYs). For plants with head temperatures higher than 600°F, the number of EDYs will be greater than the number of EFPYs.

While the simple time-temperature model has been used to rank plants by susceptibility, recent nondestructive testing results are showing that there are at least two other factors that can be used to assess susceptibility. These are the head fabricator and the nozzle material supplier. Inspection results in support of this finding are shown in Figures 3 and 4, respectively. These data were compiled by the EPRI Materials Reliability Program (MRP).

As more inspection results become available it is possible to refine predictions of time to PWSCC or time to leaks. These predictions can be performed using a Weibull statistical model as shown in Figure 5. Since there are seldom repeat inspections, the slope is often assumed to be 3 based on other Alloy 600 PWSCC experience such as with steam generator tubing. For lead plants which have performed a nonvisual nondestructive examination of all nozzles without finding indications of PWSCC, it can be conservatively assumed that there is one nozzle with a PWSCC crack at the limit of NDE detectability immediately upon plant startup.

RISK OF LEAKS

The risk of leaks is calculated assuming that a preexisting flaw at the limit of NDE detectability grows by PWSCC. Figure 6 shows the types of flaws that are modeled. The crack growth is calculated using the current NRC guidance.¹ This model involves calculation of the crack tip stress intensity factor from finite element stress analysis results and crack growth rates for Alloy 600 established by an industry expert panel.² The crack growth rate curves used are shown in Figure 7, including the curve for Alloy 182 weld metal presented in report MRP-21.³ The data in Figure 7 show that the crack growth rate through the J-groove weld can be higher than through the base metal. However, field experience has shown that most cracks are in the base metal rather than the welds.

Deterministic calculations show that cracks growing through the base metal that are just detectable by NDE can develop into leaks after 3.5–10 years and that cracks growing through welds that are just detectable by NDE can develop into leaks after 1–3 years of operation, depending upon assumptions.

Probabilistic calculations show the risk of leaks for an example plant operating near 600°F to be about 5% during the third year after completing a nonvisual nondestructive examination of all nozzles and welds. This risk is based on the conservative assumption that there is a nozzle with a growing weld crack just below the limit of detectability at the time of the inspection.

FLAW TOLERANCE

Figure 8 shows the tolerance of a typical CRDM nozzle to axial flaws above the J-groove weld, circumferential flaws above the J-groove weld, and axial-circumferential (lack of fusion type) flaws between the nozzle and J-groove weld. These calculations show that axial flaws of about 5 inches length and circumferential through-wall or loss-of-fusion type cracks of about 270–280° total arc can be tolerated with a safety factor of 2.7 on the pressure load. This factor of safety is based on the level specified by Section XI of the ASME Boiler & Pressure Vessel Code for continued service with actual flaws.

Figure 9 shows that, for corrosion progressing from the outer head surface downward such as might have occurred at Davis-Besse, large volumes of low-alloy steel material in the RPV head can be lost

¹ Letter from R. Barrett (NRC) to A. Marion (NEI) dated April 11, 2003, *Flaw Evaluation Guidelines*.

² *Materials Reliability Program (MRP) Crack Growth Rates for Evaluating Primary Water Stress Corrosion Cracking (PWSCC) of Thick-Wall Alloy 600 Materials (MRP-55) Revision 1*, EPRI, Palo Alto, CA: 2002, 1006695.

³ *Crack Growth of Alloy 182 Weld Metal in PWR Environments (PWRMRP-21)*, EPRI, Palo Alto, CA: 2000, 1000037.

without exceeding ASME Code allowable stress values in the remaining ligament. For the case evaluated, about 150 in³ of material can be lost without exceeding ASME Code allowable stresses.

In summary, these analyses show that the RPV head and nozzles are quite flaw tolerant.

RISK OF RUPTURE AND CORE DAMAGE DUE TO NOZZLE EJECTION

The main concern regarding nozzle ejection is the potential for a circumferential crack through the nozzle wall above the J-groove weld to grow to a critical length. There is less concern with ejection due to a "lack-of-fusion" type flaw since this flaw would have to be perfectly concentric for the nozzle to eject. Any deviation from a pure cylinder would create protrusions that would tend to "pin" the nozzle in place and prevent ejection.

It is conservatively assumed that a 30° through-wall circumferential crack exists in the nozzle above the J-groove weld immediately after a leak occurs. As shown in Figure 10, this flaw can grow to about 330° prior to the nozzle being ejected from the vessel head. The crack is assumed to be driven by the stresses in the nozzle perpendicular to the crack plane, which are also shown in Figure 10.

Development work has recently been completed to integrate a fracture mechanics model into the welding residual stress model. The objective of this approach is to be able to account for relaxation of the welding residual stresses as cracks grow in length. Figure 11 shows a typical model with a 180° crack above the J-groove weld, and Figure 12 shows the effect of the crack in reducing axial stresses.

The fracture mechanics module calculates the J-integral using numerical volume integration. This approach captures the effects of Modes I, II and III crack opening displacements. The J-integrals are averaged across the nozzle wall and the equivalent stress intensity factor (K) is calculated from the J-integral using the following expression:

$$K_{eq} = \sqrt{\frac{J_{avg} E}{1 - \nu^2}}$$

where E is Young's modulus and ν is Poisson's ratio for the Alloy 600 material.

Figure 13 shows a comparison of these calculations relative to other references sources for the case of a through-wall circumferential crack above the J-groove weld on the downhill side of an outer row CRDM nozzle. It should be noted that the results are similar to results obtained by EMC², and reported in NUREG/CP-0180.

Figure 14 shows example results of a deterministic calculation for growth of a circumferential through-wall crack above the J-groove weld from the assumed 30° starting flaw. The allowable size of approximately 280° includes a factor of safety of 2.7 on rupture as specified in Section XI of the ASME Code. This type of calculation provides assurance that rupture is unlikely.

The actual risk of rupture is quantified using a probabilistic analysis as shown in simplified form in Figure 15. Additional details regarding this model were described during the recent NRC workshop

on Alloy 600.⁴ This model includes distributions on each of the main analysis input variables. For example, Figure 16 shows the distribution of heat-to-heat crack growth rate variability for Alloy 600 base metal based on the industry expert panel work (MRP-55).

The acceptance criterion of an increase in the core damage frequency (CDF) of 1×10^{-6} per reactor year is taken from Reg. Guide 1.174. The increase in CDF is determined by multiplying the probability of nozzle ejection times the conditional core damage probability (CCDP) for the appropriately sized loss of coolant accident (LOCA). For one example plant with about 20 EDYs that performed nonvisual nondestructive examinations that revealed no reportable indications, Monte Carlo calculations showed that the increase in CDF remains below 1×10^{-6} per reactor year for more than three years after the baseline inspection. This supports inspection intervals every second refueling outage for this plant.

Sensitivity analyses are run to show that the results are not too dependent upon the particular input assumption and distributions. Parameters assessed in the sensitivity studies include:

- Inspection probability of detection (POD) curves
- Crack geometry and location
- Weibull crack initiation reference
- Crack growth rate (CGR) assumptions including weld CGR
- Credit for bare metal inspections to show leaks at outages when NDE is not performed

RISK OF RUPTURE AND CORE DAMAGE DUE TO BORIC ACID WASTAGE

In addition to the risk of nozzle ejection due to a circumferential flaw above the J-groove weld, there can be a risk of rupture and core damage due to boric acid wastage of the type seen at Davis-Besse. Probabilistic analyses for wastage have been performed using the methodology given in Appendices C, D, and E of MRP-75⁵ (see Figure 17), which considers relatively wide tolerance bands for the key model parameters of

- Point within the operating cycle that wastage begins
- Stress intensity factor driving crack growth
- Crack growth rate distribution
- Leak rate as a function of axial crack length
- Wastage rate as a function of leak rate
- Sensitivity of the bare metal visual inspections

The analysis results in Figure 18 show that the probability of a leaking nozzle producing wastage greater than the typical 150 in³ allowable volume is less than 1×10^{-4} given bare metal visual inspections performed during each refueling outage. The effect on CDF may be estimated by multiplying the probability of the wastage volume exceeding the allowable size given a leaking nozzle times the probability of leakage per year times the CCDP for the appropriately sized LOCA.

⁴ G. White, S. Hunt, and N. Nordmann, "Risk-Informed Evaluation of PWR Reactor Vessel Head Penetration Inspection Intervals." *Vessel Head Penetration Inspection, Cracking and Repairs Conference*, U.S. NRC and ANL, September 29 – October 2, 2003.

⁵ *PWR Reactor Pressure Vessel (RPV) Upper Head Penetrations Inspection Plan (MRP-75): Revision 1*, EPRI, Palo Alto, CA: 2002. 1007337.

CONCLUSIONS REGARDING INSPECTION INTERVALS

The above described approach provides a rational basis for setting re-inspection intervals that result in a low probability of leakage and an extremely low probability of core damage as defined by Reg. Guide 1.174.

Because the nozzles and vessel head are rather flaw tolerant, typical results show that re-inspection of nozzles and J-groove welds every second or third refueling outage, in combination with bare metal visual inspection for leaks every refueling outage, maintains the requisite level of nuclear safety with a low risk of leakage.

INPUTS AND CONSTRAINTS TO SELECTING AN OPTIMUM STRATEGIC PLAN

There are a number of constraints that apply to establishing a cost-effective strategic plan. Issues that should be addressed include:

- The current condition of the vessel head must be established by non-destructive examination. The head must be free of cracking to remain in the moderate susceptibility category.
- The rate of future PWSCC initiation and growth should be predicted based on industry experience and modeling that accounts for differences between the subject plant and relevant industry peers.
- Non-destructive examination intervals should be selected such that there is a low risk of leakage and extremely low risk of core damage.
- Planned refueling outage durations can have a significant effect on establishing a strategic plan. For example, plants with short refueling outages will have little time for inspections or repairs without extending the outage, and plants in a long outage, such as for steam generator replacement or 10 year ISI, may have longer time available for inspections or repairs.
- The time and cost for nozzle inspections and repairs.
- The time and cost for replacement head procurement and installation. For example, inspections may show the need for immediate replacement while there may be a long delay to obtain a suitable replacement head.
- Potential remedial measures, including an assessment of their cost and effectiveness.
- Special attention should be given to the possibility of discovering leaks from a nozzle at an inopportune time such as during a mid-cycle outage conducted for another purpose, during system leak checks at the end of a refueling outage, or during a regular outage when a leak is discovered but no provisions have been made in advance for inspections or repairs.

NRC inspection requirements such as EA-03-009, *Issuance of Order Establishing Interim Inspection Requirements for Reactor Pressure Vessel Heads at Pressurized Water Reactors*, are obviously significant inputs to strategic planning. It is necessary to comply with the order or to obtain relaxation from the requirements based on appropriate technical assessments.

ALTERNATIVE MANAGEMENT APPROACHES

There are four main alternative management approaches for RPV heads. These are:

- Continue to inspect and make repairs as necessary to ensure a low risk of leakage and an extremely low risk of core damage.
- Perform remedial measures to reduce the risk of PWSCC and possibly to increase the inspection intervals.
- Replace the head as soon as possible after discovery of the first PWSCC.

- Replace the vessel head as quickly as possible and perform NDE at longer intervals based on the materials in the new head.

Comments on each of these approaches are as follows:

Inspect and Repair as Necessary

Inspection and repair methods are currently available to support the first alternative. The main nondestructive examination methods are volumetric NDE (UT) of nozzles plus volumetric examination for leakage paths through the annulus, or eddy current examination of the entire wetted surface of the nozzle and weld to show absence of cracks. Repair methods that have been used include removing shallow surface flaws, embedding deeper flaws, and removing the lower part of the nozzle and rewelding the bottom of the remaining nozzle to the head using a temper bead technique.

Remedial Measures

A number of remedial measures have been proposed for RPV head nozzles including:

- Modification of the internals flanges to increase bypass flow and thereby reduce the temperature of the vessel head. Some utilities have already performed this modification.
- Surface treatment of the nozzle and weld surfaces by shot peening or water jet conditioning to reduce the tensile stresses and, in the case of water jet conditioning, to remove small preexisting flaws.
- Nickel plating the nozzle and weld surfaces to keep the primary water coolant from contacting the Alloy 600 materials.
- Applying Alloy 152 weld overlays on the nozzles and welds.
- Roll expanding the nozzles into the vessel head to provide a redundant load path above the J-groove weld, and then conditioning the rolled surface to reduce the potential for new cracks.
- Application of a new structural weld between the nozzle and low-alloy steel vessel head, either on the top surface of the head or after boring out the lower part of the nozzle.
- Mechanical stress improvement.
- Zinc injection.

EPRI has sponsored testing of many of these remedial measures.⁶ Upon completion of the testing, the remedial measures were ranked in terms of effectiveness. The three main categories were:

- Most Effective
 - Water jet conditioning
 - Electro mechanical nickel brush plating
 - Shot peening
- Intermediate Effectiveness
 - Electroless nickel plating
 - GTAW weld repair
 - Laser weld repair

⁶ *Materials Reliability Program: An Assessment of the Control Rod Drive Mechanism (CRDM) Alloy 600 Reactor Vessel Head Penetration PWSCC Remedial Techniques (MRP-61)*, EPRI, Palo Alto, CA: 2003, 1008901.

- Least Effective
 - EDM skim cutting
 - Laser cladding
 - Flapper wheel surface polishing

To date, the main remedial measure applied in the field has been modification of the internals to increase the bypass flow and thereby reduce the head temperature. The lower head temperature should reduce the rates of crack initiation and growth based on the thermal activation energy. However, experience in France suggests that PWSCC may occur at head temperatures close to the reactor cold leg temperature. This is especially significant given the PWSCC at the South Texas Project Unit 1 bottom mounted instrument nozzles at a temperature of about 565°F. The South Texas Project experience shows that poor material properties and weld defects can result in PWSCC at temperatures lower than otherwise expected.

Finally, while remedial measures may reduce the rates of PWSCC initiation and growth, and thereby reduce the cost of future repairs, it may be difficult to take credit for the improvement in the form of increased inspection intervals.

Head Replacement

Installation of a new RPV head with improved nozzle and weld materials is a clear success path that has been taken in France and has been announced by many plants in the United States. The Alloy 690 nozzles and Alloy 52 J-groove welds in these heads should provide better service life than the original heads with Alloy 600 nozzle base material and Alloy 182 welds. In addition to the cost of the new head, consideration must be given to:

- Access provisions for getting the new head into containment.
- Whether the head will be installed with new CRDM drives.
- Disposal of the old head.

One variation on head replacement is to use this as an opportunity to replace the original design reactor head service structure with an improved service structure that requires less effort to disassemble and reassemble every outage. Figure 19 shows a typical original design head service structure and one possible configuration for an improved head service structure. As shown, the original design requires disassembly and removal of the following parts at the beginning of every refueling outage:

- Head insulation
- Head cooling ductwork
- CRDM cables
- Head cooling fans
- Head missile shield

An integrated head service structure, such as shown in Figure 19, can be developed for most plants. In this arrangement, most of the above listed components are integrated in such a manner that only one main lift is required after disconnecting the electrical cables to the CRDM drives.

While an integrated head service structure can reduce the required manpower, it may not result in a reduction of refueling outage critical path time since other constraints can establish the point in time

at which the head can be removed and replaced. Nevertheless, there are a number of significant benefits of an integral head service structure including:

- Freeing up labor and crane time inside containment during normal refueling outages.
- Reducing the risk of personnel injury by eliminating many crane lifts.
- Cutting several days off of the time required to perform a rapid head disassembly and reassembly such as for a leaking RPV flange o-ring seal or internals inspection after a slow rod drop test, etc.

ECONOMIC EVALUATIONS

In most cases, strategic plans will include some level of economic evaluation. A deterministic "best-estimate" approach can be used for these evaluations, provided the analysis includes sufficient detail and includes costs over the remaining plant life. In some cases, utilities may elect to perform a Monte Carlo type probabilistic analysis to provide better information of the range and probability of possible costs.

Regardless of the type of economic evaluation, the analysis should include the following:

- The risk of future cracks and leaks for each alternative considered.
- The cost of performing planned (preventive maintenance) work.
- The cost of making repairs (corrective maintenance).
- The value of lost production.
- The value of consequential risks.
- The potential risk that leaks will be discovered at inopportune times such as during a mid-cycle outage or during a system leak check at the end of an outage.
- The planned operating life, including life extension.
- The discount and inflation rates.

Guidance on developing strategic plans is provided in EPRI report 1000806, *Demonstration of Life Cycle Management Planning for Systems, Structures, and Components with Pilot Applications at Oconee and Prairie Island Nuclear Stations*. Deterministic type economic analyses can be performed using the LcmVALUE version 1.0 software prepared as part of the EPRI LCM demonstration program.

Figure 20 shows typical results of net present value calculations for a moderate susceptibility plant. The figure shows the discounted net present value cost over the remaining plant life including preventive maintenance, corrective maintenance, value of lost production and consequential costs.

CONCLUSIONS

For the sample strategic planning case presented, the optimum alternative appears to be bare metal visual inspections of the RPV head every refueling outage with nondestructive examinations of the nozzles and J-groove welds every second refueling outage.

- As future inspection data become available and predictive models are refined, there may be a technical basis for retaining inspections every second outage when the plant enters the high susceptibility category based on EDYs.
- Volumetric examination every outage and immediate head replacement appear significantly more expensive.

- Remedial measures such as reducing head temperature or waterjet conditioning may be attractive provided inspection intervals can be increased as a result of the effort.
- A reasonable longer term plan is to replace the vessel head the second outage after identifying PWSCC.

These results are plant specific, and other plants may have different constraints that would affect the optimum solution.

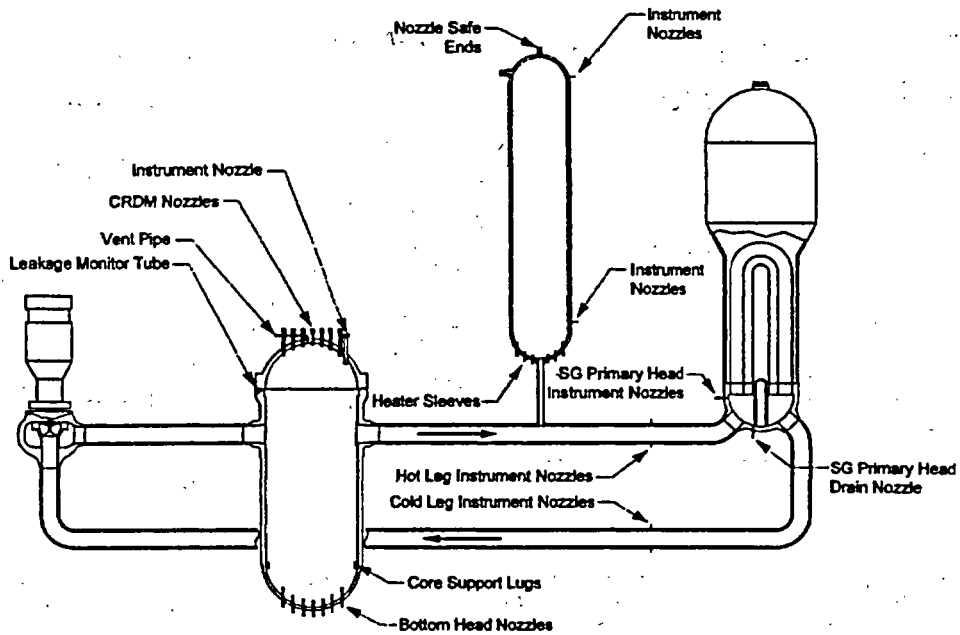


Figure 1
Locations of Thick Section Alloy 600 Materials

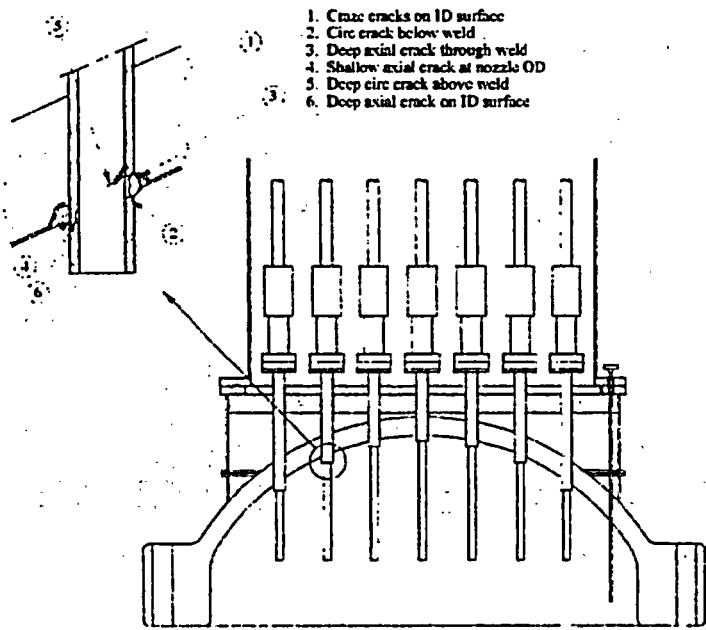
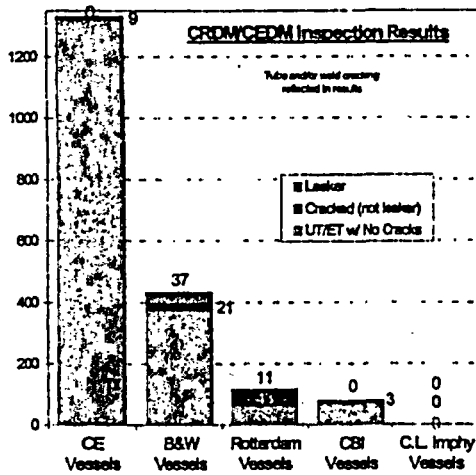
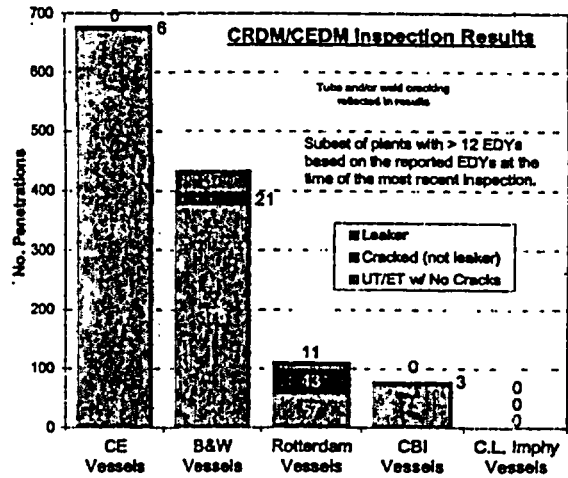


Figure 2
Typical PWR Reactor Vessel Head (RVH) Nozzle PWSCC



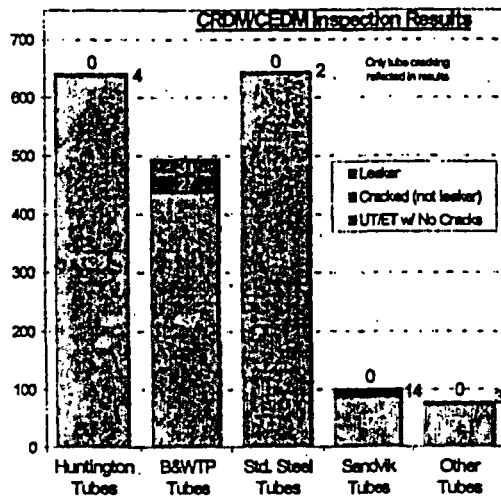
All Plants



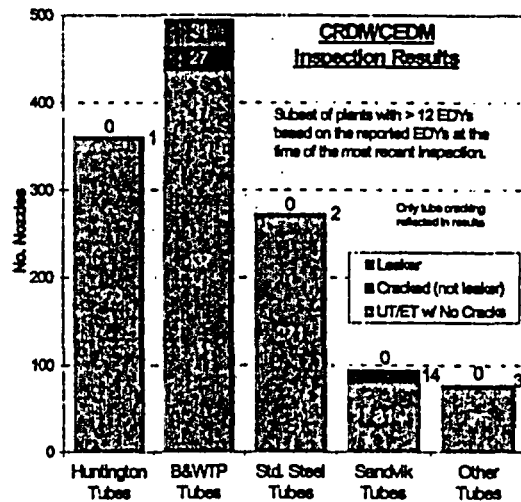
Plants >12 EDY

* Results compiled under EPRI sponsorship (see G. White, N. Nordmann, L. Mathews, and C. King, "Summary of U.S. PWR Reactor Vessel Head Nozzle Inspection Results," NRC-ANL Conference on Vessel Head Penetration Inspection, Cracking, and Repairs, September 29 - October 2, 2003, Gaithersburg, Maryland)

Figure 3
Inspection Results by Vessel Head Fabricator*



All Plants



Plants >12 EDY

* Results compiled under EPRI sponsorship

Figure 4
Inspection Results by Nozzle Material Supplier*

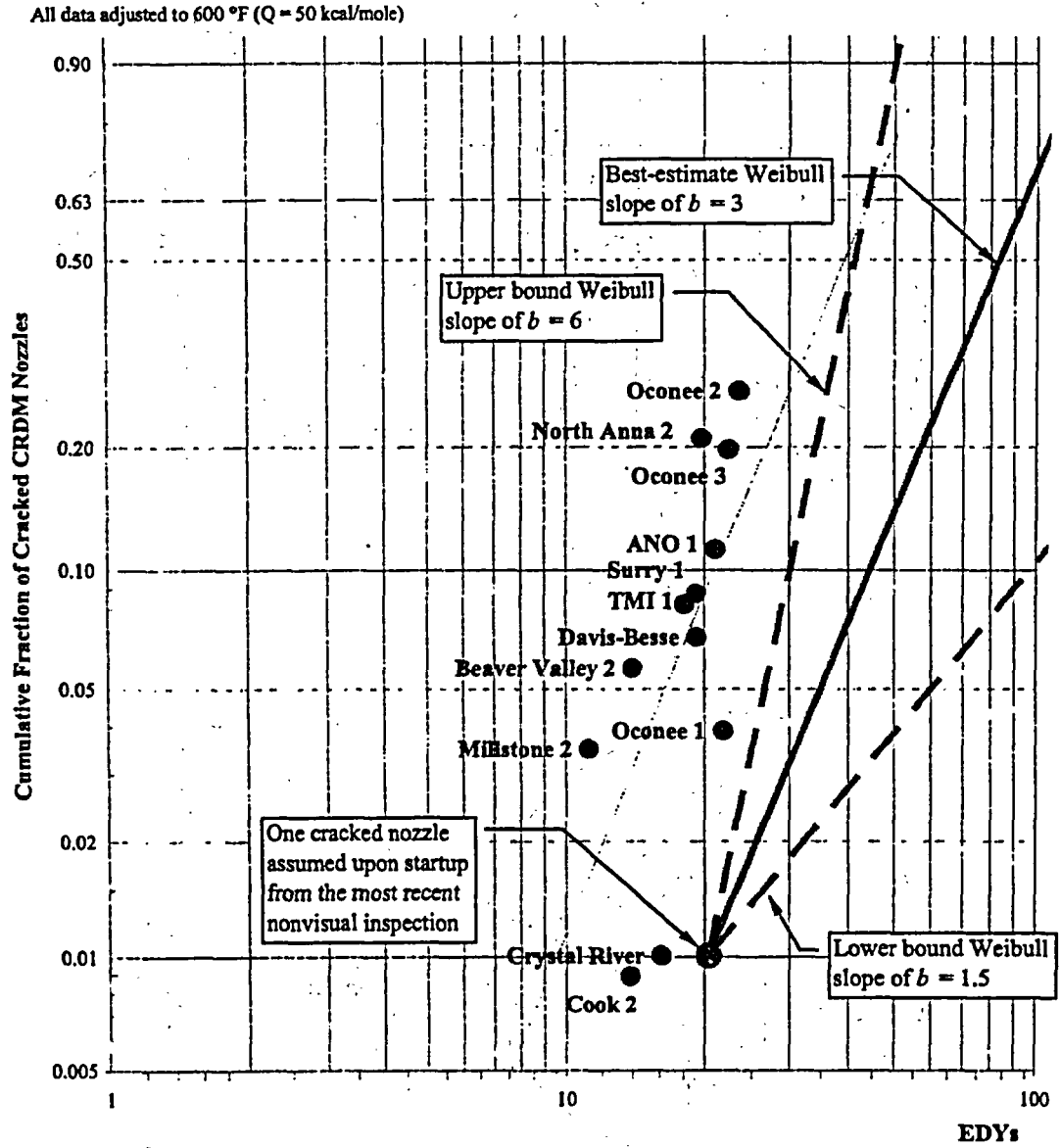


Figure 5
Weibull Statistical Model for Time to Cracks/Leaks

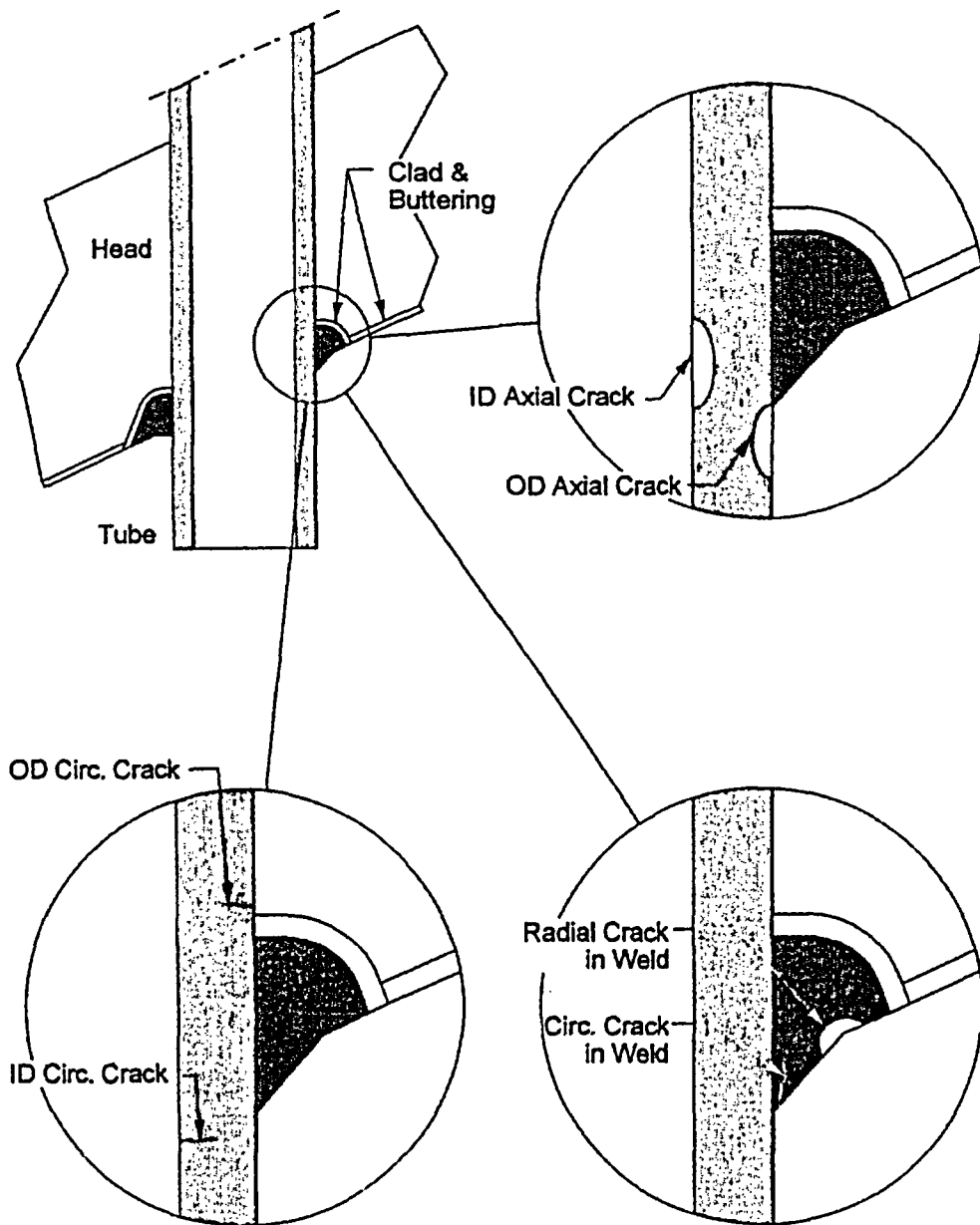


Figure 6
Modeled Flaw Geometries

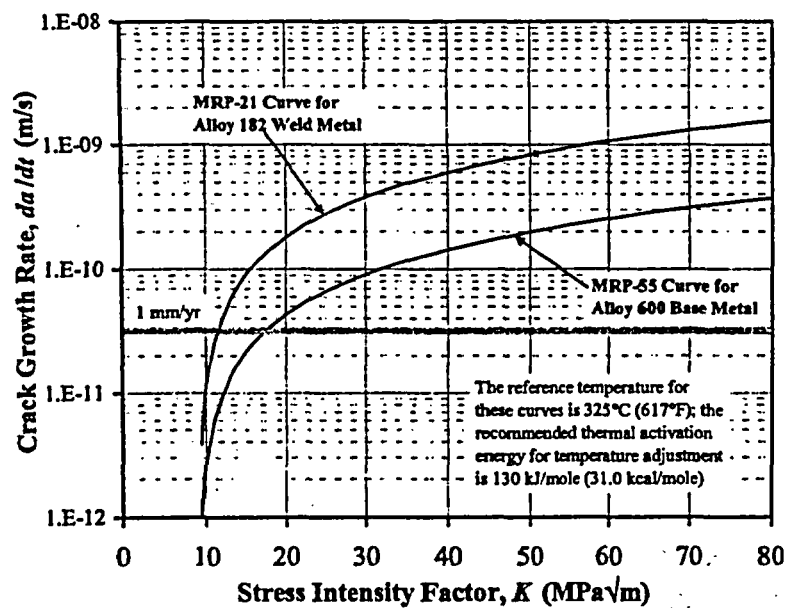
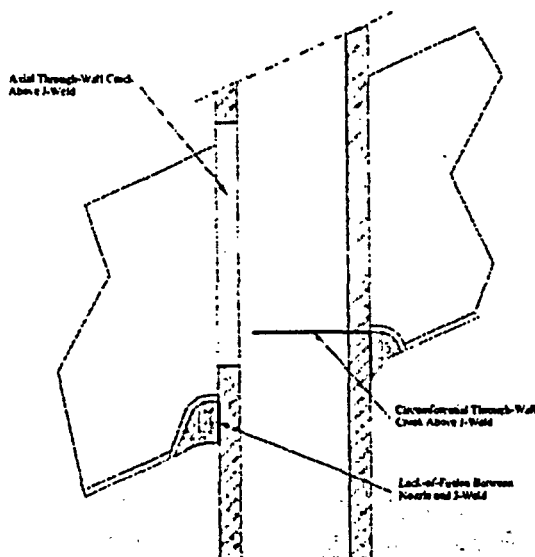


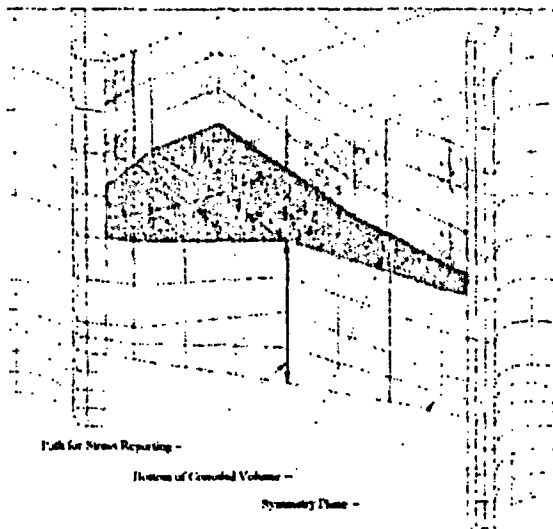
Figure 7
Crack Growth Rates for Alloy 600 Base Metal and Alloy 182 Weld Metal



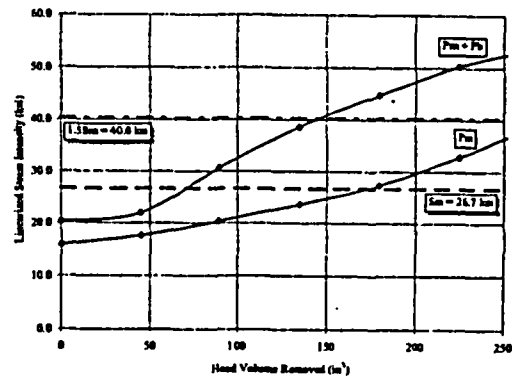
Typical Results for CRDM Nozzle

	2500 psi	6750 psi
Axial through-wall flaw in nozzle above J-weld	14.3 inches	5.3 inches
Circ. through-wall flaw above J-weld	330°	284°
Lack of fusion between nozzle and weld	327°	271°

Figure 8
Tolerance to Axial and Circumferential Cracks

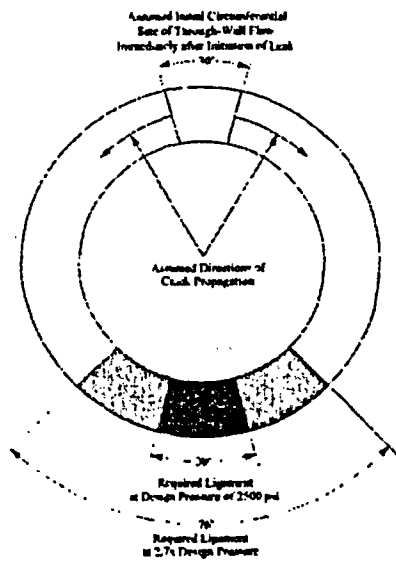


Finite Element Model of Representative Head



Primary Membrane and Membrane Plus Bending Stress as Function of Wastage Volume

Figure 9
Tolerance to Boric Acid Wastage



Typical Critical Flaw Size of 330°



Example of Operating Stress Perpendicular to Circ Crack Plane

Figure 10
Crack Growth Around Nozzle Circumference Above J-Groove Weld

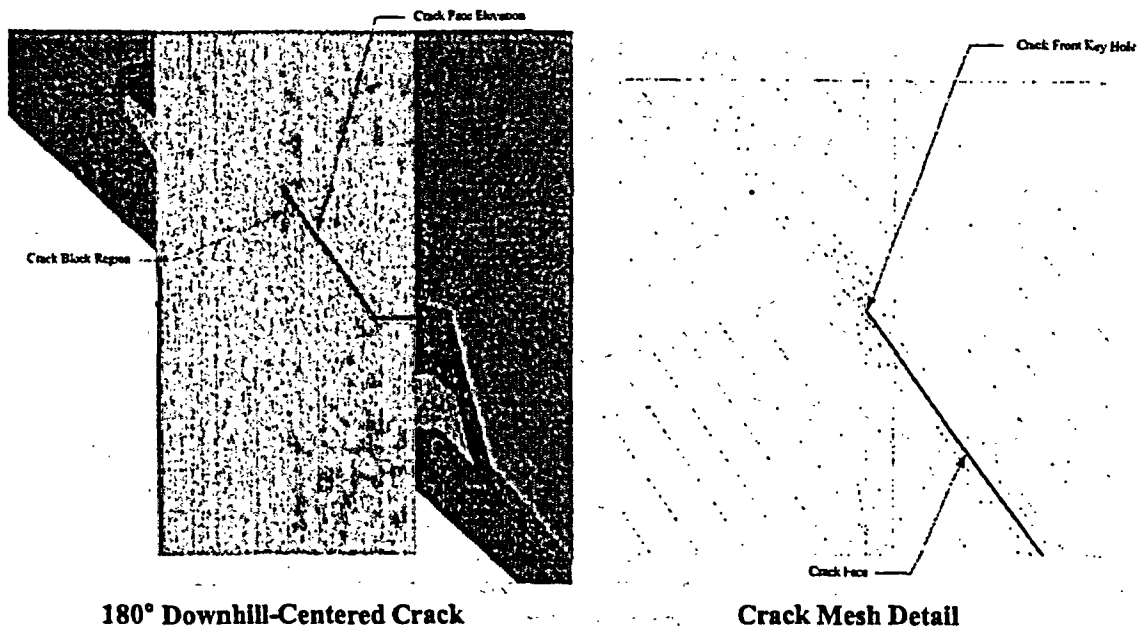


Figure 11
 Example Fracture Mechanics Model for Nozzle Circumferential Cracks

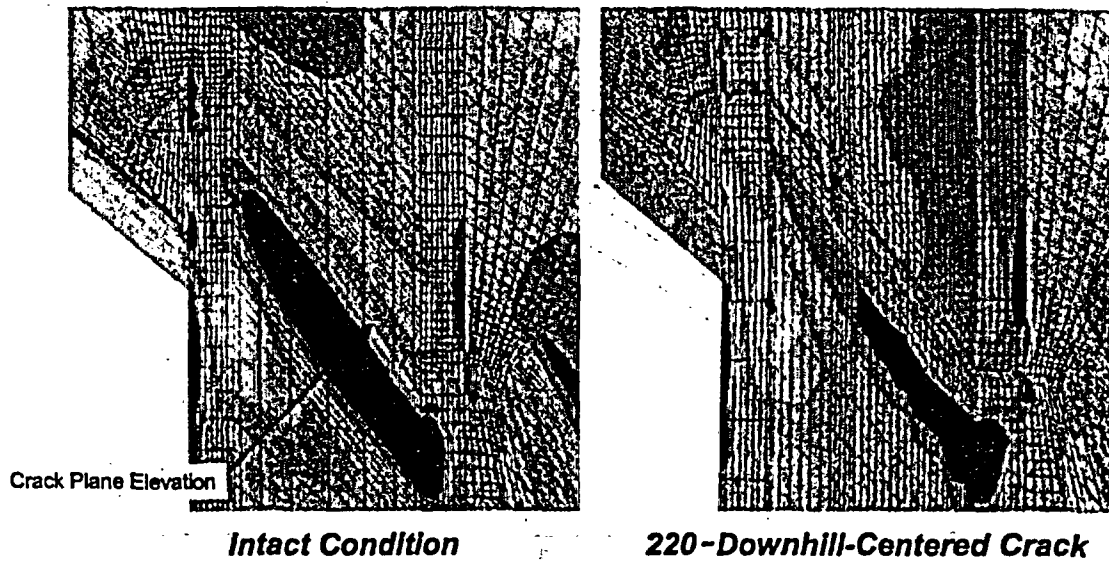


Figure 12
 Relief of Welding Residual Stress with Circumferential Crack Growth – Operating Condition Axial Stress

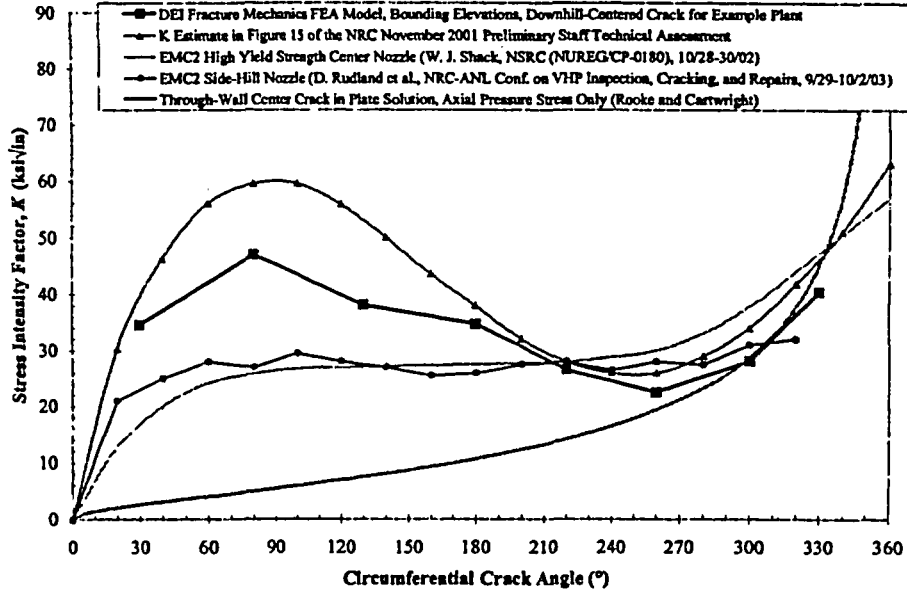


Figure 13
Stress Intensity Factor Calculation Results for Downhill Centered Circumferential Crack

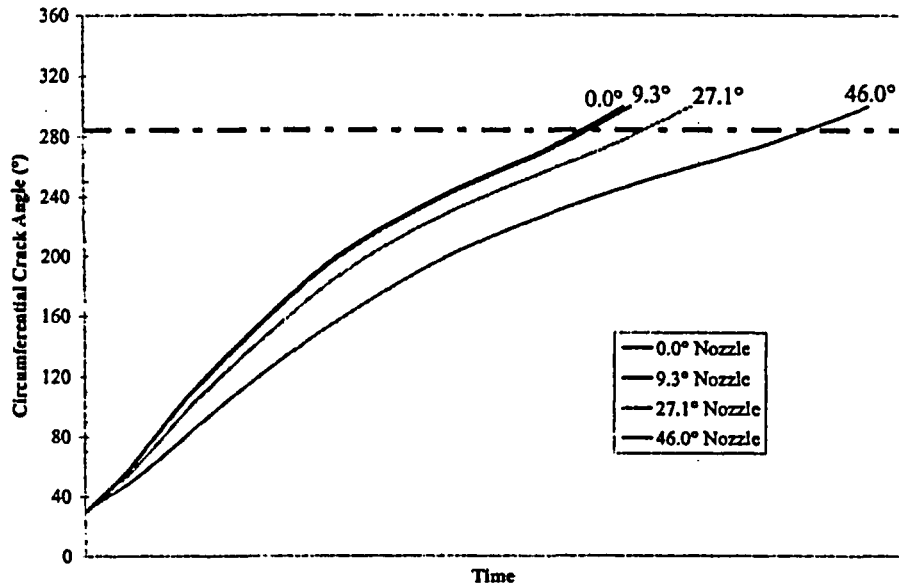


Figure 14
Example Deterministic Results for Circumferential Crack Growth

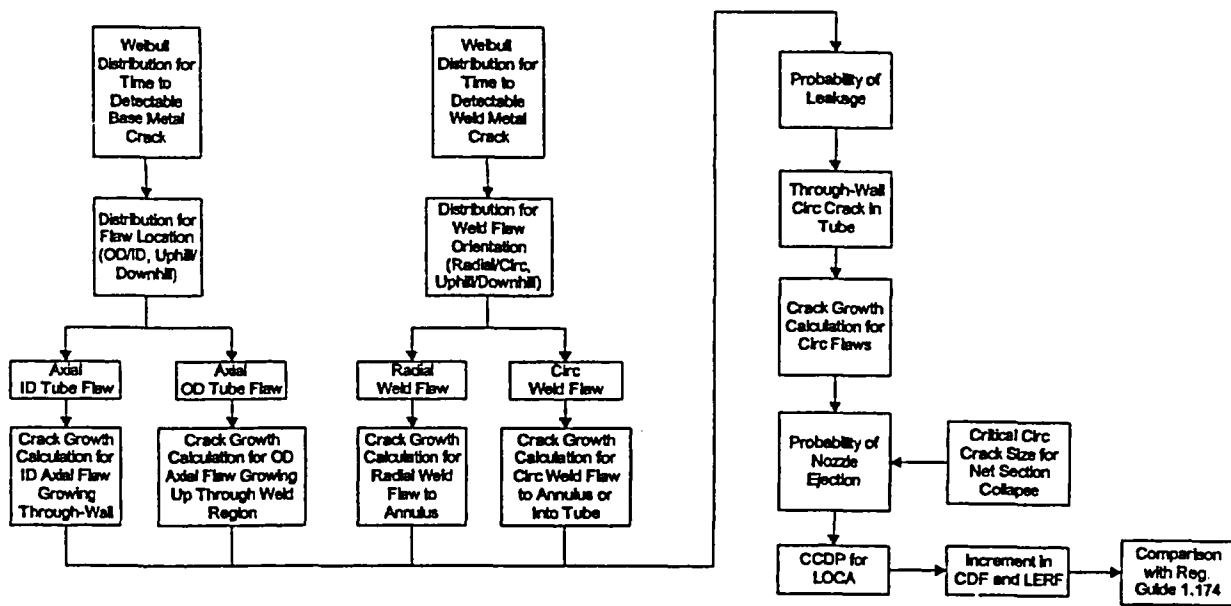


Figure 15
Simplified Monte Carlo Probabilistic Model for Nozzle Ejection

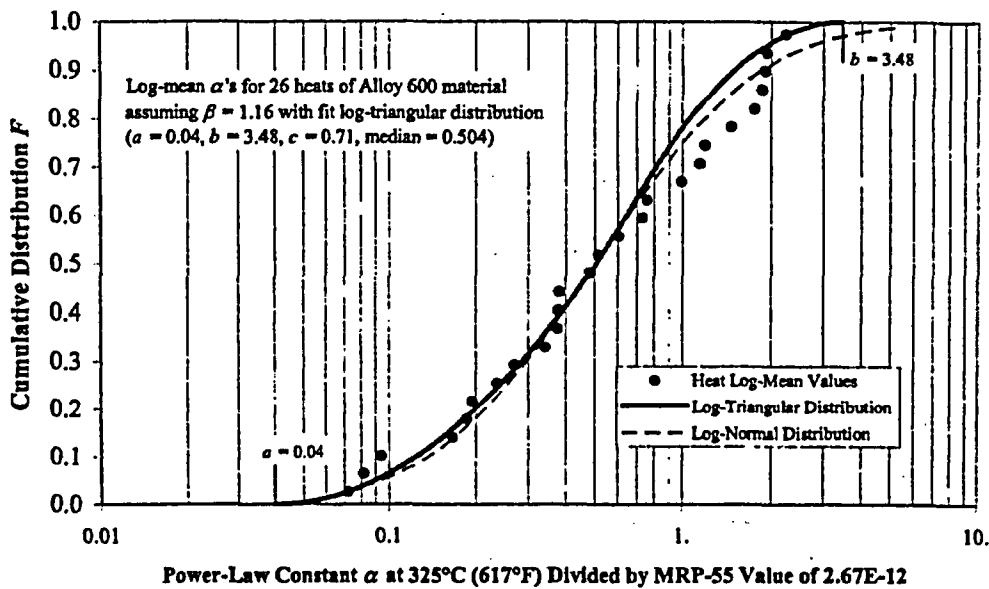


Figure 16
Crack Growth Rate Distribution for Alloy 600 Base Metal (MRP-55)

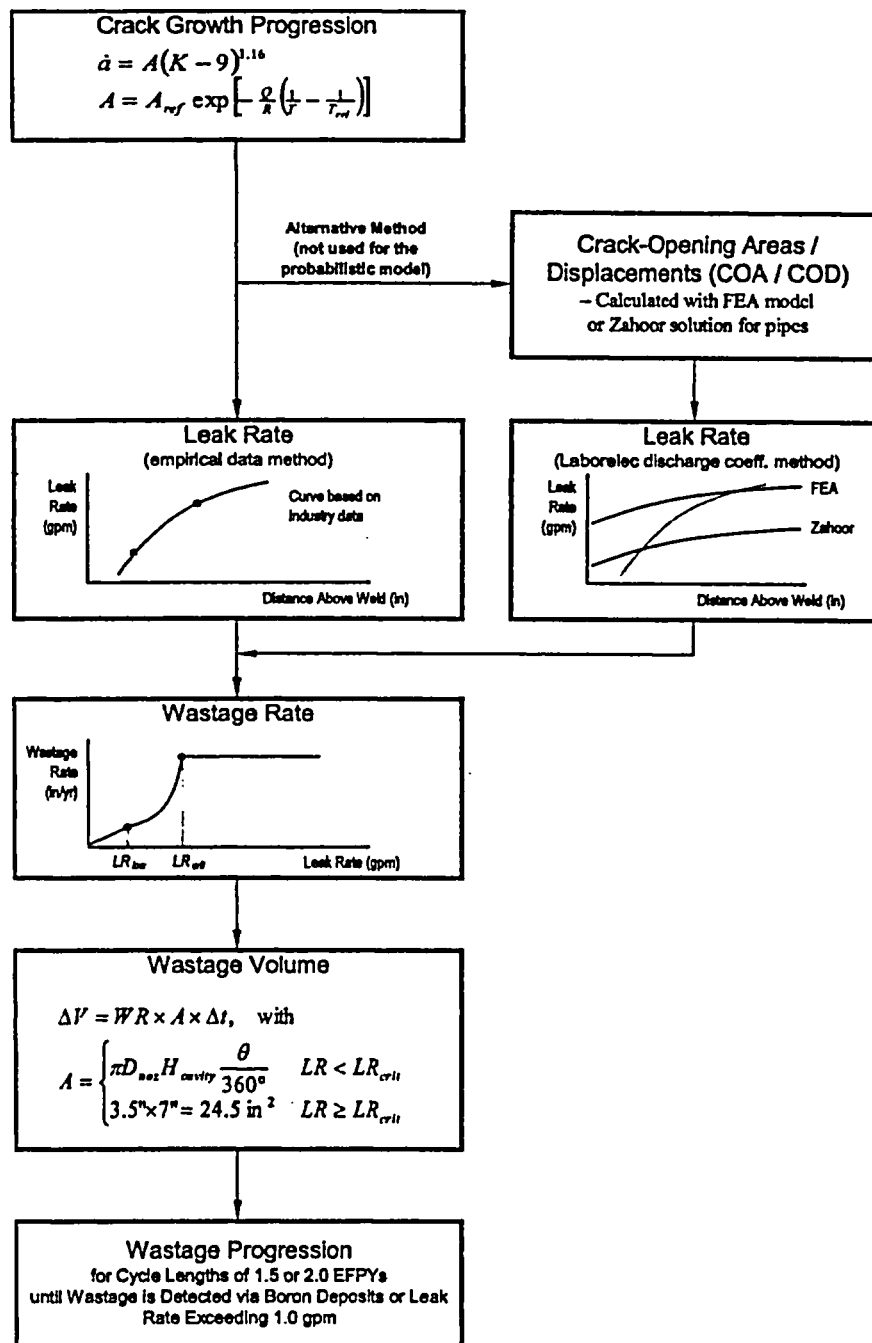


Figure 17
Boric Acid Wastage Model (MRP-75)

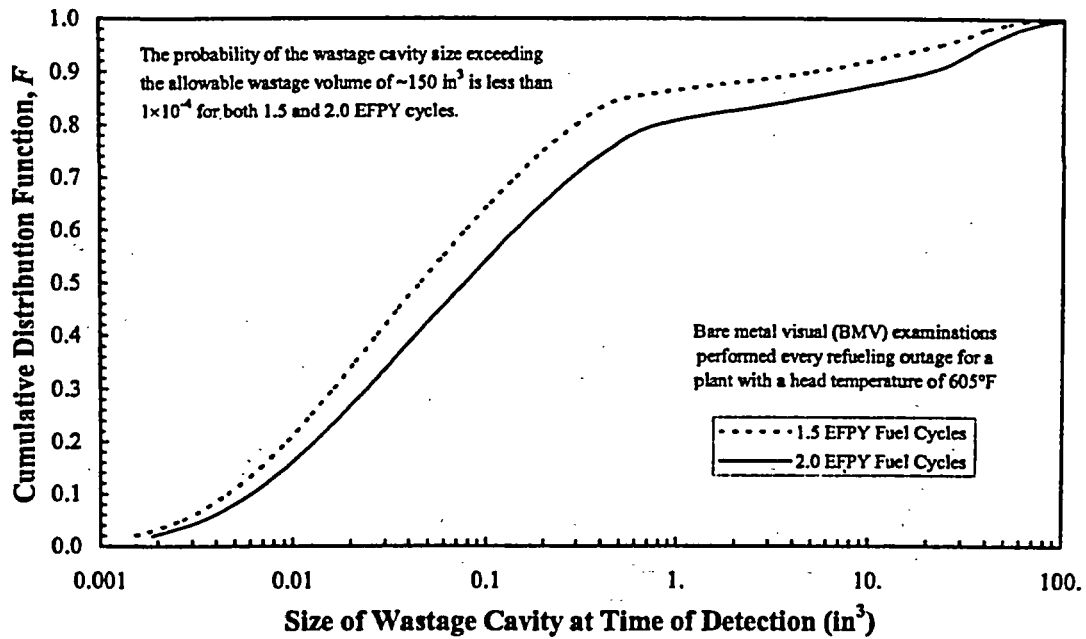
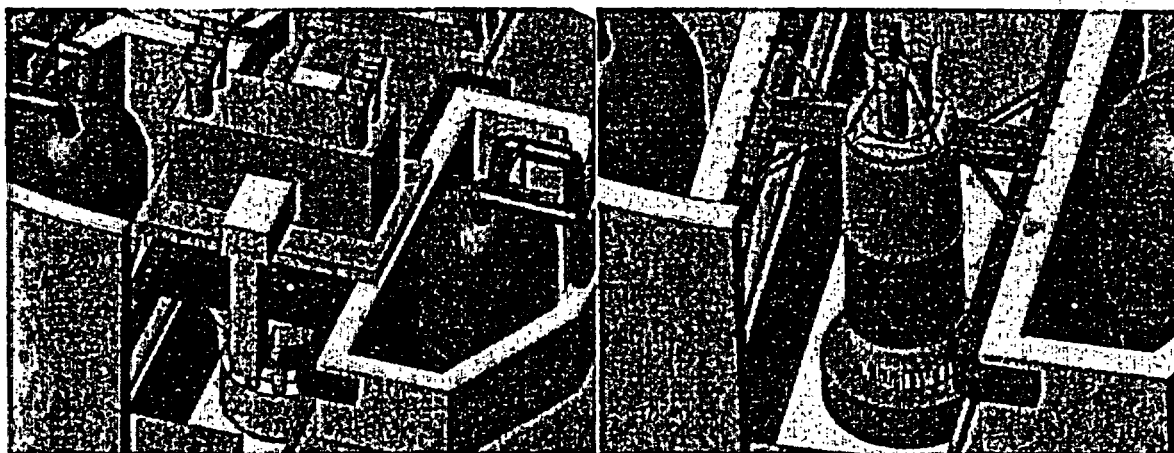


Figure 18
 Results of Probabilistic Wastage Analysis for a Single Leaking Nozzle (Assuming Bare Metal Visual Inspections are Performed During Each Refueling Outage)



Typical Original Structure

Conceptual Integrated Structure

Figure 19
 Head Replacement – Integrated Head Service Structure Option

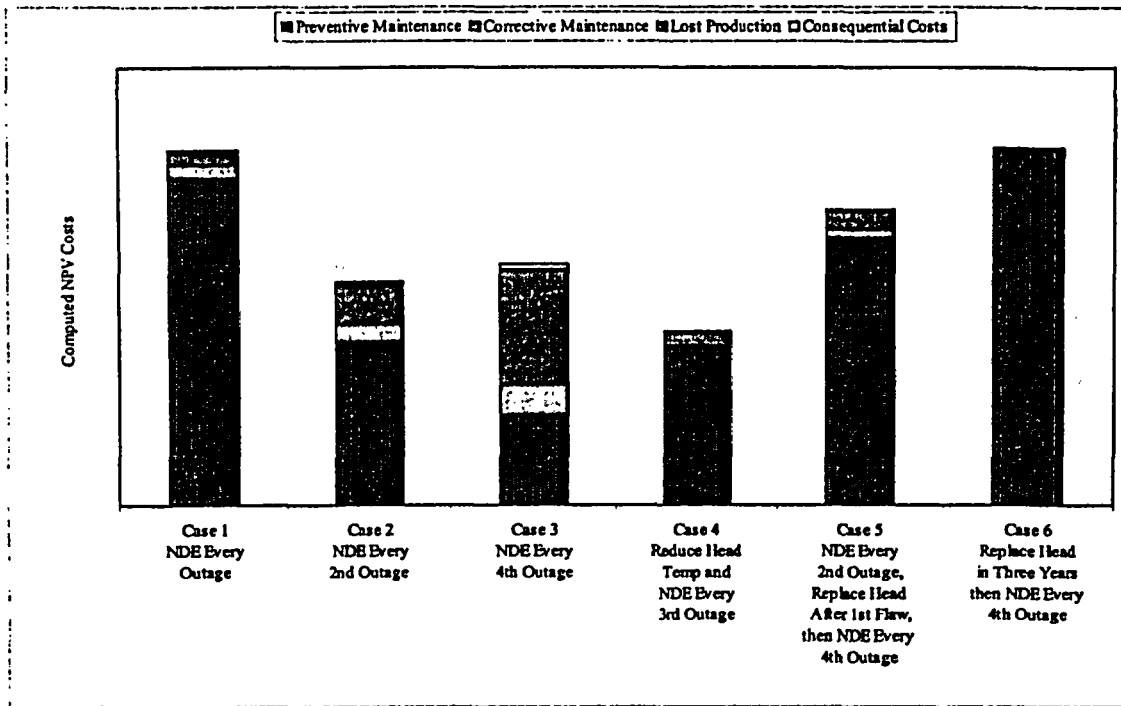


Figure 20
Typical Life Cycle Management Economic Results for Moderate Susceptibility Plant

Latest Results of the United States Nuclear Regulatory Commission Pressurized Thermal Shock Rule Re-evaluation Project¹

T.L. Dickson, Computational Science and Engineering Division, Oak Ridge National Laboratory,
Oak Ridge, Tennessee, USA

M.T. Kirk, C.G. Santos, Office of Nuclear Regulatory Research,
U.S. Nuclear Regulatory Commission, Washington, DC

ABSTRACT

The current federal regulations to insure that nuclear reactor pressure vessels (RPVs) maintain their structural integrity when subjected to transient loading conditions such as pressurized thermal shock (PTS) events were derived from computational models developed in the early-mid 1980s. Since that time, there have been advancements in relevant technologies associated with the modeling of PTS events that impact RPV integrity assessment. These updated computational models have been implemented into the FAVOR (Fracture Analysis of Vessels: Oak Ridge) computer code. An objective of the United States Nuclear Regulatory Commission (USNRC) PTS rule re-evaluation project is to determine if application of improved technology can provide a technical basis to reduce the conservatism in the current regulations while continuing to provide reasonable assurance of adequate protection to public health and safety. A relaxation of PTS regulations could have profound implications for plant license renewal considerations. As part of the re-evaluation project, the FAVOR code has been applied to three domestic commercial pressurized water reactors (PWRs). This paper discusses the application of the updated integrated computational methodology to the three PWRs and discusses the results and interpretation of those results.

PROBLEM DEFINITION, CURRENT REGULATIONS, AND PTS ANALYSIS RESULTS

The issue of pressurized thermal shock (PTS) arises because cumulative neutron irradiation exposure makes the reactor pressure vessel (RPV) more brittle (i.e., reduced ductility and fracture toughness) and, therefore, increasingly susceptible to cleavage (brittle) fracture over its operating life. The degree of embrittlement of RPV steel is quantified by changes in the reference nil-ductility transition temperature, RT_{NDT} . The radiation-induced shift in RT_{NDT} is a function of the chemical composition of the steel, the neutron irradiation exposure, RPV operating temperature, and the initial unirradiated transition temperature, RT_{NDT_0} .

¹ Research Sponsored by the Office of Nuclear Regulatory Research, U.S. Nuclear Regulatory Commission under Interagency Agreement 1886-N011-9B with the U.S. Department of Energy under Contract DE-AC05-00OR22725 with UT-Battelle LLC. The submitted manuscript has been authored by a contractor of the U.S. Government. Accordingly, the U.S. Government retains a nonexclusive, royalty-free license to publish or reproduce the published form of this contribution, or allow others to do so, for U.S. Government purposes. This report was prepared as an account of work sponsored by an agency of the United States government. Neither the United States government nor any agency thereof, nor any of their employees, makes any warranty, express or implied, or assumes any legal liability or responsibility for the accuracy, completeness, or usefulness of any information, apparatus, product, or process disclosed, or represents that its use would not infringe privately owned rights. Reference herein to any specific commercial product, process, or service by trade name, trademark, manufacturer, or otherwise, does not necessarily constitute or imply its endorsement, recommendation, or favoring by the United States government or any agency thereof. The views and opinions of authors expressed herein do not necessarily state or reflect those of the United States government or any agency thereof.

In PWRs, transients can occur that result in severe overcooling (thermal shock) of the RPV concurrent with or followed by high repressurization. Thermal transients in which the temperature of the coolant in contact with the inner surface of the RPV decreases with time results in time-dependent gradients and resulting tensile stresses across the RPV wall. Both pressure and thermal stresses are tensile stresses that tend to open existing cracks located on or near the inner surface of RPV. If an aging RPV is subjected to a PTS event, flaws on or near the inner surface could potentially initiate in cleavage fracture and propagate through the RPV wall, thus introducing the possibility of RPV failure.

In the early to mid 1980's, working from the state-of-the-art technology at that time, the nuclear industry, the NRC staff, and others performed a number of investigations aimed at assessing the risk imposed by PTS. These efforts led to the publication by the staff of SECY 82-465 [1], which provided the technical basis for what has come to be known as the PTS rule [2]. Results from these analyses, combined with the judgement that a 5×10^{-6} yearly probability of developing a through-wall crack due to PTS is acceptable, led to the establishment of the current screening limits or maximum values of RT_{NDT} permitted during the operating life of the plant. The maximum values of RT_{NDT} allowed by the current PTS rule are 270 °F for axial welds, plates, and forgings and 300 F for circumferential welds. The PTS rule requires plants that desire to operate beyond the screening criteria to submit an integrated plant-specific safety analysis to the NRC three years before the PTS screening limit is anticipated to be reached for any material in the RPV beltline. The NRC subsequently developed Regulatory Guide 1.154 [3] regarding the format and content of analyses that could be used to demonstrate the continued safe operation of RPVs that exceeding the PTS screening criterion.

Figure 1 is a curve from SECY 82-465, from which the current PTS screening criteria was derived, which established a correspondence between a value of RT_{PTS} of 270 °F and a thru-wall crack frequency of 5×10^{-6} failed RPVs per year. Here, RT_{PTS} is the metric currently used to quantify the embrittlement of the RPV and is defined as the maximum value of RT_{NDT} in the entire RPV beltline plus a margin term to account for uncertainties. Figure 1 also includes the results of PTS analyses recently performed for three commercial PWRs as part of the PTS re-evaluation study, i.e., the mean value of the thru-wall crack frequency (TWCF) as a function of increasing RT_{PTS} . These TWCF are considerably less than those generated in SECY 82-465. Specifically, figure 1 illustrates that the values of TWCF corresponding to the current screening criteria of 270 °F are approximately $7.0e-09$, $7.0e-08$, and $5.0e-07$ for the Beaver Valley, Oconee, and Palisades plants, respectively. The results of these analyses will be discussed in more detail below.

When a flaw is predicted to initiate in cleavage fracture, it has two possible outcomes during the duration of the transient. It either propagates through the RPV wall thickness causing RPV failure, or it experiences a stable arrest at a location in the wall. In either case, the advancement of the crack tip through the RPV wall may involve a sequence of *initiation / arrest / reinitiation* events. The failure criterion used in the analyses discussed in this paper are that a RPV is considered as failed if a flaw propagated through 90 per cent of the wall thickness or fails due to plastic instability of the remaining ligament.

OVERVIEW OF PTS RE-EVALUATION PROJECT

Preliminary studies [4] performed in 1999 suggested that the application of improved technology could reduce the conservatism in the current PTS regulations while continuing to provide reasonable assurance of adequate protection to public health and safety. Based on the above, in 1999, the USNRC initiated a comprehensive project, with the nuclear power industry as a participant, to develop an improved integrated computational methodology that eliminated known conservatisms and provides a more realistic characterization of risk associated with PTS. Figure 2 illustrates elements of the improved fracture-related technology that have been integrated into the FAVOR computer code [5].

Analogous to the Integrated Pressurized Thermal Shock studies [6-8] performed in the 1980s, the PTS Re-evaluation Project plan included the analysis of a number of commercial PWRs with the objective to cover the range of various system designs, operational procedures, and training programs. To date, analyses have been performed for the Westinghouse-designed Beaver Valley plant, the Babcock and Wilcox designed Oconee plant, and the Combustion Engineering designed Palisades plants. Additional analyses will be performed as necessary to insure that any revision to the PTS rule may be applied generically to all commercial PWRs. The PTS analysis results presented in this paper were generated by the 02.4 version of FAVOR.

DETAILED NEUTRON FLUENCE MAPS AND RVID

In the PTS analyses performed in SECY 82-465, from which the current PTS regulations were derived, a single value of neutron fluence and chemistry were assumed to apply to the entire RPV beltline, which conservatively assumes that all of the RPV materials were made of the most brittle of its constituent material.

FAVOR utilizes a methodology that allows the RPV beltline (defined to include the RPV material from one foot below the active core to one foot above the active core) to be divided into major regions such as axial welds, circumferential welds, and plate regions. These major regions may be further discretized into subregions to accommodate very detailed neutron fluence maps provided by Brookhaven National Laboratory (BNL) that include the azimuthal and axial variations in neutron fluence. Detailed neutron fluence maps were provided for each of the three plants corresponding to 32 and 40 effective full power years (EFPY).

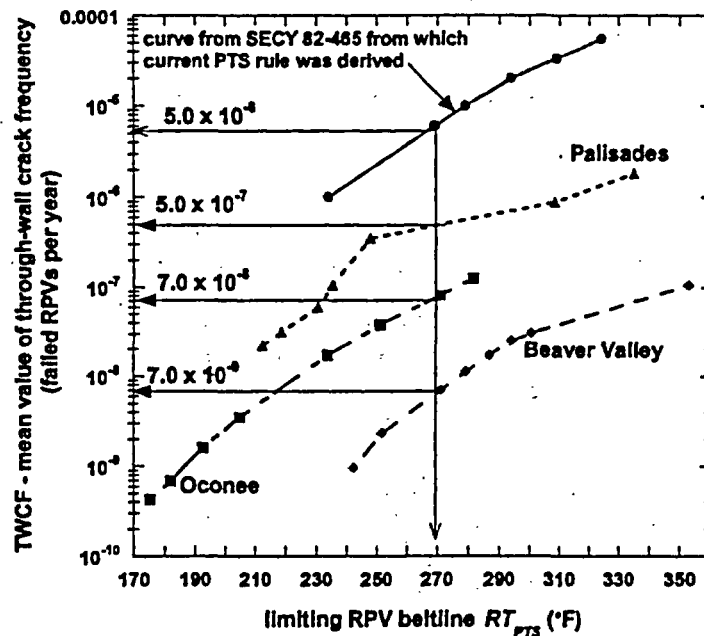


Figure 1 - Results of current PTS re-evaluation program compared to results from SECY 82-465 from which the current PTS screening criteria was derived in early 1980s

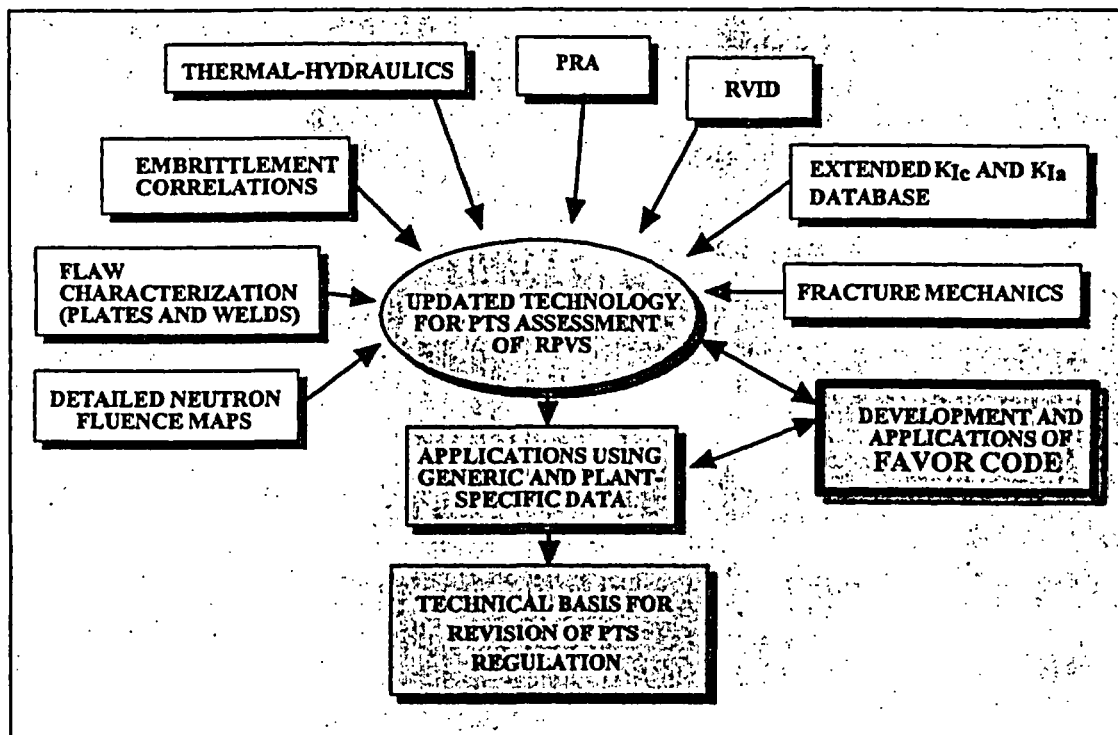


Figure 2 – Elements of improved fracture-related technology are integrated through the application of the FAVOR computer code, which has been applied in the USNRC PTS re-evaluation program.

As an example, the fluence map provided by BNL for the Oconee plant contained 13,080 discrete values of neutron fluence (60 azimuthal x 218 axial) corresponding to one-eighth of the RPV azimuth (45 degree sector); therefore, the entire 360 degree beltline region would have to be discretized into 104,640 subregions to accommodate the level of detail provided by the BNL. In practice, one may take advantage of symmetry to include this amount of detail with a considerably smaller number of subregions. The discretization used to model the level of detail of neutron fluence for Oconee, Beaver Valley, and Palisades was 19651, 15280, and 67076 subregions.

The modeling and procedures used in generating these neutron fluence maps were based on the guidance provided in the NRC Draft Regulatory Guide DG-1053 [9]. The calculations were performed using the DORT discrete ordinates transport code [10] and the BUGLE-93 [11] forty-seven neutron group ENDF/B-VI nuclear cross sections and fission spectra.

The Reactor Vessel Integrity Database, RVID [12], developed by the NRC, provides a key source of input data for FAVOR. RVID summarizes the properties for the RPV beltline materials for each operating commercial nuclear power plant. The chemistries (copper, nickel, and phosphorus) and values of RT_{NDT0} (initial unirradiated values of RT_{NDT}) for each of the RPV major regions used as input to FAVOR were taken from RVID.

IMPROVED FLAW CHARACTERIZATION

The single largest improvement in the updated computational methodology is the establishment of a technical basis for the postulation of flaws. The probabilistic fracture mechanics (PFM) model utilized in SECY 82-465 conservatively postulated all fabrication flaws to be inner-surface breaking flaws. Specifically, the model assumed the RPV had six axially oriented infinite length inner-surface breaking flaws with their size distributed according to the OCTAVIA distribution.

The USNRC-sponsored research at Pacific Northwest National Laboratory (PNNL) has resulted in the postulation of fabrication flaws based on the non-destructive and destructive examination of actual RPV material. Such measurements have been used to develop characterizations of the number, size, and location of flaws in various types of weld and base metal used to fabricate vessels. This has provided a technical basis for the flaw data that is critical input data into FAVOR. These measurements have been supplemented by expert elicitation [13]. Separate distributions have been developed to characterize the number and size of flaws in weld and plate regions. The reader is referred to References 14-16 for the details of this research. The flaw depth distributions used in these analyses were truncated at 23 per cent and 5 per cent of the RPV wall thickness for flaws in weld and plate regions, respectively.

A major result of the PNNL flaw characterization research is that RPV material has a much higher density of flaws than was postulated in the model utilized in the PFM analyses from which the current PTS regulations were derived; however, all of the flaws detected thus far have been embedded. Application of the improved PNNL flaw characterization results in an average of 7937, 4848, and 5772 postulated flaws for Oconee, Beaver Valley, and Palisades, respectively, in each stochastically generated RPV modeled in the Monte Carlo PFM analysis. Nearly all of the postulated flaws are embedded flaws distributed uniformly through the first 3/8 of the RPV wall thickness.

During the Monte Carlo PFM analysis, the fracture response of each postulated flaw in a RPV is assumed to be physically and statistically independent of all other flaws postulated in that RPV.

IMPROVED EMBRITTLEMENT CORRELATION

Embrittlement correlations are used to predict the neutron-irradiation-induced increase in embrittlement, as characterized by a shift in the nil-ductility transition temperature (ΔRT_{NDT}), over the operating life of the RPV. The current regulatory correlation, described in Regulatory Guide 1.99, Revision 2 [17] is based on analysis of Charpy V-notch impact-energy test data available in 1984. Since then, a significantly larger body of Charpy surveillance data has become available, and the understanding of embrittlement mechanisms has advanced. The result is that improved embrittlement correlations have recently been developed by research sponsored by the NRC. These improved correlations have been published by researchers from Modeling and Computing Services and the University of California at Santa Barbara [18].

IMPROVED THERMAL HYDRAULICS AND PRA

The PTS analyses performed in SECY 82-465 were based on a highly simplified treatment of plant transients (very coarse groupings of many operational sequences), necessitated by limitations in computational resources required to perform multiple thermal hydraulic and PFM analyses. Also, no significant credit was given for operator action.

For the current PTS analyses, a comprehensive search was performed for each plant for transients that are both probabilistically credible and physically significant. The base case transients were identified by

development of a PRA model for each plant that addressed possible over-cooling transients that could occur. The identification of the possible over-cooling scenarios for each plant consisted of a review of the current plant design, recent operating history, latest procedures, present-day operator training, and feedback from the ongoing thermal-hydraulic analyses. The PRA model development for each plant involved two visits to the plant, where plant staff input was obtained and plant staff comments on the PRA, including the human reliability assessments, were received and incorporated. Additionally, during the first visit, over-cooling events were simulated on the plant simulator to gain insights about operator responses to such events.

Sandia National Laboratory generated a probability distribution of the transient frequency (events per reactor operating year) for each of the base case transients. The SAPHIRE Version 7 [19] code was used to generate the probability distributions. Hence, the scenarios modeled in the PRA and quantified using the SAPHIRE code, included a cooperative effort with plant staff to ensure that the model reflected current design and practices, and appropriate estimates for the means and uncertainties for the initiator frequencies as well as equipment and human failure probabilities.

Information Sciences Laboratories (ISL) provided thermal hydraulic boundary conditions for the 55, 61, and 29 base case transients for Oconee, Beaver Valley, and Palisades, respectively. The selection of these transients was based not only on thermal hydraulic and anticipated fracture mechanics considerations, but also on PRA input regarding scenarios of sufficient likelihood to be of potential concern to PTS. The thermal-hydraulic calculations were performed using the RELAP5/MOD3 code [20].

IMPROVED FRACTURE TOUGHNESS MODEL

The computational model for quantification of fracture toughness uncertainty is improved in two ways: (1) the fracture initiation toughness (K_{Ic}) and crack arrest (K_{Ia}) databases were extended by 83 and 62 data values, respectively, relative to the databases in the EPRI report [21] and (2) the statistical representations for K_{Ic} and K_{Ia} were derived through the application of rigorous mathematical procedures. Bowman and Williams [22] provide details regarding the data and mathematical procedures. A Weibull distribution, in which the parameters were calculated by the *Method of Moments* point-estimation technique, forms the basis for the new K_{Ic} statistical model. The new K_{Ia} model is based on a lognormal distribution.

IMPROVED FRACTURE MECHANICS

One particularly significant improvement in fracture mechanics modeling capability is the addition of the phenomena known as warm-prestress (WPS) which is now available in FAVOR as a user-option. The concept of the WPS effect is that a crack tip cannot initiate in cleavage fracture in a stress field that is decreasing with respect to time. The results reported in this paper for Oconee, Beaver Valley, and Palisades included warm-prestress. The analyses performed in SECY 82-465, from which the current PTS screening criteria was derived, did not include WPS. A limited number of sensitivity analyses were performed for Oconee and Beaver Valley to quantify the impact of WPS on TWCF. The impact of the inclusion of WPS was to reduce the TWCF by between a factor of 2 and 5. The impact decreases over the operating life of the plant.

IMPROVED PFM METHODOLOGY

The PFM model in SECY 82-465 [1] utilized a methodology that produced a Boolean result for cleavage fracture initiation and RPV failure, i.e., the outcome for each RPV in the Monte Carlo analysis was fracture or no fracture and failure or no failure. The conditional probability of crack initiation (CPI) was calculated simply by dividing the number of RPVs predicted to experience cleavage fracture by the total number of simulated RPVs. Similarly, the conditional probability of RPV failure CPF was calculated by

dividing the number of RPVs predicted to fail by the total number of simulated RPVs. The final results were discrete values for *CPI* and *CPF*, without any quantification of the uncertainty in the solution. The improved PFM model provides for the calculation of probability distributions of *CPI* and *CPF* and thus for the quantification of uncertainty in the results. The reader is referred to reference 23 for a more detailed explanation of the improved PFM model.

The overall PRA methodology for PTS integrates these probability distributions of *CPI* and *CPF* with distributions of transient initiating frequencies (events per reactor year) derived from plant system and human interaction considerations. Output from this process includes probability distributions for *CIF* and *TWCF*. It is the mean of these distributions that are illustrated in Figures 1 and 3.

PTS ANALYSIS RESULTS, TRENDS, AND INSIGHTS

As previously discussed, Figure 1 illustrates the mean value of *TWCF* for each of the three US commercial PWRs plotted as a function of RT_{PTS} . The improved embrittlement correlation discussed above was used in the calculation of RT_{PTS} for the three plants. The neutron fluence maps utilized for the higher levels of embrittlement were obtained by extrapolating beyond the two maps provided by BNL corresponding to 32 and 40 EFPY. Some of these extrapolations are far beyond the range of EFPY for which these plants would ever actually operate. These analyses were performed at the higher levels of embrittlement to establish the relationship between *TWCF* and values of RT_{PTS} at and above the current screening criteria.

Figure 3 illustrates the *TWCF* for each of the three PWRs plotted as a function of operating life. Tables 1 and 2 contain results that would be relevant as these three PWRs approach the end of their 40-year operating licenses and consider requesting a 20-year license renewal.

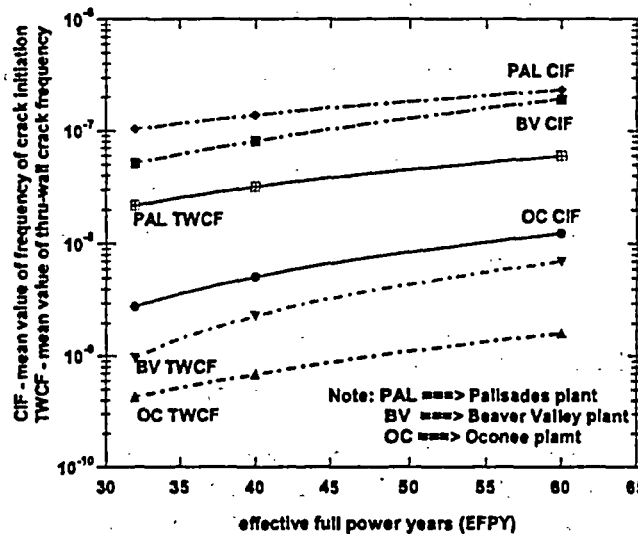


Figure 3 – Results of current PTS re-evaluation program as a function of reactor operating life

Tables 1 and 2 contain results that would be relevant as these three PWRs approach the end of their 40-year operating licenses and consider requesting a 20-year license renewal. Table 1 expresses the relationship between operating life and the current embrittlement metric RT_{PTS} . Based on these results, Oconee and Palisades are not expected to exceed the current PTS screening criteria within 60 EFPY. While Beaver Valley is projected to exceed the current PTS screening criteria, at 60 EFPY, the integrated

risk analysis illustrates that TWCF at 60 years is considerably less than the currently acceptable 5.0×10^{-6} . In addition to illustrating that these three PWRs satisfy the current PTS criteria for a license extension from 40 to 60 years, the results of the analysis provide a technical basis for a relaxation to the current PTS screening criteria.

Table 1 – Relationship between RPV operating life and RT_{PTS}

EFPY	Oconee RT_{PTS} (°F)	Beaver Valley RT_{PTS} (°F)	Palisades RT_{PTS} (°F)
32	175.3	242.4	212.5
40	181.9	251.8	218.5
0	192.6	271.1	230.5

Table 2 – Results from PTS analyses relevant to license extension considerations

EFPY	Oconee CIF ⁽¹⁾	Beaver Valley CIF ⁽¹⁾	Palisades CIF ⁽¹⁾	Oconee TWCF ⁽²⁾	Beaver Valley TWCF ⁽²⁾	Palisades TWCF ⁽²⁾
32	2.80E-09	5.15E-08	1.04E-07	4.29E-10	9.49E-10	2.18E-08
40	5.12E-09	8.05E-08	1.38E-07	6.86E-10	2.31E-09	3.17E-08
60	1.23E-08	1.93E-07	2.33E-07	1.61E-09	6.98E-09	5.94E-08

(1) mean value of probability distribution of crack initiation frequency (cracked RPVs per EFY)

(2) mean value of probability distribution of thru-wall crack frequency (failed RPVs per EFY)

Operationally, the events that dominate TWCF are all associated with primary coolant system failures. These include both loss of coolant accidents (LOCAs) and stuck open safety relief valves that produce a sudden repressurization when the valve does close. By far the greatest contribution to PTS risk arises from loss-of-coolant accidents (LOCAs).

In each of the three PWRs analyzed, the dominant contributing material to PTS-induced risk of failure was axial welds. Postulated flaws in plate regions contributed one per cent or less to the PTS-induced risk of failure owing to the smaller flaw size distribution of plate flaws relative to weld flaws.

For Oconee, a circumferential weld is the most embrittled material, i.e., has the highest value of RT_{PTS} . The most embrittled material for Beaver Valley is a plate and for Palisades is an axial weld. The fact that the dominant contributing material to PTS-induced risk of failure was axial welds, which are not necessarily the materials with the highest values of RT_{PTS} , suggests that an improved embrittlement metric can possibly be defined that more directly correlates with the factors affecting the likelihood of PTS-induced failure.

SUMMARY

In 1999, the USNRC initiated a comprehensive project to establish an updated technical basis for PTS regulation and to determine if it would lead to a relaxation in the current regulations. An updated technical basis has been established within the framework established by modern probabilistic risk

assessment techniques and the advances in technologies associated with the physics of the PTS. During this project, an improved risk-informed computational methodology was developed that provides a more realistic characterization of PTS risk. This updated methodology has been applied to three commercial PWRs. The results of these analyses provide encouragement that a technical basis can be established to reduce the conservatism in the current regulations while continuing to provide reasonable assurance of adequate protection to public health and safety. Work is continuing to insure that that any proposed revision to the PTS rule may be applied generically to all commercial PWRs.

REFERENCES

1. U.S. Nuclear Regulatory Policy Issue, 1982, NRC Staff Evaluation of Pressurized Thermal Shock, SECY 82-465.
2. Code of Federal Regulations, Title 10, Part 50, Section 50.61 and Appendix G.
3. U.S. Nuclear Regulatory Commission, *Regulatory Guide 1.154, Format and Content of Plant-Specific Pressurized Thermal Shock Safety Analysis Reports for Pressurized Water Reactors*, 1987.
4. T.L. Dickson, S. N. M. Malik, J. W. Bryson, and F. A. Simonen, "Revisiting the Integrated Pressurized Thermal Shock Studies of an Aging Pressurized Water Reactor," ASME PVP-Volume 388, *Fracture, Design Analysis of Pressure Vessels, Heat Exchangers, Piping Components, and Fitness for Service, ASME Pressure Vessels and Piping Conference*, August, 1999.
5. P.T. Williams and T.L. Dickson, *Fracture Analysis of Vessels - Oak Ridge, FAVOR, v02.4, Computer Code: Theory and Implementation of Algorithms, Methods, and Correlations*, draft NUREG, November, 2002.
6. Selby, D.L., et al., *Pressurized-Thermal-Shock Evaluation of the Calvert Cliffs Unit 1 Nuclear Power Plant*, NUREG/CR-4022 (ORNL/TM-9408), Oak Ridge National Laboratory, Oak Ridge, TN, September 1985.
7. Selby, D.L., et al., *Pressurized-Thermal-Shock Evaluation of the H.B. Robinson Nuclear Power Plant*, NUREG/CR-4183 (ORNL/TM-9567), Oak Ridge National Laboratory, Oak Ridge, TN, September 1985.
8. Burns, T.J., et al., *Preliminary Development of an Integrated Approach to the Evaluation of Pressurized-Thermal-Shock as Applied to the Oconee Unit 1 Nuclear Power Plant*, NUREG/CR-3770 (ORNL/TM-9176), Oak Ridge National Laboratory, Oak Ridge, TN, May 1986.
9. Office of Nuclear Regulatory Research, "Calculational and Dosimetry Methods for Determining Pressure Vessel Neutron Fluence," Draft Regulatory Guide DG-1053, U.S. Nuclear Regulatory Commission, September 1999.
10. "DORT, Two-Dimensional Discrete Ordinates Transport Code," RSIC Computer Code Collection, CCC-484, Oak Ridge National Laboratory, 1988.
11. D. T. Ingersoll, J. E. White, R. Q. Wright, H. T. Hunter, C. O. Slater, N. M. Greene, R. E. MacFarlane, R. W. Roussin, "Production and Testing of the VITAMIN-B6 Fine-Group and the BUGLE-93 Broad-Group Neutron/Photon Cross-section Libraries Derived from ENDF/B-VI Nuclear Data," ORNL-6795, NUREG/CR-6214, January 1995.
12. RVID Reactor Vessel Integrity Database, NUREG-1511, U.S. Nuclear Regulatory Commission, December, 1994, NUREG-1511, Supplement 1, October, 1996; RVID Version 2.0, August, 1997.
13. Jackson, D.A., and Abramson, L., 1999, *Report on the Results of the Expert Judgment Process for the Generalized Flaw Size and Density Distribution for Domestic Reactor Pressure Vessels*, U.S. Nuclear Regulatory Commission Office of Research, FY 2000-2001 Operating Milestone 1A1ACE.
14. Schuster, G.J., Doctor, S.R., Crawford, S.L., and Pardini, A.F., 1998, *Characterization of Flaws in U.S. Reactor Pressure Vessels: Density and Distribution of Flaw Indications in PVRUF*, USNRC Report NUREG/CR-6471, Vol. 1, U.S. Nuclear Regulatory Commission, Washington, D.C..

15. Schuster, G.J., Doctor, S.R., and Heasler, P.G., 2000, Characterization of Flaws in U.S. Reactor Pressure Vessels: Validation of Flaw Density and Distribution in the Weld Metal of the PVRUF Vessel, USNRC Report NUREG/CR-6471, Vol. 2, U.S. Nuclear Regulatory Commission, Washington, D.C.
16. Schuster, G.J., Doctor, S.R., Crawford, S.L., and Pardini, A.F., 1999, *Characterization of Flaws in U.S. Reactor Pressure Vessels: Density and Distribution of Flaw Indications in the Shoreham Vessel*, USNRC Report NUREG/CR-6471, Vol. 3, U.S. Nuclear Regulatory Commission, Washington, D.C.
17. U.S. Nuclear Regulatory Commission, Regulatory Guide 1.99, Revision 2, "Radiation Embrittlement of Reactor Vessel Materials", May 1988.
18. E. D. Eason, J.E. Wright, and G.R. Odette, Improved Embrittlement Correlations for Reactor Pressure Vessel Steels, NUREG/CR-6551, November, 1998.
19. Smith, C. L., et al, Testing, Verifying and Validating SAPHIRE Versions 6.0 and 7.0, NUREG/CR-6688, October 2000.
20. RELAP5 / MOD3 Code Manual (RELAP5/MOD3.2.2Gamma), U.S. Nuclear Regulatory Commission, NUREG/CR-5535, June, 1999.
21. EPRI Report EPRI Special Report, 1978, Flaw Evaluation Procedures: ASME Section XI, EPRI NP-719-SR, Electric Power Research Institute, Palo Alto, CA.
22. Bowman, K.O. and Williams, P.T., Technical Basis for Statistical Models of Extended K_{Ic} and K_{Ia} Fracture Toughness Databases for RPV Steels, ORNL/NRC/LTR-99/27, Oak Ridge National Laboratory, Oak Ridge, TN, February, 2000.
23. T.L. Dickson, P.T. Williams, and B.R. Bass, An Improved Probabilistic Fracture Mechanics Model for Pressurized Thermal Shock, 16th International Structural Mechanics in Reactor Technology (SmiRT) Conference, Washington, D.C., August 2001.

The Effects of Aliovalent Elements on Nodular Oxidation of Zr-Base Alloys

H. M. Chung
Argonne National Laboratory
Argonne, IL 60439, USA

Abstract

Under loss-of-coolant-accident situations, postquench mechanical properties of fuel cladding are profoundly influenced by oxidation and concomitant H uptake. Unlike Zircalloys, under high-temperature LOCA situations, some Nb-containing alloys are susceptible to nodular oxidation, which leads to excessive H uptake and premature embrittlement at oxidation significantly below the 17% oxidation limit. Other Nb-containing alloys, of nominally the same or similar compositions, are resistant to nodular oxidation under similar conditions. To provide insight useful to the understanding of this strange behavior, a mechanistic model has been developed. The model is based on the effect of aliovalent elements (i.e., alloying or impurity elements that exhibit a valency that differs from the valency of tetravalent Zr in Zr oxide) on charge balance, O ion vacancy, stoichiometry, crystal structure, and fracture toughness of Zr oxide. Because of the overvalent nature of Nb, oxide formed on a Zr-Nb alloy at high temperatures is more susceptible than Zircaloy to lower oxygen vacancy, higher stoichiometry, monoclinic structure, lower toughness, and tendency to develop microcracks. The model predicts that susceptibility of a Zr-Nb alloy to high-temperature nodular oxidation is suppressed by pickup of undervalent impurities, such as Mg, Ca, and Al, during Hf purification and Zr metal production. In some fabrication processes, pickup of such impurities is inherently absent, and significant F contamination occurs. Such processes are predicted to lead to higher susceptibility to nodular oxidation.

Introduction

For loss-of-coolant-accident (LOCA) situations, Code of Federal Regulation 10CFR50.46 specifies a peak-cladding-temperature limit of 1204°C and a maximum-cladding-oxidation limit of 17% [1]. In establishing these criteria in 1973, excessive degradation of postquench ductility of Zircaloy-4 due to high-temperature oxidation, as reported by Hobson and Rittenhouse [2], was the key consideration [3,4]. In addition to the oxidation-related embrittlement, it was found in later investigations [5-8] that excessive H uptake also leads to significant degradation of postquench ductility [6-8] and impact properties [5,6]. The large H uptake in these investigations was due to exposure of the inner surface of the short sections near the burst opening to H-rich gas that is produced in the small gap between the fuel pellet and the cladding inner diameter. This type of H embrittlement was, therefore, limited to the relatively short "necks" immediately above and below the burst opening. Most cladding sections that were further from the burst opening are protected from excessive H uptake because an adherent compact oxide layer forms on the outer surface and the inner surface is exposed to fission gas. Neither nodular nor breakaway oxidation relevant to LOCA situations, which could lead to excessive H uptake in general from the outer-diameter surface, was reported. These properties, characteristic of Zircaloy cladding, are addressed in detail in Refs. 6 and 9.

Inasmuch as the current trend in the industry is increased use of advanced cladding fabricated from Nb-containing alloys, such as E110 (Zr-1Nb), M5 (Zr-1Nb), E-635 (Zr-1Nb-1.2Sn-0.4Fe), Zirlo (Zr-1Nb-1Sn-0.1Fe), and MDA (Zr-0.5Nb-0.8Sn-0.2Fe-0.1Cr), performance of these alloys under LOCA-like situations has been investigated in an increasing number of laboratories [10-21]. Although corrosion resistance of these alloys under normal operating conditions is excellent or superior to that of Zircaloy-4, some of them have been known to be susceptible to nodular oxidation in steam at 850-1100°C under LOCA-like conditions. Such nodular oxidation leads to excessive H uptake and premature loss of postquench ductility [10-18]. For example, E110 Zr-1Nb [10-18] and E635 [16] have been reported to be susceptible to nodular oxidation and premature loss of ductility under LOCA-like conditions, even though the oxidation environment was steam containing negligible amount of H gas. In contrast, despite the fact that M5 cladding is fabricated from nominally the same type of Zr-1Nb alloy, it has been reported to be resistant to nodular oxidation under similar conditions, and neither excessive H uptake nor premature ductility loss was observed [20]. Test results reported for Zirlo indicate behavior similar to that of M5 [21].

Because excessive H uptake associated with nodular oxidation at high temperatures is the primary factor that leads to premature embrittlement, susceptibility to high-temperature nodular oxidation is the key to understanding the contrasting performance of E110 and E635 on the one hand and M5 and Zirlo on the other. In particular, the contrasting behavior of E110 and M5 has been a mystery to the fuel community, because both are fabricated from nominally the same and seemingly simple alloy Zr-1Nb. An intuitive consideration suggests that the fabrication procedure used to produce the two types of cladding may play an important role. Therefore, an investigation was performed to carefully evaluate the contrasting fabrication characteristics and to develop a mechanistic model of the effects of aliovalent elements on the susceptibility of Zr-based alloys to high-temperature nodular oxidation. Based on the model and through an understanding of the contrasting fabrication characteristics, this paper is intended to provide insights that are useful to identify the root causes that lead to high-temperature nodular oxidation in Nb-containing cladding.

Characteristics of Nodular Oxidation in E110

It is helpful to gain an overview of the characteristics that are important for the high-temperature nodular oxidation for E110. Similar oxidation in E635 has also been reported [16,17]; however, information on this alloy is rather limited.

Occurrence of high-temperature nodular oxidation in E110 can be deduced from the observation of premature embrittlement caused by excessive H uptake. Boehmert reported such a phenomenon in steam at 850, 900, 950, 1000, 1050, and 1100°C [10]. Similar observations have been reported by Griger et al. [12] and Maroti [13] at 900, 1000, 1100, and 1200°C; by Vrtilkova et al. [15] at 1000°C; by Aslomov et al. [16] at 1100°C; and by Yegorova and Lioutov [17] at 1000 and 1100°C.

Premature embrittlement due to nodular-oxidation-induced excessive H uptake was also reported by Aslomov et al. [16] for irradiated E110 fuel during oxidation in steam at 1000, 1100, or 1200°C. This indicates that irradiation does not mitigate the susceptibility of E110 to nodular oxidation.

Visual appearance [14,16-18] and morphology [18] of nodular oxide produced on E110 have been reported. In the early stage of oxidation, separate white or grayish-white nodules of various size form more or less randomly on the cladding surface. Subsequently, the nodules coalesce to form a continuous white oxide layer. Eventually, the continuous white oxide layer delaminates and flakes off. These

characteristics, reported recently by Billone and coworkers [18], are shown in Fig. 1. Frequently, nonuniform color and partial flakeoff of the oxide layer lead to a messy-looking surface [14,16].

Modeling the Effects of Aliovalent Elements

Major Undervalent and Overvalent Elements

An aliovalent element refers to an element with a valency that differs from the valency of tetravalent Zr (Zr^{4+}), as in ZrO_2 . Some undervalent elements that are important in the consideration of the properties of Zr oxide are double-valent elements, e.g., Ni^{++} , Ca^{++} , Mg^{++} as in NiO, CaO, MgO. Some are triple-valent elements, such as Fe^{+++} , Cr^{+++} , and Al^{+++} as in Fe_2O_3 , Cr_2O_3 , and Al_2O_3 . An important overvalent element in all Nb-containing cladding alloys is the pentavalent element Nb^{5+} , as in Nb_2O_5 .

Oxide Charge Balance, Valency, Defects, and Stoichiometry

It is well known that the rate-controlling step of the oxidation of Zr-base alloys at high temperatures ($>800^\circ C$) is the transport of O ions through Zr dioxide from the outer diameter (OD) or steam side toward the Zr metal. Because O ions transport is controlled by their diffusion in the oxide via a vacancy-exchange mechanism at high temperatures, several factors play important roles: concentration of O vacancies, temperature, diffusivity of O^- , crystallographic structure of the oxide unit cell, and microstructure of the oxide layer (e.g., cracks, pores, columnar grain of oxide, equiaxed grain, and the state of grain boundaries). A fundamental assumption in this model is that, during such high-temperature oxidation, the overall electric charge of an oxide unit cell remains balanced (neutral). A direct inference from this assumption is that the number and valency of substitutional cation elements in the oxide unit cell (e.g., Nb or Mg) determine the population of anion (O^-) vacancy in the unit cell, and hence, the stoichiometry of the oxide. This concept was originally proposed by Wagner as early as 1943 [22,23].

An overvalent element (i.e., Nb^{5+}) in the oxide unit cell leads to less O^- vacancy, and therefore, makes the oxide more stoichiometric. In contrast, an undervalent element (such as, Ca, Mg, Al, Fe, Cr, or Ni) in the oxide unit cell leads to a higher density of O^- vacancy and keeps the oxide understoichiometric. These characteristics of a Zr oxide unit cell are shown schematically in Fig. 2.

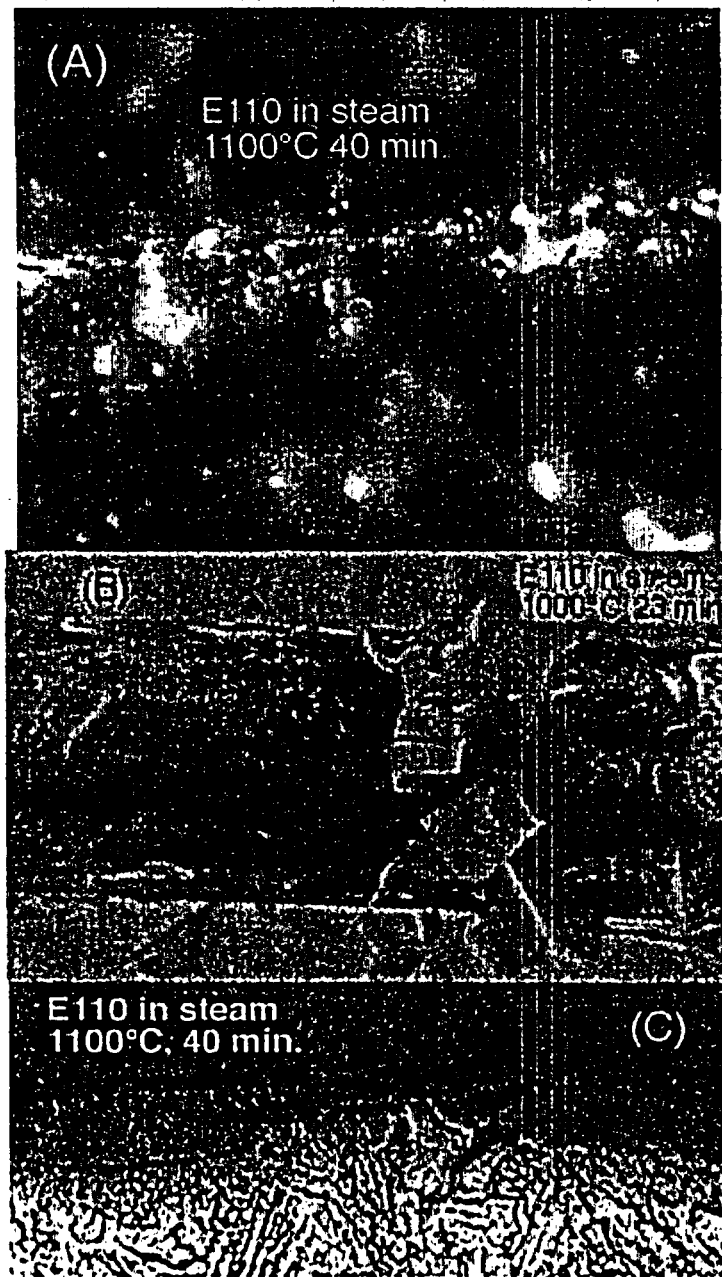


Figure 1.
Morphology of nodular oxides formed on unirradiated E110, from Billone [18]: (A) separate nodules, (B) oxide delamination and flakeoff, and (C) nodule cross section.

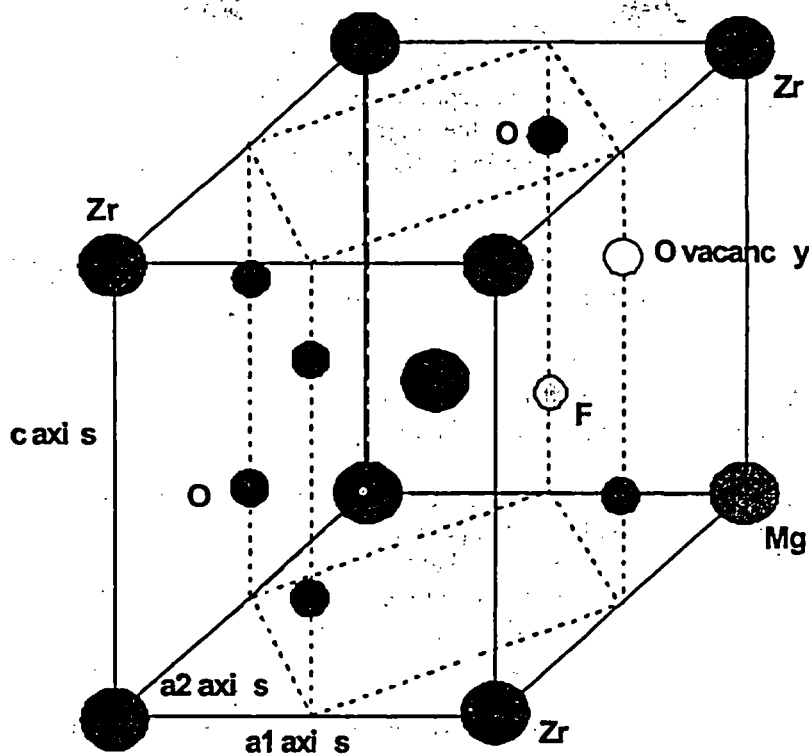


Figure 2.
Unit cell of Zr dioxides and occupation sites of O, O vacancy, and some aliovalent elements.

Properties of Zr Dioxide Formed at 800-1500°C

The crystallographic structure of Zr dioxide produced in steam at 800-1490°C, is either monoclinic, tetragonal, or mixed monoclinic-tetragonal. Under otherwise similar conditions (i.e., similar temperature, stress, and impurity concentration), the relative stability of the monoclinic (vs. tetragonal) structure is strongly influenced by stoichiometry of the oxide.

To keep the charge balance in the oxide unit cell neutral, an undervalent element incorporated in the unit cell increases the concentration of O vacancies, therefore, the oxide unit cell is maintained understoichiometric. This in turn promotes a higher volume fraction of tetragonal oxide in the growing oxide layer. As a consequence of the higher volume fraction of tetragonal oxide, the fracture toughness of the oxide layer remains higher. In this situation, microcracking in the oxide layer is more difficult, the oxide maintains its compact adherent structure, and the cladding is resistant to nodular oxidation.

In contrast, an overvalent element (e.g., Nb) incorporated in the unit cell promotes a lower concentration of O vacancies, and therefore of stoichiometric oxide. This promotes a lower volume fraction of tetragonal phase in the oxide layer. Because of the lower volume fraction of tetragonal oxide, the fracture toughness of the oxide layer becomes significantly lower. In this situation, the oxide layer is susceptible to local microcracking, the oxide loses its adherent protective structure, and the cladding becomes susceptible to nodular oxidation.

Effective Undervalent Impurities in Suppressing Nodular Oxidation

In light of the fundamental properties of Zr dioxide described above, it is possible to deduce that pure binary Zr-Nb alloys are inherently more susceptible to nodular oxidation at high temperatures than Zircalloys that contain Sn (instead of Nb) as the major alloying element. However, all Zr-Nb alloys contain various impurities that may help to either offset the effect of Nb or exacerbate the susceptibility to nodular oxidation.

Based on the same consideration, it is deduced that an undervalent impurity effective in suppressing the susceptibility to nodular oxidation is an element that exhibits the following properties:

- (1) Double or triple valency.
- (2) Affinity to O that is stronger than that of Zr.
- (3) Diffusion to the metal/oxide boundary that is fast.

To evaluate these properties, the free energy of oxidation (per mole of O₂ gas) was plotted in Fig. 3 for various elements as a function of oxidation temperature. The figure shows that oxidation of Ca and Mg atoms is preferred to oxidation of Zr atoms and that the affinity of Al for O is similar to that of Zr in the range of temperatures of our interest. At the same time, considering that the atomic sizes of Ca, Mg, and Al are significantly smaller than that of Zr, diffusion of these impurities in the beta or alpha phase of the cladding metal will be sufficiently fast in the range of temperatures of our interest.

Therefore, Ca and Mg, and to a lesser extent, Al are predicted to be the most effective impurities in promoting formation of tetragonal oxide, and hence in increasing the resistance to nodular oxidation. The role of double-valent Ca or Mg will be especially important, because they produce more O vacancies per atom in the oxide unit cell, thereby being more effective in keeping the oxide understoichiometric and tetragonal. This view is consistent with the well-known role of Ca and Mg as the most effective of the doping elements used to produce stabilized zirconia in the ceramic industry.

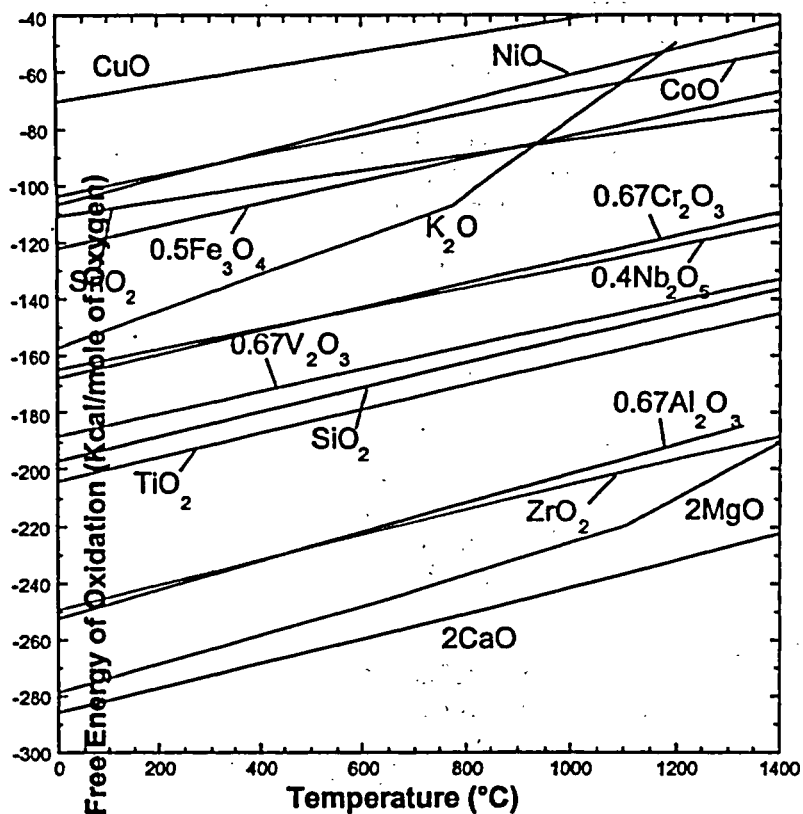


Figure 3.
Free energy of oxidation (per mole of O_2 gas) of impurity and alloying elements as function of oxidation temperature.

Alloy Fabrication and Impurity Pick-Up

The primary time for pickup of beneficial or deleterious impurities is during fabrication of the cladding tube, i.e., production of nuclear-grade Zr metal, production of Zr-1Nb ingot, fabrication of cladding tube, and final surface finishing of the tube. It was noted that the methods of producing nuclear-grade Zr used for E110 and M5 claddings greatly differ; therefore, details of both processes were critically examined. Production of nuclear-grade Zr metal involves more than ≈ 25 steps but is divided basically into four stages [24-28]:

- (1) Decomposition of zircon ore.
- (2) Production of feedstock compound for Hf purification, i.e., $(ZrCl_4 + HfCl_4)$ or $(K_2ZrF_6 + K_2HfF_6)$. Before purification of Hf, the feedstock typically contains $\approx 15,000 - 25,000$ wppm Hf.
- (3) Separation of the Zr and Hf compounds, i.e., production of low-Hf $ZrCl_4$ or low-Hf K_2ZrF_6 .
- (4) Reduction of the low-Hf compounds into low-Hf Zr metal. After this step, the Hf content is typically reduced to < 500 wppm.

Individual steps in these processes may change with time, driven by a desire to reduce production cost or to simplify the operation. Therefore, the type and quantity of impurity pickup associated with alloy production could change with time, and then influence the high-temperature oxidation behavior.

Impurity Pickup during Decomposition of Zircon Ore $ZrO_2 \cdot SiO_2$

The basic process for the decomposition of zircon ore used to produce nuclear-grade Zr metal for E110 cladding, involves F chemistry, i.e., conversion of the ore to potassium fluozirconate via the reaction [26]



This operation, typically carried out at 700-800°C, is conducive to eventual contamination of Zr metal by F, most likely in the form ZrF_4 residue in the metal.

In contrast, in western countries, the basic process for the decomposition of ore, used to produce Zr metal for Zircalloys, M5, and Zirlo, involves Cl chemistry [24,25]. In this process, a mixture of $ZrO_2 \cdot SiO_2$ and graphite is chlorinated with $SiCl_4$, $TiCl_4$, or $AlCl_3$. The ore is converted to $ZrCl_4$ and $SiCl_4$, typically at >1150°C. This zirconium-chloride product contains minor amounts of $HfCl_4$. Then, the $ZrCl_4$ and $HfCl_4$ are separated, mostly by the MIBK process described below.

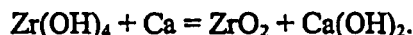
Impurity Pickup during Hf Separation

Because the thermal neutron cross section of Hf at 105 barn is almost 600 times greater than that of Zr, separation of Zr and Hf is essential for the production of low-Hf nuclear-grade Zr metal. The three processes most commonly used for this purpose are the methyl isobutyl ketone (MIBK) process [24], extractive distillation [25], and fractional crystallization of Zr and Hf salts [28].

The fractional crystallization method is used to produce low-Hf nuclear-grade Zr destined for E110 and E635 cladding. The feedstock potassium fluozirconate (K_2ZrF_6) obtained from decomposition of zircon ore typically contains 1.5-2.5 wt.% potassium fluohafnate (K_2HfF_6) as impurity. The fractional crystallization process takes advantage of the fact that the solubility of K_2HfF_6 in distilled water is slightly higher than that of K_2ZrF_6 . When the mixture is dissolved in water at <90°C, a slight accumulation of Hf occurs in the mother solution and the Hf content is slightly decreased in the undissolved feedstock mixture of K_2ZrF_6 and K_2HfF_6 . The mother solution is then cooled slowly, and fractional crystallization of the compounds occurs at differing rates. After ≈15 steps of fractional crystallization, the concentration of K_2HfF_6 in the final mixture is reduced to ≈400-500 wppm. Then, the low-Hf K_2ZrF_6 compound is reduced to Zr metal by an electrolytic process.

The most common and the most traditional method of Hf purification used to produce Zircalloys, M5, and Zirlo in western countries, is the MIBK process. This process starts with the $ZrCl_4 + HfCl_4$ mixture obtained from decomposition of the zircon ore; it involves many steps that are summarized as follows:

- (1) Convert the $ZrCl_4+HfCl_4$ mixture to $ZrOCl_2+HfOCl_2$ in demineralized water.
- (2) Convert the oxychloride compounds to $ZrO(SCN)_2+HfO(SCN)_2$ using thiocyanate $SCNNH_4$.
- (3) Remove $HfO(SCN)_2$ by liquid-liquid extraction using methyl isobutyl ketone (MIBK).
- (4) Treat remaining $ZrO(SCN)_2$ with HCl to convert it to $ZrOCl_2$.
- (5) Convert $ZrOCl_2$ to $Zr(OH)_4$ using NH_4OH and H_2SO_4 .
- (6) Calcinate the Zr hydroxide to produce ZrO_2 via the reaction



- (7) Chlorinate the ZrO_2 to convert it to $ZrCl_4$.
- (8) Reduce the $ZrCl_4$ to Zr metal by the Kroll process.

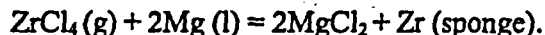
Once treated by the MIBK process, the final low-Hf $ZrCl_4$ product picks up Ca, the most efficient aliovalent element that helps stabilize tetragonal or cubic form of Zr dioxide.

Another method of Hf purification is the extractive distillation process, developed relatively recently [25] and probably used extensively in the production of more recent heats of M5. The feedstock mixture of $ZrCl_4$ and ≈ 2.5 wt.% $HfCl_4$ is separated by extractive distillation with a solvent of molten KCl and $AlCl_3$. The final product from this process ($ZrCl_4$) typically contains <100 wppm Hf, which is then fed to the Kroll process to reduce the $ZrCl_4$ to Zr metal. This anhydrous process does not involve a calcination step, and the low-Hf $ZrCl_4$ produced by this process does not pick up Ca. The Hf-purified $ZrCl_4$ product, instead, picks up Al, which is an efficient aliovalent element that helps stabilize tetragonal oxide.

Impurity Pickup during Zr Reduction

Zirconium metal used in the production of E110 and E635 cladding is typically a mixture of electrolytic Zr and iodide Zr, e.g., in 60%-40% proportion. Iodide Zr is produced by decomposition of ZrI_4 on a hot tungsten filament heated to $\approx 1500^\circ C$, a process known as the van Arkel and de Boer process. Large-scale production by this process is difficult, but the purity of the Zr metal is high. Electrolytic Zr is produced by electrolysis of Hf-purified K_2ZrF_6 in a molten bath of KCl , $NaCl$, mixed $KCl-NaCl$, or other halides [24, 28]. Zirconium metal produced by this process inherently contains F impurities that were picked up during ore decomposition and Hf purification.

Practically all Zr metal used to fabricate Zircaloy, Zirlo, and M5 in western countries is produced by the Kroll process [24]. In this process, Hf-purified $ZrCl_4$ in gaseous form is reduced by molten Mg to produce "sponge" Zr, i.e.,



The sponge Zr contains $MgCl_2$ residue and excess Mg. The concentrations of $MgCl_2$ and Mg are reduced by vacuum degassing or vacuum distillation; however, complete removal of the residues is difficult. Therefore, Zircaloy, Zirlo, and M5 produced with sponge Zr contains, as an important impurity, Mg, one of the most efficient aliovalent elements that help stabilize tetragonal Zr dioxide.

Discussion

It appears clear that the processes of alloy fabrication (i.e., decomposition of zircon ore, Hf purification, and Zr metal reduction) used to produce E110 and E635 on the one hand and Zircaloy, M5, and Zirlo on

the other differ substantially. Of particular importance is the contrasting type and nature of impurities that are picked up during fabrication of the two groups of cladding alloys. Information about the fabrication-related impurity pickup is summarized in Table 1.

Also described in Table 1 are the type and nature of impurities that can be picked up during surface finishing of cladding tubes, i.e., final cleaning and surface polishing with hard oxides. However, during surface finishing, impurities are picked up near room temperature; therefore, their presence is limited to a thin layer near the surface. Consequently, the effect of surface-finish-related impurity pick up is limited to the delay of the onset of nodular oxidation.

The primary findings from the analysis of fabrication processes of the two groups of alloys, i.e., E110 and E635 on one hand and Zircalloys, M5, and Zirlo on the other, can be summarized as follows:

- (1) The fabrication procedures used to produce Zircalloys, Zirlo, and M5 alloys inherently promote pick up of two strongly beneficial impurities, namely, Ca and Mg, in one procedure (i.e., Hf purification by the MIBK process followed by sponge Zr production by the Kroll process), or Al and Mg in the other (i.e., Hf purification by the extractive-distillation process followed by sponge Zr production by the Kroll process).
- (2) Pickup of beneficial impurities such as Ca, Mg, or Al is inherently absent during fabrication of E110 and E635 alloys.
- (3) The fabrication procedure used to produce E110 and E635 is inherently susceptible to pickup of the deleterious impurity F.
- (4) Pickup of the deleterious impurity F is inherently absent in the fabrication of Zircalloys, Zirlo, and M5.

Table 1. Summary of presence and absence of deleterious or beneficial impurity picked up during major fabrication steps.

Process	Important Impurities Present	Deleterious or Beneficial
Decomposition of zircon ore, conversion to K_2ZrF_6	F	deleterious
Hf separation, fractional crystallization of K_2ZrF_6 and K_2HfF_6	F	deleterious
Zr reduction, electrolysis of K_2ZrF_6 , electrolytic Zr	F	deleterious
Zr reduction, iodide Zr	-	-
Decomposition of zircon ore, conversion to $ZrCl_4$	-	-
Hf separation, MIBK process, calcination of $Zr(OH)_4$ to convert to ZrO_2	Ca	beneficial
Hf separation, extractive distillation	Al	beneficial
Zr reduction, Kroll process, sponge Zr	Mg	beneficial
Degreasing or cleaning in HF-containing solution	F	deleterious
Surface finishing with Al_2O_3 , Fe_2O_3 , or Y_2O_3	Al, Fe, Y	beneficial

The behavior of F atoms is similar to that of O in some respect. Fluorine is readily incorporated in a metal oxide, and once incorporated, it can migrate rapidly through the oxide. Such behavior, which is consistent with the fact that the size of F ions is significantly smaller than that of O^- ions, has been reported for Ta oxide by Shimizu et al. [29] and for Zr oxide by Welton [30].

Shimzu et al. [29] analyzed the distribution of F atoms in their Ta oxide by secondary ion mass spectroscopy (SIMS) and showed that the concentration of F is high in the oxide and that the F atoms tend to accumulate at the metal/oxide boundary. This behavior is consistent with the fact that the solubility of F is extremely small or negligible in most metals [31]. Because of the negligible solubility, F atoms can be incorporated in most metals only in the form of metallic fluorides, whose melting points are relatively low, e.g., 39°C for RbF, 843°C for YbF₂, 1086°C for SmF₂, 232°C for SnF₂, 1100°C for MoF₃, and 640°C for ZrF₄ [31].

The boiling point of ZrF₄ is ≈905°C. Because of this low boiling point, localized ZrF₄ residues that were picked up during fabrication (i.e., decomposition of zircon ore for E110 and E635 alloys) become unstable and breakup during oxidation at high temperatures. Consequently, rapid diffusion of the unstable F atoms occurs in the alloy matrix at temperatures higher than ≈900°C, i.e., the temperatures of importance under LOCA conditions. Under such conditions, the F atoms supersaturated in the metal diffuse toward the surface oxide layer in which they are thermodynamically more stable, and eventually are incorporated in the oxide unit cell or degassed out of the cladding. Fluorine ions incorporated in the oxide occupy O vacancy sites (see Fig. 2), therefore, they promote more stoichiometric oxide, in effect decreasing the stability of the tetragonal oxide. This process, consequently, exacerbates the susceptibility of some local spots to nodular oxidation, as is illustrated schematically in Fig. 4. Similar illustrations in Figs. 5 and 6 show how the beneficial aliovalent elements Ca, Mg, and Al work to suppress the susceptibility to nodular oxidation.

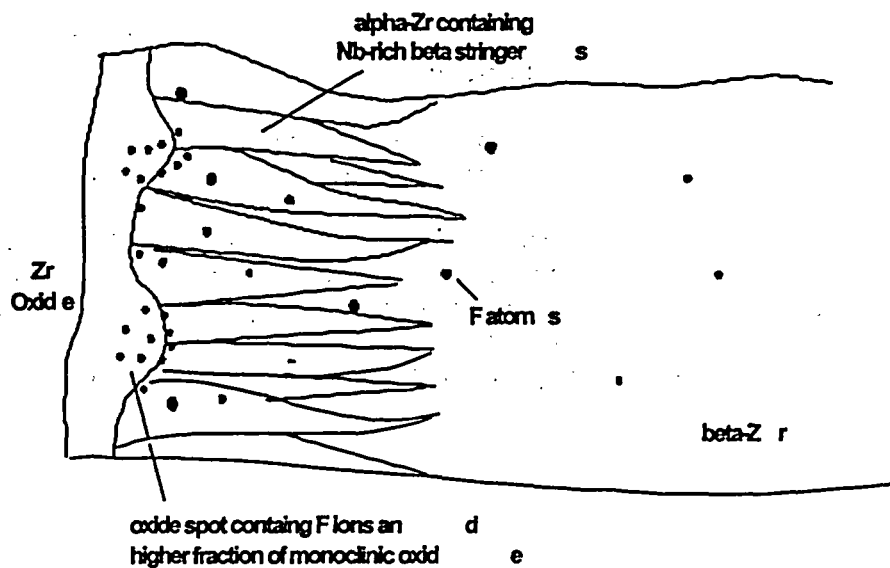
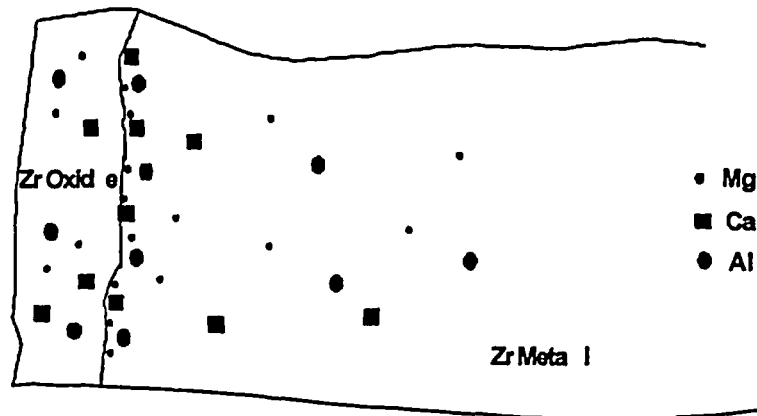


Figure 4.
Schematic illustration of formation of monoclinic nodular oxide promoted by F contamination.

Vrtilkova et al. reported that susceptibility of E110 to nodular oxidation in steam is insignificant at oxidation temperatures <750°C [15]. Consistent with this observation, Boehmert reported that embrittlement of E110 was insignificant after oxidation at 700 and 800°C, indicating that the material was not susceptible to nodular oxidation or large H uptake at these temperatures [10]. Vrtilkova et al. also reported that susceptibility of E110 to nodular oxidation becomes high at oxidation temperatures in which the beta phase is stable, i.e., >860°C [15]. These observations seem to agree well with a prediction based on the model described above.

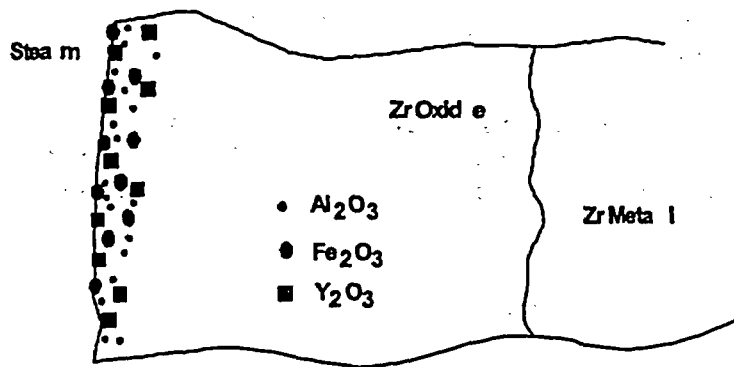


Affinity to O of Mg, Ca, or Al is far greater than that of Zr. Mg, Ca, or Al diffuses to and accumulates at an oxide/metal boundary where O is concentrated.

Mg, Ca, or Al is oxidized preferentially at the oxide/metal boundary. Although average concentration is low, Mg, Ca, or Al is preferentially incorporated in the oxide unit cell.

Figure 5.
Schematic illustration of fabrication-related pickup of Ca, Mg, or Al suppressing nodular oxidation of Zr-1Nb.

Effects of F contamination on the properties of oxide layers formed on austenitic stainless steels have been reported by several investigators in conjunction with studies on F effects on stress corrosion cracking of steel weldments [32-35]. A peculiar phenomenon observed in these investigations is that the oxide layers formed on the F-contaminated steels tend to delaminate and flake off, in a manner similar to that shown in Fig. 1 for E110. In the former investigations, this phenomenon was known as "oxide slough off." Shimzu et al. reported a similar phenomenon in their investigation of F effects on Ta oxide [29]. The phenomenon is explained well by a process in which F atoms accumulate at the boundary between the metal and the oxide, subsequently forming a thin film of low-melting-point metal fluoride.



Surface polishing with fine powders of a hard oxide removes surface rough spots.

Oxide of divalent element such as Al, Fe, or Y, incorporated in the surface layer, tends to make the Zr oxide understoichiometric and helps the oxide remain in tetragonal phase.

Overall effect is to delay the onset of nodular oxidation

Figure 6.
Schematic illustration of surface-finishing-related pickup of Al, Fe, or Y suppressing nodular oxidation of Zr-1Nb

Following the same ore-decomposition and Hf-purification processes summarized in Table 1, raw Zr metal for fabrication of E110 could be produced by the Kroll process instead of the electrolytic process. In this route, it would be necessary to convert K_2ZrF_6 to $Zr(OH)_4$ and then calcinate the $Zr(OH)_4$ to obtain ZrO_2 . Then, the nuclear-grade raw Zr metal would have picked up Ca and Mg as well as F. In this situation, it is expected that Ca and Mg trap F atoms in the metal to form clusters of Ca-O-F, similar to those reported in stainless steel welds [36], or Mg-O-F. It is also likely that the oxide unit cells contain some Ca or Mg as substitutional impurities (as depicted in Fig. 2). Then, the end effect would be that the deleterious effect of F is suppressed by the beneficial effect of Ca and Mg.

Because the typical fabrication procedures used to produce Zircalloys, Zirlo, and M5 inherently promote contamination by Ca and Mg but prevent F pickup, it is predicted that susceptibility of these alloys to high-temperature nodular oxidation is inherently suppressed.

Conclusions

A mechanistic model was developed that can explain the contrasting susceptibility of Zr-1Nb class E110 and M5 fuel cladding to high-temperature nodular oxidation in steam in LOCA situations. The model is based on effects of aliovalent elements on the properties of Zr oxide.

The model predicts that Ca and Al pickup, related to Hf purification by the process of methyl isobutyl ketone and extractive distillation, respectively, and Mg pickup, related to the production of sponge Zr by the Kroll process, are beneficial, because they lead to suppression of the susceptibility to nodular oxidation. Absence of such pickup is predicted to be deleterious.

Fluorine pickup, related to zircon ore decomposition by use of potassium fluozirconate, Hf purification by the fractional-crystallization process, and Zr reduction by the electrolytic process, is predicted to be deleterious, leading to increased susceptibility to nodular oxidation. Such F pickup, combined with the

absence of fabrication-related pickup of Ca, Mg, or Al, is predicted to conjointly exacerbate the susceptibility to nodular oxidation.

It is recommended to verify the above predictions by testing oxidation behavior of several model Zr-1Nb ingots. Such ingots can be fabricated with non-nuclear-grade iodide Zr that was produced without going through an Hf-purification process and can be doped with various combinations and amounts of Ca, Mg, Al, and F.

Acknowledgements

The author thanks R. O. Meyer for helpful discussions. This work was supported by the U.S. Nuclear Regulatory Commission, Office of Nuclear Regulatory Research.

References

- (1) Code of Federal Regulation, Title 10, Part 50.46 and Appendix K, (Revised January 1, 1981) Government Printing Office, 1981.
- (2) D. O. Hobson and P. L. Rittenhouse, "Embrittlement of Zircaloy-Clad Fuel Rods by Steam During LOCA Transients," ORNL-4758, Oak Ridge National Laboratory, January 1972.
- (3) U. S. Atomic Energy Commission Rulemaking Hearing on Acceptance Criteria for Emergency Core Cooling Systems for Light-Water-Cooled Nuclear Power Reactors, Opinion of the Commission, Docket No. RM-50-1, December 28, 1973, pp. 1085-1138.
- (4) G. Hache and H. M. Chung, "The History of LOCA Embrittlement Criteria," Proc. 28th Water Reactor Safety Information Meeting, October 23-25, 2000, Bethesda, MD, NUREG/CP-0217, U.S. Nuclear Regulatory Commission, 2001, pp. 205-237.
- (5) H. M. Chung and T. F. Kassner, "Development of an Oxygen Embrittlement Criterion for Zircaloy Cladding Applicable to Accident Conditions in Light-Water Reactors," Zirconium in the Nuclear Industry, Fourth Conference, ASTM STP 681, American Society for Testing and Materials, 1979, pp. 600-627.
- (6) H. M. Chung and T. F. Kassner, "Embrittlement Characteristics of Zircaloy Cladding Applicable to Accident Situations of Light-Water Reactors: Summary Report," NUREG/CR-1344, ANL-79-48, Argonne National Laboratory, January 1980.
- (7) H. Uetsuka, et al., "Zircaloy-4 Cladding Embrittlement Due to Inner Surface Oxidation under Simulated Loss-Of-Coolant Condition," J. Nucl. Sci. Tech. 18 (1981) 705-717.
- (8) H. Uetsuka, et al., "Embrittlement of Zircaloy-4 Due to Oxidation in Environment of Stagnant Steam," J. Nucl. Sci. Tech. 19 (1982) 158-165.
- (9) Compendium of ECCS Research for Realistic LOCA Analysis – Final Report, NUREG-1230, U. S. Nuclear Regulatory Commission, December 1988.
- (10) J. Boehmert, "Embrittlement of Zr-Nb1 at Room Temperature after High-Temperature Oxidation in Steam Atmosphere," Kerntechnik 57 (1992) 55-58.
- (11) J. Boehmert, M. Dietrich, and J. Linek, "Comparative Studies on High-Temperature Corrosion of ZrNb1 and Zircaloy-4," Nucl. Engr. Design 147 (1993) 53-62

- (12) A. Griger, L. Maroti, L. Matus, and P. Windberg, "Ambient and High-Temperature Mechanical Properties of ZrNb1 Cladding with Different Oxygen and Hydrogen Content," Proc. Enlarged Halden Program Group Meeting, May 24-29, 1999, Loen, Norway.
- (13) L. Maroti, "Ring-Compression Test Results and Experiments Supporting LOCA PCT, Oxidation and Channel Blockage Criteria," Proc. OECD Topical Mtg. on LOCA Fuel Safety Criteria, March 22-23, 2001, Aix-en-Provence, France.
- (14) Yu. K. Bibilashvili, N. B. Sokolov, L. N. Andreeva-Andrievskaya, V. Yu. Tonkov, A. V. Salatov, A. M. Morosov, and V. P. Smirnov, "Thermomechanical Properties of Oxidized Zirconium-Based Alloy Claddings in Loss of Coolant Accident Conditions," Proc. OECD Topical Mtg. on LOCA Fuel Safety Criteria, March 22-23, 2001, Aix-en-Provence, France.
- (15) V. Vrtilkova, M. Valach, and L. Molin, "Oxidation and Hydriding Properties of Zr-1Nb Cladding Material in Comparison with Zircalloys," Proc. IAEA Technical Committee Mtg. on Influence of Water Chemistry on Fuel Clad Behavior, October 4-8, 1993, Rez, Czech Republic; also in IAEA TECDOC-927, Vienna, 1997, pp. 227-251.
- (16) V. Asmolov, L. Yegorova, K. Lioutov, A. Konoveyev, V. Smirnov, A. Goryachev, V. Chesanov, and V. Prokhorov, "Understanding LOCA-Related Ductility in E110 Cladding," Proc. Nuclear Safety Research Conference, October 28-30, 2002, Washington, D.C.
- (17) L. Yegorova and K. Lioutov, "LOCA Behavior of E110 Alloy," Proc. Nuclear Safety Research Conference, October 20-22, 2003, Washington, D.C.
- (18) M. Billone, "Overview of Advanced Alloy Post-Quench Ductility Program," Review Mtg. of LOCA and Dry-Cask-Storage Programs, July 16-17, 2003, Argonne, Illinois.
- (19) Y. Yan, T. Burtseva, and M. Billone, "LOCA Results for Advanced-Alloy and High-Burnup Zircaloy Cladding," Proc. Nuclear Safety Research Conference, October 20-22, 2003, Washington, D.C.
- (20) J.-C. Brachet, J. Pelchat, D. Harmon, R. Maury, P. Jacques, and J.-P. Mardon, "Mechanical Behavior at Room Temperature and Metallurgical Study of Low-Tin Zry-4 and M5 Alloys after Oxidation at 1100°C and Quenching," Proc. IAEA Technical Committee Mtg. on Fuel Behavior under Transient and LOCA Conditions, September 10-14, 2001, Halden, Norway.
- (21) W. J. Leach, "Ductility Testing of Zircaloy-4 and Zirlo Cladding after High-Temperature Oxidation in Steam," Proc. OECD Topical Mtg. on LOCA Fuel Safety Criteria, March 22-23, 2001, Aix-en-Provence, France.
- (22) C. Wagner, *Naturwissenschaften*, 31 (1943) 265.
- (23) K. Kiukkola and C. Wagner, *J. Electrochem. Soc.*, 104 (1957) 379.
- (24) W. W. Stephens, "Extractive Metallurgy of Zirconium – 1945 to the Present," *Zirconium in the Nuclear Industry: Sixth International Conference*, ASTM STP 824, D. G. Franklin and R. B. Adams, Eds., American Society for Testing and Materials, 1984, pp. 5-36.
- (25) L. Moulin, P. Thouvenin, and P. Brun, "New Process for Zirconium and Hafnium Separation," *Zirconium in the Nuclear Industry: Sixth International Conference*, ASTM STP 824, D. G. Franklin and R. B. Adams, Eds., American Society for Testing and Materials, 1984, pp. 37-44.
- (26) M. Takahashi, H. Miyazaki, and Y. Katoh, "New Solvent Extraction Process for Zirconium and Hafnium," *Zirconium in the Nuclear Industry: Sixth International Conference*, ASTM STP 824, D. G. Franklin and R. B. Adams, Eds., American Society for Testing and Materials, 1984, pp. 45-56.

- (27) P. Pint and S. N. Flengas, "Production of Zirconium Metal by Fused-Salt Electrolysis," Transactions, Institution of Mining and Metallurgy, London, Section C, Vol. 87, March 1978, pp. C29-C49.
- (28) N. P. Sajin and E. A. Pepelyaeva, "Separation of Hafnium from Zirconium and Production of Pure Zirconium Dioxide," Proc. Intl. Conf. on Peaceful Uses of Atomic Energy, Vol. 8, Presentation P/634, pp.559, August 8-20, 1955, Geneva, Switzerland.
- (29) K. Shimizu, K. Kobayashi, G. E. Thompson, P. Skeldon, and G. C. Wood, J. Electrochem. Soc. 144 (1997) 418.
- (30) R. F. Welton, private communication, November 2003; also see: "Target Material Characterization Apparatus and Measurement Techniques," presentation slides available in website of Holifield Radioactive Ion Beam Facility, Beam Development - Target Material Characterization Laboratory, Physics Division, Oak Ridge National Laboratory, 2003.
- (31) The Handbook of Binary Phase Diagrams, W. G. Moffatt, Genium Publishing Corporation, Schenectady, NY, 1984.
- (32) C. T. Ward, D. L. Mathis, and R. W. Staehle, Corrosion 25 (1969) 394.
- (33) P. E. C. Bryant and P. R. Habicht, Combustion Engineering Internal Report TIS-5065, also in Proc. IAEA Workshop on Stress Corrosion Cracking, March 29-31, 1976.
- (34) M. Takemoto, T. Shonohara, M. Shirai, and T. Shinogaya, Mater. Performance 24 (1985) 26.
- (35) H. M. Chung, W. E. Ruther, J.-H. Park, J. E. Sanecki, and N. J. Zaluzec, Paper #443, Corrosion '99, San Antonio, Texas, April 25-30, 1999.
- (36) H. M. Chung, J.-H. Park, J. E. Sanecki, N. J. Zaluzec, T. T. Yang, and M. S. Yu, "Cracking Mechanism of Type 304L Stainless Steel Core Shroud Welds," Proc. 9th Intl. Conf. on Environmental Degradation of Materials in Nuclear Power Systems - Water Reactors, Eds. S. Bruemmer, P. Ford, and G. Was, The Minerals, Metals, and Materials Society, Warrendale, PA, 1999, pp. 973-984.

LOCA Testing at Halden, Trial Runs in IFA-650

V. Lestinen, E. Kolstad, W. Wiesenack
OECD Halden Reactor Project

ABSTRACT

The current safety criteria for loss-of-coolant accidents (LOCA) are based on the earlier LOCA experiments in the 1970s, which were largely conducted with fresh fuel. Changes in fuel design, introduction of new cladding materials and moves to high burnup fuel have generated a need to re-examine safety criteria and their continued validity. For this purpose, hot cell research programs have been started in some countries. These investigations are concentrating on embrittlement and mechanical properties of high burnup cladding. The LOCA experiments in Halden are integral single pin in-pile tests on fuel behaviour under simulated LOCA conditions. It is planned to use high and medium burnup fuel rods irradiated in commercial reactors. The Halden experiments will focus on effects that are different from those studied in out-of-reactor tests.

The first LOCA trial test runs were carried out in the Halden reactor in May 2003 using a fresh, tight-gap and unpressurised PWR rod with Zr-4 cladding. The main objective was to gain experience in the operation of the rig and to determine how to run the later experiments with the pre-irradiated rodlets. The target peak cladding temperatures (PCT) were successfully achieved and the test gave a good basis for further experiments. Some pre-test calculations of the first LOCA trial test runs were performed by outside laboratories and by the Halden project. The codes produced fairly good simulations of the cladding temperature measurements. These calculations will be continued and developed for planning of further LOCA tests.

1. INTRODUCTION

The move to high burnup fuels, new fuel designs and introduction of new cladding materials have generated a need to re-examine and verify the validity of the safety criteria for LOCA accidents. LOCA tests in the Halden reactor will be integral in-pile tests using high burnup fuel rods irradiated in commercial reactors. The experiments will be single pin tests. Participating organisations in the Halden Project have offered both PWR and BWR fuels with the desired high burnup. Preparations for transportation of the fuel segments to the Kjeller hot laboratory are ongoing. It has also been proposed to include medium burnup (40-45 MWd/kg) fuel in the test series in order to bridge the gap between the low and high burnup fuel. Future testing of VVER-fuel is being considered.

The test conditions are planned to meet the following primary objectives:

- to maximise the ballooning size to promote fuel relocation and to evaluate its possible effect on cladding temperature and oxidation.
- to investigate the extent (if any) of "secondary transient hydriding" on the inner side of the cladding around the burst region.

Target peak clad temperatures (PCTs) for the pre-irradiated rods have been set at 800°C and 1100°C for high and medium burnups. The lower temperature is used because high burnup fuel is not expected to reach higher clad temperatures in a LOCA. The higher temperature is close to the current LOCA temperature limit prescribed by regulations.

Some pre-test calculations were performed by outside laboratories and by the Halden project. The codes used were FRAPTRAN/GENFLOW (VTT), TRAC-BF1 (PSI), ALGOR, SCTEMP and FTEMP3 (Halden). The codes CATHARE and ICARE by IRSN are to be used in the second phase of the experiments.

2. EXPERIMENTS

The first LOCA test was performed in the Halden reactor in May 2003. A tight-gap, unpressurised PWR fuel rod with Zr-4 cladding was used. The aim was to gain experience in the operating the rig and to test and instrumentation. The configurations and conduct of further experiments will be based on experience gained from the first test.

2.1 Fuel and rig

In the IFA-650 rig the 50 cm long fuel rod was located in the center of an insulated standard high-pressure flask. The rig with the rod was connected to a high-pressure heavy water loop and a blow-down system. The fuel rod had an outer diameter of 9.50 mm and a wall thickness of 0.57 mm. The filling gas was helium at 2 bar. The fuel rod was surrounded by a heated flow separator and the flask. A shroud with a He³-coil was also incorporated in the rig. The rig structure is presented in Figure 1, and Figure 2 shows the cross-section of the test channel.

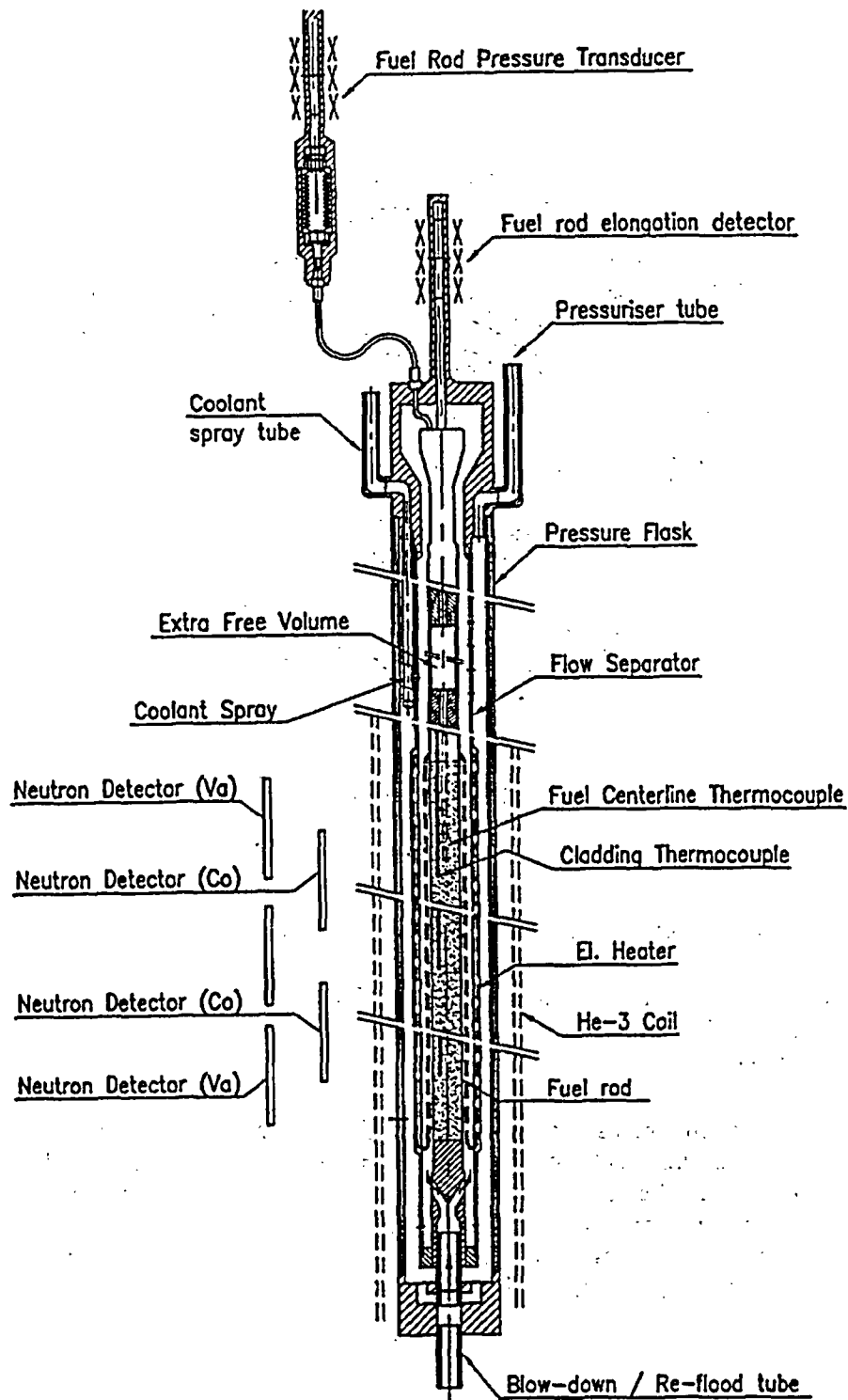


Figure 1 Schematic of test rig for LOCA experiments.

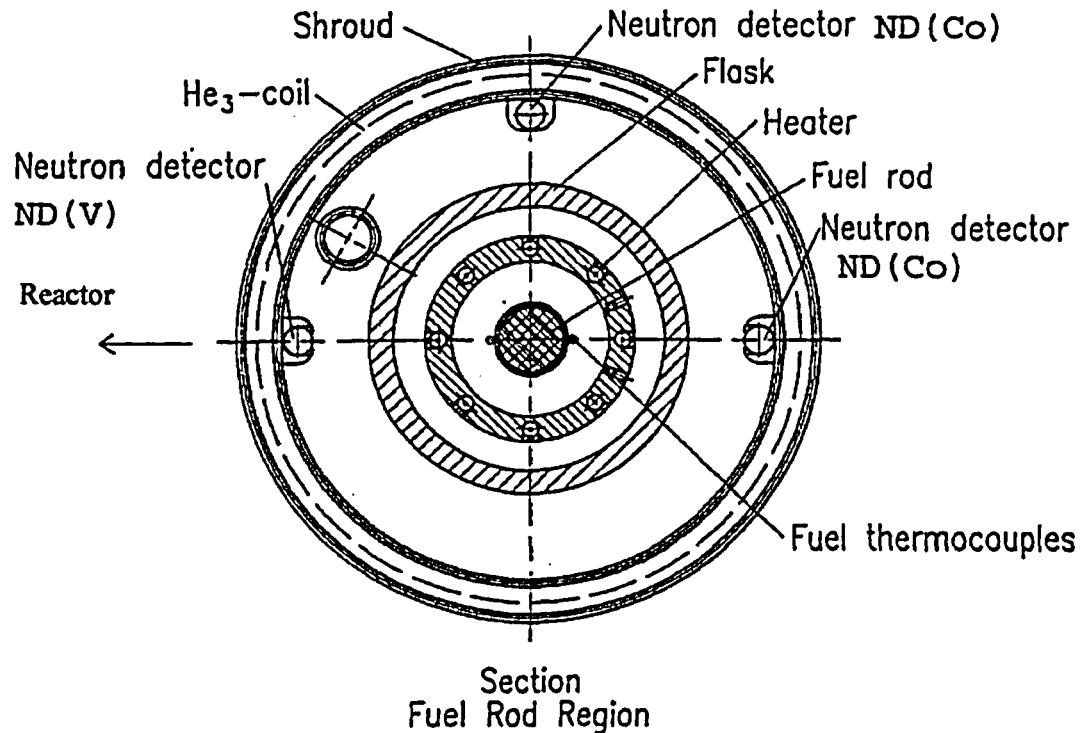


Figure 2 Cross section geometry of the LOCA test rig (scale 1:1).

Heating is provided from the fuel pellets and the heater. The cladding temperature can be controlled by the rod and heater power. The rod power can be controlled by varying the He³-coil pressure and by changing the reactor power.

The test rig instrumentation consists of two heater thermocouples, two inlet and outlet coolant thermocouples, a flow meter, three self-powered vanadium neutron detectors (ND) and two fast response cobalt NDs. The two embedded heater thermocouples are located above and below the axial mid height of the fuel rod. The volume flow rate is measured in the external loop. The axial power distribution can be observed by the three vanadium NDs, which are located at three elevations. Rapid power changes are monitored using the two fast responding cobalt NDs.

The rod instrumentation includes three cladding surface thermocouples and one fuel thermocouple, a cladding extensometer and a pressure sensor. In the first trial test (IFA-650.1) the cladding thermocouples were located at the upper and lower ends and in the middle of the fuel segment. In the next experiments with ballooning, the cladding temperature will be measured at the upper and lower ends of the fuel rod only. The fuel temperature was measured at the top of the fuel. The cladding extensometer and the pressure sensor are located at the top of the rod.

2.2 Test runs and results

A total of six trial runs were carried out in the first LOCA experiments. The peak cladding temperatures, rod linear heat generation rates (LHGR) and heater powers are presented in Table 1.

Table 1 Peak cladding temperatures with the rod LHGRs, and the heater powers.

Run [No.]	Rod LHGR [W/cm]	Heater Power [W/cm]	Peak Cladding Temperature [°C]	Note
1.	12	6	840	
2.	12	6	840	
3.	12	12	890	spray used
4.	18	6	930	
5.	23	20	1050	
6.	28	22	1140	spray used

The measured fuel temperatures during the test runs are shown in Figure 3 and the corresponding cladding temperature histories in Figure 4.

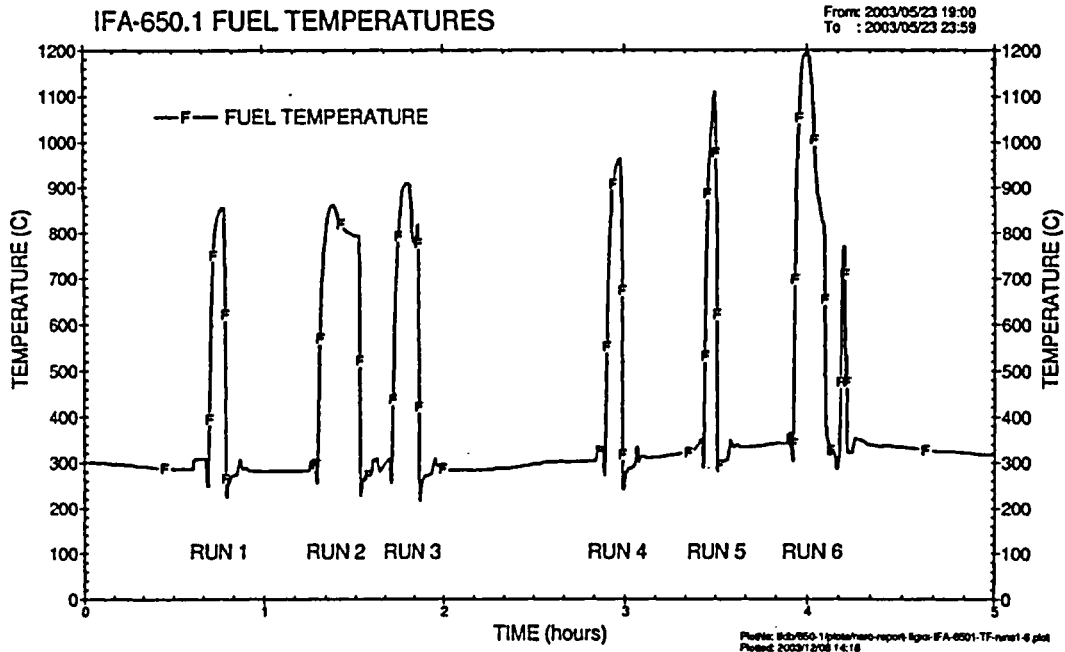


Figure 3 Measured fuel temperatures during the LOCA test runs.

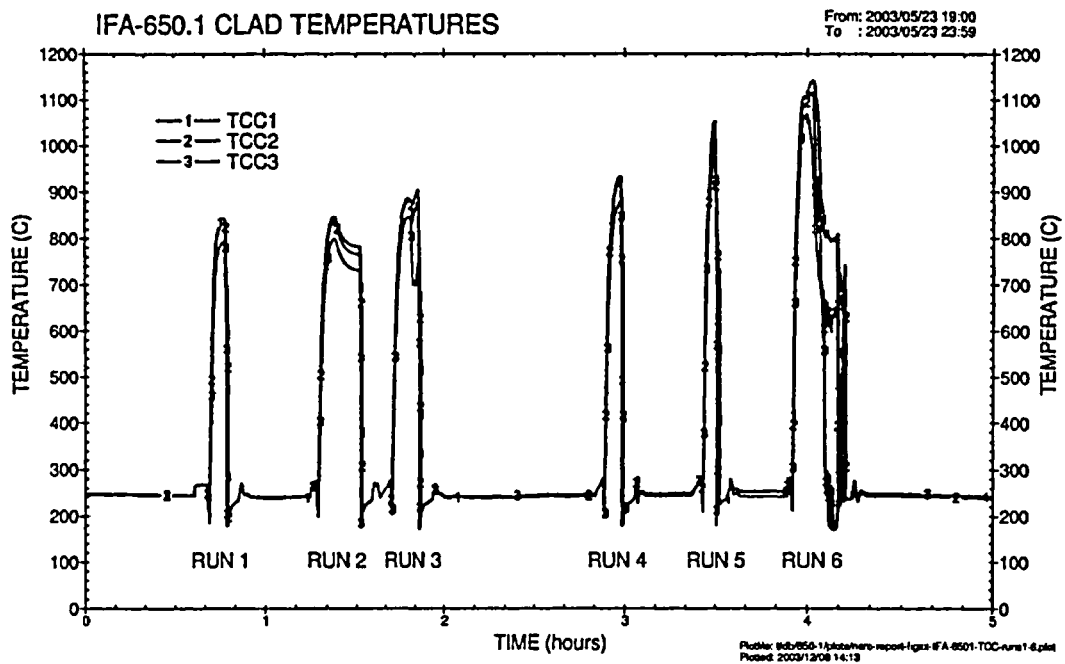


Figure 4 Measured clad temperatures during the LOCA test runs.

The target maximum cladding temperature was 800°C in first two test runs. In the subsequent four runs the cladding temperatures were gradually increased to about 1100°C by raising the rod and heater powers. The transient temperature responses can be seen in more detail in Figure 5 - Figure 7, where fuel center, cladding and heater temperatures are presented along with heater power for all runs.

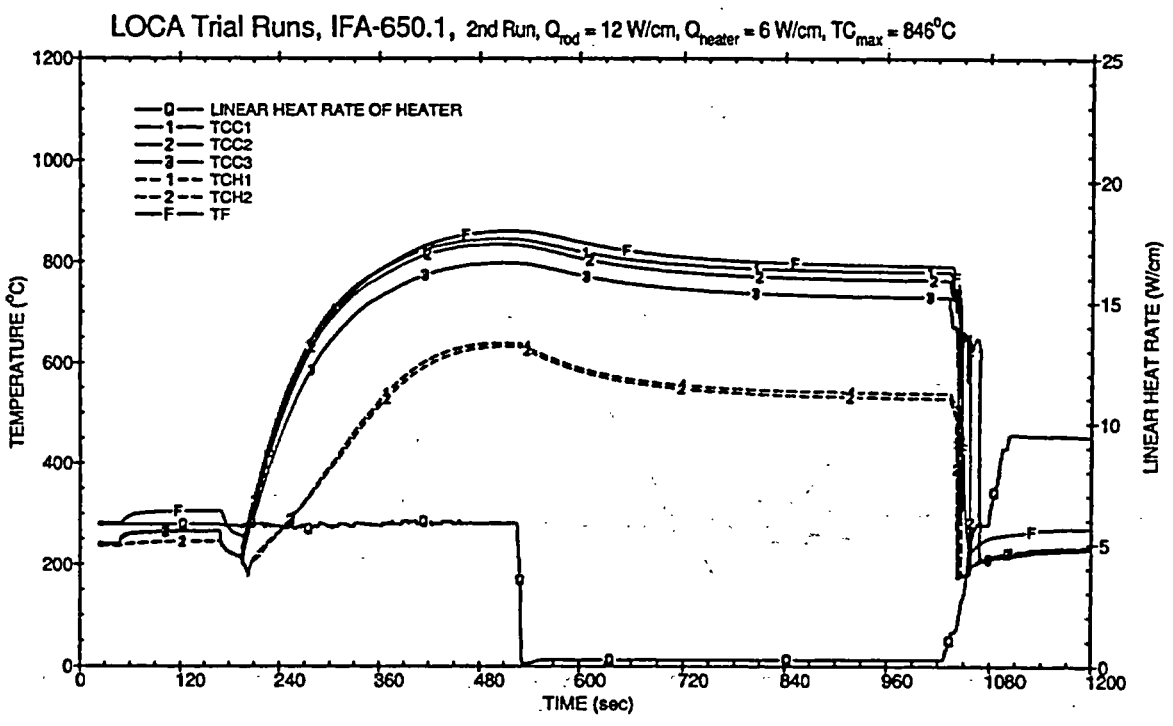
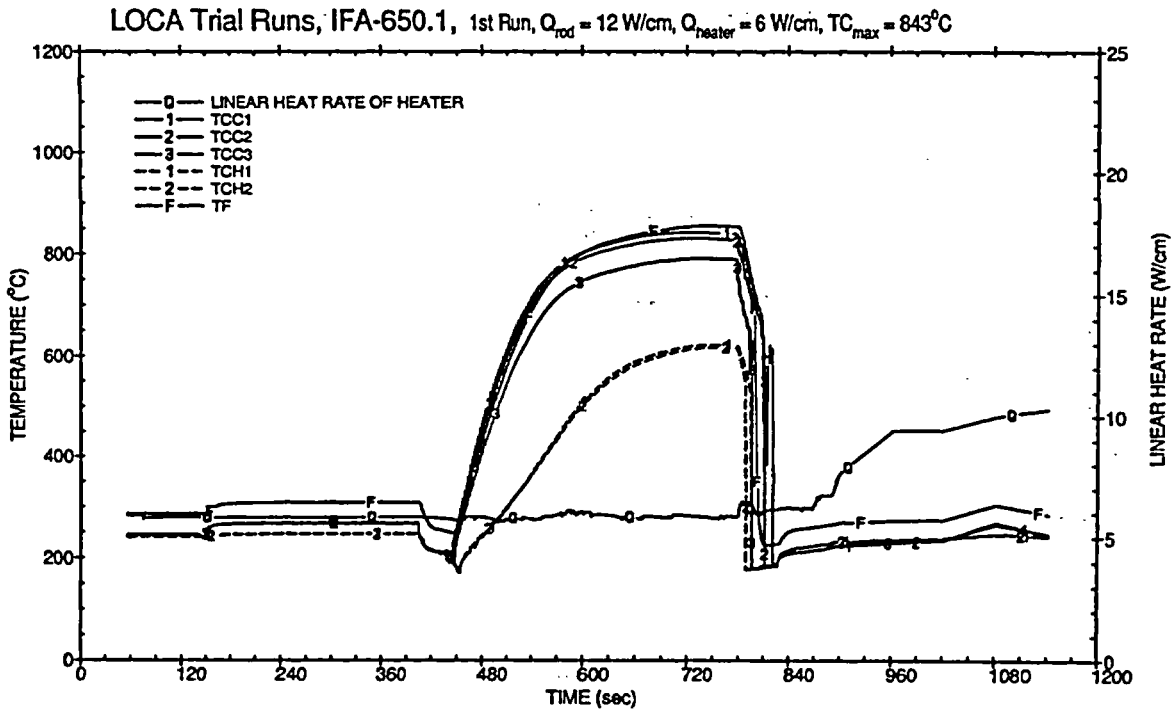


Figure 5 Cladding surface, heater and fuel temperatures during the trial test runs 1 and 2. The effect of heater power is seen. Nomenclature: F = fuel temperature, Q = linear heat rate, lines 1-3 = cladding temperatures (from bottom to top of the rod), dashed lines 1-2 = heater temperature.

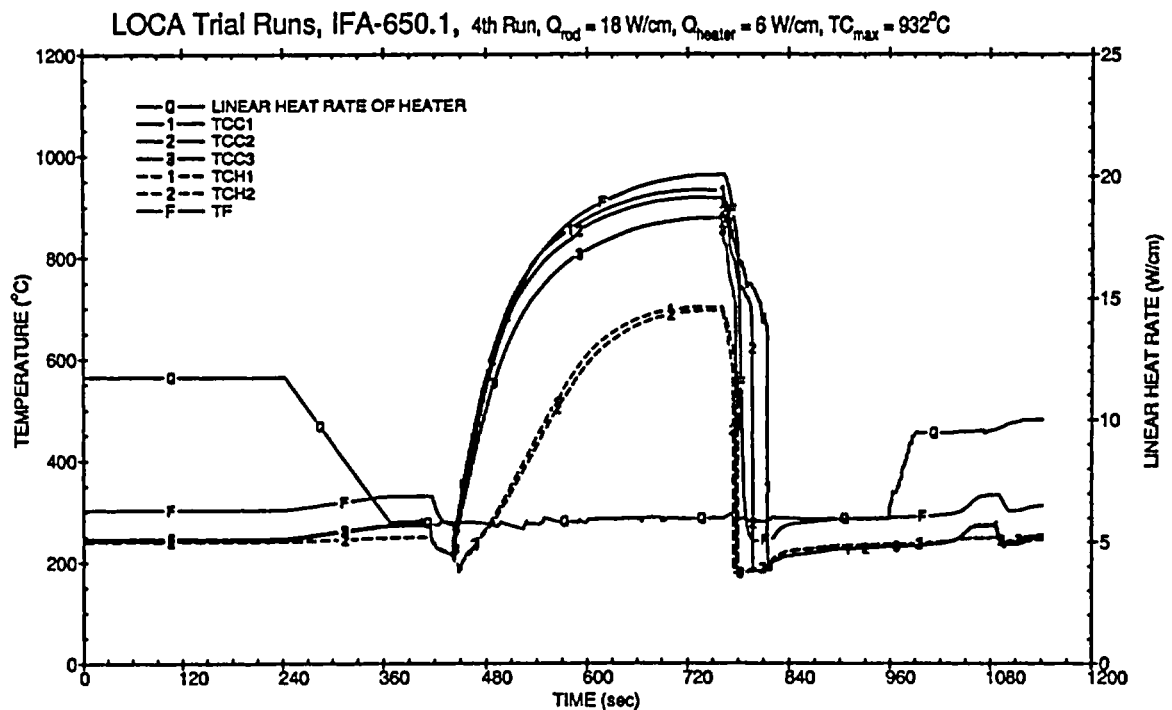
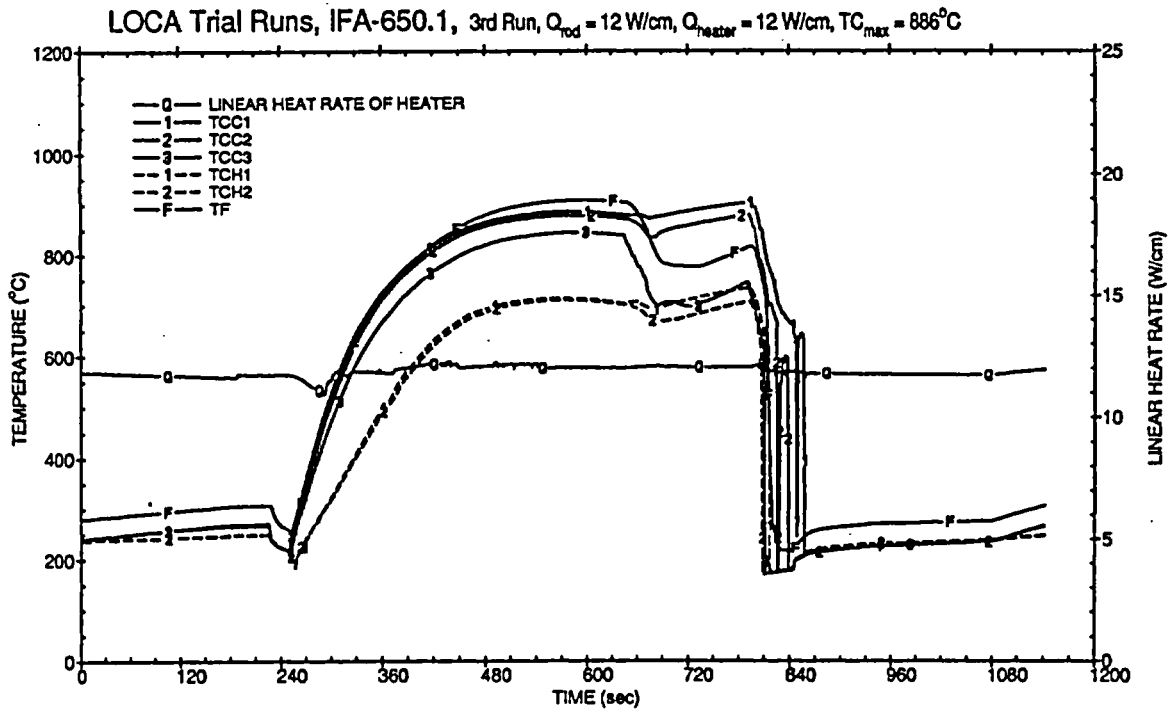


Figure 6 Cladding surface, heater and fuel temperatures during the trial test runs 3 and 4. The effect of heater power is seen. Nomenclature: F = fuel temperature, Q = linear heat rate, lines 1-3 = cladding temperatures (from bottom to top of the rod), dashed lines 1-2 = heater temperature.

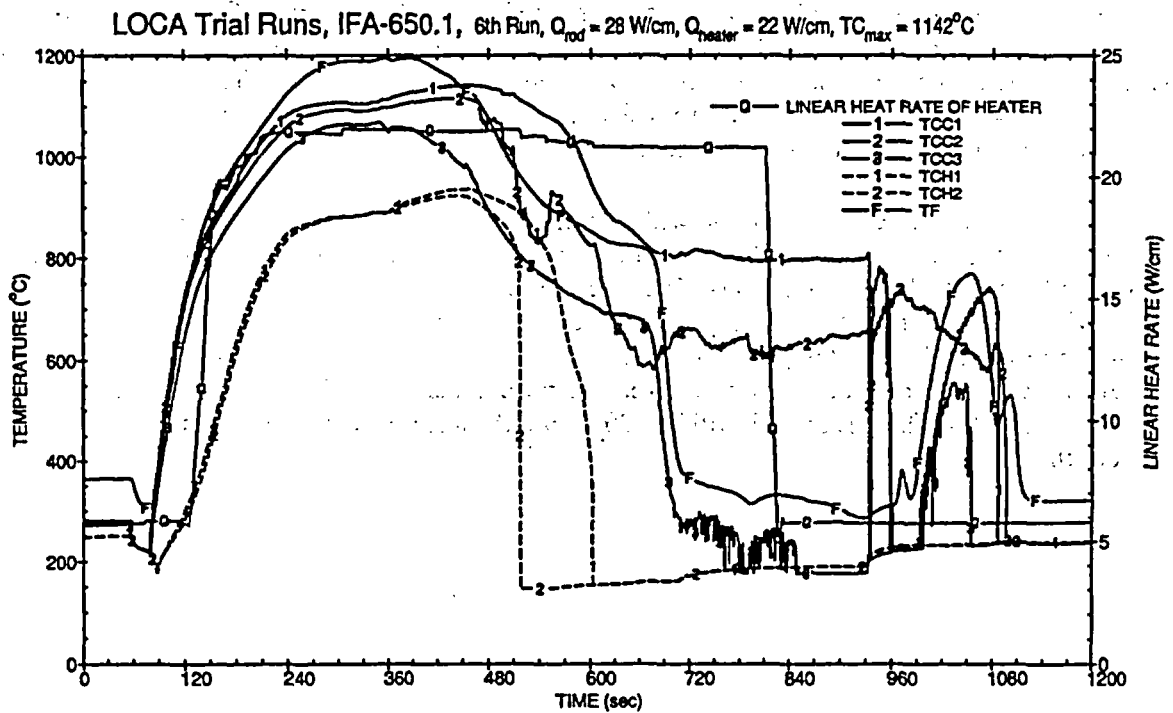
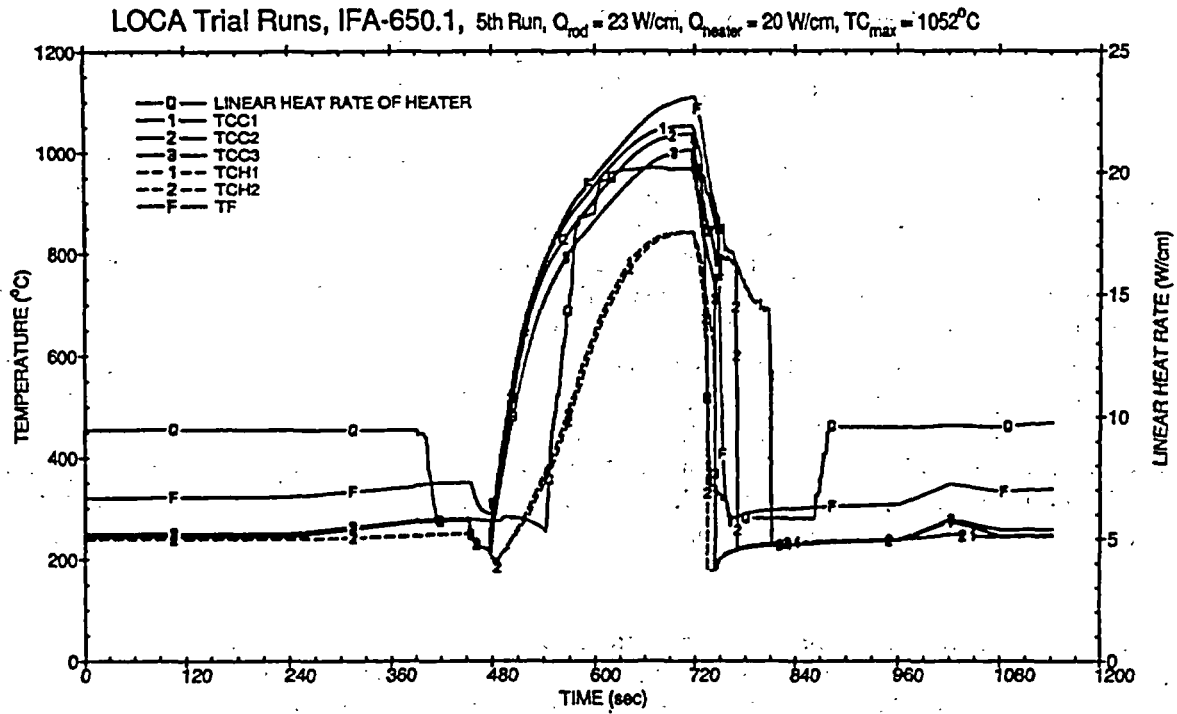


Figure 7 Cladding surface, heater and fuel temperatures during the trial test runs 5 and 6. The effect of heater power is seen. Nomenclature: F = fuel temperature, Q = linear heat rate, lines 1-3 = cladding temperatures (from bottom to top of the rod), dashed lines 1-2 = heater temperature.

In runs 1 and 2, the linear heat rate (LHR) of the fuel was about 12 W/cm and of the heater about 6 W/cm. The peak cladding temperature (PCT) in both cases was about 845°C. In run 2 the heater was shut off during the test. Reduction of the heat input reduced temperatures by about 20-30°C.

In run 3 the LHR of the rod was kept at about 12 W/cm, but the heater power was now higher, about 12 W/cm. The PCT was about 886°C. The spray system was used and it is seen that the temperature of the upper cladding thermocouple decreased, while the other two thermocouples remained almost stable. The fuel temperature measured at the top of the fuel, decreased by the same amount. In run 4 the LHR of the fuel was increased to 18 W/cm and that of the heater decreased to 6 W/cm. The resulting PCT was 932°C. In run 5 the LHR of the fuel was about 23 W/cm and the heater about 20 W/cm and the PCT was 1052°C. In the final run (6), the LHR of the fuel was 28 W/cm and the heater power 22 W/cm, resulting in a PCT of 1142°C, slightly above the target cladding temperature of 1100°C. The spray system was tested also in run 6. The effects were very similar to run 3, the temperatures of the cladding and fuel thermocouples at the top of the fuel rod tended to decrease, but the other two thermocouples did not spontaneously react to the injection of a small amount of water (6 l/h). The spray valve was opened gradually and the heater was totally quenched about 300 seconds after starting of the spray. At that point the spray valve was about 50-60% open.

The results show that the target cladding temperatures of 800°C and 1100°C were achieved in the tests. Comparing test runs 3 and 4, it can be seen that both the fuel and the heater LHRs were different, but the PCTs were quite similar. The total LHR (fuel+heater) was about the same, which explains the similarity of the temperatures. In test run 5 both fuel and heater LHRs were raised. The effect on the cladding temperatures is clear; they increased with increasing LHRs. In the last run (6) the fuel power was increased further, but the heater LHR only slightly. The measured cladding temperatures increased by almost 100°C. The influence of spraying can be seen from the test runs 3 and 6. The temperatures of the uppermost thermocouple and the fuel decreased immediately upon spraying, while the effect on the cladding lower thermocouples was smaller and delayed.

In the second experiment the test rig design will be similar to the first test apart from a few changes. The enrichment of the fuel will be 2 wt% U_{235} instead of 4 wt% U_{235} in the first test. This gives a possibility to use higher and more stable reactor powers. The filler gas will be argon instead of helium. The filler gas pressure will be about 40 bar at room temperature and about 75 bar in hot condition. Because ballooning is expected in test 2, fuel or cladding thermocouples will not be located at the rod mid-height. A six cycle PWR fuel rod with Zr-4 cladding will be used in the third experiment. The burnup of the fuel will be about 70 MWd/kg UO_2 . The target PCT will be 800°C and the test run will be terminated by a scram, not by full quench.

3. CODE ANALYSES

Some pre-test calculations were performed by outside laboratories using the codes FRAPTRAN/GENFLO (VTT) and TRAC-BF1 (PSI). FRAPTRAN/GENFLO is a coupled code where FRAPTRAN calculates fuel performance and GENFLO thermal-hydraulics. TRAC-BF1 is the LOCA code developed for BWR simulations.

FRAPTRAN/GENFLO calculations are in a good accordance with the measurements. Both the shape of the curve and the maximum temperatures are reasonable and the code will be utilised for analyses of future LOCA tests.

Calculations were also performed by the Halden project using the codes FTEMP3, SCTEMP3 and ALGOR. These codes are relatively simple in-house codes, which calculate transient thermal behaviour of fuel using different heat transfer correlations. With FTEMP3 steady-state analyses can be performed. During the power ramp up to about 18 MW, predicted fuel temperatures were in a good agreement with the measurements. Also SCTEMP3 gave useful results. The commercial finite element analysis (FEA) code ALGOR is capable of calculating heat conduction, but radiative and convective heat transfer must be calculated semi-manually.

The codes have a tendency to overestimate the cladding temperatures to some extent during the transients. All the codes do have several input parameters, which separately and in combination (e.g. emissivity factors) have a strong influence on the calculated results. They gave fairly good simulations of the clad temperatures recorded in the six runs and provided valuable input for planning this first test series.

5. SUMMARY

The first LOCA test runs were performed in the Halden reactor in May 2003 using a fresh small-gap and unpressurised PWR rod with Zr-4 cladding. Totally six test runs were carried out. The target PCTs of 800-1100°C were successfully achieved.

The cladding temperatures were increased by raising the power of the fuel and the heater. From the results it can be seen that the total LHR (fuel + heater) is the major factor determining the clad temperature transients. The spray was successfully tested at the end of the two test runs. The effect of the spray is limited to the thermocouples located at the upper end of the fuel. The spray can't be used for controlling the cladding temperature precisely and its main purpose will be to ensure right conditions for oxidation. The rig and the loop as well as the instrumentation and the data collecting systems worked well. No fuel failure occurred. The first LOCA trial runs gave a good basis for the further tests to be conducted in 2004.

In preparation for the initial tests several code calculations were performed by the outside laboratories as well as by the Project. FRAPTRAN/GENFLO (VTT) and TRAC-BF1 (PSI) calculations were made by the outside laboratories and ALGOR, SCTEMP and FTEMP3 calculations were made by the Halden project. The code calculations gave good overall simulations of the clad temperatures and they will be continued in the future.

A Scaling Method for RIA Data

R. O. Meyer
U.S. Nuclear Regulatory Commission

Background

Most of the test data for reactivity-initiated accidents (RIAs) with high-burnup pressurized water reactor (PWR) fuel rods have been obtained in the Cabri test reactor in France and the Nuclear Safety Research Reactor (NSRR) in Japan. Both test reactors have provided data on the fuel enthalpy required to produce cladding failure, which is important in some safety analyses. However, neither of these facilities reproduces conditions in a commercial reactor, so it is desirable to scale these data to PWR conditions to obtain relevant results.

There are several ways to use test reactor data for RIA analysis for commercial reactors. The traditional way is to use the data to validate a transient fuel rod code and then perform the commercial reactor analysis with that code. The difficulty with this indirect use of test reactor data is that it assumes that an appropriate failure model is available in the code and all code modeling assumptions and materials properties data are adequate for RIA analysis. Modeling assumptions (e.g., symmetric fuel pellet loading of the cladding, homogeneous and isotropic cladding mechanical properties) are not very accurate, and the mechanical properties data base for irradiated cladding is quite limited at this time. But the biggest difficulty is with the failure model; a broadly accepted understanding of RIA failures is not yet available. In fact, the failure modes observed to date range from brittle to mixed to ductile. Also, the presence of non-homogeneous hydride precipitates and blisters may have a significant impact on the failure mode.

To minimize these uncertainties, a more direct way to use test reactor data for RIA analysis has been chosen. This method uses code stress and strain predictions at the time of cladding failure in the test reactor to determine critical values associated with the fuel rod segment used in the test. In order to apply these results to predictions for the behavior of the test rod segments in a PWR environment, it is necessary to estimate how these critical values would change with test conditions – principally test temperatures and pulse width. An algorithm is described here for scaling RIA test reactor data to the RIA history relevant to a PWR. Such an approach can be refined as more material property and test reactor data become available.

Failure in the elastic region

For failures that occur in the elastic region, cladding hoop stress is probably the most important parameter. Brittle failure occurs at a critical stress intensity factor (i.e., fracture toughness), which is proportional to the product of the nominal applied stress and the square-root of the flaw size. For scaling purposes, the flaw sizes and distribution of flaws are assumed to be identical for a given specimen under test reactor or commercial reactor conditions. Using FRAPTRAN, the hoop stress is calculated as a function of time for the actual test reactor pulse.¹ The calculated hoop stress at the time of failure is taken as the critical failure stress. The calculation is then run again, but this time pulse shape, coolant temperature, coolant pressure, and rod internal pressure are changed to those that would be expected in a PWR. The previously determined value of critical failure stress is adjusted for resulting temperatures

and is then located in the new calculation of hoop stress as a function of time; the corresponding time is taken as the time of expected failure during the hypothetical PWR pulse.

Cladding in the REP-Na10 test in Cabri appears to have failed in or near the elastic region, and this test is used to illustrate the scaling method for such a failure. Measured test parameters for REP-Na10 are shown in Table 1.²

Table 1 Measured Parameters for REP-Na10	
Total Energy Input	107 cal/g
Time at Failure (arbitrary zero)	0.456 s
Pulse Width (Full Width at Half Maximum)	31 ms
Initial Coolant Temperature	553°K

Calculations performed by IRSN with the SCANAIR code show that failure in REP-Na10 occurs near the end of the elastic region.³ Our own calculations with FRAPTRAN show that plastic deformation has already begun at that time. Therefore, we used a gap size that was larger than expected and assumed that failure occurred at a slightly earlier time to ensure failure in the elastic region for the purpose of this illustration. Resulting calculated parameters for the REP-Na10 test at the assumed time of failure are shown in Table 2.

Table 2 Calculated Parameters for REP-Na10	
Fuel Enthalpy Increase at Failure	59 cal/g
Cladding Hoop Stress = Failure Stress	450 MPa
Cladding Average Temperature	740°K

Rough validation of the strain predictions made by FRAPTRAN can be made by looking at measured plastic hoop strains for tests with non-failed cladding in Cabri's REP-Na test series.⁴ (Strain could not be measured for tests with cladding failure because sodium ingress caused additional swelling and cladding strain.) These measured values are shown in Fig. 1.

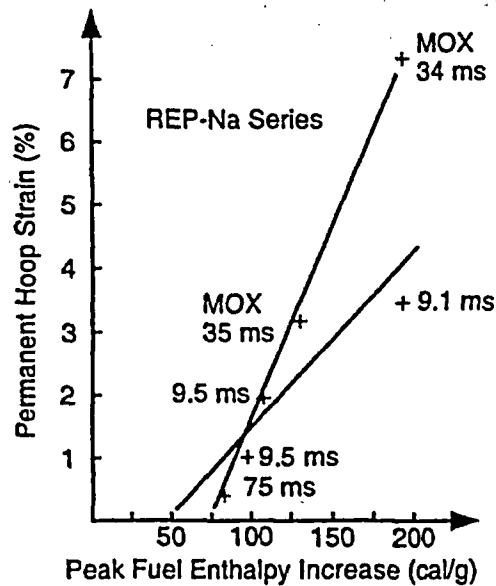


Figure 1 Permanent hoop strain as a function of enthalpy increase for Cabri data

The intercept is not well defined because it is not known if the data form a single population or should be segregated by pulse width or by fuel pellet type. Nevertheless, it is clear that between 50 and 75 cal/g are required to close any gaps and go through the elastic region such that plastic strain can begin. Our calculated value of 59 cal/g is in this range.

The deduced failure stress from Table 2 is 450 MPa at a temperature of 740°K. However, the Cabri test pulse was broad and equivalent stresses will occur at lower temperatures in a narrower PWR pulse. It was assumed that failure stress is proportional to independently measured fracture toughness, which exhibits a temperature dependence. Using such a temperature dependence (assumed for this calculation), we estimated the failure stress for this fuel rod specimen as shown in Fig. 2.

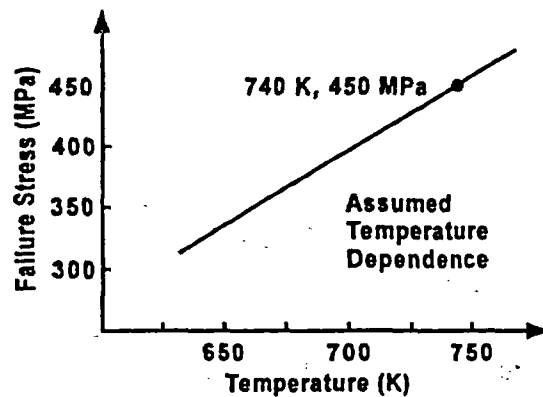


Figure 2 Estimated Dependence of Failure Stress on Temperature

A second calculation was run with a pulse shape corresponding to PWR conditions, but having the same total deposited energy as the REP-Na10 test pulse. Both power traces are shown in Fig. 3.

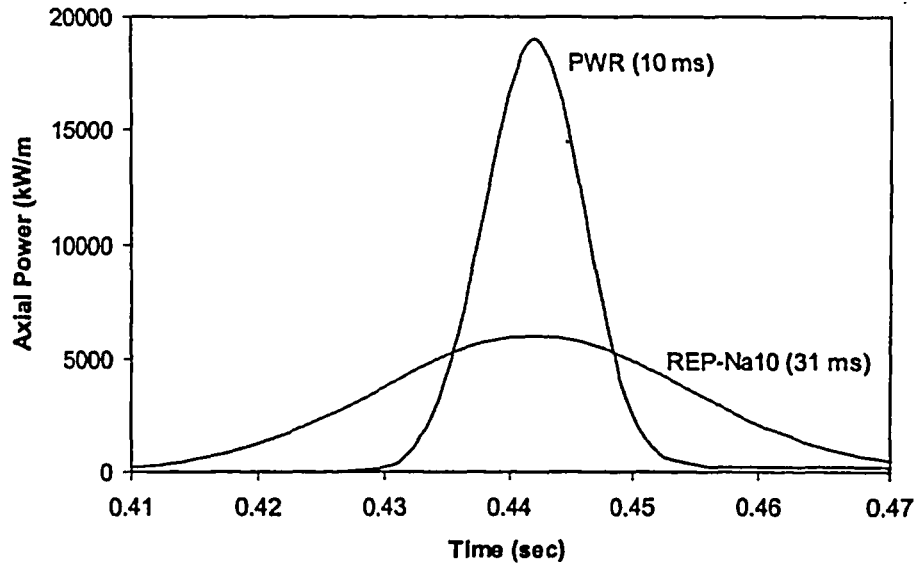


Figure 3 REP-Na10 pulse shape and corresponding PWR pulse shape

The effect of pulse width on cladding temperature can be seen clearly in Fig. 4. This figure shows average cladding temperature as a function of fuel enthalpy. Fuel enthalpy can be considered approximately equivalent to fuel pellet expansion, which is the source of both stress and strain in the cladding. Thus, a given stress or strain occurs at a higher temperature in a broader pulse.

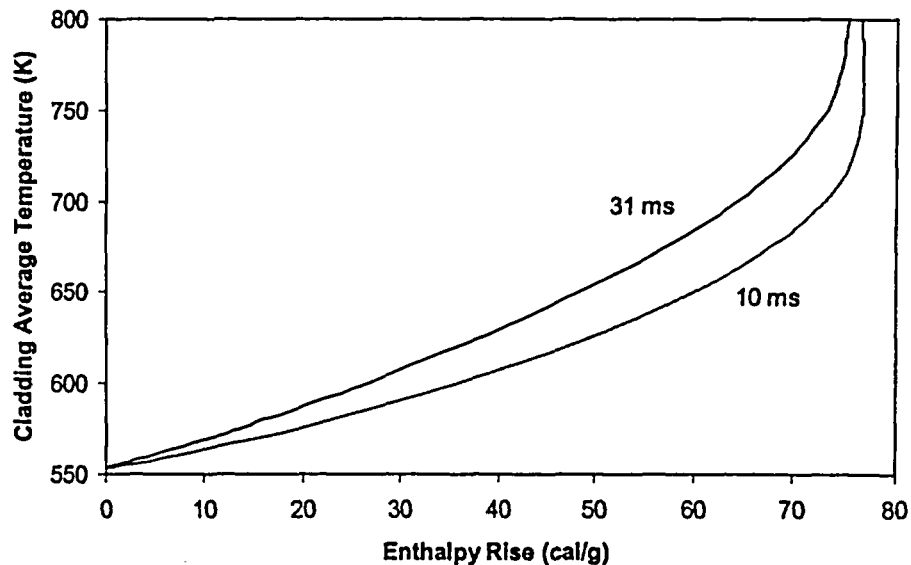


Figure 4 Average Cladding Temperature as a Function of Enthalpy Rise

A time can be found in this second calculation for which cladding temperature and applied stress fall on the failure line shown in Fig. 2. The results are given in Table 3.

Table 3 Calculated Parameters for the REP-Na10 Specimen with PWR Test Conditions	
Fuel Enthalpy Increase at Failure	40 cal/g
Cladding Hoop Stress	350 MPa
Cladding Average Temperature	660°K

The conclusion is that, if this fuel rod specimen had been subjected to a narrow PWR pulse, cladding failure would have occurred at a somewhat lower stress and lower temperature corresponding to a fuel enthalpy about 20 cal/g lower than that observed in the Cabri test.

Failure in the plastic region

For failures that occur with some plastic hoop strain, ductility is probably the most important parameter. Strength is no longer important because the loading is displacement-controlled and cladding deformation progresses beyond the plastic yield strain (yield strength) and beyond uniform elongation (ultimate tensile strength) in many cases. Using FRAPTRAN, the plastic hoop strain is calculated as a function of time for the actual test reactor pulse and for a corresponding PWR pulse. The method of comparison is the same as above except that a failure strain is determined instead of a failure stress.

Cladding in the HBO-1 test in NSRR appears to have failed in the plastic region, and this test is used to illustrate the scaling method for such a failure. Measured test parameters for HBO-1 are shown in Table 4.

Table 4 Measured Parameters for HBO-1	
Total Energy Input	93 cal/g
Time at Failure (arbitrary zero)	0.2045 s
Pulse Width (Full Width at Half Maximum)	4.4 ms
Initial Coolant Temperature	291°K

In NSRR, not only are the pulses atypical (too narrow), but the test temperature is also atypical (too low). Both atypicalities can be addressed with this method. Calculated parameters for the HBO-1 test pulse are shown in Table 5.

Table 5 Calculated Parameters for HBO-1	
Fuel Enthalpy Increase at Failure	60 cal/g
Cladding Plastic Hoop Strain = Failure Strain	0.62%
Cladding Average Temperature	340°K

Rough validation of the strain predictions made by FRAPTRAN can again be made by looking at measured plastic hoop strains for tests with non-failed cladding in NSRR's HBO test series.⁵ These measured values are shown in Fig. 5. Strain was not measured for tests with cladding failure.

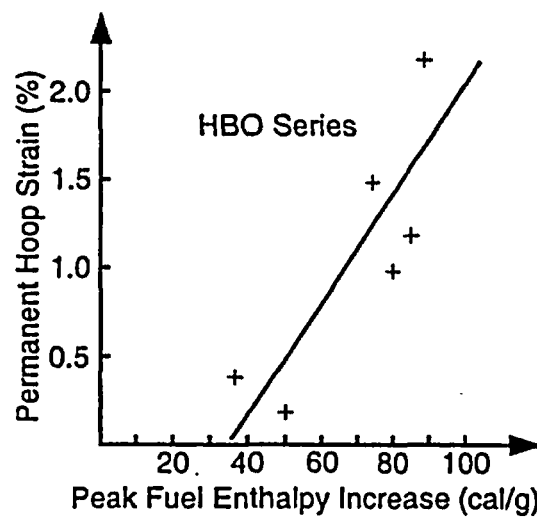


Fig. 5 Permanent Hoop Strain Versus Enthalpy Rise in NSRR

The intercept is better defined for this test series than for Cabri's REP-Na series. The plastic strain corresponding to 60 cal/g is seen to be about 0.7%, in good agreement with our calculation.

Since both pulse width and test temperature are atypical, they can be examined separately. The pulse width can be examined first by comparing calculations for the HBO-1 test pulse and a pulse of the same deposited energy and the same test temperature, but having a broader width. These two pulses are shown in Fig. 6.

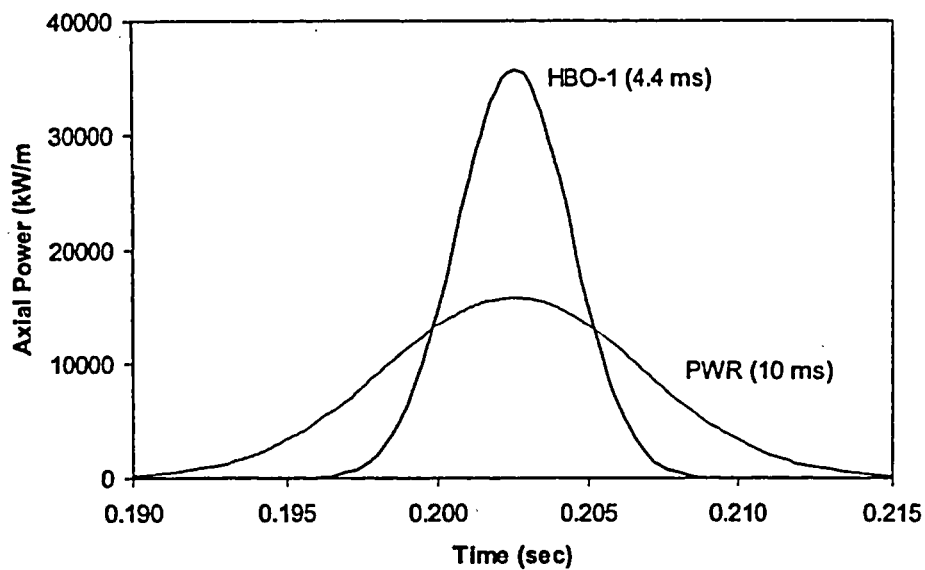


Fig. 6 HBO-1 pulse shape and corresponding PWR pulse shape

In this case the second pulse is broader and will produce equivalent strains at somewhat higher temperatures. It was assumed that failure strain is proportional to independently measured total elongation values, which exhibit a temperature dependence. Using such a temperature dependence (assumed for this calculation), we have estimated the failure strain for this fuel rod specimen as shown in Fig. 7.

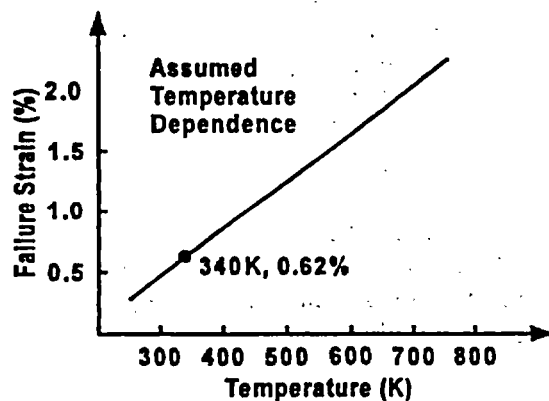


Figure 7. Estimated failure strain for HBO fuel rods

No time could be found in this calculation for which the cladding temperature and the plastic strain fall on the failure line shown in Fig. 7. The reason for this is interesting and has significant consequences. Figure 8 will illustrate this situation with a plot of cladding temperature and permanent strain on the same figure.

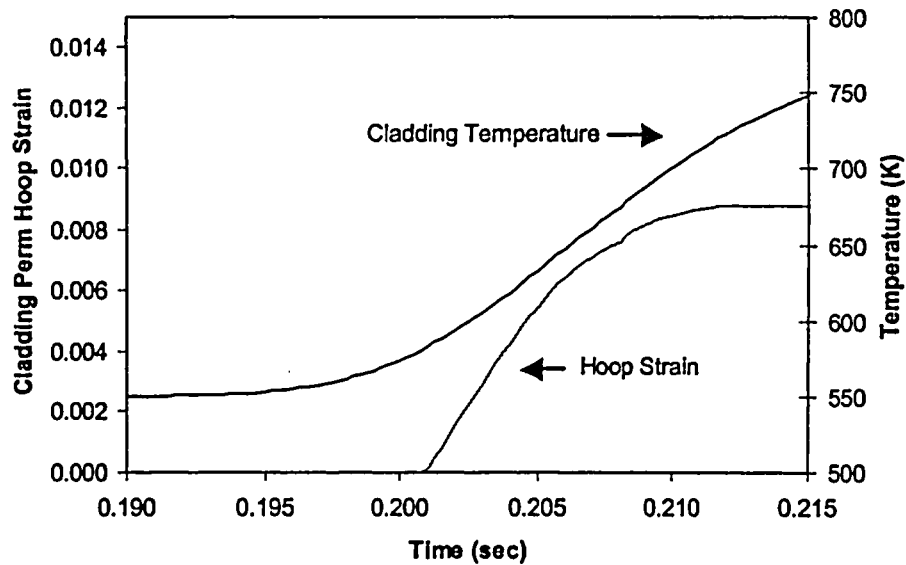


Fig. 8 Cladding Permanent Hoop Strain Versus Temperature

After exceeding the yield stress, the plastic strain increases at a rapid rate until the fuel enthalpy approaches its maximum value. While the rate of increase in strain is slowing down, the rate of increase of cladding temperature is not, because heat is continuing to flow from the pellet through the cladding. Thus, a *point of no return* is reached, beyond which failure cannot occur because cladding temperature is increasing the failure strain (total elongation, Fig. 7) faster than pellet expansion is increasing the cladding strain. This has two closely related consequences. One is that a pulse of greater total deposited energy will have to be used in our scaling calculations to determine the effect of pulse width. The other is that HBO-1, which failed at 60 cal/g with a pulse that had a total energy input of 93 cal/g, would not have failed with a pulse that had a total energy input of 60 cal/g. This is a general result and gives a source of margin that can be taken into account in applying the scaling method.

Three other 10-ms pulses were calculated to find a time at which the cladding temperature and plastic strain would fall on the failure line shown in Fig. 7. The pulse with 110% of the total energy deposition did not produce a failure either, but the pulses with 120% and 130% of the total energy deposition both produced the same result within 1 cal/g. These results are shown in Table 6.

Table 6 Calculated Parameters for the HBO-1 Specimen with a 10 ms Pulse and 291°K Test Temperature	
Fuel Enthalpy Increase at Failure	69 cal/g
Cladding Plastic Hoop Strain	0.75%
Cladding Average Temperature	380°K

Similarly, a pulse with a much larger (twice in this example) total energy deposition was used to estimate the effects of both pulse width and test temperature together. Power traces for this pulse and the HBO-1 test pulse are shown together in Fig. 9.

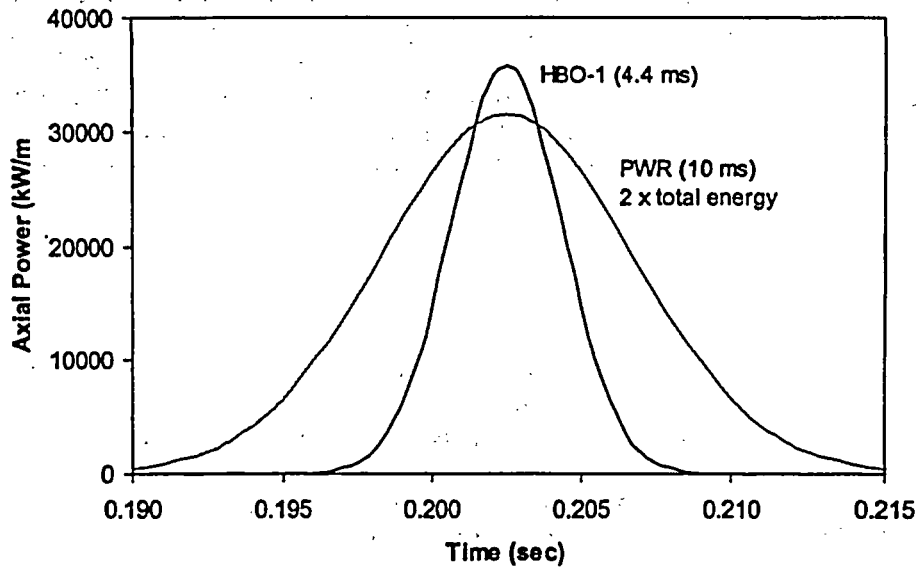


Figure 9 HBO-1 pulse shape and PWR pulse with twice the total energy

Results from comparing these calculations are given in Table 7. The combination of pulse width and test temperature atypicalities lead to a 40 cal/g increase in the expected failure enthalpy.

Table 7 Calculated Parameters for the HBO-1 Specimen with PWR Test Conditions	
Fuel Enthalpy Increase at Failure	100 cal/g
Cladding Permanent Hoop Strain	1.7%
Cladding Average Temperature	710°K

Notice that the 1.7 percent calculated strain at 100 cal/g also agrees with the experimentally determined plastic strains for the HBO series as shown in Fig. 5.

Summary

For the assumed temperature dependence of failure stress, the Cabri REP-Na10 test would be expected to fail at a fuel enthalpy 20 cal/g lower than that observed with the 31-ms pulse, if the test had been conducted with 10-ms pulse that is typical of a PWR. Although the temperature dependence assumed here was arbitrary, it was somewhat lower than the temperature

dependence of fracture toughness that we inferred from the data of Bertolino et al.⁶ For the assumed temperature dependence of failure strain, the NSRR HBO-1 test would be expected to fail at a fuel enthalpy 40 cal/g higher than that observed, had the test been conducted with 10-ms pulse and a temperature that are typical of a PWR. Of this amount, 10 cal/g is due to pulse width effects alone. Although the temperature dependence assumed here was arbitrary, it is consistent with unpublished data that are just emerging. If a much larger temperature dependence for failure strain (total elongation) were assumed, the ductility of this moderately corroded HBO rod could increase so much that cladding failure by pellet-cladding mechanical interaction (PCMI) might not occur at all. Cladding failure should not be expected to occur at or near the peak fuel enthalpy in a test reactor or in a power reactor, and this margin can be taken into account in applying the scaling method.

References

1. M.E. Cunningham, C.E. Beyer, P.G. Medvedev and G.A. Berna, *FRAPTRAN: A Computer Code for the Transient Analysis of Oxide Fuel Rods*, U.S. Nuclear Regulatory Commission Report NUREG/CR-6739 (PNNL-13576), August 2001.
2. Ch. Marquié, C. Hée, F. Hueber and E. Ragagli, *Quick Look Report of the Cabri REPNa10 Test*, Institut de Protection et de Surete Nucleaire (France) Note Technique LEAC n°3/98, October 1998.
3. H. Rigat, *Precalculations of the CABRI REP Na 10 Test Using the SCANAIR Code Version 2.3*, Institut de Protection et de Surete Nucleaire (France) Note Technique SEMAR 98/82, July 1998.
4. J. Papin, F. Lemoine and E. Fédérici, "Main Outcomes from the Cabri Test Results," *Proceedings of the Topical Meeting on RIA Fuel Safety Criteria*, Aix-en-Provence, France, 13-15 May 2002 (NEA/CSNI/R(2003)8/Vol. 2)
5. T. Nakamura, H. Sasajima and H. Uetsuka, "NSRR RIA Tests Results and Experimental Programs," *Proceedings of the Topical Meeting on RIA Fuel Safety Criteria*, Aix-en-Provence, France, 13-15 May 2002 (NEA/CSNI/R(2003)8/Vol. 2)
6. G. Bertolino, G. Meyer and J. Perez Ipiña, "Effects of Hydrogen Content and Temperature on Fracture Toughness of Zircaloy-4," *Journal of Nuclear Materials* 320 (2003) 272-279.

Recent results from LOCA study at JAERI

Fumihisa NAGASE and Toyoshi FUKETA
Department of Reactor Safety Research
Japan Atomic Energy Research Institute
Tokai-mura, Ibaraki-ken, 319-1195, Japan

Abstract

With a view to obtaining basic data to evaluate high burnup fuel behavior under loss-of-coolant accident (LOCA) conditions, a research program is being conducted at the Japan Atomic Energy Research Institute (JAERI). The program consists of integral thermal shock tests and other separate tests for oxidation rate and mechanical property of fuel claddings. Prior to the tests on irradiated claddings, the tests have been conducted on non-irradiated claddings to examine separate effects of corrosion and hydrogen absorption during reactor operation. Hydrogen effects have been especially examined because hydrogen absorption has an great impact on cladding embrittlement. The tests on irradiated claddings have recently been started and preliminary results have been obtained. The present paper summarizes recent results from those studies.

1. Introduction

Current safety criteria for LOCA were established during the late 60's and early 70's in most countries. These criteria are mainly based on experiments conducted with fresh Zircaloy fuel claddings. Although burnup effect was generally taken account of the criteria, the level of fuel burnup was rather low at that time. With burnup extension, corrosion and hydrogen absorption during the reactor operation become more significant in the fuel cladding, which causes degradation of the mechanical properties. In safety analysis for a postulated loss-of-coolant accident (LOCA) in a LWR, the fuel cladding would be exposed to high-temperature steam for several minutes and quenched by the emergency core cooling water. The cladding embrittled by severe oxidation would be subject to fracture due to thermal shock during the quench. Therefore, it is one of the most important issues to clarify the thermal shock resistance of the pre-corroded and pre-hydrated high burnup fuel rod in order to confirm the safety of LWRs in a LOCA, though peak clad temperature becomes lower with the burnup extension. The influence of burnup extension on high-temperature oxidation kinetics, rupture behavior, and mechanical properties of severely

oxidized cladding are also subjects of great concern. Under this circumstance, a systematic research program is being conducted at JAERI, which aims at a wide range database for evaluating the influence of burnup extension on fuel behavior under LOCA conditions. The program consists of integral thermal shock tests and separate effect tests such as oxidation tests and mechanical tests. In the integral thermal shock tests, short test rods were heated up, ruptured, oxidized in steam and quenched by flooding water in order to evaluate the rupture behavior and thermal shock resistance of oxidized cladding under simulated LOCA conditions.

An increase in hydrogen concentration generally reduces the ductility of the cladding at relatively low temperatures. Therefore, hydriding before LOCA transient should be the most important factor on the cladding embrittlement under LOCA conditions. The present paper describes the effects of pre-hydriding on oxidation kinetics, rupture behavior and thermal shock resistance, which have been investigated with non-irradiated cladding tubes. The integral thermal shock tests with irradiated claddings have been started since January 2003 after test apparatus was successfully equipped in the Reactor Fuel Test Facility at JAERI. The present paper reports preliminary results from those tests as well.

2. Experimental method

2.1 Sample

Non-irradiated low-Sn (1.3wt%) Zircaloy-4 claddings were used in the tests to examine the separate effect of pre-hydriding. The initial outer diameter and thickness were 9.50 and 0.57 mm, respectively. Hydrogen concentration of the as-received cladding was about 10 ppm. Artificial hydriding was done at about 620 K in mixture gas of hydrogen and argon. Four claddings of 200 mm or 580 mm long were hydrided in one batch of the hydriding and one of the claddings was subjected to hydrogen analysis to estimate the hydrogen concentration of the other three. The hydrogen analysis was also performed on tested claddings to confirm the concentration of each cladding.

Two PWR fuel rods, irradiated to 39 and 44Gwd/t (rod average) at Takahama unit-3 reactor, are currently subjected to the thermal shock tests. The cladding material is low-Sn Zircaloy-4. The fuel rod is cut into 190 mm segments and defueled claddings are subjected to the tests. Three tests have been conducted and information of the cladding tubes used is summarized in Table 1. The initial oxide layer thickness ranged 18 to 25 μm and hydrogen concentrations were estimated to be about 200 ppm though the analysis has not been performed yet.

Table 1 PWR fuel segments subjected to integral thermal shock test

Sample No.	1	2	3
Fuel Type	17×17		
Rod Average Burn up (GWd/t)	43.9	39.1	
Fuel Cladding	Low tin Zircaloy-4		
Sampling Span No. from Top	4	2	2
Corrosion Layer Thickness (μm)	20	25	18
Zircaloy Thickness Remained (μm)	558	554	629

2.2 Oxidation test

As-received and pre-hydrated claddings were cut into 15-mm ring-like specimens and were isothermally oxidized in flowing steam at temperatures ranging from 773 to 1573 K for the duration between 30s and 2.16×10^6 s in a test apparatus. The test apparatus consisted mainly of a 38 mm I.D. quartz reaction tube, an electrical resistance furnace or an infrared furnace, and a steam generator. The ring-like specimen was hang inside the reaction tube and heated in steam flow. The steam supply rate to the cladding surface was $11 \text{ g/m}^2/\text{s}$ and it was sufficient to oxidize the specimen without steam starvation [1]. The specimen was heated up to target temperatures at a rate of about 20 K/s. The electrical resistance furnace was used for oxidation temperatures lower than 1373 K and the infrared furnace was used for temperatures higher than 1373 K. Weight measurement and microstructure observation were done after cooling, and oxidation rate was evaluated for every tested temperature.

2.3 Integral thermal shock test

Figure 1 shows a schematic of the test rod and the apparatus. Al_2O_3 pellets were loaded into a 580mm-long cladding tube, and Zircaloy-4 end caps were attached to the

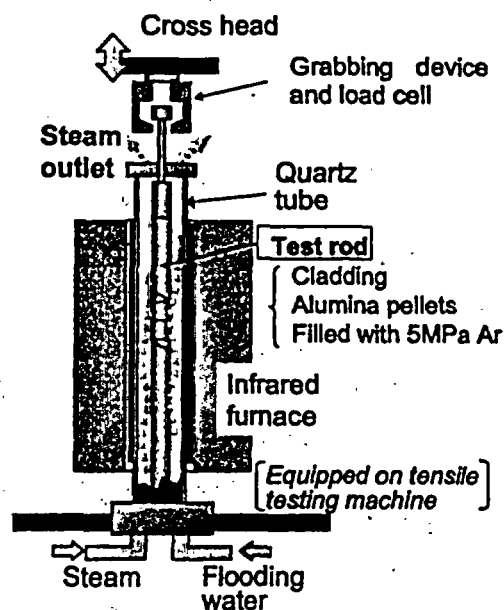


Fig. 1 Test apparatus for integral thermal shock test

cladding using Swageloc tube fittings. The rod was pressurized to about 5MPa with Ar at room temperature to cause cladding rupture with an increase of temperature. The test apparatus consists of an Instron-type tensile testing machine, a quartz reaction tube, an infrared image furnace with four tungsten-halogen lamps, a steam generator and a water supply system for flooding. The test rod was vertically mounted in the center of the reaction tube. Figure 2 shows an example of temperature history during the test. The rod is heated up at a rate of 10 K/s. Steam introduction is started prior to the heat-up, and the steam flow is maintained at a supply rate of about 36mg/s during the oxidation. The steam supply rate is sufficiently high to oxidize cladding tubes without steam starvation. During the heat up, the cladding tube balloons and ruptures at temperatures ranging 1000 to 1050 K with both an increase in rod internal pressure and a decrease in cladding strength.

The rod is isothermally oxidized after the rupture. Isothermal oxidation temperature and time ranges from 1220 to 1530 K and from 30 to 3000s, respectively. Three Pt-Pt/13%Rh thermocouples were spot-welded on the outer surface of the cladding to control and measure the cladding temperature. As shown in Fig. 2, the rod was cooled in the steam flow to about 970 K and finally quenched with water flooding from the bottom after the isothermal oxidation. Raising rate of water surface during quenching was 30 to 40 mm/s.

The test rod was quenched under non-restrained or restrained conditions. Under the restrained condition, both ends of the test rod were fixed to the tensile testing machine at the end of the isothermal oxidation for the tests. Figure 3 shows tensile load histories during the cooling and quenching phase of a test. In addition to the fully

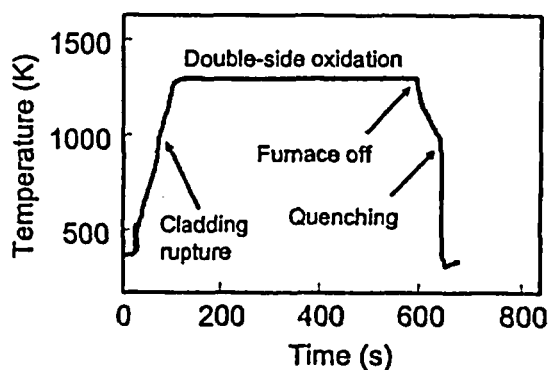


Fig. 2 Cladding temperature change during test.

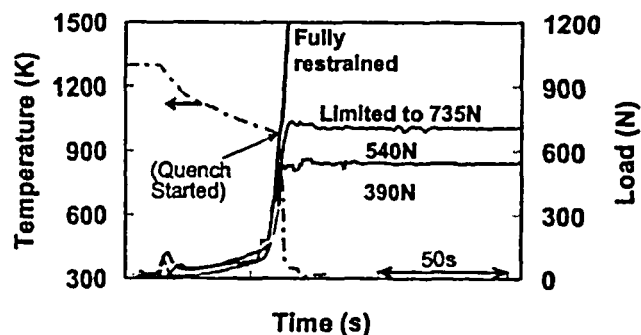


Fig. 3 Tensile load changes during cooling and quenching under axially restrained conditions

restrained condition, the rod was quenched under the intermediate restrained conditions. The maximum load was controlled at 390, 540 and 735 N with automatic load adjusting operation of the tensile testing machine.

For the irradiated cladding tube, Al₂O₃ dummy pellets were loaded in the 190mm-long defueled claddings, and Zircaloy end-plugs were welded at the both ends of the claddings. The test method was almost the same as that for the non-irradiated cladding, except for the restrained condition. The test rods were axially restrained at the maximum load of 540 N (30 to 35MPa for initial metal cross section). The maximum restraint load was conservatively determined referring to previous reports regarding the restrained conditions in bundle geometry [2-4].

3. Results and discussion

3.1 Hydrogen effect

3.1.1 Oxidation rate

The influence of pre-hydridding on the oxidation rate varies depending on temperature as well as hydrogen concentration. The weight gain ratio of pre-hydridded cladding to as-received cladding is plotted as a function of hydrogen concentration in Fig. 4. Pre-hydridding enhances oxidation above 1223 K and it is more remarkable at higher hydrogen concentrations. The largest influence is observed in the oxidation at 1223 and 1273 K. On the other hand, smaller enhancement and suppression effect of pre-hydridding are seen under specific hydrogen concentration ranges below 973 K. The phase structure of ZrO₂ formed on the Zircaloy changes from monoclinic to tetragonal between 1173 and 1273 K. Growth of oxide layer, namely diffusion of oxygen, is affected by the phase structure change of oxide layer. Therefore, the phase structure change of ZrO₂ might be connected with the different hydrogen effect on the oxidation. About 9% increase in oxidation rate at maximum was measured for the

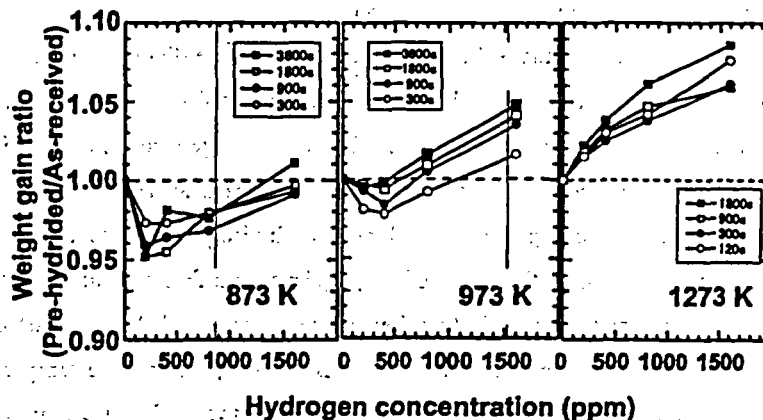


Fig. 4 Comparison of weight gain after high temperature oxidation between pre-hydridded and as-received cladding

examined ranges of hydrogen concentration and oxidation time. However, the hydrogen concentration is lower and oxidation time is shorter under the realistic conditions. Consequently, it can be said that enhancement of oxidation rate due to pre-hydrating is very small.

3.1.2 Rupture behavior

Circumferential strain due to ballooning and rupture was estimated by comparing the circumferential before and after the test. The correlation between the circumferential strain and the rupture temperature is shown in Figure 5. Data points are categorized into three groups for hydrogen concentration. The figure indicates that the circumferential strain reduces with an increase in the hydrogen concentration.

However, this is unlikely to be a general trend. It is known that the circumferential strain is strongly dependent on the phase structure of Zircaloy at rupture [5-7]. The circumferential strain shows a maximum in the temperature range where the Zircaloy transforms from α to $\alpha+\beta$, a minimum in the higher temperature range of the $\alpha+\beta$ phase region, and a second maximum in the temperature range from the $\alpha+\beta/\beta$ phase boundary to the β phase region.

Phase structure changes, based on the ternary phase diagram of the Zr-H-O system studied by Yamanaka et al. [8], are representatively shown in the figure for zirconium containing 300 (upper in the figure) and 1000 ppm hydrogen (lower in the figure). Oxygen concentration is assumed 1200 ppm. Zirconium containing 300ppm of hydrogen transforms from α to $\alpha+\beta$ at about 1100 K. The figure shows that the claddings containing 100 to 350 ppm of hydrogen rupture in the temperature range near the phase boundary. This is the cause of the higher circumferential strain of those claddings. The $\alpha/\alpha+\beta$ phase boundary drastically shifts to a lower temperature and the range of the $\alpha+\beta$ phase region expands with increase of hydrogen concentration. As a result, the rupture temperature of the claddings containing a larger amount of hydrogen is in the middle of the $\alpha+\beta$ phase region where the Zircaloy exhibits lower circumferential strains. The rupture temperature changes with the initial rod pressure. If the initial rod pressure increases and the rupture temperature of the highly hydrided cladding increases to the $\alpha/\alpha+\beta$

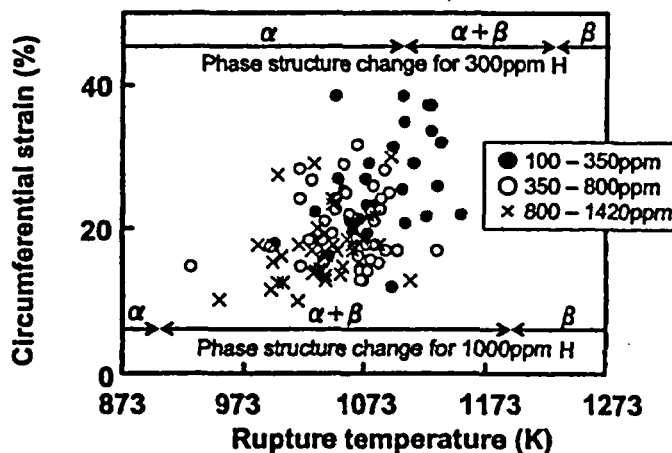


Fig. 5 Correlation between circumferential strain and rupture temperature for pre-hydrated Zircaloy-4 cladding tube

phase boundary, the circumferential strain would increase. Consequently, the present result shows that changes of phase transformation temperature with hydrogen concentration should be taken into account for estimating circumferential strain due to rupture.

3.1.3 Thermal shock resistance

Figure 6 shows the failure maps relevant to equivalent cladding reacted (ECR) and hydrogen concentration for four restrained conditions. The Baker-Just equation for oxidation rate [9] was used to estimate the amount of oxygen absorbed during oxidation. It was assumed in the estimation that the cladding was oxidized equally from the outer and the inner surfaces only during isothermal oxidation. The failure/non-failure threshold generally decreases with an increase in the initial hydrogen concentration for each restrained condition. Comparison of the maps indicates that the threshold obviously decreases with an increase in the restrained load. The threshold is very low for a wider range of hydrogen concentration above 300ppm under the fully restrained condition. Because cladding wall thickness is

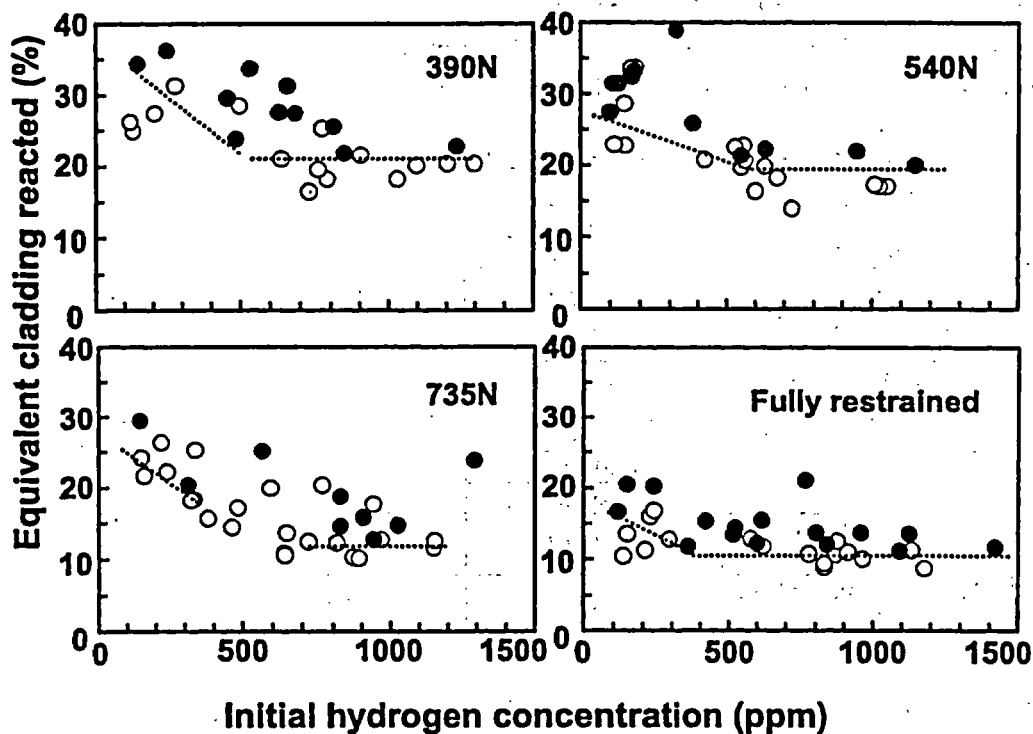


Fig. 6 Failure maps relevant to ECR and hydrogen concentration under four restraint conditions.

reduced most at the rupture position and stress by axial restraint is concentrated at the rupture opening, the cladding tubes fail at the position under the restrained conditions very often. Since no additional hydrogen absorption is observed at the rupture position, the initial hydrogen concentration is kept there. Thus, cladding embrittlement at the rupture position is more pronounced is by both oxidation and hydriding in the pre-hydrated cladding. This explains reduction of the failure threshold with an increase in the initial hydrogen concentration under the restrained conditions. On the other hand, the claddings fail away from the rupture position, where plenty of hydrogen up to about 3000ppm is analyzed, under the non-restrained condition. Therefore, pre-hydriding has negligible effect on the failure threshold [10].

3.2 Irradiation effect on thermal shock resistance

Conditions of the integral thermal shock tests for three 48GWd/t PWR claddings are summarized in Table 2. One cladding oxidized at 1453 K to about 30% ECR during the isothermal oxidation failed during quench. The post-test appearance is shown in Fig. 7. It is considered that cracking initiated at the rupture opening and propagated circumferentially. The oxidation condition is plotted in the failure map for non-irradiated claddings containing similar hydrogen concentrations (Fig. 8). Since the failure boundary of non-irradiated claddings with similar hydrogen concentrations, lies at about 28% ECR, the

Table 2 Summary of integral thermal shock test on 48GWd/t PWR cladding tubes

Test No.	1	2	3
Sample No.	A 3-1	A1-2	B L-3
Burst Temperature (K) [(C)]	1053 [780]	1053 [780]	1083 [810]
Burst Strain (%)	14.1	27.7	24.3
Oxidation Temperature (K) [(C)]	1453 [1180]	1465 [1192]	1430 [1157]
Oxidation Time (sec)	486	120	200
ECR	30.0*	17.9*	16.4*
Failed / Survived	Failed	Survived	Survived
Load at Failure (N) [(kgf)]	498 [50.8]	--	--
Maximum restraint load (N)	--	540	540

failure of the irradiated cladding agrees with the failure criteria for non-irradiated claddings. Two claddings oxidized at 1465 and 1430 K to about 16 and 18% ECR, respectively, survived the quench. This indicates that failure boundary is not reduced so significantly by irradiation to the examined burnup level.

4. Future plans

The JAERI plans to perform LOCA-related studies with PWR and BWR claddings (MDA¹, NDA², ZIRLO™, and Zircaloy-2) highly irradiated to about 70GWd/t. The influence of further burnup extension and new alloys will be investigated in detail.

5. Conclusion

- With a view to accumulating database for evaluating high burnup fuel rod behavior under LOCA conditions, a systematic research program is being conducted at JAERI with non-irradiated and irradiated claddings.
- Hydrogen effects on fuel behaviors under LOCA conditions have been especially examined and clarified.
- The tests have been started with irradiated claddings and preliminary results were obtained for 48GWd/t PWR fuel claddings.
- More tests are planned to investigate the influence of further burnup extension and new alloys on the fuel behavior under LOCA conditions in detail.

Acknowledgment

The present study regarding rupture behavior and thermal shock resistance has been performed as a cooperative research program of JAERI with Japanese PWR utilities.

REFERENCE

1. H. Uetsuka and T. Otomo, J. Nucl. Sci. Technol., Vol.26, No.2(1989)pp.240-248.
2. N. Waeckel et al, OECD/NEA SEG/FSM LOCA Meeting March 22-23, 2001, Aix-en-Provence.
3. K. Honma et al., ANS Annual Meeting, Milwaukee, Wisconsin, June 17-21, 2001.
4. T. Murata et al., ANS Annual Meeting, Milwaukee, Wisconsin, June 17-21, 2001.
5. F.J. Erbacher, Nuclear Engineering and Design 103(1987)55-64.

¹ Mitsubishi Developed Alloy (Zr-0.8Sn-0.2Fe-0.1Cr-0.5Nb) was developed by Mitsubishi Heavy Industries, Ltd.

² New Developed corrosion resistance Alloy (Zr-1.0Sn-0.27Fe-0.16Cr-0.1Nb-0.01Ni) was developed by Nuclear Fuel Industries, Ltd. and Sumitomo Metal Industries, Ltd.

6. R.H. Chapman, Fifth Water Reactor Safety Research Information Meeting, Gaithersburg, Maryland, Nov. 7-10, (1977).
7. H.M. Chung and T.F.Kassner, Argonne National Laboratory report ANL-77-31 (NUREG/CR-0344) (1978).
8. D. Setoyama and S. Yamanaka, to be published, Trans. At. Energy Soc. Japan, to be published, Vol.2, No.4 (2003), [Text in Japanese].
9. L. Baker and L.C. Just, Technical report ANL-6548 (1962).
10. F. Nagase et al., Proc. Topical Meeting on LOCA Fuel Safety Criteria, Aix-en-Provence, 22-23 March 2001, NEA/CSNI/R(2001)18 (2001), pp.197-208.

Key Input Variables for RIA Simulations: A Study Based on FRAPCON and SCANAIR Codes

F. J. Barrio, L. E. Herranz. CIEMAT-Spain

ABSTRACT

Accuracy of a transient code response during a RIA (Reactivity Insertion Accident) depends largely upon input variables, some of which come from the output of an irradiation code. In this paper the influence of the uncertainties affecting the FRAPCON-3 output variables that are transferred to SCANAIR 3.2 is analyzed. The experimental scenario taken as a reference has been the CIP02 test of the CABRI project.

The sensitivity of SCANAIR 3.2 results has been explored by examining output magnitudes of both a thermal nature (i.e., coolant and fuel temperature and enthalpy) and a mechanical one (clad elongation, hoop strain and strain energy density). The study has indicated that input variables might be split in two groups: "hard" and "soft" ones. Hard variables do affect drastically code estimates, either thermally and/or mechanically; hardness parameter, gap width and the so-called rim burst option are good examples of this group. Soft variables slightly affect code predictions; some of them are burn-up, EOL temperature, porosity, gas concentration and oxide layer width.

As a final remark, it should be underlined that the validity of the results here outlined are subject to the code interface analyzed, the present status of the codes and the experimental scenario taken as a reference.

1.- INTRODUCTION

The intention of nuclear industry to reach a higher burnup in the nuclear fuel has reopened some safety issues that were already solved for current burnups. This fact, together with some rod failures recorded in experimental programmes on RIA (Reactivity Initiated Accidents), has emphasised the need to carry out a comprehensive investigation of high burnup fuel response to a sharp energy deposition. One of these experimental set-ups is the CABRI project, where fuel rods irradiated to high burnup in commercial reactors are submitted to power pulses.

One important task linked to the CABRI project is the development of the SCANAIR code. Its purpose is to simulate the thermo-mechanical behaviour of a fuel rod under RIA conditions. As in the case of any other code, SCANAIR accuracy depends upon the models it contains and their coupling, as well as upon the description of the scenario made through the initial and boundary conditions in the input deck. In other words, the uncertainties in the fuel rod characterisation (coming from a steady state code) just at the beginning of the power pulse may play a major role in the SCANAIR code accuracy.

The objective of the work here presented has been to carry out an importance analysis of SCANAIR 3.2 input variables to determine which of them become critical for the code output accuracy. In order to do so, an uncertainty range has been defined for each variable studied. Worth to mention that this study is code and version specific; that is, the same conclusions could not be guaranteed for substantially upgraded versions. The scope of the study has been restricted to the experimental scenario provided by the CIP02 test of the CABRI International project.

This paper has been done under CIEMAT participation in the CABRI project through the agreement on "Thermomechanical Behaviour of High Burnup Fuel" established with CSN (Consejo de Seguridad Nuclear), who is a member of the International CABRI Project Consortium.

2.- BASIS FOR THE STUDY.

2.1.- CIP02.

The CIP02 experiment was carried out in November 2002 in the frame of the international CABRI Programme (Vallejo, et al 2003). A 0.5 m long piece from a rod containing UO₂ pellets in a cladding made of M5 alloy was submitted to a RIA in the CABRI experimental reactor. The father rod had been irradiated for six cycles in Gravelines 5 reactor. In span 5, the maximum burnup is 74.2 GWd/tU (rodlet average burnup of 74 GWd/tU). During the test, the rodlet underwent a power pulse 28.2 ms long (at middle height) that deposited 88.7 cal/g (369.6 KJ/Kg) on the rod after 1.2 s.

2.2.- SCANAIR.

The purpose of the SCANAIR code (Lamare, 2001) is to simulate the thermo-mechanical behaviour of a PWR rod in postulated RIA, for high burnup UO₂ and MOX fuels. It has been developed by IRSN and is still under improvement. The code is grouped in three main modules: thermal dynamics, fission gas and structural mechanics, with high coupling characteristics among them. The physical modelling mainly relies on global test interpretation of the CABRI experimental programme, including both in-reactor and separate effect tests. So far, the aim of the tests in the sodium loop of the CABRI reactor was to investigate only the first phase of the accident (until DNB), so the thermal-hydraulics modulus of SCANAIR was developed in order to deal with Na flow. Further extension of the code in order to deal with water thermal-hydraulics in RIA conditions has been considered thanks to the PATRICIA separate effect program. Additional improvement up to the fuel-coolant interaction phase is foreseen.

This code needs, as input deck, the definition of certain parameters and the description of the rodlet state after the irradiation period. Using an irradiation code such as FRAPCON-3 can perform the last task.

2.3.- FRAPCON-3

The steady state rod behaviour has been simulated with FRAPCON-3. The code performs a 2D analysis of the fuel rod by assuming that it is azimuthally symmetrical and by nodalising it along the axial and across the radial direction. It was enabled to deal with long periods of irradiation at constant power and/or slow power ramps up to 65 GWd/tU (rod average), (Berna, et al, 1997). As a result, many material properties and models were re-examined and upgraded when needed to account for the effects of high burnup. Examples are the fission gas release model, the fuel thermal conductivity equation, the cladding mechanical properties, etc.

3.- FRAPCON-3 -SCANAIR 3.2 INTERFACE.

The main source of information to work out the SCANAIR input-deck has come from the FRAPCON-3 calculations (Vallejo et al, 2003). Nonetheless, some variables required by SCANAIR are not readily available from the steady state analysis and they have been taken from the experimental values. In those

cases where FRAPCON-3 does not provide information and there are not measurements, a survey of related literature has been carried out to find out values as representative as possible.

Among the parameters obtained via FRAPCON-3 code, the most relevant are: fuel density, plutonium concentration, burnup, fission gas concentrations, EOL temperatures and pressure, clad oxide thickness and geometry dimensions of fuel and clad. Important variables settled thanks to data provided by literature are in particular: critical coverage fraction of grain boundaries by inter-granular bubbles, porosity, grain radius, rim width and intra-granular and inter-granular bubbles radius.

As mentioned before, variables coming from FRAPCON-3 code are subjected to uncertainties. Coping with those uncertainties is not a straight task. There are only a few variables whose range of uncertainty is referred to in FRAPCON manual (Lanning et al, 1997), these are the oxide layer width, the burnup and the gas concentration. For the others, such range must be decided attending to some physical considerations. Nevertheless, considering that this study is mainly exploratory, and in order to simplify the situation and to achieve a sufficient conservative determination, the uncertainty interval has been taken widely enough. It is worth to say that most of uncertainty ranges are considered much bigger than expected for a code like FRAPCON-3, and it will be clear later that if these huge ranges produce small variations in SCANAIR predictions, the expected errors will be of less importance.

The variables and their range of uncertainty are listed below:

1. Gap width: $\pm 50\%$
2. Oxide thickness: $\pm 50\%$
3. Porosity: up to 25% for pellet radius bigger than 0.38 cm (last seven nodes in the nodalisation, slightly wider than the rim area)
4. Gas concentration: $\pm 50\%$
5. Rim width: $\pm 90\%$
6. End of life temperatures: $\pm 20\%$
7. Power radial profile: $\pm 30\%$ (in the last seven nodes)
8. Burnup: $\pm 30\%$ (in the last seven nodes)
9. Plutonium concentration: $\pm 30\%$ (in the last seven nodes)

In SCANAIR input deck there are also some user options that need to be settled before running the code. One of these is the so-called "rim-burst", that can be either activated or not. This option notably influences the gas release modelling. With the rim-burst activated the total porosity is not conserved, and the fuel may swell. When the rim-burst is not activated the total porosity is maintained, so that no fuel swelling takes place. Some fuel swelling during the power burst is physically reasonable. Fission gas release modelling in SCANAIR is effect-driven and designed to maximise clad loading even further than expected on physical grounds (IRSN, 2003).

Another important option is the hardness value. It represents the resistance of a material to be penetrated under pressure. It means that it is a key parameter in the conditions of heat transmission between to materials in contact. When its value is set to zero, the contact is perfect and there is continuity in temperatures between both materials, contrarily, when it is set to infinity the contact is worst and the heat transmission is reduced. The simulation of the CIP02 experiment shows a better agreement with the experimental data when the hardness is set to zero (Vallejo et al, 2003), but it is not clear that this is a realistic physical case.

The variation of these two options in the study is:

1. Rim-burst option: activated or non-activated.

2. Fuel and clad hardness: zero or infinite.

4.- RESULTS AND DISCUSSION

The procedure to investigate the uncertainties transmission in SCANAIR output has been starting with a base case that is the case with the standard FRAPCON-3 results, rim burst non-activated and hardness zero, and modify each variable to its limits. In some cases two variables have been modified at the same time since there is a clear link between them.

4.1.- Reference variables.

The sensitivity was assessed through examining several output magnitudes of SCANAIR, some of a thermal nature (coolant and fuel temperatures and enthalpy) and others of a mechanical one (clad elongation, hoop strain and strain energy density (SED)). The selection was done considering two criteria. On the one hand variables for which there are experimental data (coolant temperature, clad elongation and remaining hoop strain) so a comparison with experimental results can be done, on the other hand magnitudes particularly important in safety evaluations of fuel integrity after a RIA (fuel temperature, enthalpy and SED).

4.2.- Test cases.

The variables and options considered in this study have been those whose uncertainty, as it has been observed in previous studies, could notably affect SCANAIR predictions. Anyhow, there are other magnitudes that could have some effect and it could be worth to investigate. We mean, for example, pore opening pressure, bubble and grain radius, some material properties, etc.

In Table 1 the results of the simulations are summarized. In this table the first, second and third columns contain the variable, its number and its variation in the uncertainty study. The fourth column indicates any relevant observation in the case considered (for example the values of any parameter that has been modified). The rest of the columns are the magnitudes to assess the sensitivity, containing their value and the percentage of variation with respect to the base case. Those cases with a notorious deviation with respect to the base case have been remarked in black.

Given the limited scope of this study only a few cross effects have been analyzed. Anyhow, in a previous sensitivity analysis, some of the potential cross effects were considered particularly relevant. Those cases have been the subject of this study.

TABLE 1. SCANAIR input deck sensitivity assessment

Modified variable			Observations	Enthalpy J/g	Coolant Temp. °C	Fuel max. Temp. °C	Cladding Hoop stra. %	Clad elong. cm	SED J/cm ³
Experimental results					383		0.31	0.25	
BASE CASE	1		Hard=0 Rim=NO	342.9	387.6	1263	0.37	0.32	1.65
Hardness	2	∞		375.6 9.5%	353.2 -8.8%	1365 8%	0.44 18.9%	0.32 0%	3.21 94.5%
Rim-burst	3	YES	Hard=0	353.8 3.2%	377.3 -2.6%	1286 1.8%	1.12 202%	0.32 0%	5.36 224%
	4		Hard=∞	380.4 10.9%	348.8 -10%	1370 8.4%	1.11 200%	0.33 3.1%	6.81 312%
Gap width	5	+50%		343.1 0.06%	387.6 0%	1264 0%	0.2 -45.9%	0.22 -31.2%	0.82 -50%
	6	-50%		342.8 -0.03%	387.5 -0.03%	1263 0%	0.51 37.8%	0.38 18.7%	2.67 162%
Oxide thickness	7	+50%		344.7 0.5%	384.1 -0.9%	1265 0.2%	0.42 13.5%	0.33 3%	1.62 -1.8%
	8	-50%		340.9 -0.6%	391.1 0.9%	1262 0%	0.34 -8%	0.3 -6%	1.77 7%
Porosity	9	up to 25% in the rim zone	Rim=NO	352.9 2.9%	376.4 -2.8%	1278 1.2%	0.35 -5.4%	0.32 0%	1.9 15%
	10		Rim=YES	362.8 5.8%	367.5 -5.1%	1321 4.6%	0.63 70%	0.32 0%	3.54 114%
Gas conc.	11	+50%		342.9 0%	387.6 0%	1263 0%	0.38 2.7%	0.32 0%	1.66 0.6%
	12	-50%		342.9 0%	387.6 0%	1263 0%	0.36 -2.7%	0.32 0%	1.64 -0.6%
Rim width	13	+90%	Rim=NO	342.9 0%	387.6 0%	1263 0%	0.39 5.4%	0.32 0%	1.64 -0.6%
	14		Rim=YES	355.1 3.5%	376.2 -2.9%	1291 2.2%	1.72 364%	0.33 3.1%	8.31 403%
	15	-90%	Rim=NO	342.9 0%	387.6 0%	1263 0%	0.36 -2.7%	0.32 0%	1.65 0%
	16		Rim=YES	348.3 1.5%	382 -1.4%	1270 0.5%	0.73 97%	0.33 3.1%	3.52 113%
EOL Temp.	17	+20%		342.9 0%	387.6 0%	1263 0%	0.35 -5.4%	0.32 0%	1.64 -0.6%
	18	-20%		343.1 0%	387.5 0%	1264 0%	0.36 -2.7%	0.32 0%	1.37 -16.9%
Power radial profile	19	+30%		339.9 -0.8%	397.3 2.5%	1380 9%	0.39 5.4%	0.29 -9%	1.26 -23%
	20	-30%		354.4 3.3%	375.6 -3%	1322 4.6%	0.36 -2.7%	0.34 6.2%	2.31 40%
Burnup	21	+30%	Rim zone	345.2 0.6%	384.9 -0.7%	1266 0.2%	0.37 0%	0.31 -3%	1.68 1.8%
	22	-30%		339.7 -0.9%	391.2 0.9%	1259 -0.3%	0.38 2.7%	0.32 0%	1.55 -6%
Pu Conc.	23	+30%		342.9 0%	387.6 0%	1263 0%	0.37 0%	0.32 0%	1.65 0%
	24	-30%		342.9 0%	387.6 0%	1263 0%	0.36 -2.7%	0.32 0%	1.64 -0.6%

In Figure 1 the deviation of two magnitudes, SED and Enthalpy, regarding to the base case are plotted for the 24 cases considered. The range of variations in both variables are 0.8-8.3 MJ/m³ for SED and 81-90.8 cal/g for enthalpy. It is easy to see, from this figure, that some cases produce large deviations, while others scarcely affect the results. In addition, one should note that variations in the plot are given in absolute terms; however, in sight of Table 1 the base case might be seen as a kind of averaged case, since some of the cases are shown to result in negative variations with respect to the base case.

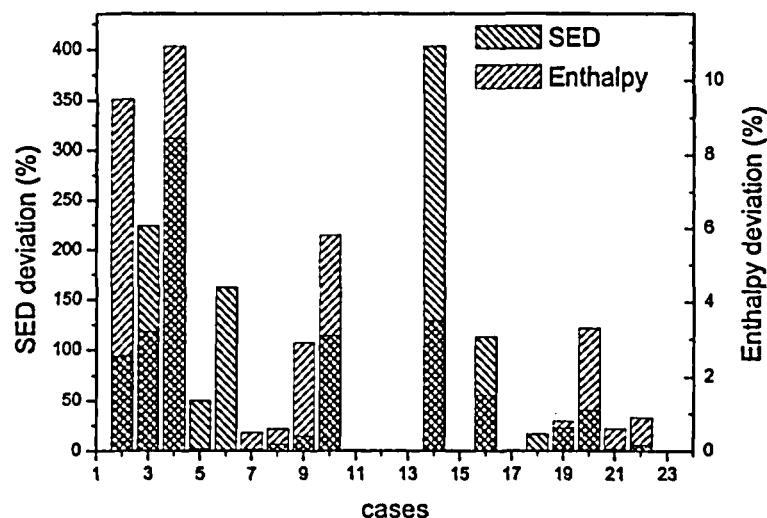


Figure 1. Deviation of SED and Enthalpy of the cases considered with respect to the base case

4.3.- Major observations

Those values significantly different from the base case are remarked in black in the table. From the table, the following comments arise:

1. The base case fits reasonably well to the experimental results.
2. There are variables or parameters whose effect in the results is quite huge, while others have much less influence.
3. Hardness, Rim-burst option and Gap width have strong influence in the results.
4. Gap width and rim-burst affect mainly mechanical response, hardness affects both thermal and mechanical response.
5. Comparison with available experimental results shows that in CIP02 simulation the input with the parameter hardness set to zero and rim-burst non-activated produces a closer result.
6. The rest of the variables do not have so high influence.
7. User options can make some variables become important. For example, porosity or rim width has a strong influence when including the rim-burst option activated.

4.4.- Remarks

It is important to emphasise that the calculations do not imply whether the variables do have or not an important influence in a RIA event. They only suggest that their accuracy in the input deck of SCANAIR is or not an important factor in the simulation.

The option with hardness zero and rim-burst non-activated produce closer values to experimental results in CIP02 simulation. The hardness zero implies a perfect thermal contact between fuel and cladding and is supported by the fact that for high burn-up fuel, the gap is closed at the end of the base irradiation and that there is a bonding between the 2 materials due to the internal zirconia layer. For the rim burst option not activated, this assumption is supported by the fact that the cladding temperature is still "low" in this first phase of the transient (i.e. no DNB) and restrains the gases inside the pellet for such a low energetic test (typical PCMI behaviour).

Only in few cases cross effects have been studied. In this respect this study should be taken as a first step to see which parameters or variables must be specially considered in both the irradiation and SCANAIR codes.

5.- SUMMARY AND CONCLUSIONS

The effect of the uncertainties in variables and parameters in the input deck of SCANAIR 3.2 code has been investigated. Some of these variables come from a steady state irradiation code (FRAPCON-3). These are fuel density, plutonium concentration, burnup level, fission gas concentrations, EOL temperatures and pressure, clad oxide thickness and geometry dimensions of fuel and clad. Two user options are directly implemented in SCANAIR input deck. These are the material hardness and the so-called rim burst option.

An accuracy interval has been established for each variable and the deviation of SCANAIR result with respect to the base case has been quantified. Two major groups have been identified regarding the value of this deviation. A group that can be called "hard" variables which produces a huge deviation. These are the gap width; the hardness parameter and the rim burst option. The rest of variables produce much less deviation and can be called "soft" variables.

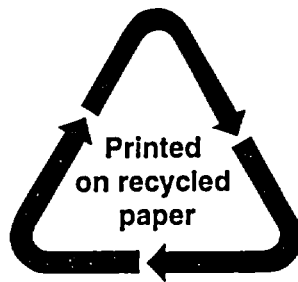
It is important to remark that this study is limited to the input deck of SCANAIR, and no considerations are done about the physical modelling. The work has been done with the SCANAIR 3.2 version, so the conclusions can differ for updated versions. As a final point, the simulation has been carried out based in the CIP02 experiment so no extension to other CABRI tests follows necessarily.

6.- REFERENCES.

1. Berna G.A. Lanning D.D., Beyer C.E., Davis K.L. 1997. *FRAPCON-3: A Computer Code for the Calculation of Steady State, Termal-mechanical Behaviour of Oxide Fuel Rods*. NUREG/CR-6534, Vol. 2.
2. Lamare F., 2001. *The SCANAIR Code Version 3.2: Reference Documentation*. Laboratoire d'Etudes Physiques des Accidents de Reactivité. Note Technique SEMAR 01/37.
3. Lanning D.D., Beyer C.E., Painter C.L., 1997. *FRAPCON-3: Modifications to Fuel Rod Materials Properties and Performance Models for High-Burnup Application*. NUREG/CR-6534, Vol.1

4. Vallejo I., Barrio F.J., García J.C., Herranz, L.E., 2003. *Simulation of the CIP02 Experiment of the CABRI Program*. DFN/SN-02/OP-02. CIEMAT.

NRC FORM 335 (2-89) NRCM 1102, 3201, 3202	U.S. NUCLEAR REGULATORY COMMISSION	1. REPORT NUMBER (Assigned by NRC, Add Vol., Supp., Rev., and Addendum Numbers, if any.)
BIBLIOGRAPHIC DATA SHEET		NUREG/CP-0185
<i>(See instructions on the reverse)</i>		
2. TITLE AND SUBTITLE		3. DATE REPORT PUBLISHED
Proceedings of the 2003 Nuclear Safety Research Conference		MONTH YEAR
		June 2004
5. AUTHOR(S)		4. FIN OR GRANT NUMBER
Conference Papers by various authors; Compiled by Susan Monteleone, BNL		A3988
		6. TYPE OF REPORT
Proceedings of conference on safety research		7. PERIOD COVERED <i>(Inclusive Dates)</i>
		October 20-22, 2003
8. PERFORMING ORGANIZATION - NAME AND ADDRESS <i>(If NRC, provide Division, Office or Region, U.S. Nuclear Regulatory Commission, and mailing address; if contractor, provide name and mailing address.)</i>		
Office of Nuclear Regulatory Research U.S. Nuclear Regulatory Commission Washington, DC 20555-0001		
9. SPONSORING ORGANIZATION - NAME AND ADDRESS <i>(If NRC, type "Same as above"; if contractor, provide NRC Division, Office or Region, U.S. Nuclear Regulatory Commission, and mailing address.)</i>		
Same as Item 8 above.		
10. SUPPLEMENTARY NOTES		
S. Nesmith, NRC Project Manager; Proceedings prepared by Brookhaven National Laboratory		
11. ABSTRACT <i>(200 words or less)</i>		
<p>This report contains papers presented at the 2003 Nuclear Safety Research Conference at the Marriott Hotel at Metro Center in Washington, DC, October 20-22, 2003. The papers were presented in each of the conference's technical sessions and at poster sessions over the course of the three days. They describe progress and results of programs in nuclear safety research conducted in this country and abroad. International participation in the meeting included papers presented by researchers from France, Germany, Japan, Norway and Russia.</p>		
<p>The titles of the papers and the names of the authors have been updated and may differ from those that appeared in the final program of the meeting.</p>		
12 KEY WORDS/DESCRIPTORS <i>(List words or phrases that will assist researchers in locating the report.)</i>		13. AVAILABILITY STATEMENT
reactor safety research nuclear safety research		Unlimited
		14. SECURITY CLASSIFICATION
<i>(This Page)</i> Unclassified		<i>(This Report)</i>
Unclassified		15. NUMBER OF PAGES
16. PRICE		



Federal Recycling Program

**UNITED STATES
NUCLEAR REGULATORY COMMISSION
WASHINGTON, DC 20555-0001**

OFFICIAL BUSINESS